THE EFFECT OF COMPOSITION ON THE BOILING RATES OF LIQUEFIED NATURAL GAS FOR CONFINED SPILLS ON WATER

by

Jaime A. Valencia-Chávez

B.S., University of Maryland (December, 1973)

Submitted in Partial Fulfillment
of the Requirements for the
Degree of Doctor of Science

at the

MASSACHUSETTS INSTITUTE OF TECHNOLOGY

February, 1978

Signature of Author: _____
Department of Chemical Engineering

Certified by: _____
Professor R. C. Reid
Thesis Supervisor

Accepted by: _____
Chairman, Departmental Committee on
Graduate Theses

Abstract

THE EFFECT OF COMPOSITION ON THE BOILING RATES OF LIQUEFIED NATURAL GAS FOR CONFINED SPILLS ON WATER

by

Jaime A. Valencia-Chávez

Submitted to the Department of Chemical Engineering on February 14, 1978, in partial fulfillment of the requirements for the degree of Doctor of Science.

The effect of composition on the boiling rates for confined spills of LNG on water was studied. Addition of heavier hydrocarbons to pure methane changed the boiling rates significantly, specifically increasing them in the initial period of time, thus leading to a higher maximum heat flux.

Upon contact with water, a preferential evaporation of the more volatile components takes place. The composition of the vapors evolved, as well as the temperature of the residual LNG, were experimentally determined at various times after the spill. Predictions made for the vapor composition and saturation temperature based on vapor-liquid equilibria considerations agreed well with the experimental data.

Initially, LNG mixtures film boil on water. A theory has been developed for the collapse of this film resulting in the high heat fluxes and boiling rates observed in the initial period. Consideration is given to the rise in saturation temperature following the depletion of methane, as well as to the amount of energy required to warm the residual LNG to this rising temperature.

Based on the above considerations, a heat transfer model that draws information from the vapor-liquid equilibria model has been developed. This combined heat transfer/vapor-liquid equilibria model predicts successfully the evaporation of confined spills of LNG on water.

Thesis Supervisor: Robert C. Reid
Professor of Chemical Engineering

Department of Chemical Engineering
Massachusetts Institute of Technology
Cambridge, Massachusetts 01239

February, 1978

Professor Irving Kaplan
Secretary of the Faculty
Massachusetts Institute of Technology
Cambridge, Massachusetts 02139

Dear Professor Kaplan:

In accordance with the regulations of the Faculty, I herewith submit a thesis, entitled "The Effect of Composition on the Boiling Rates of Liquefied Natural Gas for Confined Spills on Water," in partial fulfillment of the requirements for the degree of Doctor of Science in Chemical Engineering at the Massachusetts Institute of Technology.

Respectfully submitted,

Jaime A. Valencia-Chávez

To my parents

Luis and Julia

ACKNOWLEDGEMENTS

Generally a doctoral thesis represents a painstaking process and quite often difficult times. I would like to thank my thesis supervisor Professor Robert C.Reid; his encouragement and enthusiasm not only reduced the difficulties, they almost made it fun to work on this thesis.

I would also like to express my gratitude to the members of my thesis committee, Professors T. Drew, W. Rohsenow and K.A. Smith for their technical comments.

To my friends in the Department, too numerous to mention all of them here, go my thanks for their help in the many facets of my work, but mostly for their friendship. In particular, I would like to thank Kenton Griffis and Ross Wilcox for their technical suggestions. Most of all I am indebted to Mary Jane Garry who not only helped me through the rough spots but also labeled all of my graphs, edited and proof-read the thesis.

Finally I would like to thank Debbie Hackel for typing the manuscript.

TABLE OF CONTENTS

I. Summary 21

Introduction 21
Experimental 25
Vapor-Liquid Equilibria 29

Development of the VLE Model 30
Results 34

Boiling of LNG on Water 35

Results 38
Discussion of Results 43

Heat Transfer Models 46

Regression of Surface Temperatures by Using Convolution Integrals 46
Variable Grid Size Heat Transfer Model 50

Conclusions 56

II. Previous Work Relevant to the Boiling of LNG on Water 58

Regimes of Boiling 58
Effect of Surface Roughness on Pool Boiling 60
Boiling of Liquid-Liquid Interfaces 65
Boiling Heat Transfer to Liquid Mixtures 68
Boiling of Cryogenic Liquids on Solid Surfaces 75
Boiling of Cryogenic Fluids on Water 86

III. Experimental 107

Equipment for Spills of LNG on Water 107
Preparation of Cryogens 114
Analysis of Chemical Composition 117

IV. Vapor-Liquid Equilibria 121

Introduction 121
Development of the VLE Model 122
Applicability of the SRK Equation of State 133
Experimental Vapor Sampling 145
Experimental Results and VLE Model Predictions 148

TABLE OF CONTENTS - cont.

V. Boiling of LNG on Water 173

Results 173

Methane 173
Ethane 178
Propane 182
Nitrogen 186
Methane-Ethane Mixtures 187
Ethane-Propane Mixtures 191
Methane-Ethane-Propane Mixtures 191
Mixtures Containing Nitrogen 206
Water Temperatures 212
Vapor Temperatures 212

Discussion of Results 213

Methane 213
Ethane 218
Propane 220
Mixtures 221
Comparison of Results 227

VI. Heat Transfer Models 230

Previous Models 230
Semi-Infinite Solid 236
Moving Boundary Model 245
Regression of Surface Temperature by Using Convolution Integrals 255

Boiling on Ice 255
Boiling on Water 261

Variable Grid Size Heat Transfer Model 270
Combined VGS/VLE HTM Model for LNG Mixtures 279

VII. Secondary Observations Regarding the Evaporation of Light Hydrocarbons on Water 300

Foaming 300
Solid Phase (Ice) Composition 304
Water Pick-Up 309

TABLE OF CONTENTS - cont.

VIII. Conclusions and Recommendations 313

Conclusions 313
Recommendations 316

Appendices 317

A. Experimental 317

Electronic Balance 318
Real Time Computer 324
Computer Programs to Monitor Data Acquisition 327
Thermocouples 334
Gas Chromatograph 339

B. Vapor-Liquid Equilibria 342

The Soave-Redlich-Kwong Equation 343
Determination of the SRK Interaction Parameters, k_{ij} 347
Logic Diagram: Evaluation of Residual Liquid Composition 357
Vapor Sampling Time 359
Computer Programs 361

C. Computation of Boiling Rates 379

Procedure 380
Computer Programs 382

D. Heat Transfer Models 392

Properties of Ice 393
Properties of Water 394
Computer Programs 395

Convolution Integral 395
Variable Grid Size Heat Transfer Model 403
VGS/VLE HTM 408

Bibliography 421

TABLE OF CONTENTS - cont.

Location of Original Data 427

Biographical Note 428

LIST OF FIGURES

1-1	Experimental Set-up for the Study of LNG Boiling on Water	27
1-2	Boiling Vessel	28
1-3	Pressure Composition Diagram for the Methane-Ethane System (k_{ij} = 0.0)	33
1-4	Vapor Composition as a Function of Mass Evaporated (85.2% Methane, 10.1% Ethane, 4.7% Propane)	36
1-5	Temperature as a Function of Mass Evaporated (85.2% Methane, 10.1% Ethane, 4.7% Propane)	37
1-6	Mass Evaporated for Methane Boiling on Water	39
1-7	Boiling Rates for Methane	40
1-8	Mass Evaporated for Run R-20, Ternary Mixture	41
1-9	Boiling Rates for Run R-20, Ternary Mixture	42
1-10	Drop in Surface Temperature of Ice after a Methane Spill	48
1-11	Drop in Surface Temperature of Ice after a Spill of Methane on Water	49
1-12	Boiling of a Methane-Ethane Mixture on Water (R-1). VGS/VLE HTM Predictions and Experimental Data (τ_{cf} = 25 s)	52
1-13	Evaporation Rates of a Methane-Ethane Mixture on Water (R-1). VGS/VLE HTM Predictions and Experimental Data (τ_{cf} = 25 s)	53
1-14	Boiling of a Methane-Ethane-Propane Mixture on Water (R-20). VGS/VLE HTM Predictions and Experimental Data (τ_{cf} = 5 s)	54
1-15	Evaporation Rates of a Methane-Ethane-Propane Mixture on Water (R-20). VGS/VLE HTM Predictions and Experimental Data (τ_{cf} = 5 s)	55

LIST OF FIGURES - cont.

2-1	Regimes of Boiling	61
2-2	Effect of Surface Conditions on Boiling Heat Transfer	62
2-3	Effect of Roughness on Boiling Characteristics. Pentane Boiling on Copper (Berenson, 1962)	64
2-4	Effect of Heating Surface on the Nucleate Boiling of Pentane	67
2-5	Peak Nucleate Heat Fluxes for Water-Methyl Ethyl Ketone Mixtures (Van Wijk, 1956)	69
2-6	Peak Nucleate Heat Fluxes for Water-1-Pentanol Mixtures (Van Wijk, 1956)	70
2-7	Boiling of Liquid Nitrogen on Solid Surfaces at Atmospheric Pressure	76
2-8	Boiling of Methane on Solid Surfaces at Atmospheric Pressure	78
2-9	Boiling of Ethane on a Gold Plated Surface at Atmospheric Pressure	80
2-10	Boiling of LNG and Methane on a Gold Plated Surface at Atmospheric Pressure	81
2-11	Boiling of LPG and Propane on a Gold Plated Surface at Atmospheric Pressure	83
2-12	Effect of Composition on ΔT for Propane-n-Butane Mixtures at a Reduced Pressure of 0.3 - or 12.7 bar - (Clements, 1973)	84
2-13	Effect of Composition on Nucleate Boiling of Propane-n-Butane Mixtures, P_r = 0.3 (Clements, 1973)	85
2-14	Effect of LNG Composition on Evaporation Rate (Boyle and Kneebone, 1973)	91
2-15	Boiling of Methane and LNG on Gold and Water	94
2-16	Effect of Addition of Heavier Hydrocarbons on the Boiling of Methane on Water (Jeje, 1974)	98
2-17	Effect of Composition on the Boiling Heat Transfer of LNG on Water (Jeje, 1974)	100

LIST OF FIGURES - cont.

3-1	Experimental Set-up for the Study of LNG Boiling on Water	108
3-2	Boiling Vessel	110
3-3	Cryogen Distributor	112
3-4	Temperature Measurement. a) Vapor Thermocouple b) Typical Locations of Vapor and Liquid Thermocouples	113
3-5	Methane Liquefaction Apparatus	115
3-6	Ethane and Propane Liquefaction Apparatus	115
3-7	Sampling Bulb and Scoop for Chromatographic Analysis	119
4-1	Logic Diagram to Insure a Value of $\Delta\hat{L} \leq 0.01$ Moles is Used Throughout the VLE Model	132
4-2	Pressure Composition Diagram for the Methane-Ethane System ($k_{ij} = 0.0$)	134
4-3	Pressure Composition Diagram for the Methane-Ethane System. Low Pressure Range ($k_{ij} = 0.0$)	135
4-4	Pressure Composition Diagram for Methane-Propane System ($k_{ij} = 0.01$)	137
4-5	Pressure Composition Diagram for the Ethane-Propane System ($k_{ij} = 0.0$)	138
4-6	Pressure Composition Diagram for the Nitrogen-Methane System ($k_{ij} = 0.035$)	139
4-7	Pressure Composition Diagram for Nitrogen-Ethane System ($k_{ij} = 0.035$)	140
4-8	Pressure Composition Diagram for the Nitrogen-Propane System ($k_{ij} = 0.120$)	141
4-9	Vapor Sampling Bulb	147
4-10	Schematic of the Vapor Sampling Procedure	149
4-11	Temperature Composition Diagram for the Methane-Ethane System	152

LIST OF FIGURES - cont.

4-12	Temperature Composition Diagram for the Ethane-Propane System	154
4-13	Temperature Composition Diagram for the Methane-Propane System	155
4-14	Vapor Composition as a Function of Mass Evaporated (83.5% Methane, 16.5% Ethane)	156
4-15	Vapor Composition Composition as a Function of Mass Evaporated (89.7% Ethane, 10.3% Propane)	157
4-16	Temperature as a Function of Mass Evaporated (89.7% Ethane, 10.3% Propane)	158
4-17	Vapor Composition as a Function of Mass Evaporated (84.0% Methane, 9.4% Ethane, 6.6% Propane)	160
4-18	Temperature as a Function of Mass Evaporated (84.0% Methane, 9.4% Ethane, 6.6% Propane)	161
4-19	Vapor Composition as a Function of Mass Evaporated (88.9% Methane, 10.2% Ethane, 0.9% Propane)	162
4-20	Temperature as a Function of Mass Evaporated (88.9% Methane, 10.2% Ethane, 0.9% Propane)	163
4-21	Vapor Composition as a Function of Mass Evaporated (83.9% Methane, 8.1% Ethane, 8.0% Propane)	164
4-22	Temperature as a Function of Mass Evaporated (83.9% Methane, 8.1% Ethane, 8.0% Propane)	165
4-23	Vapor Composition as a Function of Mass Evaporated (51.8% Methane, 30.0% Ethane, 18.2% Propane)	166
4-24	Vapor Composition as a Function of Mass Evaporated (70.1% Methane, 20.5% Ethane, 9.4 Propane)	167
4-25	Temperature as a Function of Mass Evaporated (70.1% Methane, 20.5 Ethane, 9.4% Propane)	168
4-26	Vapor Composition as a Function of Mass Evaporated (85.2% Methane, 10.1% Ethane, 4.7% Propane)	169
4-27	Temperature as a Function of Mass Evaporated (85.2% Methane, 10.1% Ethane, 4.7% Propane)	170

LIST OF FIGURES - cont.

4-28	Vapor Composition as a Function of Mass Evaporated (91.0% Methane, 6.5% Ethane, 2.5% Propane)	171
4-29	Temperature as a Function of Mass Evaporated (91.0% Methane, 6.5% Ethane, 2.5% Propane)	172
5-1	Mass Evaporated for Methane Boiling on Water	175
5-2	Boiling Rates for Methane	177
5-3	Mass Evaporated for Ethane Boiling on Water	180
5-4	Boiling Rates for Ethane	181
5-5	Mass Evaporated for Propane Boiling on Water	184
5-6	Boiling Rates for Propane	185
5-7	Mass Evaporated for Methane-Ethane Mixtures Boiling on Water	189
5-8	Boiling Rates for Methane-Ethane Mixtures	190
5-9	Mass Evaporated for Ethane-Propane Mixtures Boiling on Water	193
5-10	Boiling Rates for Ethane-Propane Mixtures	194
5-11	Mass Evaporated for Run R-15, Ternary Mixture	196
5-12	Boiling Rates for Run R-15, Ternary Mixture	197
5-13	Mass Evaporated for Run R-20, Ternary Mixture	198
5-14	Boiling Rates for Run R-20, Ternary Mixture	199
5-15	Mass Evaporated for Run R-37, Ternary Mixture	200
5-16	Boiling Rates for Run R-37, Ternary Mixture	201
5-17	Mass Evaporated for Run R-41, Ternary Mixture	202
5-18	Boiling Rates for Run R-41, Ternary Mixture	203
5-19	Mass Evaporated for Run R-64, Ternary Mixture	204

LIST OF FIGURES - cont.

5-20	Boiling Rates for Run R-64, Ternary Mixture	205
5-21	Mass Evaporated for Methane-Nitrogen Mixtures Boiling on Water	208
5-22	Boiling Rates for Methane-Nitrogen Mixtures	210
5-23	Mass Evaporated for Methane-Ethane-Propane-Nitrogen Mixtures	211
5-24	Mass Evaporated for Methane Boiling on Water and on Ice	217
5-25	Mass Evaporated for Ethane Boiling on Water and on Ice	219
5-26	Mass Evaporated for Propane Boiling on Water and on Ice	222
5-27	Sequence of Events leading to the Collapse of the Vapor Film During Boiling of a Methane Ethane Mixture	225
6-1	Comparison of Previous Models for Evaporation of LNG on Water with Experimental Data	232
6-2	Comparison of Previous Models for Evaporation Rates of LNG on Water with Experimental Data	233
6-3	Semi-Infinite Solid Model	238
6-4	Boiling of Methane on Ice. Semi-Infinite Solid Model and Experimental Data	242
6-5	Boiling of Ethane on Ice. Semi-Infinite Solid Model and Experimental Data	243
6-6	Boiling of Propane on Ice. Semi-Infinite Solid Model and Experimental Data	244
6-7	Moving Boundary Model	246
6-8	Boiling of Methane on Water. Moving Boundary Model and Experimental Data	252
6-9	Boiling of Ethane on Water. Moving Boundary Model and Experimental Data	253
6-10	Boiling of Propane on Water. Moving Boundary Model and Experimental Data	254

LIST OF FIGURES - cont.

6-11	Drop in Surface Temperature of Ice after a Methane Spill	259
6-12	Drop in Surface Temperature of Ice after an Ethane Spill	260
6-13	Drop in Surface Temperature of Ice after a Spill of Methane on Water	262
6-14	Drop in Surface Temperature of Ice after a Spill of Ethane on Water	263
6-15	Transient Boiling of Methane on Water Compared to Steady State Boiling on Metal Surfaces	265
6-16	Transient Boiling of Ethane on Water Compared to Steady State Boiling on Metal Surfaces	266
6-17	Transient Boiling of a Methane-Ethane Mixture on Water	268
6-18	Transient Boiling of an LNG Mixture (C_1 82.5%, C_2 13.1%, C_3 4.4%) Compared to Steady State Boiling of LNG (C_1 87.5%, C_2 4.3%, C_3 1.6%, $C_4^+/N_2/CO_2$ 6.6%) on a Metal Surface	269
6-19	Variable Grid Size Scheme	272
6-20	Boiling of Methane on Water. Variable Grid Size Heat Transfer Model and Experimental Data (τ_{cf} = 45 s)	277
6-21	Evaporation Rates of Methane Boiling on Water. Variable Grid Size Heat Transfer Model and Experimental Data (τ_{cf} = 45 s)	278
6-22	Boiling of Ethane on Water. Variable Grid Size Heat Transfer Model and Experimental Data (τ_{cf} = 13 s)	280
6-23	Evaporation Rates of Ethane Boiling on Water. Variable Grid Size Heat Transfer Model and Experimental Data (τ_{cf} = 13 s)	281
6-24	Variable Grid Size/Vapor Liquid Equilibria Heat Transfer Model (VGS/VLE HTM)	282
6-25	Times for Collapse of Vapor Film (τ_{cf}) for Binary Methane-Ethane Mixtures	284

LIST OF FIGURES - cont.

6-26	Boiling of a Methane-Ethane Mixture on Water (R-1). VGS/VLE HTM Predictions and Experimental Data (τ_{cf} = 25 s)	286
6-27	Evaporation Rates of a Methane-Ethane Mixture on Water (R-1). VGS/VLE HTM Predictions and Experimental Data (τ_{cf} = 25 s)	287
6-28	Boiling of a Methane-Ethane Mixture on Water (R-17). VGS/VLE HTM Predictions and Experimental Data (τ_{cf} = 25 s)	288
6-29	Evaporation Rates of a Methane-Ethane Mixture on Water (R-17). VGS/VLE HTM Predictions and Experimental Data (τ_{cf} = 13 s)	289
6-30	Boiling of a Methane-Ethane Mixture on Water (R-35). VGS/VLE HTM Predictions and Experimental Data (τ_{cf} = 11 s)	290
6-31	Evaporation Rates of a Methane-Ethane Mixture on Water (R-35). VGS/VLE HTM Prediction and Experimental Data (τ_{cf} = 11 s)	291
6-32	Boiling of an Ethane-Propane Mixture on Water (R-30). VGS/VLE HTM Predictions and Experimental Data (τ_{cf} = 5 s)	292
6-33	Evaporation Rates of an Ethane-Propane Mixture on Water (R-30). VGS/VLE HTM Predictions and Experimental Data (τ_{cf} = 5 s)	293
6-34	Boiling of an LNG Mixture on Water (R-15). VGS/VLE HTM Predictions and Experimental Data (τ_{cf} = 5 s)	294
6-35	Evaporation Rates of an LNG Mixture on Water (R-15). VGS/VLE HTM Predictions and Experimental Data (τ_{cf} = 5 s)	295
6-36	Boiling of an LNG Mixture on Water (R-20). VGS/VLE HTM Predictions and Experimental Data (τ_{cf} = 5 s)	296
6-37	Evaporation Rates of an LNG Mixture on Water (R-20). VGS/VLE HTM Predictions and Experimental Data (τ_{cf} = 5 s)	297

LIST OF FIGURES - cont.

6-38	Boiling of an LNG Mixture on Water (R-41). VGS/VLE HTM Predictions and Experimental Data (τ_{cf} = 10 s)	298
6-39	Evaporation Rates of an LNG Mixture on Water (R-41). VGS/VLE HTM Predictions and Experimental Data (τ_{cf} = 10 s)	299
A-1	Block Diagram for the METTLER P11 Electronic Balance	319
A-2	Response Time of the Balance, 128 g Dropped from 5 cm	322
A-3	Response Time of the Balance, 1000 g Dropped from 2.5 cm	322
A-4	Response Time of the Balance, 128 g Dropped from 18 cm	323
A-5	Response Time for a 25 μm Thick, 2.3 cm Long Ribbon Thermocouple	337
A-6	Response Time for 150 μm Thick, 0.2 cm Long Lead Thermocouple	337
A-7	Response Time of a 150 μm Thick, 0.3 cm Long Lead Thermocouple. Base of Leads in 308 K Water and Leads in Liquid Nitrogen	338
B-1	Effect of the Interaction Parameter on the Accuracy of VLE Predictions by the SRK Equation. Methane-Ethane System	348
B-2	Effect of the Interaction Parameter on the Accuracy of VLE Predictions by the SRK Equation. Methane-Propane System	350
B-3	Effect of the Interaction Parameter on the Accuracy of SRK Predictions. Ethane-Propane System	352
B-4	Flow Chart to Insure a Value of $\Delta\hat{L} \leq 0.01$ Moles is Used Throughout the VLE Model	358

LIST OF TABLES

2-1	Burgess' Results for Boiling of Cryogenic Fluids	87
2-2	Boiling of Nitrogen on Water	103
2-3	Boiling of Liquid Methane on Water	104
2-4	Boiling of LNG on Water	105
4-1	Binary Interaction Parameter, k_{ij}, for the SRK Equation	126
4-2	Hypothetical Evaporation of a Hydrocarbon Mixture Using Various Mole Decrements	130
4-3	Comparison of SRK Predictions for Pressure and Vapor Composition with Experimental Data by Price and Kobayashi. Methane-Ethane-Propane System (283 K)	142
4-4	Comparison of SRK Predictions for Pressure and Vapor Composition with Experimental Data by Price and Kobayashi. Methane-Ethane-Propane System (172 K)	146
4-5	Experimental Conditions for LNG Spills Related to the VLE Model	151
5-1	Experimental Conditions for Methane Spills	174
5-2	Experimental Conditions for Ethane Spills	179
5-3	Experimental Conditions for Propane Spills	183
5-4	Experimental Conditions for Methane-Ethane Mixtures	188
5-5	Experimental Conditions for Ethane-Propane Mixtures	192
5-6	Experimental Conditions for Methane-Ethane-Propane Mixtures	195
5-7	Experimental Conditions for Mixtures Containing Nitrogen	207
5-8	Isothermal Vapor Pressures for Methane-Ethane Mixtures (113 K)	223
5-9	Boiling of Liquid Methane on Water	229

LIST OF TABLES - cont.

6-1	Thermophysical Properties Used in the Semi-Infinite Solid Model	240
6-2	Thermophysical Properties Used in the Moving Boundary Model	250
7-1	Analysis of Ice for Presence of Hydrocarbons	307
A-1	Performance and Design Specifications for the Electronic Balance	320
A-2	Input Ranges Available for the Multi-Range Analog Input Modules	325
A-3	Retention Times in Chromatographic Analysis	340
B-1	Effect of the Interaction Parameter, k_{ij}, on the Accuracy of VLE Predictions by the SRK Equation. Methane-Ethane System	349
B-2	Effect of the Interaction Parameter, k_{ij}, on the Accuracy of VLE Predictions by the SRK Equation. Methane-Propane System	351
B-3	Effect of the Interaction Parameter, k_{ij}, on the Accuracy of VLE Predictions by the SRK Equation. Ethane-Propane System	353
B-4	Effect of the Interaction Parameter, k_{ij}, on the Accuracy of VLE Predictions by the SRK Equation. Nitrogen-Methane System	354
B-5	Effect of the Interaction Parameter, k_{ij}, on the Accuracy of VLE Predictions by the SRK Equation. Nitrogen-Ethane System	355
B-6	Effect of the Interaction Parameter, k_{ij}, on the Accuracy of VLE Predictions by the SRK Equation. Nitrogen-Propane System	356

I. SUMMARY

Introduction

The supply of fuels in the USA decreased in the recent past. As a consequence, increasing amounts of LNG may be imported to meet the demand for energy. Questions have been raised, by both public and private interests, regarding the safety of the marine transportation of LNG. A collision involving an LNG tanker or a failure in the loading/unloading system could result in the accidental spillage of LNG on water. LNG is a mixture of methane, some ethane, small amounts of propane and traces of heavier hydrocarbons. It is usually transported at a temperature near its normal boiling point ($\sim$115 K) and close to atmospheric pressure. When LNG contacts a hot surface, water, at a higher temperature than its saturation temperature, it will boil and form a hydrocarbon vapor cloud. This cloud when mixed with air could form a flammable mixture.

As part of safety evaluation programs, several studies (Burgess, 1970, 1972; Boyle and Kneebone, 1973; Vestal, 1973; Jeje, 1974) were made to determine the rates of evaporation of LNG on water and the factors that influence such rates.

Burgess used an aquarium which was placed on a load cell. About 19 liters of water were placed in the aquarium and 4 to 8 liters of cryogen were spilled on it. As the cryogen evaporated, the time for each 50 g loss was recorded. For the first 20-40 seconds, the boiling rate of LNG was reported to be relatively constant with an average value of 0.018 g/cm^2-s. The maximum observed rate of evaporation was

0.030 g/cm^2-s, 65% higher than the average value. The aquarium was later replaced by a polystyrene ice chest (1972). The reported boiling rates for the first 20 seconds were 0.015 g/cm^2-s. No explanation was given for the discrepancy with the value reported in 1970. The boiling rates were found to decrease after ice formation took place on the water surface.

Similar spills using pure methane yielded boiling rates ranging from 0.010 to 0.016 g/cm^2-s. The higher value corresponds to a spill twice the amount of that represented by the lower rate. The boiling rates of methane were reported to have increased with time.

The higher boiling rate exhibited by LNG when compared to methane was believed to be due to the exothermic formation of hydrates. This idea, however, was abandoned after measuring rates of hydrate formation; they were much too slow to account for the difference in boiling rate.

Boyle and Kneebone (1973) performed LNG evaporation experiments both on confined and unconfined pools of water. The restricted area experiments were carried out on tanks, 0.836 m^2 and 3.72 m^2, placed on a load cell. It was found that boil-off rates increased with time reaching a maximum at the point of "pool break-up". This point is attained when the amount of LNG is no longer sufficient to cover completely the water surface. Evaluation of the LNG layer thickness at pool break-up yielded a value of 1.8 mm for many experiments.

The maximum rate observed in any one experiment was 0.02 g/cm^2-s. An increase in the initial quantity of LNG spilled was reflected in

an increase in boil-off rate. Interestingly enough, for a very large spill, the evaporation rate reached a maximum of 0.02 g/cm^2-s, and then declined even though the water was still completely covered with LNG. Decreasing the initial water temperature also caused an increase in boiling rate.

Boyle and Kneebone found a strong dependence of evaporation rate on the chemical composition of the LNG. Increasing the amount of heavier hydrocarbons such that the methane fraction dropped from 0.99 to 0.95 caused a threefold increase in the rate of evaporation. The following explanation was given for these results. As LNG is spilled on water, the large temperature difference causes film boiling. Heat is supplied by cooling a thin layer of water. Once this layer reaches the freezing point of water, ice forms and cools down very fast. The temperature difference between the ice surface and the LNG decreases enormously; nucleate boiling is promoted thereby causing a rise in heat flux and evaporation rate with time.

Although Boyle and Kneebone's explanation for the observed rates is a very logical one, their data cannot be completely trusted. Most of the spills corresponded to an equivalent non-boiling hydrostatic head of only 0.4 to 0.6 cm, barely 2 to 3 times the pool break-up thickness of 0.18 cm. Furthermore, these spills were carried out on large water surfaces of 3700 and 8400 cm^2 (4 and 9 ft^2). Since the volumes spilled were relatively small, the spreading effects become significant and should be accounted for, but they were not.

Vestal (1973) used a glass Dewar flask coupled to a load cell to study the heat transfer between cryogenic liquids and water. The maximum rates of evaporation were reported to be 0.04 g/cm^2 for pure methane and 0.11 g/cm^2 for LNG. These values are considerably higher than those given by Burgess and by Boyle and Kneebone. The flask used by Vestal had an inside diameter of only 48 mm. Thus, a significant amount of heat is believed to have been supplied by the cooling of the thick glass walls of the flask.

Jeje (1974) studied the transient boiling of light liquid hydrocarbons on water. Liquid methane and liquid ethane did not show much sensitivity to the amount spilled nor to the initial water temperature. Ice formation took place for both hydrocarbons, although in the case of ethane it formed more rapidly.

The heat fluxes for ethane were higher than those observed for methane. The boil-off rate of methane increased continuously with time, whereas ethane started boiling slowly and then rapidly increased.

Addition of heavier hydrocarbons increased the boiling rate of methane significantly. After 10 seconds, the mass evaporated for mixtures of methane containing 1.6 mole percent ethane and 0.1 mole percent propane, was twice that for pure methane. For mixtures containing 8.2% ethane and 2.0% propane, the mass evaporated after 10 seconds was nearly three times that for pure methane.

The boiling rates for LNG mixtures increased with time and decreased slightly with increased initial water temperature.

The most important conclusion that can be reached after reviewing previous research efforts is that the chemical composition of the LNG plays the most important role in determining the boiling behavior of the mixture. Only qualitative explanations had been offered which are not completely satisfactory. No attempts were made to explain quantitatively the boiling of LNG on water.

Determination of boiling rates of LNG spilled on open sea is extremely difficult. There are no techniques available for accurately determining these rates. So far, any attempts to measure these rates have been based on aerial observation of the LNG pool area as a function of time. In addition to the composition of LNG, two other factors play an important role in the evaporation of LNG on the open sea: the spreading of the LNG pool and the wave motion of the water. Before these effects can be incorporated in a scheme to predict the boiling rates, one must have a clear understanding of how the composition affects the boiling of LNG on water. Furthermore, one must be able to quantify these effects. Such has been the goal of this study.

Experimental

The spillage of LNG on water results in a highly transient process of evaporation. In order to study the characteristics of this process, one must be able to measure, or otherwise determine, the mass evaporated, the composition of the liquid and vapor, and the system temperatures as a function of time. In the present work this was accomplished by spilling the cryogen on quiescent distilled water contained in a

boiling vessel placed on an electronic balance. The output of this balance was monitored by a NOVA-840 real time computer. Water, cryogen, and vapor temperatures were measured by thermocouples whose output was also fed into the real time computer. A schematic representation of this setup is given in Figure 1-1.

The boiling vessel, shown in Figure 1-2, was a triple wall cylindrical container. It was transparent to allow visual observation and was designed to minimize heat leaks. The outer wall was made of 0.32 cm thick acrylic tube; the inner walls were made of 25 μm Mylar sheets. The three walls were separated by 2 mm thick polyurethane spacers. These spacers were wound horizontally and were positioned at different heights around the walls. They not only kept the thin walls in place but minimized natural convection of the air present within the wall gaps.

In most spills the cryogen evaporated completely within 2 to 3 minutes. In this short period of time the most important heat leaks are due to the cooling of the walls of the container and, therefore, it was necessary to use very thin inner walls to minimize their thermal mass.

A cryogen distributor was used to reduce disturbances to the water surface, and to prevent overshoots on the mass recorded by the balance due to the inertia of the cryogen spilled.

Three vapor thermocouples were fed through the steel tube guide for the cryogen distributor. The first thermocouple was placed about 2 cm above the cryogen surface; the other two were placed at 1.5 cm

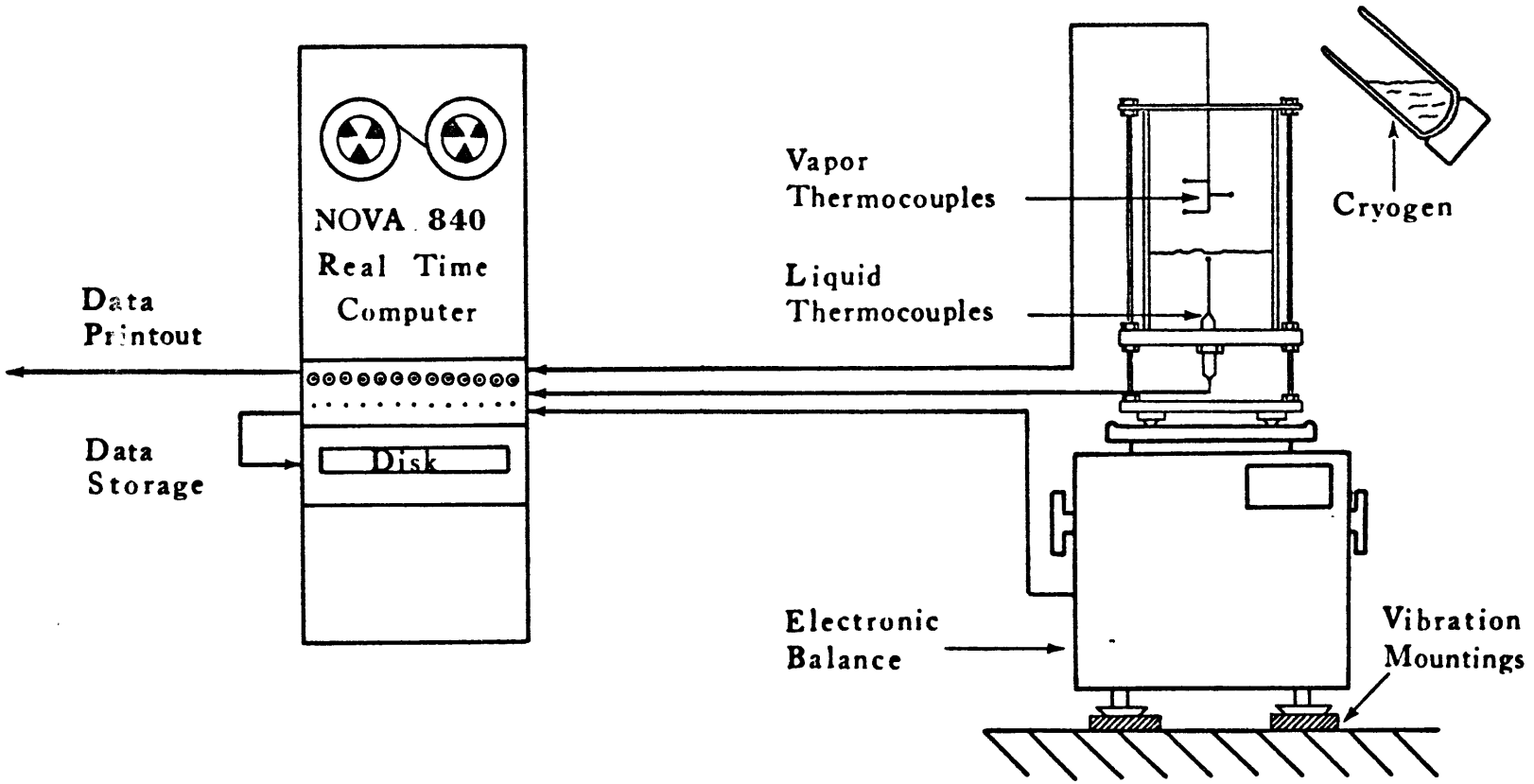

Figure 1-1 Experimental Set-up for the Study of LNG Boiling on Water

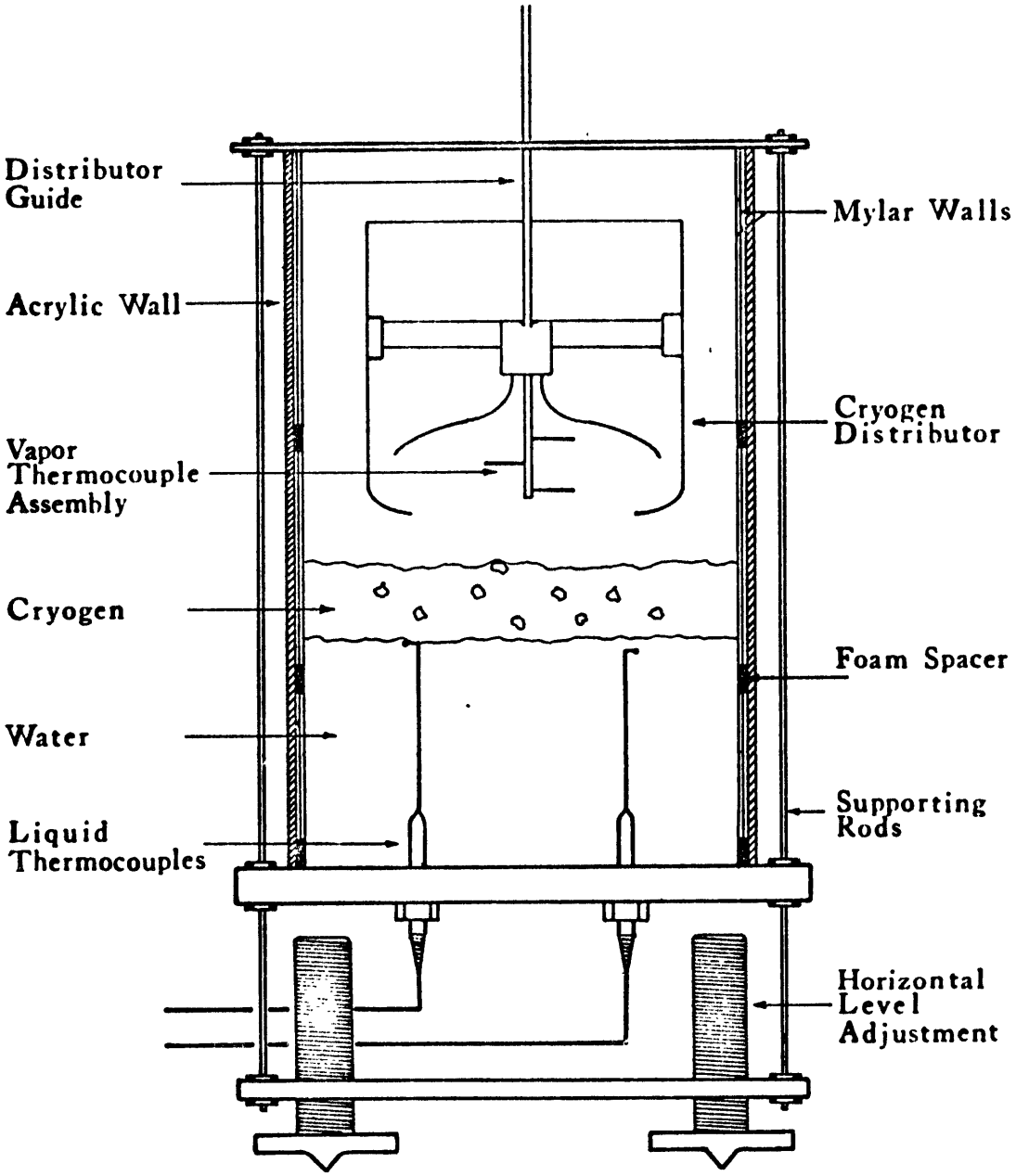

Figure 1-2 Boiling Vessel

intervals above the first one. Six liquid thermocouples were used to monitor water and LNG temperatures.

In general, the liquid hydrocarbons were prepared by cooling the hydrocarbon gases below their boiling point either with liquid nitrogen or with a pentane-nitrogen slush bath.

The composition of the hydrocarbon mixture was determined by two methods: gravimetric and chromatographic. The gravimetric method consisted of accurately weighing the amount of each component added to the mixture. For the chromatographic method, a sample of the liquid mixture was removed with a pre-cooled sampling scoop and introduced into a sampling bulb. After the liquid evaporated, a sample was removed and analyzed with a gas chromatograph.

Vapor-Liquid Equilibria

LNG is a cryogenic fluid comprised of components which differ significantly in volatility. Thus, in a transient boiling experiment, the vapor evolved varies in composition as the liquid becomes enriched in the less volatile components. This time-dependent vapor composition would show a maximum in nitrogen, if present, followed by methane, ethane, propane, etc. It is important to be able to estimate the composition of the vapor during a spill of LNG because each component may affect the dispersion characteristics of the cloud. It is also important to estimate the liquid composition since the saturation temperature of the residual liquid depends on its composition. Changes in the saturation temperature could significantly affect the heat transfer characteristics.

One could assume that vapor-liquid equilibrium existed at all times; the vapor composition could then be computed as a function of the residual liquid composition. Before proceeding with this assumption, however, it is imperative to demonstrate its validity. To this end the vapor composition was measured experimentally as a function of time and compared with results obtained from theory assuming vapor-liquid equilibria. In addition, temperature measurements in both the liquid and vapor are compared with those predicted from theory.

Development of the VLE Model

For a mixture at thermodynamic equilibrium, the fugacity coefficients ϕ_i can be related to pressure, total volume and temperature by the following thermodynamic relationship (Prausnitz et al., 1967)

$$\ln \phi_i = \ln \frac{\hat{f}_i}{y_i P} = \frac{1}{RT} \int_V^\infty \left[\left(\frac{\partial P}{\partial n_i} \right)_{T,V,n_j} - \frac{RT}{V} \right] dV - \ln Z \qquad (1\text{-}1)$$

where n_i = number of moles of component $\underline{i}$

$Z = PV/n_T RT$

The Soave (1972) modification of the Redlich-Kwong (1949) equation of state (SRK)

$$P = \frac{RT}{v - b} - \frac{a}{v(v + b)} \qquad (1\text{-}2)$$

where v = molar volume

a = temperature dependent term

b = constant

can be used to relate pressure, temperature and volume. Thus the fugacity coefficients can be evaluated by combining Eqs. (1-1) and (1-2),

$$\ln \phi_i = \frac{b_i}{b}(Z-1) - \ln(Z-B) + \frac{A}{B}\left[\frac{b_i}{b} - 2\sum_j \frac{(1-k_{ij})(a_i a_j)^{0.5}}{a} x_j\right] \ln \frac{Z+B}{Z} \tag{1-3}$$

where

$$A = \frac{aP}{R^2T^2} \tag{1-4}$$

$$B = \frac{bP}{RT} \tag{1-5}$$

$$a = \sum_i \sum_j x_i x_j (1 - k_{ij})(a_i a_j)^{1/2} \tag{1-6}$$

$$b = \sum_i x_i b_i \tag{1-7}$$

k_{ij} = binary interaction parameter

To determine the values of the interaction parameters, only binary equilibrium data are required. The method involves fitting k_{ij} to experimental vapor-liquid equilibrium data and minimizing the differences between the predicted and experimental values. Experimental data reported by various researchers (Price and Kobayashi, 1959; Chang and Lu, 1967; Stryjek et al., 1974; Poon and Lu, 1974) were used in selecting the values of k_{ij}. The following values were selected for the interaction parameter, $k_{C_1\text{-}C_2} = 0.000$, $k_{C_1\text{-}C_3} = 0.010$, $k_{C_2\text{-}C_3} = 0.000$, $k_{N_2\text{-}C_1} = 0.035$, $k_{N_2\text{-}C_2} = 0.035$ and $k_{N_2\text{-}C_3} = 0.120$.

The system variables are pressure, temperature, liquid and vapor composition. If temperature and liquid composition are taken as the independent variables, then the pressure and vapor composition are calculated by combining Eq. (1-3) which gives the fugacity coefficient ϕ_i and the vapor-liquid distribution coefficient K_i,

$$K_i = \frac{y_i}{x_i} = \frac{\phi_i^L}{\phi_i^V} = \frac{\dfrac{\hat{f}_i^L}{P\,x_i}}{\dfrac{\hat{f}_i^V}{P\,y_i}} \tag{1-8}$$

The SRK equation, used as described, coupled with the interaction parameters given above, yielded predictions that agreed well with reported experimental VLE data for systems containing methane, ethane, propane and nitrogen. The SRK predictions for one such system, methane-ethane, are compared to experimental data in Figure 1-3.

The procedure to determine vapor-liquid equilibria compositions can be used in conjunction with a mass balance to determine the temperature of the residual liquid LNG as well as the composition of the vapor evolved during the boiling of LNG on water.

For every component $\underline{i}$ in the mixture, a mass balance over a differential period of time can be written:

$$-d(x_i L) = y_i dV \tag{1-9}$$

where L = number of moles in the liquid phase

V = number of moles in the vapor phase

Since $dL = -dV$, Eq. (1-9) can be rewritten as

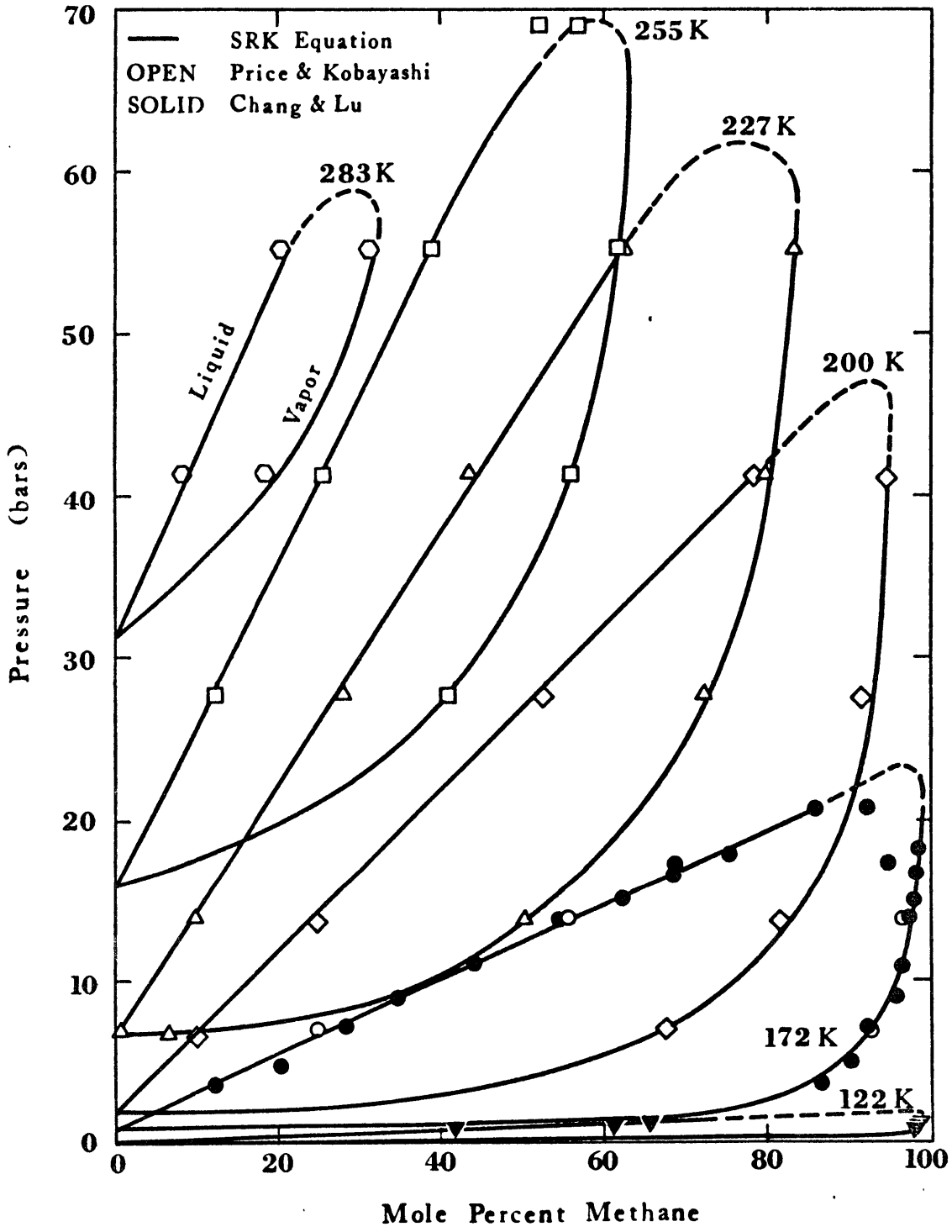

Figure 1-3 Pressure Composition Diagram for the Methane-Ethane System (k_{ij} = 0.0)

$$\frac{dL}{L} = \frac{dx_i}{y_i - x_i} \tag{1-10}$$

In an evaporation process dL is negative. A more convenient variable to be used is the moles evaporated $d\hat{L}$,

$$d\hat{L} = -dL \tag{1-11}$$

which is positive. Equation (1-10) can be approximated by a difference equation, which incorporates the moles evaporated $d\hat{L}$,

$$-\frac{\Delta\hat{L}}{L} = \frac{\Delta x_i}{y_i - x_i} \tag{1-12}$$

provided that small enough values of $\Delta\hat{L}$ are used. During spills of LNG on water, experimental data were recorded at $\Delta\tau$ = 1 s intervals. In Eq. (1-12), at any time τ, L, x_i and y_i are known. For instance, at τ = 0 s, L is the number of moles in the initial charge of LNG, x_i the mole fraction of i in this charge and y_i the mole fraction of i in the vapor in equilibrium with the given composition for the liquid. Furthermore, $\Delta\hat{L}$ can be determined from the experimentally-measured mass that was evaporated, during the period of time $\Delta\tau$. Thus the only unknown in Eq. (1-12) is the value of x_i at time $\tau + \Delta\tau$,

$$x_i(\tau + \Delta\tau) = x_i(\tau) - \frac{L(\tau) - L(\tau + \Delta\tau)}{L(\tau)} \cdot [y_i(\tau) - x_i(\tau)] \tag{1-13}$$

Results

The values predicted by the VLE model, using Eq. (1-13), the experimentally-measured mass evaporated and the SRK equation, are

compared to experimental data in Figures 1-4 and 1-5. As was expected, a preferential evaporation takes place. The initial saturation temperature is close to that of methane (111.7 K), and methane evaporates preferentially. Once it has been nearly exhausted in the residual liquid, the saturation temperature begins to rise approaching the boiling point of ethane (184.5 K). Ethane, then becomes the major constituent of the vapor. Finally, after the ethane has been depleted, a propane layer is left boiling at the propane saturation temperature (231.3 K).

The close agreement between the experimental data and the predicted values assuming vapor-liquid equilibria proves the validity of the assumption. Thus the VLE model, described above, can be used to determine the vapor composition and the saturation temperature of the residual liquid.

Boiling of LNG on Water

Pure hydrocarbons, methane, ethane and propane were spilled on water and the mass evaporated was recorded as a function of time. Similarly, tests were carried out with binary mixtures of methane-ethane and ethane-propane and with ternary mixtures of methane-ethane-propane. Finally, the effect of small amounts of nitrogen added to methane and LNG was also studied (nitrogen is occasionally present in small amounts <2% in LNG).

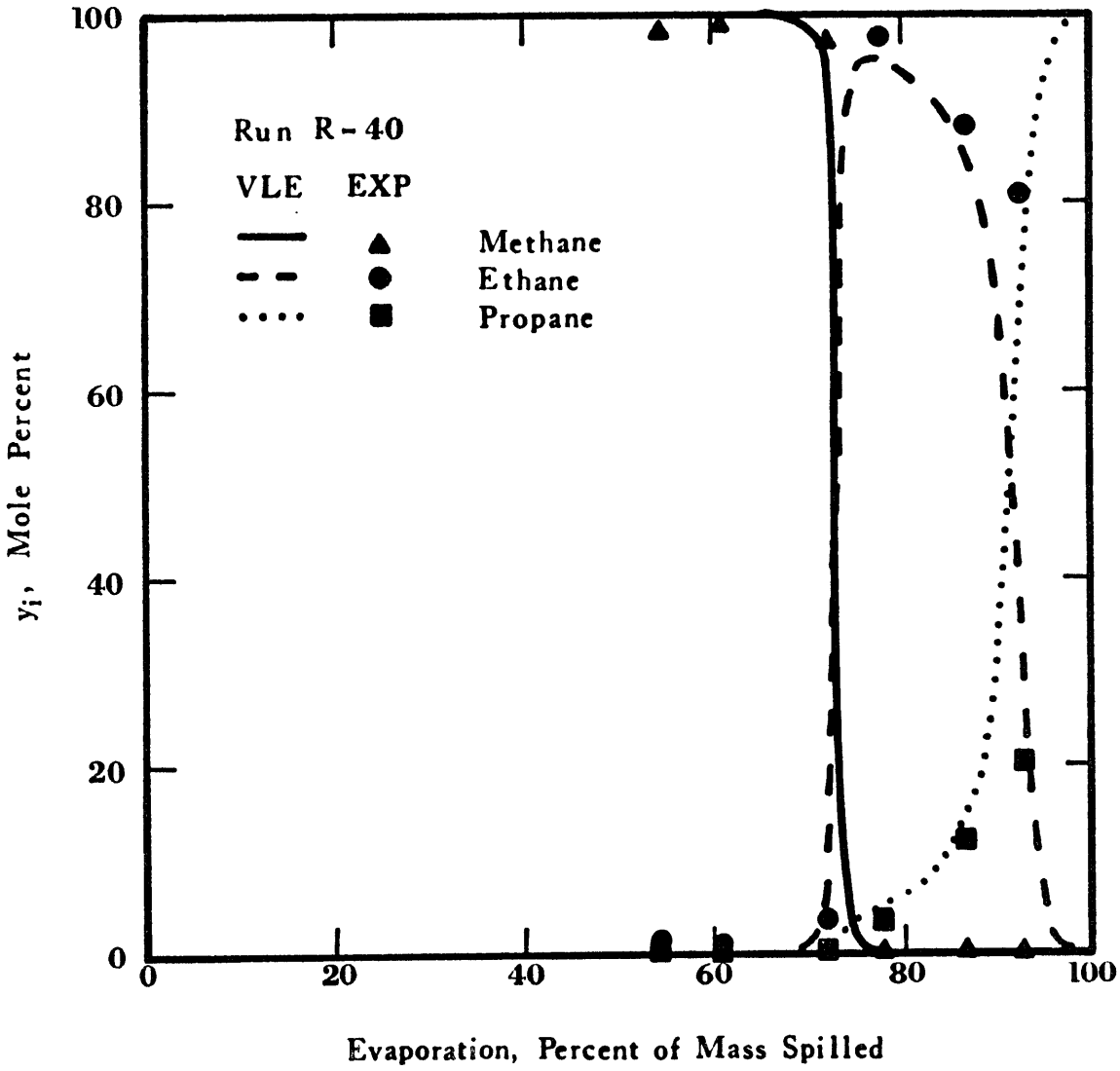

Figure 1-4 Vapor Composition as a Function of Mass Evaporated (85.2% Methane, 10.1% Ethane, 4.7% Propane)

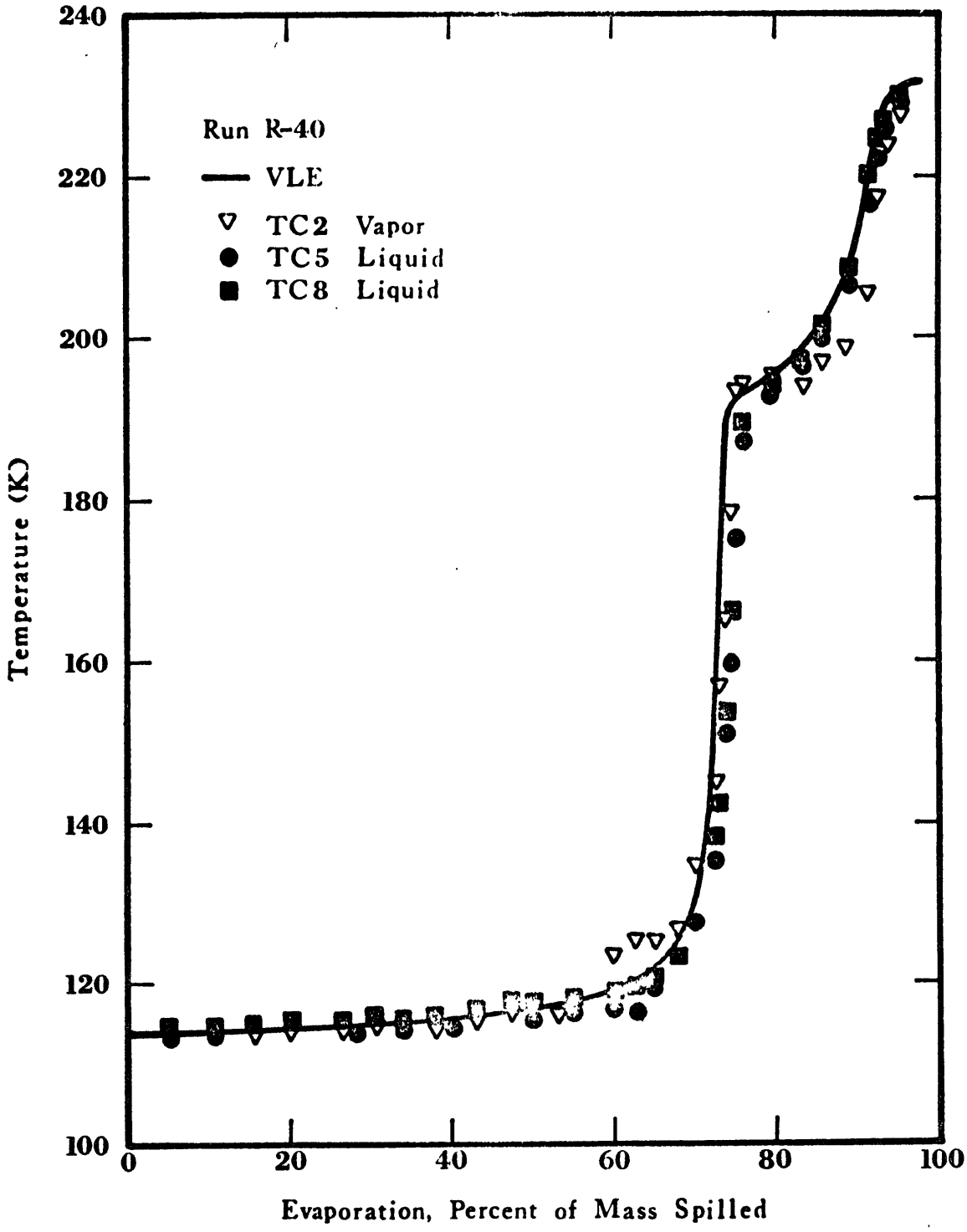

Figure 1-5 Temperature as a Function of Mass Evaporated (85.2% Methane, 10.1% Ethane, 4.7% Propane)

Results

The mass of methane evaporated as a function of time is shown in Figure 1-6. As can be seen, methane evaporated slowly at first but then the rate of evaporation increased and reached a peak after about 40 seconds (Figure 1-7). Ice patches began to form after a few seconds ($\sim$5 s) and these grew radially, eventually covering the water surface ($\sim$20 s).

Ethane displayed initial boiling rates (and heat fluxes) higher than those for methane. As in the case of methane, the boiling rates increased with time reaching a peak after about 15 seconds. Subsequently, the boiling rates decreased significantly. Ice formation took place at a faster rate than with methane.

Propane boiled very rapidly during the first few ($\sim$5) seconds. The boiling rates then dropped to considerably lower values. Highly irregular ice was formed very quickly (<1 s).

Methane-ethane mixtures ($0.80 \leq x_{C_1} \leq 0.985$) displayed high initial boiling rates. These rates increased with time reaching a peak within 10 to 25 seconds. A layer of ice covered the water surface in about 5 seconds. Extensive amounts of foam were generated.

When methane-ethane-propane mixtures were spilled on water, rapid boiling took place in the first few seconds and was accompanied by extensive foam, 10 to 15 cm high. In most cases, the maximum boiling rate was achieved within the first 8 seconds; the boiling rates then decreased with time. In many tests secondary peaks in the boiling rates were observed; their magnitudes were, however, much lower than the initial peak. These effects can be seen in Figures 1-8 and 1-9.

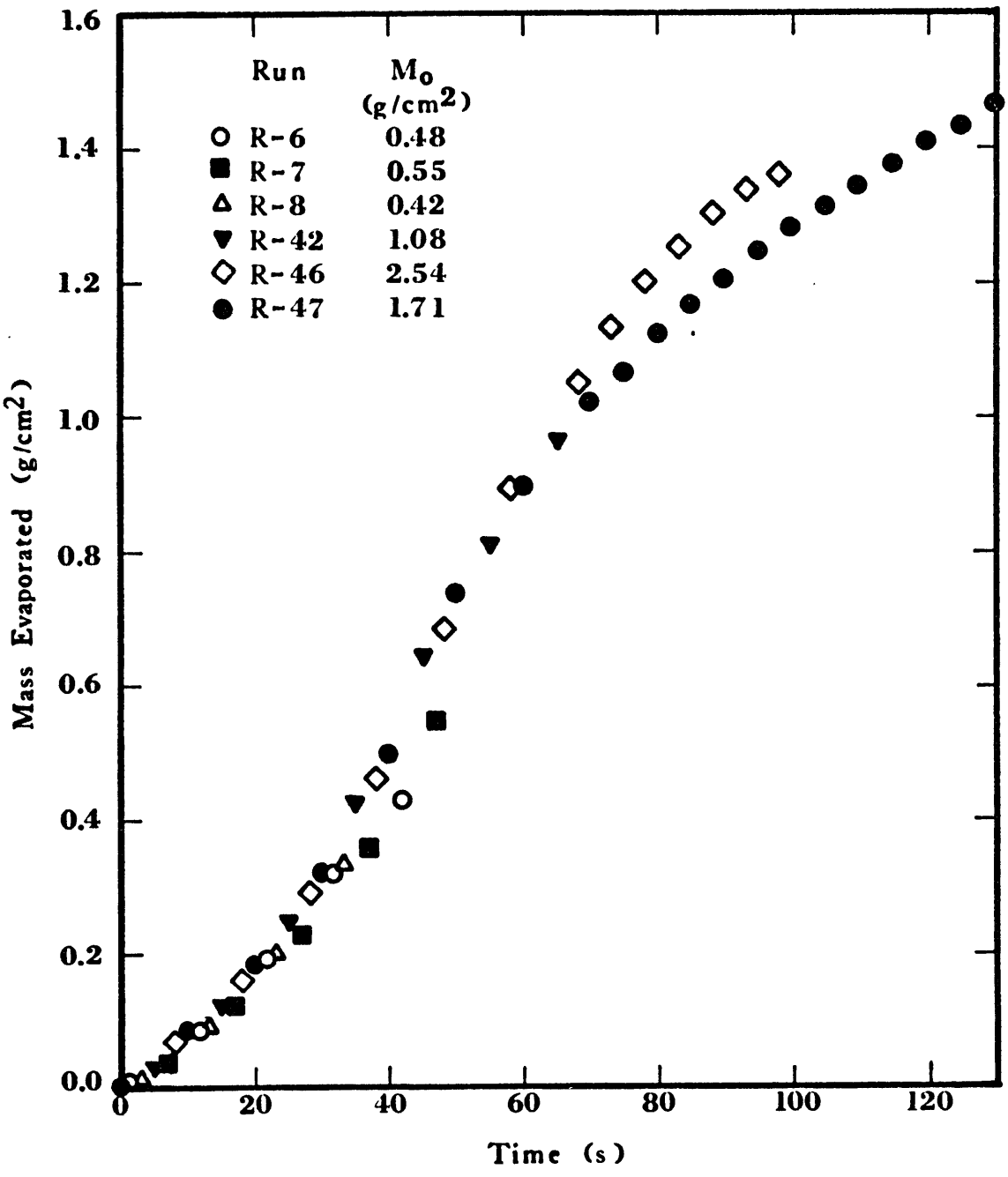

Figure 1-6 Mass Evaporated for Methane Boiling on Water

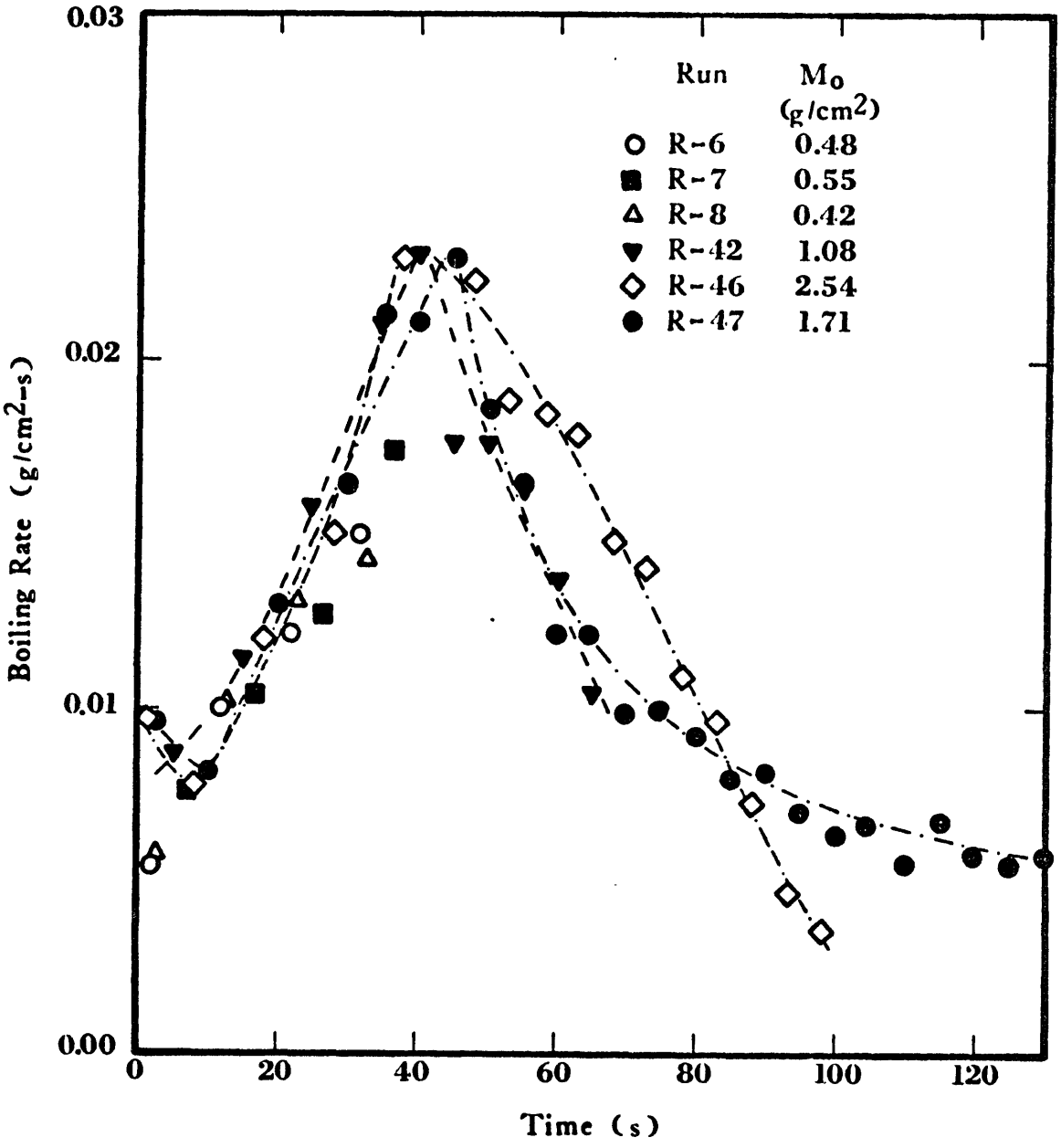

Figure 1-7 Boiling Rates for Methane

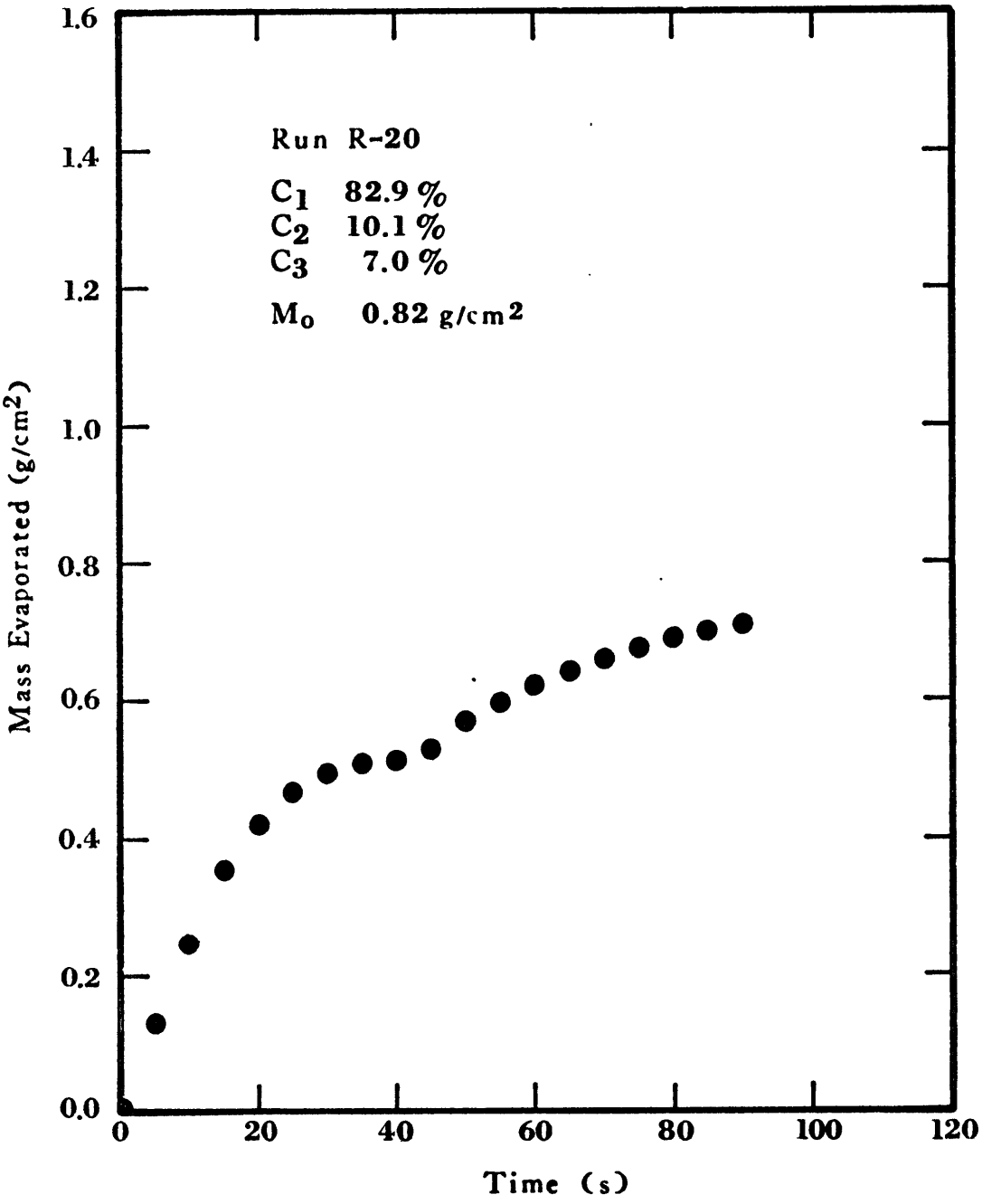

Figure 1-8 Mass Evaporated for Run R-20, Ternary Mixture

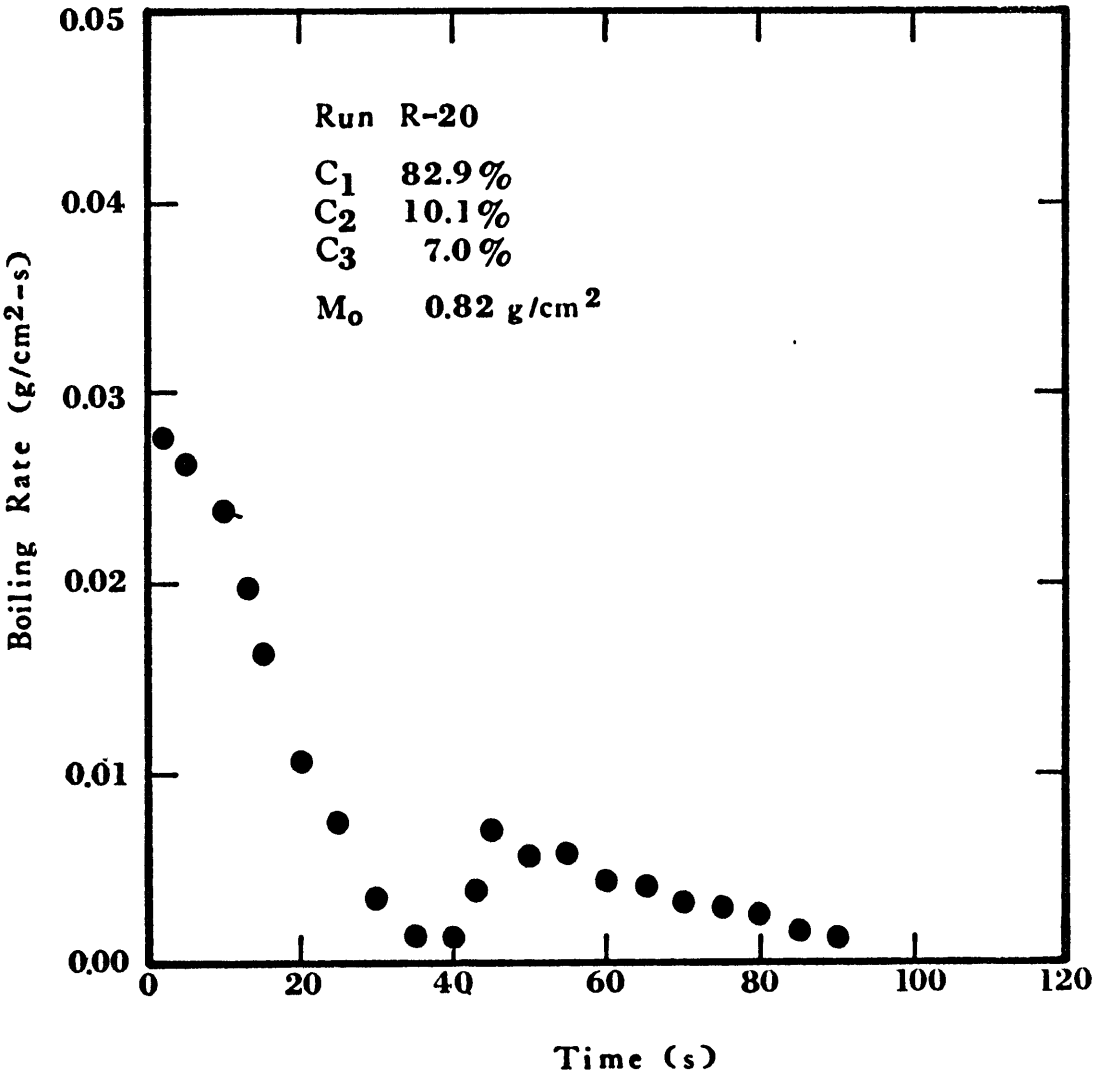

Figure 1-9 Boiling Rates for Run R-20, Ternary Mixture

The addition of small amounts of nitrogen to methane and to methane-ethane-propane mixtures did not affect their boiling rates significantly.

Discussion of Results

Upon initial contact with water, a surface at a temperature approximately 180 K above its boiling point, methane film boils. The insulating behavior of the film results in the low initial heat fluxes observed. As energy is removed, the upper layers of water cool and ice forms. The temperature of the ice surface continues to decrease until the difference in temperature is no longer high enough to maintain stable film boiling. Transitional boiling begins and the heat fluxes increase, reaching a peak when nucleate boiling (direct methane-ice contact) is fully established. Thereafter, the heat fluxes, and the boiling rates, decrease.

Initially, ethane transition boils on water. Nucleate boiling, and the peak boiling rate, is attained faster than with methane. Propane, with a saturation temperature only 42 K below the freezing point of water, nucleate boils upon initial contact. The heat flux, and boiling rates, are therefore highest at the initial contact time.

The evaporation of mixtures is a far more complicated situation. In addition to shifts in boiling regimes, one must consider the change in composition and saturation temperature of the residual liquid as preferential evaporation of the more volatile components takes place.

Consider a binary mixture of 90% methane and 10% ethane. The saturation temperature is close to that of methane. As in the case of pure methane, a vapor film is formed. As a vapor bubble is formed,

the liquid at the base of the bubble becomes depleted in methane since the vapor bubble is made up primarily of the most volatile component. The liquid remains essentially isothermal but a thin liquid layer at the base of the bubble has changed significantly in composition (heat transmission and evaporation being much faster than diffusional mass transfer). This means that for this thin liquid layer to be in equilibria the pressure must drop. Or in other words, the vapor pressure of this thin layer at the base of the bubble becomes less than one atmosphere. As some of the vapor in the film evaporates into the growing vapor bubble, the low vapor pressure of this thin surface layer hinders the replenishment of the vapor film. Thus, the vapor film collapses. The bubble pinches off and carries in its wake the ethane-rich layer which then mixes with the bulk of the liquid. Fresh liquid rushes in and a temporary liquid-liquid contact is made which allows for high heat fluxes. The vapor film is reformed and the cycle begins again. The direct contact causes the water and the ice, when formed, to cool more rapidly. Soon, the surface temperature of the ice drops enough that the difference in temperature with the boiling liquid is no longer large enough to regenerate the film, and nucleate boiling is established. Thereafter, the heat fluxes and boiling rates begin to decrease.

In the case of mixtures richer in heavier hydrocarbons, the decrease in vapor pressure is even more dramatic, so the film around a bubble collapses more easily, and the peak flux can be attained at shorter times.

This theory presents a plausible mechanism to explain why there is an increase in initial boiling rates upon addition of heavier hydrocarbons to methane.

The eventual enrichment of the bulk liquid in heavier hydrocarbons due to the preferential evaporation of methane plays a very important role in the latter part of the boiling process. The saturation temperature of a mixture of methane and ethane, for instance, will not change appreciably until the residual methane is less than about 20%. The saturation temperature then quickly rises to the saturation temperature of ethane.

Consider again the 90% methane, 10% ethane mixture spilled on water; after the ice has formed it begins to cool and approach the saturation temperature of the mixture. The bulk of the liquid is being depleted in methane and when nearly all the methane has evaporated, the saturation temperature of the cryogen begins to increase towards that of pure ethane. Considering the situation from the ice point of view, its surface is placed in contact with a body at a very low temperature. As the surface of the ice is approaching this low temperature, the temperature of the cold body begins to increase. Obviously, this upsets the temperature gradient near the interface resulting in very low heat fluxes.

Furthermore, the residual liquid must be warmed to the (continuously increasing) saturation temperature. Thus, most of the modest amount of energy being transferred goes into heating the residual mixture and very little into actual evaporation. The overall result is a very low rate of evaporation.

A similar situation develops with methane-ethane-propane mixtures. Once the methane is depleted, the mixture is primarily ethane and propane. A new plateau in saturation temperature is reached, and the heat flux preferentially evaporates ethane, yielding a secondary, small peak in the boiling rate. The difference in volatility between ethane and propane is not as drastic. Thus, although the behavior upon exhaustion of ethane will be similar to the previous exhaustion of methane, it is not as pronounced; in fact, a third peak is not necessarily expected.

Heat Transfer Models

The first step in a scheme to predict the evaporation of LNG on water is to determine the amount of energy that is transferred across the water (ice)/LNG interface. This can be accomplished by solving the equations for transient conduction involving solidification (Stefan's Problem). In the present case, the boundary condition at $x = 0$ (water/ice-LNG interface) must yield the temperature at that point. Since a vapor film is formed initially, the temperature at $x = 0$ will not reach the temperature of the cryogen until the film collapses.

Regression of Surface Temperatures by Using Convolution Integrals

Pure methane was spilled on a solid block of ice and the following convolution integral was used to determine the ice surface temperature as a function of time:

$$\theta(0,\tau) = \frac{1}{k}\sqrt{\frac{\alpha}{\pi}}\int_0^{\tau} q(\lambda)(\tau - \lambda)^{-1/2}\, d\lambda \qquad (1\text{-}14)$$

which can be rewritten as follows

$$\theta(0,\tau) = \frac{1}{k}\sqrt{\frac{\alpha}{\pi}}\int_0^{2\sqrt{\tau}} q(\tau - \frac{u^2}{4})\, du \qquad (1\text{-}15)$$

where θ is the change in surface temperature from the initial ice temperature and k and α are the temperature-averaged thermal conductivity and diffusivity of ice, respectively. The experimental values of heat flux (evaporation rate × heat of vaporization) were used in the integrand. The results are shown in Figure 1-10.

Similarly for methane spilled on water, the following convolution integral was used.

$$\theta(0,\tau) = \frac{\text{erf}\ (K\beta/2\sqrt{\alpha_1})}{k_1}\sqrt{\frac{\alpha_1}{\pi}}\int_0^{-2\sqrt{\tau}} q(\tau - \frac{u^2}{4})\, du \qquad (1\text{-}16)$$

where θ is the departure of the surface temperature from the freezing point, k_1 and α_1 are the temperature-averaged thermal conductivity and diffusivity, respectively, of ice. β is the ratio of the density of water to that of ice and K is a parameter which depends on the properties of ice, water, heat of fusion of ice, water and cryogen temperatures. Again the experimental heat fluxes, q, are used in the integrand. The results are shown in Figure 1-11.

As can be seen in these figures, the surface temperature drop can be approximated by a linear drop over a period of time τ_{cf}, the time for the total collapse of the vapor film.

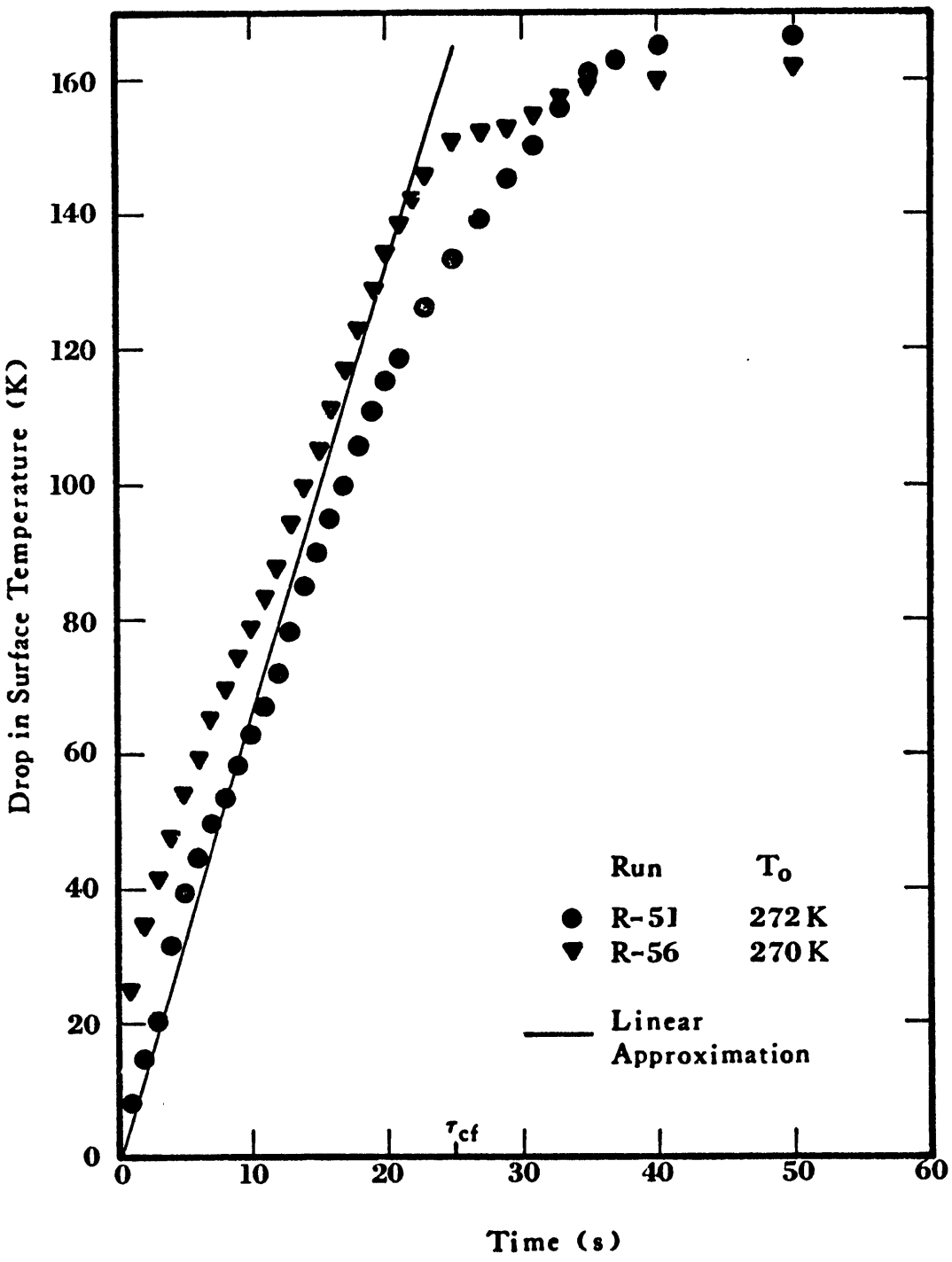

Figure 1-10 Drop in Surface Temperature of Ice after a Methane Spill

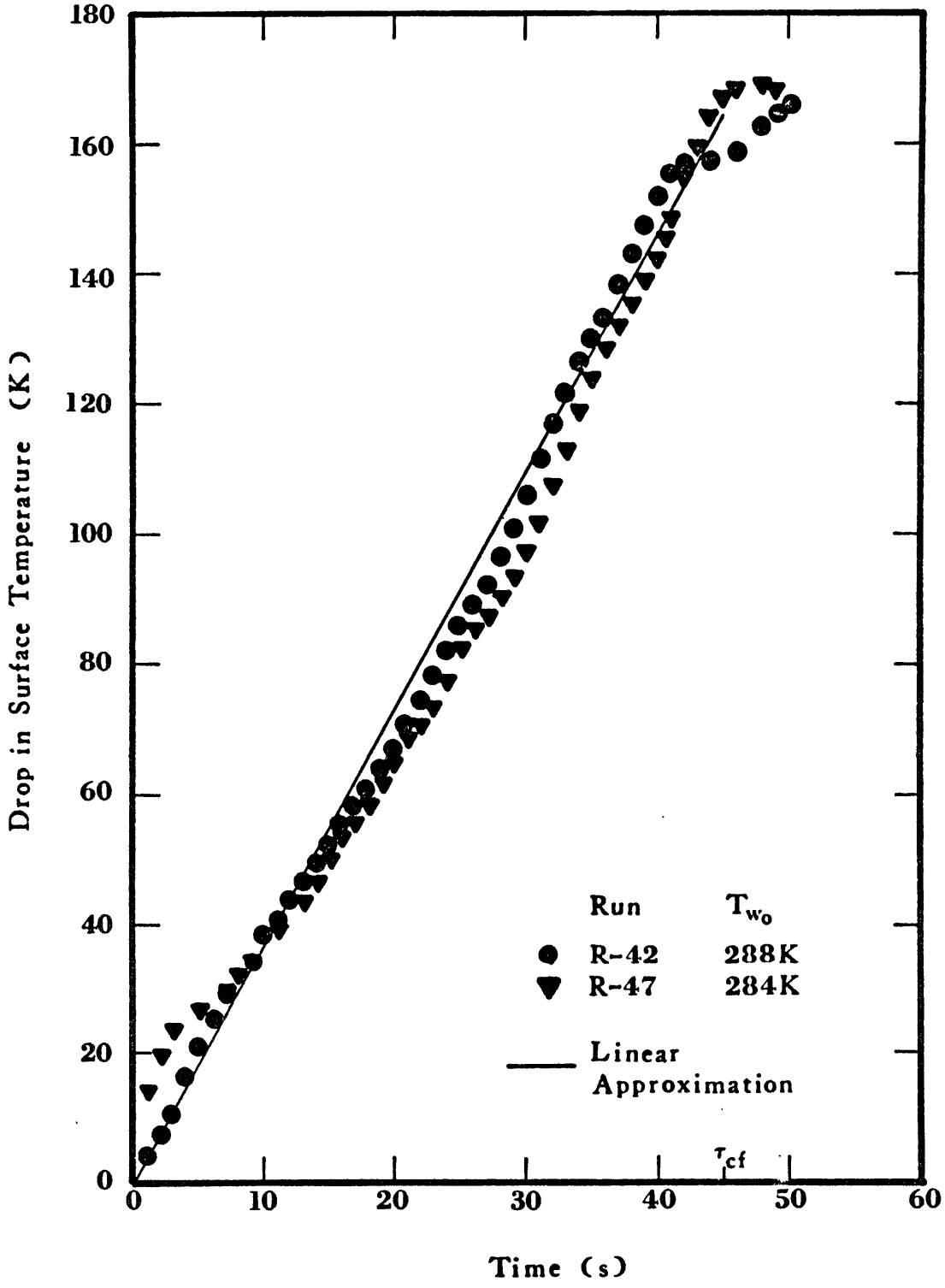

Figure 1-11 Drop in Surface Temperature of Ice after a Spill of Methane on Water

Variable Grid Size Heat Transfer Model

In order to allow for the time-varying surface temperature condition, and for the variation in thermal properties of ice with temperature, a numerical, variable grid size heat transfer model was developed. In such a model, the differential equations are replaced by difference equations.

The substrate of thickness E is, at all times, divided into an ice layer of thickness e, and a water layer of thickness E - e. In turn, each layer is divided into m points. Consequently, the spacing between grid points in the ice layer will be $\Delta x_S = e/m$ and in the water layer $\Delta x_L = (E - e)/(M - m)$ where M is the total number of grid points equal to 2 m. As time progresses, the depth, e, of the freezing front increases but the freezing front always corresponds to the m-th grid point.

The movement of the freezing front is given by

$$\frac{de}{d\tau} = \frac{1}{\rho \Delta H_{fus}} \left\{ k_i \frac{\theta_{m-2} - 4\theta_{m-1} + 3\theta_m}{2(e/m)} + k_w \frac{\theta_{m+2} - 4\theta_{m+1} + 3\theta_m}{2(E - e)/(M - m)} \right\} \quad (1\text{-}16)$$

The temperature at the n-th grid point in the ice layer is given by

$$\frac{d\theta_n}{d\tau} = \frac{n}{e} \left(\frac{\theta_{n+1} - \theta_{n-1}}{2} \right) \frac{de}{d\tau} + \frac{1}{\rho_n C_{p_n}} \left(\frac{k_{n-1/2}(\theta_{n-1} - \theta_n) - k_{n+1/2}(\theta_n - \theta_{n+1})}{(e/m)^2} \right) \quad (1\text{-}17)$$

and in the water layer by

$$\frac{d\theta_n}{d\tau} = \frac{M-n}{E-e}\left(\frac{\theta_{n+1} - \theta_{n-1}}{2}\right)\frac{de}{d\tau} + \alpha_w\left(\frac{\theta_{n-1} + 2\theta_n + \theta_{n+1}}{(E-e)^2/(N-m)^2}\right) \qquad (1\text{-}18)$$

Finally,

$$e_{\tau+\Delta\tau} = e_\tau + \Delta\tau\ de/d\tau \qquad (1\text{-}19)$$

and

$$\theta_{n,\tau+\Delta\tau} = \theta_{n,\tau} + \Delta\tau\ d\theta_n/d\tau \qquad (1\text{-}20)$$

The properties of ice are allowed to vary with temperature, whereas those of water were taken as constants since they vary little in the range of interest.

Making use of the results obtained with the convolution integral, the temperature at the surface is allowed to approach the cryogen temperature linearly over a period of time τ_{cf}.

The model as described thus far, can be used only with pure components. For mixtures it must be coupled with the VLE model previously described. The VLE model provides the Variable Grid Size (VGS) model with the cryogen temperature. The VGS model computes the total heat flux across the substrate/cryogen interface. After subtracting the heat required to raise the temperature to the new saturation temperature, the mass evaporated is determined. This evaporation is fed to the VLE model which then determines the new residual liquid composition and saturation temperature. The cycle is then repeated.

The results obtained with the VGS/VLE HTM for a binary methane-ethane mixture and for an LNG mixture are shown in Figures 1-12

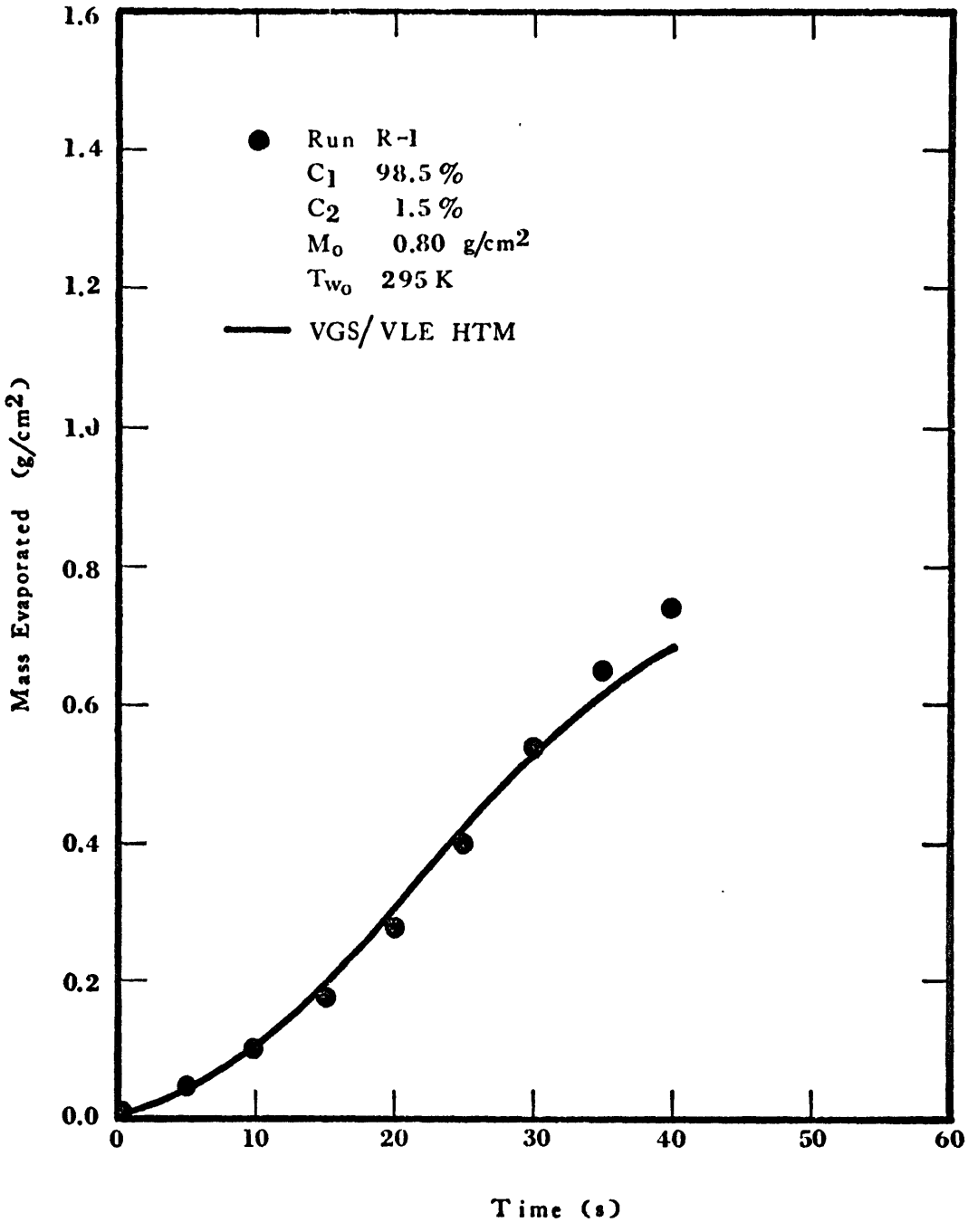

Figure 1-12 Boiling of a Methane-Ethane Mixture on Water (R-1). VGS/VLE HTM Predictions and Experimental Data (τ_{cf} = 25 s)

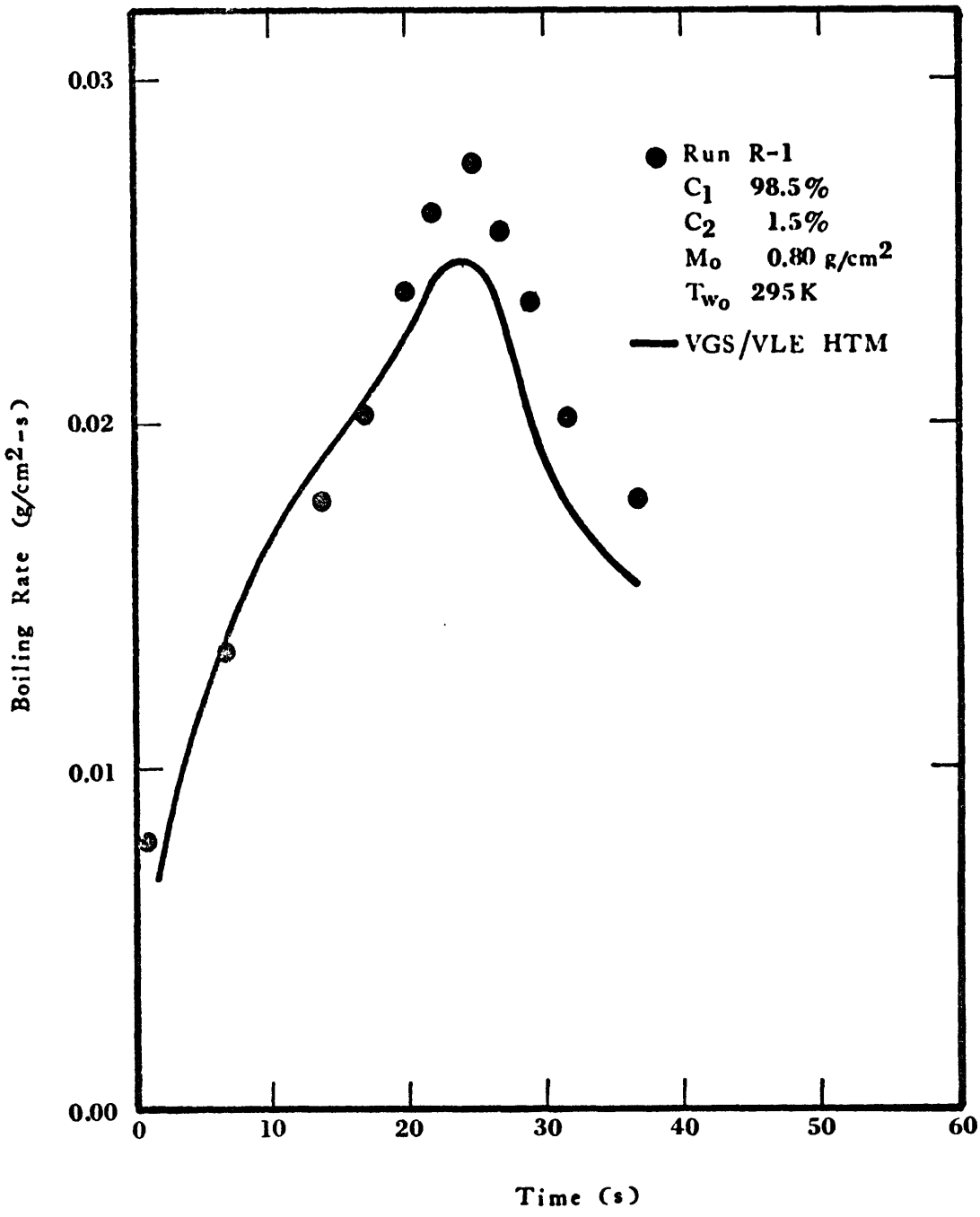

Figure 1-13 Evaporation Rates of a Methane-Ethane Mixture on Water (R-1). VGS/VLE HTM Predictions and Experimental Data (τ_{cf} = 25 s)

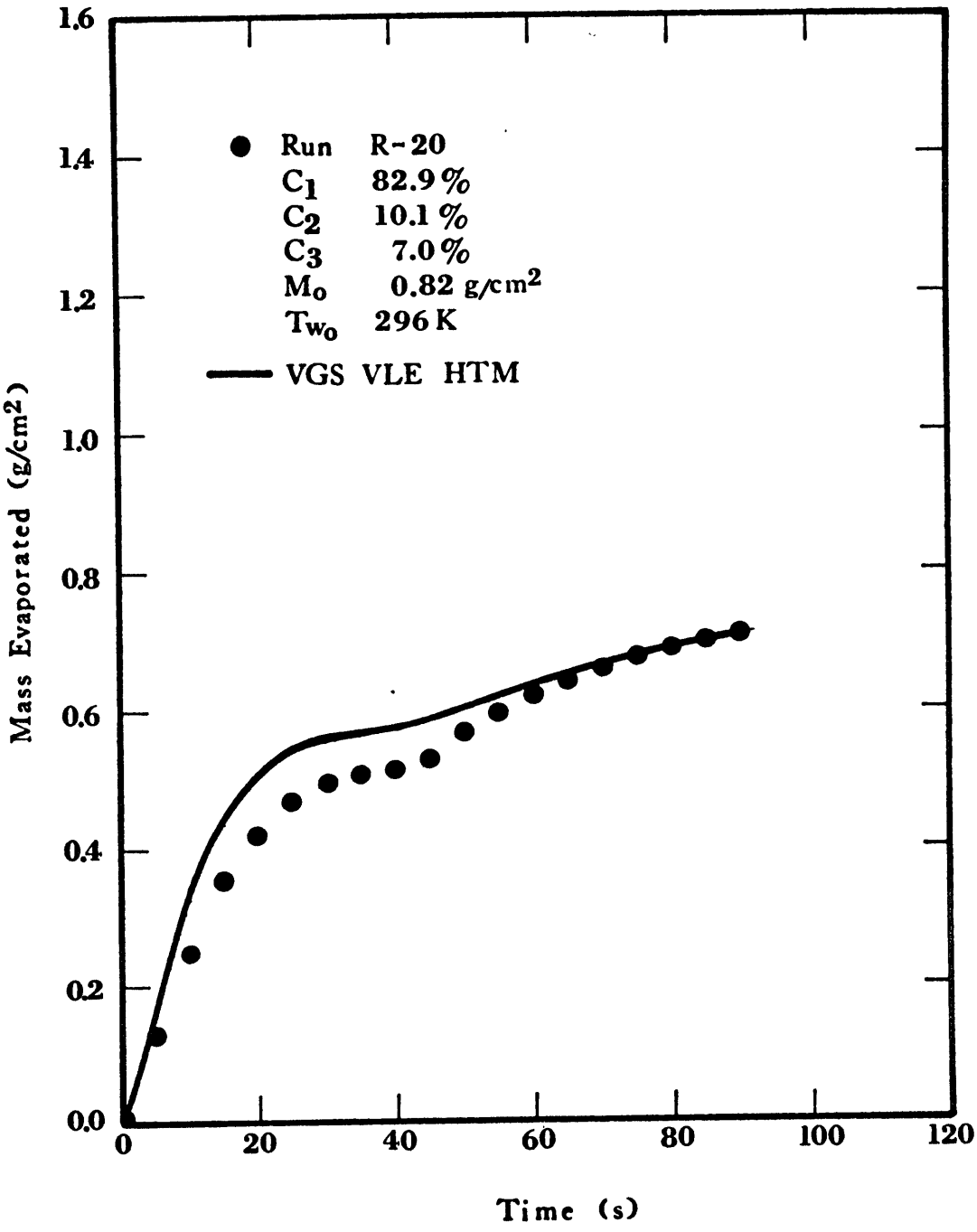

Figure 1-14 Boiling of a Methane-Ethane-Propane Mixture on Water (R-20). VGS/VLE HTM Predictions and Experimental Data (τ_{cf} = 5 s)

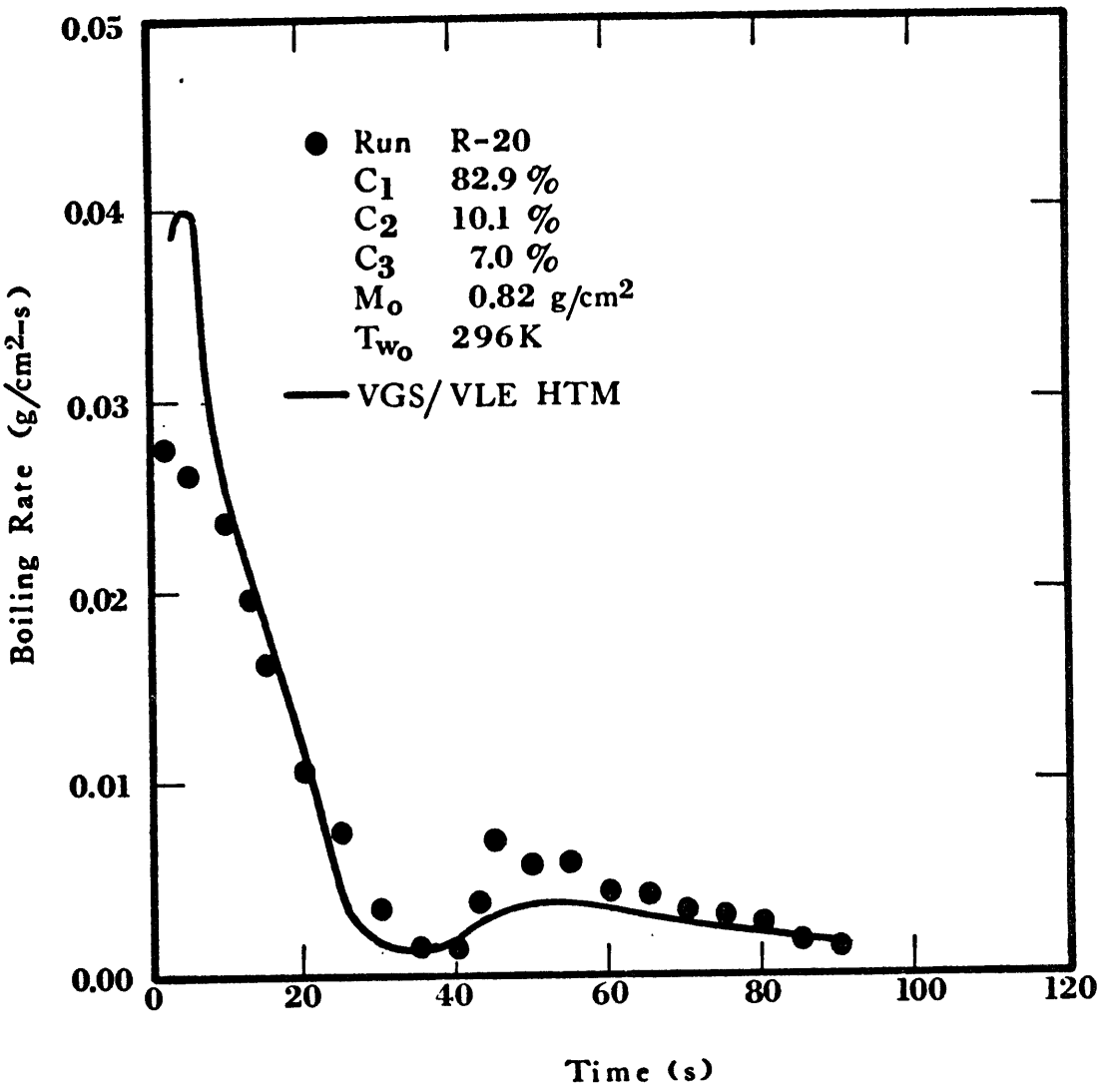

Figure 1-15 Evaporation Rates of a Methane-Ethane-Propane Mixture on Water (R-20). VGS/VLE HTM Predictions and Experimental Data (τ_{cf} = 5 s)

through 1-15. The VGS/VLE HTM predictions agree well with the experimental data; thus reinforcing the qualitative explanations previously given.

The only variable parameter in the model, τ_{cf}, the time for the collapse of the vapor film, has been correlated as follows

$$\tau_{cf} = 45\ x_{C_1} - 40\ x_{C_2}^{0.2} - 10\ x_{C_3}^{0.1}\ (s)$$

where x's are mole fractions. The following restrictions are made: $\tau_{cf} \geq 0$, and it should only be used within the LNG compositional range ($x_{C_2} \leq 0.20$, $x_{C_3} \leq 0.10$).

Thus, the VGS/VLE HTM model becomes the first successful scheme to predict a priori, the evaporation of confined spills of LNG on water.

Conclusions

The following conclusions are made regarding the evaporation of confined spills of liquefied natural gas (LNG) on water.

- Methane film boils on water until the ice layer which forms cools sufficiently to promote nucleate boiling. The heat fluxes, and boiling rates, increase with time until nucleate boiling is achieved, thereafter they decrease.
- LNG mixtures undergo a preferential evaporation of the more volatile components. This evaporation causes a rise in the saturation temperature of the residual liquid. The composition of the vapor and the

residual liquid, as well as the saturation temperature, can be determined from vapor-liquid equilibria and mass balance considerations.

- LNG mixtures film boil on water upon initial contact. The preferential evaporation of methane causes a drop in the vapor pressure of the liquid at the base of the bubbles being formed; such a pressure drop results in the collapse of the vapor film around the bubble.
- The higher the heavier hydrocarbons content in the LNG mixture, the faster the vapor film collapses and the sooner nucleate boiling is established.
- As methane is exhausted, the saturation temperature increases, causing a decrease in the heat flux across the ice/LNG interface. Furthermore, most of the energy transferred at this time goes into warming up the cryogen to the rising saturation temperature.
- The decrease in the surface temperature of the substrate, approaching the cryogen temperature, may be approximated by a linear drop over a period of time τ_{cf}. This period of time τ_{cf} is a function of the chemical composition of the cryogen.
- Based on the above considerations, a heat transfer model that draws information from the vapor liquid equilibria model has been developed. This model predicts successfully the evaporation of confined spills of LNG on water.

Now that the effect of composition on the boiling of LNG on water is understood, research efforts can be directed towards the determination of the effect of spreading and wave motion on the boiling of LNG in an open sea spill.

II. PREVIOUS WORK RELEVANT TO THE BOILING OF LNG ON WATER

Regimes of Boiling

When a liquid at its saturation temperature contacts a hot surface at a temperature above that of the liquid, a phase transformation from liquid to vapor, i.e. boiling, takes place. This phenomenon is known as saturated or bulk boiling as opposed to subcooled or local boiling in which the bulk of the liquid is below the saturation temperature.

If the temperature of the hot surface is only slightly above the saturation temperature of the liquid, heat transfer takes place by convection and evaporation occurs at the free surface of the liquid. Increasing the hot surface temperature causes the liquid near the hot surface to superheat slightly; bubbles form at the hot surface and rise through the liquid. This form of boiling is called nucleate boiling. In this regime the boiling liquid is in direct contact with the hot surface, and its boundary layer is intensely disturbed by the vapor bubbles. Furthermore, as the bubbles detach and begin to rise, they drag some superheated liquid from the layer adjacent to the hot surface into the core of the rising stream, creating an intensive macroscopic transport of heat from the hot surface into the bulk of the boiling liquid. Thus, essentially all the heat is transferred directly to the liquid which divests itself of the energy by evaporation into the vapor (Kutateladze, 1963). The bubbles in this regime are formed at certain favored spots on the surface, the so called *active sites* or *cavities*; some gas or vapor is present in these active sites. Upon heating, the vapor pocket grows by evaporation at the liquid-vapor

interface near the heated wall. As a bubble pinches off and detaches from the surface, some vapor is trapped in the cavity. This vapor initiates the generation of a new bubble (Rohsenow and Choi, 1961).

For a spherical bubble of radius R, the liquid and vapor pressures are related by equilibrium thermodynamics.

$$p_{vap} - p_{liq} = \frac{2\sigma}{R}$$

Using the Clausius-Clapeyron equation, it can be shown that the vapor temperature for such a bubble is

$$T_v = T_{sat}\left(1 + \frac{2\sigma}{R}\frac{\Delta V^{vap}}{\Delta H^{vap}}\right)$$

A minimum degree of superheat is then required for the generation of bubbles in a given cavity. As the temperature of the heating surface is increased, more and smaller nucleation sites are activated, thus increasing the rate of bubble production. This increase in bubble generation as well as the macroscopic agitation near the hot surface are responsible for the high heat fluxes observed in this regime. The increase in heat flux does not continue indefinitely. As the bubbles depart dragging some superheated liquid, a mass of cold liquid must flow from the bulk to the hot surface. When bubble generation is large enough that their rise interferes with the flow of the replenishing liquid, a blanket of vapor essentially covers the hot surface. In most boiling studies an electrically heated filament is used as the hot surface; the formation of a vapor blanket decreases the heat

transfer to the liquid and the filament temperature increases from point *a* towards point c in the boiling curve shown in Figure 2-1. Generally the temperature at point c is higher than the melting point of most metals and the wire melts before reaching this point. Thereafter, point *a* is called the burnout point or peak nucleate flux (Rohsenow and Choi, 1961).

Increasing the temperature of the heating surface past point *b* results in a stable vapor blanket; this is the film boiling regime. Heat must be transferred through the vapor film and the vapor bubbles are formed at the vapor film-boiling liquid interface. The low thermal conductivity of the vapor is responsible for the low heat transfer rates observed in the film boiling regime. The lowest temperature capable of sustaining a stable film is called the Leidenfrost point.

Between the nucleate burnout and the Leidenfrost points lies the transition regime, in which the vapor film collapses intermittently. The random nature of the collapse of the film makes this regime extremely hard to characterize.

Effect of Surface Roughness on Pool Boiling

The degree of smoothness of the heating surface affects the boiling characteristics in the nucleate regime. There is both a change in position as well as slope of the nucleate boiling curve. As shown in Figure 2-2, the nucleate regime expands to higher temperature differences for smoother surfaces and the transition regime shrinks. But, the film boiling regime remains essentially unaffected.

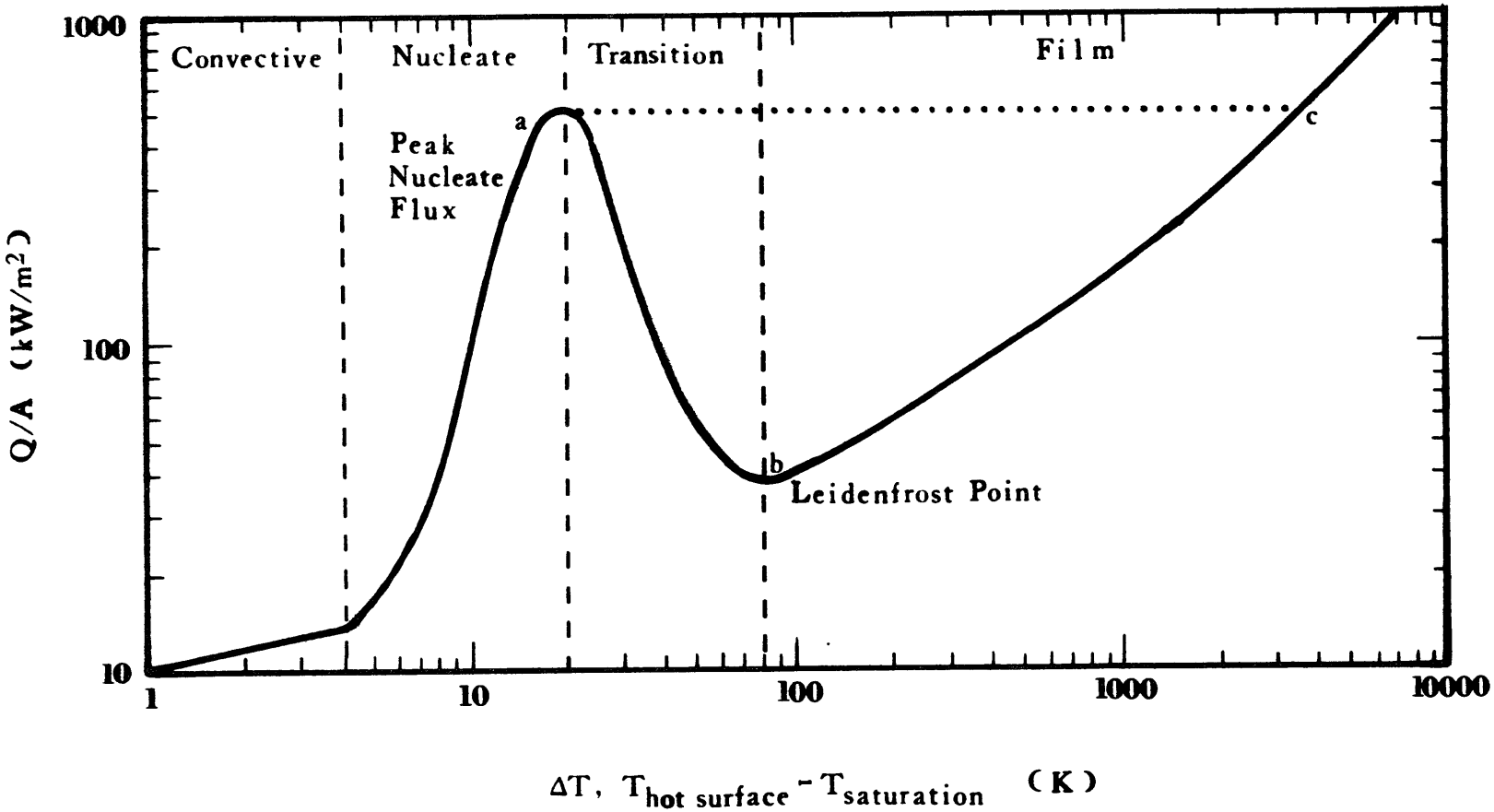

Figure 2-1 Regimes of Boiling

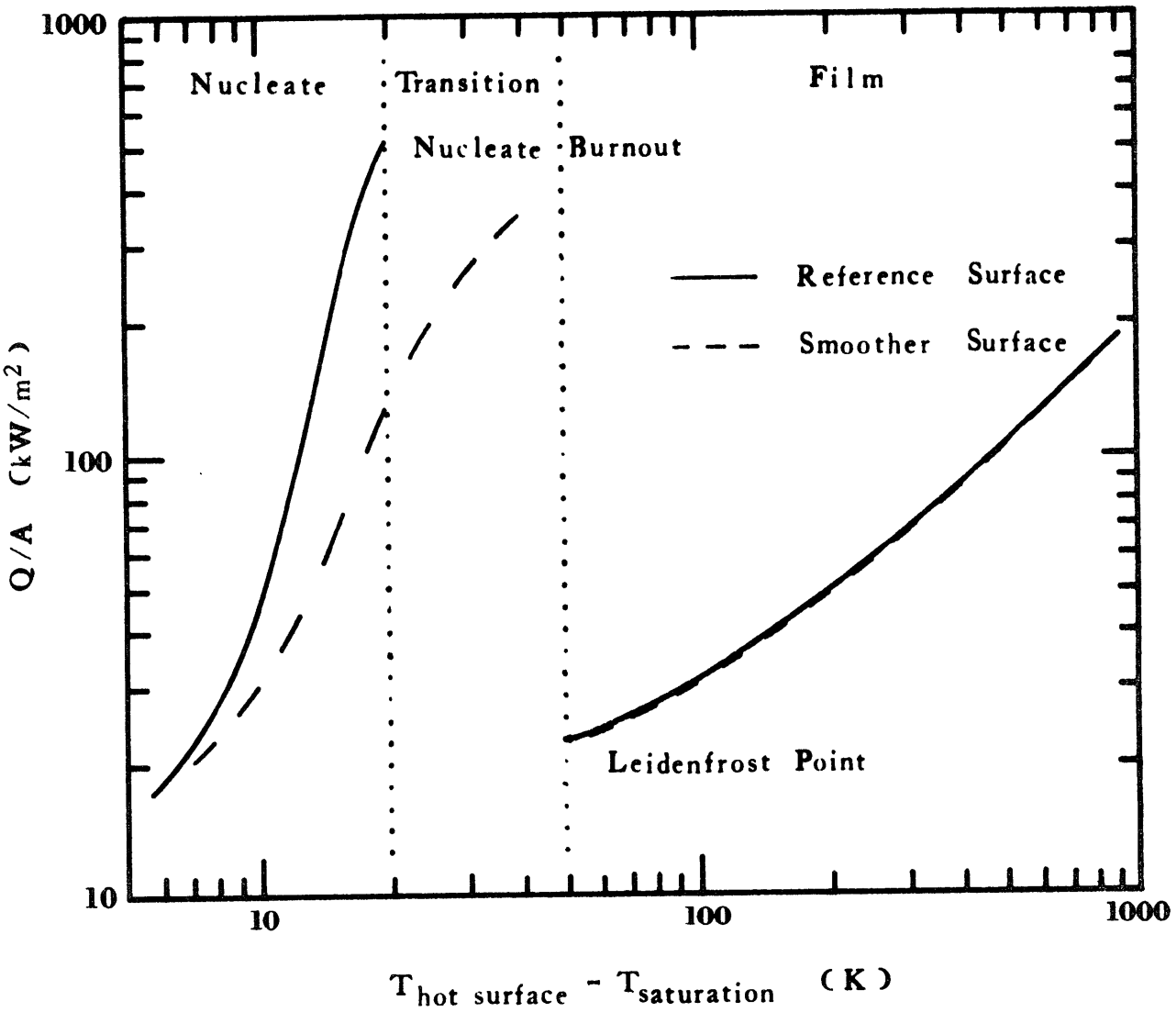

Figure 2-2 Effect of Surface Conditions on Boiling Heat Transfer

Berenson (1960, 1962) carried out a comprehensive study of the effect of roughness on boiling characteristics. The results, presented in Figure 2-3, clearly show the shift in the nucleate regime. The term *roughness* used in reference to boiling surfaces can be misleading since it often has the implication of mechanical roughness finish, i.e., the greater the rms roughness height, the greater the roughness. A rough surface, with regard to boiling, is that which has a large number of cavities of appropriate size for nucleation, regardless of the mechanical roughness (Berenson, 1960). As indicated previously, for a cavity to be active it must contain some entrapped vapor. If the cavity is too small, it will need a large superheat to be activated; if it is too large, it will not be able to entrap any vapor. The difference between mechanical and boiling roughness is clearly illustrated in Figure 2-3. The lapped surface was mechanically smoother than either of the emery-finished surfaces, yet the boiling characteristics correspond to those of a "rougher" surface. The lapping compound contains small pieces of grit suspended in oil which essentially saturate the surface with small cavities. This condition, while corresponding to a small rms roughness, is ideal for bubble nucleation (Berenson, 1962).

Although there is general agreement in the shift of the nucleate curve with surface conditions, such is not the case with the peak nucleate flux. Berenson concludes that the peak flux is, for practical purposes, independent of surface material, roughness and cleanliness. Porchey et al. (1972) report increases by as much as 50% with increasing

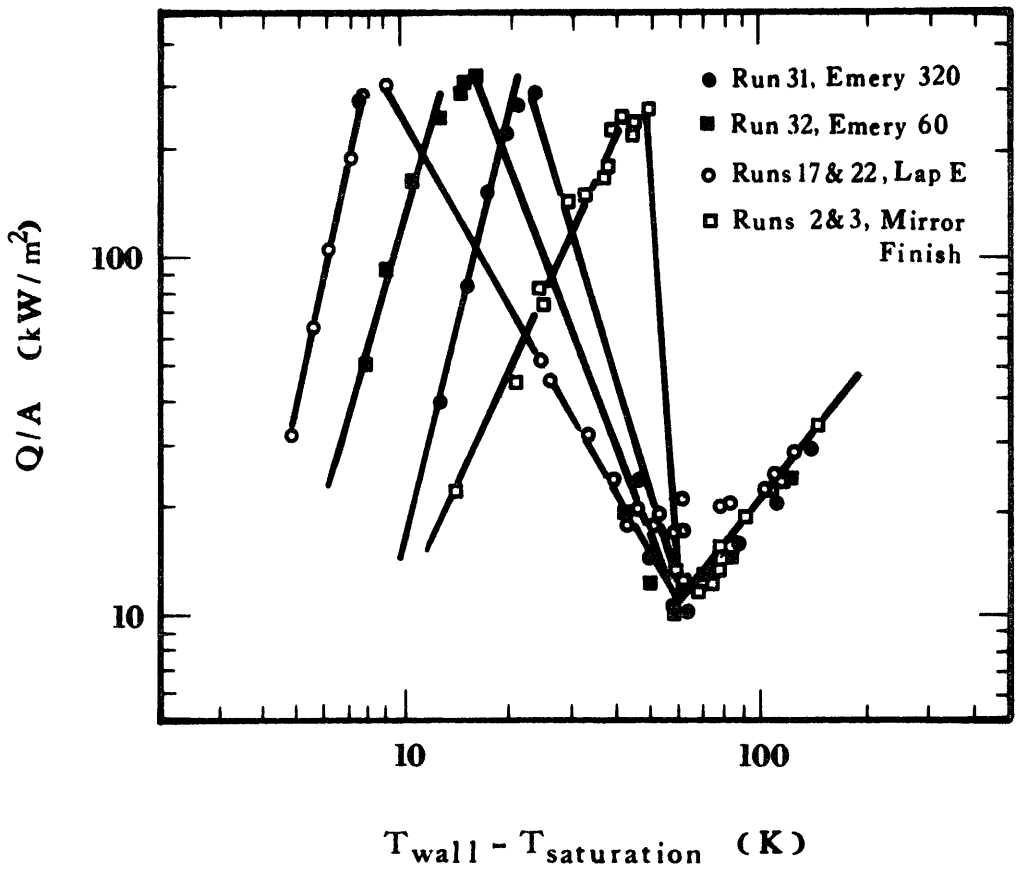

Figure 2-3 Effect of Roughness on Boiling Characteristics. Pentane Boiling on Copper (Berenson, 1962)

roughness on surfaces characterized by scanning electron microscopy. A closer look at Berenson's results (Figure 2-3) will reveal a change in the peak flux of 20% with surface conditions. Tong (1965) surveys the literature and indicates that changes of as much as 50% are reported particularly in cases involving oxidized heating surfaces. It is apparent then that a change in the maximum nucleate flux might be expected; however, it is unlikely that such a change will exceed 50 percent.

Berenson's work indicates that the film boiling regime is independent of the surface roughness unless this roughness is great enough to disturb the vapor film. This is to be expected, since in film boiling bubble formation does not originate in the surface cavities.

Boiling of Liquid-Liquid Interfaces

In most applications boiling takes place on a hot solid surface; consequently, the thrust of boiling studies has been on the boiling of a liquid from a solid surface. Very little is known about the boiling of a liquid in contact with a denser, immiscible and hotter liquid. The mechanism for boiling in the latter case is by far more complicated. Microscopically, the hot fluid surface is smooth and provides very few nucleation sites. Such "surface smoothness" can cause large shifts in the nucleate and transition portions of the boiling curve. Furthermore, if the cold liquid boils at a temperature lower than the freezing point of the hot fluid, a third solid phase could form between the two liquids. Complications arise not only due to the change in characteristics

of the heating surface but also due to a new thermal resistance. The mobility of the heating surface increases the complexity of the system since heat transfer in this layer can take place by conduction as well as convection.

Fortuna and Sideman (1968) determined heat fluxes between immiscible liquid layers with simultaneous boiling and stirring. Pentane was boiled on the top of a water layer, which in turn, was heated by a brass, chrome plated heating surface. Independent stirrers were used for the agitation of each phase. Fortuna and Sideman's results are compared to those reported by Berenson (1962) and Novakovic and Stefanovic (1964) in Figure 2-4. Berenson's experiments were on solid surfaces of varying degree of smoothness. Novakovic and Stefanovic studied the boiling of pentane on a mercury surface. Theoretically, as the surface becomes smoother, the nucleate boiling curve should shift to the right. This shift is in fact observed in Figure 2-4. Mercury has thermal properties intermediate between those of a normal liquid such as water and solid metal, thus the curve for pentane boiling on water is expected to shift to the right of metal and mercury surfaces. However, the double stirrer agitation in Fortuna's experiments would tend to increase the heat transfer for a given ΔT thereby counteracting the shift in the nucleate curve that would otherwise occur. Further analysis is very limited, particularly concerning the maximum nucleate boiling heat transfer since Fortuna and Sideman, as well as Novakovic and Stefanovic, had physical limitations; either the bottom layer would begin boiling or the boiling in the upper layer became vigorous enough

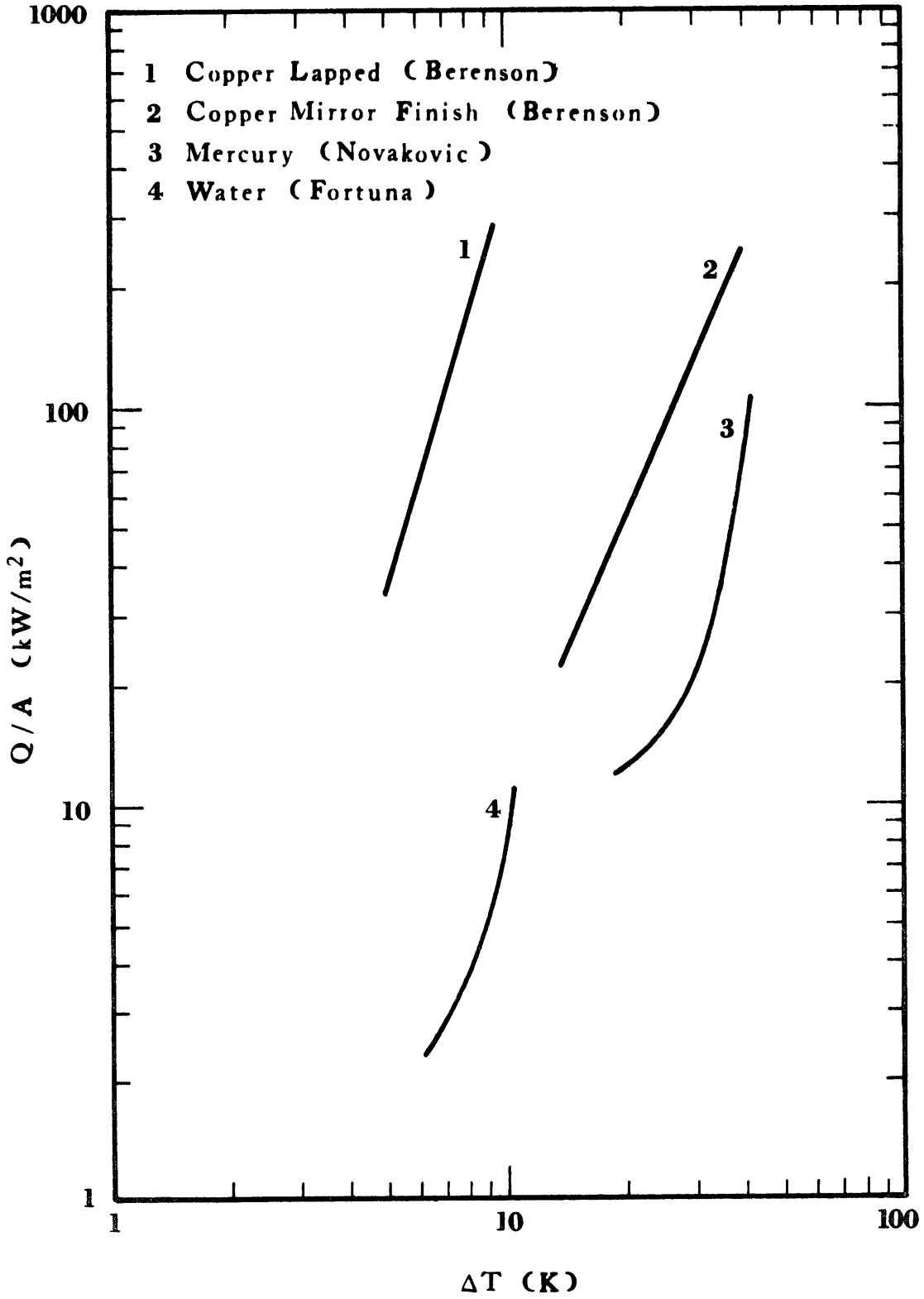

Figure 2-4 Effect of Heating Surface on the Nucleate Boiling of Pentane

to disrupt the thin bottom layer. The most important point, however, has been demonstrated by the experiments of boiling on solid and liquid surfaces: nucleation on a smooth liquid surface can occur at higher ΔT's than on a rough solid surface.

Boiling Heat Transfer to Liquid Mixtures

Van Wijk et al. (1956) investigated the effect of concentration upon the maximum heat flux in nucleate boiling. Mixtures of methyl ethyl ketone and water yielded a maximum value for the burnout nucleate heat flux at a concentration of 4.2 weight percent methyl ethyl ketone. This heat flux was 150% higher than that for pure water. Figure 2-5 shows the peak nucleate heat fluxes as a function of composition. The boiling of mixtures of 1-pentanol and water are illustrated in Figure 2-6. A second peak was observed at high alcohol concentrations. Acetone-water and 1-butanol-water systems also exhibited two peaks.

The onset of film boiling is aided by large bubbles merging in the neighborhood of the surface. Thus, the smaller the average size of the bubbles leaving the heating surface, the more the onset of film boiling is shifted towards a higher heat flux. For a pure liquid the vapor bubbles, which are at their dew point, continue to grow during their passage through the bulk of the superheated liquid. For a mixture the dew point of the vapor bubbles is the same as the boiling point of the remainder of the mixture. Since the liquid is locally being depleted of the volatile component, the dew point of the bubbles is higher than the boiling point of the original mixture. As the

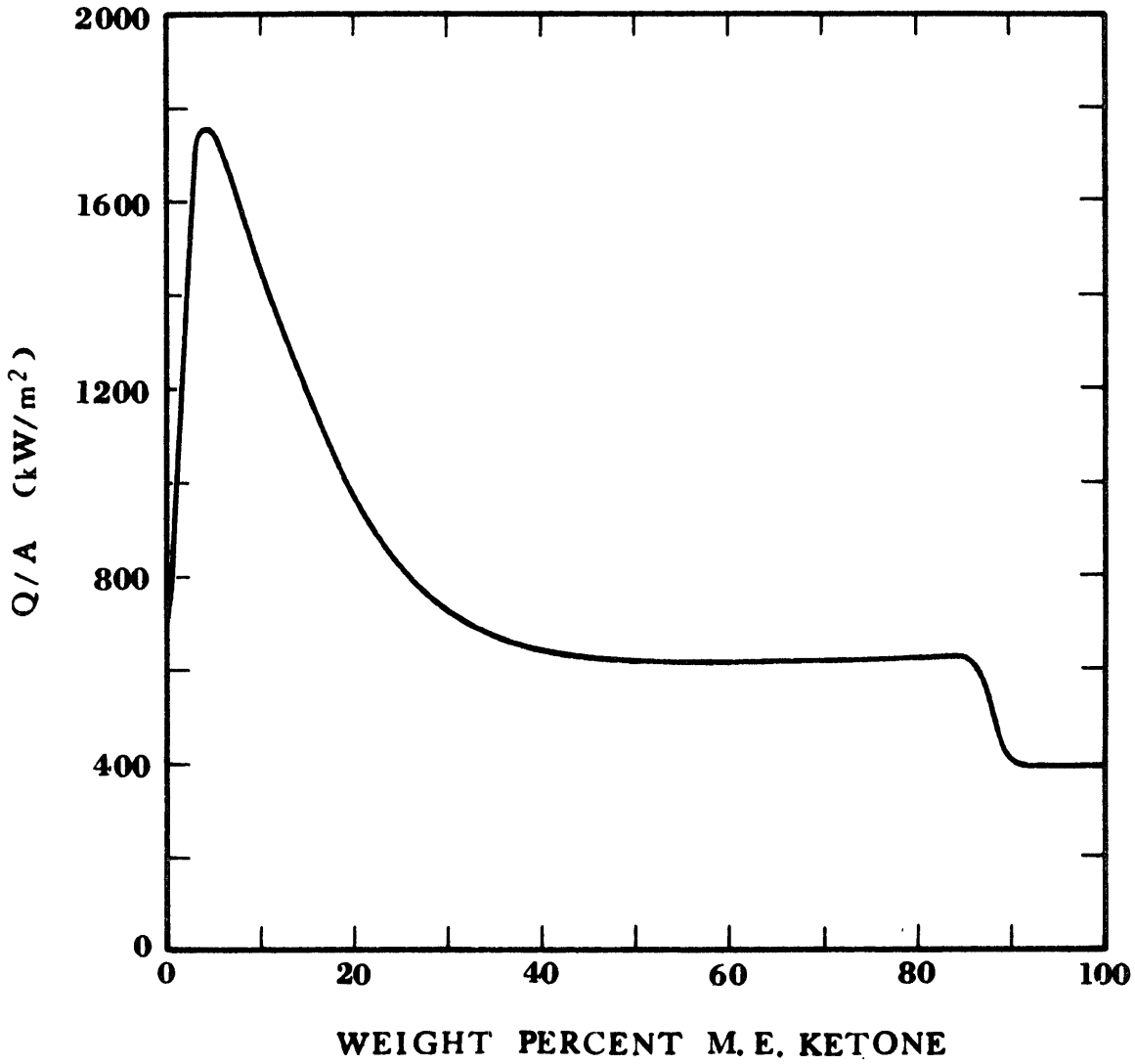

Figure 2-5 Peak Nucleate Heat Fluxes for Water-Methyl Ethyl Ketone Mixtures (Van Wijk, 1956)

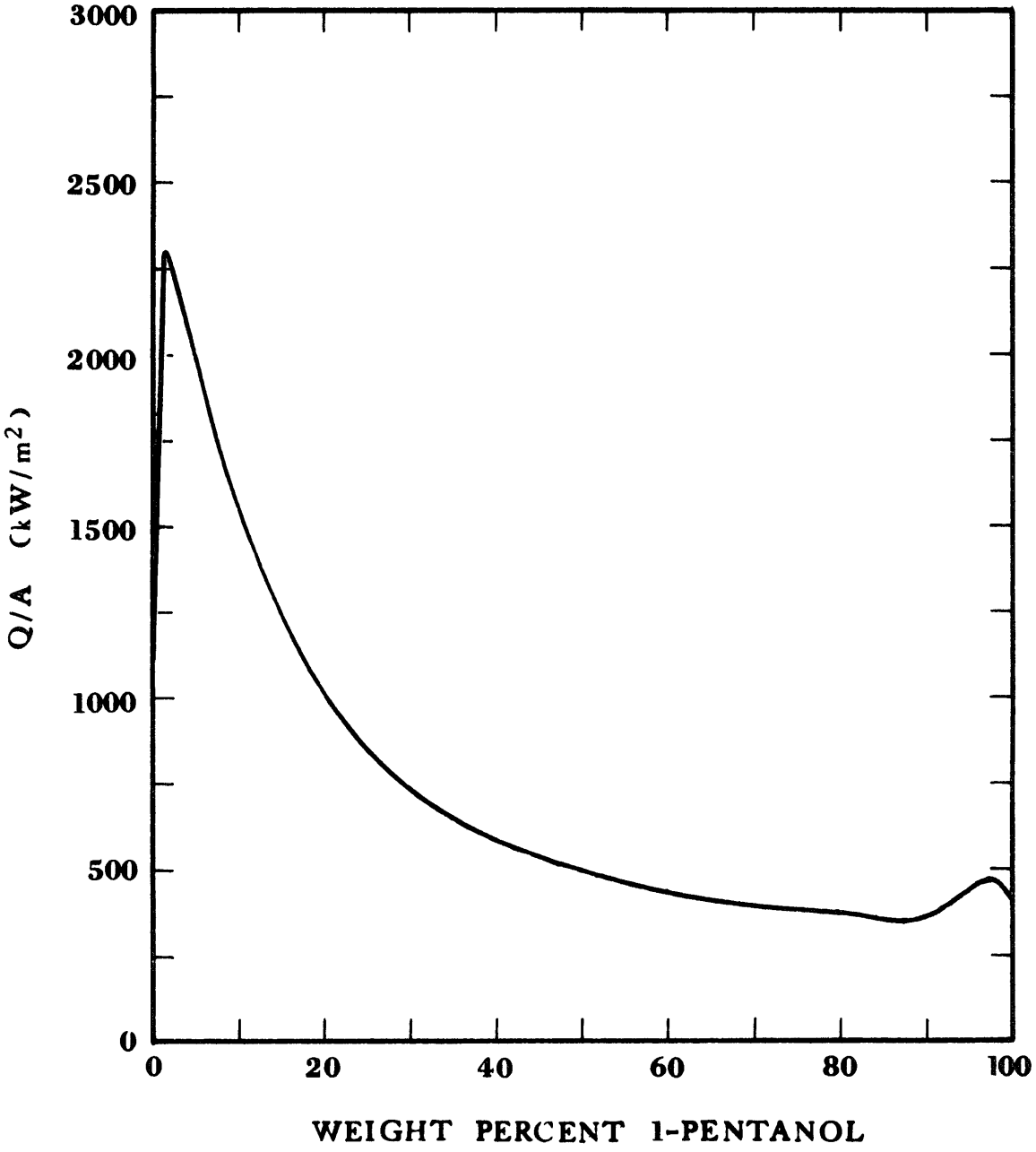

Figure 2-6 Peak Nucleate Heat Fluxes for Water-1-Pentanol Mixtures (Van Wijk, 1956)

bubble travels upward through a mass of superheated liquid of the original composition, a point is reached in which the dew point of the bubble equals the temperature of the bulk superheated liquid. At this location, the driving force ($T_{bulk} - T_{bubble}$) becomes zero and only diffusional interchange takes place. This mechanism results in the size of the bubble being considerably smaller than for pure boiling liquids.

In cases in which the mixture forms are azeotrope, two peaks in heat flux are expected since the component that is the more volatile at one side of the azeotrope becomes the least volatile at the other side. Such was the case with 1-butanol-water and 1-pentanol-water mixtures. The second peak reported for the acetone-water system could not be explained by this theory since this system does not form an azeotrope.

Although Van Wijk's theory for the boiling of a mixture explains the slowing down in the growth of an individual bubble, it does not explain why the bubbles do not merge together.

Hovestreijdt (1963) proposed an interesting explanation for the increase of maximum heat fluxes in mixtures. Aside from the slowing down of bubble growth considered by Van Wijk, he considered the influence of surface phenomena on the boiling of mixtures. As the volatile component evaporates, the liquid in the immediate neighborhood of the bubble becomes deficient in this component. A concentration gradient originates and diffusion from the bulk liquid takes place. However, if two bubbles are close together, the diffusion of volatile component

from the bulk to the zone between the bubbles becomes limited. If the surface tension of the more volatile component happens to be the lower one (positive systems), there is then an increase of surface tension at the bubble walls between the bubbles. Liquid is drawn between the bubbles as a consequence of the surface tension gradient (Marangoni effect) thus stabilizing the bubbles against merging. A similar effect would take place at the heating surface since replenishment of the volatile component also becomes highly limited. Furthermore, for a positive mixture, the bubbles are pinched off at a smaller diameter due to the surface tension gradient at the base of the bubbles that draws liquid between the bubble and the heating surface. Through this effect, the frequency at which bubbles are generated at an active site increases, thus increasing the heat transfer at the wall. The bubble stabilization at the wall also retards the onset of film boiling.

Hovestreijdt found that the stabilization of bubbles in positive mixtures not only increased the heat flux but it caused foaming at the liquid surface. This foam is only an indication that a large number of small bubbles are being generated and stabilized against merging. The foam in itself does not affect the heat flux.

The surface-tension effect explained the presence of the maximum for the burnout nucleate boiling flux in a mixture for a number of systems. It failed, however, for the methanol-heptane system in which case the surface tension decreased as evaporation took place and yet a peak in the heat flux was observed. Similarly, Van Wijk's theory explained the observations for this last system and some others, but it

also failed in some cases. It is quite possible that both effects can be present simultaneously. The relationship between the two, co-operating or counteracting, is unknown and needs to be investigated.

Van Stralen (1966, 1970) modified existing theories for the explanation of the "boiling paradox" (coincidence of the maximal peak flux and a minimal bubble growth rate) and proposed a new "relaxation microlayer" theory for nucleate boiling. According to this theory, bubble formation is a relaxation phenomenon resulting from the superheating of the thermal boundary layer at the heating surface. This thin liquid layer is periodically pushed away from the heating surface due to the rapid initial growth of succeeding bubbles on active sites. Colder liquid at saturation temperature flows to the surroundings of the nucleation site and is superheated during the delay time before formation of a new bubble. Based on Van Wijk's theory, Van Stralen shows the occurrance of a maximum in bubble frequency at the peak flux. Convection is augmented by the action of the bubbles and the heat flux increases. A combination of the theories formulated by Van Wijk, Hovestreijdt and Van Stralen provide a satisfactory qualitative explanation for the maxima in peak nucleate fluxes observed at some intermediate composition in boiling mixtures.

The surface tension effect (Marangoni effect) at the heating surface causes the bubbles to be pinched off at a small diameter. Thus the frequency of bubble generation at an active site increases. As the bubble is quickly formed and released, convection is augmented; this results in an increased heat flux.

Furthermore, the growth of these small bubbles is hindered by Van Wijk's equilibrium considerations and their coalescence prevented by the Marangoni effect. As a consequence, the formation of a vapor film is retarded to higher ΔT's thus allowing higher peak nucleate fluxes.

Film boiling of binary mixtures was studied by Van Stralen et al. (1972). As noted earlier, Van Wijk showed that a 4.2 weight percent methyl ethyl ketone in water mixture exhibited a maximum nucleate boiling flux 150% higher than that for pure water. For the same mixture Van Stralen was able to reach film boiling fluxes exceeding the value of the peak nucleate flux by a factor of two. Similarly, the maximum film boiling flux attained (the heating element burned out) for this 4.2 weight percent methyl ethyl ketone exceeded the maximum film boiling flux attained with pure water by a factor of two. The increased heat fluxes of the mixture in comparison with pure water were said to be due to mass diffusional effects and ultimately to an increase of the boiling temperature of the liquid in the immediate neighborhood of the vapor film. Such an increase in temperature is due to the local exhaustion of the more volatile component in the liquid. A temperature gradient is established in an adjacent liquid layer causing a heat flow in the direction of the bulk liquid. Van Stralen observed that the direct vapor production at the film in pure liquids accounts for 95% of the total heat flux (radiation heat excluded). However, for 4.1 percent methyl ethyl ketone it accounted only for 53%. Apparently the rest of the heat flux is transmitted through the vapor film into the bulk of the liquid by the temperature gradient above mentioned.

Boiling of Cryogenic Liquids on Solid Surfaces

The use of cryogenic liquids in nuclear reactors, rocket engines and some industrial processes as heat transfer fluids motivated the study of their heat transfer properties. The discussion here shall be restricted to those fluids of interest, namely liquid nitrogen and liquefied hydrocarbons.

Nucleate and film boiling of nitrogen was studied by Park et al. (1966). An electrically heated, gold plated, cylindrical assembly was used as the heating element. The heat flux and temperatures were measured under steady state conditions. Park's results at atmospheric pressure are compared to those reported by Lyon (1968), Bewilogua et al. (1975) and Ackermann et al. (1976) in Figure 2-7. Lyon's experiments were conducted on a flat, horizontal, platinum plated surface. Bewilogua et al. used a horizontal copper disk for their heating surface while Ackermann et al. made use of a horizontal cylinder, the material of which is not specified.

The nucleate data is rather consistent, with the exception of Lyon's. Although the geometry of the heating surface has an effect on the heat flux (Ackermann et al., 1976; Tong, 1965), the discrepancy with Lyon's data seems too large to be accounted for only on geometrical grounds. Furthermore, Kosky and Lyon (1968) indicated the choice of platinum as the heating surface was an unfortunate one due to the possible formation or decomposition of a surface layer of platinum oxides and adsorption of oxygen. The reproducibility of Lyon's data was very poor. On these grounds one should pay limited attention to

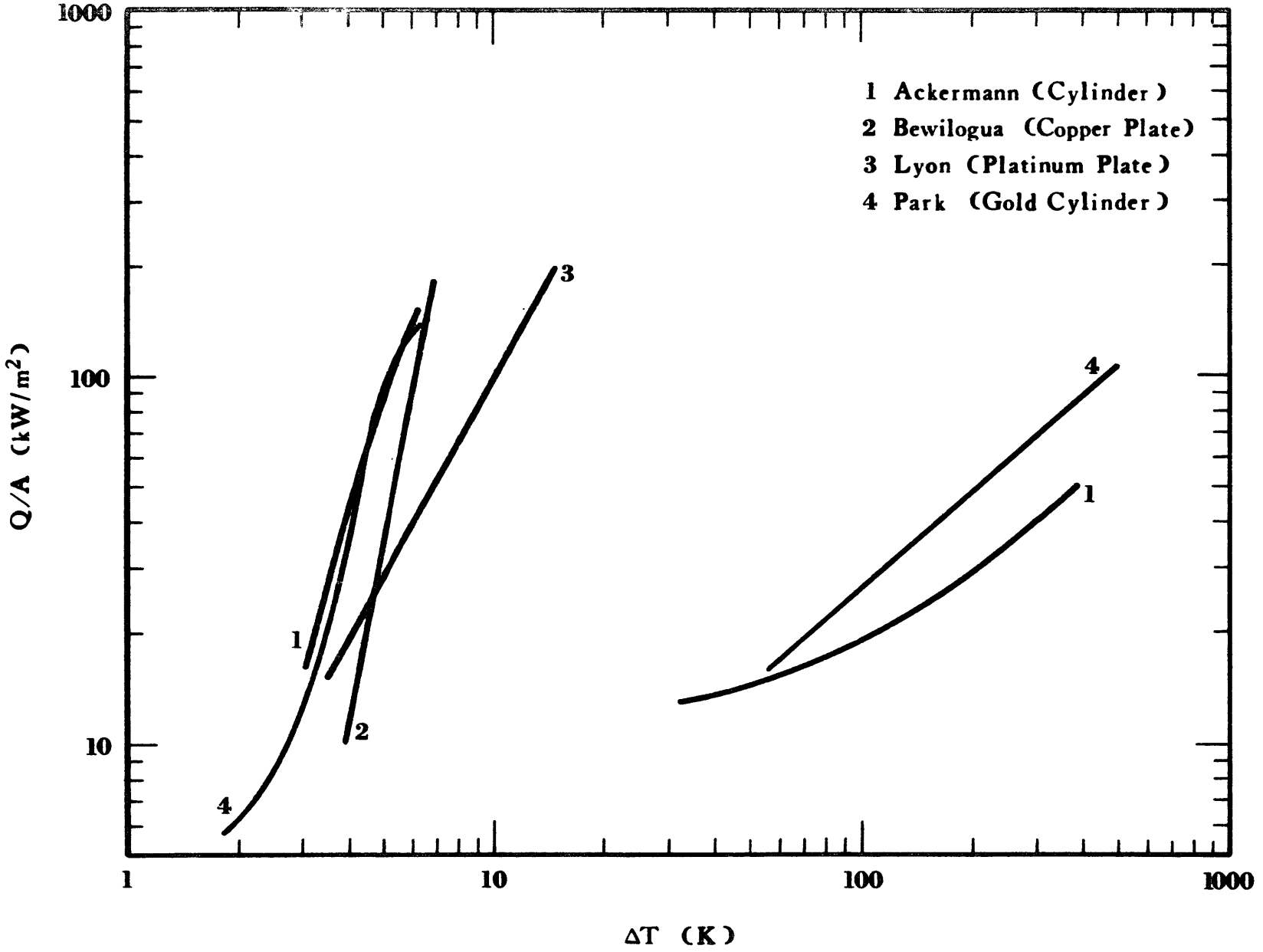

Figure 2-7 Boiling of Liquid Nitrogen on Solid Surfaces at Atmospheric Pressure

Lyon's data. Only two investigators, Park and Ackermann, covered the film boiling regimes, both in a cylindrical configuration. From the above data it can be concluded that the nucleate burnout flux for nitrogen is around 150 kW/m^2 corresponding to a ΔT of 6 K and the Leidenfrost flux is about 15 kW/m^2 corresponding to a ΔT between 30 and 55 K.

Park and Lyon also studied the boiling of methane on the same gold and platinum plated surfaces used for the boiling of nitrogen. In addition, Sciance et al. (1967-c) investigated the pool boiling of methane on a gold plated cylinder, Kravchenko et al. (1975) using a vertical stainless steel tube and Ackermann (1976) with a horizontal cylinder. Their data, at atmospheric pressure, are shown in Figure 2-8. For the same reasons given in the discussion of nitrogen data, Lyon's results are questionable. Considering Sciance's and Kravchenko's results, the nucleate burnout for methane boiling on a horizontal surface is about 220 kW/m^2 corresponding to ΔT's of 13-16 K. In turn Sciance's and Ackermann's film boiling data yield a Leidenfrost flux of about 25 kW/m^2 for a ΔT of 70 K. Although Park's data were taken at 1.65 bar, it is shown so as to compare the fluxes at the Leidenfrost point. Seven pressure lines (range 1.65 - 36 bar) converged to the same minimum film boiling flux of 55 kW/m^2 at a ΔT of about 150 K. Due to the equipment design, it is possible that the internal cooling coils used (with liquid nitrogen) caused the bulk of the liquid to be subcooled. Since Park used $(T_{\text{hot surface}} - T_{\text{liquid}})$ as ΔT $(T_{\text{hot}} - T_{\text{sat}})$, the reported ΔT would be higher for the same heat flux. In addition, a thermal surface resistance was neglected in computing the surface

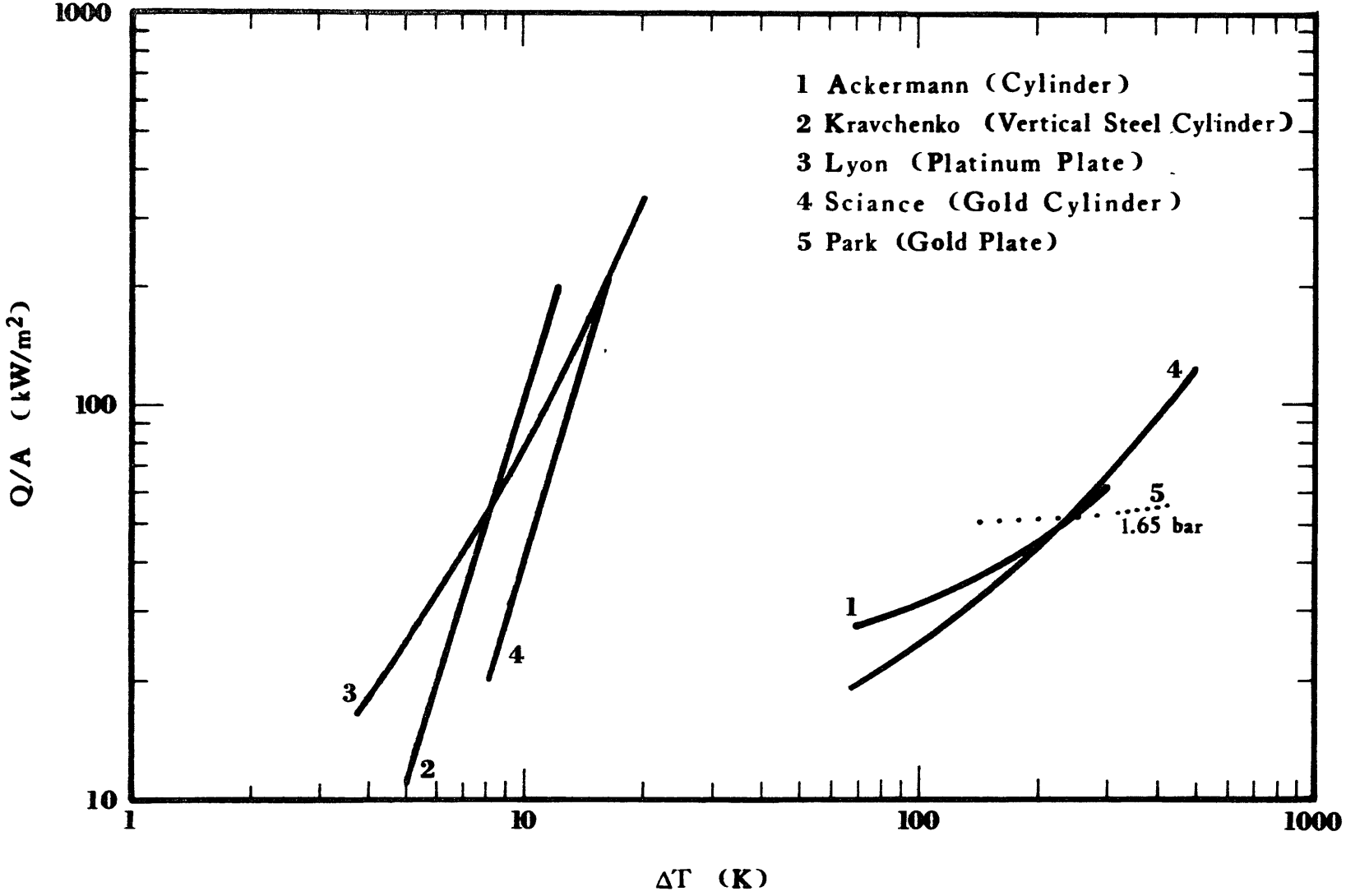

Figure 2-8 Boiling of Methane on Solid Surfaces at Atmospheric Pressure

temperature of the heating element. Nevertheless, as pointed out by Sciance, these errors could add up to 2-3 K, which is significant for the nucleate regime but not for film boiling.

As it will become more apparent in the next section, small amounts of heavier hydrocarbons can cause significant changes in the boiling fluxes. Unfortunately, the extent to which this factor could be responsible for the above discrepancies cannot be determined since only two investigators reported the purity of materials used; Sciance, 99.7 mole percent methane; and Lyon, 99.95 percent methane.

The above information leads to the conclusion that not enough data is available to specify the heat flux and corresponding ΔT at the methane Leidenfrost point with any degree of certainty.

Sciance et al. (1967a) studied the nucleate boiling of ethane on a gold plated cylinder. Wright and Colver (1969) studied ethane-ethylene systems on the same heating element used by Sciance. Sliepcevich (1968) presents the only data available on film boiling of ethane. The corresponding boiling curves are shown in Figure 2-9.

Liquefied natural gas and liquefied petroleum gas were tested at various pressures by Brown (1967). The results for LNG are compared to methane curves in Figure 2-10. Due to equipment limitations, nucleate burnout for LNG was not achieved. For the same ΔT LNG exhibited higher nucleate fluxes. However, at a flux of 100 kW/m^2 the slope for LNG tends to flatten out, whereas that for methane remains quite steep with the heat fluxes for methane becoming higher than those for LNG. In film boiling the LNG curve almost overlaps Sciance's methane curve.

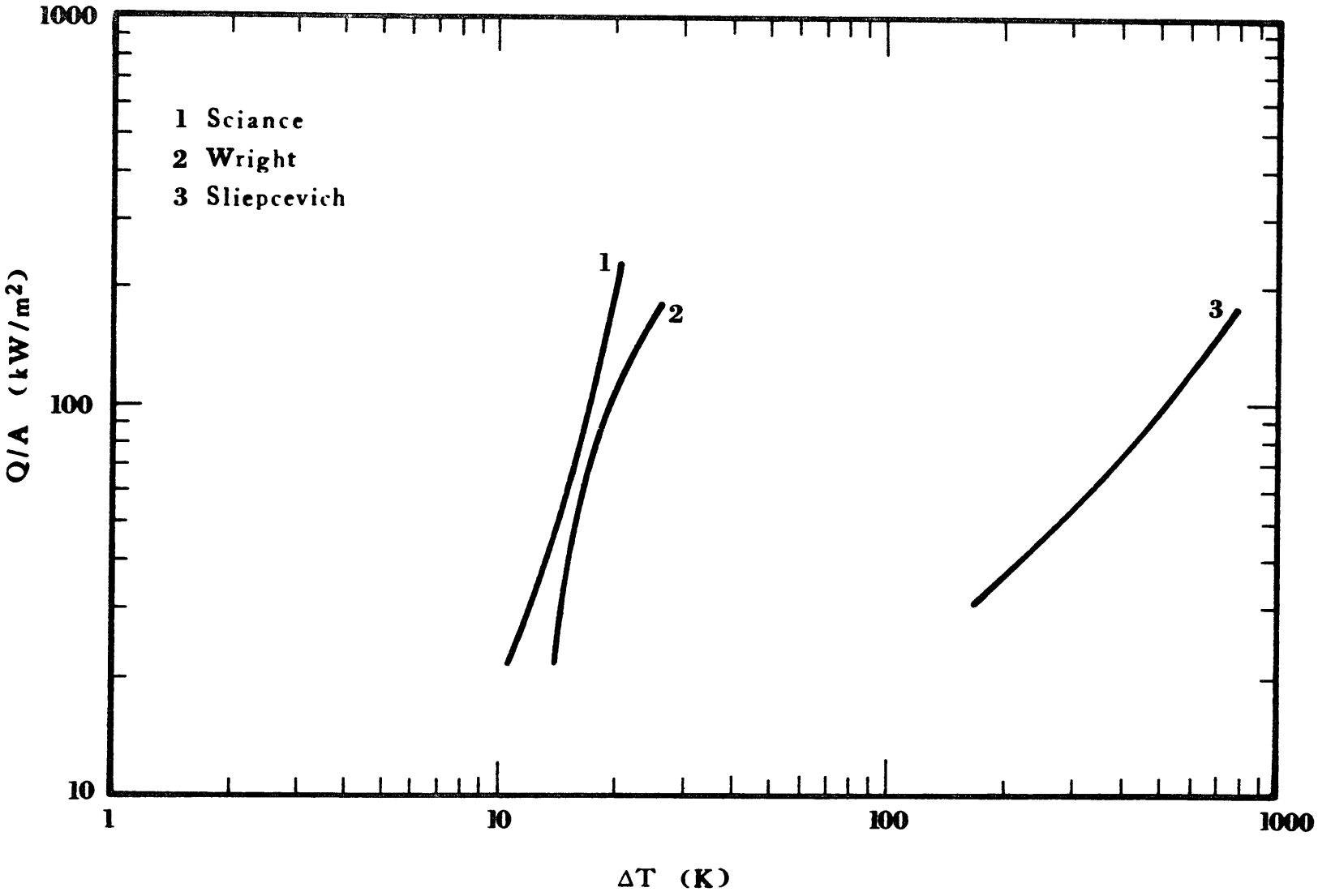

Figure 2-9 Boiling of Ethane on a Gold Plated Surface at Atmospheric Pressure

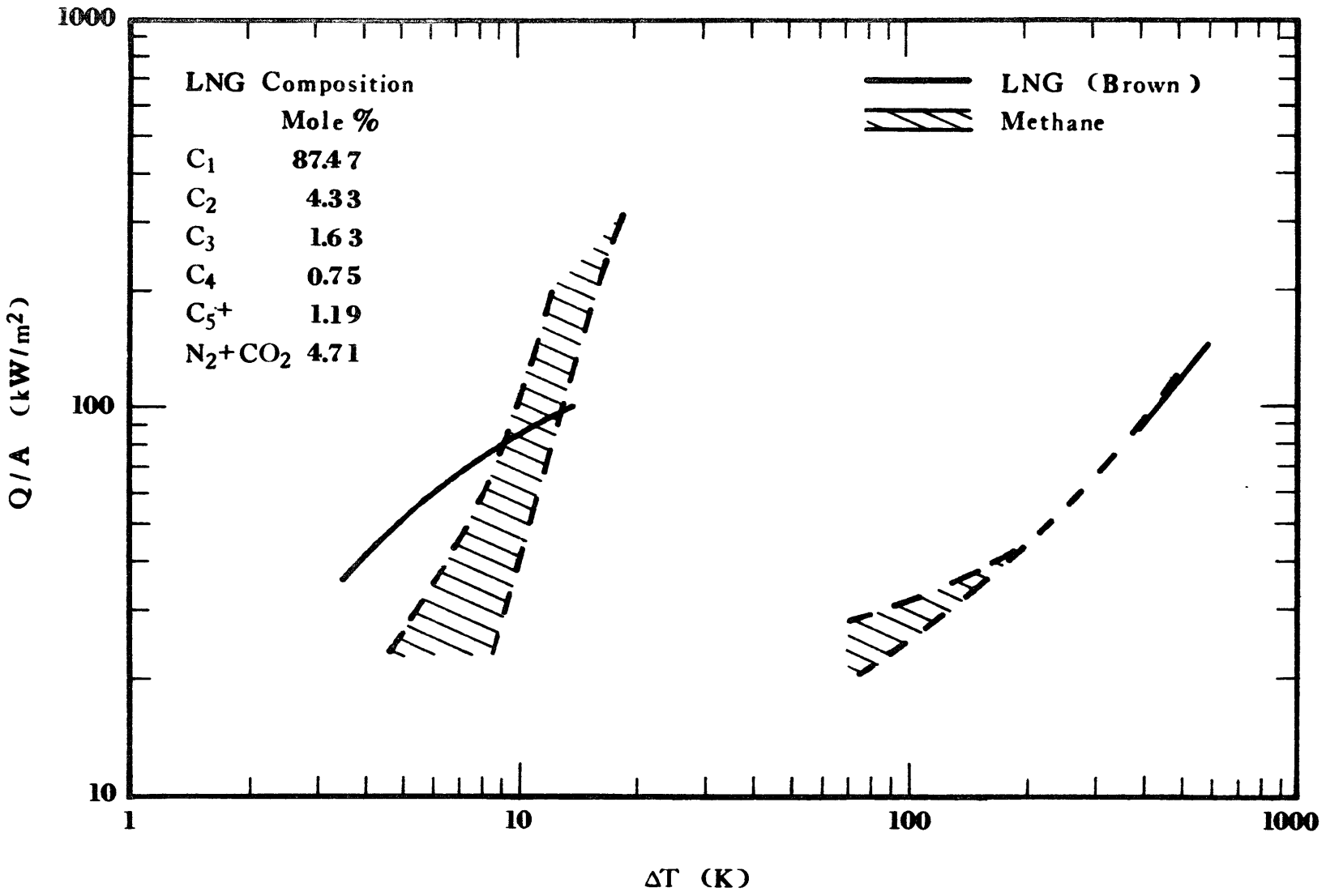

Figure 2-10 Boiling of LNG and Methane on a Gold Plated Surface at Atmospheric Pressure

The Leidenfrost point for LNG was quite high, 210 K, compared to Sciance's value for methane of 70 K. Although the bulk of the liquid might have remained at a constant composition, the layer in the immediate neighborhood of the heating surface will become deficient in methane as it is the main constituent of the vapor bubbles due to its high volatility. Thus, a thin liquid layer becomes enriched in heavier hydrocarbons. The saturation temperature of this layer increases with a subsequent decrease in ΔT, which is no longer high enough to maintain a stable film and, consequently, the film collapses. This theory then explains why the LNG Leidenfrost point reported by Brown is so much higher than that for pure methane.

A similar comparison is made between LPG (a mixture of mainly propane and higher hydrocarbons) and propane curves in Figure 2-11. For a given ΔT, the nucleate heat fluxes for LPG are about twice as high as those for propane.

Clements (1973) studied pressure and composition effects in steady state pool boiling of propane, n-butane, n-pentane and their mixtures. It must be pointed out that the ΔT's were based on the temperature of the bulk liquid rather than the saturation temperature. Unfortunately, the pressure in all cases was above atmospheric and therefore the results are of limited use in this study. Nevertheless, the effect of composition on the boiling of propane - n-butane mixtures is shown in Figure 2-12. A cross-plot of ΔT and composition is shown in Figure 2-13. Similar results were observed by Wright et al. (1971) who experimented with mixtures of ethane and ethylene. ΔT was a maximum at some

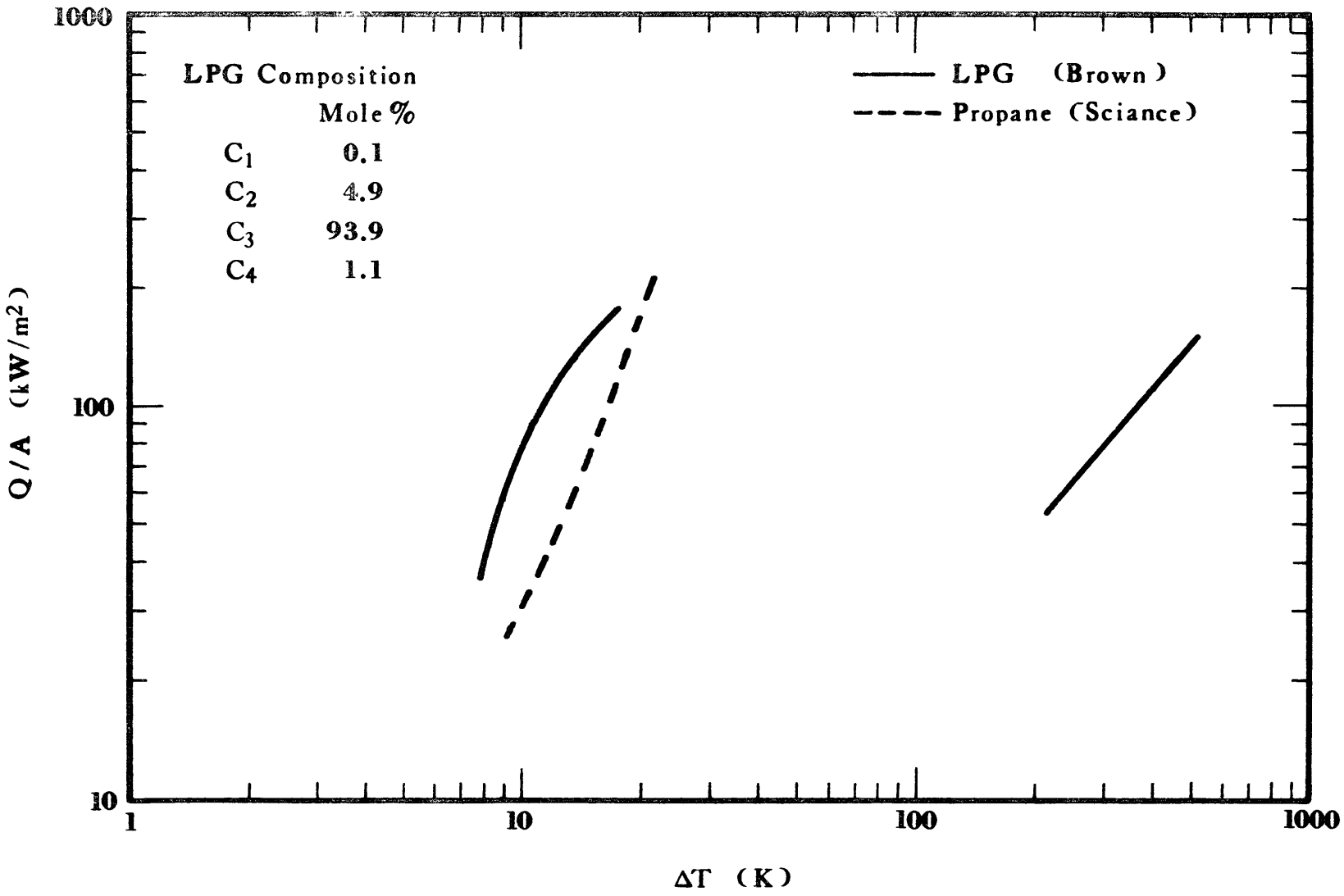

Figure 2-11 Boiling of LPG and Propane on a Gold Plated Surface at Atmospheric Pressure

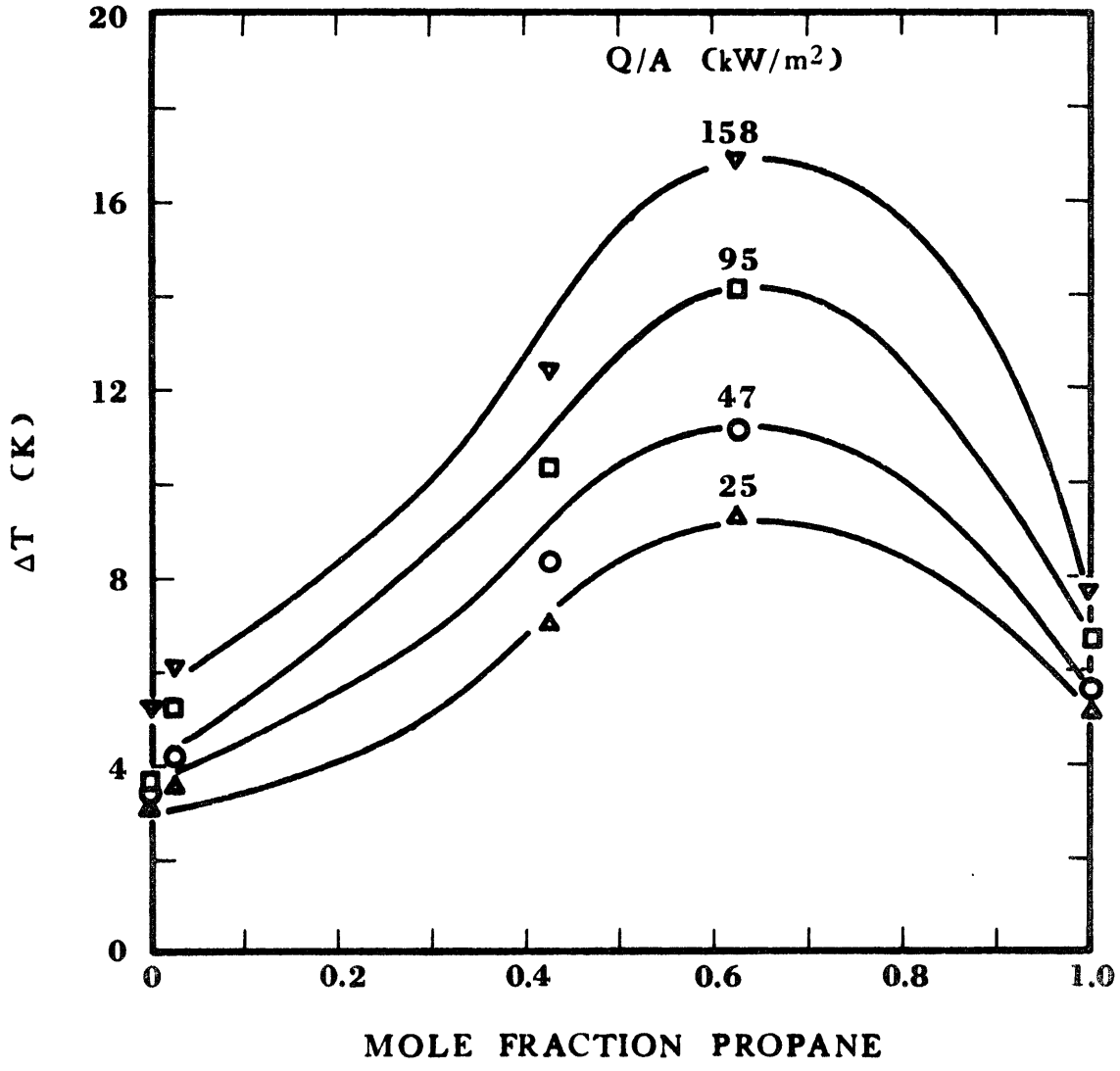

Figure 2-12 Effect of Composition on ΔT for Propane-n-Butane Mixtures at a Reduced Pressure of 0.3 - or 12.7 bar - (Clements, 1973)

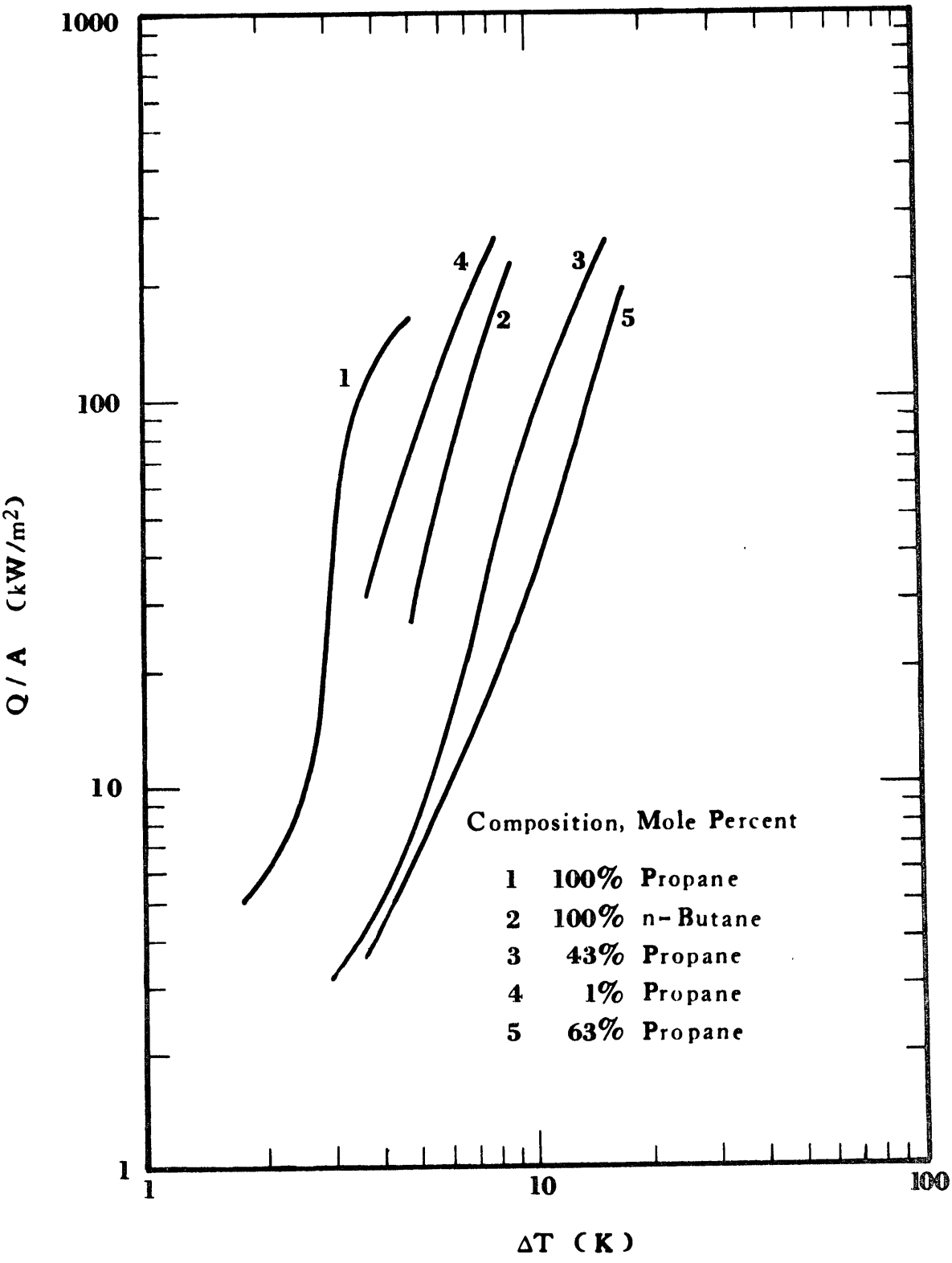

Figure 2-13 Effect of Composition on Nucleate Boiling of Propane - n-Butane Mixtures, P_r = 0.3 (Clements, 1973)

intermediate composition of the mixture. Furthermore, it was found that this maximum occurred when the difference in composition between the liquid and the corresponding vapor in equilibrium was a maximum. The same observation is made by Ackermann et al. (1976) for nitrogen-methane mixtures.

All of the above observations resemble the results reported by Van Wijk, Hovestreidjt and Van Stralen for boiling mixtures. And the occurrence of a maximum in the nucleate fluxes as a function of chemical composition can be explained by exactly the same theories that explain the boiling of liquid mixtures in the previous section.

Boiling of Cryogenic Fluids on Water

Increases in marine transportation of cryogens motivated several studies trying to determine the safety of such transportation.

Burgess et al. (1970, 1972) conducted an investigation to evaluate the hazards associated with the spillage of LNG on water. Spills were made both in a confined and unconfined area.

A 61 x 30.5 x 30.5 cm aquarium was used in the confined spills (1970). The aquarium was placed on a load cell and the time observed when each 50 g loss occurred. Four to eight liters of cryogen were spilled on 19 liters of water. These quantities correspond to initial (non-boiling) hydrostatic heads of 2.15 to 4.30 cm. Table I shows the experimental results.

For the first 20-40 seconds, the boiling rate of LNG was relatively constant with an average value of 0.018 g/cm^2-s. The corresponding heat

TABLE I

BURGESS' RESULTS FOR BOILING OF CRYOGENIC FLUIDS

CRYOGEN	SURFACE	EVAPORATION RATE g/cm^2-s		HEAT FLUX kW/m^2	
1970		Avg. 20 sec.	Max.	Avg. 20 sec.	Max.
LNG	Water	0.018	0.030	92	153
LNG	Ice	0.018	0.051	92	260
LNG	Brine	0.019	0.025	97	127
LN_2	Water	0.013	0.034	26	68
1972					
LNG	Water	0.015		77	
LNG	Al Foil	0.007		36	
LN_2	Water	0.016		32	
LN_2	Al Foil	0.013		26	
LCH_4/2.7 cm head	Water	0.01		50	
LCH_4/4.0 cm head	Water	0.012		61	
LCH_4/6.0 cm head	Water	0.016		82	
LCH_4	Al Foil	0.005		25	

LNG composition:

1970: C_1 = 94.5%, C_2 = 3.4%, C_3 = 0.9%, C_4^+ = 1.2%

1972: C_1 = 92%, C_2 = 6.3%, C_3 = 0.1%, $C_4^+ + O_2 + N_2 + CO_2$ = 1.6%

fluxes were in the order of 92 kW/m^2 (ΔH_{vap} = 511 J/g). However, this rate decreased after a layer of ice was formed. Oddly enough, the boiling rate of LNG on water, ice and brine was about the same. On the other hand, in the unconfined experiments no ice formation was noted and the boiling rate of LNG was nearly constant throughout the run.

Similar confined spills using liquid nitrogen revealed a heat flux of only 26 kW/m^2. It was also observed that LNG foamed on water whereas nitrogen did not. Although ice was also formed in the nitrogen spills, its formation was less rapid than for LNG. The aquarium was later replaced by a polystyrene ice chest (1972). Approximately 2 to 4.5 liters of cryogen were spilled on 6 liters of water; this corresponded to initial hydrostatic heads of 2.7 to 6 cm of LNG. Such spills yielded a heat flux of about 77 kW/m^2. No explanation was given for the difference between this value and the value of 92 kW/m^2 obtained in 1970.

Liquid nitrogen boiling on water yielded results close to those reported for boiling on solids. Yet LNG and methane boiling on water showed much higher heat fluxes. In order to explain this large difference, it was thought that a chemical interaction between hydrocarbon and water was taking place, i.e., hydrate formation. An aluminum sheet was placed on the top of the water thus eliminating the possibility of any direct water-cryogen interaction. The heat flux to LNG decreased from 77 to 36 kW/m^2. For liquid methane it decreased from 82 to 25 kW/m^2. Finally, for nitrogen the decrease was from 32 to 26 kW/m^2.

Hydrate formation could have been inhibited by the aluminum sheet if it indeed took place in regular spills of hydrocarbon on water. However, Burgess also measured rates of methane hydration. No hydrate formation was observed at a temperature of -120°C. At -138°C a rate of absorption of 0.42 ml of methane (gas at 20°C and 1.013 bars) per gram of ice was measured. Such low rate of hydrate formation could not account for the differences in heat fluxes of methane boiling on water and on an aluminum sheet. Thus a firm conclusion could not be arrived at from the aluminum sheet experiments.

Burgess also found that the boiling rate of methane on water increased with time and with the amount spilled. For LNG the rate was independent of the amount spilled and constant with time until ice formed, then it decreased. No data were given to show the dependence of liquid nitrogen boiling rates. The interface between nitrogen and water was very turbulent whereas for LNG it was quite calm. It must be noted that heat fluxes were calculated based only on the heat of vaporization of pure methane. No vapor temperatures were recorded to calculate any sensible heat stored as vapor superheat.

Boyle and Kneebone (1973) from Shell Research Ltd. performed LNG evaporation experiments both on a confined and unconfined pool of water.

The restricted area experiments were carried out on tanks 0.836 m^2 and 0.372 m^2 placed on a load cell. It was found that boil-off rates increased with time reaching a maximum at the point of "pool break-up". This point is attained when the amount of LNG is no longer sufficient to completely cover the water surface. Evaluation of the LNG layer

thickness at pool break-up yielded a value of 1.8 mm for many experiments. The maximum rate observed in any one experiment was of 0.02 g/cm^2-s or 100 kW/m^2 (ΔH_{vap} = 511 J/g).

An increase in the initial quantity of LNG spilled was reflected in an increase in boil-off rate. Interestingly enough, for a very large spill, the evaporation rate reached a maximum of 0.02 g/cm^2-s and then declined even though the water was still completely covered with LNG.

Decreasing the water temperature increased the evaporation rate significantly. For a given mixture of LNG the maximum evaporation rate was of 67 kW/m^2 for an initial water temperature of 15°C. This rate went up to 92 kW/m^2 when the initial water temperature was reduced to 0.5°C.

In general, boil-off rates were higher when ice formation took place. This suggested carrying out experiments in which the water was agitated so as to reduce ice formation. A series of experiments revealed that agitation reduced significantly the boil-off rates. At the same time ice formation was reduced to about half the amount formed on a still water surface.

Like other research centers, the Shell laboratories found a strong dependence of evaporation rate on the chemical composition of the liquefied natural gas. Figure 2-14 illustrates those results. An increase in heavies causes an increase not only on the rate of evaporation at any given time, but also in the rate of change of this evaporation rate.

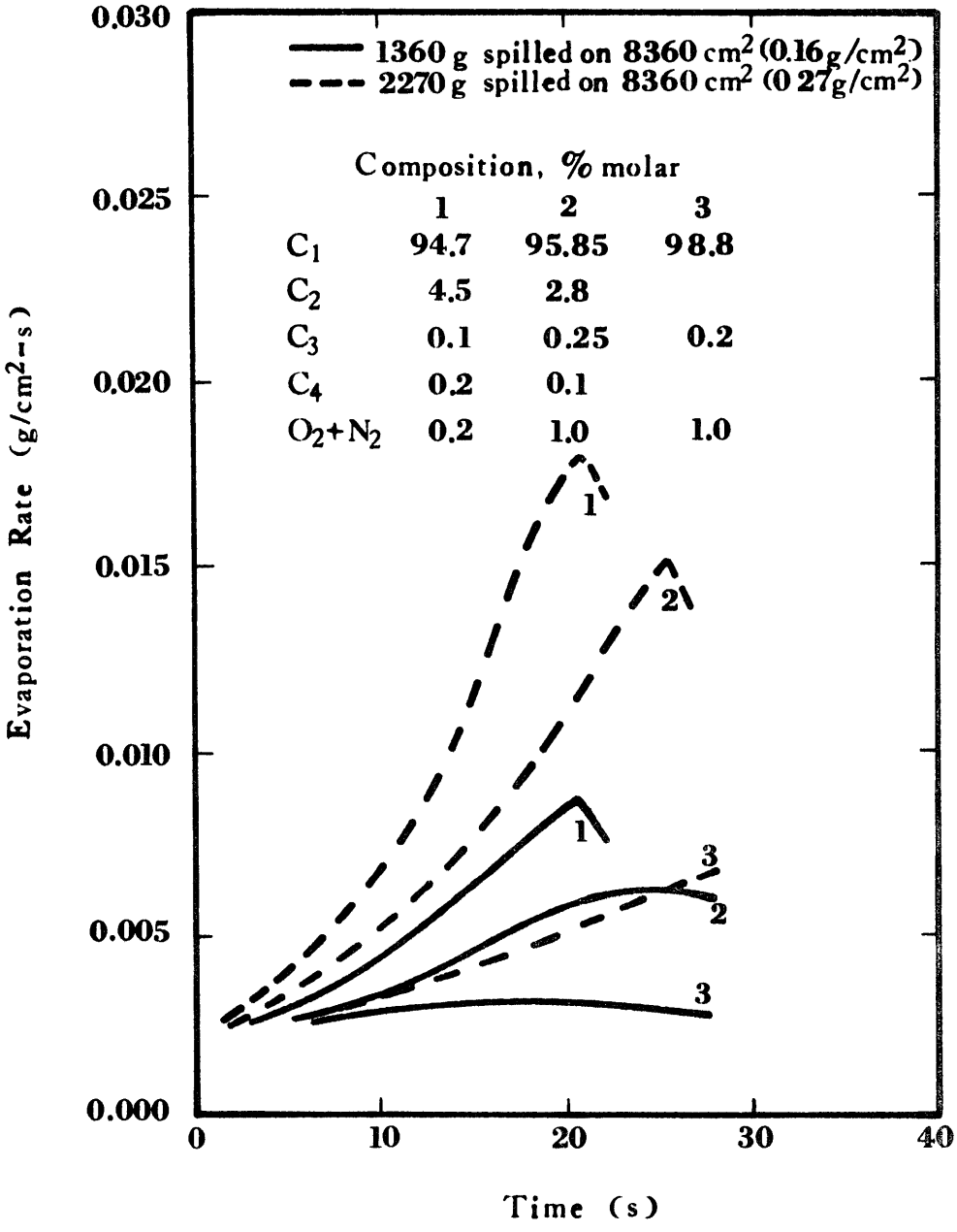

Figure 2-14 Effect of LNG Composition on Evaporation Rate (Boyle and Kneebone, 1973)

The following explanation was given for these results. As LNG is spilled on water, the large temperature difference causes film boiling. Heat is supplied by cooling of a thin layer of water. Eventually, this layer reaches the freezing point of water, ice forms and due to its high conductivity it cools down very fast. The temperature difference decreases enormously and nucleate boiling is promoted bringing as a consequence a rise in heat flux with time. The fact that heat is supplied by a thin upper layer of water is supported by thermocouple readings indicating little change in water temperature 5 mm below the interface.

Although Boyle and Kneebone's explanation for the observed rates is a very logical one, their data cannot be completely trusted. Most of the spills corresponded to an equivalent non-boiling hydrostatic head of only 0.4 to 0.6 cm, barely two to three times the pool break up thickness of 0.18 cm. Furthermore, these spills were carried out on large water surfaces of 3700 and 8400 cm^2 (4 and 9 ft^2). Since the volumes spilled were relatively small, the spreading effects become significant and should be accounted for, but they were not. In addition, integration of the boiling rates does not yield the initial amounts spilled. Between 10 to 25 percent of the amount spilled is unaccounted for.

Another important observation made by Boyle and Kneebone is that of water pick up. When pure methane and nitrogen were spilled, a net loss of weight of water was observed immediately after evaporation was completed. With LNG, however, there was a gain in weight which changed

to a weight loss after the ice melted. Either some LNG was entrained in the ice and it evaporated as ice melted, or hydrate formation took place. Nevertheless, when LNG was spilled on ice no weight change was observed. The water pick up ranged from 0.8 to 6.7 percent of the amount of LNG spilled. The weight of water lost is nearly constant for a given container regardless of the amount of LNG spilled. This is to be expected since the water is picked up from the water surface and therefore is a function of its area.

Film boiling heat transfer between cryogenic liquids and water was studied by Vestal (1973). A glass dewar flask coupled to a load cell was used in the experiments. Thermocouples were located at various heights in the water; one at the interface and one in the cryogenic liquid. Thus, mass and temperature could be monitored continuously.

Liquid nitrogen boiled without foaming, but there was an unstable interface. On the other hand, methane and LNG foamed and the interface was rather smooth. Rapid ice formation took place with LNG. Lowering the initial temperature of water increased the heat flux for nitrogen. The opposite effect was observed for methane and LNG. The heat flux for all of the cryogens decreased with time.

Liquid nitrogen exhibited a maximum heat flux of 88 kW/m^2 for an interfacial temperature difference of 254 K. For methane this maximum was of 197 kW/m^2 corresponding to a ΔT of 196 K. Finally, LNG boiled at a maximum heat flux of 550 kW/m^2 for a ΔT ranging from 200 to 220°C.

Heat fluxes for methane and LNG are compared to those of Sciance and Brown, respectively, in Figure 2-15. Boiling on water yields much higher heat fluxes than those on solid surfaces.

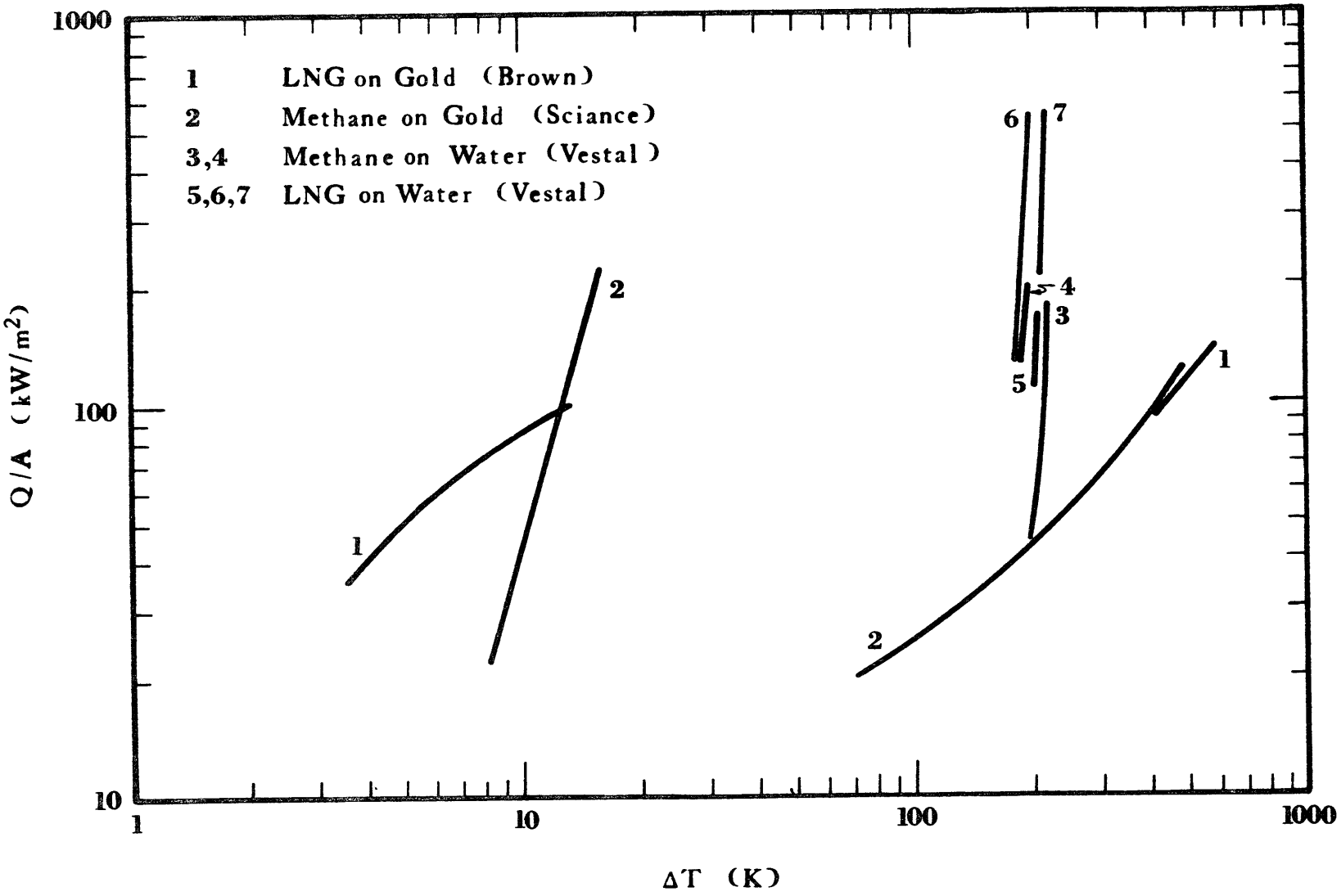

Figure 2-15 Boiling of Methane and LNG on Gold and Water

Vestal based much of his analysis on the interfacial temperature which was measured with a grounded thermocouple. That is, the junction of the thermocouple was welded to the protective sheath. The result was that the temperature recorded corresponded to an average of the temperatures in the neighborhood of the junction rather than a point temperature. This comes as a consequence of heat conduction through the protective sheath since large temperature gradients exist at the interface. Furthermore, the interface was not stationary. As smoothly as boiling might take place, there is always an original disturbance of the water interface at the moment of pouring the cryogenic fluid. Consequently, the assumption that a fixed thermocouple located at the original water surface will continue to read interfacial temperatures is a rather tenuous one. Furthermore, the experiments were carried out in a flask 48 mm in inside diameter. This raises the question of the presence of end effects. Boyle and Kneebone found that for the same hydrostatic head of cryogen the boiling rate on a vessel half the area of a second one yielded higher boil off rates by about 20 %. A significant amount of cryogen can be evaporated in cooling the walls, particularly when the ratio of the wall area to the cross sectional area of the container becomes very high as in Vestal's equipment.

The transient boiling of liquefied hydrocarbons on water was investigated by Jeje (1974) and Drake et al. (1975). A well-insulated triple wall container was used in the experiments. The two outer walls were made from acrylic plastic. Ther innermost wall was made from 127 μm cellulose acetate sheets. Vertical polyurethane spacers

separated the acetate sheet from the acrylic walls. The inside diameter of the boiling vessel was 9.92 cm. This assembly was placed on a load cell to measure continuously the mass of the system. An acrylic double-cone was hung at the open end of the vessel. It allowed an even distribution of the cryogen at the start of the test and it held the vapor thermocouples. The cone also prevented the flow of ambient air into the vessel during the test. Six thermocouples inserted through the bottom of the vessel at different heights and distance from the center monitored water temperatures. Vapor temperatures were recorded by three heat-stationed thermocouples. Vapor temperature measurements are very important since some heat might be removed as sensible heat by the vapor. Therefore, not all of the heat flux has to be directed to the vaporization of cryogen. Some heat can be directed to the "superheating" of the vapors produced.

Liquid nitrogen exhibited a strong sensitivity to the initial hydrostatic head of cryogen. Initial water temperature had little effect on the boil-off rates. Ice was formed rapidly but it did not form a continuous layer. The interface was quite rough except in the areas covered with ice. Water temperatures a few mm below the surface registered very little change. This result supports the hypothesis that most of the heat is extracted from the uppermost layers of water. Nitrogen vapors were quite superheated. For large spills the superheat ranged from 40-50°C but small spills ranged from 90-100°C.

Liquid methane and liquid ethane did not show sensitivity to the original amount of hydrocarbon spilled as did nitrogen. Similarly,

the initial water temperature had little effect on the boil-off rates. Although ice formation took place for both hydrocarbons, in the case of ethane it was more rapid. Again the temperature of the water a few mm below the interface did not change significantly. Vapor superheats for methane were in the order of 10-30°C, whereas for ethane, none were exhibited. These vapor superheat data seem to indicate that nitrogen and methane film boil on water whereas ethane nucleate boils. This argument is further supported by the rapid ice formation which would promote nucleate boiling.

The heat fluxes observed for ethane were higher than those observed for methane which in turn were higher than nitrogen. The boil-off rate of methane increased continuously with time. Ethane, however, started boiling slowly then it rapidly increased.

Addition of small amounts of heavier hydrocarbons increased the boiling rate of methane significantly. These results are illustrated in Figure 2-16. The heavier the hydrocarbon, the less amount of it needed to enhance the boil-off rate by a given factor.

Two ranges of composition of LNG were studied. The first contained 98.2 mole percent methane, 1.6% ethane and the remaining was 0.2% propane and trace butanes. As expected, heat fluxes were higher than those for pure methane. Decreasing the initial water temperature increased the boil-off rate slightly. Boil-off rates increased with time and foaming took place, especially at the beginning of the tests.

The second series involved mixtures containing 82-89 mole percent methane and ethane/propane ratios of 4 to 5. Trace butanes were also

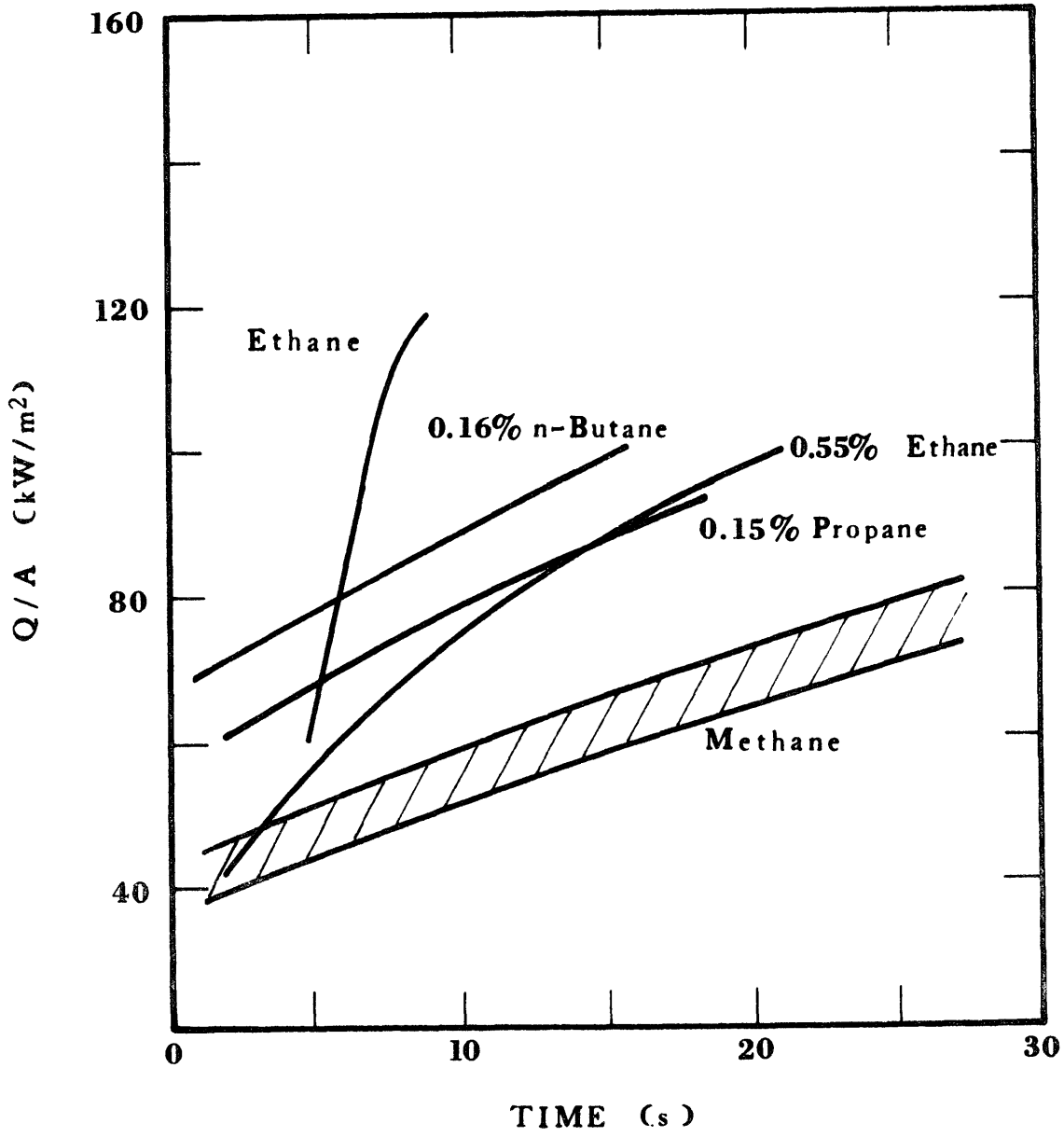

Figure 2-16 Effect of Addition of Heavier Hydrocarbons on the Boiling of Methane on Water (Jeje, 1974)

present. The individual effect of initial hydrostatic head and water temperature could not be determined since both parameters were changed from run to run. As in the previous series of tests, the boiling rates increased with time and significant foaming occurred. Although the water surface temperature dropped drastically, the temperature a few mm below the surface did not change appreciably. A solid crust of ice was formed when water temperatures were low ($\sim$10°C). For higher temperatures ice also formed but not in a continuous crust.

The heat fluxes for both ranges of LNG composition are compared to pure methane in Figure 2-17. It is clear that the higher the concentration of heavier hydrocarbons, the higher the effect on the heat flux.

Thermal fluctuations in water and their effect on the boiling rate of methane and nitrogen were the subject of an investigation by Dincer (1975). Aside from minor modifications, the experimental apparatus was the same used by Jeje.

Boil-off rates for liquid nitrogen were the same as those found by Jeje. These rates were found to increase with initial hydrostatic head of cryogen and to decrease with time. The initial water temperature did not have a significant effect on boil-off rates. Ice formation was found to take place after 30 seconds for initial water temperatures of 30°C and above. For water temperatures below 20°C, ice formed within a few seconds.

Boil-off rates for liquid methane were higher than those reported by Jeje. This discrepancy, however, is easily explained by the fact

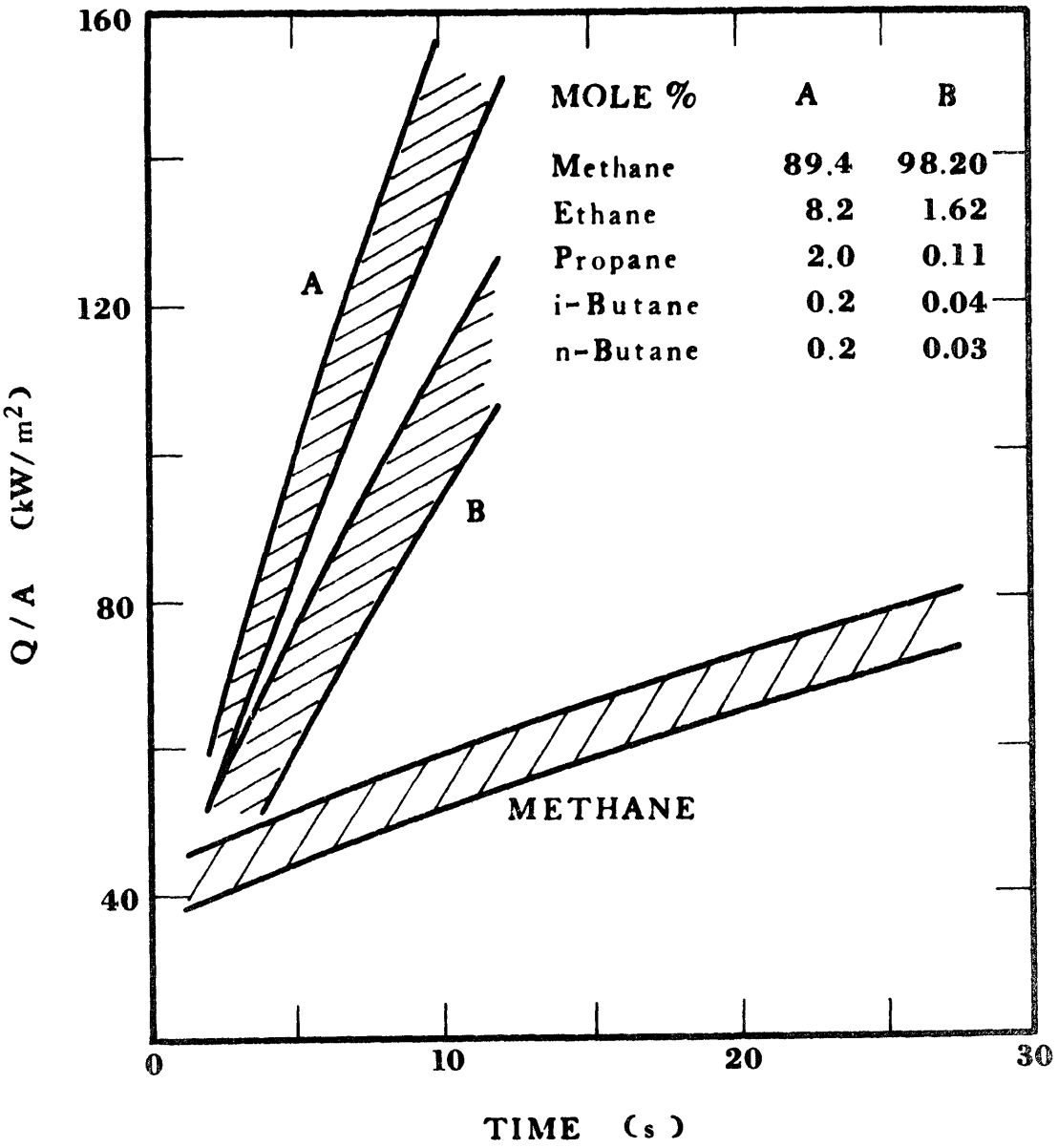

Figure 2-17 Effect of Composition on the Boiling Heat Transfer of LNG on Water (Jeje, 1974)

that Jeje used 99.98% pure methane, whereas Dincer used lower purity methane containing some higher hydrocarbons as impurities. From previous studies, it would be predicted that there would be an increase in boil-off rates.

Boiling rates for methane increased with time but were unaffected by initial water temperature or hydrostatic head. Ice formed almost instantaneously for initial water temperatures below 20°C.

When ice was formed, there was a sharp drop in temperature only for the water in the immediate neighborhood of the interface. When ice was not formed, or it was formed slowly, the bulk of the water exhibited a drop in temperature. Furthermore, temperatures along the sides of the vessel were found to change somewhat more than those at the center. These observations coupled with nitrogen spills on water gel allowed the determination of the main resistance to heat transfer.

Dincer assumed that water-gel, prepared by the addition of agar to water, retained the thermal properties of water. The purpose of these experiments was to inhibit convective motions in the water and determine the consequent effect on boil-off rates. Liquid nitrogen was poured onto water-gel and the observed boil-off rates were close to those of nitrogen boiling on water. A gradual change in temperature was recorded away from the interface.

These observations suggest that for low initial water temperatures heat is supplied by ice formation. For higher water temperatures, heat is supplied by cooling the upper layers of water with some agitation of the bulk of the water. Furthermore, the mode of heat transfer in the

water phase does not seem to affect the overall boiling process. Thus, it can be said that the main resistance to heat transfer lies elsewhere, either in the interface or in the cryogenic fluid.

A summary of the information gathered on boiling of cryogens on water is given in Tables II, III and IV. Different investigators agree on the evaporation characteristics of liquid nitrogen; the boiling rate is highly sensitive to the amount spilled, decreases with time and is independent of initial water temperature. No foaming is observed, and the water-nitrogen interface is a rough one. Vapor superheats ranging from 40 to 100 K are reported.

In the case of methane, Burgess reports an increase in heat flux with amount spilled, whereas Jeje and Dincer claim no effect at all. The boiling rate increases with time; Vestal is the only investigator that disagrees with this statement. The initial water temperature has no effect on the evaporation rates. The interface is a smooth one and superheat of 10-30 K are reported. Vestal reports foaming, whereas Jeje did not observe any.

The disagreement is more pronounced when considering LNG mixtures. A decrease in water temperature increases the rate. Boyle and Jeje found the boiling rate to be independent of amount spilled. A maxima is observed for the boiling rate with time. Boyle reported it to occur at the time of pool break-up, Burgess after ice formation and Jeje does not report a maxima. With the exception of Vestal (550 kW/m^2), the heat fluxes reported range from 50-150 kW/m^2.

TABLE II

BOILING OF NITROGEN ON WATER

INVESTIGATOR		BURGESS	VESTAL	JEJE	DINCER
Q (kW/m^2)	High	68	88(60°C)*	50	**
	Low (Avg)	(26)	28(10°C)*	20	**
Effect on Q due to an increase in:					
Water Temperature		--	up	same	same
Cryogen Mass		--	--	up	up
Time		--	down	down	down
Area		--	--	--	--
Foaming?		no	no	no	--
Rough Interface?		yes	yes	yes	--
Vapor Superheat?		--	--	40-100 K	--

* Number in parenthesis refers to initial water temperatures.

** Dincer's boil-off rates were the same as those reported by Jeje. If the same vapor superheats are assumed, then Dincer's heat fluxes are the same as Jeje's.

TABLE III

BOILING OF LIQUID METHANE ON WATER

INVESTIGATOR		BURGESS	VESTAL	JEJE	DINCER
Q (kW/m^2)	High	82(Avg)	197	95	
	Low (Avg)	51(Avg)		30	*
Effect on Q due to an increase in:					
Water Temperature		--	same	same	same
Cryogen Mass		up	--	same	same
Time		up	down	up	up
Area		--	--	--	--
Foaming?		--	yes	no	--
Rough Interface?		--	no	no	--
Vapor Superheat?		--	--	10-30 K	--

* Dincer's boil-off rates were 25% higher than those reported by Jeje. If we assume the same contribution of vapor superheat to the total heat flux, then Dincer's heat fluxes would be 25% higher than Jeje's.

TABLE IV

BOILING OF LNG ON WATER

INVESTIGATOR		BURGESS		BOYLE	JEJE		VESTAL
Q (kW/m^2)	High		153	100	120	150	550
	Low (Avg)	(92)	(77)		50	50	
LNG Composition	C_1	94.5	92.0	94.7	98.2	89.4	92.58
	C_2	3.4	6.3	4.5	1.6	8.2	6.27
	C_3	0.9	0.1	0.1	0.11	2.0	0.40
	C_4			0.2	0.07	0.4	
	Other	1.2	1.6	0.5			0.77
Effect on Q due to an increase in:							
Water Temperature		--		down	down		same
Cryogen Mass		same		up	up		--
Time		same, down after ice formation		up, down after pool break up	up		down
Area		--		down	--		--
Water Agitation		--		down	--		--
Foaming?		yes		--	yes		yes
Rough Interface?		no		--	no		no
Vapor Superheat?		--		--	5-10 K		--

Prior to the present work and "as a result of this sensitivity (to LNG composition), it is not possible to predict in an *a priori* manner the boiling rate of an LNG of a given composition" (Jeje, 1974).

III. EXPERIMENTAL

Equipment for Spills of LNG on Water

The spillage of LNG on water results in a highly transient process of evaporation. In order to study the characteristics of this process, one must be able to measure, or otherwise determine, the mass evaporated, the composition of the liquid and vapor, and the system temperatures as a function of time. In the present work this was accomplished by spilling the cryogen on quiescent distilled water contained in a boiling vessel placed on an electronic balance. The output of this balance was monitored by a NOVA-840 real time computer. Water, cryogen, and vapor temperatures were measured by thermocouples whose output was also fed into the real time computer. A schematic representation of this setup is given in Figure 3-1.

A Mettler P-11 analog balance was used to measure the weight of the boiling vessel and its contents. This balance had a typical response time of less than 100 ms. When severe oscillations were present, such as those caused by dropping a large weight from a significant height, a 0-100% response time took as long as 1 second. The balance accuracy was ±100 mg; however, due to limitations in the computer's analog-to-digital convertor, the accuracy was reduced to ±125 mg. Further details can be found in Appendix A.

Because of the response time of the balance, and for ease in calculations, the voltage outputs from the balance and thermocouples were sampled by the computer every second.

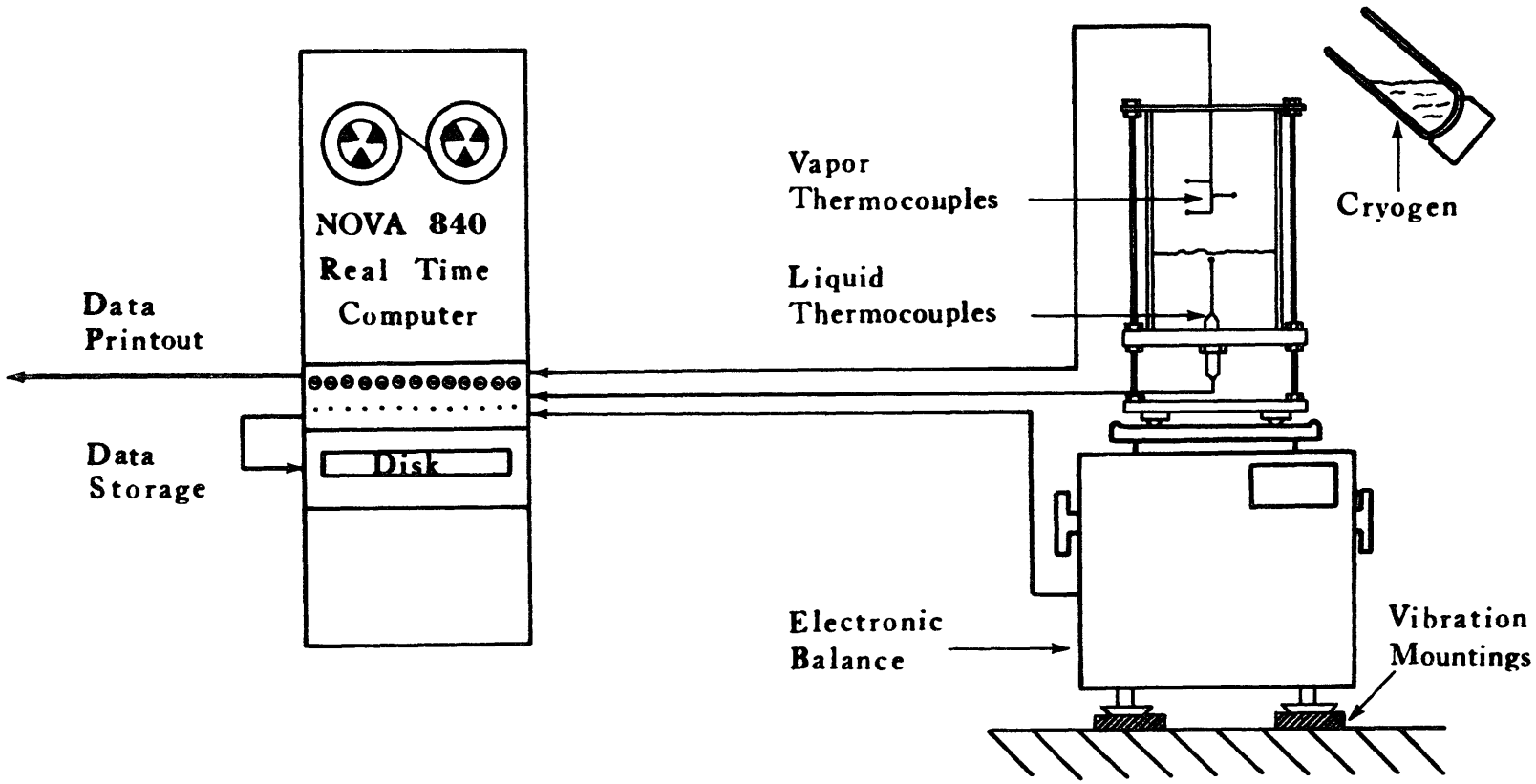

Figure 3-1 Experimental Set-up for the Study of LNG Boiling on Water

The boiling vessel, shown in Figure 3-2, was a triple wall cylindrical container. It was transparent to allow visual observation and was designed to minimize heat leaks. The outer wall was made of 0.32 cm thick acrylic tube; the inner walls were made of 25 μm Mylar sheets. The three walls were separated by 2 mm thick polyurethane spacers. These spacers were wound horizontally and were positioned at different heights around the walls. They not only kept the thin walls in place but minimized natural convection of the air present within the wall gaps.

In most spills the cryogen evaporated completely within 2 to 3 minutes. In this short period of time the most important heat leaks are due to the cooling of the walls of the container and, therefore, it was necessary to use very thin inner walls to minimize their thermal mass.

Several boiling vessels were built. Stresses due to the formation of ice caused the inner wall seam to eventually fail. Foaming mixtures presented a problem when they overflowed the vessel and taller containers had to be built. Depending on the diameter of the acrylic tube, the inside cross-sectional areas of the vessels were 133, 139 and 143 cm^2, and the heights were 20 and 35 cm. Typically the water level was about 12 cm and the amount of cryogen spilled ranged from 150 to 1000 cm^3.

Simply spilling the cryogen from the top of the container would cause a severe disruption on the surface of the water and increase, in an unknown fashion, the area for heat transfer in the first few seconds. Furthermore, the inertial impacting forces would cause an erroneous

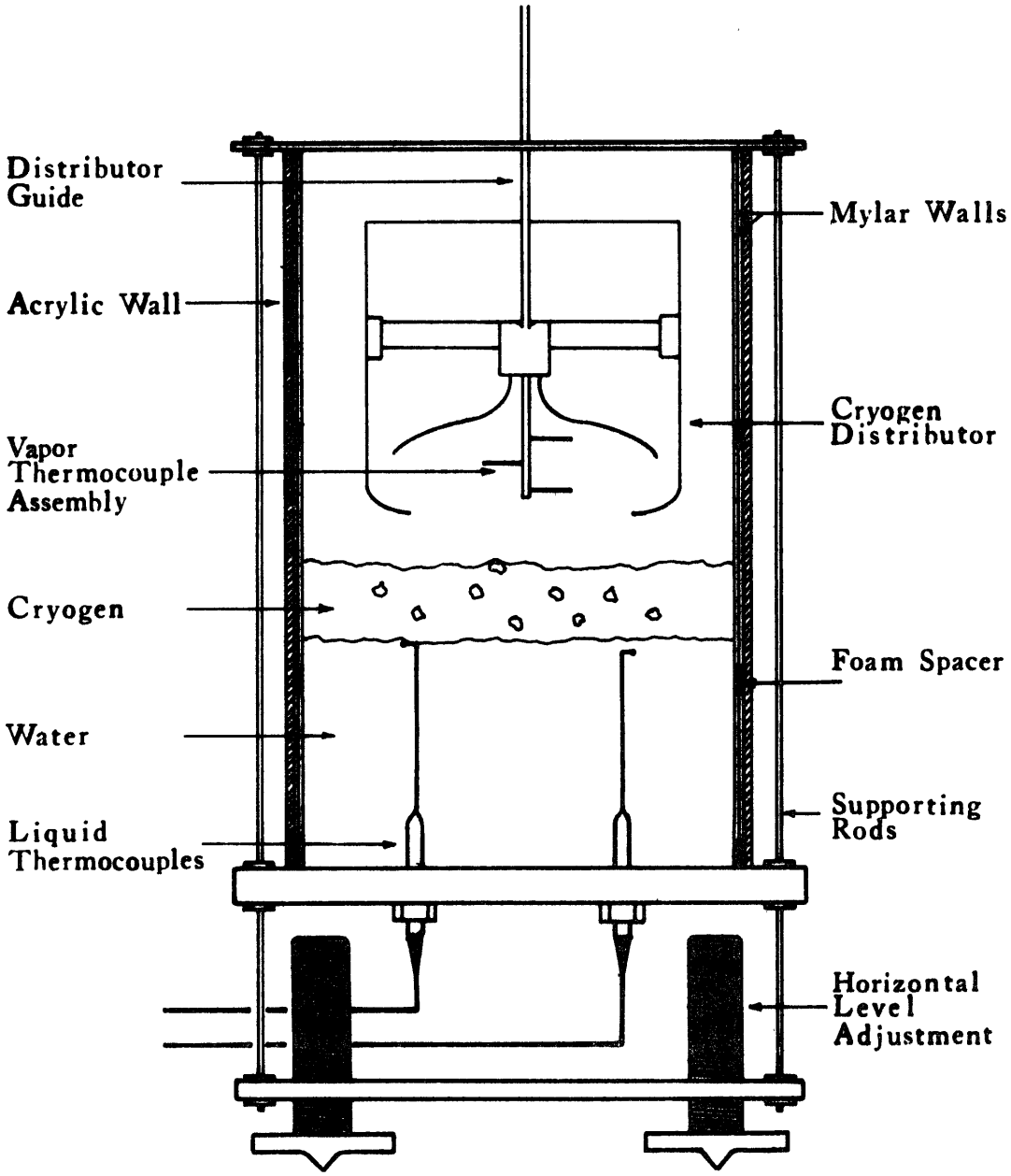

Figure 3-2 Boiling Vessel

overshoot on the mass recorded by the balance. In order to reduce these effects, a cryogen distributor, shown in Figure 3-3, was used. It consisted of a conical section and a wall. The conical section directed the flow of cryogen against the wall of the cryogen distributor. The cryogen then flowed down the wall which had a curvature at the bottom. As the cryogen passed over this curvature, it was directed tangentially across the water surface thus minimizing any splashing and disturbances of the interface. After the cryogen had been poured, the distributor was raised by means of pulleys. The bottom part of the distributor was made to line up with the top of the vessel. In this configuration the cryogen distributor did not affect the flow of cryogen vapor out of the container, and it inhibited ambient air flow into the boiling vessel.

The cryogen distributor rode on the outside of a 0.64 cm o.d. stainless steel tube which was suspended externally to the boiling vessel. Thus the distributor was free to be moved vertically without affecting the mass of the vessel and its contents.

Three vapor thermocouple wires were fed through the steel tube guide for the cryogen distributor. Thin 25 μm chromel-constantan wires were used in the vapor thermocouples. To insure a fast response and accurate readings (minimize axial heat conduction through the wires) a length of 2 cm of bare wire was exposed. The thin leads were supported by a Teflon structure as shown in Figure 3-4a. Response times (0-100%) for these thermocouples were less than 90 ms for step changes of 180 K. The first vapor thermocouple was placed about 2 cm above the cryogen surface. The other two were placed at 1.5 cm intervals as shown in

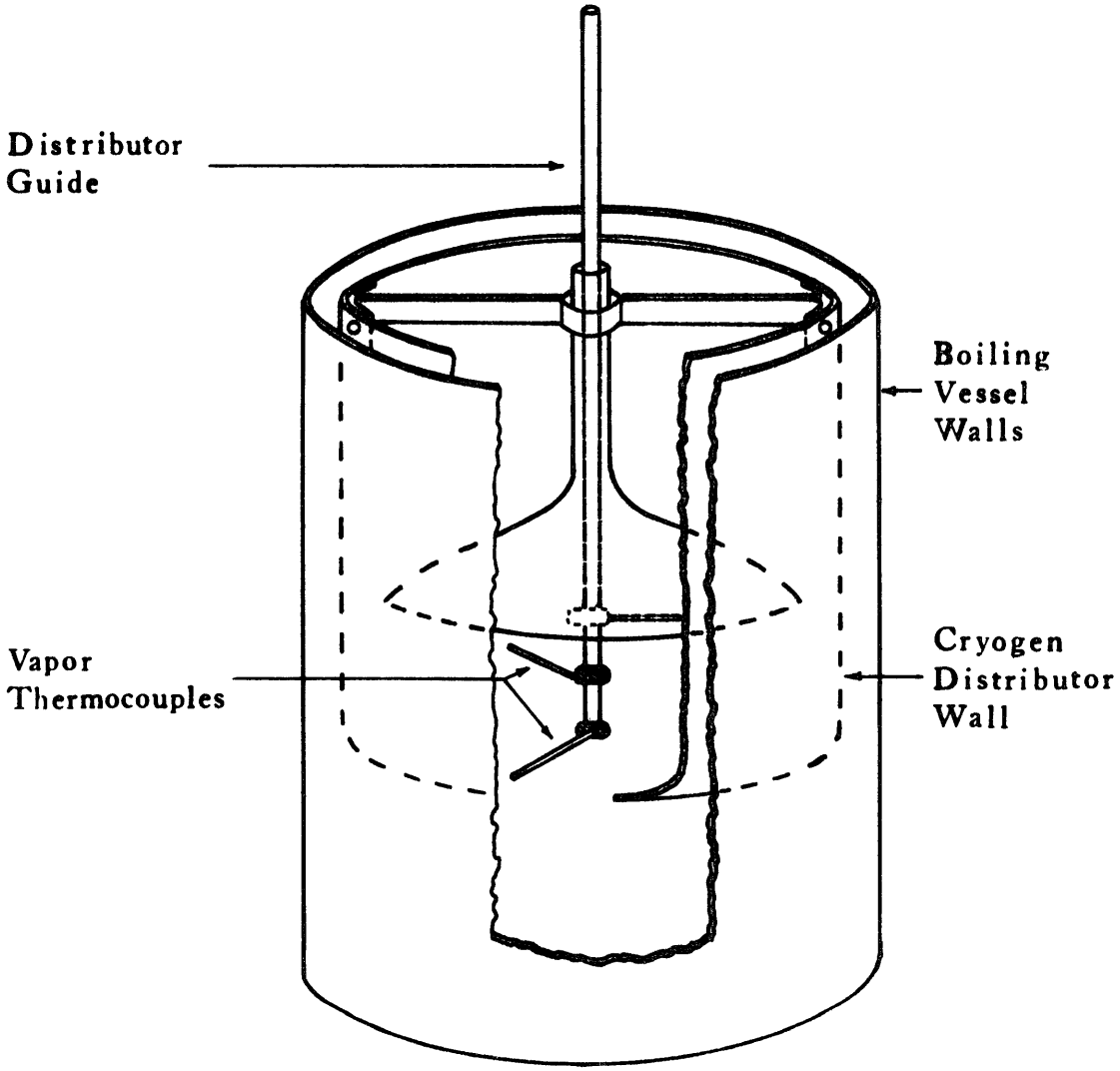

Figure 3-3 Cryogen Distributor

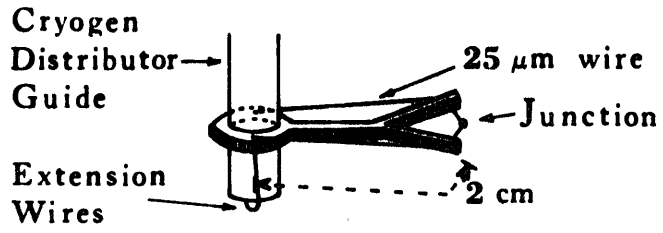

a

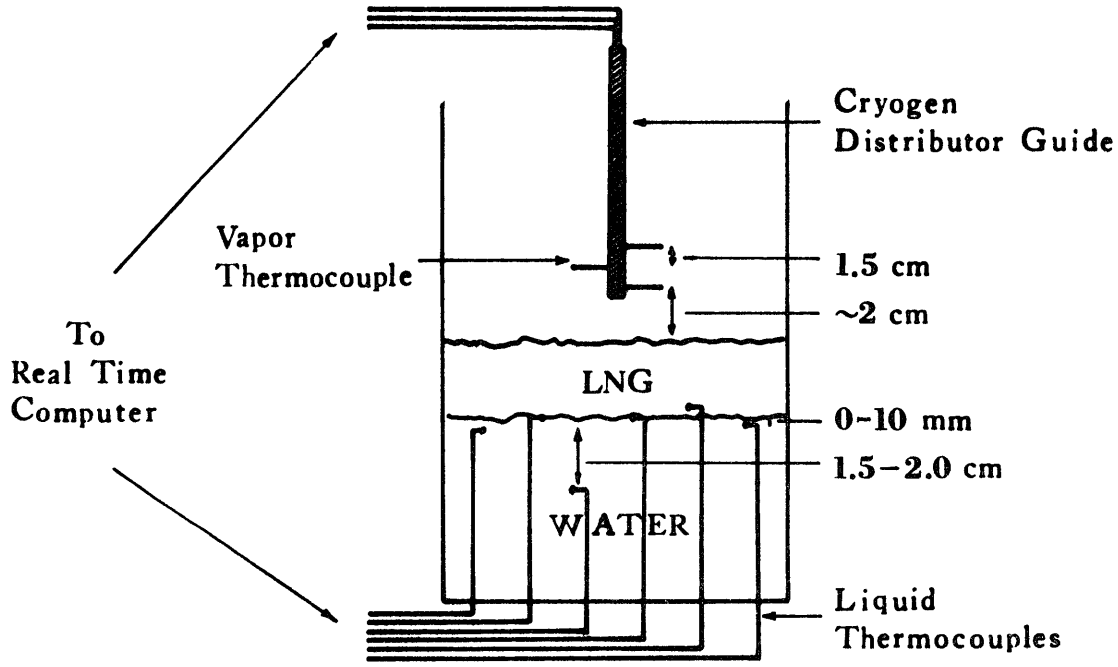

b

Figure 3-4 Temperature Measurement. a) Vapor Thermocouple b) Typical Locations of Vapor and Liquid Thermocouples

Figure 3-4b. Further details in the design and performance of these thermocouples are given in Appendix A.

Six liquid thermocouples were used to monitor water and LNG temperatures. A typical spatial arrangement of these thermocouples is shown in Figure 3-4b. The thickness of the lead wires varied from 25 μm to 250 μm, and their length from 2 mm to 23 mm. They were all tested for response in the event of a rapid and large change in temperature. Typical response times (0-100%, 180 K step change) ranged from 100 to 600 ms. It must be emphasized that the values recorded for water temperatures are limited to qualitative analyses only. Ice formation and motion of the interface made it impossible to determine the true distance of the thermocouple from the cryogen/ice-water interface. More details on the construction and testing of the liquid thermocouples can be found in Appendix A.

Preparation of Cryogens

In general, the liquid hydrocarbons were prepared by cooling the hydrocarbon gases below their boiling point either with liquid nitrogen or with a pentane-nitrogen slush bath.

Liquid methane was prepared by flowing methane gas through a 0.63 cm copper tubing into a 1000 cm^3 Pyrex beaker which in turn was immersed in a Dewar flask filled with liquid nitrogen. This arrangement is shown in Figure 3-5. Since the temperature of liquid nitrogen is 78 K and methane liquefies at 111.7 K, the liquid methane was subcooled. After sufficient methane had been collected, the feed of

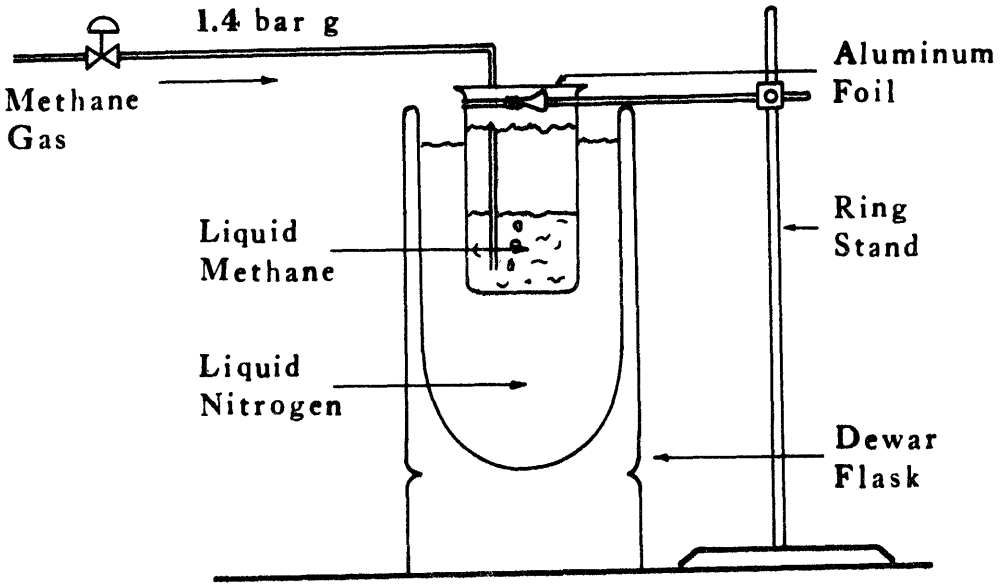

Figure 3-5 Methane Liquefaction Apparatus

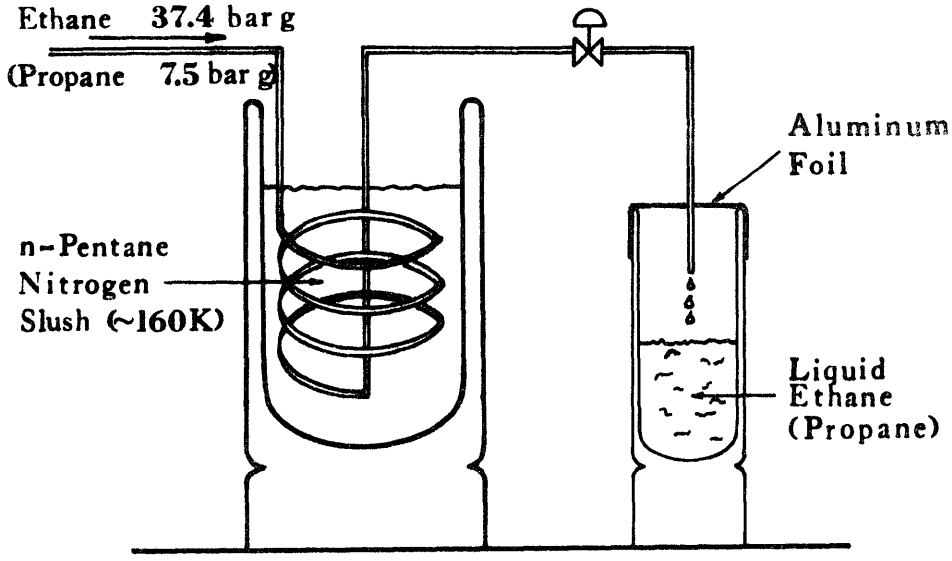

Figure 3-6 Ethane and Propane Liquefaction Apparatus

liquid nitrogen was discontinued and methane gas was allowed to bubble through the subcooled liquid until it reached the saturation temperature.

Methane gas of two purities was used, Matheson Ultra High Purity Grade with a minimum methane content of 99.97 mole percent and Matheson Certified Purity Grade with a minimum methane content of 99 mole percent. Typically, the impurities were: ethane 0.1%, carbon dioxide 0.2%, and nitrogen 0.6%. UHP methane was used in studying the boiling of pure methane and preparing some mixtures when the composition was believed to be particularly important. Generally, however, the mixtures were prepared with C.P. grade methane. Nitrogen, the major impurity and the most volatile component, was driven off while heating the subcooled methane to saturation temperature.

Liquid ethane was prepared by flowing ethane gas through a stainless steel coil immersed in a n-pentane - nitrogen slush bath, as shown in Figure 3-6. n-Pentane freezes at 143 K and the bath temperature was kept at approximately 160 K by replenishment of the nitrogen. Ethane boils at 189.5 K so the liquid was subcooled. In a procedure similar to that used for methane, the liquid ethane was heated to saturation temperature. C.P. grade ethane, typically 99.5 mole percent pure, was used. The major impurity was hydrogen at 0.4 mole percent.

Liquid propane was prepared in a similar setup to that of ethane and following the same procedure. C.P. grade propane, 99.4 mole percent pure, was used. The major impurity was isobutane at 0.5 mole percent.

The liquid nitrogen, used both as coolant and as a mixture component, was supplied by the MIT Cryogenics Laboratory. Typical purity was better than 99.95 mole percent.

The preparation of LNG mixtures required a special procedure. All the components had to be cooled to approximately the boiling point of the final desired mixture. For instance, if propane were to be added to a 90% methane, 10% ethane solution it first had to be cooled to about 112 K. If propane were added at its boiling point of 231.3 K, some of the existing mixture would boil (sometimes violently). By cooling the components so that there was no boiling upon mixing, one could use a gravimetric method to determine the composition of the mixture in addition to the chromatographic analysis.

Caution had to be exercised in cooling down the components. This was usually done by immersing a container in liquid nitrogen; however, should they be subcooled too much, the mixture itself would be subcooled. Any attempt to bring the mixture to saturation temperature would cause localized boiling of the more volatile component with a subsequent change in composition. If a component were subcooled too much, it would have to be warmed to the proper temperature before mixing.

Analysis of Chemical Composition

The composition of the hydrocarbon mixtures was determined by two methods: gravimetric and chromatographic.

The gravimetric method consisted of accurately weighing the amount of each component added to the mixture. The molar percentage was then calculated by the simple relationship

$$\text{mole percent}_i = \frac{\text{Mass}_i/\text{Mol. wt.}_i}{\sum_j \text{Mass}_j/\text{Mol. wt.}_j} \times 100$$

For the chromatographic method, a sample of the liquid mixture was removed with a sampling scoop and introduced into a sampling bulb. These devices are shown in Figure 3-7. The sampling scoop was essentially a female ground-glass connector with a receptacle ($\sim$1 cm^3) for the liquid sample and a glass rod for a handle. The sampling bulb ($\sim$1000 cm^3) had a male ground-glass connector separated from the body of the bulb by a stopcock. Prior to the preparation of the mixtures, the bulb was evacuated. After cooling the sampling scoop with liquid nitrogen, the mixture was stirred and a liquid sample removed. The ground-glass connection between the bulb and the scoop allowed an easy transfer of the sample into the bulb. This gas-tight connection was maintained until the liquid in the scoop had been drawn into the bulb and recondensed on the liquid nitrogen cold fingers. After the liquid in the sampling bulb had evaporated, a vapor sample (100-500 μl) was removed and run through a chromatograph. This technique has been satisfactorily employed by Porteous (1975).

A Hewlett-Packard 700 gas chromatograph was used. The chromatograph outputs a peak for each component; the area under a peak is proportional to the amount present in the sample. The composition of

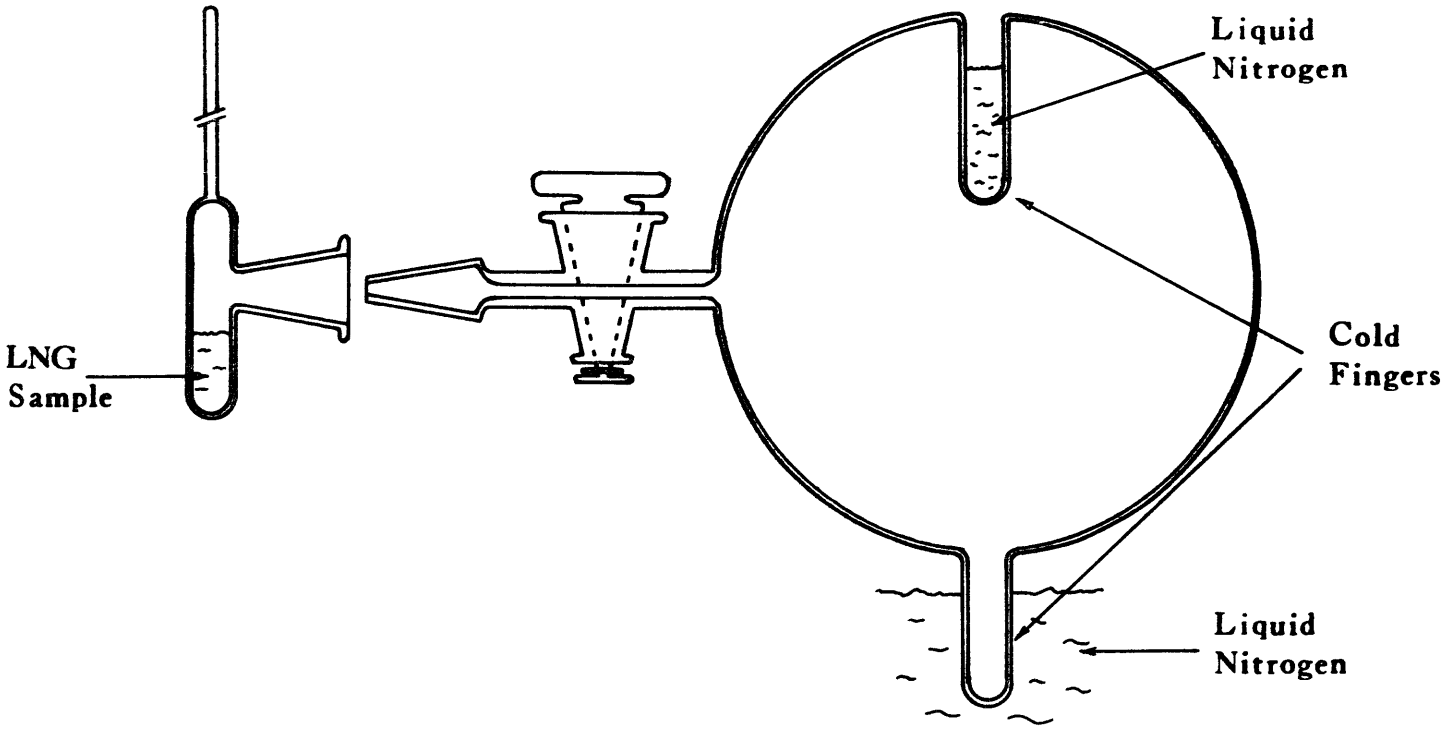

Figure 3-7 Sampling Bulb and Scoop for Chromatographic Analysis

the mixtures could then be determined after calibrating the chromatograph for the specific response to each component.

Despite precautions taken, a minor change in composition could take place during the short interval of time between sampling and spilling. However, after consideration of all sources of error, both gravimetric and chromatographic, it is estimated that the reported compositions were within 1.5% of the actual composition or 0.15 mole percent, whichever is largest.

IV. VAPOR-LIQUID EQUILIBRIA

Introduction

LNG is a cryogenic fluid comprised of components which differ significantly in volatility. Thus, in a transient boiling experiment, the vapor evolved would vary in composition as the liquid becomes enriched in the less volatile components. This time dependent vapor composition would show a maximum in nitrogen, if present, followed by methane, ethane, propane, etc. It is important to be able to estimate the composition of the vapor during a spill of LNG because each component may affect the dispersion characteristics of the cloud and lead to different hazardous zones for ignition or even detonation. It is also important to estimate the liquid composition since the saturation temperature of the residual liquid depends on its composition. Changes in the saturation temperature could significantly affect the heat transfer characteristics.

One could assume that vapor-liquid equilibrium existed at all times; the vapor composition could then be computed as a function of the residual liquid composition. However, it is conceivable that the transient nature of the test or the boiling characteristics would interfere with the attainment of equilibrium. For example, the vapor generation rate is large in LNG spills in water. As a consequence the bubbles formed at the interface could deplete the interfacial layer in the more volatile components. Then, depending upon the residence time and mass transfer rate of the ascending bubbles, vapor-liquid equilibrium with the bulk liquid may or may not be achieved by the time the vapor bubble breaks clear of the liquid.

Under these circumstances, it is imperative to demonstrate the validity of the vapor-liquid equilibrium assumption before it is used in any theory or model. To this end the vapor composition was measured experimentally as a function of time and compared with results obtained from theory assuming vapor-liquid equilibrium. In addition, temperature measurements in both the liquid and vapor are compared with those predicted from theory.

Development of the VLE Model

For thermodynamic equilibria to exist between two phases which are at the same temperature and pressure, the fugacity of every component i in the mixture, $\hat{f}_i$, must be the same in both phases,

$$\hat{f}_i^L = \hat{f}_i^V \qquad (4\text{-}1)$$

where L = liquid

V = vapor

For a mixture of ideal gases, the fugacity $\hat{f}_i^V$ is equal to the partial pressure of component i, $y_i P$. To account for deviations from ideality, the fugacity coefficient ϕ_i is used,

$$\hat{f}_i^V = \phi_i^V y_i P \qquad (4\text{-}2)$$

Although the fugacity in the liquid phase is usually related to the liquid mole fractions by means of an activity coefficient, γ_i, it is often more convenient to use the same form of Eq. (4-2),

$$\hat{f}_i^L = \phi_i^L x_i P \tag{4-3}$$

The fugacity coefficients ϕ_i can be related to pressure, total volume and temperature by the following thermodynamic relationship (Prausnitz et al., 1967)

$$\ln \phi_i = \ln \frac{\hat{f}_i}{y_i P} = \frac{1}{RT}\int_V^\infty \left[\left(\frac{\partial P}{\partial n_i}\right)_{T,V,n_j} - \frac{RT}{V}\right] dV - \ln Z \tag{4-4}$$

where n_i = number of moles of component i

$Z = PV/n_T RT$

Several equations of state that relate pressure, temperature and volume have been proposed (Benedict-Webb-Rubin, Lee-Erbar-Edmister, Soave-Redlich-Kwong, Sugie-Lee, etc.). The Soave (1972) modification of the Redlich-Kwong (1949) equation of state has been found to be particularly successful with hydrocarbon mixtures (Reid et al., 1977) and is widely used in industry (Erbar, 1977). The pressure explicit form of the Soave-Redlich-Kwong (SRK) equation is

$$P = \frac{RT}{v - b} - \frac{a}{v(v + b)} \tag{4-5}$$

where v = molar volume

a = temperature dependent term

b = constant

The fugacity coefficients can now be evaluated by combining Eqs. (4-4) and (4-5), as described in Appendix B.

$$\ln \phi_i = \frac{b_i}{b}(Z-1) - \ln(Z-B) + \frac{A}{B}\left[\frac{b_i}{b} - 2\sum_j \frac{(1-k_{ij})(a_i a_j)^{0.5}}{a} x_j\right] \ln \frac{Z+B}{Z} \quad (4\text{-}6)$$

where

$$A = \frac{aP}{R^2T^2} \quad (4\text{-}7)$$

$$B = \frac{bP}{RT} \quad (4\text{-}8)$$

$$a = \sum_i \sum_j x_i x_j (1 - k_{ij})(a_i a_j)^{1/2} \quad (4\text{-}9)$$

$$b = \sum_i x_i b_i \quad (4\text{-}10)$$

k_{ij} = binary interaction parameter

In the SRK equation, the mixture parameters a and b are a function of the pure component parameters a_i and b_i, and they must be related by a suitable mixing rule. In the case of the parameter b, the arithmetic rule given by Eq. (4-10) has been found to be satisfactory (Chueh and Prausnitz, 1967; Soave, 1972). For the parameter a, a classic geometric mean rule is often used,

$$a = \sum_i \sum_j y_i y_j a_{ij} \quad (4\text{-}11)$$

where

$$a_{ij} = (a_i a_j)^{1/2} \quad (4\text{-}12)$$

which is equivalent to

$$a = \left(\sum_i x_i a_i^{0.5}\right)^2 \quad (4\text{-}13)$$

This geometric-mean assumption can be too restrictive and, in order to relax it, Zudkevitch and Joffe (1970) suggested the use of a binary interaction parameter k_{ij},

$$a_{ij} = (1 - k_{ij})(a_i a_j)^{0.5} \qquad (4\text{-}14)$$

Using the value of a_{ij} in Eq. (4-11) yields Eq. (4-9) which is the expression for the parameter a to be used in this work. The binary interaction parameter k_{ij} is assumed to be independent of pressure, temperature and composition.

To determine the values of the interaction parameters, only binary equilibrium data are required. The method involves fitting k_{ij} to experimental vapor-liquid equilibrium data and minimizing the differences between the predicted and experimental values. Experimental data reported by various researchers (Price and Kobayshi, 1959; Chang and Lu, 1967; Stryjek et al., 1974; Poon and Lu, 1974) were used in selecting the values of k_{ij}. The selected values for the interaction parameter are given in Table 4-1. In this table they are also compared to values for k_{ij} found in the literature. Details on the procedure to select the values for k_{ij} can be found in Appendix B.

The values of k_{ij} are then in reasonable agreement with other published values. The differences observed with the values of Kato et al. (1976) and Joffe et al. (1970) might be due in part to the different temperature dependency used for the parameters a and b. Both Kato and Joffe modify the original Redlich-Kwong equation by

TABLE 4-1

Binary Interaction Parameter k_{ij} for the SRK Equation

Binary System	This Work	Erbar	Kato et al.*	Joffe et al.*
Methane-Ethane	0.000	0.000	0.003	0.009
Methane-Propane	0.010	0.000	0.010	0.073
Ethane-Propane	0.000	0.000		0.027
Nitrogen-Methane	0.035	0.020	0.045	
Nitrogen-Ethane	0.035	0.060		
Nitrogen-Propane	0.120	0.080		

*Original Redlich-Kwong Equation

letting a and b be temperature dependent; whereas Soave incorporated all the temperature dependency in the term a while leaving b independent of temperature.

For a nonreacting system of m chemical components and π phases there are F degrees of freedom

$$F = 2 - \pi + m \tag{4-15}$$

In the present case two phases are present, consequently, the degrees of freedom are equal to the number of components. Thus specifying m independent variables fixes, thermodynamically, the system. In the case of LNG boiling on water, the independent variables are determined by the experimental conditions: atmospheric pressure and liquid composition. The dependent variables are temperature and vapor composition. In equilibria studies, however, it is customary to fix the temperature rather than the pressure since a constant temperature can be maintained more easily than constant pressure. Therefore, in the next section where the applicability of the SRK equation to light hydrocarbons' equilibria is assessed, the temperature and liquid composition are taken as the independent variables. The dependent variables, pressure and vapor composition, are calculated by combining Eq. (4-6) which gives the fugacity coefficient ϕ_i and the vapor-liquid distribution coefficient K_i,

$$K_i = \frac{y_i}{x_i} = \frac{\phi_i^L}{\phi_i^V} = \frac{\dfrac{\hat{f}_i^L}{P\,x_i}}{\dfrac{\hat{f}_i^V}{P\,y_i}} \tag{4-16}$$

The above procedure for vapor-liquid equilibria compositions can be used in conjunction with a mass balance to determine the temperature of the residual liquid LNG as well as the composition of the vapor evolved during the boiling of LNG on water.

For every component $\underline{i}$ in the mixture, a mass balance over a differential period of time can be written:

$$-d(x_i L) = y_i dV \tag{4-17}$$

where L = number of moles in the liquid phase

V = number of moles in the vapor phase

Since $dL = -dV$, Eq. (4-17) can be rewritten as

$$\frac{dL}{L} = \frac{dx_i}{y_i - x_i} \tag{4-18}$$

In an evaporation process dL is negative. A more convenient variable to be used is the moles evaporated $d\hat{L}$,

$$d\hat{L} = - dL \tag{4-19}$$

which is positive. Equation (4-18) can be approximated by a different equation, which incorporates the moles evaporated $d\hat{L}$,

$$- \frac{\Delta\hat{L}}{L} = \frac{\Delta x_i}{y_i - x_i} \tag{4-20}$$

provided that small enough values of $\Delta\hat{L}$ are used. During spills of LNG on water, experimental data were recorded at $\Delta\tau$ = 1 sec. intervals. In Eq. (4-20), at any time τ, L, x_i and y_i are known. For instance,

at τ = 0 sec. L is the number of moles in the initial charge of LNG, x_i the mole fraction of i in this charge and y_i the mole fraction of i in the vapor in equilibrium with the given composition for the liquid. Furthermore, $\Delta\hat{L}$ can be determined from the experimentally-measured mass that was evaporated, during the period of time $\Delta\tau$. Thus the only unknown in Eq. (4-20) is the value of x_i at time $\tau + \Delta\tau$,

$$x_i(\tau + \Delta\tau) = x_i(\tau) - \frac{L(\tau) - L(\tau + \Delta\tau)}{L(\tau)} \cdot [y_i(\tau) - x_i(\tau)] \qquad (4\text{-}21)$$

As previously indicated, for the difference approximation to be valid, the value of $\Delta\hat{L}$ must be sufficiently small. The maximum value of $\Delta\hat{L}$ that can be used satisfactorily in the difference equation was obtained after studying the hypothetical evaporation of a mixture. A liquid mixture was assumed to have an initial composition of 90% methane and 10% ethane, and an initial mass of 100 grams (5.732 g moles). A molar mass $\Delta\hat{L}$ was then assumed to have evaporated. The new liquid composition was calculated from Eq. (4-21). The equilibrium vapor composition and temperature were calculated with the SRK equation. The procedure was repeated until the liquid was completely evaporated. Various values of $\Delta\hat{L}$ were used, and for given values of residual molar mass, the temperature, composition and mass were compared. The point at which a further decrease in $\Delta\hat{L}$ did not significantly change the results was selected as the value of $\Delta\hat{L}$ to be used in the VLE model. The results obtained with the various $\Delta\hat{L}$'s are given in Table 4-2. The ethane fractions were used in this table since they make the observation of differences in compositions easier.

TABLE 4-2

Hypothetical Evaporation of a Hydrocarbon Mixture Using Various Mole Decrements

Initial Mass 100 grams

Initial Liquid Composition C_1 = 90%, C_2 = 10%

Molar Mass	$\Delta\hat{L}$ = 0.1 mole				$\Delta\hat{L}$ = 0.05 mole				$\Delta\hat{L}$ = 0.01 mole				$\Delta\hat{L}$ = 0.001 mole			
	T, K	x_{C_2}	y_{C_2}	Mass g	T, K	x_{C_2}	y_{C_2}	Mass g	T, K	x_{C_2}	y_{C_2}	Mass g	T, K	x_{C_2}	y_{C_2}	Mass g
5.732	113.07	0.100	.00018	100.	113.07	0.100	.00018	100.	113.07	0.100	.00018	100.	113.07	0.100	.00018	100.
5.032	113.24	0.114	.00020	88.77	113.24	0.114	.00020	88.77	113.24	0.114	.00020	88.77	113.24	0.114	.00020	88.76
4.032	113.58	0.141	.00026	72.72	113.58	0.142	.00026	72.72	113.59	0.142	.00020	72.72	113.59	0.142	.00026	72.73
3.032	114.14	0.186	.0036	56.68	114.16	0.187	.00036	56.68	114.18	0.189	.00037	56.67	114.18	0.189	.00036	56.68
2.032	115.32	0.273	.00059	40.63	115.38	0.277	.00060	40.63	115.43	0.281	.00061	40.63	115.44	0.282	.00061	40.62
1.032	119.72	0.513	.00184	24.57	120.19	0.532	.00203	24.57	120.63	0.549	.00221	24.57	120.73	0.553	.00226	24.58
0.532	148.18	0.916	.07461	16.51	172.22	0.979	.47642	16.46	183.09	0.997	.91180	16.10	182.71	0.997	.89315	16.01
0.432	184.77	1.000	1.0000	14.80	184.77	1.000	1.0000	13.82	184.77	1.000	1.0000	13.12	184.77	1.000	1.0000	13.02

The difference in values obtained with $\Delta\hat{L} = 0.1$ and $\Delta\hat{L} = 0.001$ moles in quite significant; whereas between $\Delta\hat{L} = 0.01$ and $\Delta\hat{L} = 0.001$ moles there is little difference. Thus the value of $\Delta\hat{L} = 0.01$ was selected to be used in the VLE model.

In applying the VLE model, so far described, to the experimental data, it is likely that the mass evaporated during the interval of time (1s) between two consecutive mass readings represents a molar change greater than 0.01 moles. In such a case, an alternative procedure to the direct use of Eq. (4-21) is to be followed; a logic diagram of this procedure is given in Figure 4-1.

Essentially, this method involves breaking the mass evaporated, ΔM, in that period of time in smaller decrements in mass corresponding to $\Delta\hat{L}$'s of 0.01 moles or less. An initial value of $\Delta\hat{L}' = 0.01$ is taken and the new liquid fraction for component i is calculated from an alternate version of Eq. (4-21):

$$x_i'^{new} = x_i' - \frac{\Delta\hat{L}'}{L'}(y_i' - x_i') \qquad (4\text{-}22)$$

The mass evaporated corresponding to this $\Delta\hat{L}'$ is then computed and subtracted from ΔM to yield a ΔM^{new}. The value of $\Delta\hat{L}'$ equivalent to evaporating ΔM^{new} in one step is calculated; if smaller than 0.01 moles, this value of $\Delta\hat{L}'$ is used directly in Eq. (4-22). Otherwise a value of $\Delta\hat{L}' = 0.01$ is assumed and the procedure repeated. The x_i^{new} corresponding to the total evaporation of ΔM becomes $x_i(\tau + \Delta\tau)$; and the vapor in equilibrium with this liquid composition becomes $y_i(\tau + \Delta\tau)$. A detailed flow diagram of the computer algorithm for the above procedure is given in Appendix B.

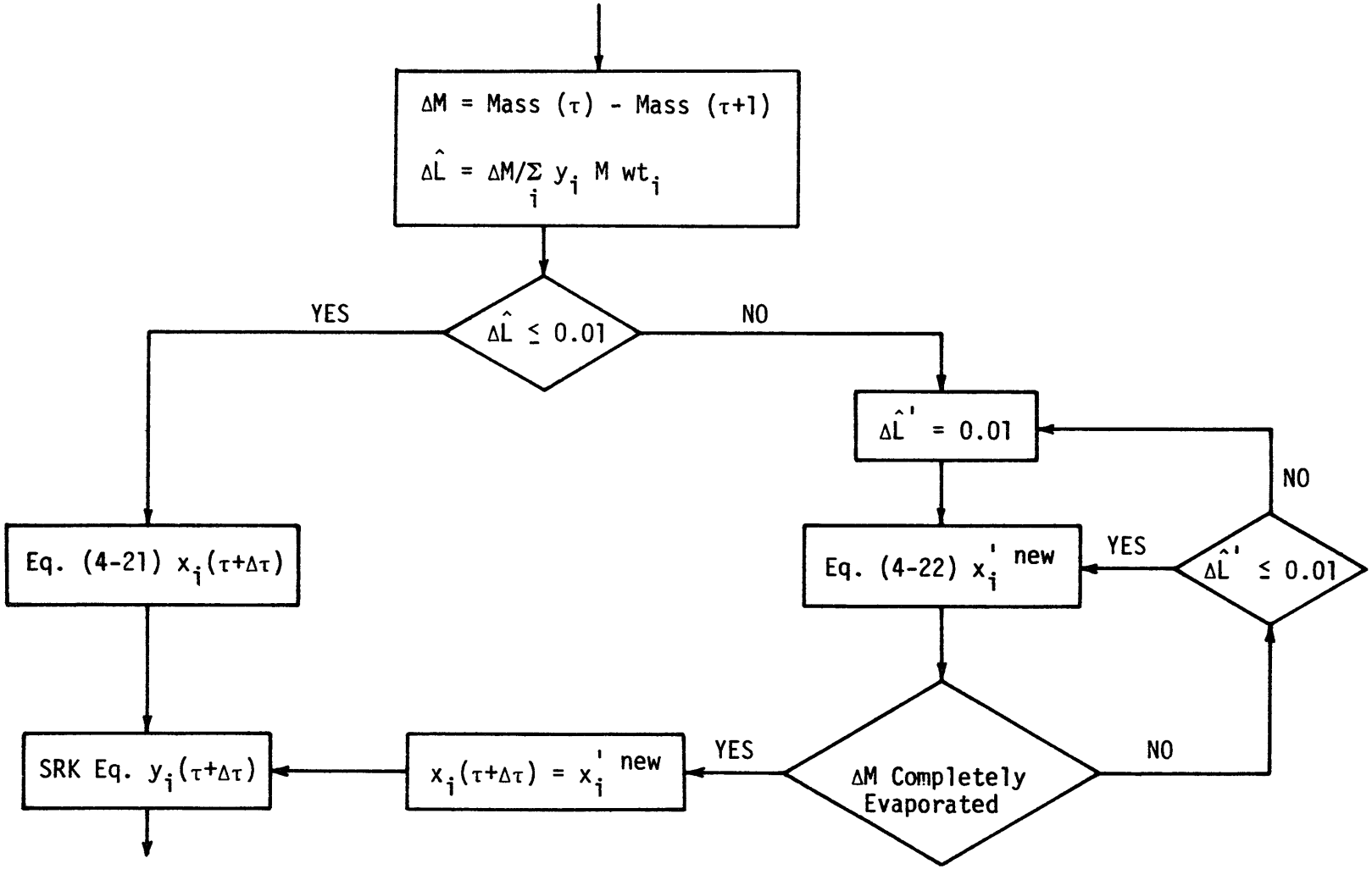

Figure 4-1 Logic Diagram to Insure a Value of $\Delta\hat{L} \leq 0.01$ Moles is Used Throughout the VLE Model

Applicability of the SRK Equation of State

Before the Soave-Redlich-Kwong equation of state can be used, it must be shown that it is applicable in predicting low-temperature vapor-liquid equilibria of light hydrocarbon systems. To this end predictions made with the SRK equation were compared with experimental light-hydrocarbon equilibria data reported by various investigators.

The methane-ethane system has been studied experimentally by Price and Kobayashi (1959) over a temperature range of 144-283 K and a pressure range of 6.9-69.0 bar. In their experiments a given mixture was placed in a equilibrium cell maintained at constant temperature. After equilibrium was attained, the liquid and vapor composition were determined as well as the system pressure. In using the SRK equation, the experimental conditions are followed--which is to say that the temperature and liquid composition are taken as the independent variables, and pressure and vapor composition are determined from thermodynamic equilibrium considerations. Chang and Lu (1967) also investigated the methane-ethane system. The experimental procedure was similar to that of Price and Kobayashi. Two isotherms were studied, 172 K (3.6-20.8 bars) and 122 K (1.3-2.2 bars). SRK predictions are compared to the data reported by Price and Kobayashi, and by Chang and Lu in Figure 4-2. The SRK predictions are in excellent agreement with Price and Kobayashi's data. In general, the SRK predictions match Chang and Lu's data closely except near the critical point for the 172 K isotherm. Since the pressure of interest in this work is 0.987 bar (1 atm), the low pressure range (0-10 bar) results are shown in more detail in Figure 4-3. The agreement between SRK predictions and experimental data is seen to be quite good.

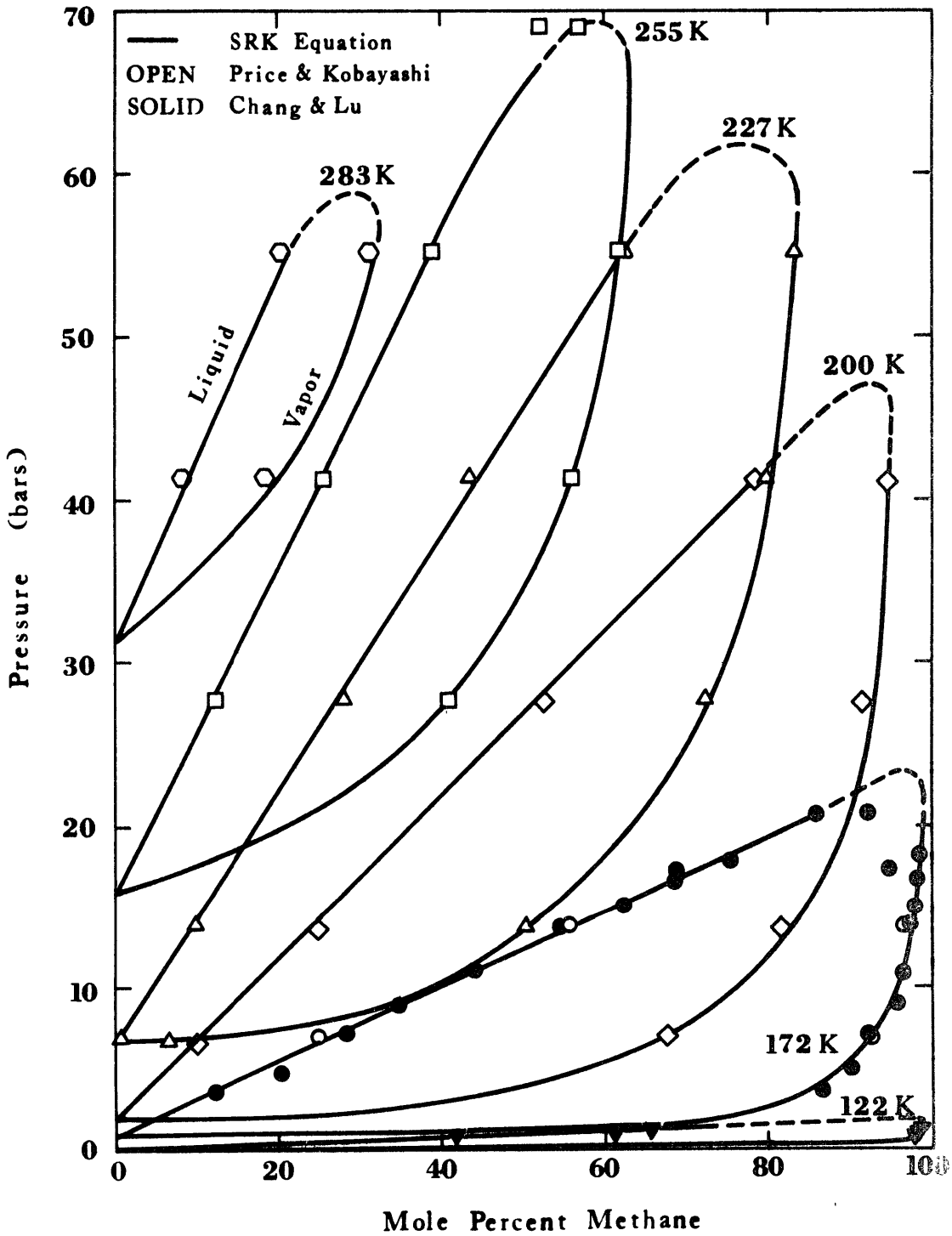

Figure 4-2 Pressure Composition Diagram for the Methane-Ethane System (k_{ij} = 0.0)

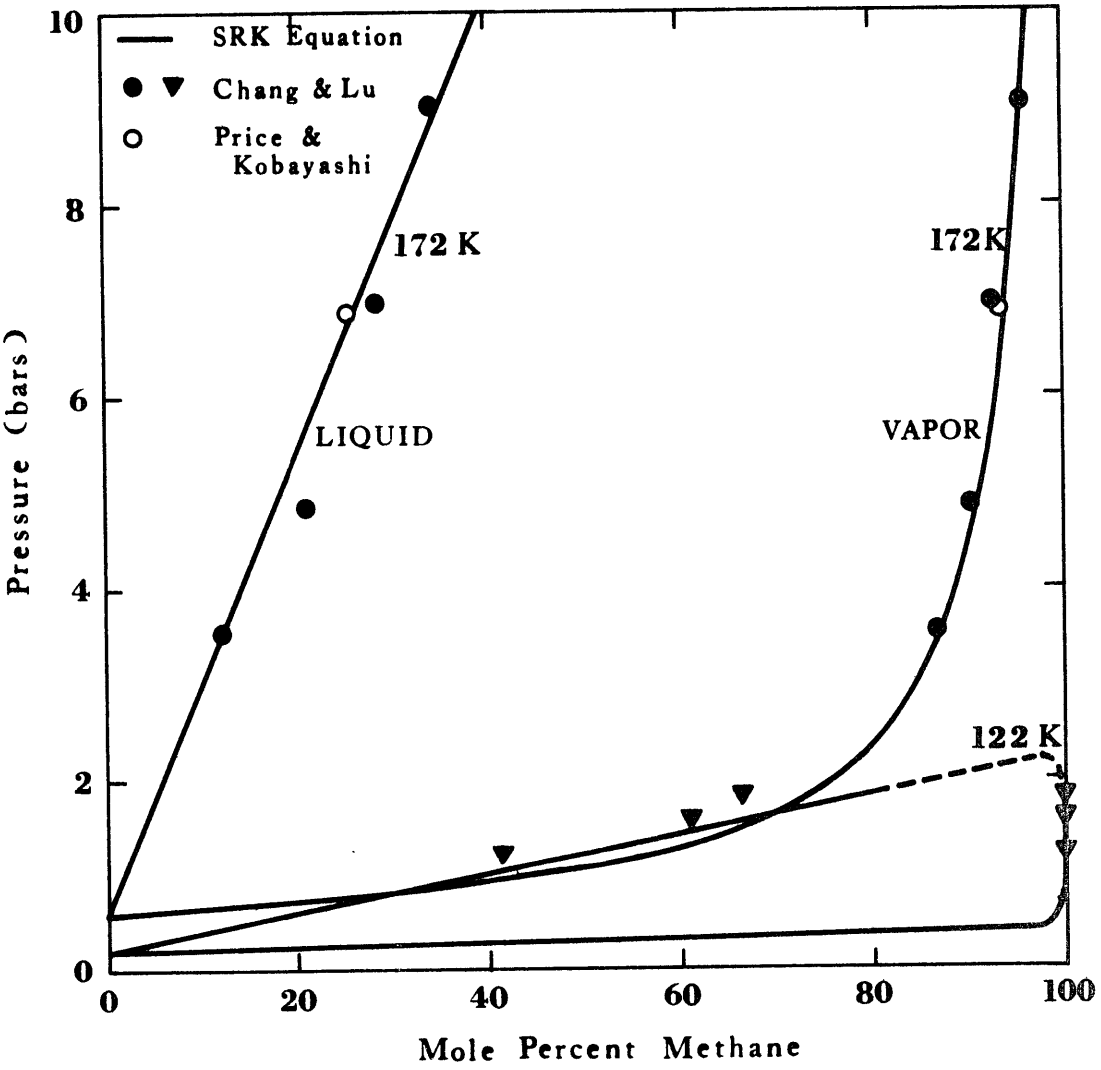

Figure 4-3 Pressure Composition Diagram for the Methane-Ethane System. Low Pressure Range (k_{ij} = 0.0)

The binaries methane-propane and ethane-propane were also studied by Price and Kobayashi. Methane-propane in the range 172-283 K and 6.9-89.6 bar; ethane-propane in the range 255-283 K and 6.9-27.6 bar. SRK predictions are compared to these experimental data in Figures 4-4 and 4-5. The agreement, again, is quite good.

Even though nitrogen is present in LNG in small amounts (<2 mole percent), it is an important component since it is the most volatile. Thus, the binaries involving nitrogen were also considered. Stryjek et al. (1974a) studied experimentally the equilibrium in the nitrogen-methane system (114-183 K, 3.4-48.8 bar). Stryjek et al. (1974b) considered the system nitrogen-ethane (139-194 K, 3.4-125 bar). Poon and Lu (1974) evaluated the equilibria for the nitrogen-propane binary (114-122 K, 1.5-28 bar). Predictions made with SRK equation are compared to these experimental equilibrium data for the nitrogen binaries in Figures 4-6, 4-7 and 4-8. The SRK values are seen to match the experimental data quite closely.

Prediction of vapor-liquid equilibria for a ternary system becomes more difficult since the interaction parameters determined to best fit binary data must apply without further change. Predictions made using the SRK equation are compared in Table 4-3 to isothermal (283 K) data for the methane-ethane-propane system reported by Price and Kobayashi (1959). As was the case for the binary systems, the temperature and liquid composition are the independent variables; the predicted values for pressure and vapor composition are then compared to the experimentally measured values. For 32 points considered, the

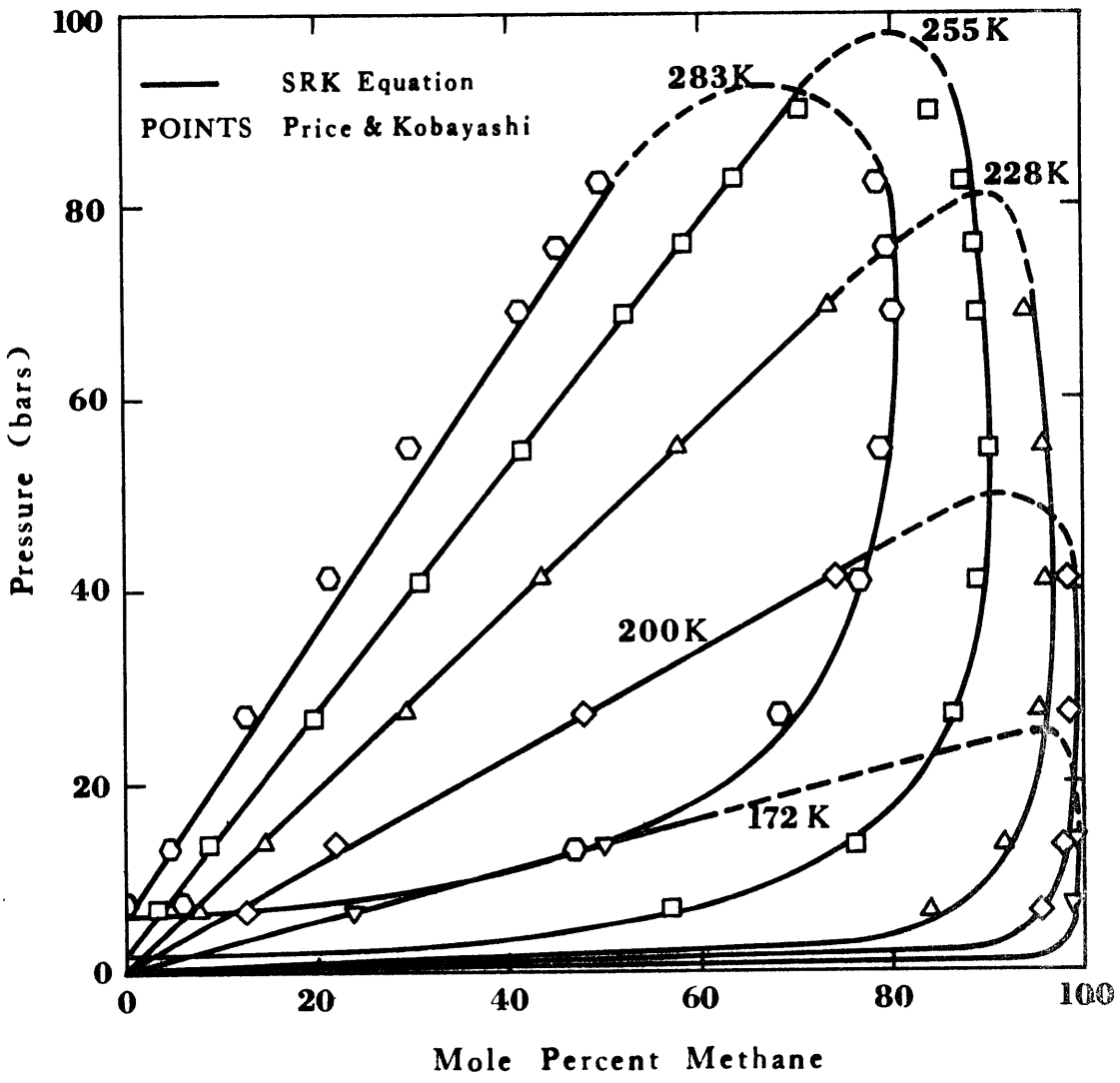

Figure 4-4 Pressure Composition Diagram for Methane-Propane System (k_{ij} = 0.01)

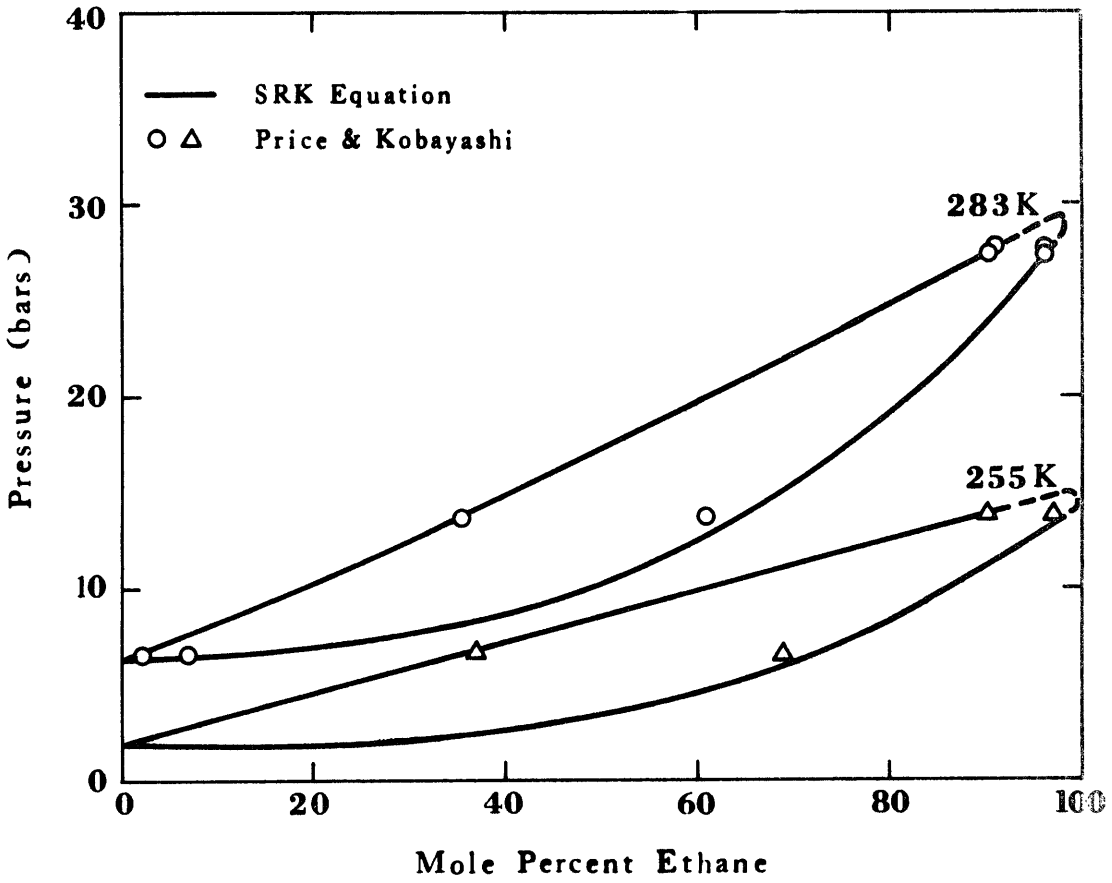

Figure 4-5 Pressure Composition Diagram for the Ethane-Propane System (k_{ij} = 0.0)

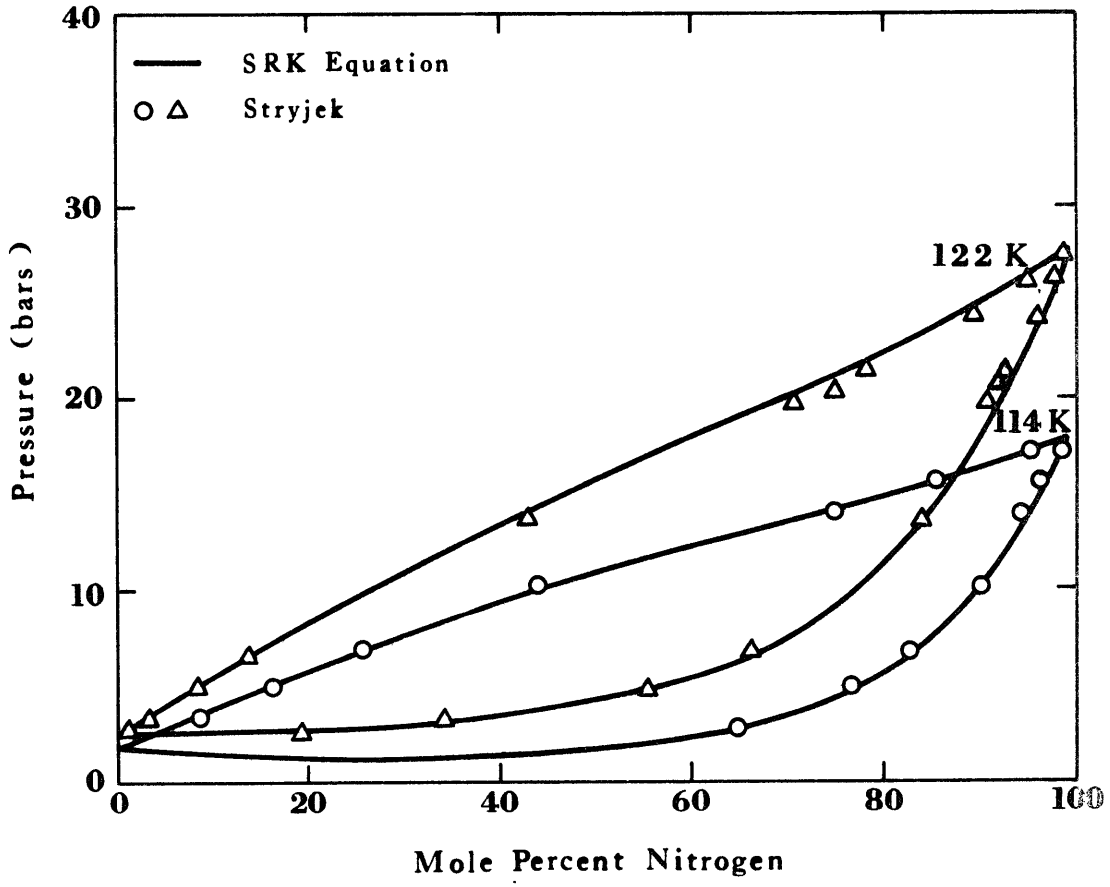

Figure 4-6 Pressure Composition Diagram for the Nitrogen-Methane System (k_{ij} = 0.035)

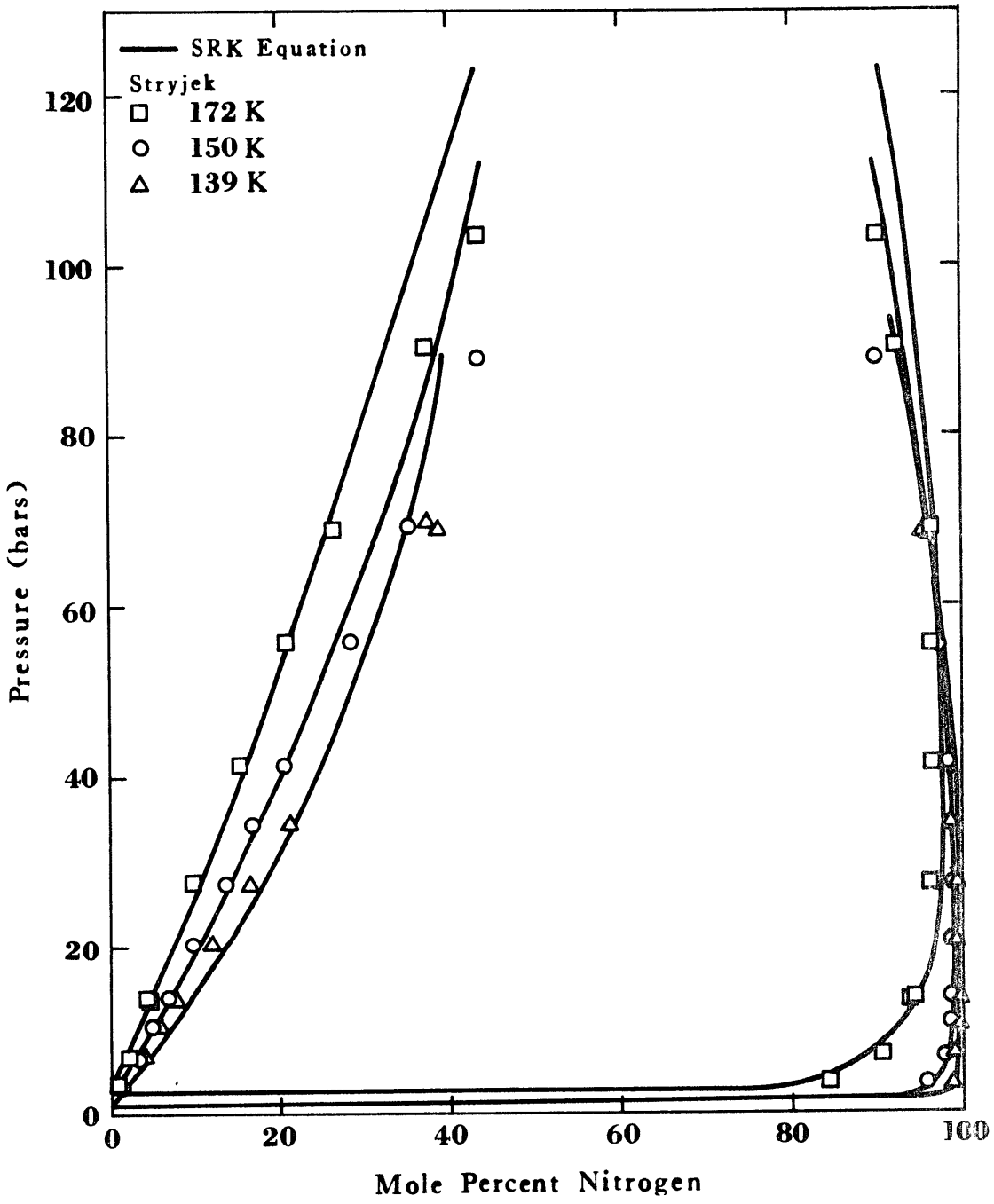

Figure 4-7 Pressure Composition Diagram for Nitrogen-Ethane System (k_{ij} = 0.035)

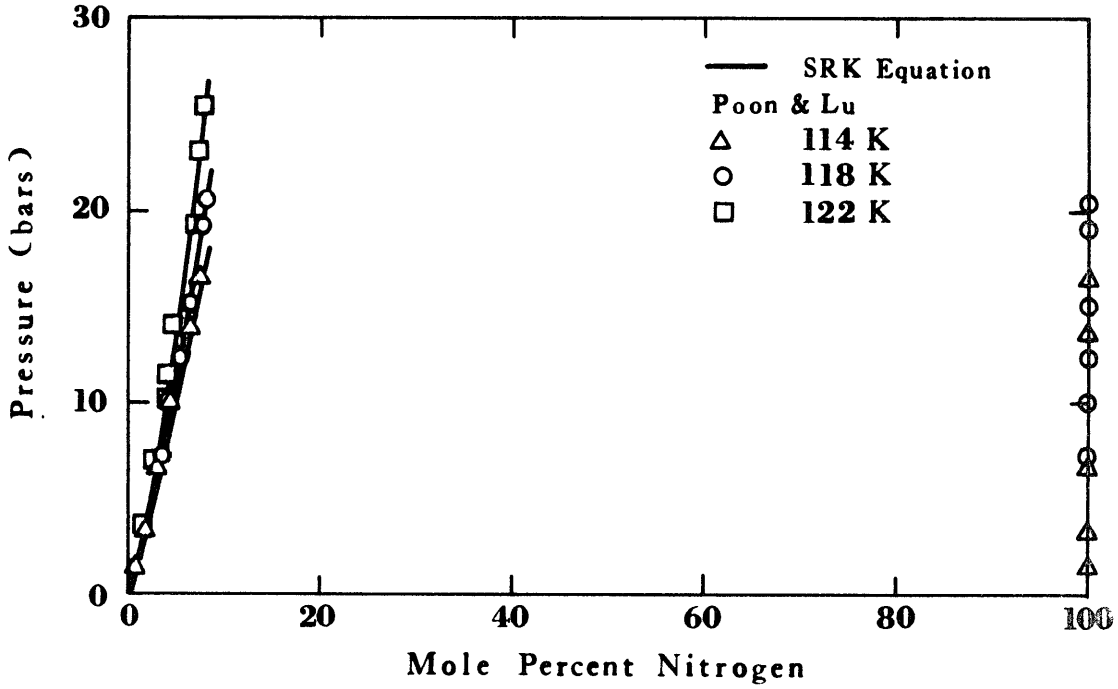

Figure 4-8 Pressure Composition Diagram for the Nitrogen-Propane System (k_{ij} = 0.120)

TABLE 4-3

Comparison of SRK Predictions for Pressure and Vapor Composition
with Experimental Data by Price and Kobayashi.
Methane-Ethane-Propane System (283 K)

		EXPERIMENTAL			SRK			
TEMPERATURE (K)	COMPONENT (I)	LIQUID MOLE % X(I)	VAPOR MOLE % Y(I)	PRESSURE (N/M2)	VAPOR MOLE % Y(I)	DEVIATION (%)	PRESSURE (N/M2)	DEVIATION (%)
283.15	1	0.2200	4.5200	689476	4.1780	-7.57	673653	-2.29
	2	0.8000	2.8000		2.7195	-2.87		
	3	98.9800	92.6800		93.1025	0.46		
283.15	1	3.9600	41.2000	1378952	38.7210	-6.02	1327874	-3.70
	2	6.5500	11.2000		12.3003	9.82		
	3	89.4900	47.6000		48.9787	2.90		
283.15	1	2.7000	27.5000	1378952	25.6143	-6.86	1336835	-3.05
	2	16.0000	28.4000		29.7586	4.78		
	3	81.3000	44.1000		44.6271	1.20		
283.15	1	1.2800	12.7000	1378952	11.7096	-7.80	1348041	-2.24
	2	26.4000	47.6000		48.4993	1.89		
	3	72.3200	39.7000		39.7911	0.23		
283.15	1	11.0000	55.7000	2757903	54.6480	-1.89	2589975	-6.09
	2	17.5000	19.3000		19.4472	0.76		
	3	71.5000	25.0000		25.9048	3.62		
283.15	1	6.9700	30.6000	2757903	29.9068	-2.27	2715269	-1.55
	2	50.0000	53.5000		53.8223	0.60		
	3	43.0300	15.9000		16.2710	2.33		
283.15	1	6.2000	28.2000	2757903	25.9720	-7.90	2728207	-1.08
	2	55.3000	57.0000		59.3237	4.08		
	3	38.5000	14.8000		14.7043	-0.65		
283.15	1	3.0200	11.5000	2757903	11.4008	-0.86	2781528	0.86
	2	75.7800	79.8900		80.1314	0.30		
	3	21.2000	8.6100		8.4678	-1.65		
283.15	1	21.4000	66.3000	4136855	67.7195	2.14	4099049	-0.91
	2	15.1000	13.3000		12.6275	-5.06		
	3	63.5000	20.4000		19.6531	-3.66		
283.15	1	20.4000	65.4000	4136855	65.5688	0.26	4004224	-3.21
	2	17.8000	15.0000		15.0895	0.60		
	3	61.8000	19.6000		19.3418	-1.32		
283.15	1	17.8000	52.1000	4136955	53.0135	1.75	4038549	-2.38
	2	37.6000	33.2000		32.1158	-3.27		
	3	44.6000	14.7000		14.8706	1.16		

TABLE 4-3 CONT

MP	I	X(I)	Y(I)	PRESS	Y(I)	% DEV	PRESS	%DE
15	1	17 4000	48 7000	4136855	48 5955	-0 21	4160669	0
	2	45 7000	38 2000		38 7155	1 35		
	3	36 9000	13 1000		12 6891	-3 14		
15	1	13 7000	37 1000	413:855	35 8708	-3 31	4071022	-1
	2	64 7000	55 0100		56 0745	1 94		
	3	21 6000	7 8900		8 0548	2 09		
15	1	11 3000	28 6000	4136855	27 8884	-2 49	4037772	-2
	2	76 8000	66 6800		67 3923	1 07		
	3	11 9000	4 7200		4 7193	-0 01		
15	1	28 6000	72 2400	5515806	72 5983	0 50	5125554	-7
	2	12 1000	9 0600		9 1656	1 17		
	3	59 3000	18 7000		18 2361	-2 48		
15	1	26 8000	58 8000	5515806	59 2175	0 71	5326530	-3
	2	35 9000	28 2000		27 7264	-1 68		
	3	37 3000	13 0000		13 0561	0 43		
15	1	25 5000	53 4000	5515806	53 5727	0 82	5331:09	-3
	2	45 4000	35 7000		35 6005	-0 28		
	3	29 1000	10 9000		10 8268	-0 67		
15	1	23 7000	46 3200	5515806	46 6894	0 80	5312663	-3
	2	56 6000	45 5000		45 3531	-0 32		
	3	19 7000	8 1800		7 9575	-2 72		
15	1	38 9000	70 4000	6894 58	71 4905	1 12	6 28720	-2
	2	16 9000	12 6000		12 3277	-2 16		
	3	44 2000	16 7000		16 1818	-3 10		
15	1	38 5000	68 6000	6894.58	68 2824	0 41	6754111	-2
	2	22 5000	16 4000		16 6731	1 67		
	3	39 0000	15 6000		15 0440	-3 56		
15	1	37 3000	70 0000	6894.58	70 3680	0 45	6767345	-1
	2	35 7000	26 8000		27 6884	3 32		
	3	27 0000	13 2000		12 0436	-8 76		
15	1	34 9000	48 2600	6894.58	50 2805	4 19	6:3:532	-3
	2	50 5000	43 1000		41 7765	-3 02		
	3	14 6000	8 4400		7 7229	-8 30		

TABLE 4-3 CONT

TEMP	I	X(I)	Y(I)	PRESS	Y(I)	% DEV	PRESS	%DEV
283 15	1	37 5500	43 4500	6894758	46 9048	7 95	6889935	-0 07
	2	52 4100	49 0000		46 2907	-5 53		
	3	10 0400	7 5500		6 8044	-9 87		
283 15	1	43 6500	77 4600	7584234	78 4771	1 31	7226983	-4 71
	2	4 0900	3 0600		2 9029	-5 13		
	3	52 2600	19 4800		18 6200	-4 41		
283 15	1	43 0000	73 4100	7584234	74 6692	1 72	7225420	-4 73
	2	11 0000	8 4900		7 9624	-6 21		
	3	46 0000	18 1000		17 3684	-4 04		
283 15	1	43 8000	69 2000	7584234	69 7286	0 76	7427373	-2 07
	2	19 2000	14 3000		14 4180	0 83		
	3	37 0000	16 5000		15 8534	-3 92		
283 15	1	43 8000	66 5000	7584234	67 7818	1 93	7455108	-1 70
	2	22 3000	17 3000		17 0006	-1 73		
	3	33 9000	16 2000		15 2176	-6 06		
283 15	1	43 5000	63 0000	7584234	65 4755	3 93	7446122	-1 82
	2	25 9000	20 9000		20 0873	-3 89		
	3	30 6000	16 1000		14 4372	-10 33		
283 15	1	44 0000	50 4000	7584234	56 3611	11 83	7516435	-0 89
	2	37 6000	35 1000		32 0879	-8 58		
	3	18 4000	14 5000		11 5510	-20 34		
283 15	1	49 9700	75 5600	8273709	77 9692	3 16	8108838	-1 99
	2	3 7500	3 0200		2 7409	-9 24		
	3	46 2800	21 4000		19 2897	-9 85		
283 15	1	50 4000	67 3000	8273709	69 0102	2 54	8217432	-0 68
	2	17 6000	14 3000		14 0051	-2 06		
	3	32 0000	18 4000		16 9847	-7 69		
283 15	1	50 8000	58 4000	8273709	63 6507	8 99	8218213	-0 67
	2	24 3000	21 9000		20 5997	-5 94		
	3	24 9000	19 7000		15 7497	-20 05		

AVERAGE OF ABSOLUTE PERCENT DEVIATION

PRESSURE	2 46%
Y(1)	3 25%
Y(2)	3 16%
Y(3)	4 72%

average of the absolute percent deviation in pressure was 2.5%. The deviation in the vapor fraction of methane was 3.3%, for ethane, 3.2% and for propane, 4.7%. The SRK predictions for this isotherm are excellent. A similar comparison for a lower temperature isotherm, 172 K, is given in Table 4-4. For 7 points the average deviation in pressure is 0.9%. For the methane fraction in the vapor, the deviation is 0.8%. For the vapor fractions of ethane and propane, the deviations are much larger, 20 and 55%, respectively. These large deviations are due to the small amounts of these heavies in the vapor, ethane <6.8% and propane <0.4%. Thus any deviation will tend to show a large percent error. Consequently, the actual absolute errors are smaller and have much less significance in the present work.

It can be concluded that the Soave-Redlich-Kwong equation yields good vapor-liquid equilibria predictions for light hydrocarbon mixtures, and it is applicable in predicting low temperature - low pressure equilibria for LNG systems.

Experimental Vapor Sampling

During the transient boiling of LNG on water, vapor samples were taken at various times. The composition of these samples was determined chromatographically and compared to those predicted by the VLE model.

Small (125 cm^3) glass bulbs were used to sample the vapor. One such bulb is shown in Figure 4-9. These sampling bulbs were evacuated prior to the tests. Then, during the ebullition of LNG on water, one of the bulbs was placed at the mouth of the boiling vessel (see

TABLE 4-4

Comparison of SRK Predictions for Pressure and Vapor Composition
with Experimental Data by Price and Kobayashi.
Methane-Ethane-Propane System (172 K)

		EXPERIMENTAL			SRK			
TEMPERATURE (K)	COMPONENT (I)	LIQUID MOLE % X(I)	VAPOR MOLE % Y(I)	PRESSURE (N-M2)	VAPOR MOLE % Y(I)	DEVIATION (%)	PRESSURE (N-M2)	DEVIATION (%)
172.04	1	24.2000	96.8600	689476.	97.5425	0.70	685732	-0.54
	2	25.8000	2.8200		2.1947	-22.17		
	3	50.0000	0.3200		0.2628	-17.89		
172.04	1	24.0000	96.5300	689476	97.3862	0.89	679476	-1.45
	2	27.5000	3.0800		2.3572	-23.47		
	3	48.5000	0.3900		0.2566	-34.20		
172.04	1	24.9000	95.3800	689476	96.0416	0.69	692354	0.42
	2	44.6000	4.3300		3.7960	-12.33		
	3	30.5000	0.2900		0.1624	-44.01		
172.04	1	25.2000	92.9900	689476	94.0548	1.15	681905	-1.10
	2	67.6200	6.8200		5.9055	-13.41		
	3	7.1800	0.1900		0.0398	-79.06		
172.04	1	51.4000	98.0600	1378952	98.6999	0.65	1369476	-0.69
	2	20.8000	1.6700		1.1790	-29.40		
	3	27.8000	0.2700		0.1210	-55.17		
172.04	1	52.8000	97.4200	1378952	98.0732	0.67	1370318	-0.63
	2	31.9000	2.3400		1.8566	-20.66		
	3	15.3000	0.2400		0.0701	-70.77		
172.04	1	55.3200	96.9000	1378952	97.5858	0.71	1398749	1.44
	2	40.0000	2.9400		2.3913	-18.66		
	3	4.6800	0.1600		0.0229	-85.68		

AVERAGE OF ABSOLUTE PERCENT DEVIATION

PRESSURE	0.89%
Y(1)	0.78%
Y(2)	20.01%
Y(3)	55.25%

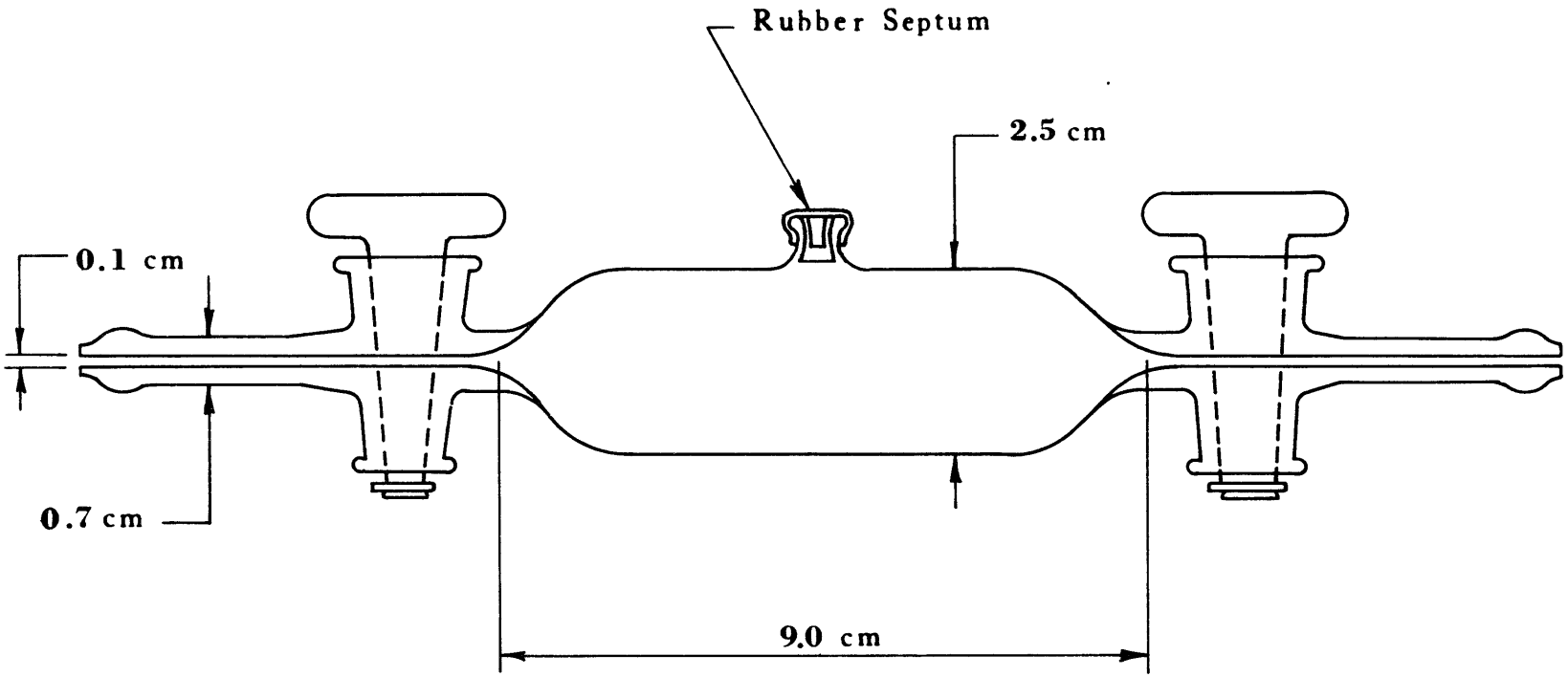

Figure 4-9 Vapor Sampling Bulb

Figure 4-10) and one of the stopcocks was opened, thus sucking a sample of the vapor into the sampling bulb. Assuming the pressure in the evacuated bulbs is 1 mm Hg, the time required to fill the bulb is between 0.4-0.7 sec. (see Appendix B). Thus the stopcock was opened for about 1 second.

Six such samples were taken at various times during a run and subsequently analyzed in a gas chromatograph.

Experimental Results and VLE Model Predictions

Eleven experiments were performed aimed at determining the degree to which vapor-liquid equilibrium is achieved during the boiling of LNG on water. The experimental results of these tests were then compared to predictions made by the VLE model.

The amount of methane initially present in the LNG mixtures ranged from 0 to 91 mole percent, ethane 6.5-89.7% and propane 0-18.2%. The amounts spilled varied between 0.5 and 2.1 g/cm^2, corresponding to non-boiling hydrostatic heads of 1.1 to 4.2 cm.

Tests R-30 through R-34 and R-39 through R-41 were made in a triple wall container with a cross-sectional area of 143 cm^2 and a height of 35 cm. For the vapors to be sampled they had to travel about 15-20 cm once they broke through the LNG liquid layer. Since the time it took for the vapor to travel upwards depends on the rate of vapor generation, the sampling time was adjusted to reflect the time at which the vapor sample was actually released from the liquid. This was accomplished by estimating the linear velocity of the vapor, assuming

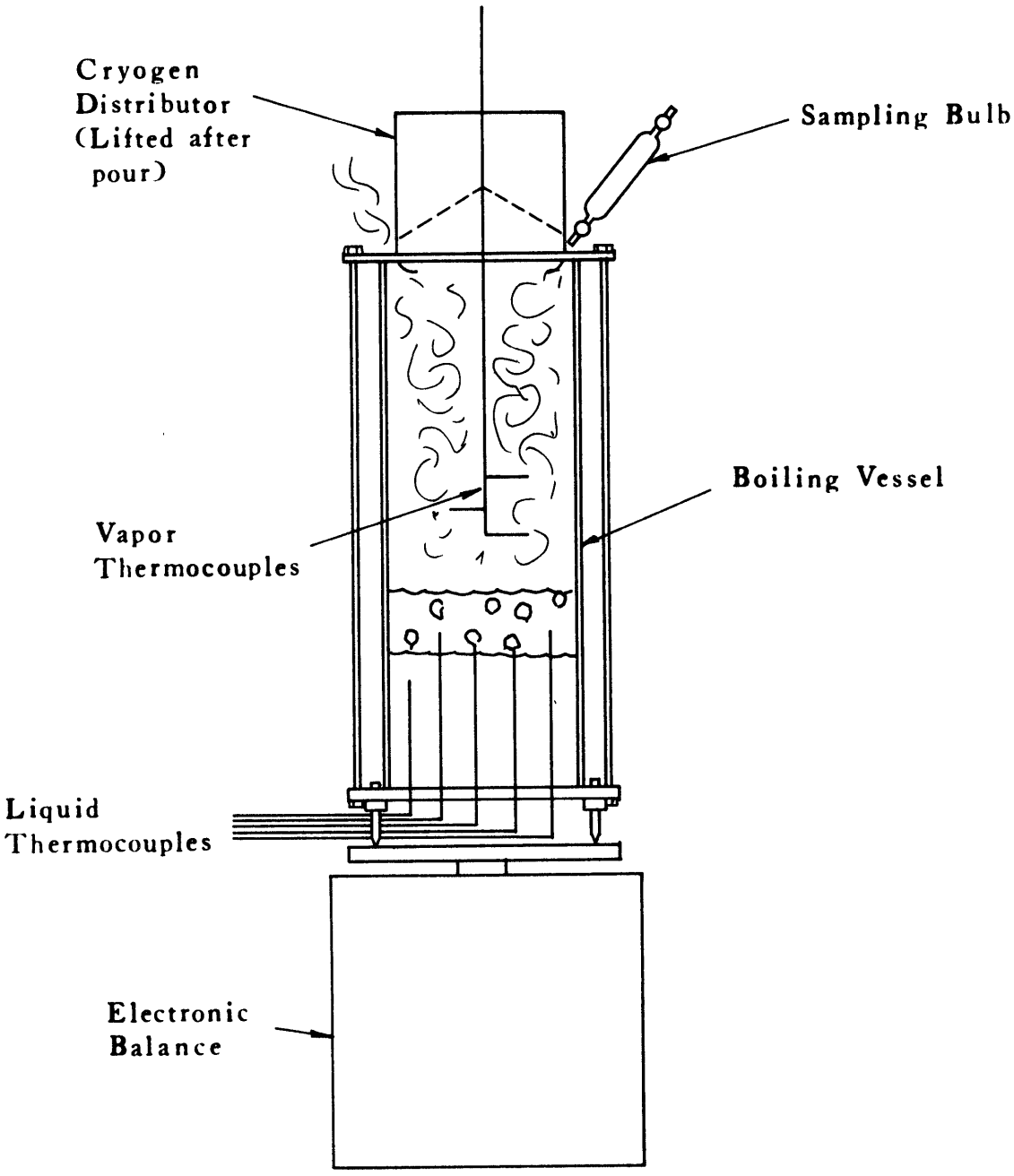

Figure 4-10 Schematic of the Vapor Sampling Procedure

plug flow. It can easily be determined from the boiling rate which gives the volumetric rate of vapor generation and the cross-sectional area of the container. For boiling rates of 0.1 mole/s, the correction in time was only 1 to 3 seconds. For boiling rates of 0.01 mole/s, it took between 10 to 30 seconds for the vapor to travel 15-20 cm, depending upon the vapor temperature and hence the vapor molar volume.

In tests R30-R34 and R39-R41, four thermocouples were used to monitor vapor temperatures. They were located 4 to 7 cm above the water surface. In tests R39-R41, five thermocouples were used to monitor the residual LNG liquid temperatures; these thermocouples were located 3 to 8 mm above the water surface. Tests R35-R38 were made in a 133 cm^2 triple wall vessel 20 cm in height. A summary of the experimental conditions for these spills is given in Table 4-5.

The experimental results can be better understood if one looks first at the T - x diagrams for the hydrocarbon binaries at atmospheric pressure. The methane-ethane T - x diagram is shown in Figure 4-11. Methane, being the more volatile of the two, is the primary constituent of the vapor. For methane liquid mole fractions of 0.2 and greater, the vapor is essentially pure methane. Even at a low 0.05 liquid mole fraction, methane makes up 82% of the vapor. It is only when the methane fraction in the liquid drops below 0.05 that the fraction of ethane in the vapor becomes large.

Thus if a methane-ethane mixture is allowed to evaporate, one would expect the vapor to be made up of methane until its mole fraction

TABLE 4-5

Experimental Conditions for LNG Spills

Related to the VLE Model

Test	Initial Composition Mole Percent C_1	C_2	C_3	Mass Spilled (g/cm^2)	Initial Molar Mass	Initial Water Temperature (K)
R-30		89.7	10.3	0.75	3.4	15.2
R-31	84.0	9.4	6.6	0.58	4.3	15.8
R-33	88.9	10.2	0.9	0.87	7.1	14.5
R-34	83.9	8.1	8.0	0.84	6.2	14.7
R-35	83.5	16.5		0.53	3.9	20.0
R-36	78.5	15.3	6.2	1.46	9.8	14.8
R-37	51.8	30.0	18.2	1.51	7.9	15.5
R-38*	80.3	19.7		2.06	14.6	15.4
R-39	70.1	20.5	9.4	1.42	9.4	16.8
R-40	85.2	10.1	4.7	1.97	15.0	16.0
R-41	91.0	6.5	2.5	1.20	9.7	14.0

*Extensive foaming. Partial loss of LNG charge due to overflow.

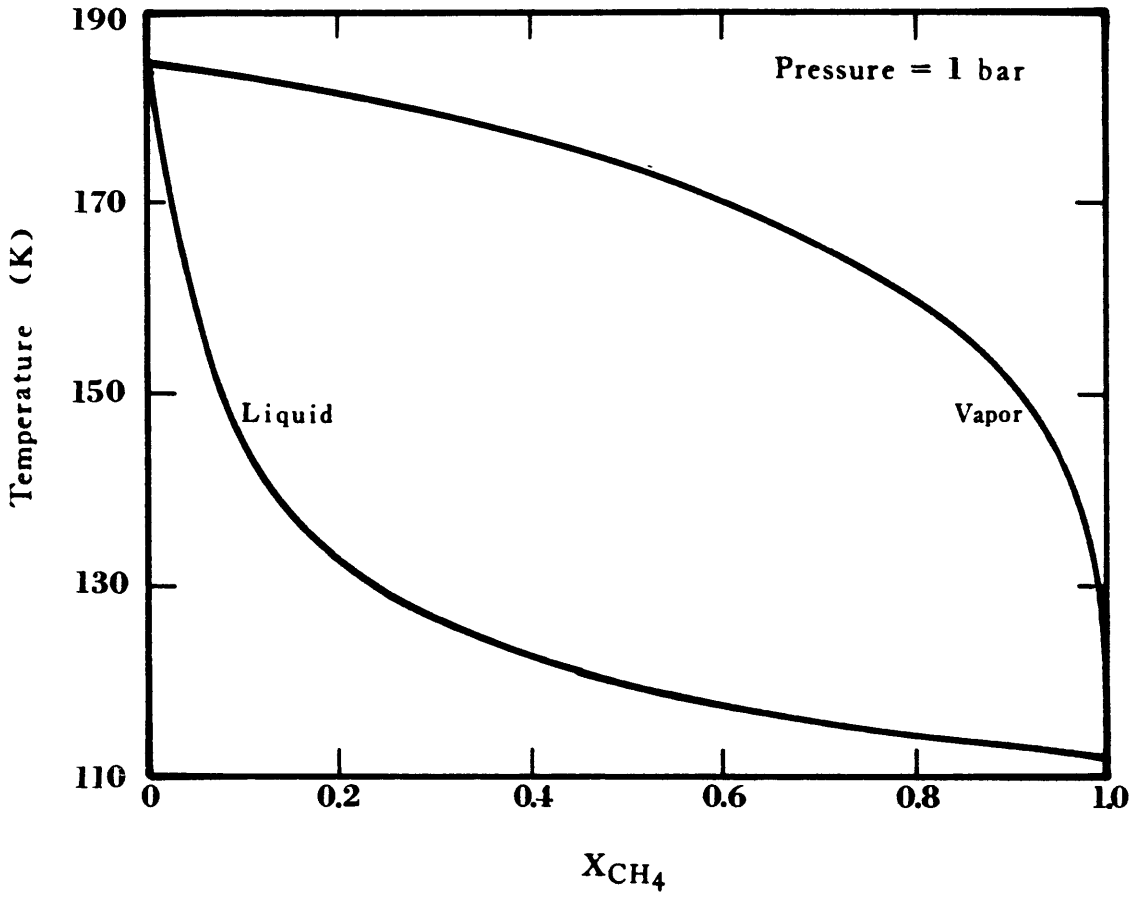

Figure 4-11 Temperature Composition Diagram for the Methane-Ethane System

in the liquid dropped below 0.1. Further evaporation would reduce the methane present in the liquid, and vapor-liquid equilibrium dictates then a sharp increase in the ethane fraction in the vapor.

Similarly, the saturation temperature of the liquid increases only 20 K going from pure methane to a liquid mixture containing 20% methane. But reducing the methane liquid-mole-fraction from 0.1 to 0.0 (pure ethane) causes a sharp increase of 40 K in temperature.

A similar behavior is observed for ethane-propane and methane-propane binaries. However, the changes in the ethane-propane system (Figure 4-12) are very progressive ones whereas in the methane-propane (Figure 4-13) they are very pronounced.

The experimental vapor compositions are compared in the next figures to predictions made with the Soave-Redlich-Kwong equation assuming vapor-liquid equilibria is attained during the evaporation process. Likewise, experimental liquid and vapor temperatures are compared to those predicted by the VLE model.

The vapor composition for a binary methane-ethane mixture is shown in Figure 4-14. The high methane content, at first, is followed by a sharp decrease and this is, indeed, observed experimentally.

As previously indicated, the transition in vapor composition in ethane-propane mixtures is a more progressive one. This can be observed in Figure 4-15. Experimental and VLE predicted temperatures for the same ethane-propane mixtures are shown in Figure 4-16.

In the case of ternary mixtures, at first, methane is expected to be the primary component in the vapor; upon its depletion in the

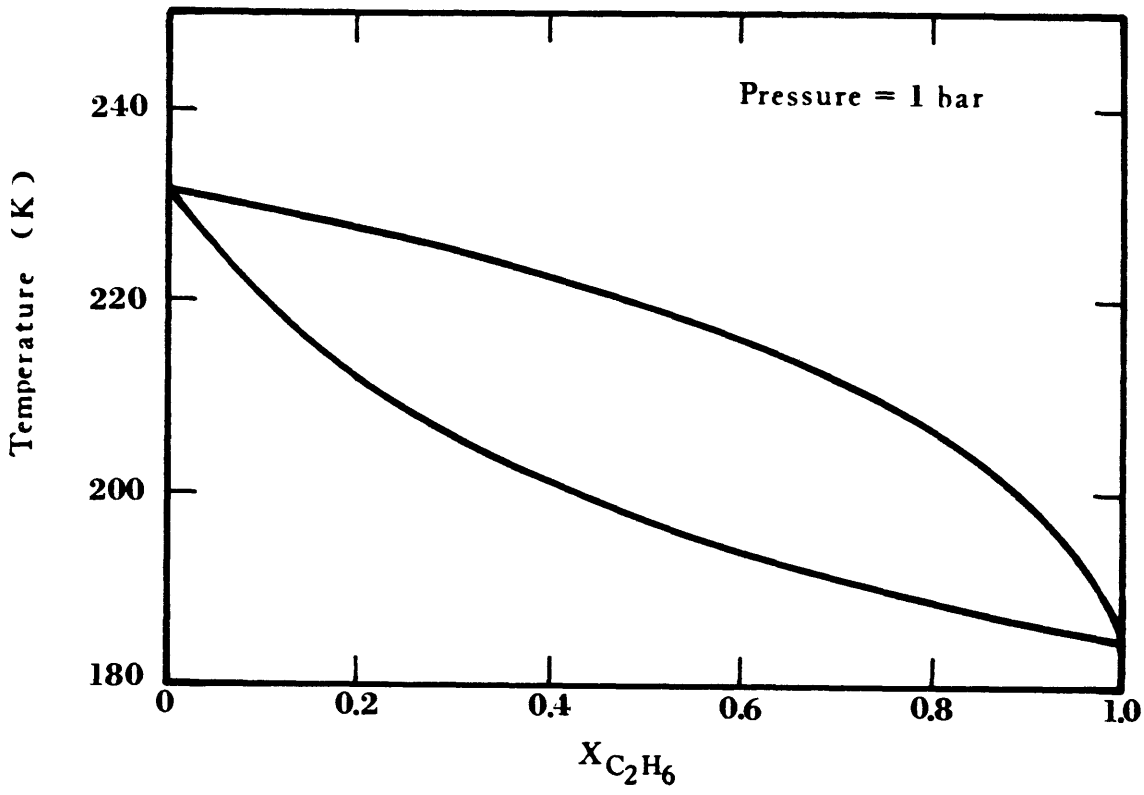

Figure 4-12 Temperature Composition Diagram for the Ethane-Propane System

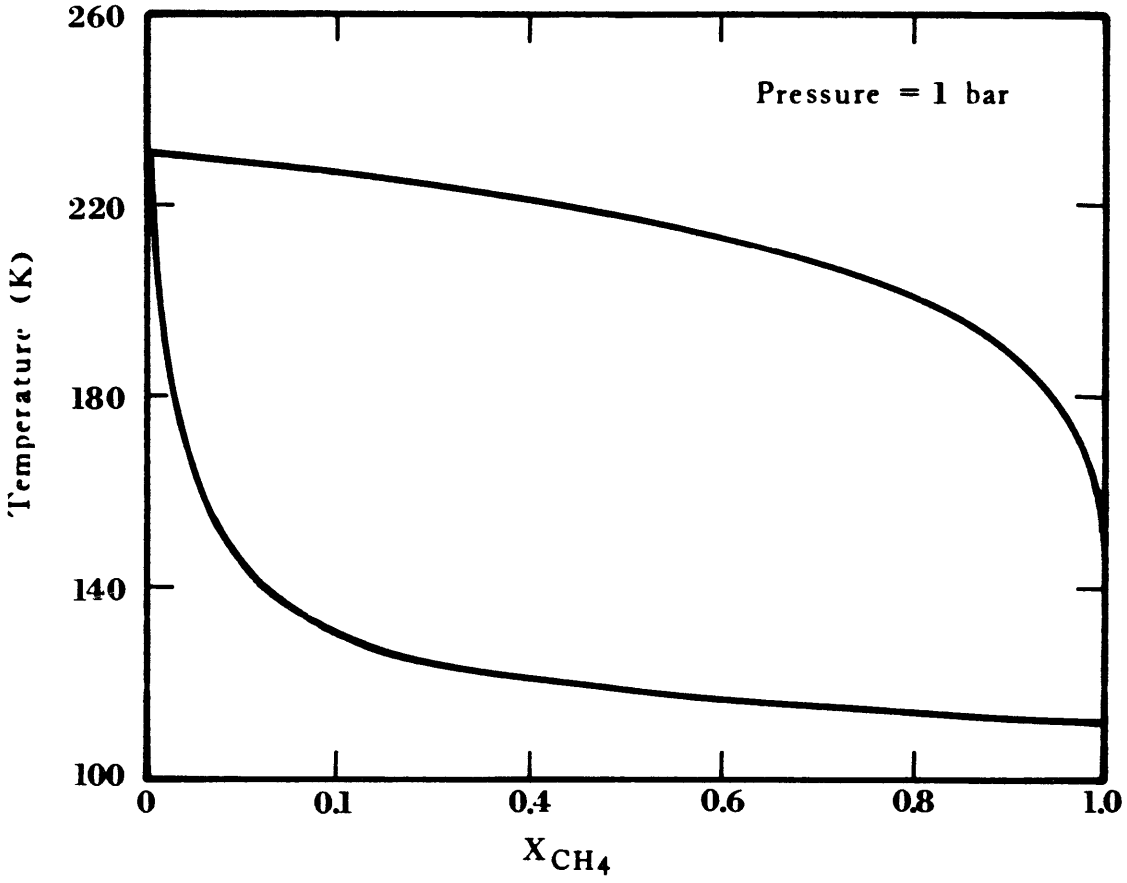

Figure 4-13 Temperature Composition Diagram for the Methane-Propane System

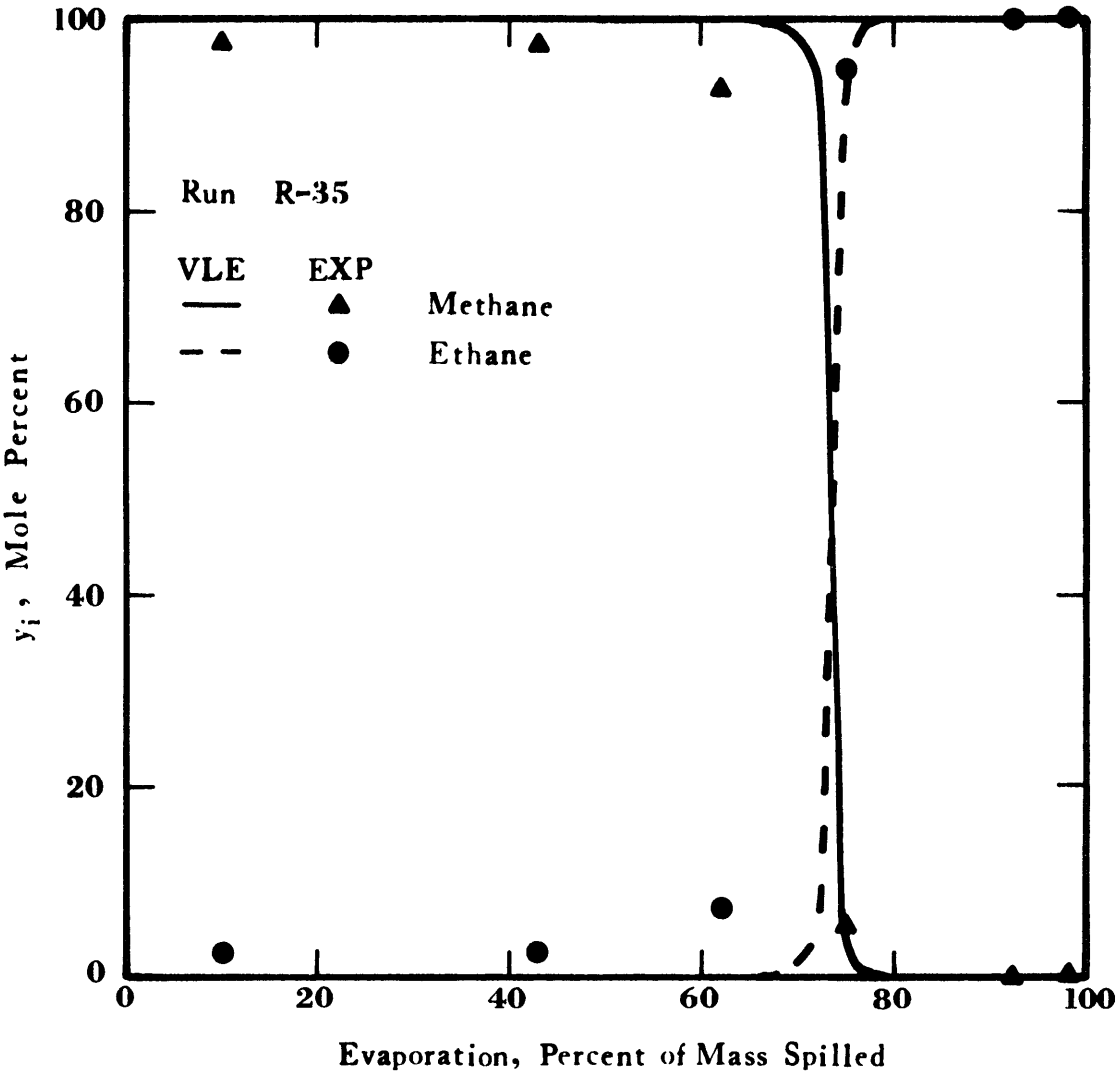

Figure 4-14 Vapor Composition as a Function of Mass Evaporated (83.5% Methane, 16.5% Ethane)

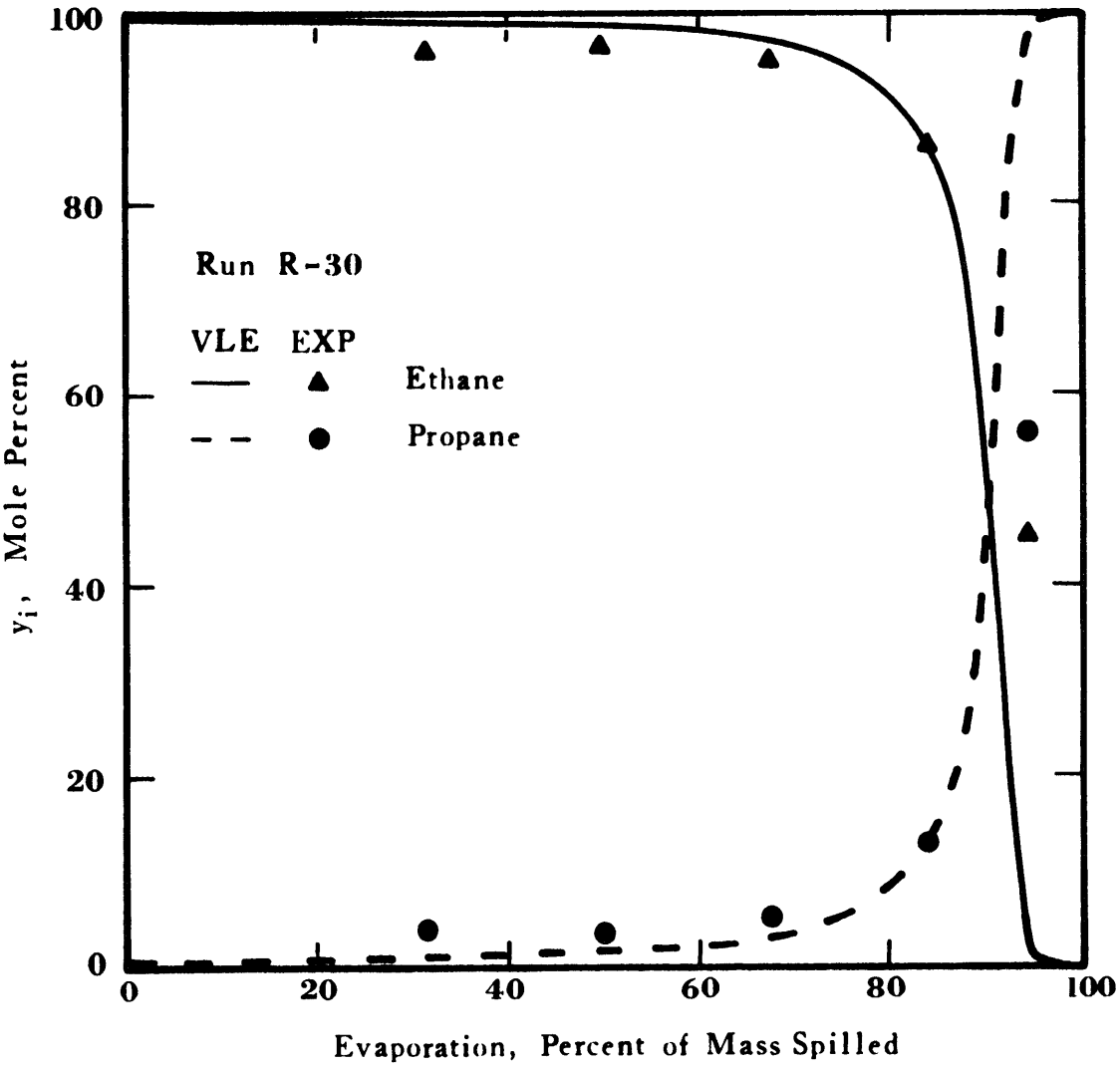

Figure 4-15 Vapor Composition as a Function of Mass Evaporated (89.7% Ethane, 10.3% Propane)

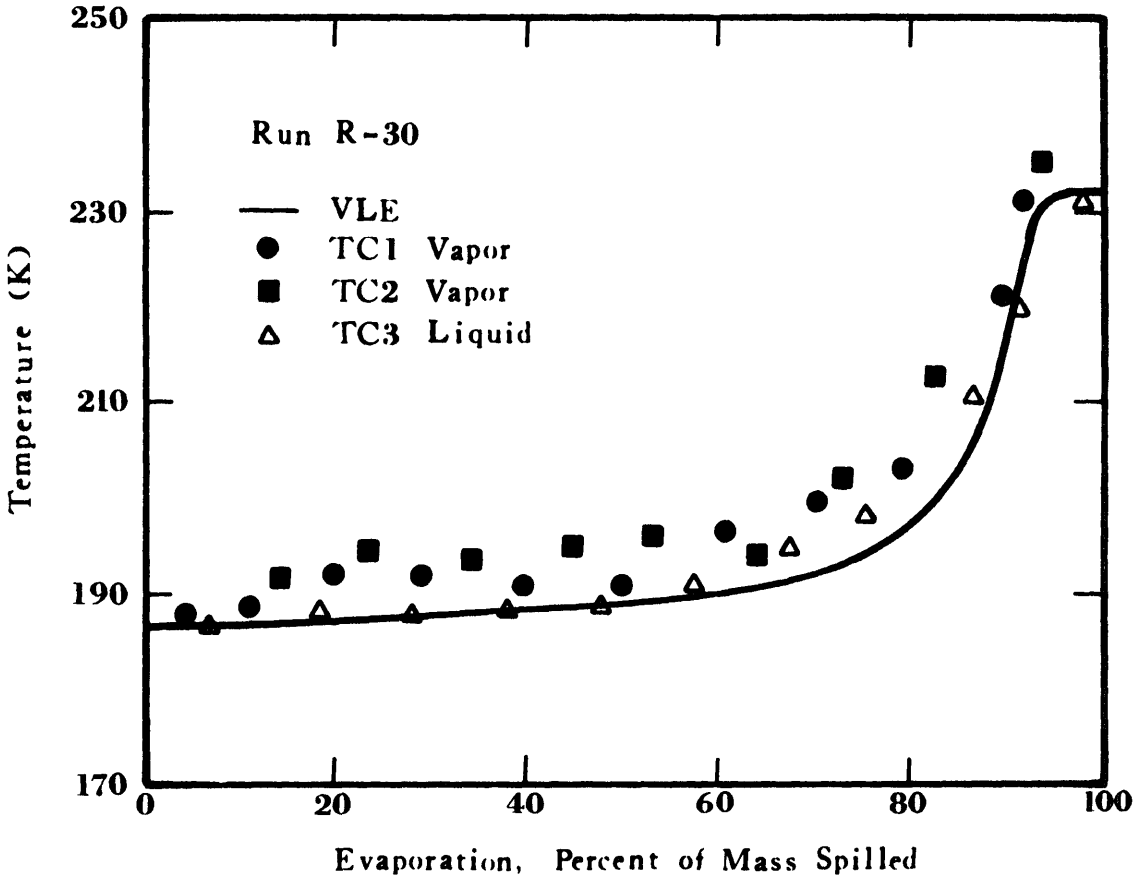

Figure 4-16 Temperature as a Function of Mass Evaporated (89.7% Ethane, 10.3% Propane)

liquid phase, ethane becomes the major component in the vapor although not to the extent of methane (∿100%). Finally, propane becomes the main component in the vapor. The transition from ethane to propane is a more progressive one than the transition from methane to ethane.

Similarly, the initial temperatures are close to the saturation point of methane. Upon exhaustion of methane in the liquid, the saturation temperature rises sharply to the vicinity of the ethane boiling point. Finally, when ethane is exhausted a second, more gradual rise to the propane boiling point is expected.

The vapor compositions for the ternary mixtures and the saturation temperatures, whenever measured, are given in Figures 4-17 through 4-29.

The agreement between the experimental data and the predictions made with the VLE model are excellent. Thus, it can be concluded that during the evaporation of LNG on water, the vapor is in equilibrium with the residual liquid, and the saturation temperature of this residual liquid can be predicted from vapor-liquid equilibria considerations.

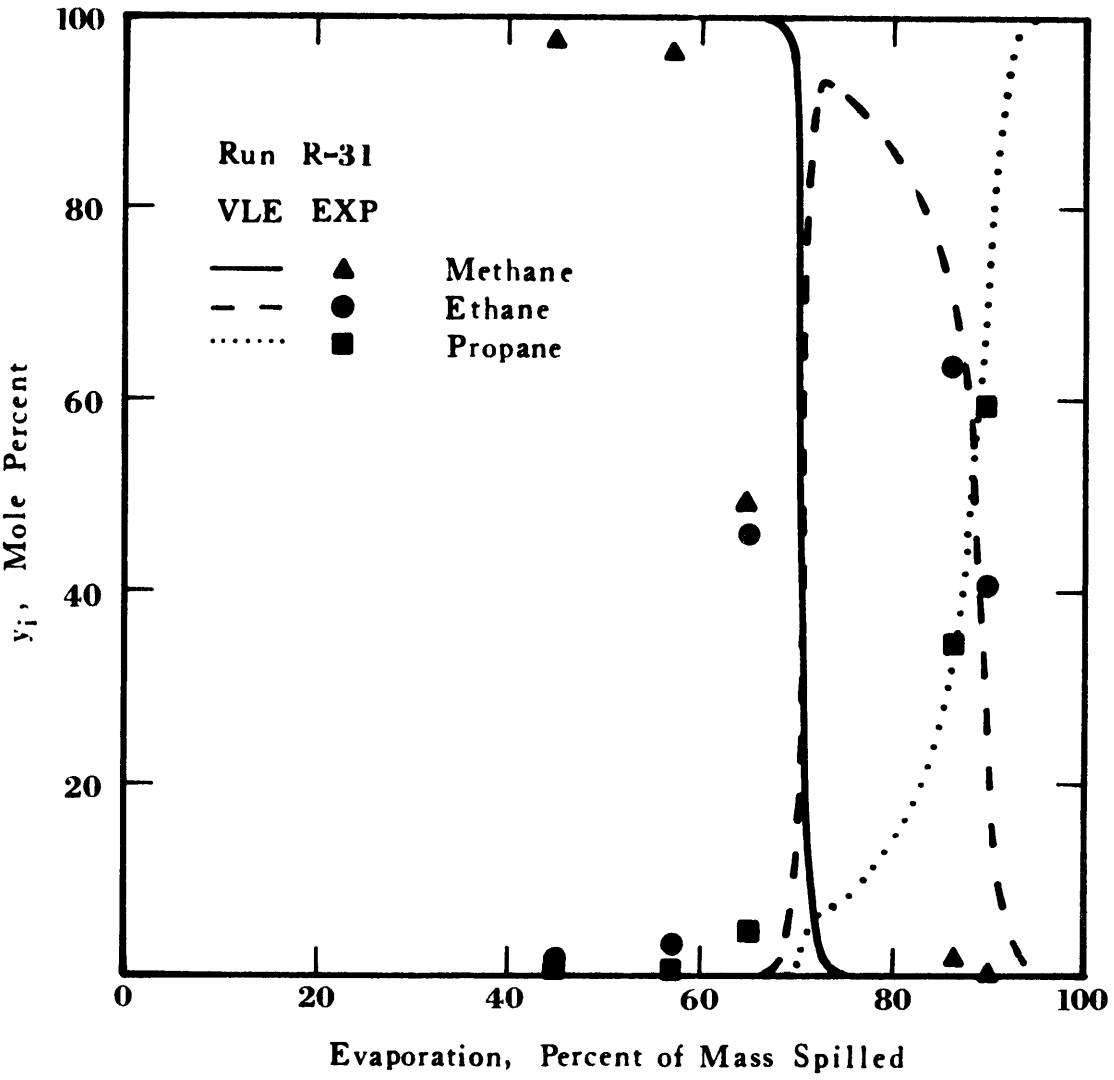

Figure 4-17 Vapor Composition as a Function of Mass Evaporated (84.0% Methane, 9.4% Ethane, 6.6% Propane)

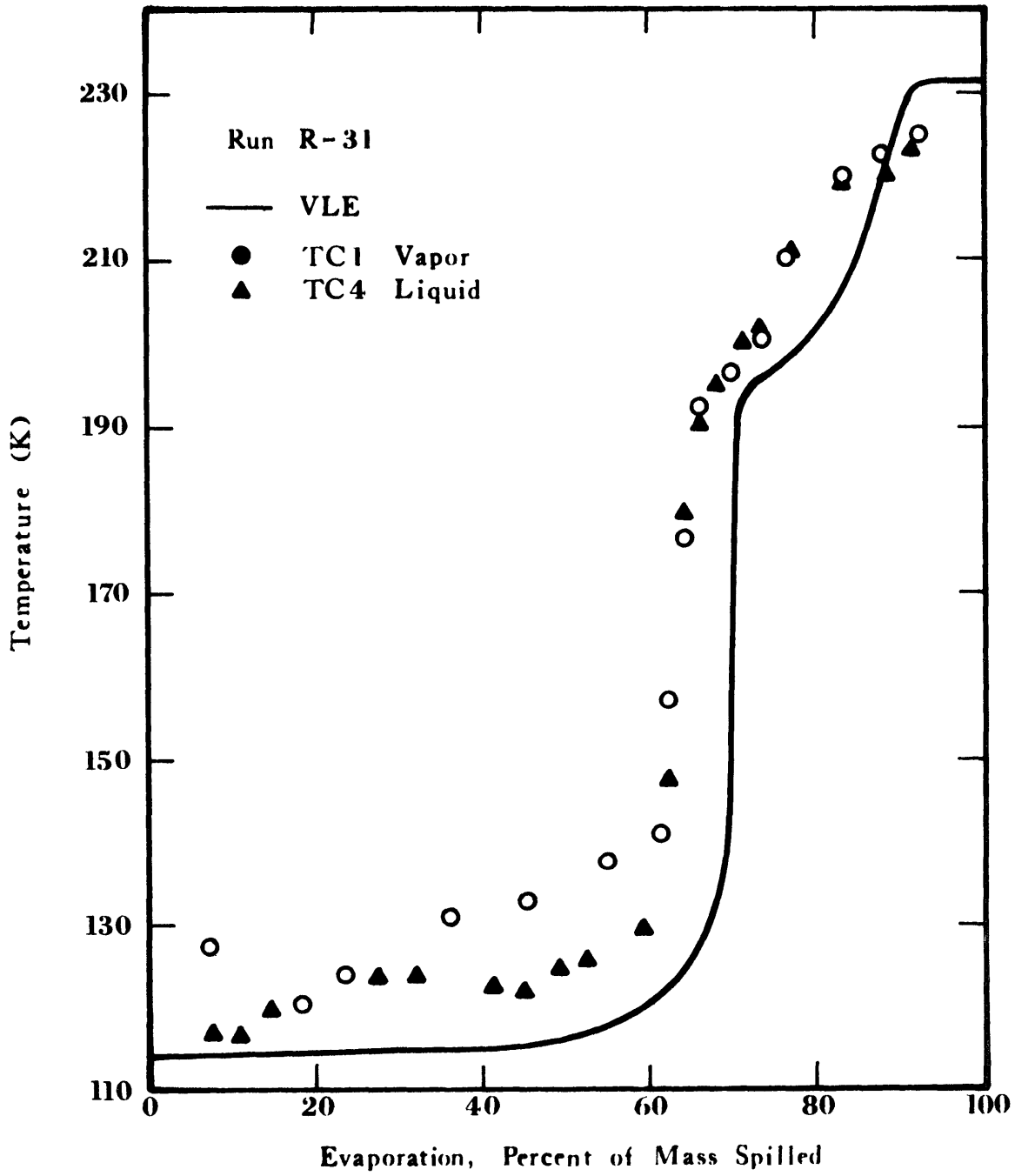

Figure 4-18 Temperature as a Function of Mass Evaporated (84.0% Methane, 9.4% Ethane, 6.6% Propane)

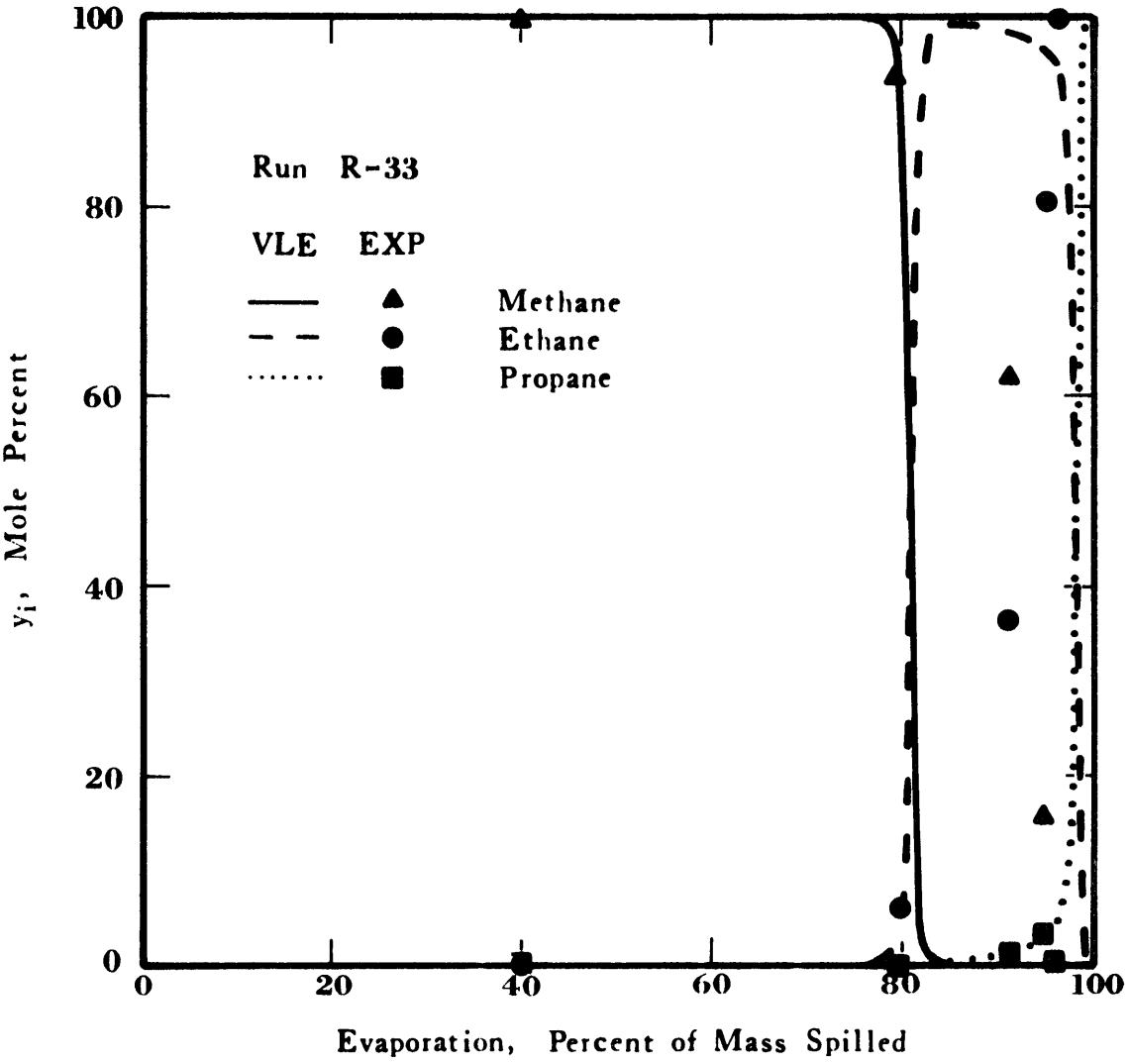

Figure 4-19 Vapor Composition as a Function of Mass Evaporated (88.9% Methane, 10.2% Ethane, 0.9% Propane)

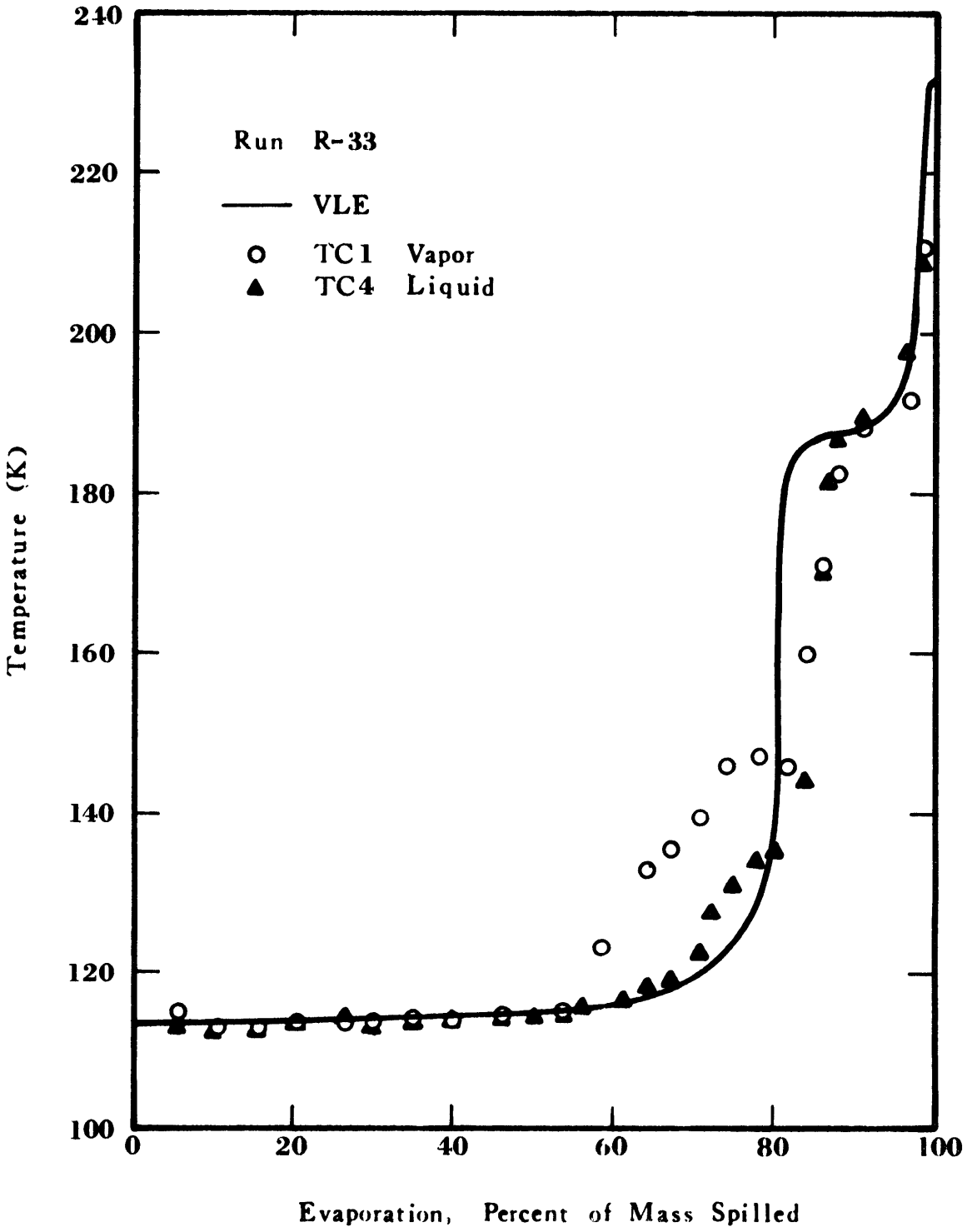

Figure 4-20 Temperature as a Function of Mass Evaporated (88.9% Methane, 10.2% Ethane, 0.9% Propane)

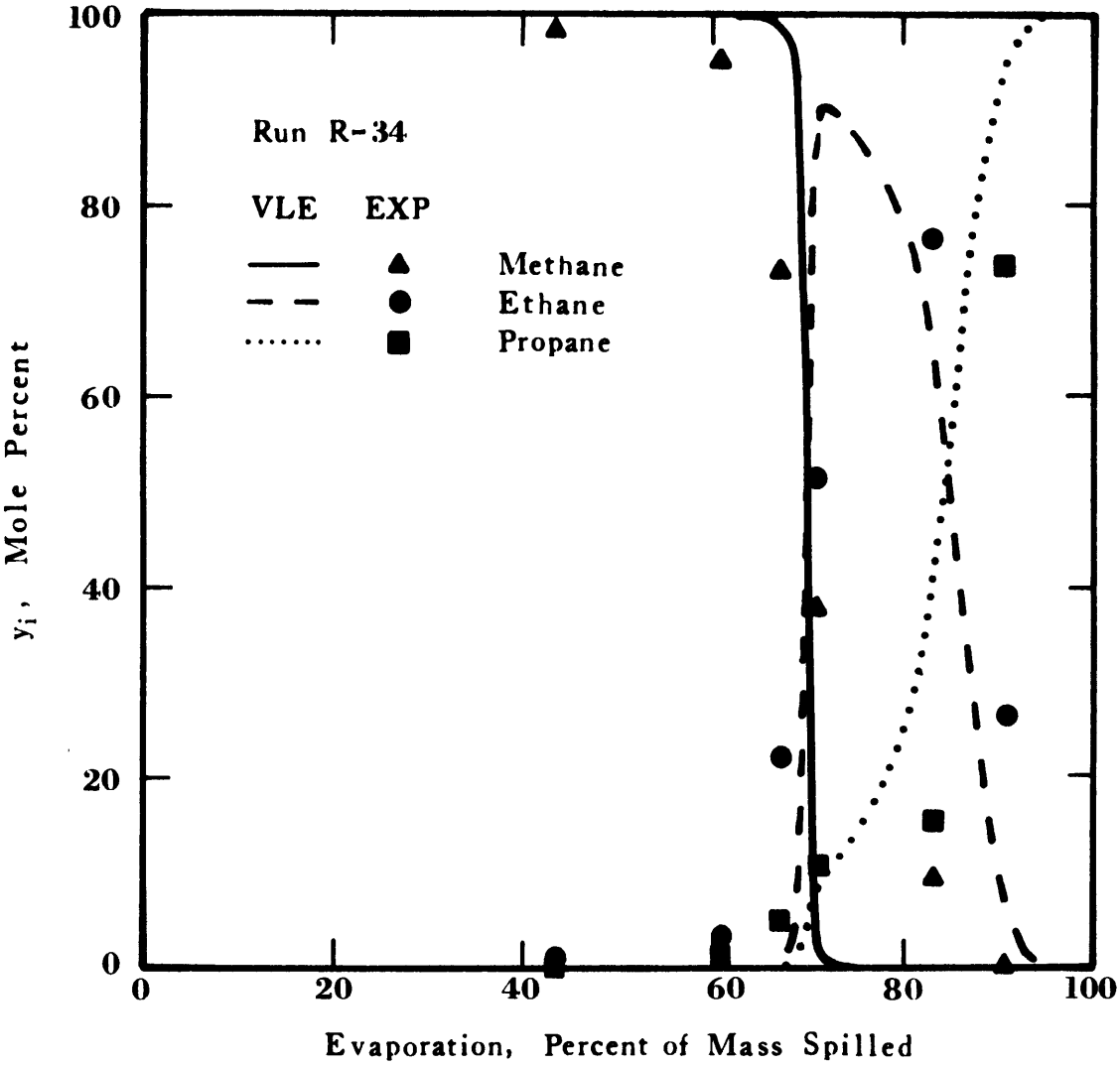

Figure 4-21 Vapor Composition as a Function of Mass Evaporated (83.9% Methane, 8.1% Ethane, 8.0% Propane)

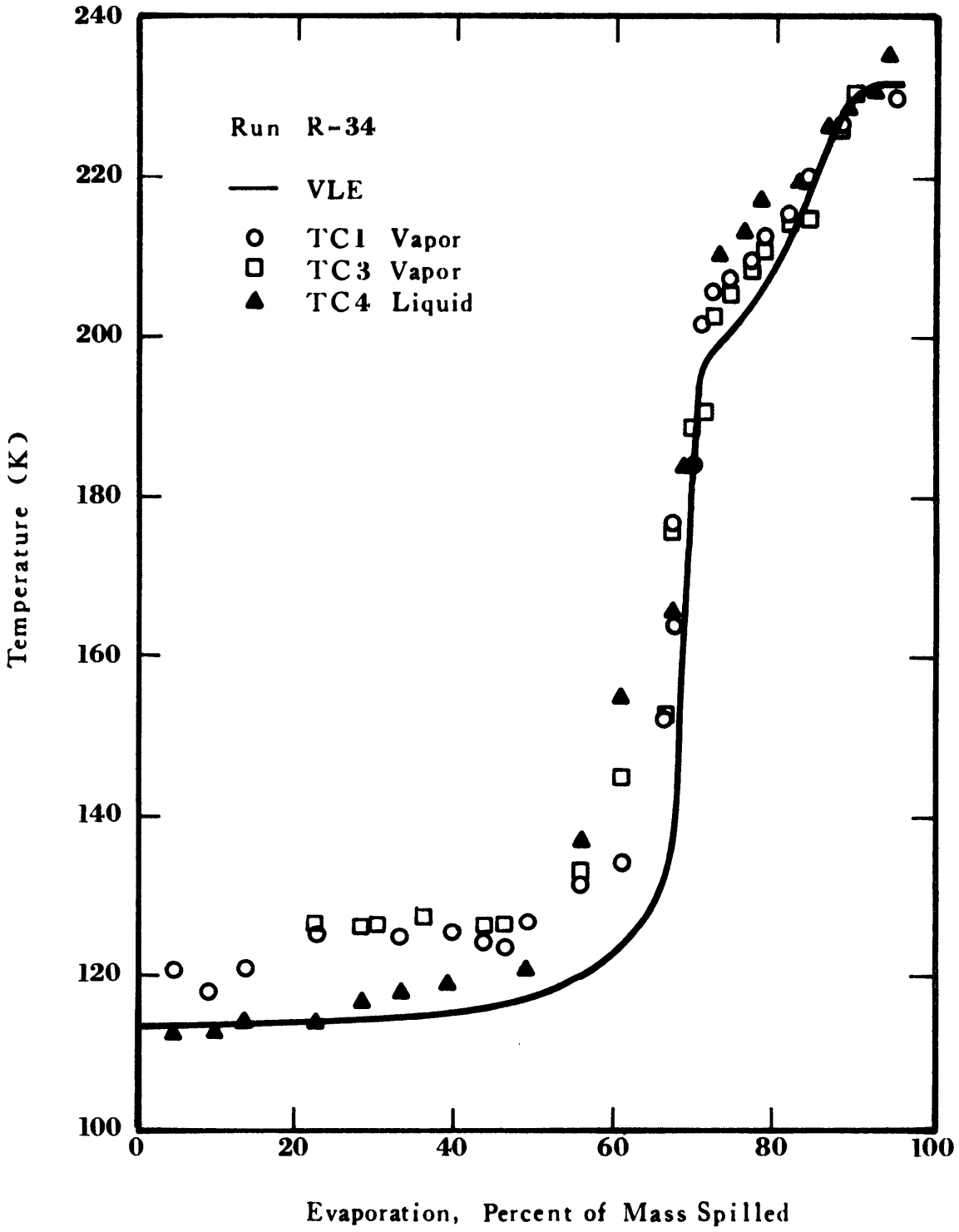

Figure 4-22 Temperature as a Function of Mass Evaporated (83.9% Methane, 8.1% Ethane, 8.0% Propane)

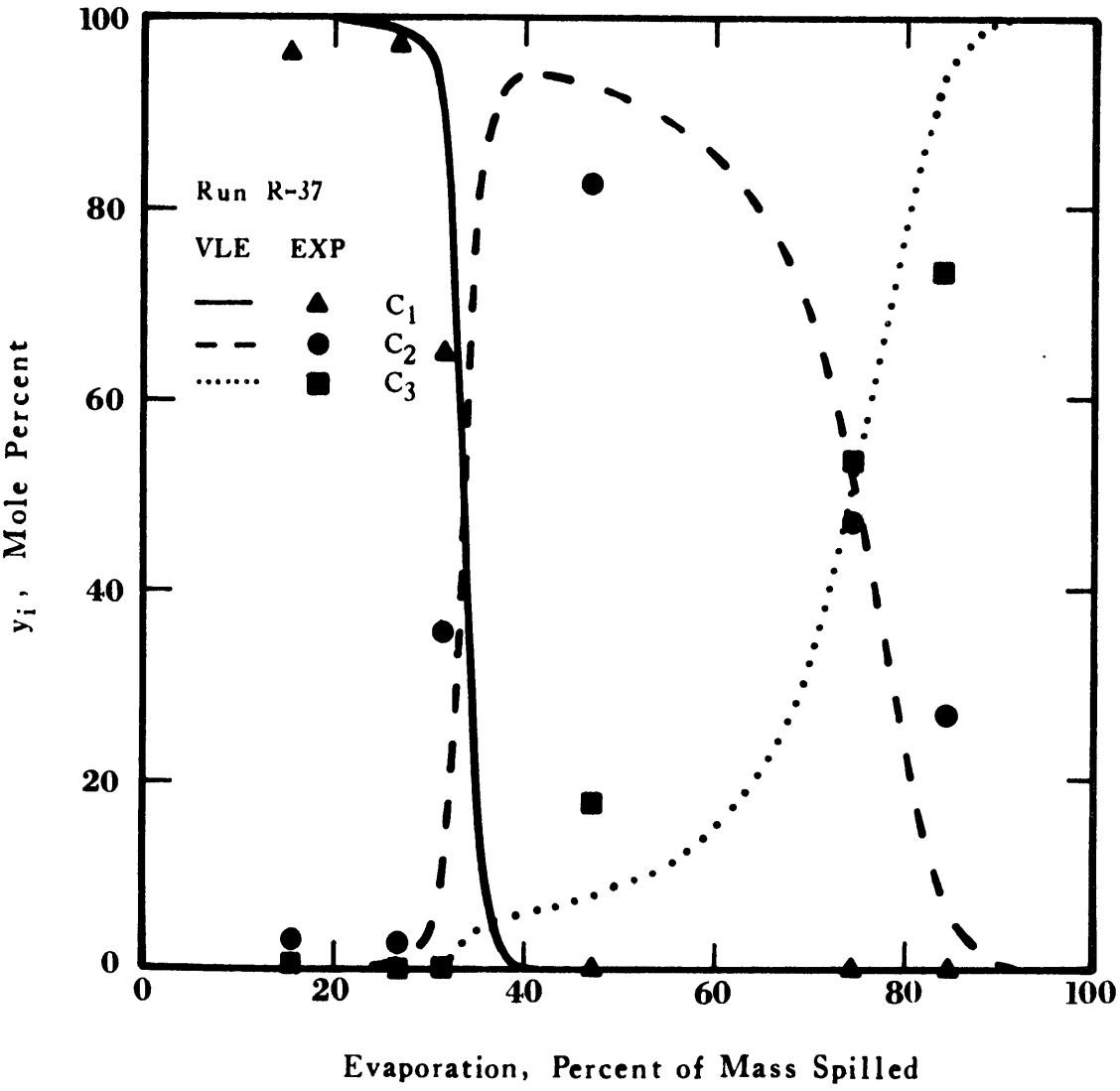

Figure 4-23 Vapor Composition as a Function of Mass Evaporated (51.8% Methane, 30.0% Ethane, 18.2% Propane)

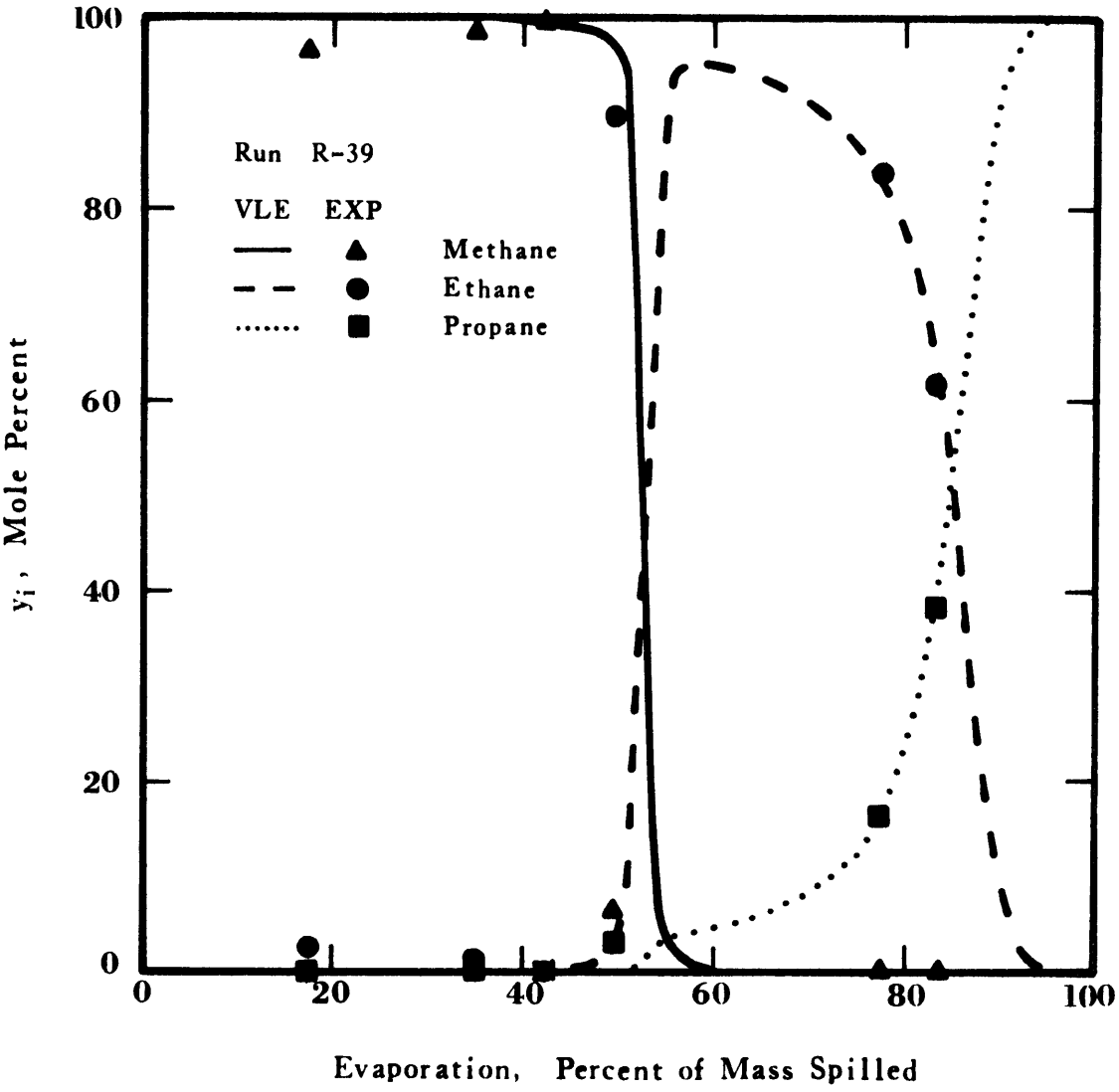

Figure 4-24 Vapor Composition as a Function of Mass Evaporated (70.1% Methane, 20.5% Ethane, 9.4% Propane)

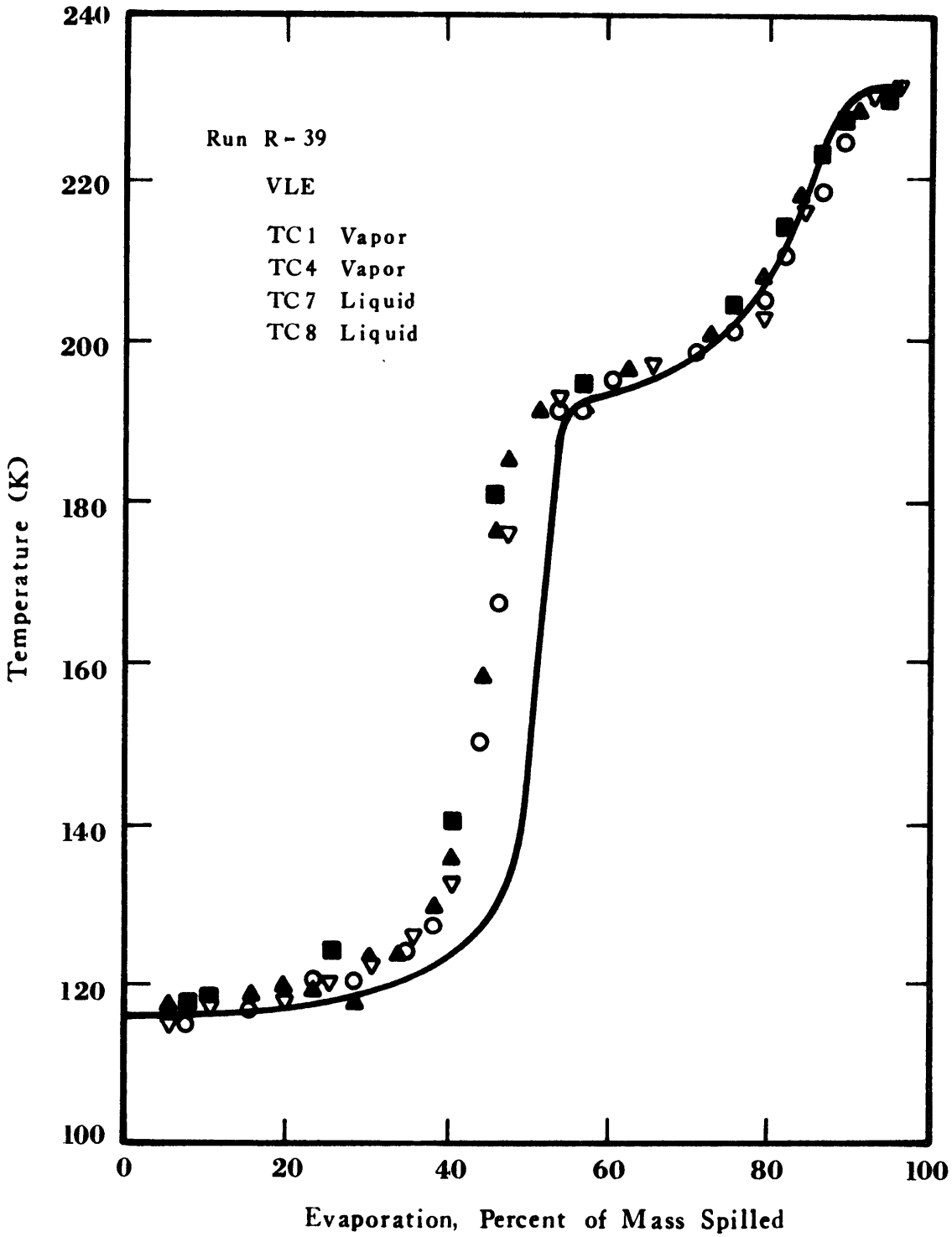

Figure 4-25 Temperature as a Function of Mass Evaporated (70.1% Methane, 20.5% Ethane, 9.4% Propane)

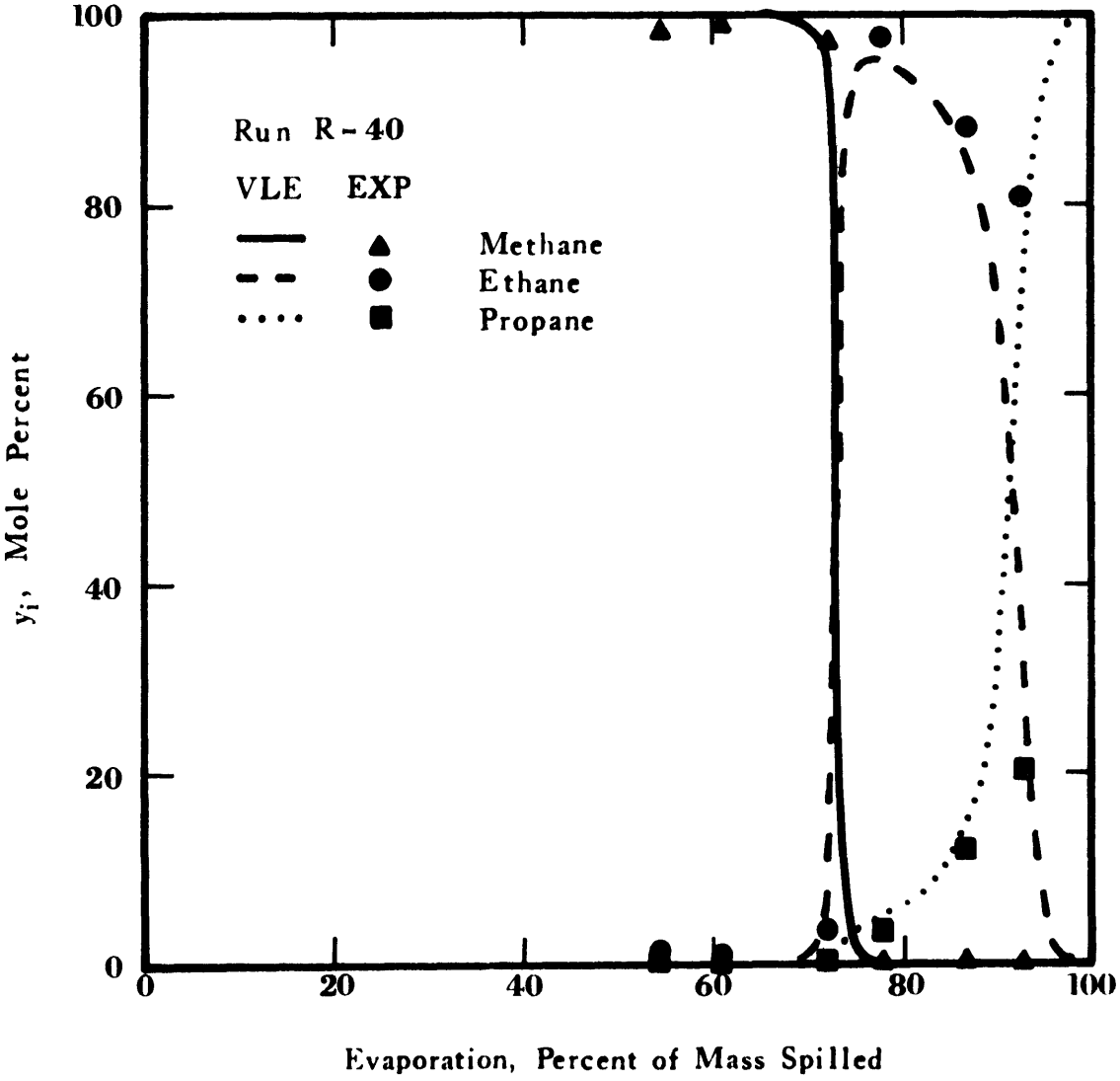

Figure 4-26 Vapor Composition as a Function of Mass Evaporated (85.2% Methane, 10.1% Ethane, 4.7% Propane)

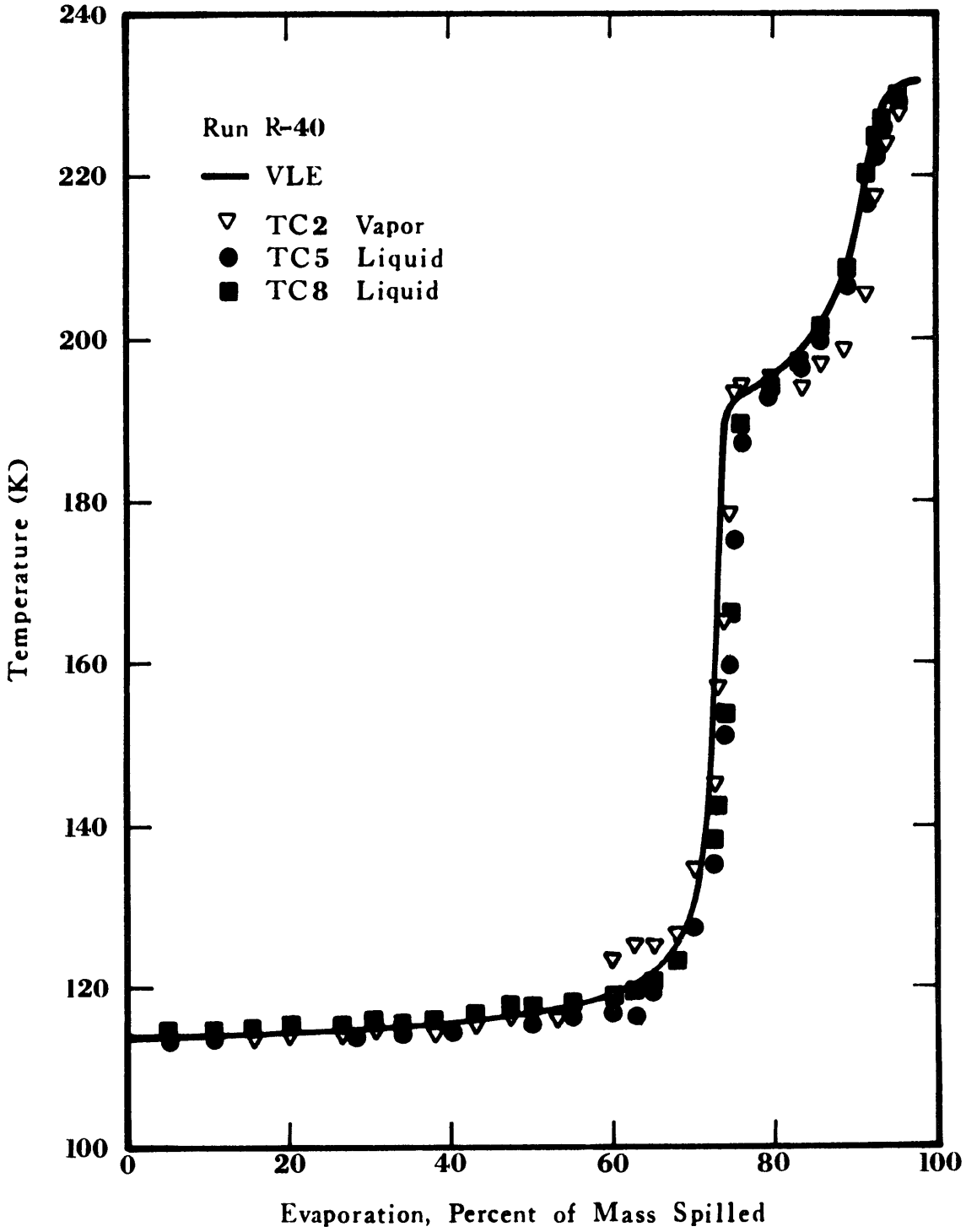

Figure 4-27 Temperature as a Function of Mass Evaporated (85.2% Methane, 10.1% Ethane, 4.7% Propane)

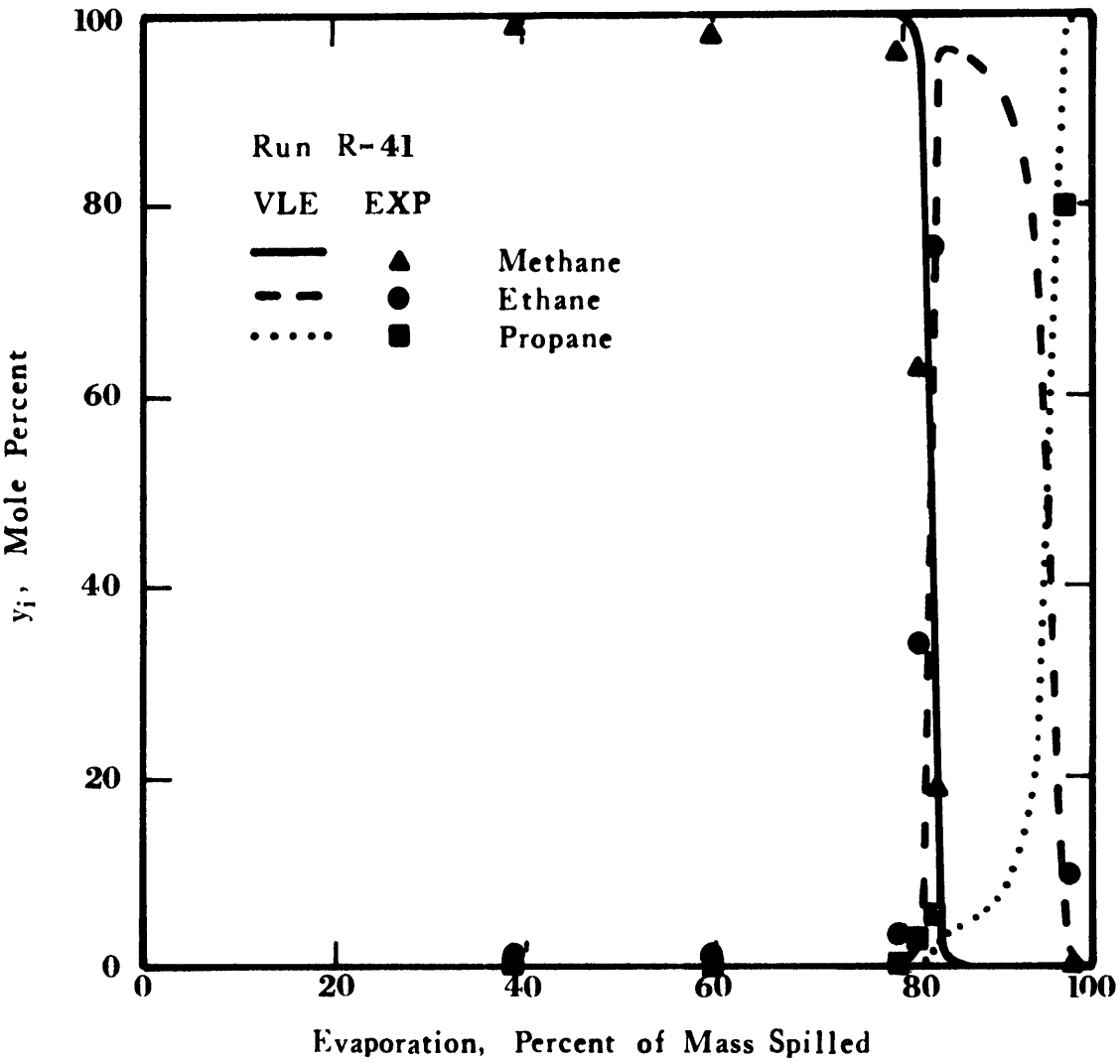

Figure 4-28 Vapor Composition as a Function of Mass Evaporated (91.0% Methane, 6.5% Ethane, 2.5% Propane)

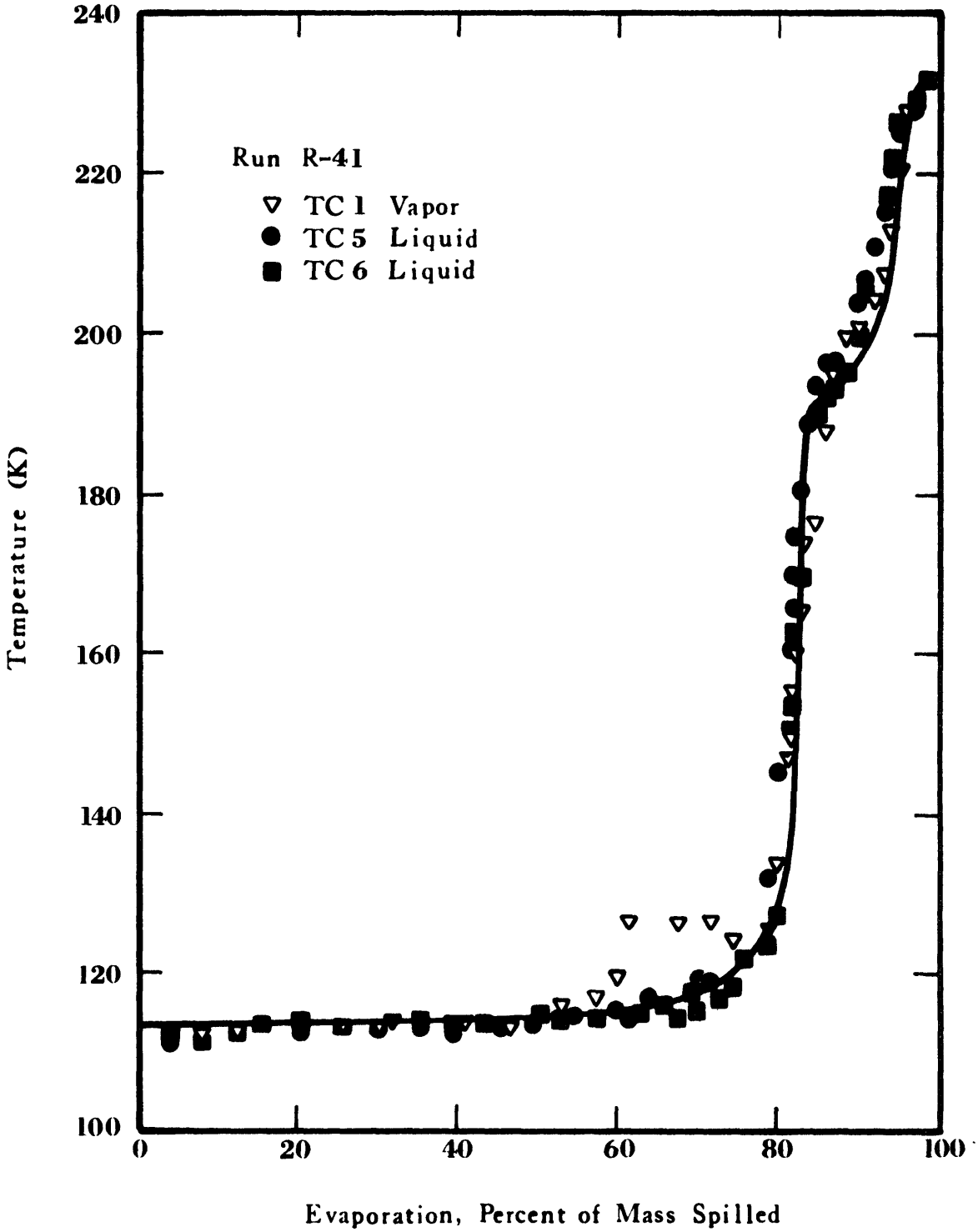

Figure 4-29 Temperature as a Function of Mass Evaporated (91.0% Methane, 6.5% Ethane, 2.5% Propane)

V. BOILING OF LNG ON WATER

Previous studies (Burgess et al., 1970, 1972; Boyle and Kneebone, 1973; Jeje, 1974) on the boiling of LNG on water gave a clear indication that the evaporation characteristics of LNG were a strong function of chemical composition. It was claimed that addition of heavier hydrocarbons to methane caused a significant increase in the rate of evaporation of the cryogen. Yet the phenomenon itself was not clearly understood. It is the purpose of the present work to elucidate such observations.

Results

The equipment and procedure described in Chapter III were utilized to carry out experiments. Pure hydrocarbons, methane, ethane and propane were spilled on water and the mass evaporated was recorded as a function of time. Similarly, tests were carried out with binary mixtures of methane-ethane and ethane-propane and with ternary mixtures of methane-ethane-propane. Finally, the effect of small amounts of nitrogen added to methane and LNG was also studied.

Methane

Ten spills of methane on water were performed. The experimental conditions for these tests are given in Table 5-1. The mass of methane evaporated as a function of time is shown in Figure 5-1. It can be seen that methane evaporated slowly at first, then the rate of evaporation increased reaching a peak after about 40 seconds. A plot of

TABLE 5-1

Experimental Conditions for Methane Spills

Test	Mass Spilled (g/cm^2)	Initial Water Temperature (K)	Area (cm^2)
T-8*	0.35	292.	139
T-9*	**	291.	139
R-6	0.48	294.	139
R-7	0.55	294.	139
R-8	0.42	294.	139
R-42	1.08	288.	143
R-43	1.79	288.	143
R-44	1.66	288.	143
R-46	2.54	288.	143
R-47	1.71	284.	143

*C. P. Grade Methane. All others U.H.P. Grade Methane.

**Possible external contact of boiling vessel at spill time resulted in an unknown spill mass.

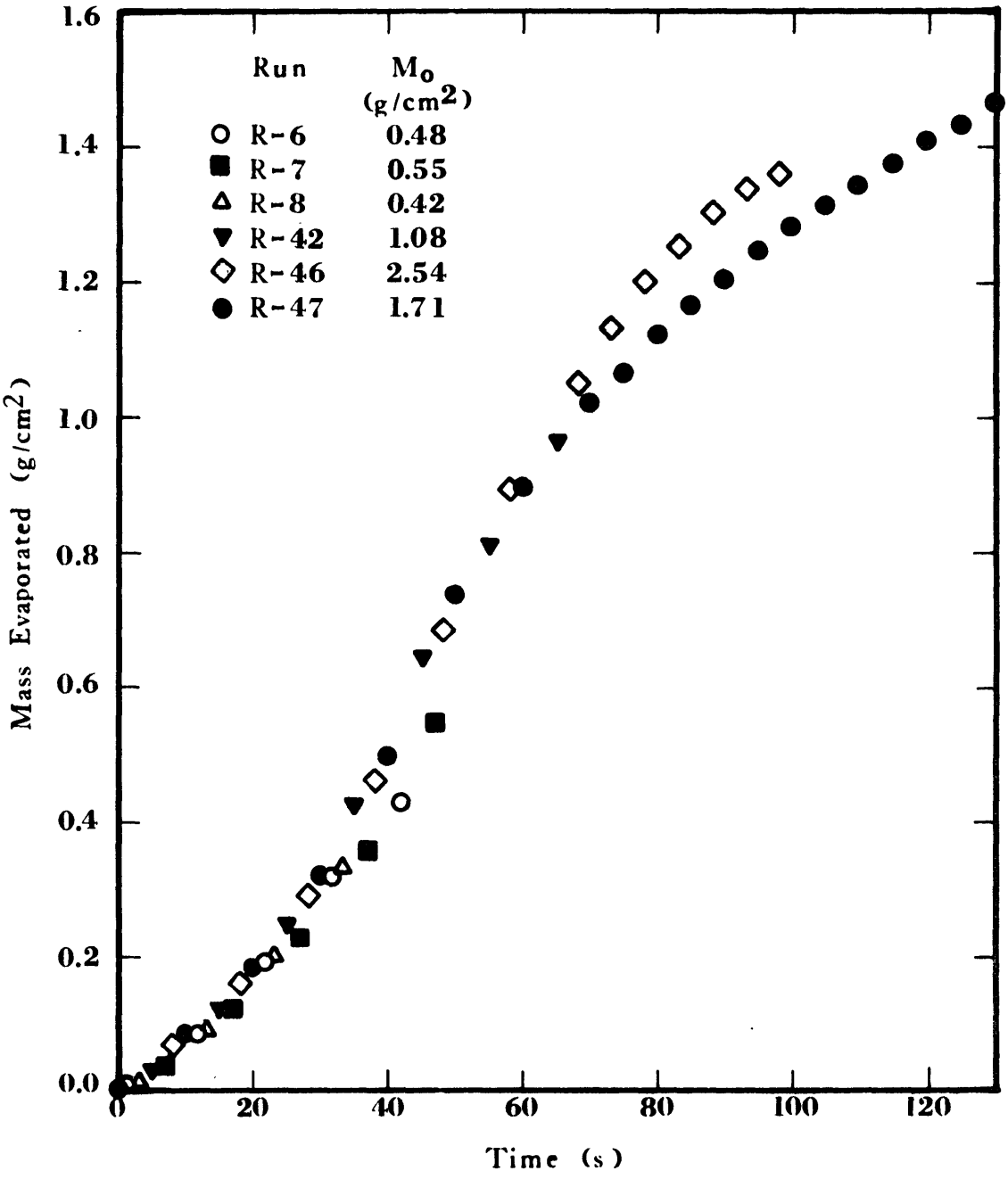

Figure 5-1 Mass Evaporated for Methane Boiling on Water

boiling rates as a function of time, Figure 5-2, reveals this behavior more clearly.

Boiling of methane on water took place in a smooth fashion; ice patches began to form after a few seconds (∿5 s) and these grew radially, eventually covering the whole water surface (∿20 s). The upper side of the ice layer was uniform but the bottom side had some concavities, as shown in the following illustration.

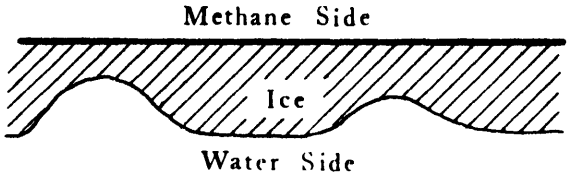

Apparently, as the ice began to cover a significant portion of the water surface, any methane that seeped through small cracks in the ice vaporized and was released through those areas still uncovered by ice. Thus as the ice already formed continued to grow, ice formation and growth was delayed in these weak spots. The fact that some methane seeped through cracks was corroborated by two observations. First, the ice attached itself to the walls very tightly, effectively sealing in the water. Later in the tests the thin inner walls were seen to bulge out. This could be caused by the methane evaporating under the ice crust or by the difference in density between ice and water. Since the ice had been attached to the wall, it could only grow downward. Second, in tests R-43 and R-44 the feed hose located at the bottom of the container was attached to the side of the container to a height higher than the water level and left open to the atmosphere.

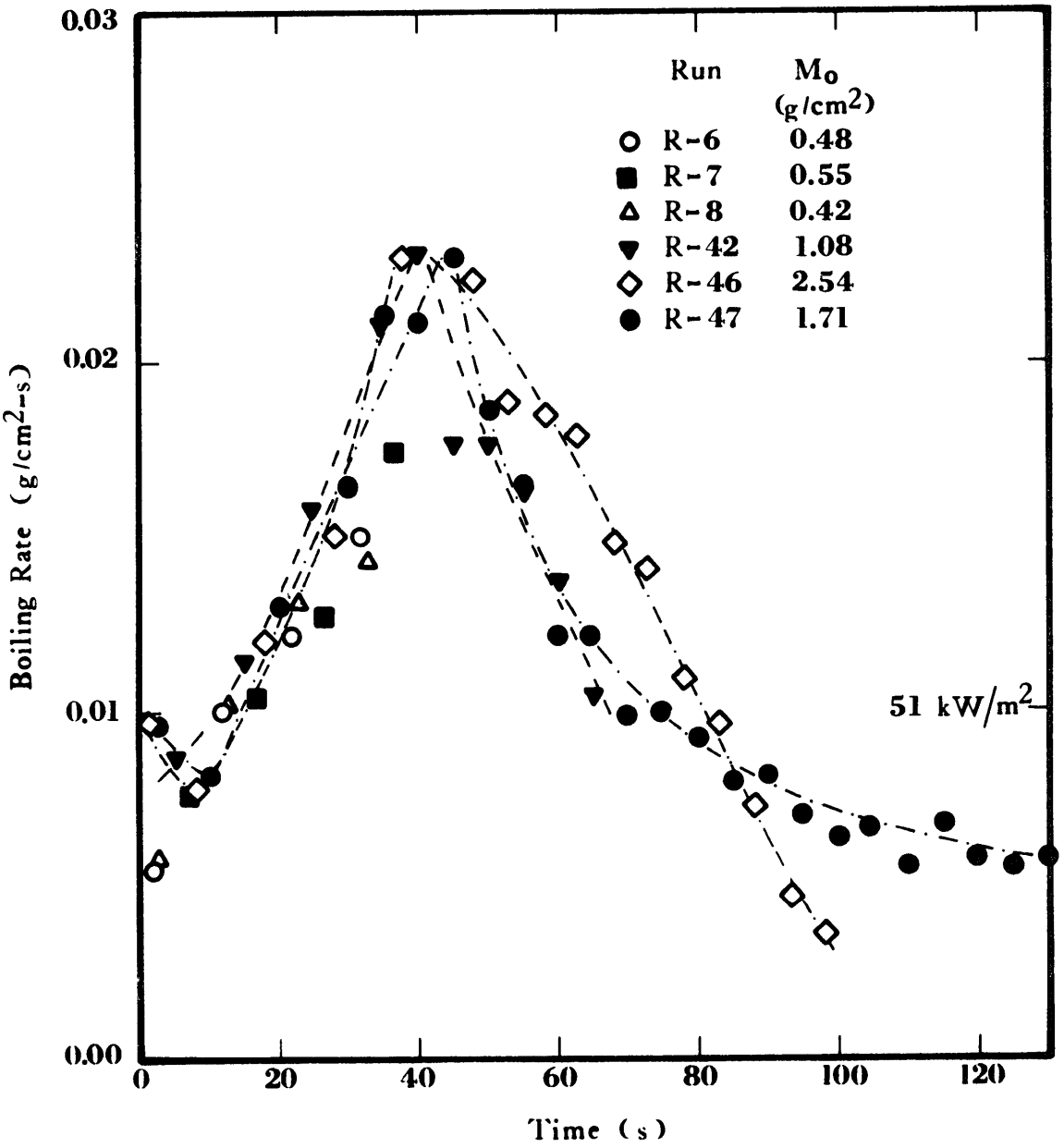

Figure 5-2 Boiling Rates for Methane

After about 100 seconds, the water level in the hose increased and eventually poured out of the hose. Although a syphon breaker was placed at the highest point in the hose, and a gap had developed between the ice and the water, the water continued to drain. Obviously, methane was seeping through the ice and upon evaporation on the water it developed some pressure between the ice and water layer that forced the water out of the container.

The size of the methane vapor bubbles was roughly 0.3-0.5 cm; these bubbles rose quickly through the boiling liquid. No foam was observed.

Ethane

Eight spills of ethane on water were carried out. The experimental conditions are given in Table 5-2. The mass of ethane evaporated as a function of time is shown in Figure 5-3. The initial boiling rates (and heat fluxes) were higher than those for methane. As in the case of methane, the boiling rates increased with time reaching a peak between 10 to 25 seconds as can be seen in Figure 5-4. Subsequently, the boiling rates decreased significantly; in fact, after about 50 seconds the <u>total mass</u> of methane evaporated became higher than that for ethane. When comparing boiling rates and mass evaporated, one should keep in mind the corresponding heats of evaporation. In this case for methane it is 510 kJ/kg and for ethane 489 kJ/kg. Thus, for the same heat flux the mass of ethane evaporated should be about 5% higher than that for ethane.

TABLE 5-2

Experimental Conditions for Ethane Spills

Test	Mass Spilled (g/cm^2)	Initial Water Temperature (K)	Area (cm^2)
T-13	0.50	284.	139
T-14	0.40	293.	139
T-15	0.91	292.	139
T-16	1.08	293.	139
R-32	0.81	289.	143
R-53	2.01	295.	143
R-62	1.17	287.	143
R-63	1.73	287.	143

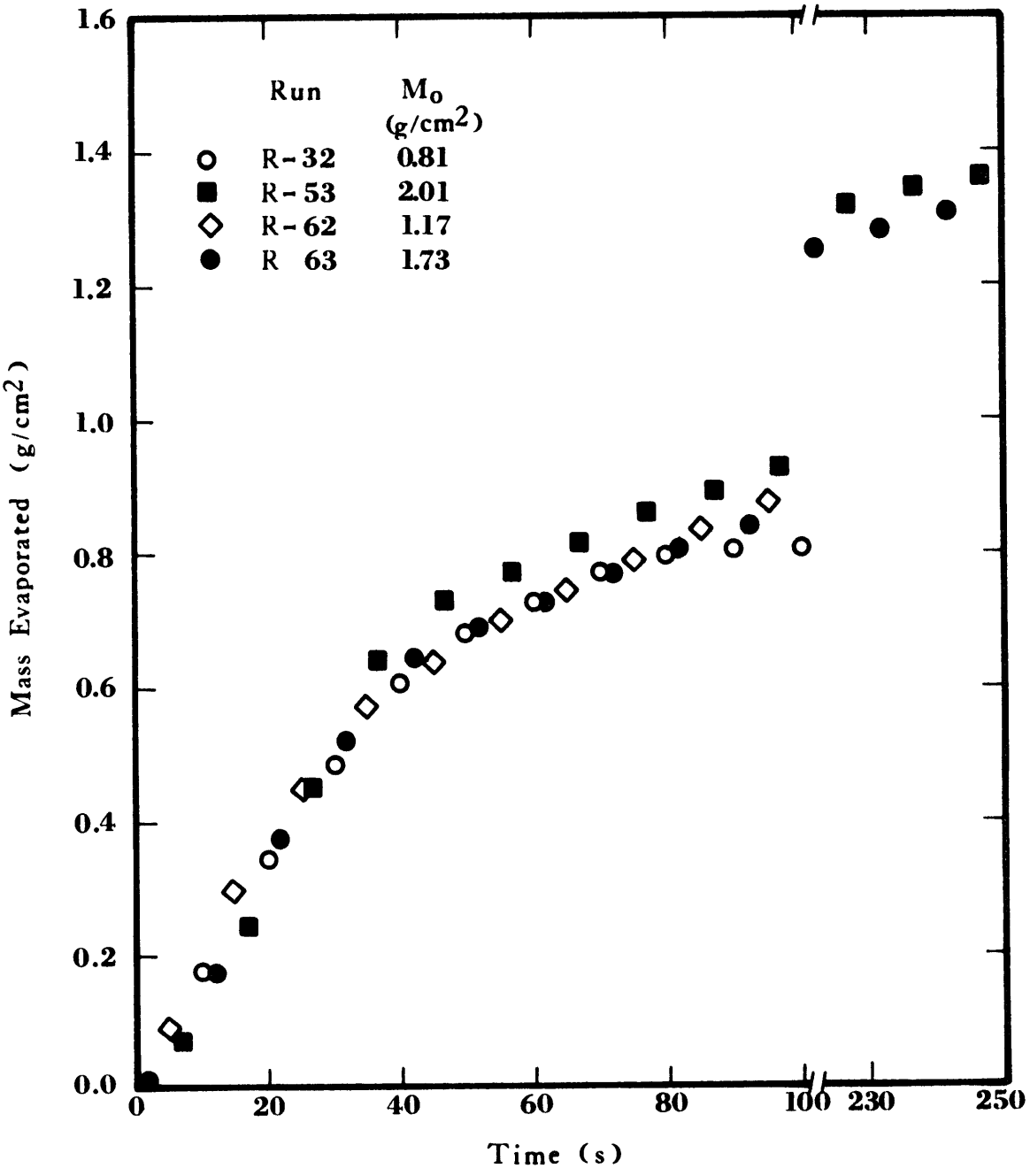

Figure 5-3 Mass Evaporated for Ethane Boiling on Water

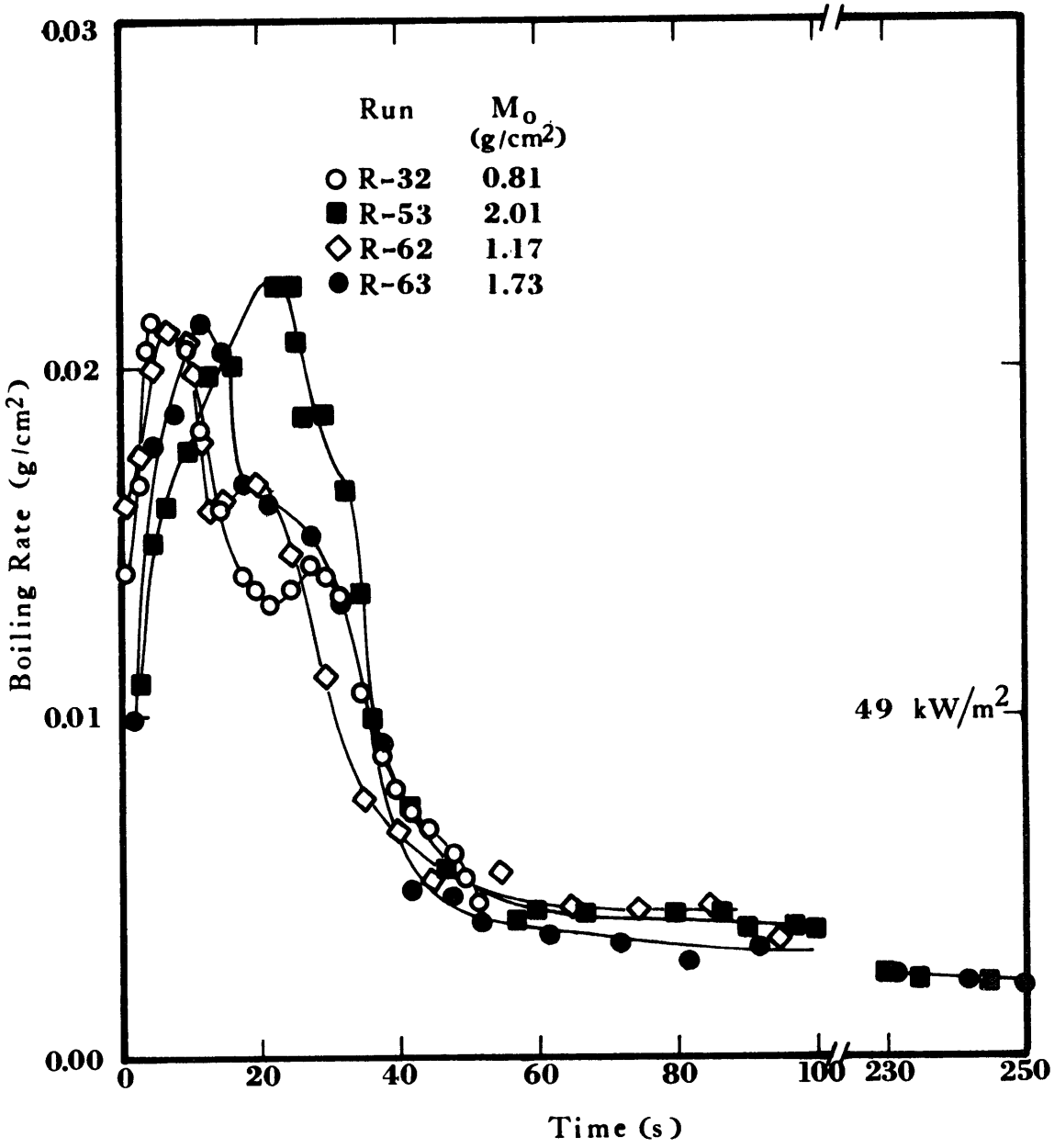

Figure 5-4. Boiling Rates for Ethane

Ice formation took place at a faster rate than in the case of methane. Usually the water surface was covered with ice within 10 seconds. The ice is highly irregular. It appeared that the rapid initial evaporation of ethane caused some water to be splashed up; as it contacted the bulk of ethane it froze in an irregular fashion. Again, the water side of the ice had a shape similar to the ice formed in methane spills. Furthermore, it seemed as though, later in the tests, ethane seeped through some cracks in the ice, evaporated and "erupted" through weak ice spots. This was observed in about a third of the tests.

Bubble formation and growth was bimodal. Large, 0.5 to 1.0 cm, and small ($\sim$2 mm) bubbles were formed. Later in the run the formation of the small bubbles became predominant.

One test, R-62, was carried out with research purity grade ethane (minimum purity, 99.96%). It essentially overlapped with tests made with certified purity grade ethane (minimum purity, 99%). These results indicate that the effect of impurities present in the C.P. grade ethane on the boiling of ethane on water is not significant.

Propane

Four spills of propane on water were made. The experimental conditions for these tests are given in Table 5-3. The total mass evaporated as a function of time is shown in Figure 5-5. Propane boiled very rapidly during the first few ($\sim$5) seconds. The boiling rates then dropped to considerably lower values as can be seen in Figure 5-6.

TABLE 5-3

Experimental Conditions for Propane Spills

Test	Mass Spilled (g/cm^2)	Initial Water Temperature (K)	Area (cm^2)
T-10	0.55	296.	139
T-11	0.63	295.	139
R-48	1.33	288.	143
R-49	2. *	289.	143

*Exact mass spilled unknown due to splashing of propane.

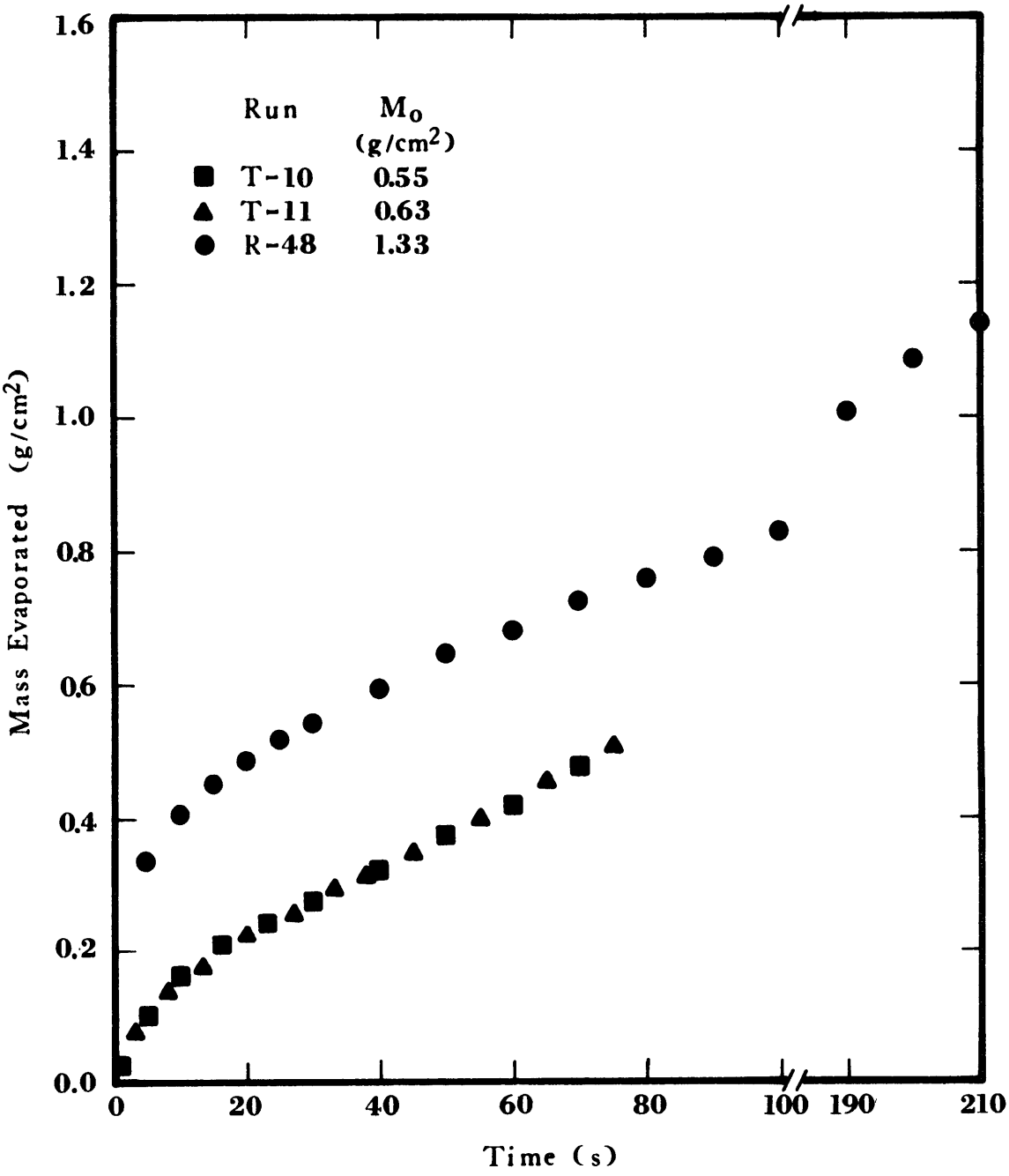

Figure 5-5 Mass Evaporated for Propane Boiling on Water

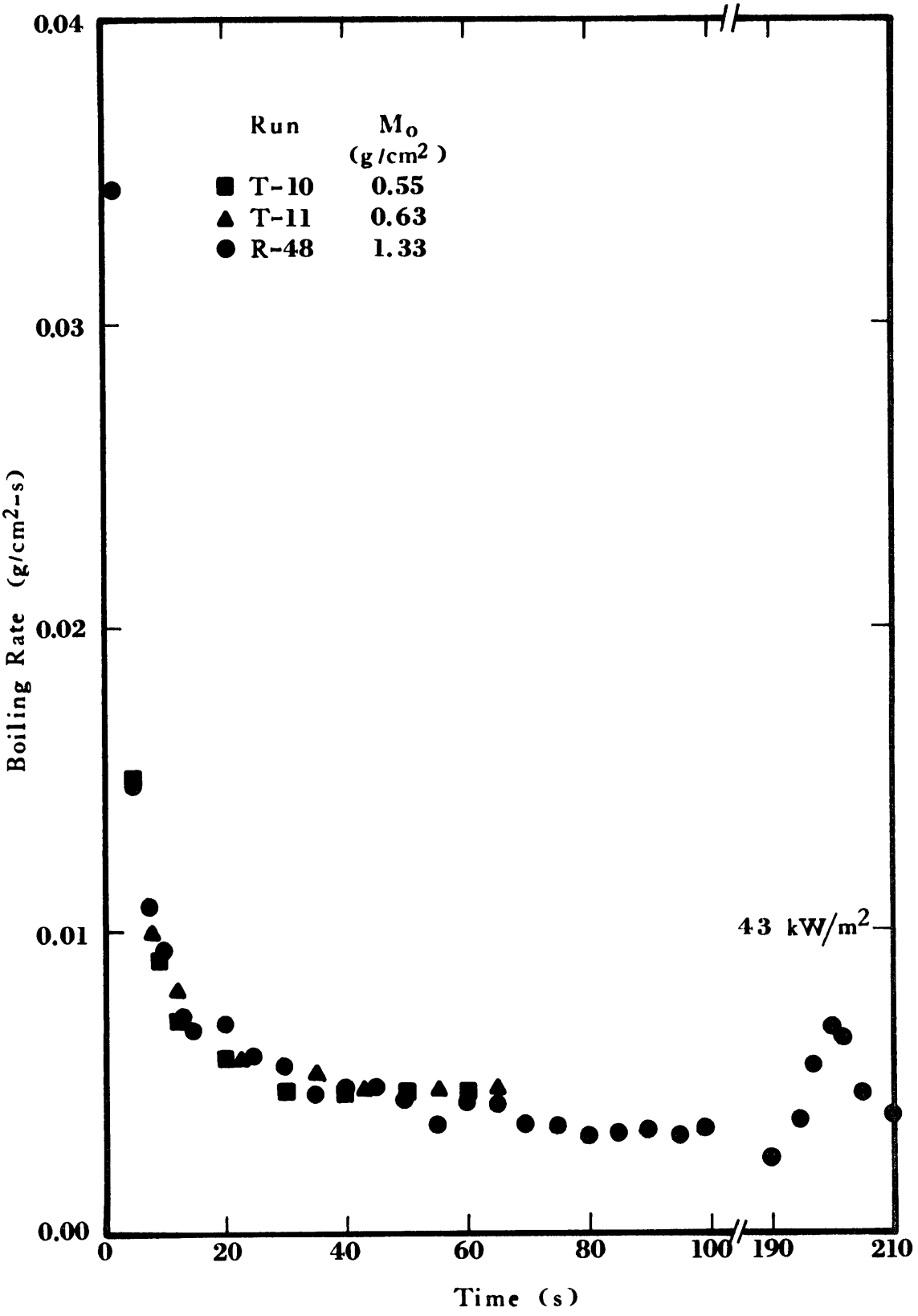

Figure 5-6 Boiling Rates for Propane

Upon contacting the water, propane boiled violently, splashing water that froze as it contacted the bulk of the liquid propane. In test R-49, splashing was so severe that water and propane were ejected from the boiling vessel; the ice reached well above the vapor thermocouple assembly, approximately 10 cm high. Once this very irregular ice completely covered the water surface, boiling became very smooth and calm. As in the case of ethane, propane occasionally seeped through cracks in the ice, with the vapors erupting through weak spots. This phenomenon manifests itself in the form of a small, but distinct, increase in boiling rate. Test R-48 displayed this effect at about 200 seconds (Figure 5-6).

Nitrogen

Initial equipment tests were made with liquid nitrogen for convenience due to its availability. It is interesting to note that the boiling rate for nitrogen decreased with time as opposed to those for methane which increased up to a certain time. Furthermore, the evaporation of nitrogen on water is strongly dependent on the amount spilled. For a spill of 0.68 g/cm^2, 0.34 g/cm^2 were evaporated in 30 s and 0.57 g/cm^2 in 60 s, whereas for a spill of 1.64 g/cm^2 the mass evaporated in the same time intervals was 0.57 and 1.07 g/cm^2, respectively. Similar observations have been made by Jeje (1974) and Dincer (1975) but a satisfactory explanation for this phenomenon has not been given. This study deals with evaporation of light hydrocarbons and their mixtures; therefore, no further investigation into the evaporation of nitrogen on water was made.

Methane-Ethane Mixtures

Seven spills of methane-ethane mixtures on water were performed. The amount of methane present in the mixtures ranged from 80.3 to 98.5 mole percent. The experimental conditions for these tests are given in Table 5-4. The mass evaporated in these tests as a function of time is given in Figure 5-7. Upon contacting the water, rapid boiling took place. The boiling rate increased with time and reached a peak within 10 to 25 seconds, as can be seen in Figure 5-8. It is important to note that the greater the amount of ethane present, the faster the peak boiling rate was reached.

The water surface was completely covered with ice in about 5 seconds. Although the ice formed was non-uniform in shape, it was not particularly rough. In fact it looked like a uniform layer with some disc shaped pieces of ice placed on its surface. These secondary ice formations were probably the result of the freezing of some water that was displaced through some portions of the water still uncovered with ice. Such displacement would be caused by pressures developed after small amounts of cryogen boil beneath the ice, thereby expanding in volume nearly three hundred fold upon evaporation. This cryogen could either seep through cracks in the ice or contact water through the uncovered areas. The ice thickness was on the order of 1 cm, but in the irregular areas, it was about twice as thick.

Extensive foam was generated in all of the LNG tests. The height of the foam was at least 10 cm. In test R-38 the foam overflowed the container and caused partial loss of the mixture charge.

TABLE 5-4

Experimental Conditions for Methane-Ethane Mixtures

Test	Methane (Mole %)	Mass Spilled (g/cm^2)	Initial Water Temperature (K)	Area (cm^2)
R-1	98.5	0.80	295.	139
R-2	98.1	0.81	294.	139
R-17	90.0	1.08	297.	143
R-18	86.9	0.69	295.	143
R-21	93.2	0.71	296.	143
R-35	83.5	0.71	293.	133
R-38	80.3	2.06	289.	133

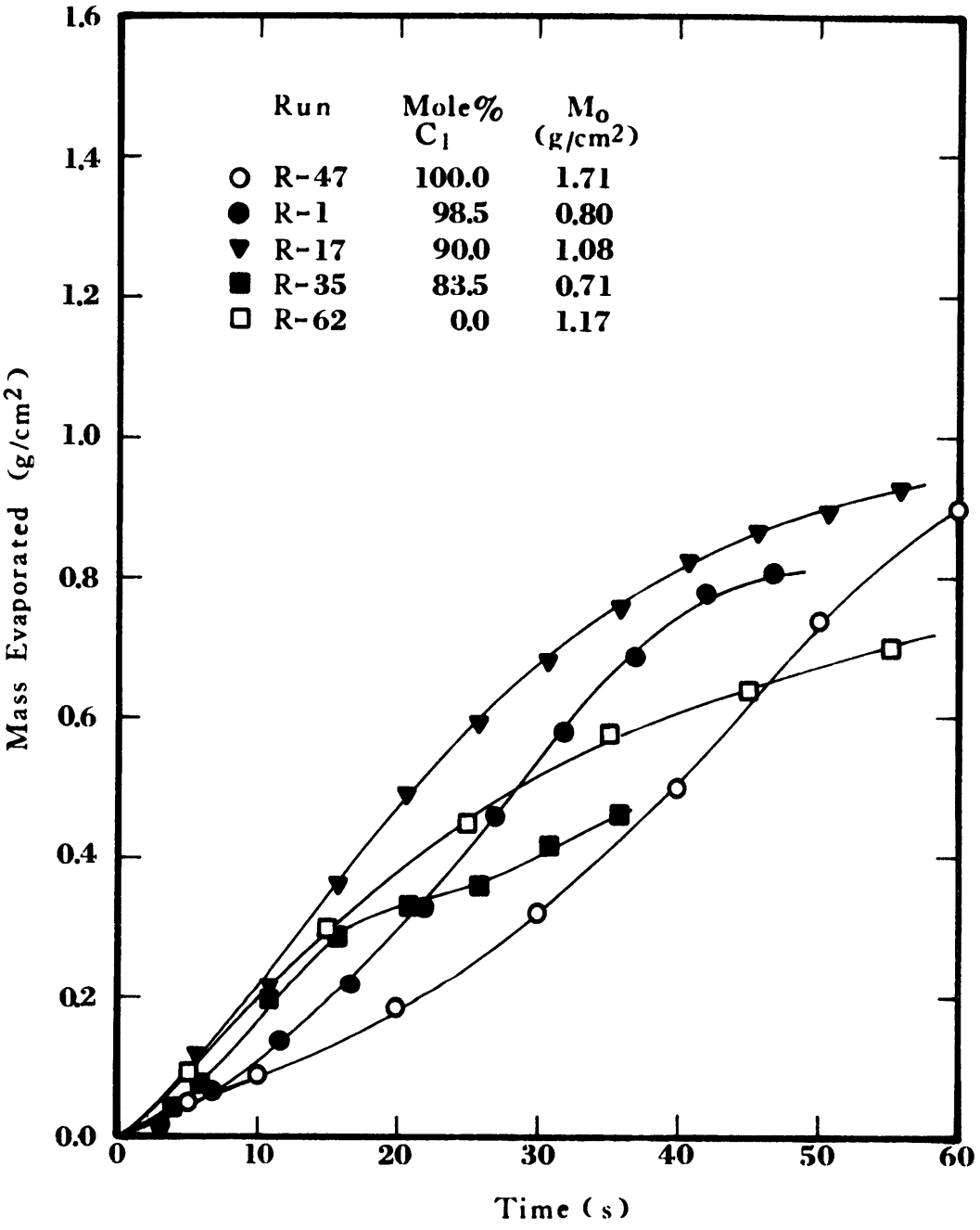

Figure 5-7 Mass Evaporated for Methane-Ethane Mixtures Boiling on Water

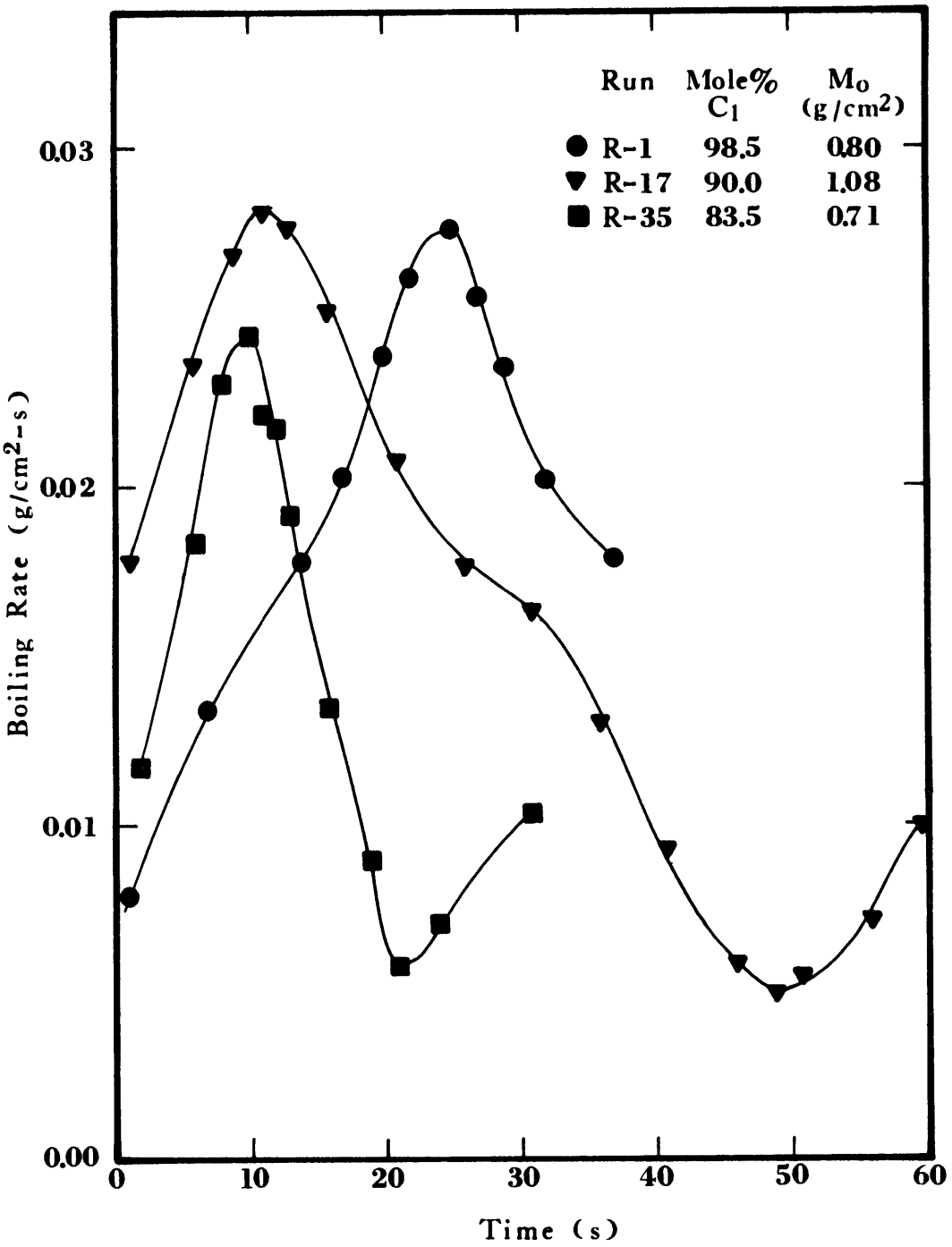

Figure 5-8 Boiling Rates for Methane-Ethane Mixtures

The container was a short one, about 10-12 cm head room over the water surface. Foaming stopped, consistently, at nearly the time that a mass equivalent to the amount of methane present in the mixture had evaporated.

The bubbles had a bimodal size distribution. Large bubbles, maybe 1 to 2 cm in diameter, rose quickly through the boiling liquid whereas the smaller bubbles, approximately 1 to 2 mm in diameter, rose more slowly and often were seen to recirculate in the boiling liquid.

Ethane-Propane Mixtures

Two spills of ethane-propane mixtures on water were made. The ethane present amounted to 85.8 and 89.7 mole percent, respectively. Other experimental conditions are given in Table 5-5. The evaporation curve as a function of time is shown in Figure 5-9. The initial rate of boiling (Figure 5-10) was very high; in fact, a violent pop was heard in test R-23.

Ice formation took place very quickly, after which boiling proceeded in a smooth and uneventful fashion. No foaming was observed with these mixtures.

Methane-Ethane-Propane Mixtures

Twenty-six ternary mixtures were spilled on water. The initial compositions of the cryogen, as well as other experimental conditions, are given in Table 5-6. Evaporation and boiling rate curves for some selected tests are given in Figures 5-11 through 5-20. Rapid boiling took place in the first few seconds and was accompanied by extensive

TABLE 5-5

Experimental Conditions for Ethane-Propane Mixtures

Test	Ethane (Mole %)	Mass Spilled (g/cm^2)	Initial Water Temperature (K)	Area (cm^2)
R-23	85.8	0.50	296.	143
R-30	89.7	0.75	294.	143

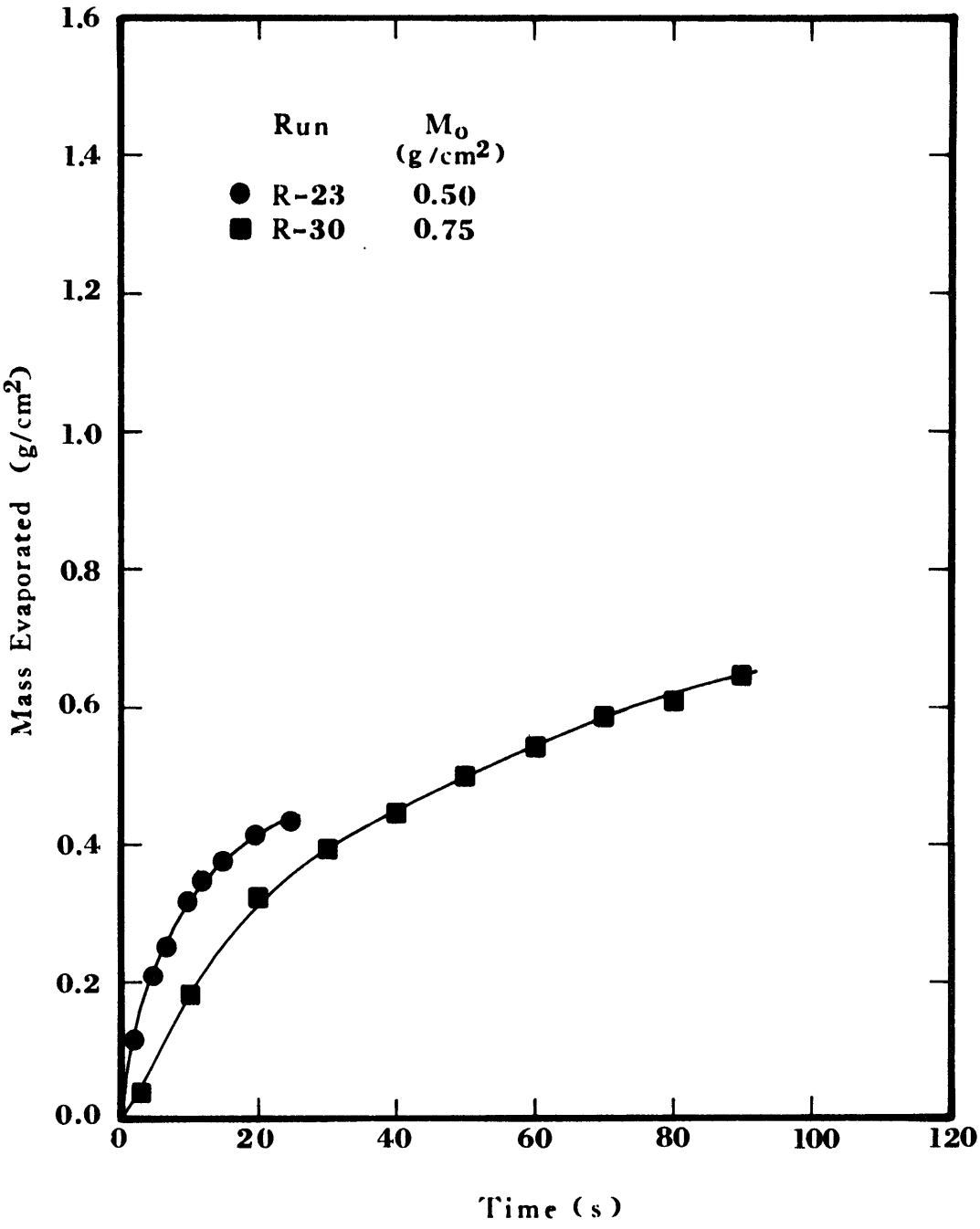

Figure 5-9 Mass Evaporated for Ethane-Propane Mixtures Boiling on Water

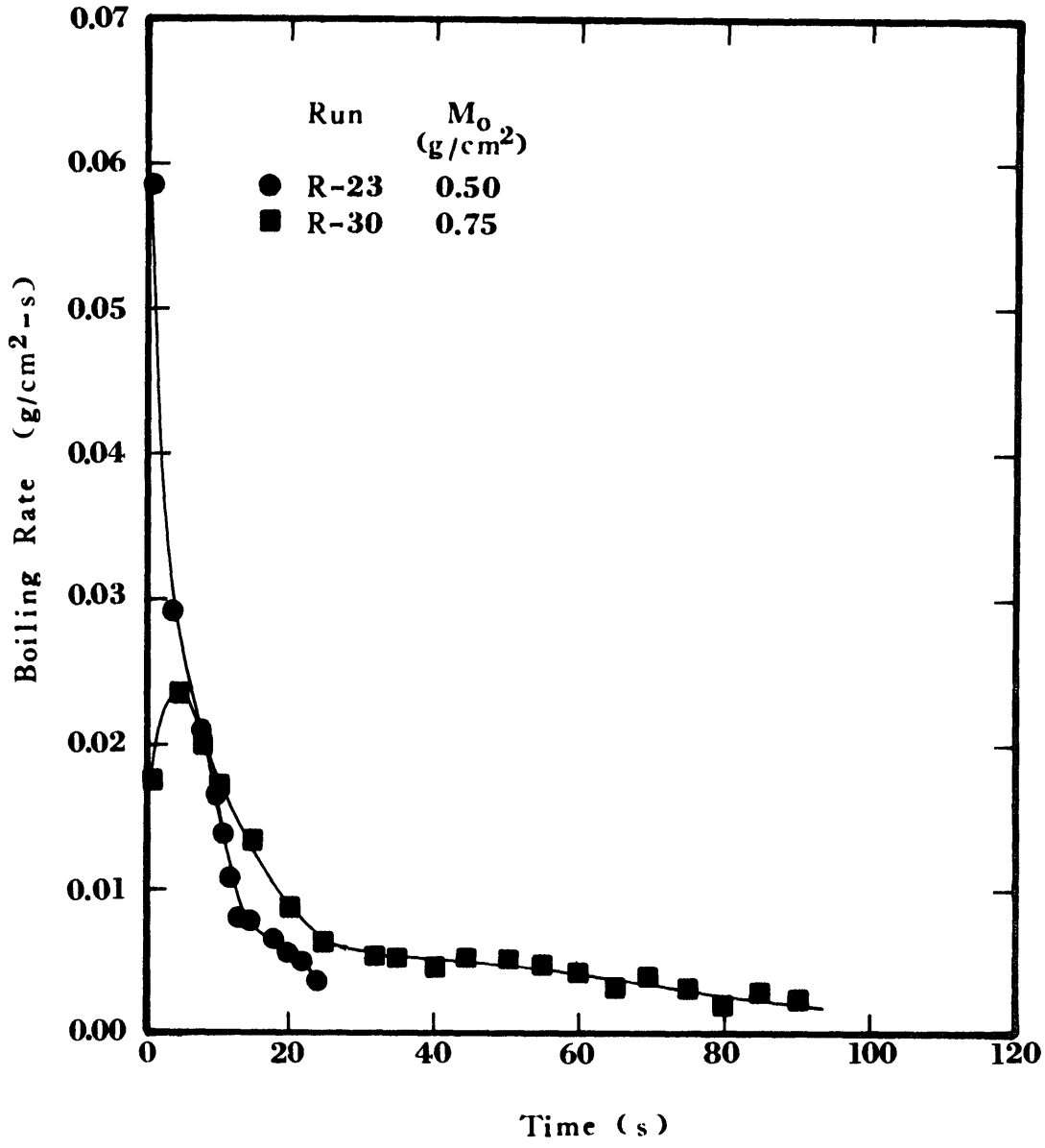

Figure 5-10 Boiling Rates for Ethane-Propane Mixtures

TABLE 5-6

Experimental Conditions for Methane-Ethane-Propane Mixtures

Test	Composition (Mole %) C_1	C_2	C_3	Mass Spilled (g/cm^2)	Initial Water Temperature (K)	Area (cm^2)
R-4	98.3	1.7	0.02	0.63	294.	139
R-5	92.7	7.2	0.04	0.30	289.	139
R-9	95.1	3.5	1.4	0.68	295.	139
R-10	89.0	5.7	5.3	0.99	295.	139
R-11	92.3	5.8	2.0	0.74	296.	139
R-12	89.6	7.8	2.6			
R-13	72.2	23.1	4.7	0.58	296.	143
R-14	75.3	21.9	2.8	0.81	296.	143
R-15	82.5	13.1	4.4	0.80	298.	143
R-16	88.3	0.2	11.5	0.69	298.	143
R-19	51.2	28.3	20.5	0.92	295.	143
R-20	82.9	10.1	7.0	0.82	296.	143
R-22	89.4	6.5	4.1	0.90	295.	143
R-24	81.2	10.8	8.0	0.83	294.	143
R-25	94.6	0.2	5.2	0.87	294.	143
R-26	78.9	13.6	7.5		294.	143
R-31	84.0	9.4	6.6	0.58	289.	143
R-33	88.9	10.2	0.9	0.87	288.	143
R-34	83.9	8.1	8.0	0.84	288.	143
R-36	78.5	15.3	6.2	1.46	288.	133
R-37	51.8	30.0	18.2	1.51	289.	133
R-39	70.1	20.5	9.4	1.42	290.	143
R-40	85.2	10.1	4.7	1.97	289.	143
R-41	91.0	6.5	2.5	1.20	288.	143
R-64	84.9	10.1	5.0	1.15	287.	143
R-66	85.1	9.9	5.0	1.52	287.	143

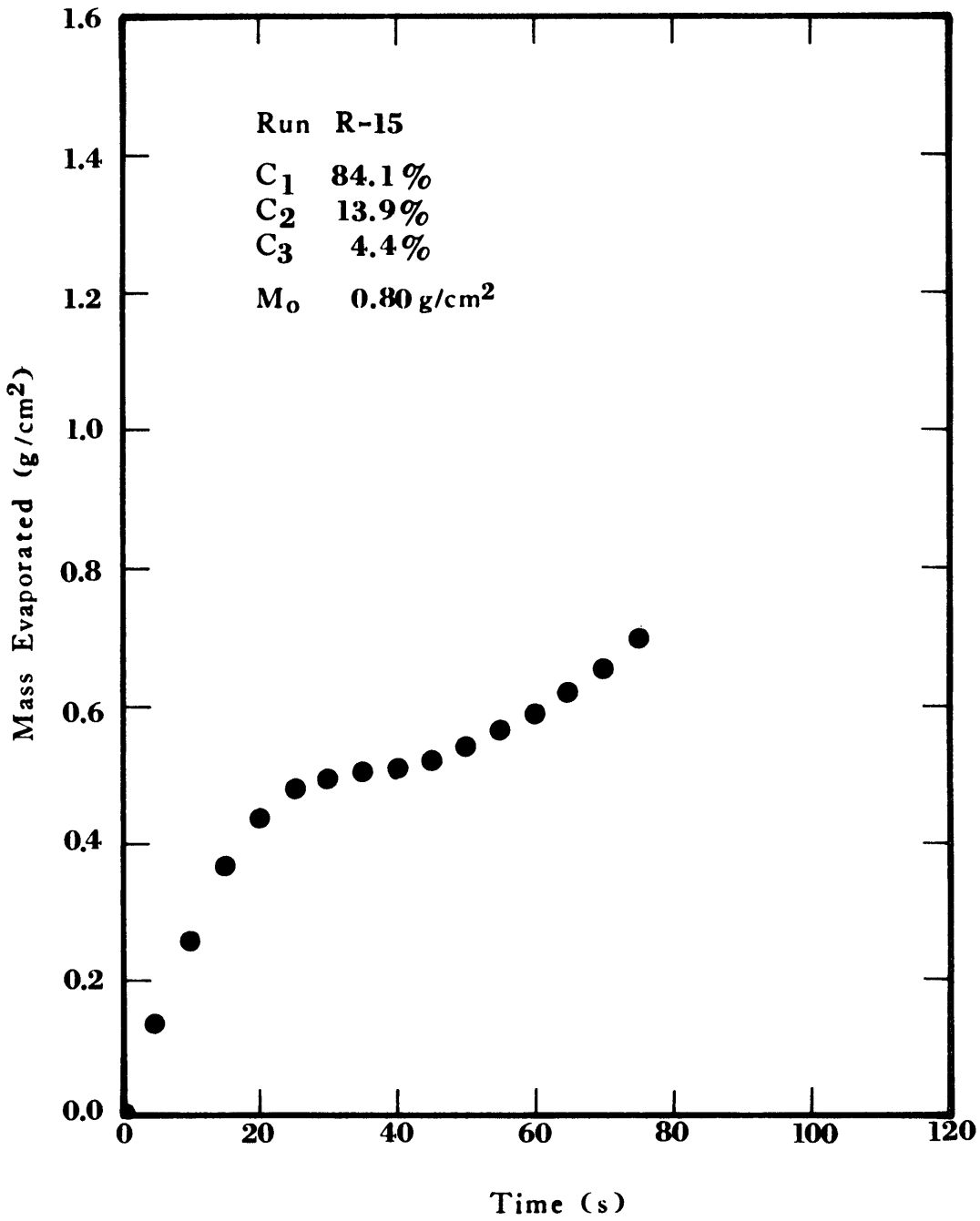

Figure 5-11 Mass Evaporated for Run R-15, Ternary Mixture

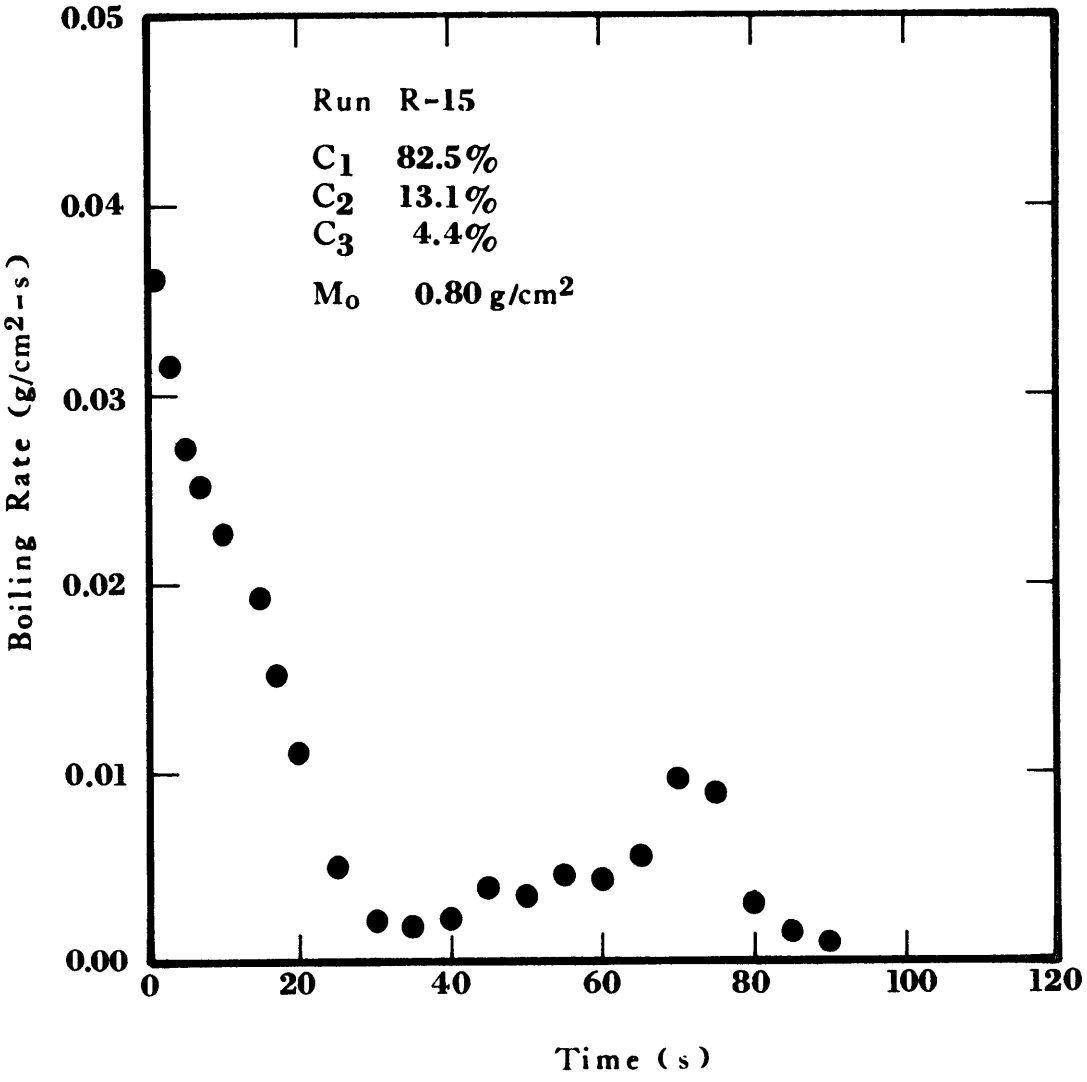

Figure 5-12 Boiling Rates for Run R-15, Ternary Mixture

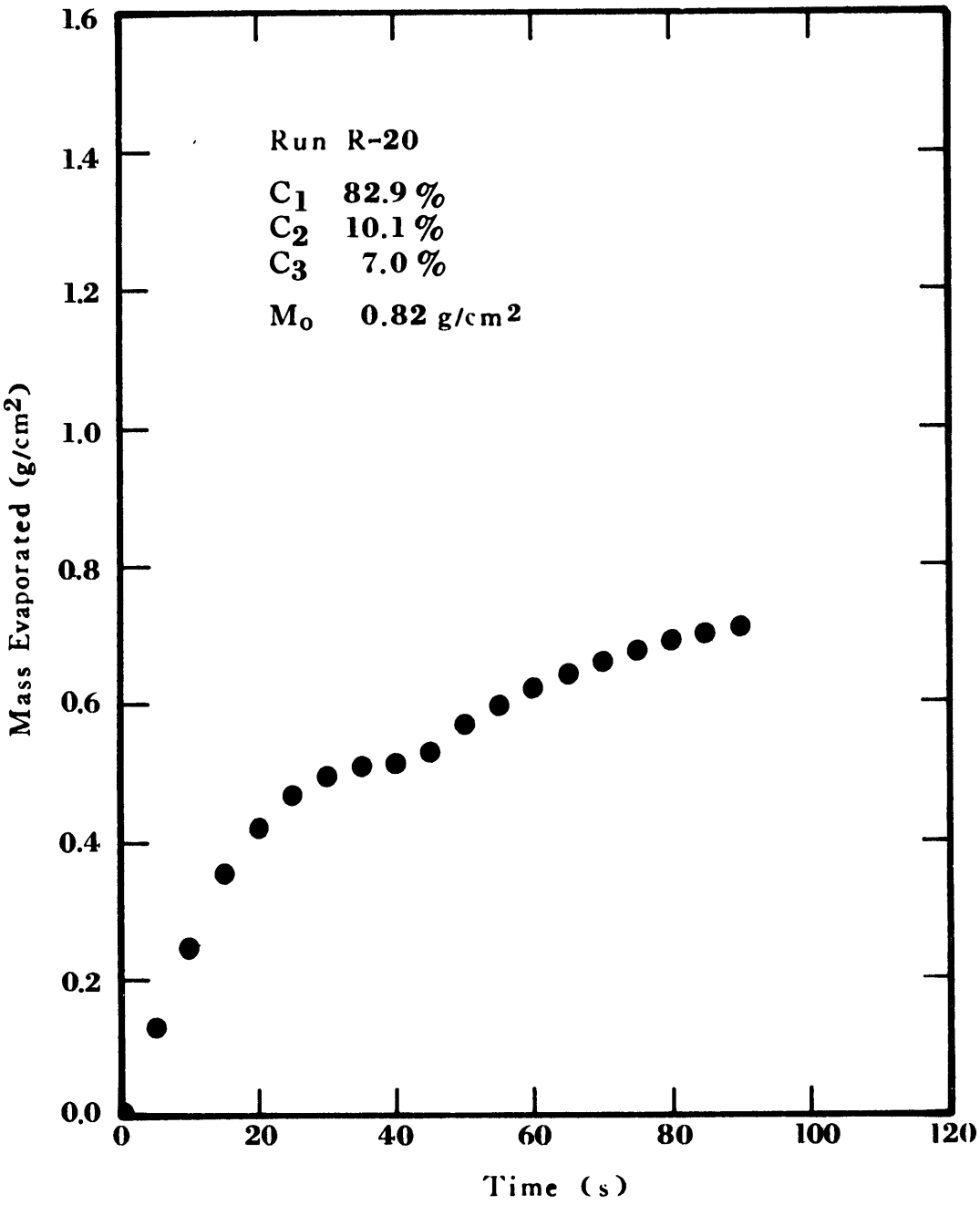

Figure 5-13 Mass Evaporated for Run R-20, Ternary Mixture

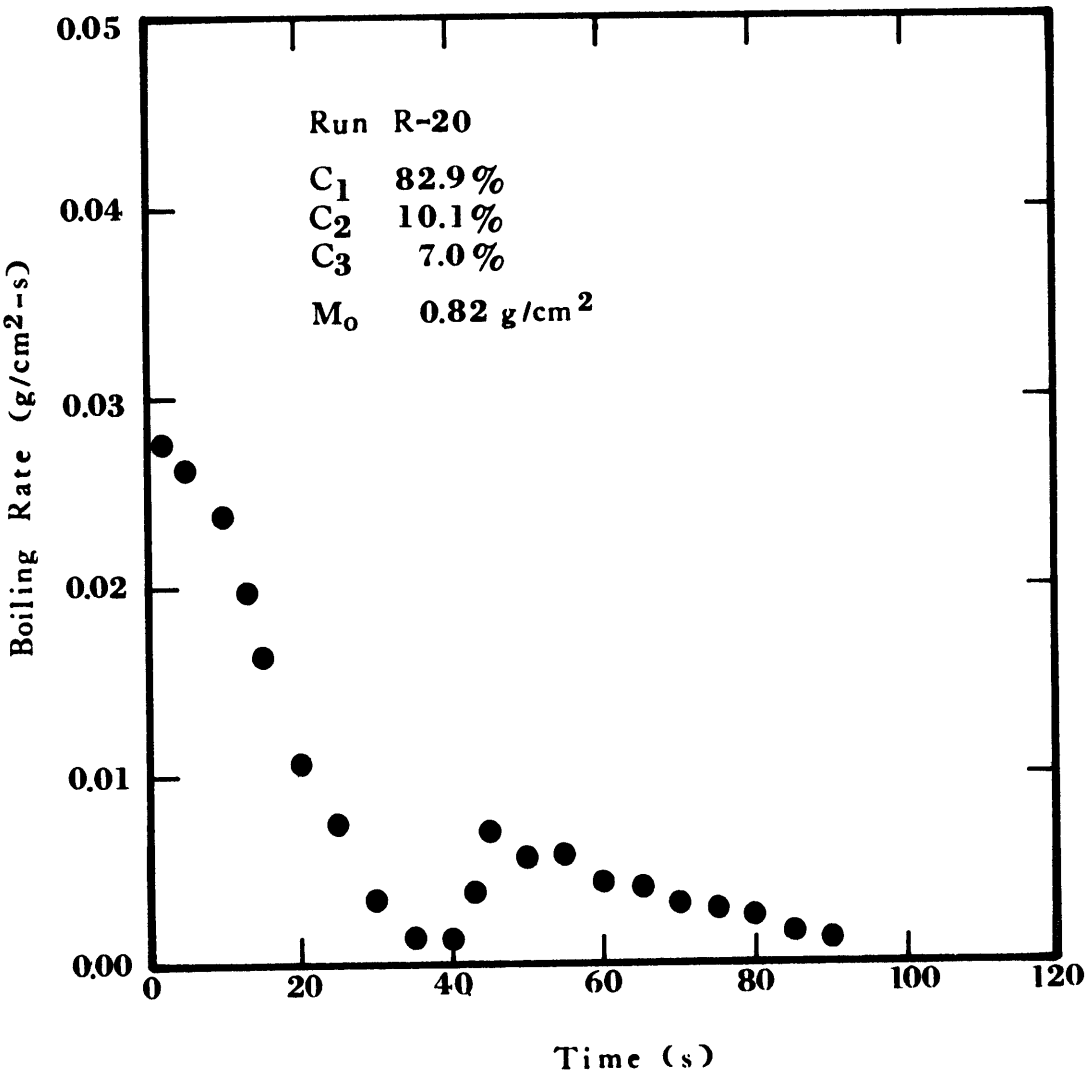

Figure 5-14 Boiling Rates for Run R-20, Ternary Mixture

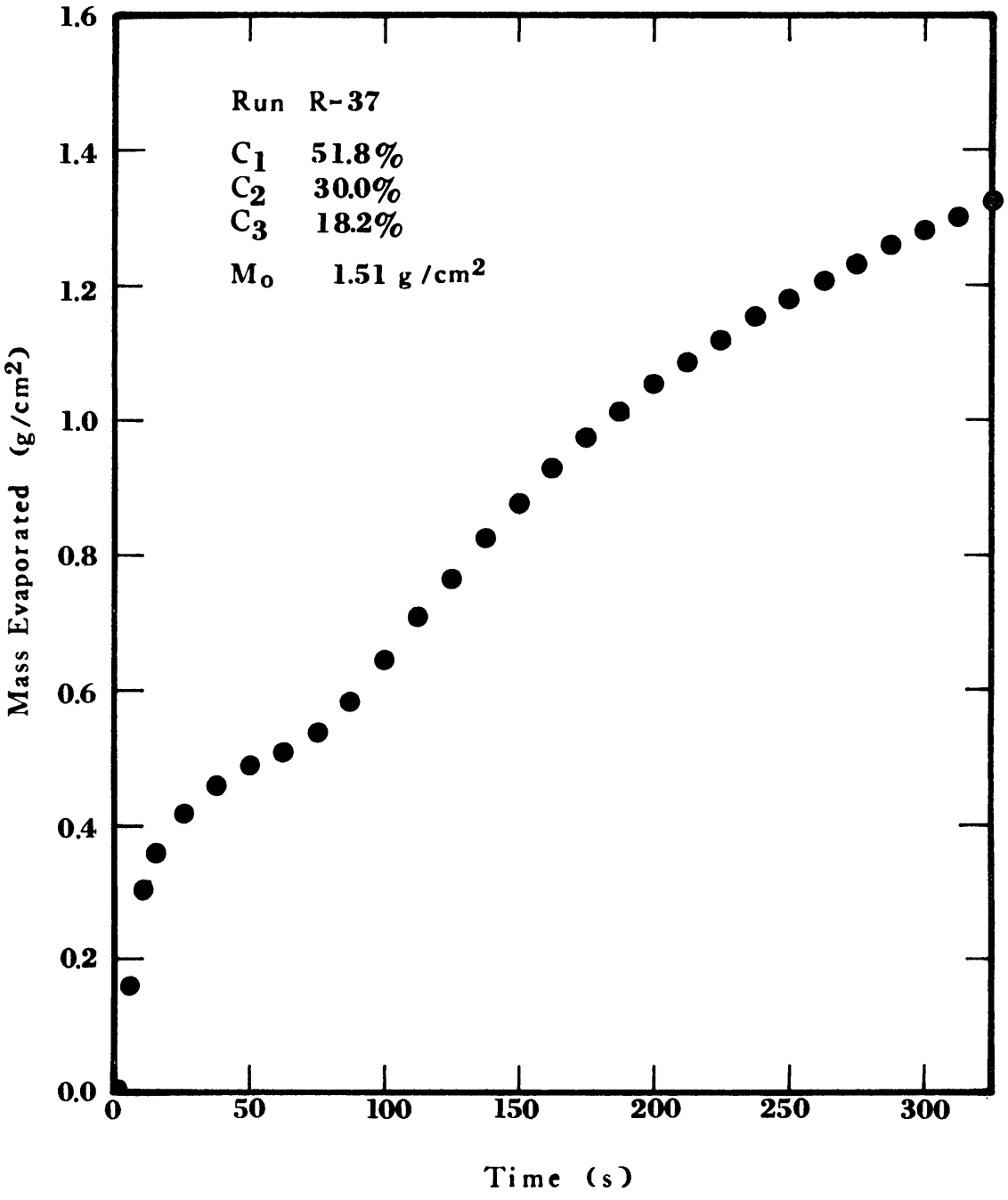

Figure 5-15 Mass Evaporated for Run R-37, Ternary Mixture

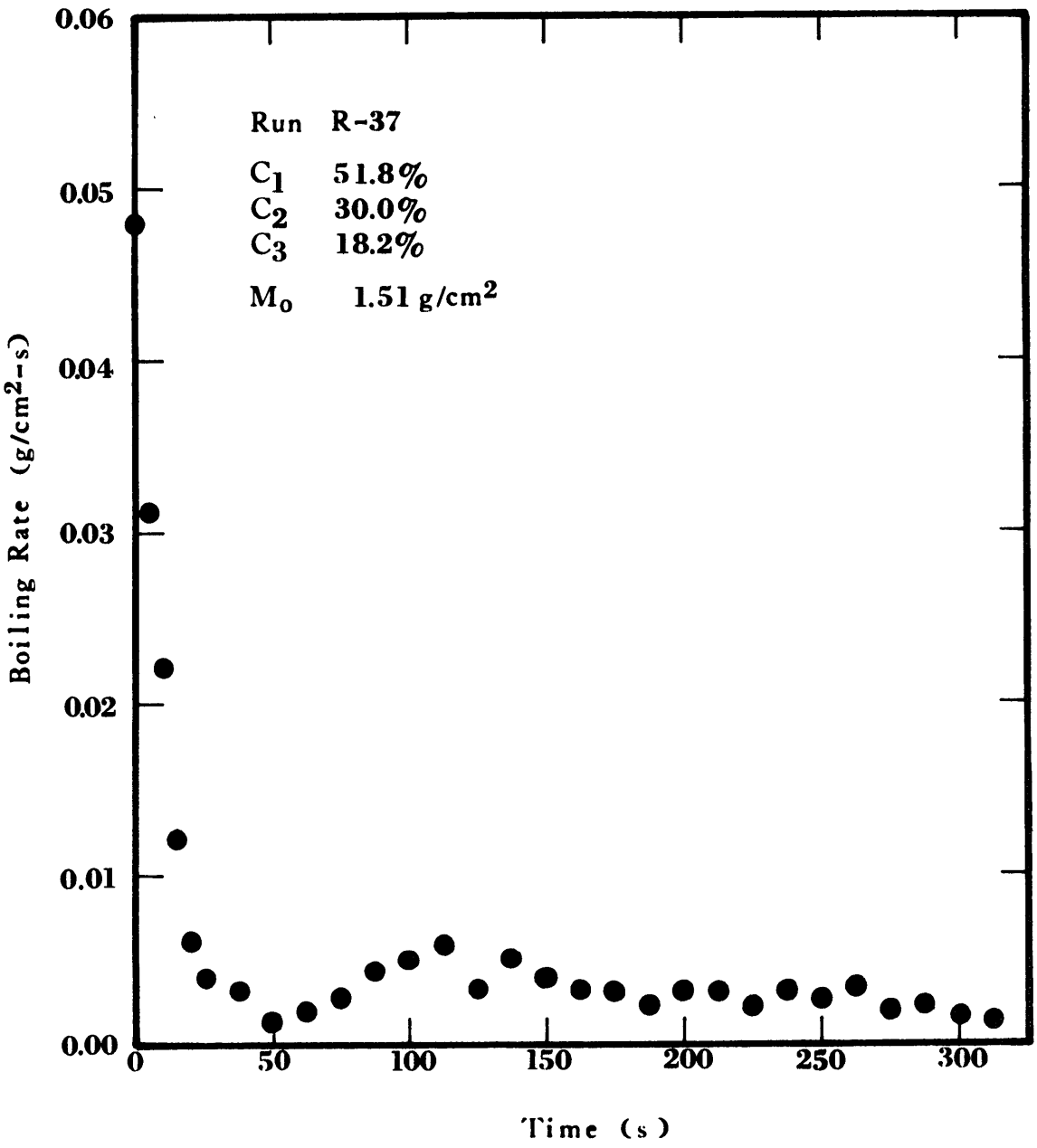

Figure 5-16 Boiling Rates for Run R-37, Ternary Mixture

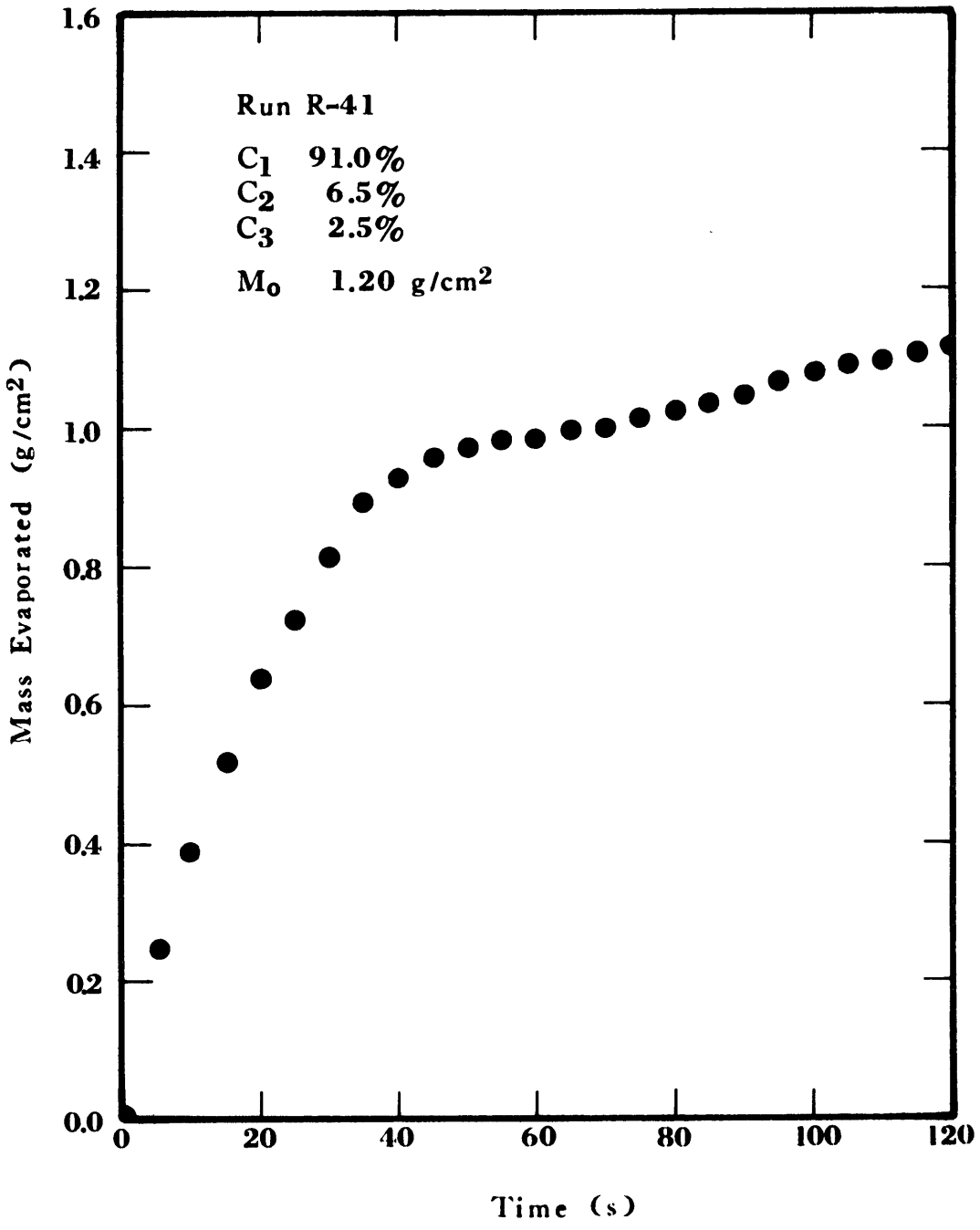

Figure 5-17 Mass Evaporated for Run R-41, Ternary Mixture

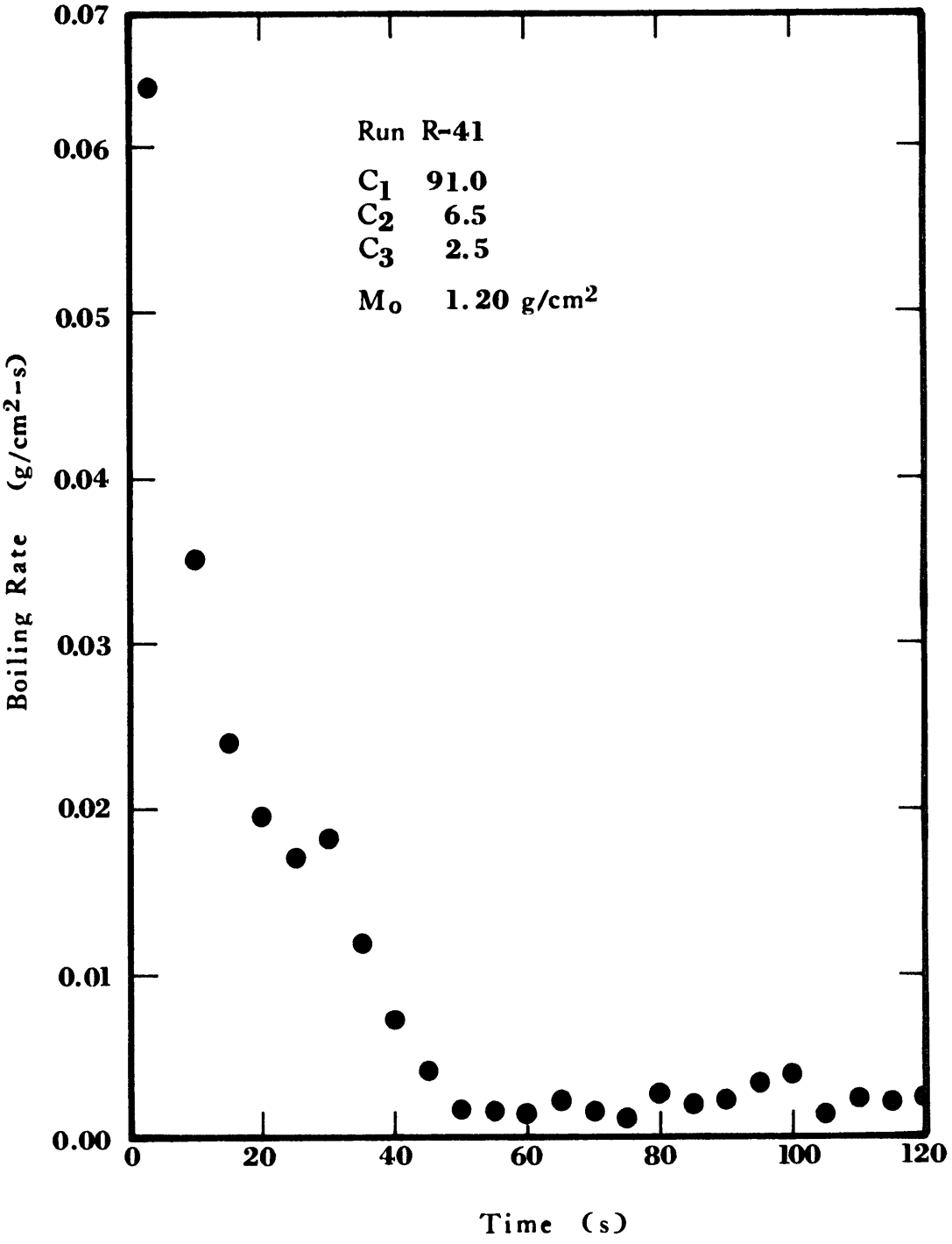

Figure 5-18 Boiling Rates for Run R-41, Ternary Mixture

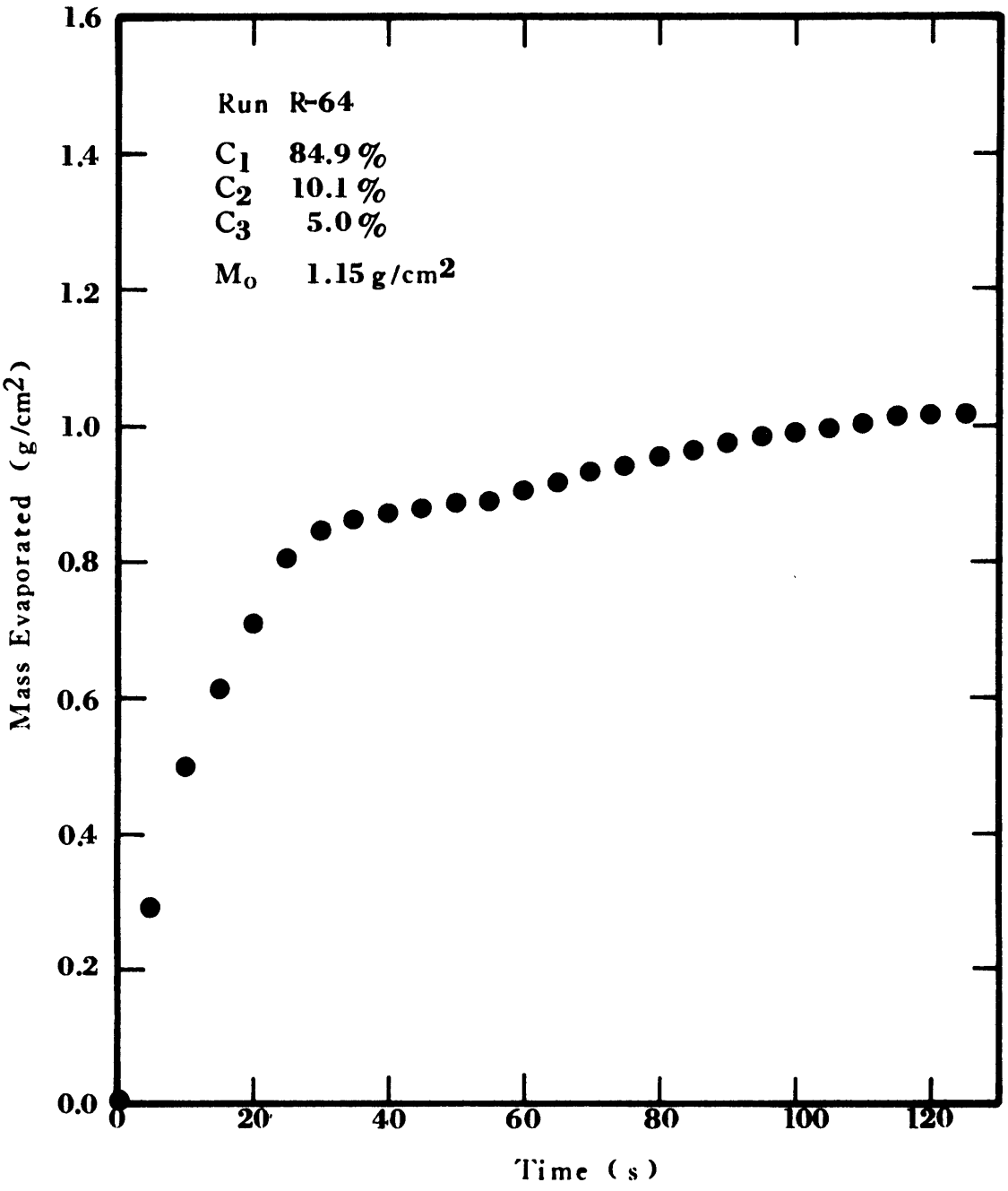

Figure 5-19 Mass Evaporated for Run R-64, Ternary Mixture

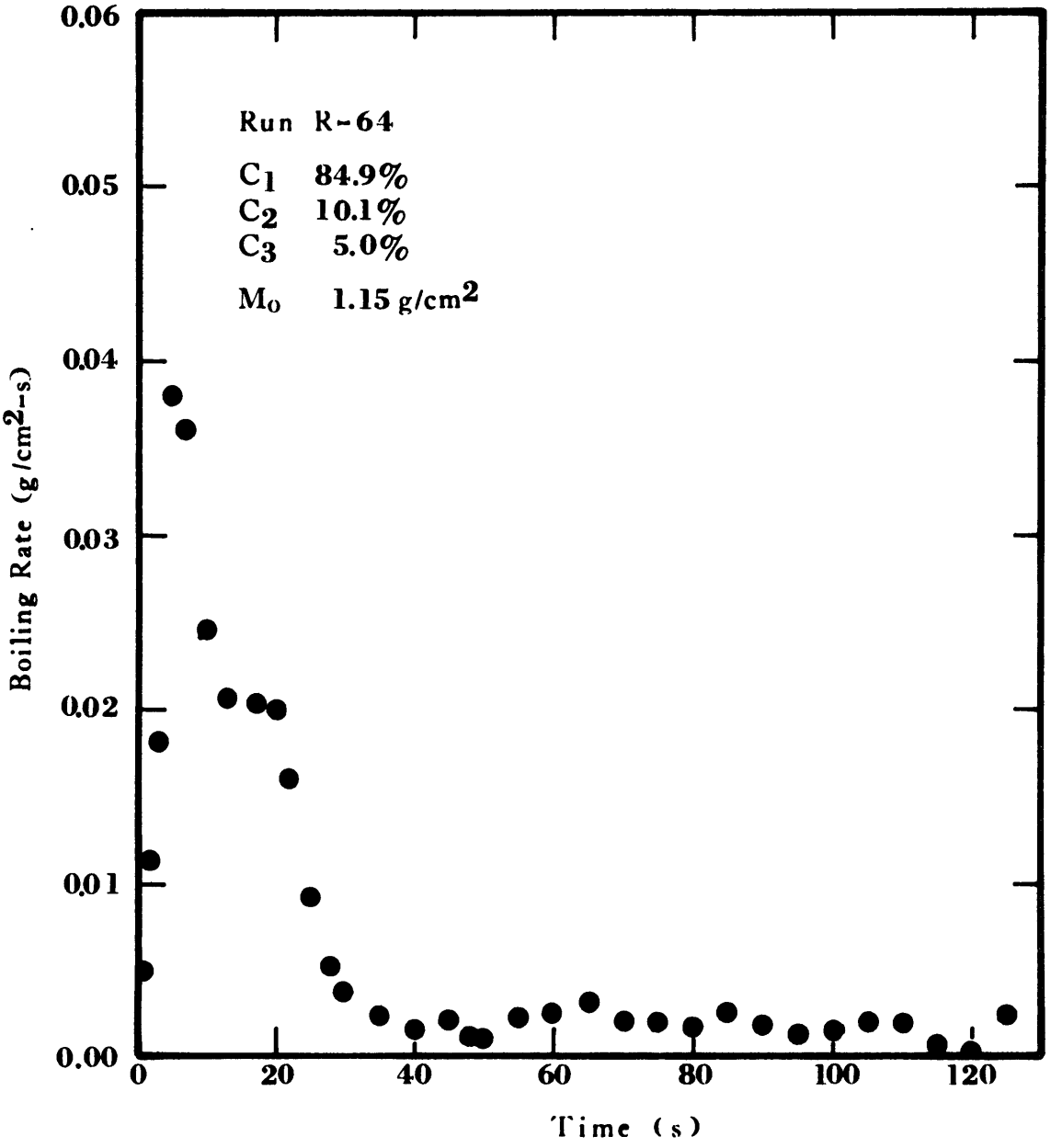

Figure 5-20 Boiling Rates for Run R-64, Ternary Mixture

foam 10 to 15 cm high. The height of the foam receded with time and eventually died out. Again, foaming stopped when the mass evaporated was nearly equivalent to the amount of methane initially present in the mixture.

The water surface was covered with ice, usually in less than 5 seconds. In most cases, the maximum boiling rates were achieved within the first 8 seconds. The boiling rates then decreased with time to very low values. In many tests secondary peaks in the boiling rates were observed, their magnitudes were, however, much lower than the initial peak.

Occasionally, a sudden burst of water squirted through the ice, sometimes to heights of 5 cm over the ice. The bubble size distribution was bimodal, very small bubbles about 1 mm in diameter were the main constituent of the foam. Large bubbles, sometime over 1 cm in diameter, quickly broke through the foam.

Mixtures containing Nitrogen

Although nitrogen is present only in small amounts in LNG, its effect on boiling characteristics has not been previously investigated; therefore, a few experiments were made to determine the influence of nitrogen.

Nitrogen was added to pure methane and, also, to LNG mixtures. These mixtures were then spilled on water. Experimental conditions are given in Table 5-7. Plots of mass evaporated as a function of time for methane-nitrogen mixtures (Figure 5-21) reveal slightly higher evaporation rates in the first few seconds when compared to evaporation

TABLE 5-7

Experimental Conditions for Mixtures Containing Nitrogen

Test	Composition (Mole %) C_1	C_2	C_3	N_2	Mass Spilled (g/cm^2)	Initial Water Temperature (K)	Area (cm^2)
R-27*	94.6	0.25		5.2	0.91	294.	143
R-59	85.0			15.0	0.98	288.	143
R-60	89.7			11.3	1.88	288.	143
R-61	92.0			8.0	1.68	287.	143
R-28	83.6	8.3	5.0	3.1	1.20	295.	143
R-65	83.0	9.6	4.9	2.5	1.06	287.	143
R-67	83.2	9.3	4.8	2.7	1.00	287.	143

*C.P. Grade Methane

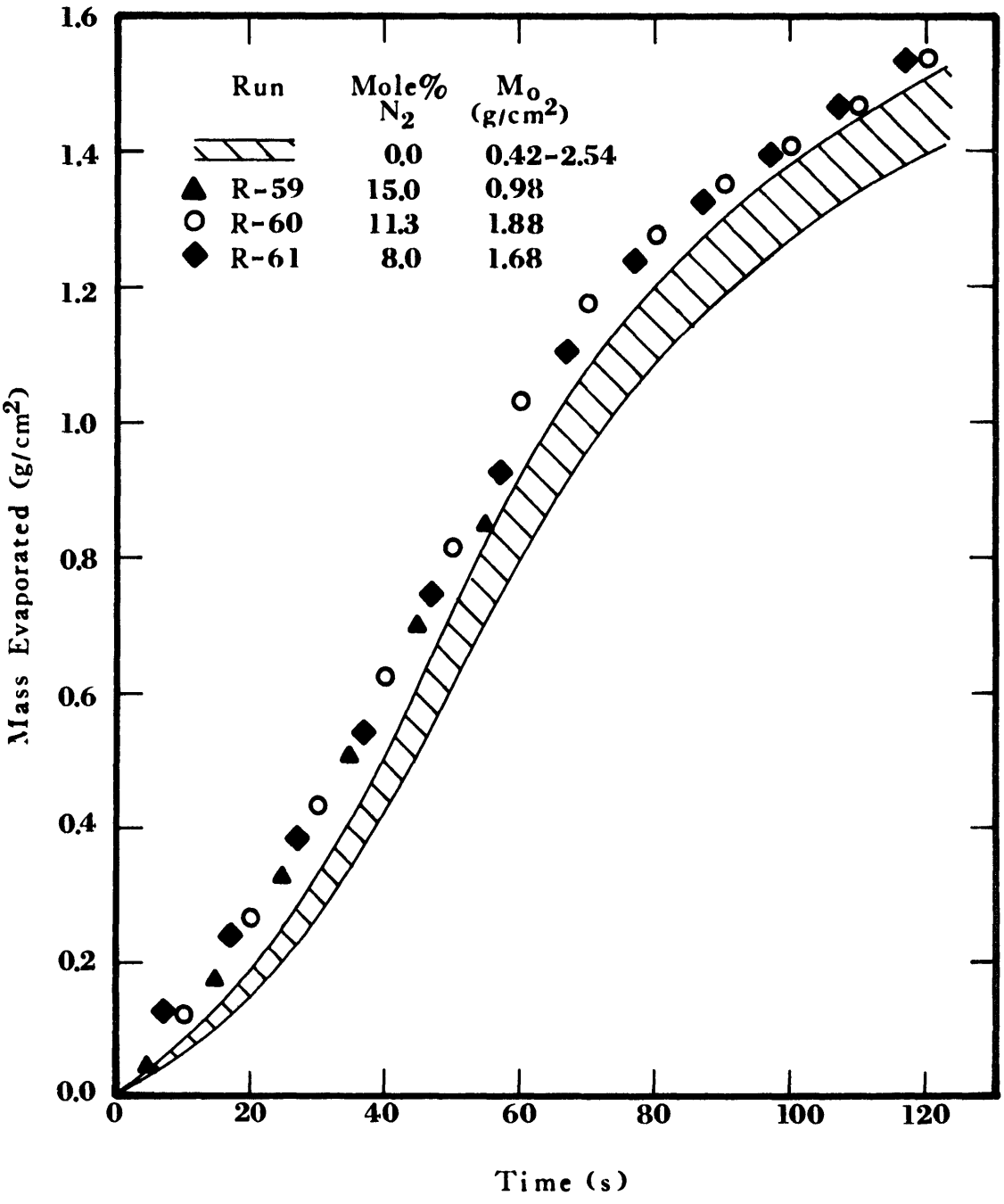

Figure 5-21 Mass Evaporated for Methane-Nitrogen Mixtures Boiling on Water

of pure methane. Afterwards, the rates of evaporation for the methane-nitrogen mixtures are very close to those of pure methane (Figure 5-22). Thus, the boiling curves for methane-nitrogen mixtures lie slightly above and parallel to the methane boiling curves. This initial difference could be due to the lower heat of vaporization of nitrogen (199 kJ/kg) when compared to that of methane (510 kJ/kg). Therefore, for the same heat fluxes a greater amount of the mixture containing nitrogen would evaporate in the initial period of time.

No significant difference in visual observations of the boiling of methane-nitrogen and pure methane was noted. It is important to note that methane-nitrogen mixtures did not foam.

Nitrogen was added to a typical LNG mixture (85% methane, 10% ethane, 5% propane) in an amount equivalent to 2.5 mole percent of the final mixture. The mass evaporated as a function of time is shown in Figure 5-23. During the first 10 seconds, the mass evaporated for the mixtures with and without nitrogen essentially overlap each other. After 10 seconds, however, the nitrogen-free mixture exhibited higher evaporation rates for 10 or 20 seconds. The boiling curves then become almost parallel to each other. It must be noted that test R-67 yielded lower boiling rates than R-65 even though both had very similar compositions. The only difference was the amount spilled, 1.06 g/cm^2 in R-65 and 1.00 in R-67. During test R-67, a sizzling sound was heard about 60 s after the spill; this corresponded to the high boiling rate exhibited at that time.

Extensive foam, on the order of 15 cm, was seen in the first few seconds. This foam, as previously described, decayed after the

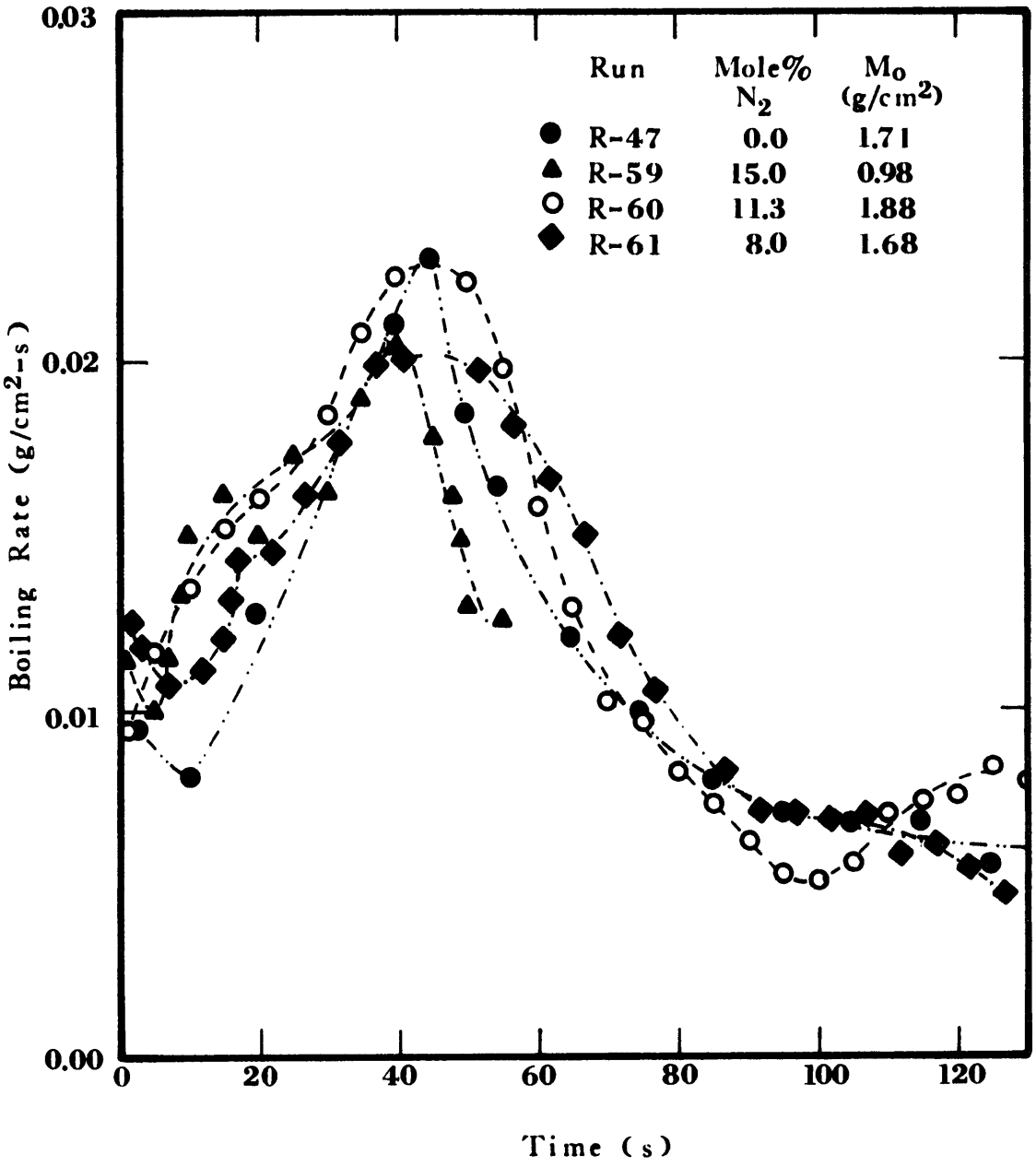

Figure 5-22 Boiling Rates for Methane-Nitrogen Mixtures

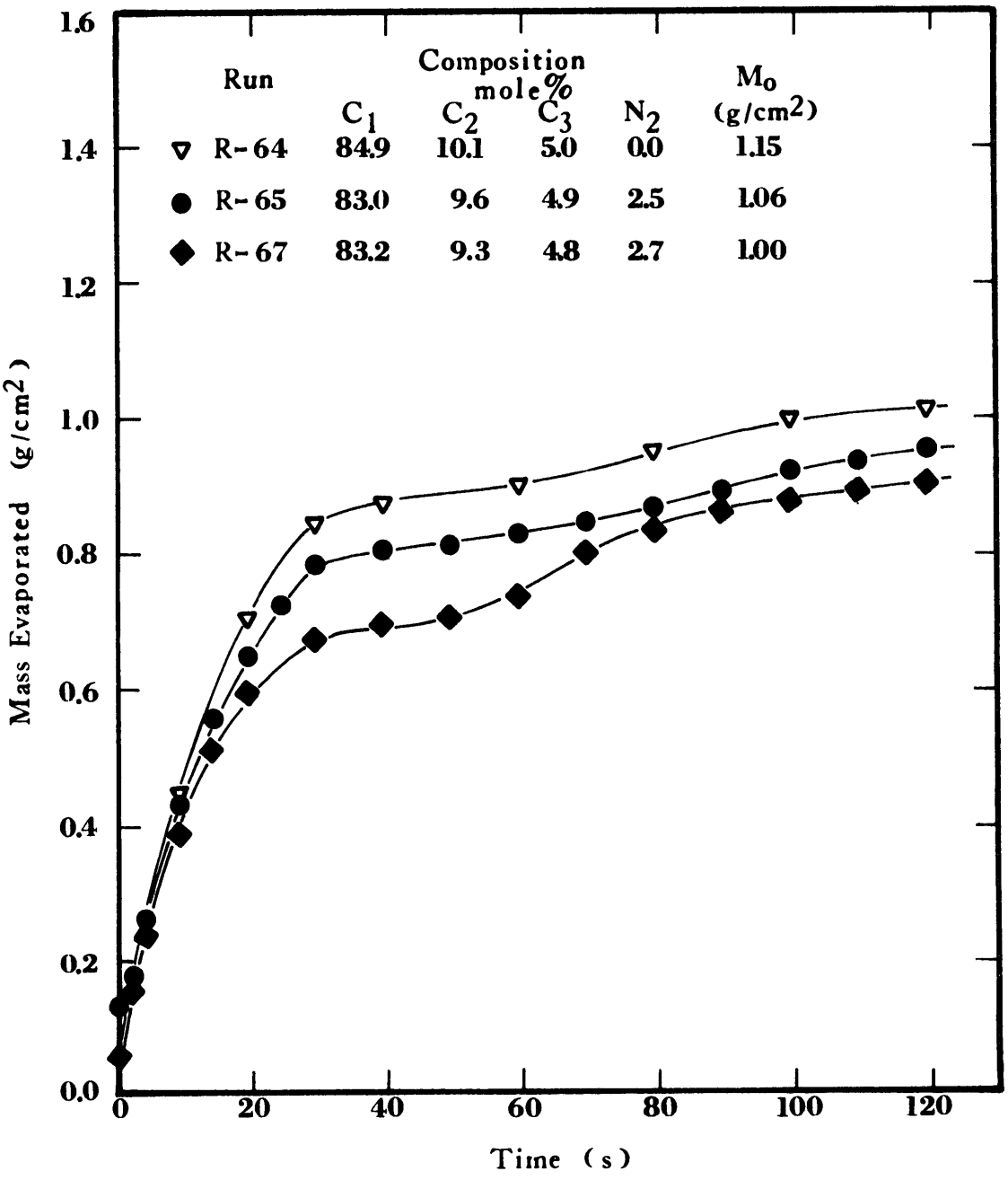

Figure 5-23 Mass Evaporated for Methane-Ethane-Propane-Nitrogen Mixtures

preferential evaporation of methane. The crackling sound, often heard while spilling LNG mixtures, was not heard when nitrogen was present. No other differences could be noticed between boiling of nitrogen-containing and nitrogen-free LNG mixtures.

Water Temperatures

The most significant portion of the temperature gradient in the water layer was in the upper centimeter or two. Thermocouples located 2 cm or more below the water surface recorded temperature changes in the neighborhood of 2 K. Thermocouples located closer to the surface (2-3 mm) almost invariably reached the freezing point and lower temperatures as ice began to encapsulate them. Obviously, the depth to which significant changes were observed depended on the amount of cryogen spilled. It is this amount which determines the energy to be removed from the water/ice substrate.

Vapor Temperatures

During the evaporation of pure methane on water, the vapor thermocouples recorded temperatures 10-20 K higher than the saturation temperature for spills of $\sim$0.5 g/cm^2. For spills higher than 1.5 g/cm^2 the superheat was reduced to 0-5 K. Jeje (1974) reported superheats of 10-30 K but with similar trends. When the amount spilled was higher than 1.5 g/cm^2, the vapors were superheated between 0 and 10 K. Obviously, the vapors produced at the vapor film/cryogen interface are superheated and are brought back to saturation temperature as they rise through the boiling methane. If the methane layer is a shallow

one, as is the case of spills of less than 0.5 g/cm^2, the vapors do not have enough time to return to the saturation temperature therefore breaking through the methane surface still superheated. On the other hand, if the amount spilled is greater than 1.5 g/cm^2 (non-boiling hydrostatic head of about 3 cm) the vapors are essentially at the saturation point.

Ethane vapors exhibited superheats of less than 5 K for spills of about 0.8 g/cm^2. Where the amount spilled was greater than 1.0 g/cm^2, the vapors were evolved at the saturation temperature.

Propane vapors were evolved at the saturation temperature of propane.

In the case of mixtures, the vapor temperatures followed the composition-dependent saturation temperature. Extensive evidence to this extent was given in Chapter IV. Therefore, no significant superheats were recorded for LNG mixtures boiling on water.

Discussion of Results

The following discussion of results will be qualitative in nature. The formulation of mathematical models based on these qualitative observations (as well as theoretical heat transfer considerations) will be made in Chapter VI.

Methane

The rates of evaporation exhibited by very pure liquefied methane boiling on water are puzzling at first. They increased with time,

reached a peak and then decreased. Intuition dictates that the rates should be high at first and then decrease with time. Such conclusions can be reached by considering the heat fluxes in the water layer whose surface suddenly undergoes a step change in temperature. The surface temperature would change from the initial water temperature to one near the saturation temperature of methane. Energy from the water would be transferred across the water-methane interface to evaporate methane. The heat flux would be proportional to the interfacial temperature gradient in the water layer. This gradient would be high upon initial contact of the two liquids and the heat fluxes would also be initially high, and ice would form; as the gradient decreased, due to cooling of the ice, the heat flux and, consequently, the rate of evaporation would decrease. Given an infinite time the gradient would vanish, no heat would flow across the interface and boiling would stop. The experimental results, however, disagree with the above intuitive concept.

A closer look at how methane boils on water was necessary. Small amounts ($\sim$1 cm^3) were spilled on water. The small methane "island" floated on and skated across the water surface. Eventually, water cooled down and froze under the methane island. The island remained on the surface of the ice where it suddenly evaporated. This suggests that methane was <u>film</u> boiling on the water surface, and a vapor film that separated the methane from the water allowed the methane freedom to roam. Once the ice formed, its surface temperature dropped and the vapor film collapsed, thus immobilizing the methane on the ice surface.

Boiling of methane on solid surfaces was described in Chapter II. Since no studies have been reported on the determination of boiling curves (Q/A vs ΔT) for methane on water or ice, the curves on solid metals will be taken as a starting point. As can be seen in Figure 2-8, methane film boils at a difference in temperature as low as 180 K, corresponding to methane (112 K) contacting water at 292 K. The insulating behavior of the film results in the low initial heat fluxes observed. As energy is taken from the upper layers of water, the temperature drops and ice is formed. The ice temperature continues to drop, thus decreasing the ΔT ($T_{sat} - T_{hot\ surface}$). (The saturation temperature of methane does not change.) This difference in temperature is no longer high enough to sustain a stable film. The film begins to collapse; liquid-ice direct contact is made thus allowing higher heat fluxes and boiling rates. Further cooling of the ice layer promotes nucleate boiling. Intimate contact is made between the boiling methane and the ice, effectively eliminating the surface resistance to boiling. The major resistance to heat transfer becomes one of conduction through the growing ice layer. Then, the heat transfer rates decrease as the temperature gradient at the ice surface decreases with time.

At first it was thought that the increase in heat flux for methane boiling on water was due to a progressive shift to nucleate boiling caused by a progressive coverage of the water surface with ice, as suggested by Boyle and Kneebone (1973). The assumption is made that the cryogen would nucleate boil on ice as soon as the ice was formed.

(It must be noted that Boyle and Kneebone report a constant rate of evaporation for methane; the above concept was given as an explanation for the increase in heat fluxes for LNG boiling on water). However, when methane was spilled on a solid block of ice, it was also found to film boil at first. As can be seen in Figure 5-24, during the first 30-40 seconds it makes little difference whether boiling is taking place on ice or on water. Such an observation is consistent with the idea that the surface on which boiling takes place has little effect on film boiling since a layer of vapor separates the boiling fluid from the heating surface. For spillages on water, a large amount of energy is liberated during ice formation and this energy is conducted through a thin layer of ice. For the spillages on ice, only conductive processes are possible; the additional source of energy, i.e., solidification of ice, is no longer available. Therefore, once nucleate boiling is approached and the surface resistance becomes negligible, one would expect higher heat fluxes for methane spilled on water than for spills on a solid block of ice.

Therefore, it is concluded that when methane is spilled on water it initially film boils; as the water cools beyond the freezing point, ice is formed. The temperature of this ice continues to decrease until the ΔT is no longer high enough to maintain stable film boiling. Transitional boiling takes place and the heat fluxes begin to increase reaching a peak which is limited by the internal conductive resistance to heat transfer in the substrate (ice or water).

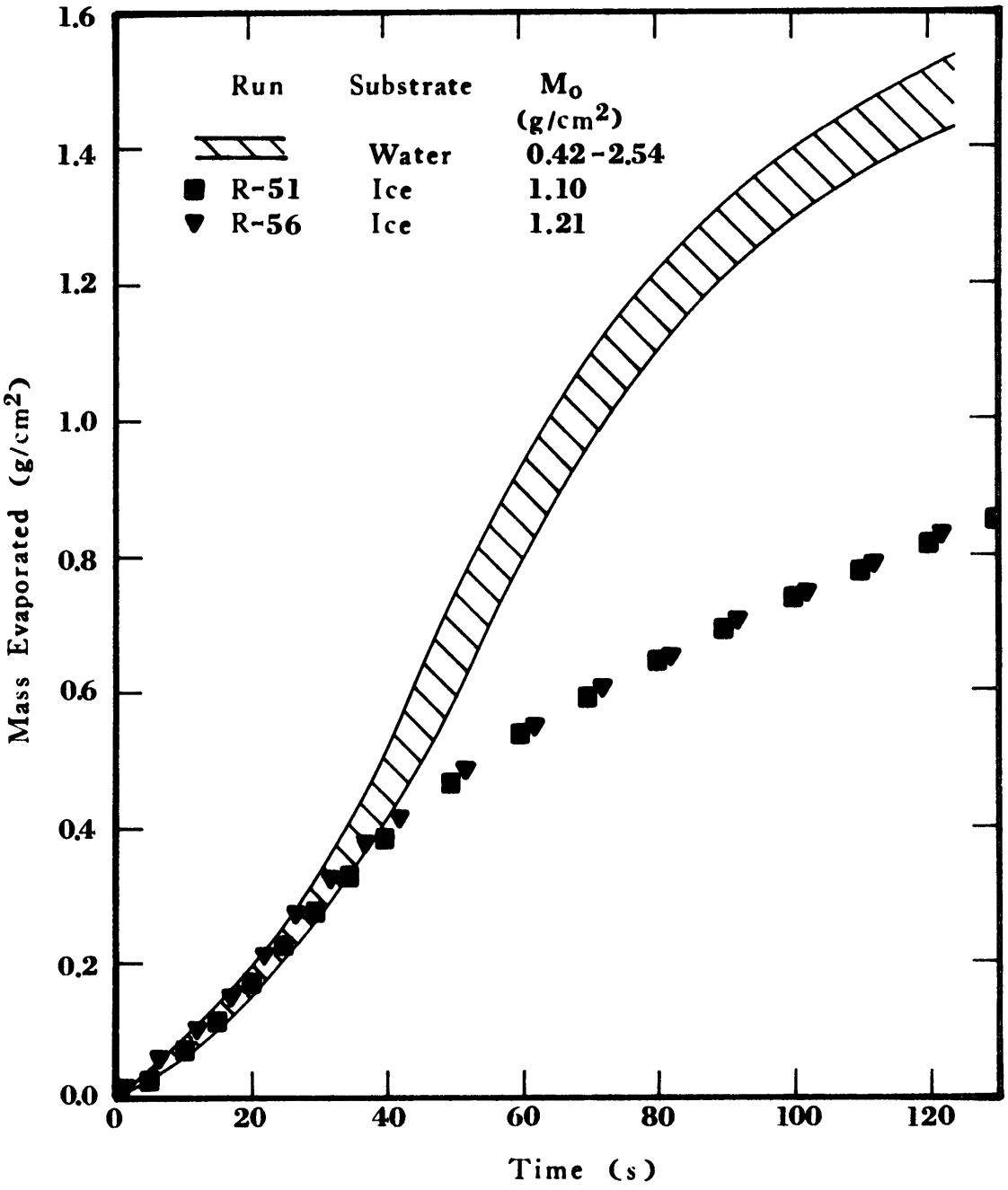

Figure 5-24 Mass Evaporated for Methane Boiling on Water and on Ice

Ethane

The rates of evaporation of ethane on water resemble those exhibited by methane. The rates increase with time and then decline after reaching a peak. This peak, however, is attained much sooner than in the case of methane. Ethane takes about 10 seconds whereas methane peaks at around 40 seconds.

The explanation for this behavior follows that given for methane. According to Figure 2-9, for a difference in temperature of 205 K (ethane at 184.5 K and water at 290 K), ethane is in the transition regime. Thus, the initial heat fluxes are higher than the corresponding ones for methane. As the nucleate regime is approached, higher heat fluxes are attained. Ice formation takes place within 5 to 10 seconds. The ice surface cools down and, once its thickness begins to grow, it becomes the major thermal resistance. As the surface temperature of the ice approaches that of ethane, the temperature gradient near the surface begins to decrease as do the heat fluxes and boiling rates.

Ethane was also boiled on a solid block of ice (Figure 5-25). It exhibited a decreasing boiling rate with time. In this case the surface of the ice cooled down very quickly, unlike spills on water in which transition boiling is maintained for several seconds. During this time ice is being formed and severe drops in surface temperature delay for a few seconds. Essentially then, ethane boiling on ice is controlled by heat conduction through the ice motivated by a step change in temperature on the ice surface.

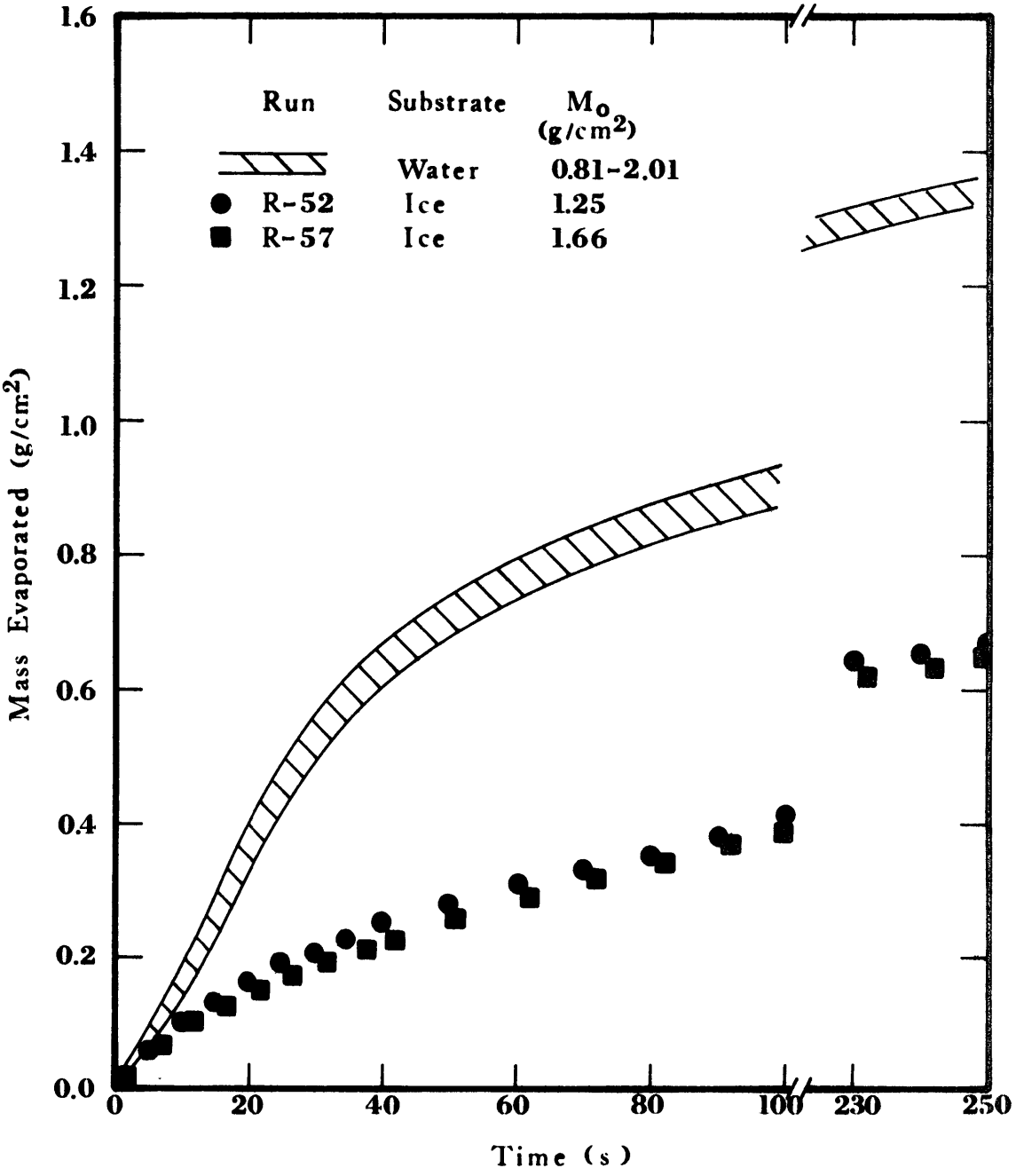

Figure 5-25 Mass Evaporated for Ethane Boiling on Water and on Ice

Propane

The boiling rates for propane are also explained by following the same line of thought and with methane and ethane. The initial temperature difference corresponds to the neighborhood of the high peak nucleate flux for propane (Figure 2-11). An intimate liquid-liquid contact is established upon spilling the propane on water; high heat fluxes are achieved. Furthermore, when any liquid cryogen is spilled on water, it inevitably penetrates the water surface due to inertial forces. Propane evaporates quickly under the water, and the rapid expansion and movement upward of the vapor splashes the water. This water interacts with the still falling propane and results in a further disturbance on the surface of the water. As a result, the area for heat transfer is increased significantly. Furthermore, the water that is thrown upward freezes in situ upon contacting the liquid propane. All these chaotic phenomena result in the violent initial boiling of propane. And, since these events are chaotic in nature, the amount evaporated in the first few ($\sim$3) seconds varies significantly from run to run. This variation has also been observed by Mohammadi (1977) and Reid and Smith (1977).

The initial disturbance of the water does not play such an important role in the case of methane since the initial film boiling rates are very low. No splashing of water takes place and the interface recovers quickly. Ethane is an intermediate case but the interface seems to have enough time to recover; the splashing of water is not nearly as severe as with propane.

Once a coherent ice layer covers the interface completely, heat transfer becomes controlled by conduction through the ice and the boiling rates decrease to very low values consistent with heat conduction through the growing ice layer. In fact, boiling of propane on a solid block of ice (Figure 5-26) took place in a very smooth fashion and at very low boiling rates. Unlike spills on water, the surface area for heat transfer was very well defined and no water was splashed up to evaporate propane.

Mixtures

The evaporation of mixtures is a far more complicated situation. In addition to shifts in boiling regimes, one must consider the change in composition and saturation temperature of the residual liquid as preferential evaporation of the more volatile components takes place.

Consider a binary mixture of 90% methane and 10% ethane. The saturation temperature is close to that of methane (Figure 4-11). As in the case of pure methane, a vapor film is formed. As the vapor bubble is being formed, the liquid at the base of the bubble becomes depleted in methane since the vapor bubble is made up primarily of the most volatile component (see Chapter IV on Vapor-Liquid Equilibria). The liquid remains essentially isothermal but a thin liquid layer at the base of the bubble has changed significantly in composition, heat transmission and evaporation being much faster than diffusional mass transfer. This means that for this thin liquid layer to be in equilibrium the pressure must drop. Or, in other words, the vapor pressure of this thin layer becomes less than one atmosphere (see Table 5-8).

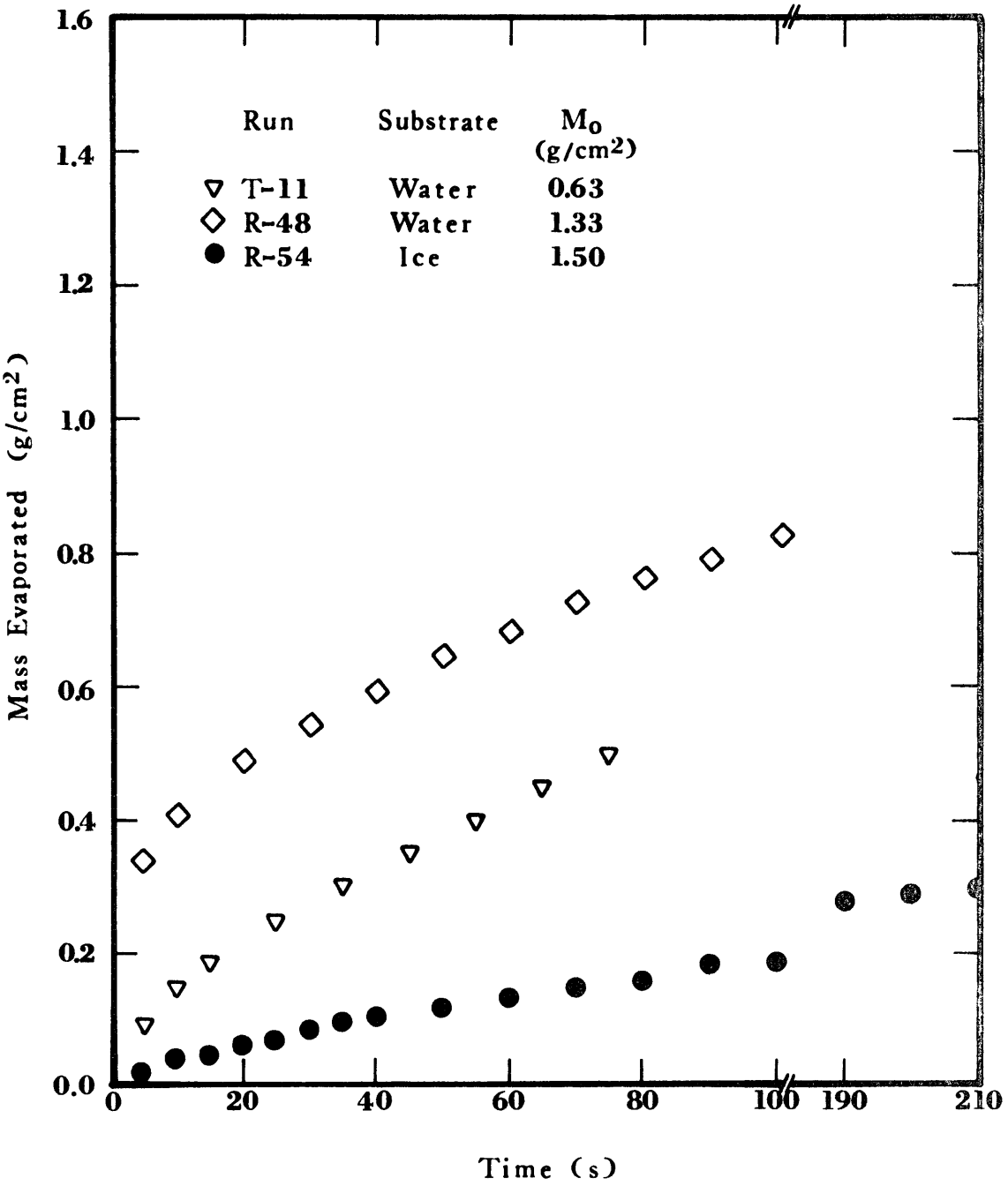

Figure 5-26 Mass Evaporated for Propane Boiling on Water and on Ice

TABLE 5-8

Isothermal Vapor Pressures for Methane-Ethane Mixtures (113 K)

Methane Mole %	Pressure 10^{-5} N/m^2 *
90	1.01
80	0.91
70	0.82
60	0.72
50	0.62

*1 atm = 1.01×10^5 N/m^2

As some of the vapor in the film evaporates into the growing vapor bubble, the low vapor pressure of the thin surface layer (richer in ethane) hinders the replenishment of the vapor film. Thus, the vapor film collapses. The bubble is pinched off and carries in its wake the ethane-rich layer which then mixes with the bulk of the liquid, as shown in Figure 5-27. Fresh liquid rushes in and a temporary liquid-liquid contact is made, which allows for high heat fluxes. The vapor film is reformed and the cycle begins again. Because some liquid-liquid contact is made, the water cools faster and ice is formed faster than with pure methane.

The small size of the bubbles is explained by the Marangoni effect taking place at the base of the bubble. The enrichment of a thin liquid layer in ethane causes an increase in surface tension at the base of the bubble ($\sigma_{C_2} > \sigma_{C_1}$). This increase in surface tension causes the bubble to be pinched off at a smaller diameter than in the case of pure methane. Furthermore, the surface tension gradient at the base of the bubble "pulls" fresh liquid in as the bubble detaches.

In the case of mixtures richer in heavier hydrocarbons, the decrease in vapor pressure of the thin rich layer is even more dramatic, so the film collapses much more easily. This not only increases the rate of ice formation but accelerates the cooling of the ice once it is formed. The difference in temperature between the ice and LNG decreases rapidly to the point where the vapor film cannot be regenerated. These factors result in the attainment of the peak flux at shorter times for mixtures containing heavier hydrocarbons.

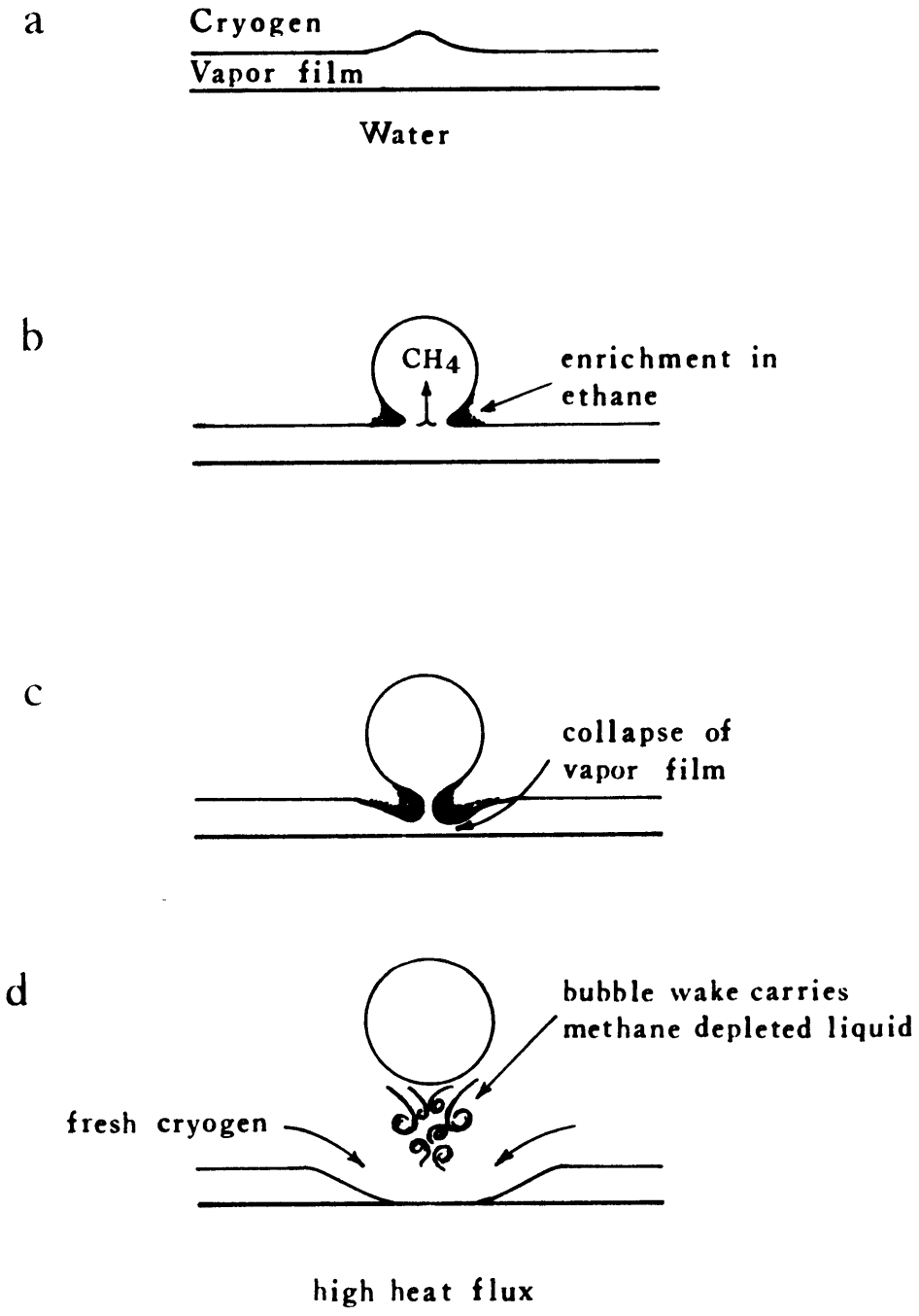

Figure 5-27 Sequence of Events Leading to the Collapse of the Vapor Film During Boiling of a Methane-Ethane Mixture

This theory presents a plausible mechanism to explain why there is an increase in initial boiling rates upon addition of heavier hydrocarbons to methane.

The eventual enrichment of the bulk liquid in heavier hydrocarbons due to the preferential evaporation of methane plays a very important role in the latter part of the boiling process. It was previously indicated, in Chapter IV, that the saturation temperature of a mixture of methane and ethane will not change appreciably until the residual methane is less than about 20%. The saturation temperature then quickly rises to that of ethane (Figure 4-11).

Consider the 90% methane, 10% ethane mixture spilled on water. After the ice has formed it begins to cool down and approach the saturation temperature of the mixture. The bulk of the liquid is being depleted in methane and, when almost all the methane is gone, the saturation temperature of the cryogen begins to increase towards that of pure ethane. Considering the situation from the ice point of view, its surface is placed in contact with a body at a very low temperature; as the surface of the ice is approaching this low temperature, the temperature of the cold body begins to increase. This upsets the temperature gradient near the interface and results in very low heat fluxes. Furthermore, the residual liquid must be warmed to the continuously increasing saturation temperature. Thus, most of the modest amount of energy being transferred goes into heating the residual mixture and very little into actual evaporation. The overall result is a very low rate of evaporation.

When an LNG mixture rich in heavier hydrocarbons is spilled on water, one would initially expect high heat fluxes and boiling rates. After ice is formed, it cools down and approaches the saturation point of mixture. Once the methane has been depleted significantly in the bulk of the residual liquid, the saturation temperature begins to rise and the heat flux decreases. Most of this small amount of energy goes to heat up the residual liquid to the new saturation temperature. Once all the methane is gone, the mixture is primarily ethane and propane. A new plateau in saturation temperature is reached as the heat flux goes toward preferentially evaporating the ethane yielding a secondary yet small peak in boiling rate. However as can be seen in Figure 4-12, the difference in volatility between ethane and propane and the change in saturation temperature are not as drastic as in the case in which methane was present; thus, although the behavior upon exhaustion of ethane will be similar to the previous exhaustion of methane, it is not as pronounced; in fact, a third peak is not necessarily expected.

Comparison of Results

Comparison with results reported by previous researchers is limited in scope. As indicated in Chapter II, Burgess (1970, 1972) used a very simplistic technique and reported only average values. Results reported by Boyle and Kneebone (1973) are questionable since very small amounts of cryogen were spilled in large confined pools; thus the exact area for heat transfer is debatable. In addition, boiling was accompanied by spreading in the initial period, a fact

which was unaccounted for. Because Vestal (1973) used a very small flask in his experiments, it is possible that a large amount of the energy for evaporation was supplied by the walls of the flask. Jeje used a more sophisticated technique and his results are the only ones that could be used in a quantitative comparison.

A qualitative comparison with reported results for pure methane boiling on water is given in Table 5-9. The water temperature did not have a significant effect in the evaporation of methane. This conclusion is in general agreement with other investigators. Similarly, the amount spilled does not play an important role in the evaporation of methane. The heat flux and boiling rate increases with time, a point with which only Vestal disagrees. This study, however, provides evidence that the increase in boiling rate does not continue indefinitely. It reaches a peak when the vapor film collapses completely and subsequently decreases monotonically.

Ultra high purity methane does not foam; the vapors are superheated 10-20 K when the amounts spilled are less than 0.5 g/cm^2; the superheat decreases as the amount spilled increases.

A similar comparison cannot be made with LNG. Evaporation of LNG is a far more complicated situation in which the composition plays the most important role. Each spill would have to be compared on the basis of the amount of each hydrocarbon present.

It's worthwhile to note that in a few experiments with methane-ethane mixtures in which the conditions were similar (composition, mass spilled), results in this study were comparable to those obtained by Jeje.

TABLE 5-9

Boiling of Liquid Methane on Water

Investigator		Burgess	Vestal	Jeje	Dincer	Valencia
Q (kW/m^2)	High	82(Avg)	197	95	110	120
	Low (Avg)	51(Avg)		30	30	25
Effect on Q due to an increase in:						
Water Temperature		--	same	same	same	same
Cryogen Mass		up	--	same	same	same
Time		up	down	up	up	up, initially down after collapse of vapor film
Foaming?		--	yes	no	--	no
Rough Interface?		--	no	no	--	no
Vapor Superheat?		--	--	10-30 K	--	0-10 K (>0.5 g/cm^2) 10-30 K (<0.5 g/cm^2)

VI. HEAT TRANSFER MODELS

Several authors have attempted to quantitatively explain the boiling of cryogenic hydrocarbons on water or even to predict a priori the boiling behavior of these hydrocarbons. Most of these models are rather simplistic and limited in their application. Therefore, it is desirable to develop appropriate mathematical models that will allow the prediction of the boiling behavior of LNG mixtures spilled on water.

Previous Models

Hoult (1972) couples evaporation and spreading rates of LNG to predict the time required for evaporation of a mass of LNG spilled on open water. Spreading is accounted for by allowing the area for heat transfer to vary with time. If the area is kept constant, Hoult's model applies to confined spills, such as those in the present study. Hoult assumes that the heat used to vaporize the LNG comes from freezing a layer, δ, of water

$$k_{ice} \frac{\Delta T}{\delta} = \rho_{water} \Delta H^{fusion} \frac{d\delta}{d\tau} \tag{6-1}$$

The solution to this equation is

$$\delta = \left(\frac{2 k_{ice} \Delta T \tau}{\rho_{water} \Delta H^{fusion}} \right)^{1/2} \tag{6-2}$$

where

$$\Delta T = T_{LNG} - T_{fusion} \tag{6-3}$$

Thus the heat flux becomes

$$q/A = \left(\frac{k_{ice}\ \Delta T\ \rho_{water}\ \Delta H^{fus}}{2}\right)^{1/2} \tau^{-1/2} \qquad (6\text{-}4)$$

or (in SI units)

$$q/A = \left(\frac{3.298 \times 10^{-3} \times 160 \times 1000 \times 333.9}{2}\right)^{1/2} \tau^{-1/2}$$

$$q/A = 297\ \tau^{-1/2}\ (kW/m^2) \qquad (6\text{-}5)$$

The rate of boiling can be obtained by dividing the heat flux by the heat of vaporization (510 kJ/kg),

$$m/A = 0.058\ \tau^{-1/2}\ (g/cm^2\text{-}s) \qquad (6\text{-}6)$$

Integrating the above expression up to time τ yields the total mass evaporated in that period of time,

$$M/A = 0.116\ \tau^{1/2}\ (g/cm^2) \qquad (6\text{-}7)$$

The mass evaporated predicted by Eq. (6-7) is compared to experimental data in Figure 6-1. Similarly, the boiling rates predicted by Eq. (6-6) are compared to experimental data in Figure 6-2.

Hoult's model ignores several factors both in the freezing and boiling processes. A linear temperature gradient across the growing ice layer is assumed, yet no provisions are made to account for the sensible cooling of ice. Sensible cooling of the water under the ice is also neglected. The major disadvantage is Hoult's assumption that

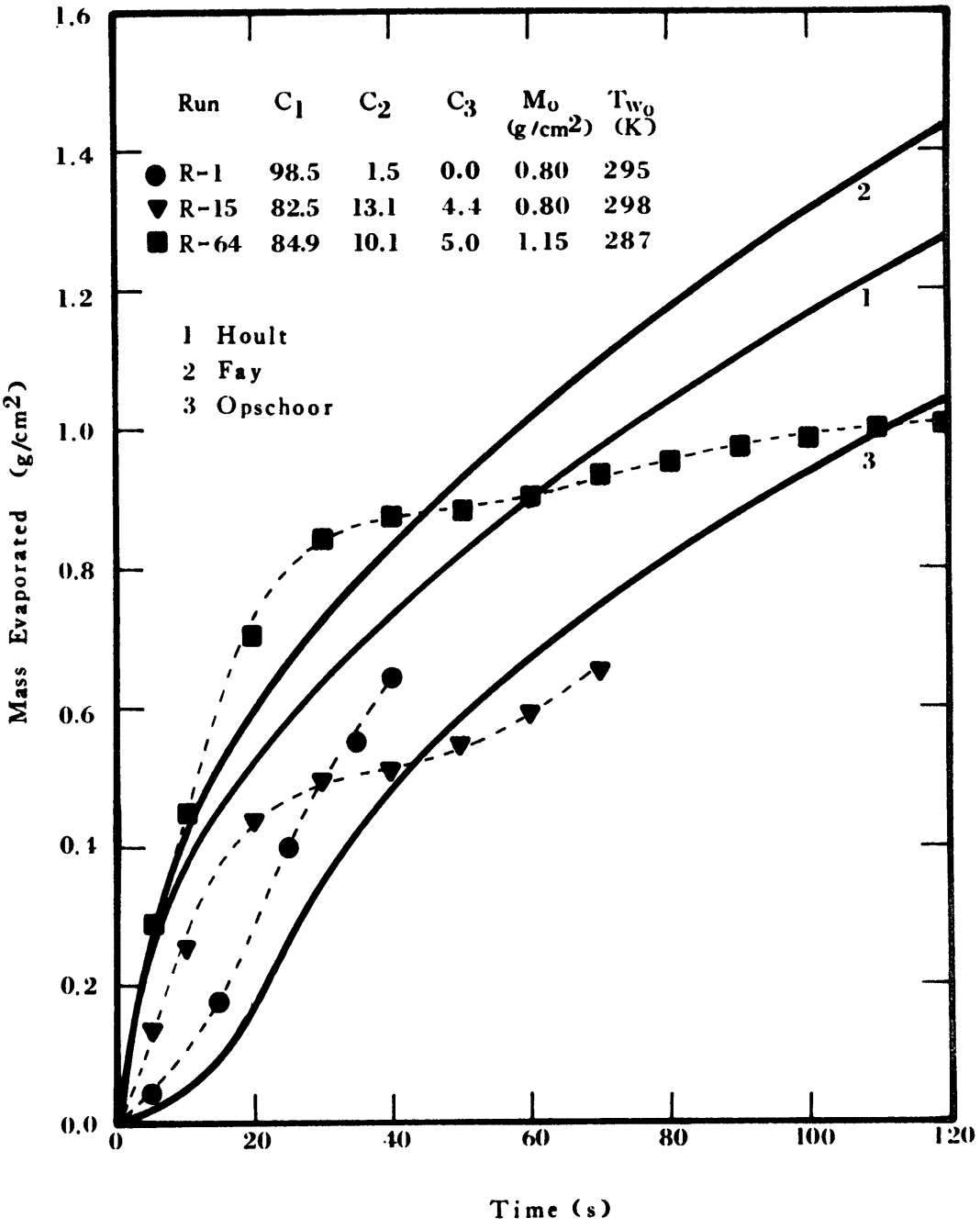

Figure 6-1 Comparison of Previous Models for Evaporation of LNG on Water with Experimental Data

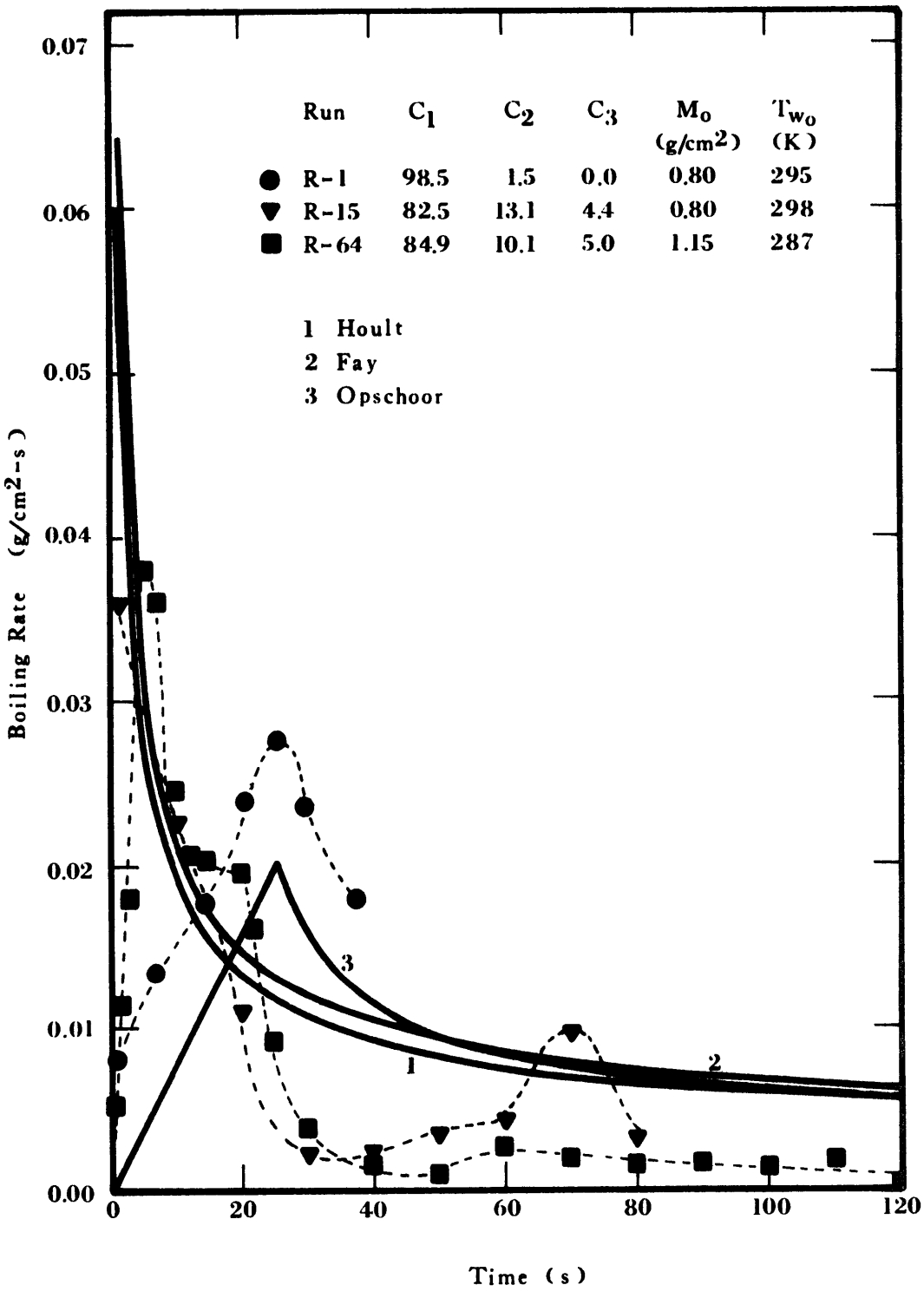

Figure 6-2 Comparison of Previous Models for Evaporation Rates of LNG on Water with Experimental Data

the only thermal resistance is within the ice layer; any surface resistance to boiling is completely neglected. This study has proven that the surface resistance is the dominant one in the early portion of the boiling process, particularly for "lean" LNG's (small amounts of heavy hydrocarbons). Furthermore, this model does not take into consideration the composition of the LNG which considerably affects the boiling behavior.

Fay (1973) improves Hoult's model by accounting for the sensible heat of cooling the ice below the freezing temperature:

$$k_{ice} \frac{\Delta T}{\delta} = \left(\rho_{ice} C_{p_{ice}} \frac{\Delta T}{2} + \rho_{ice} \Delta H^{fus} \right) \frac{d\delta}{d\tau} \qquad (6\text{-}8)$$

The thickness of the ice layer at a time τ is given by the solution to this equation,

$$\delta = \left(\frac{2 k_{ice} \Delta T \tau}{\rho_{ice} \Delta H^{fus} + \rho_{ice} C_{p_{ice}} \frac{\Delta T}{2}} \right)^{1/2} \qquad (6\text{-}9)$$

The heat flux becomes

$$q/A = \left(\frac{k_{ice} \Delta T \left(\rho_{ice} \Delta H^{fus} + \rho_{ice} C_{p_{ice}} \frac{\Delta T}{2} \right)}{2} \right)^{1/2} \tau^{-1/2} \qquad (6\text{-}10)$$

Substituting the physical constants in SI units

$$q/A = \left(\frac{3.298 \times 10^{-3} \times 160}{2} \times (921.2 \times 333.9 + 921.2 \times 1.531 \times 160/2) \right)^{1/2} \tau^{-1/2}$$

or

$$q/A = 333.05\ \tau^{-1/2}\ (kW/m^2) \qquad (6\text{-}11)$$

The boiling rate is given by

$$m/A = 0.065\ \tau^{-1/2}\ (g/cm^2\text{-}s) \qquad (6\text{-}12)$$

and the mass evaporated by

$$M/A = 0.131\ \tau^{1/2}\ (g/cm^2) \qquad (6\text{-}13)$$

The mass evaporated and boiling rates predicted by these equations are compared to experimental data in Figures 6-1 and 6-2, respectively.

Fay's model suffers from the same shortcomings of Hoult's model, with the exception that the sensible heat of cooling the ice has been accounted for.

Opschoor (1977) uses a model similar to Fay's, but realizes the fact that initially film boiling will occur and that the cryogen saturation temperature will increase as methane preferentially evaporates. Using equations similar to Fay's, Opschoor indicates the following time dependancy for the evaporation rate of LNG

$$m/A = 0.0517\ \ ^{-1/2}\ (g/cm^2\text{-}s) \qquad (6\text{-}14)$$

Opschoor indicates that an ice layer will form after about 20 s and Eq. (6-14) will apply after the ice has formed. After examining the data reported by Boyle and Kneebone (1973), Opschoor concludes that a reasonable model for the boiling rates of LNG on water is represented by the following equations:

$$\left.\begin{aligned} m/A &= 0.0008\ \tau\ (g/cm^2\text{-}s) \qquad 0 \leq \tau \leq 25\ s \\ m/A &= 0.0517/(\tau - 20)^{1/2}\ (g/cm^2\text{-}s) \qquad \tau > 25\ s \end{aligned}\right\} \tag{6-15}$$

The corresponding mass evaporated is given by

$$\left.\begin{aligned} M/A &= 0.0004\ \tau^2\ (g/cm^2 \qquad 0 \leq \tau \leq 25\ s \\ M/A &= 0.103\ (\tau - 20)^{1/2} + 0.019\ (g/cm^2) \qquad \tau > 25\ s \end{aligned}\right\} \tag{6-16}$$

The choice of values in these equations is determined by best fitting two sets of experimental data; they are not derived from any theoretical considerations. Therefore, this model is a semi-empirical one and although Opschoor recognizes two important factors, initial film boiling as well as change in saturation temperature with preferential evaporation of volatiles, he is unable to incorporate them in his model on any theoretical grounds.

Before introducing the model proposed in this study for the evaporation of LNG on a confined water surface, several simpler models will be developed to illustrate the qualitative explanations given in Chapter V. The easiest case to be treated is the evaporation of liquid hydrocarbons on a solid body such as ice; this case can be approximated by conduction through a semi-infinite solid whose surface suddenly undergoes a step change in temperature.

Semi-Infinite Solid

Consider a body whose surface is the plane x = 0, of infinite depth in the x-direction and unbounded in the other two cartesian

directions, as shown in Figure 6-3. The equation that governs the transient conduction is

$$\rho C_p \frac{dT}{d\tau} = \frac{\partial}{\partial x}\left(k \frac{\partial T}{\partial x}\right) \tag{6-17}$$

The thermophysical properties of ice do change between the freezing point of water (273 K) and the boiling point of methane (112 K), (see Appendix D). If the properties of ice are evaluated at the average of the ice and cryogen temperatures, the approximation of constant properties may be used to rewrite the differential equation as

$$\frac{dT}{d\tau} = \alpha \frac{\partial^2 T}{\partial x^2} \tag{6-18}$$

where the thermal diffusivity α is defined as

$$\alpha = \frac{k}{\rho C_p} \tag{6-19}$$

With the following boundary conditions

$$T = T_i \qquad x \geq 0 \qquad \tau = 0 \tag{6-20}$$

$$T = T_c \qquad x = 0 \qquad \tau > 0 \tag{6-21}$$

$$T = T_i \qquad x = \infty \qquad \tau > 0 \tag{6-22}$$

the solution to the differential equation is

$$\frac{T - T_c}{T_i - T_c} = \text{erf} \frac{x}{2\sqrt{\alpha\tau}} \tag{6-23}$$

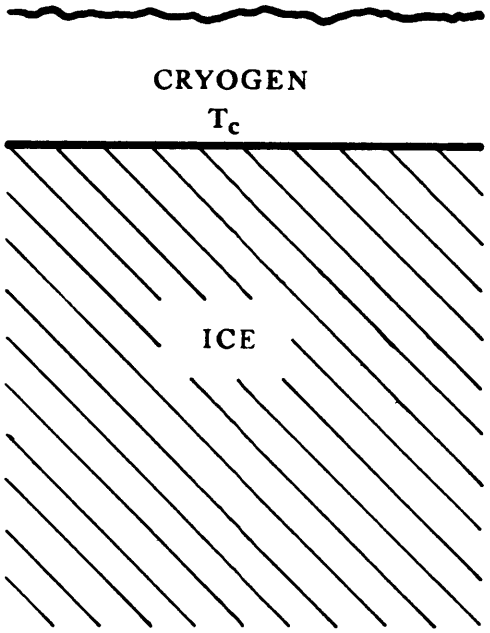

$$\frac{\partial T}{\partial \tau} = \alpha \frac{\partial^2 T}{\partial x^2}$$

$$T(x,0) = T_i$$

$$\left.\begin{aligned} T(0,\tau) &= T_c \\ T(\infty,\tau) &= T_i \end{aligned}\right\} \tau > 0$$

$$\frac{q}{A} = \frac{k(T_i - T_c)}{\sqrt{\pi \alpha}} \tau^{-1/2}$$

Figure 6-3 Semi-Infinite Solid Model

The heat flux across the interface is given by

$$q/A = k \left.\frac{dT}{dx}\right|_{x=0} \tag{6-24}$$

or

$$q/A = \frac{k(T_i - T_c)}{\sqrt{\pi\alpha\tau}} \tag{6-25}$$

Using the thermophysical properties given in Table 6-1, the following heat fluxes are obtained for methane, ethane and propane boiling on ice,

$$q/A_{methane} = 196.5\ \tau^{-1/2} \quad (kW/m^2) \tag{6-26}$$

$$q/A_{ethane} = 105.0\ \tau^{-1/2} \quad (kW/m^2) \tag{6-27}$$

$$q/A_{propane} = 49.2\ \tau^{-1/2} \quad (kW/m^2) \tag{6-28}$$

The total mass evaporated up to a time τ can be evaluated by integrating the heat flux equations and dividing by the heat of vaporization of the cryogen,

$$M/A_{methane} = 0.07706\ \tau^{1/2} \quad (g/cm^2) \tag{6-29}$$

$$M/A_{ethane} = 0.04294\ \tau^{1/2} \quad (g/cm^2) \tag{6-30}$$

$$M/A_{propane} = 0.02310\ \tau^{1/2} \quad (g/cm^2) \tag{6-31}$$

TABLE 6-1

Thermophysical Properties Used in the

Semi-Infinite Solid Model

	Methane	Ethane	Propane
T_c (K)	111.7	184.5	231.3
T_i (K)	273.2	273.2	273.2
k (kJ/s-m-K)*	3.298×10^{-3}	2.721×10^{-3}	2.439×10^{-3}
ρ (kg/m^3)*	921.2	917.5	915.2
C_p (kJ/kg-K)*	1.531	1.764	1.938
α (m^2/s)*	2.338×10^{-6}	1.681×10^{-6}	1.375×10^{-6}
ΔH^{vap} (kJ/kg)	510.	489.	426.

*Evaluated at $T = (T_c + T_i)/2$

Predictions made by these equations are compared to experimental data in Figures 6-4, 6-5 and 6-6, respectively.

The semi-infinite solid model overestimates the mass evaporated for methane boiling on ice, particularly in the first 40 seconds. Such disagreement is expected since methane film boils on ice in the initial phase. This was discussed in Chapter V. As a consequence of the formation of the vapor film, the ice surface does not come in direct contact with methane. Therefore its temperature does not approach the temperature of methane until the film collapses since a gradient exits across the vapor film. After about 20 seconds, the heat flux predicted by the model decreases significantly whereas in the actual experiments the film is beginning to collapse and high fluxes are attained; the overall result is that after about 40-50 seconds the agreement between the model and the experimental data is a reasonable one.

In the case of ethane, transitional boiling takes place; however, the ice surface temperature drops quickly and nucleate boiling is established. Thus the surface of the ice quickly approaches the temperature of ethane, and the model is a good representation of the physical situation. Propane nucleate boils on ice, so the surface temperature of the ice approaches the propane temperature rather fast and the model also gives a good representation of the physical situation.

For the more important case of evaporation of hydrocarbons on water, it would appear that a new model must be used.

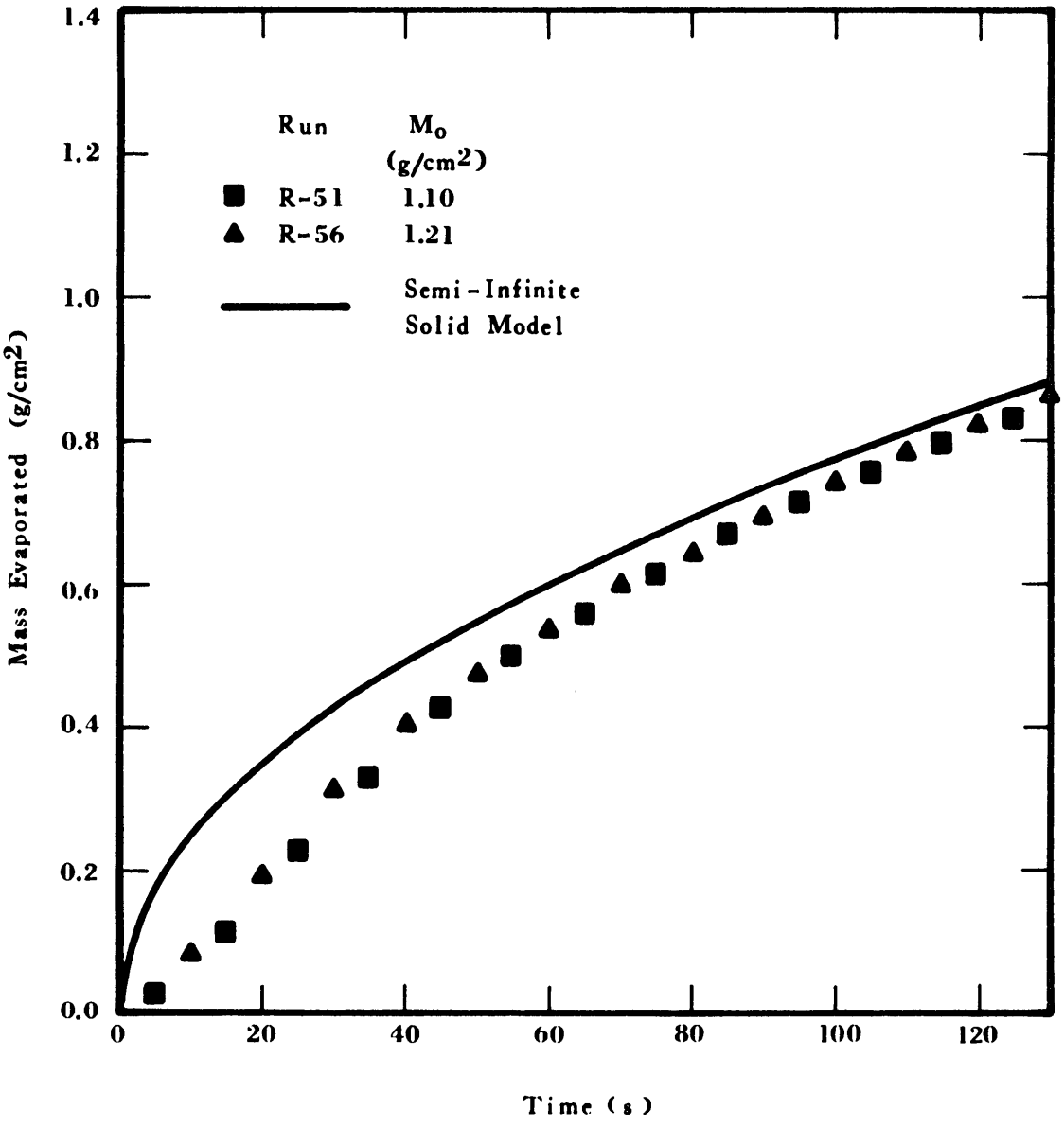

Figure 6-4 Boiling of Methane on Ice. Semi-Infinite Solid Model and Experimental Data

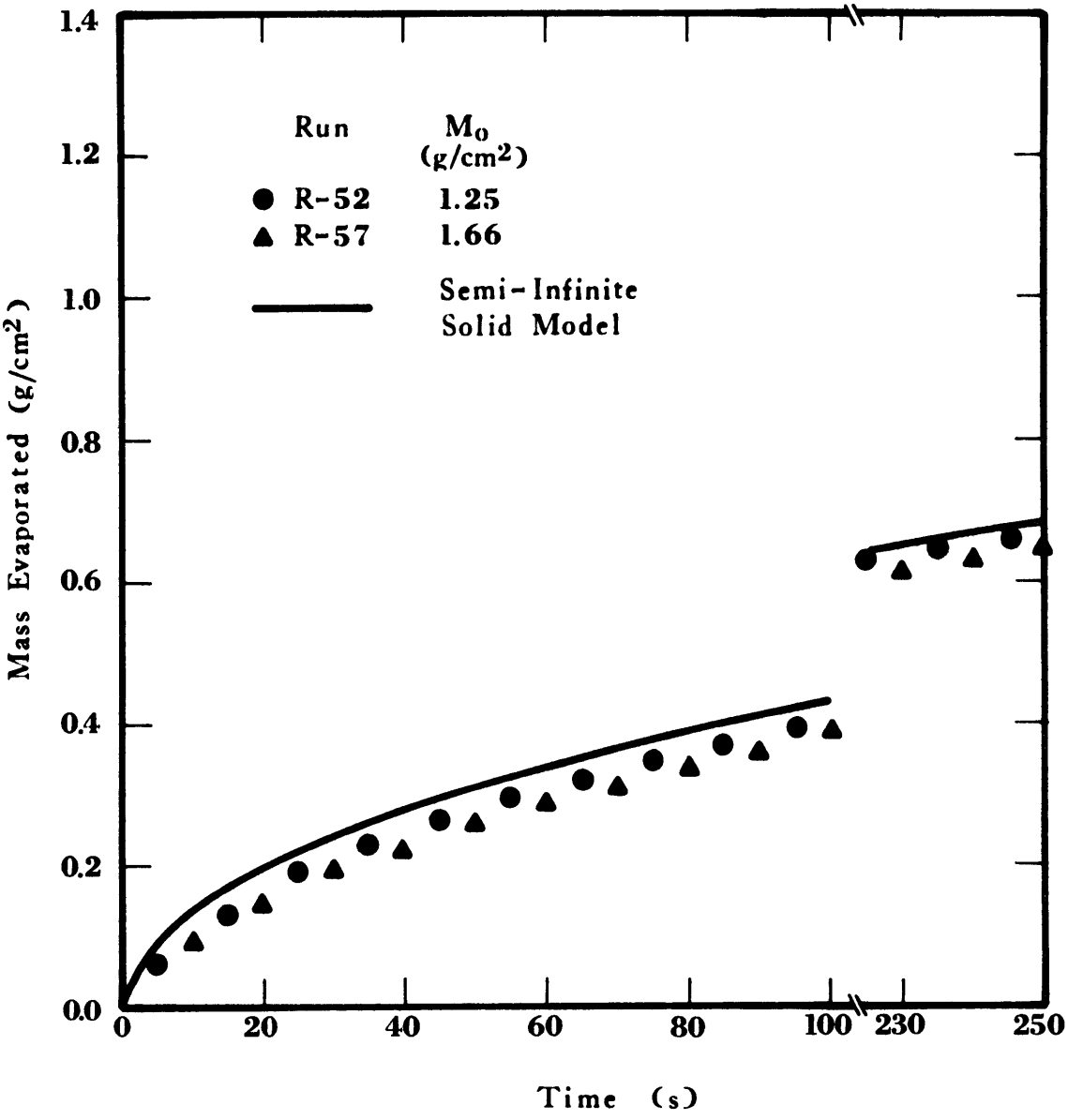

Figure 6-5 Boiling of Ethane on Ice. Semi-Infinite Solid Model and Experimental Data

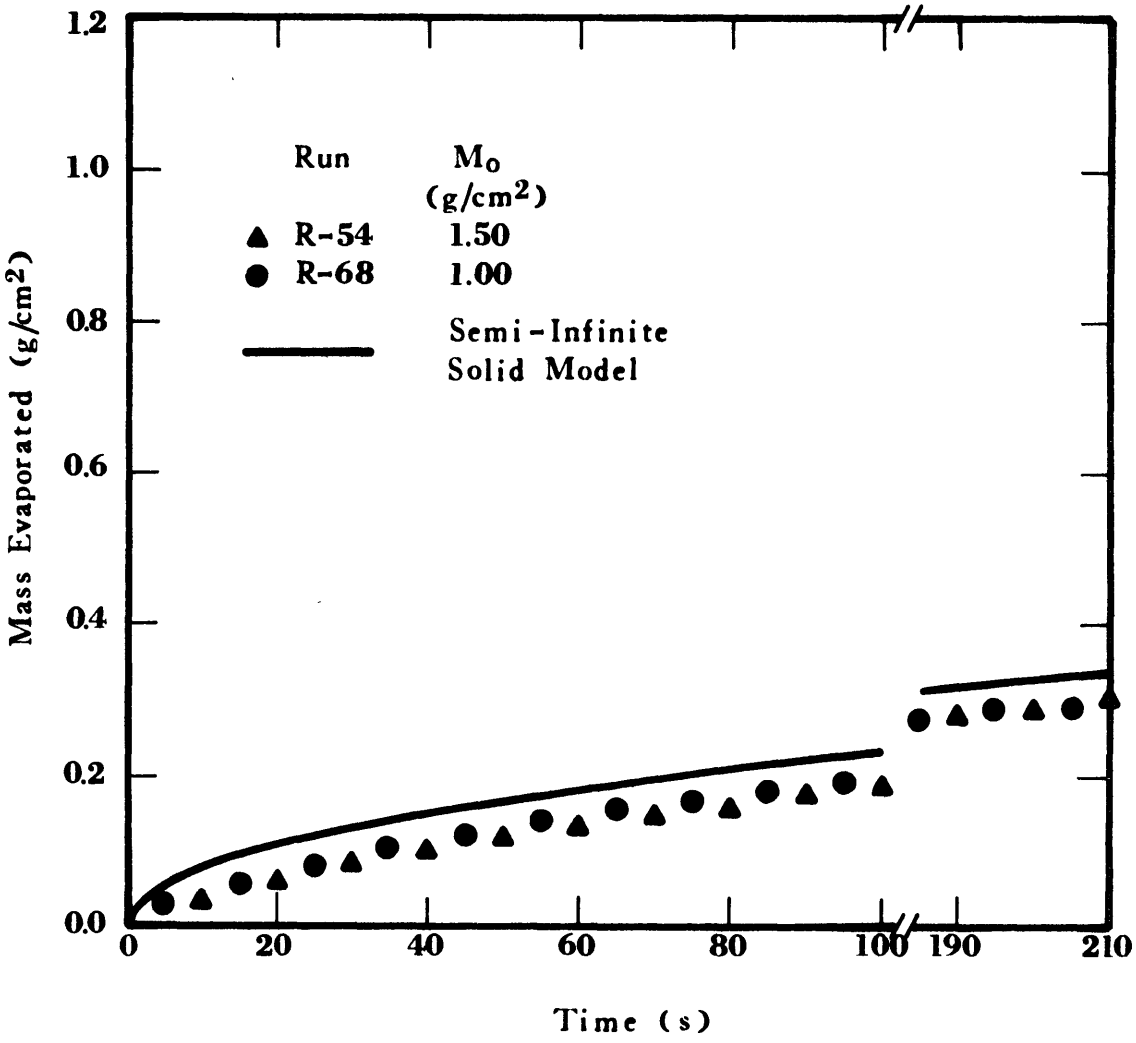

Figure 6-6 Boiling of Propane on Ice. Semi-Infinite Solid Model and Experimental Data

Moving Boundary Model

Consider the system shown in Figure 6-7. At a time $\tau = 0$ s a cryogen at a temperature T_c is placed in contact with a body of water at a uniform initial temperature T_w. Since the cryogen temperature is lower than the solidification temperature of water, T_f, ice will begin to cover the water surface. The ice layer will continue to grow in thickness as more cryogen boils on its surface. Thus the ice-water boundary moves with time. A further complication arises due to the density of ice being lower than that of water; this causes the ice-cryogen interface to be displaced from the original water-cryogen interface.

Heat transfer in the ice layer must satisfy the transient conduction equation

$$\frac{dT_1}{d\tau} = \alpha_1 \frac{\partial^2 T_1}{\partial x_1^2} \tag{6-32}$$

The same equation is assumed to apply to the water layer

$$\frac{dT_2}{d\tau} = \alpha_2 \frac{\partial^2 T_2}{\partial x_2^2} \tag{6-33}$$

At any time $\tau > 0$

$$T_1 = T_c \quad \text{at} \quad x_1 = 0 \tag{6-34}$$

and

$$T_2 = T_w \quad \text{at} \quad x_2 = \infty \tag{6-35}$$

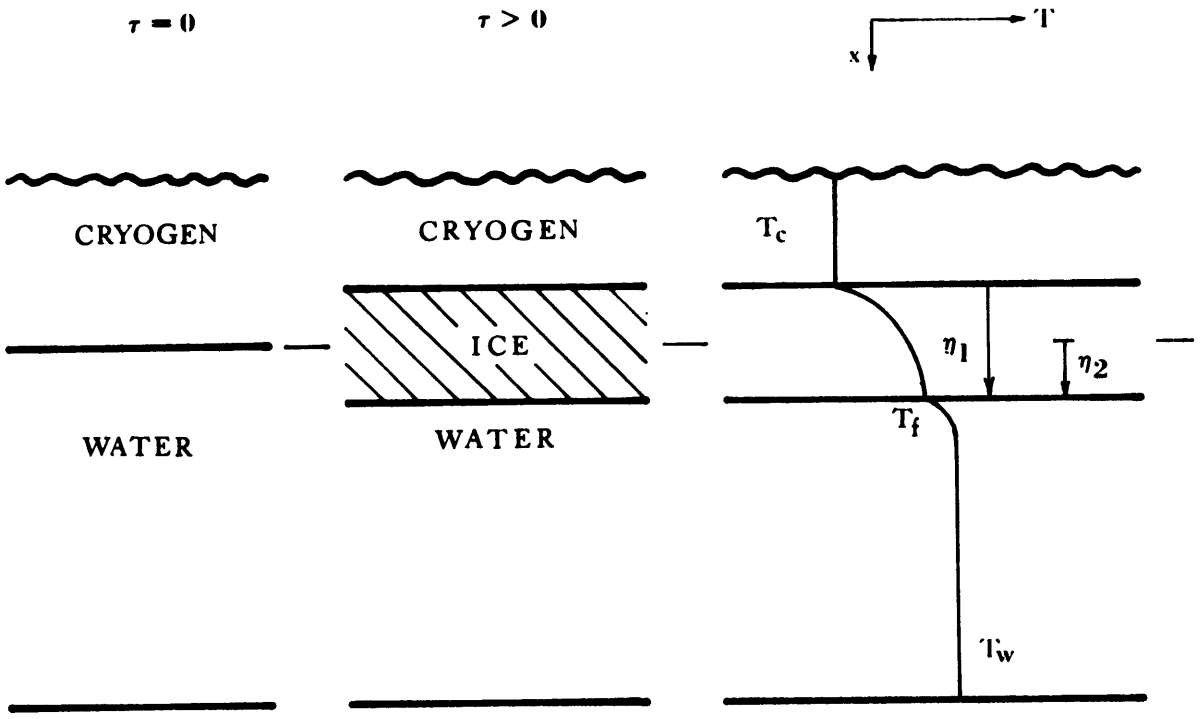

$$\frac{\partial T_1}{\partial \tau} = \alpha_1 \frac{\partial^2 T_1}{\partial x^2}$$

$$\frac{\partial T_2}{\partial \tau} = \alpha_2 \frac{\partial^2 T_2}{\partial x^2}$$

$$k_1 \left(\frac{\partial T_1}{\partial x_1}\right)_{x_1=\eta_1} - k_2 \left(\frac{\partial T_2}{\partial x_2}\right)_{x_2=\eta_2} = \rho_1 \Delta H^{fus} \frac{d\eta_1}{d\tau}$$

$$\frac{\eta_1}{\eta_2} = \frac{\rho_2}{\rho_1} = \beta$$

$$\frac{q}{A} = -\frac{(T_f - T_c)\, k_1}{\sqrt{\pi \alpha_1}\ \mathrm{erf}\,(K\beta\, 2\sqrt{\alpha_1})}\ \tau^{-1\,2} = \epsilon \tau^{-1\,2}$$

Figure 6-7 Moving Boundary Model

The displacement of the cryogen-ice interface is controlled by the ratio of the water to ice densities

$$\frac{\eta_1}{\eta_2} = \frac{\rho_2}{\rho_1} = \beta \tag{6-36}$$

The temperature of the ice-water interface must be at all times the solidification temperature of water

$$T_1 = T_2 = T_f \quad \text{at} \quad x_1 = \eta_1 \quad \text{or} \quad x_2 = \eta_2 \tag{6-37}$$

When the ice-water interface advances a distance $d\eta_1$, a quantity of heat $\rho_1 \Delta H^{fus} d\eta_1$ is liberated per unit area and must be removed by conduction

$$k_1\left(\frac{\partial T_1}{\partial x_1}\right)_{x_1=\eta_1} - k_2\left(\frac{\partial T_2}{\partial x_2}\right)_{x_2=\eta_2} = \rho_1 \Delta H^{fus} \frac{d\eta_1}{d\tau} \tag{6-38}$$

The solution to the above system of differential equations is due to Neumann (1912) although since Stefan (1891) first discussed the problem in a study of the thickness of polar ice, problems of this type are referred to as "Stefan's Problems".

Evaluation of the temperature profiles as well as heat fluxes require the determination of a parameter K, given by the equation (Eckert and Drake; Carslaw and Jaeger)

$$\frac{(T_f - T_c)k_1 \exp(-K^2\beta^2/4\alpha_1)}{\sqrt{\pi\alpha_1}\ \mathrm{erf}(K\beta/2\sqrt{\alpha_1})} - \frac{(T_w - T_f)k_2 \exp(-K^2/4\alpha_2)}{\sqrt{\pi\alpha_2}\ \mathrm{erfc}(K/2\sqrt{\alpha_2})} = \frac{\Delta H^{fus}\rho_1 K \beta}{2} \tag{6-39}$$

The temperature profile in the ice becomes

$$\frac{T_1 - T_f}{T_c - T_f} = 1 - \frac{\text{erf}(x_1/2\sqrt{\alpha_1 \tau})}{\text{erf}(K\beta/2\sqrt{\alpha_1})} \tag{6-40}$$

and the temperature profile in the liquid phase becomes

$$\frac{T_2 - T_f}{T_w - T_f} = 1 - \frac{\text{erfc}(x_2/2\sqrt{\alpha_2 \tau})}{\text{erfc}(K/2\sqrt{\alpha_2})} \tag{6-41}$$

The heat flux across the cryogen-ice interface

$$q/A = k_1 \left.\frac{\partial T_1}{\partial x_1}\right|_{x_1=0} \tag{6-42}$$

becomes

$$q/A = \frac{k_1(T_f - T_c)}{\text{erf}\left(\frac{K\beta}{2\sqrt{\alpha_1}}\right)\sqrt{\pi \alpha_1 \tau}} \tag{6-43}$$

Again if the thermophysical properties are evaluated at the average temperature between T_f and T_c, and then assumed constant, the heat loss from the ice is

$$q/A = \varepsilon\, \tau^{-1/2} \tag{6-44}$$

where

$$\varepsilon = \frac{k_1(T_f - T_c)}{\sqrt{\pi \alpha_1}\ \text{erf}\left(\frac{K\beta}{2\sqrt{\alpha_1}}\right)} \tag{6-45}$$

These constants can be evaluated with the values given in Table 6-2.

For methane

$$\frac{K\beta}{2\sqrt{\alpha_1}} = 0.507$$

and

$$q/A = 373\ \tau^{-1/2} \quad (kW/m^2) \tag{6-46}$$

Integrating over time and dividing by the heat of vaporization one obtains the mass evaporated per unit area.

$$M/A = 0.146\ \tau^{1/2} \quad (g/cm^2) \tag{6-47}$$

For ethane

$$\frac{K\beta}{2\sqrt{\alpha_1}} = 0.413$$

and

$$q/A = 238\ \tau^{-1/2} \quad (kW/m^2) \tag{6-48}$$

$$M/A = 0.097\ \tau^{1/2} \quad (g/cm^2) \tag{6-49}$$

For propane

$$\frac{K\beta}{2\sqrt{\alpha_1}} = 0.302$$

and

$$q/A = 149\ \tau^{-1/2} \quad (kW/m^2) \tag{6-50}$$

$$M/A = 0.070\ \tau^{1/2} \quad (g/cm^2) \tag{6-51}$$

TABLE 6-2

Thermophysical Properties Used in the

Moving Boundary Model

	Methane	Ethane	Propane
T_c (K)	111.7	184.5	231.3
T_f (K)	273.2	273.2	273.2
T_w (K)	288.0	288.0	288.0
k_{ice} (kJ/s-m-K)*	3.298×10^{-3}	2.721×10^{-3}	2.439×10^{-3}
ρ_{ice} (kg/m^3)*	921.2	917.5	915.2
$C_{p_{ice}}$ (kJ/kg-K)*	1.531	1.764	1.938
α_{ice} (m^2/s)*	2.338×10^{-6}	1.681×10^{-6}	1.375×10^{-6}
k_{water} (kJ/s-m-K)**	5.687×10^{-4}	5.687×10^{-4}	5.687×10^{-4}
ρ_{water} (kg/m^3)**	999.9	999.9	999.9
$C_{p_{water}}$ (kJ/kg-K)**	4.1992	4.1992	4.1992
α_{water} (m^2/s)**	1.354×10^{-7}	1.354×10^{-7}	1.354×10^{-7}
ΔH^{vap} (kJ/kg)	510.	489.	426.
ΔH_{ice}^{fus} (kJ/kg)	333.9	333.9	333.9
K ($m/s^{1/2}$)	14.30×10^{-4}	9.82×10^{-4}	6.47×10^{-4}
β	1.085	1.090	1.093

*Evaluated at $T = (T_c + T_f)/2$

**Evaluated at $T = (T_w + T_f)/2$

The mass evaporated as a function of time predicted by Eqs. (6-47), (6-49) and (6-51) were compared to experimental data in Figures 6-8, 6-9 and 6-10, respectively.

The values predicted by the Moving Boundary Model for methane boiling on water are much too high in the first 40-60 seconds. After this period of time, the predictions are closer to the experimental data but always on the high side. This is understandable since the model assumes that the surface temperature of the substrate (ice/water) approaches the cryogen's temperature immediately after the spill. The formation of the vapor film obviously prevents the substrate surface from reaching the temperature of the cryogen until the film collapses and nucleate boiling is established. This happens after about 40 seconds. Consequently, it is reasonable to expect the experimental heat fluxes, and the mass evaporated, to be lower than those predicted by the model, particularly in the early period of the test.

The predictions for ethane boiling on water are also too high in the first 20-30 seconds. As previously explained in Chapter V, ethane is not believed to nucleate boil on water upon initial contact; instead it boils in the transition regime. The surface of the substrate approaches the temperature of ethane after 10-15 seconds when nucleate boiling is fully established. The model, then, assumes a larger temperature drop than the actual one and, consequently, predicts higher initial heat fluxes and mass evaporation.

Propane is extremely difficult to characterize. The amount evaporated in the first couple of seconds is strongly dependent on

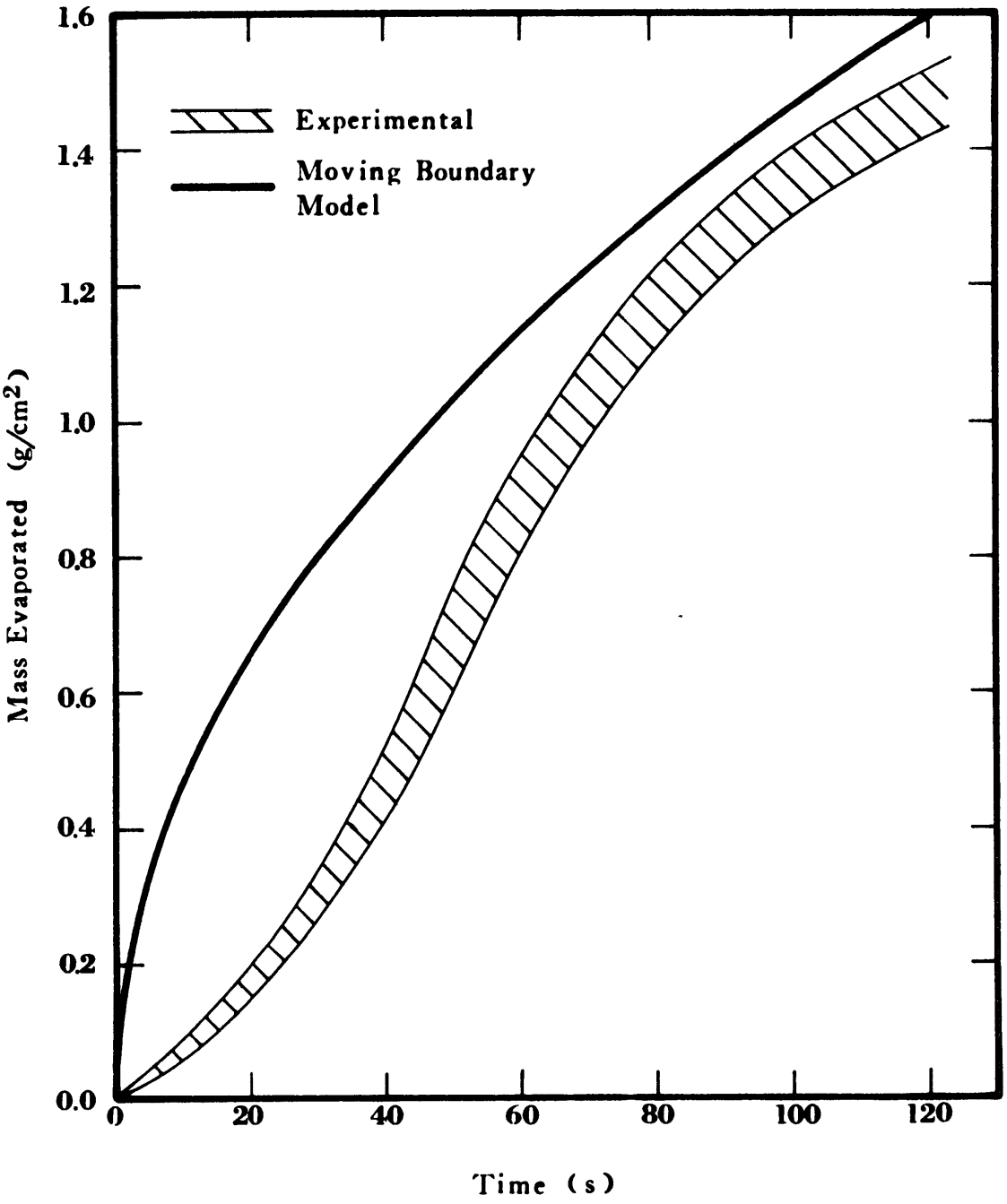

Figure 6-8 Boiling of Methane on Water. Moving Boundary Model and Experimental Data

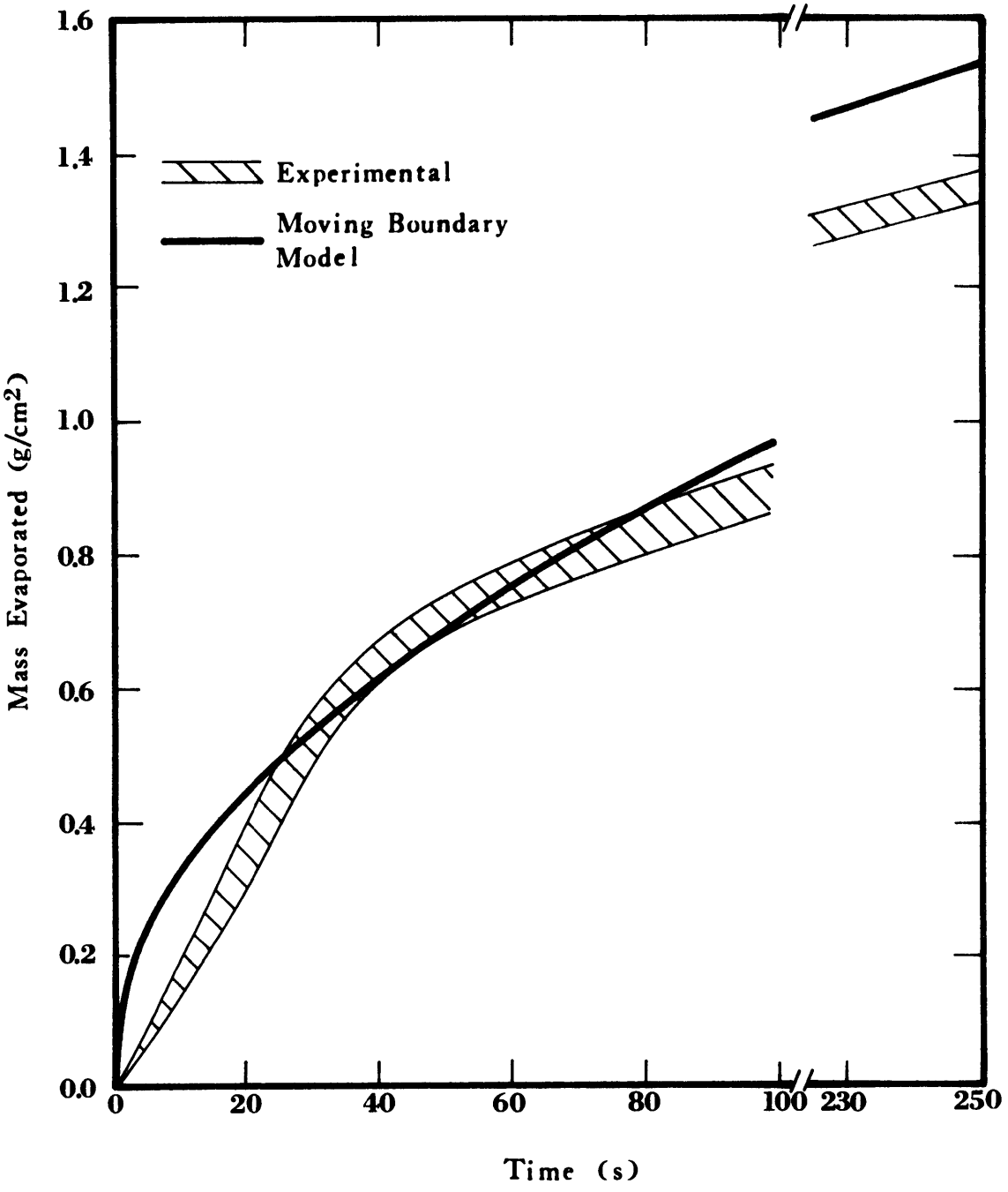

Figure 6-9 Boiling of Ethane on Water. Moving Boundary Model and Experimental Data

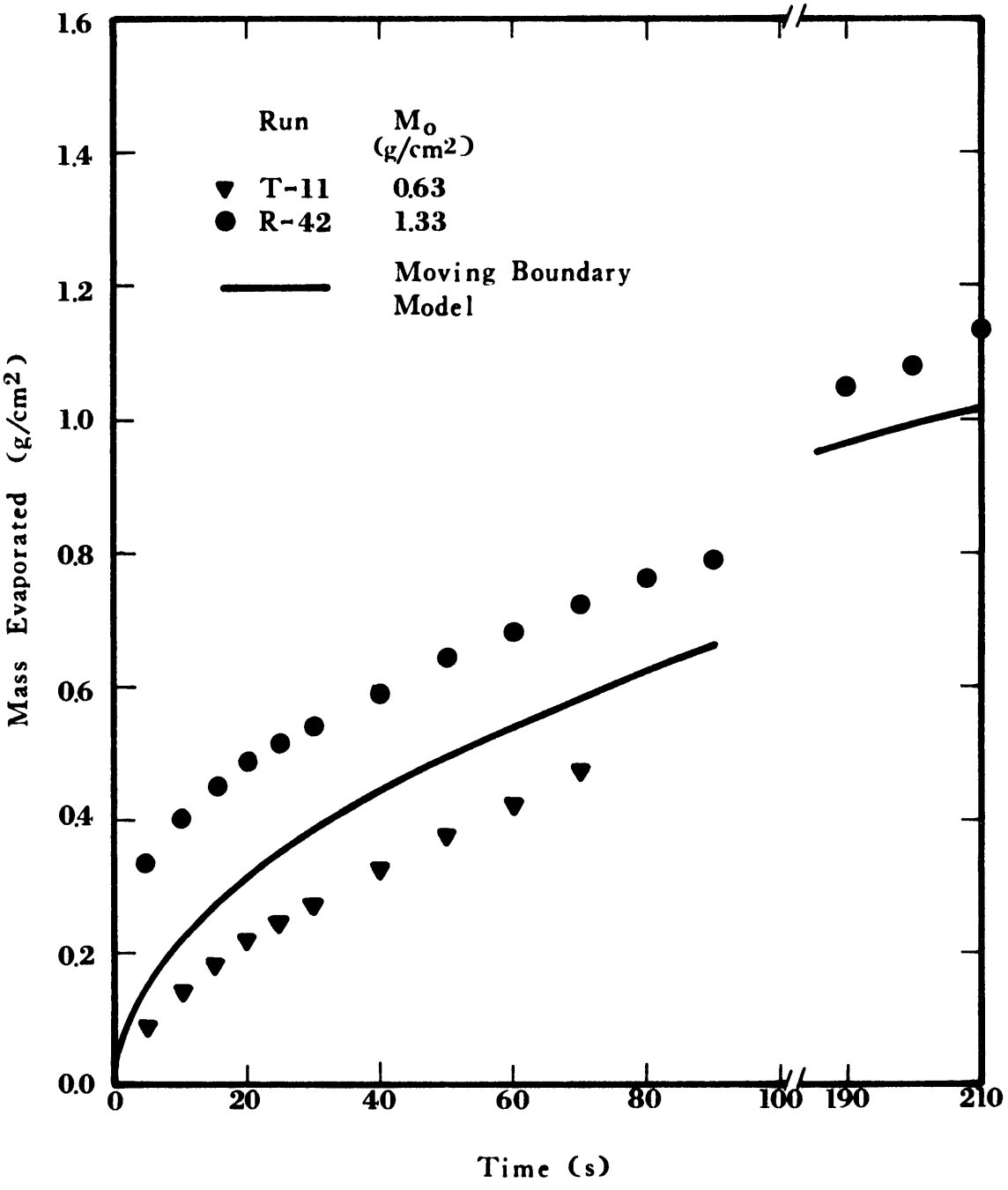

Figure 6-10 Boiling of Propane on Water. Moving Boundary Model and Experimental Data

the disturbance of the water surface caused by the spill. Propane nucleate boils on water upon initial contact, so the surface of the ice formed quickly reaches propane temperatures. Therefore, the predictions made with the Moving Boundary Model should be close to the experimental data except for the first few seconds. This can be observed in Figure 6-10; the experimental data lies parallel to the model predictions, differing only in the first few seconds.

Regression of Surface Temperature by Using Convolution Integrals

A severe limitation in the Semi-Infinite Solid and the Moving Boundary Models is the boundary condition at the surface that implies that the surface temperature undergoes a step change and remains constant thereafter. In order to develop a model closer to the physical situation, the temperature at the surface of the substrate must be allowed to vary with time. The heat fluxes obtained from experimental data are used to determine the time functionality of the variation of the surface temperature of the substrate.

Boiling on Ice

Transient conduction in a semi-infinite solid is controlled by Eq. (6-18), repeated here for convenience.

$$\frac{\partial T}{\partial \tau} = \alpha \frac{\partial^2 T}{\partial x^2} \tag{6-52}$$

or

$$\frac{\partial \theta}{\partial \tau} = \alpha \frac{\partial^2 \theta}{\partial x^2} \tag{6-53}$$

where $$\theta = T - T_i \tag{6-54}$$

and

T_i = initial temperature

Constant properties are assumed and are evaluated at the average of the initial solid and cryogen temperatures.

The following boundary conditions apply,

$$\theta = 0 \quad \text{at} \quad x \geq 0 \, , \, \tau = 0 \tag{6-55}$$

$$\frac{\partial \theta}{\partial x} = - \frac{q(\tau)}{k} \quad x = 0 \, , \, \tau > 0 \tag{6-56}$$

$$\theta = 0 \qquad x = \infty \, , \, \tau > 0 \tag{6-57}$$

Using Laplace transforms on Eq. (6-53) yields

$$s\bar{\theta} = \alpha \frac{\partial^2 \bar{\theta}}{\partial x^2} \tag{6-58}$$

Similarly, the Laplace transform of Eq. (6-56) is

$$\frac{\partial \bar{\theta}}{\partial x} = - \frac{q(s)}{k} \tag{6-59}$$

The solution to Eq. (6-58) is

$$\bar{\theta}(x,s) = C_1 \exp(- \sqrt{\frac{s}{\alpha}} \, x) + C_2 \exp(\sqrt{\frac{s}{\alpha}} \, x) \tag{6-60}$$

The condition given by Eq. (6-57) can be met only if $C_2 = 0$, thus

$$\bar{\theta}(x,s) = C_1 \exp(-\sqrt{\frac{s}{\alpha}}\, x) \tag{6-61}$$

Replacing Eq. (6-61) in Eq. (6-59) one obtains

$$\frac{\partial \bar{\theta}}{\partial x}\bigg|_{x=0} = C_1(-\sqrt{\frac{s}{\alpha}}) \exp(-\sqrt{\frac{s}{\alpha}}\, x) = -C_1 \sqrt{\frac{s}{\alpha}} = -\frac{q(s)}{k}$$

and

$$C_1 = \sqrt{\frac{\alpha}{s}}\ \frac{q(s)}{k} \tag{6-62}$$

Equation (6-61) becomes

$$\bar{\theta}(x,s) = \frac{q(s)}{k}\sqrt{\frac{\alpha}{s}}\ \exp(-\sqrt{\frac{s}{\alpha}}\, x) \tag{6-63}$$

The time dependent solution is obtained by taking the inverse Laplace transform of the above expression.

$$\theta(x,\tau) = L^{-1}\left\{\frac{q(s)}{k}\sqrt{\frac{\alpha}{s}}\ \exp(-\sqrt{\frac{\alpha}{s}}\, x)\right\} \tag{6-64}$$

At the ice surface, x = 0 and

$$\theta(0,\tau) = L^{-1}\left\{\frac{q(s)}{k}\sqrt{\frac{\alpha}{s}}\right\} \tag{6-65}$$

or

$$\theta(0,\tau) = \frac{1}{k}\sqrt{\frac{\alpha}{\pi}}\int_0^{\tau} q(\lambda)(\tau - \lambda)^{-1/2}\, d\lambda \tag{6-66}$$

Using the following substitution

$$du = (\tau - \lambda)^{-1/2}\, d\lambda \tag{6-67}$$

or

$$u = -(\tau - \lambda)^{1/2} \tag{6-68}$$

Eq. (6-66) can be rewritten as

$$\theta(0,\tau) = \frac{1}{k}\sqrt{\frac{\alpha}{\pi}}\int_0^{-2\sqrt{\tau}} q(\tau - \frac{u^2}{4})\, du \tag{6-69}$$

This equation can then be integrated numerically using the experimental heat fluxes.

The drop in surface temperature of ice after a methane spill, calculated with Eq. (6-69), is shown in Figure 6-11. These results further reinforce the qualitative explanation given in Chapter V, methane film boils on ice at first, and nucleate boils only after the surface temperature of the ice drops to the point that a vapor film can no longer be maintained. Furthermore, the temperature drop can be approximated by a linear drop in temperature over a period of time τ_{cf}, in the case of methane 25 s.

The drop in the surface temperature of ice after an ethane spill is shown in Figure 6-12. As in the case of methane, it takes a finite time before the surface reaches ethane temperatures. This also reinforces the qualitative explanation given in Chapter V that ethane boils in the transition regime first and nucleate boils subsequently. Transition boiling means some intermittent contact between the ice and ethane and, consequently, the surface temperature of the ice drops more rapidly than in the case of methane. Again, a linear drop in temperature can be used in subsequent heat transfer models. The time τ_{cf} in this case is only 5 s.

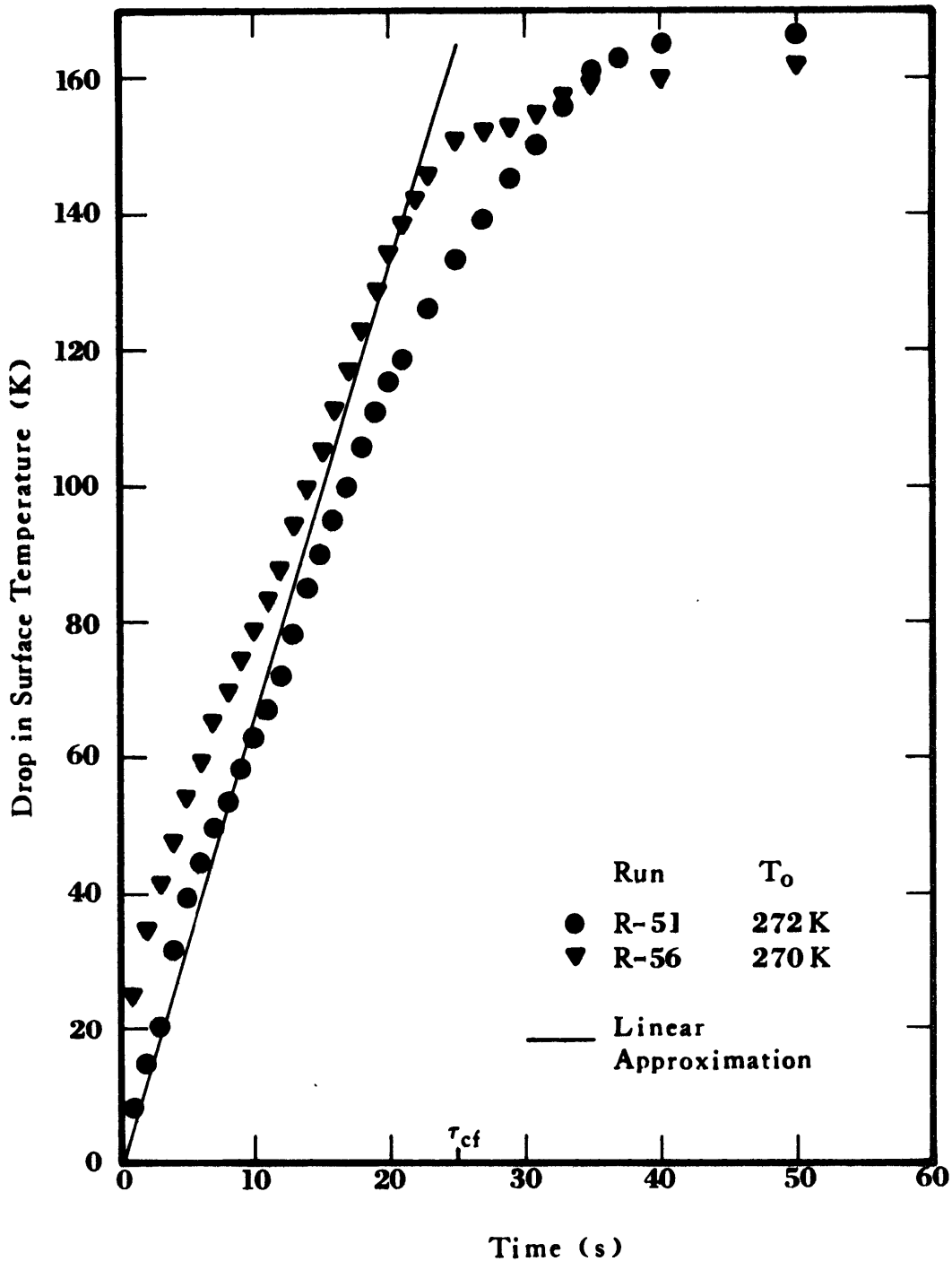

Figure 6-11 Drop in Surface Temperature of Ice after a Methane Spill

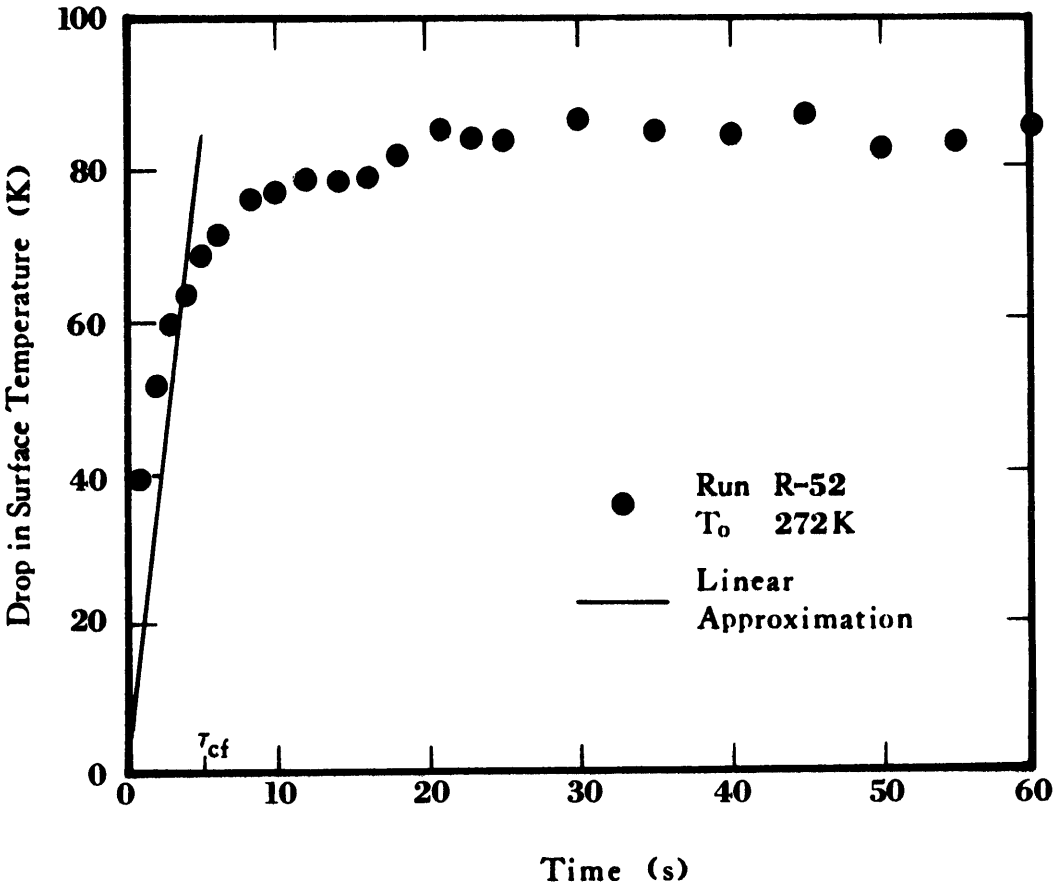

Figure 6-12 Drop in the Surface Temperature of Ice after an Ethane Spill

Boiling on Water

A convolution integral can be used to determine the drop in surface temperature after spilling a cryogen on water. The differential equations describing the Moving Boundary Model are used in a form similar to those used for spills on ice.

The difference between the surface temperature and the freezing point of water is given by the following expression:

$$\theta(0,\tau) = \frac{\mathrm{erf}(K\beta/2\sqrt{\alpha_1})}{k_1} \sqrt{\frac{\alpha_1}{\pi}} \int_0^{-2\sqrt{\tau}} q(\tau - \frac{u^2}{u})\, du \qquad (6\text{-}70)$$

where k_1 and α_1 are the temperature-averaged thermal conductivity and diffusivity, respectively, of ice. β is the ratio of the density of water to that of ice, and K is the parameter defined by Eq. (6-39).

The drop in the surface temperature of the ice formed after spilling methane on water is shown in Figure 6-13. These results are consistent with the qualitative explanations given in Chapter V. There is a shift from the initial film boiling to transition and finally to nucleate boiling after the ice cools enough to inhibit any vapor film formation. Again, the drop in surface temperature can be approximated by a linear decrease with time, a convenient result that will be employed in subsequent heat transfer models. The time for the complete collapse of the vapor film, τ_{cf}, is about 45 seconds.

The drop in surface temperature following a spill of ethane on water is shown in Figure 6-14. This drop in temperature is again a progressive one, in agreement with the theory that ethane initially transition boils on water and nucleate boils afterwards when the surface

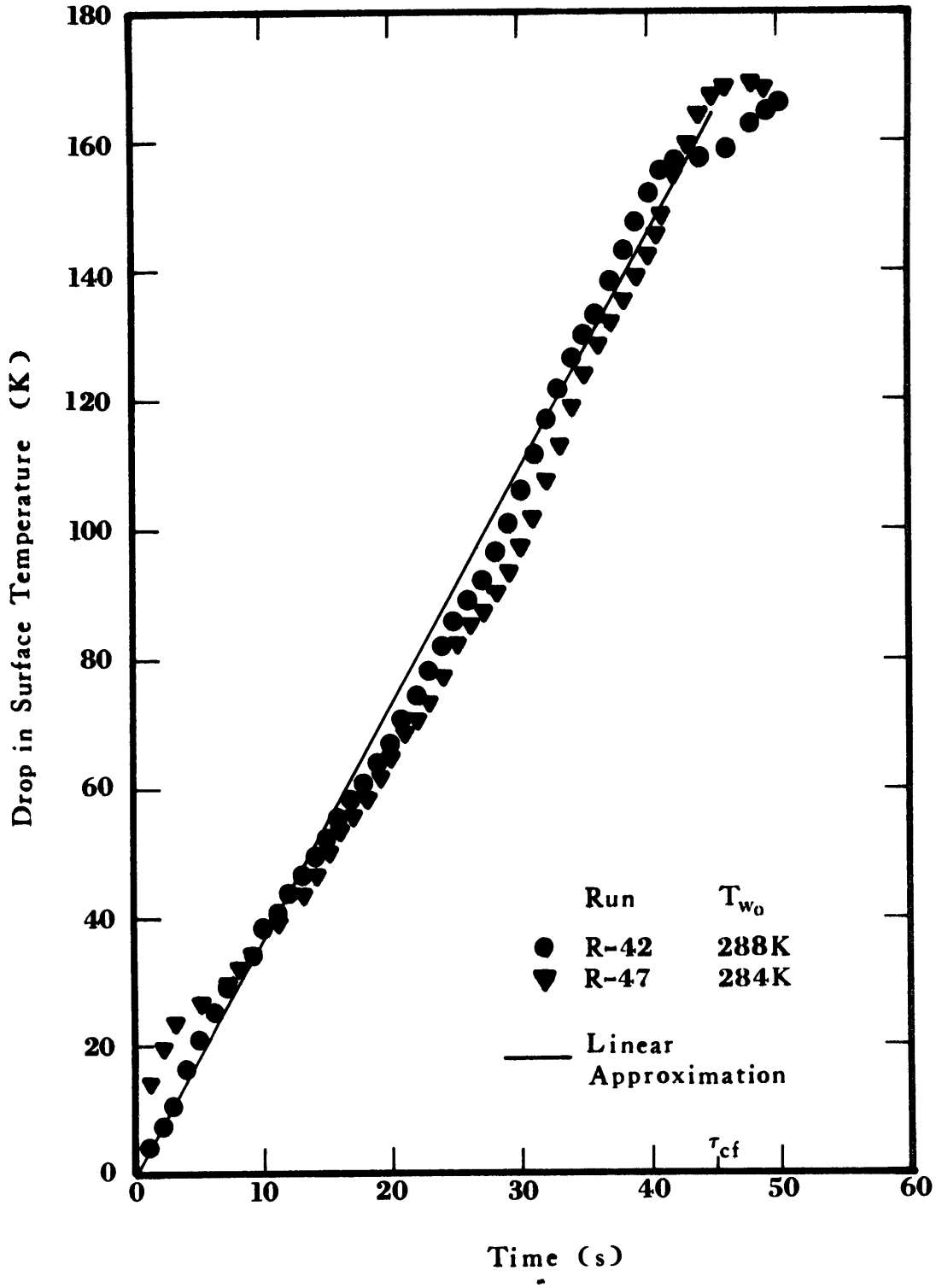

Figure 6-13 Drop in Surface Temperature of Ice after a Spill of Methane on Water

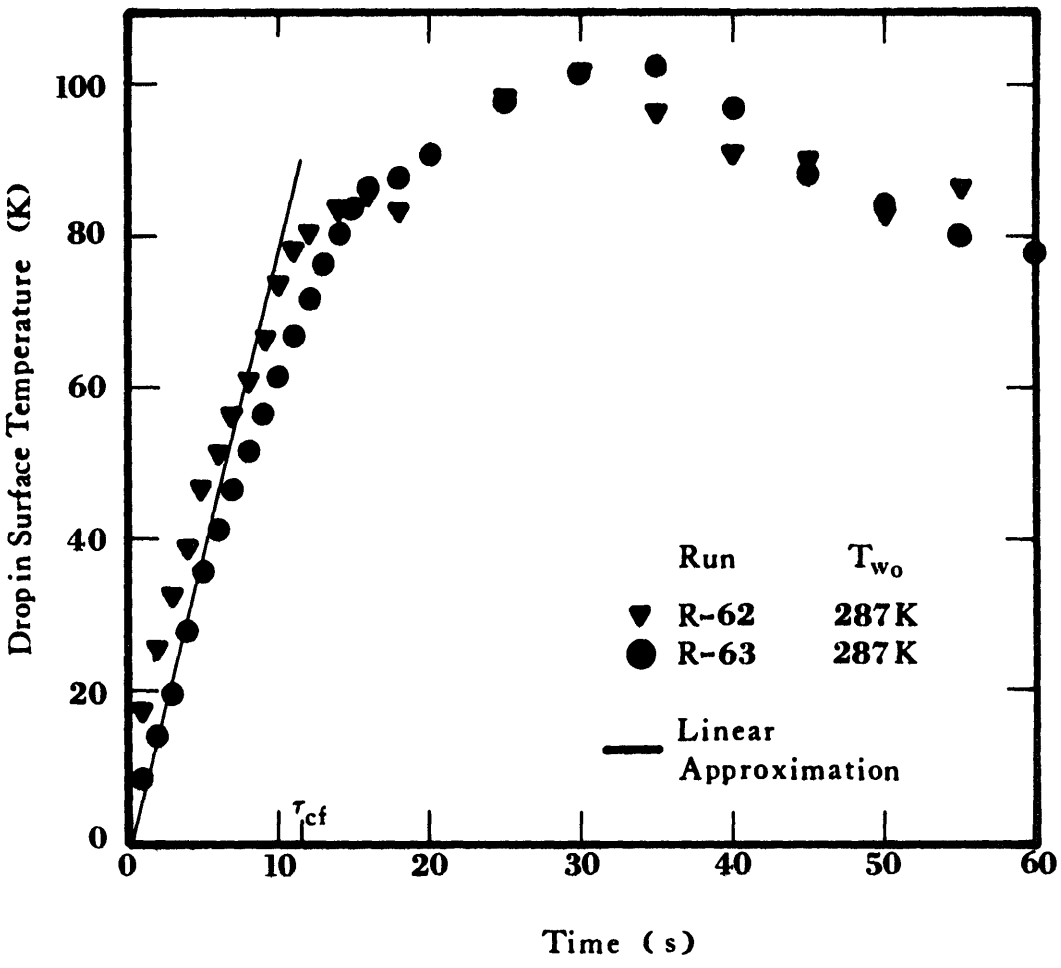

Figure 6-14 Drop in Surface Temperature of Ice after a Spill of Ethane on Water

temperature is low. A linear approximation for the temperature drop can also be made, τ_{cf} is about 13 s.

Based on the above results, new heat transfer models can be developed in which the surface temperature of the substrate (ice/water) is allowed to decrease linearly with time. The time required for the surface to reach the cryogen temperature, τ_{cf}, depends only on the cryogen and the substrate, for pure components. For mixtures, one must also consider the composition of the hydrocarbon.

The drop in surface temperature determined with convolution integrals can also be used to construct boiling curves similar to those given in Chapter II (Figures 2-8 through 2-10) for hydrocarbons boiling on metal surfaces.

The boiling curves (heat flux vs. difference in temperature between the substrate and the saturation temperature of the boiling fluid) for the transient evaporation of methane , ethane and two mixtures are given in Figures 6-15 through 6-18. The boiling curve for methane shows an increase in heat flux as the difference in temperature decreases from 160 to 20 K. The maximum nucleate flux is of 120 kW/m^2 as compared to 200 kW/m^2 reported for steady state boiling on metal surfaces. The low steady state film boiling fluxes of $\sim$25 kW/m^2 at the Leidenfrost point, ΔT = 70 K, are not observed in the transient evaporation on water. This is possibly due to the fact that a synchronization of events in the transient evaporation is highly unlikely. While film boiling is taking place at one point on the substrate surface, nucleate boiling might be occurring at another point. Therefore, the overall macroscopic result is an intermediate between film and nucleate fluxes,

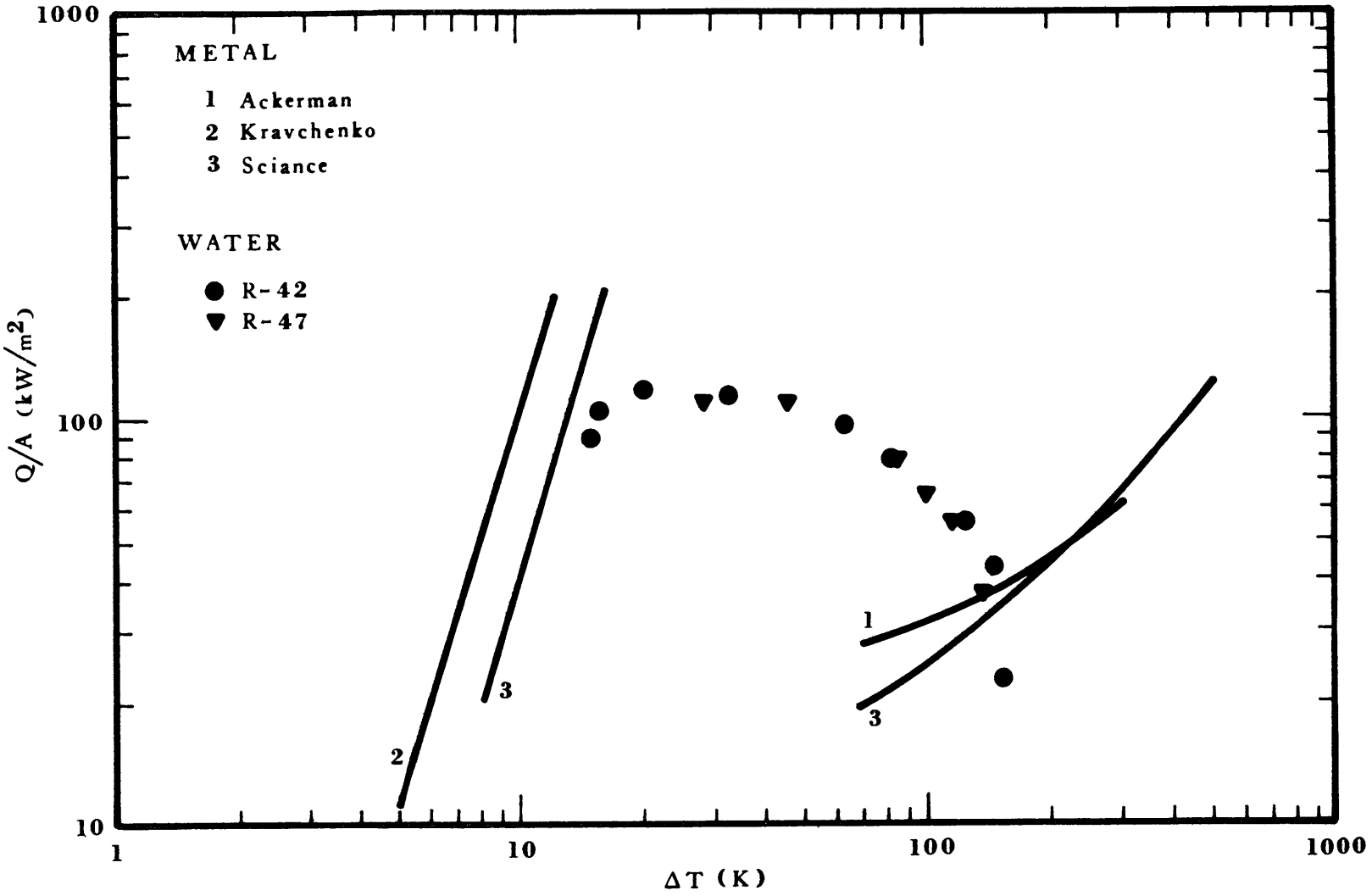

Figure 6-15 Transient Boiling of Methane on Water Compared to Steady State Boiling on Metal Surfaces

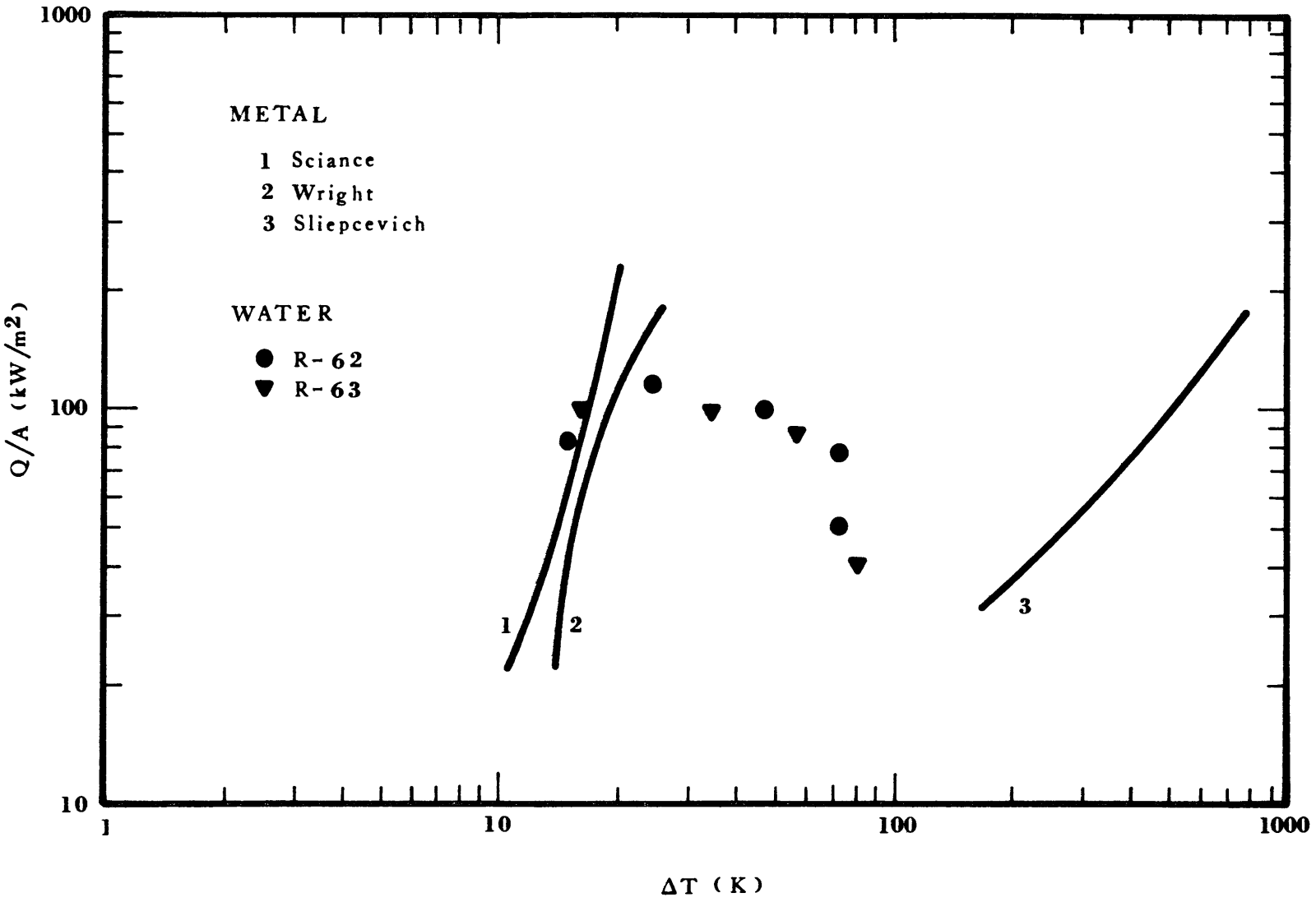

Figure 6-16 Transient Boiling of Ethane on Water Compared to Steady State Boiling on Metal Surfaces

even though each individual point on the surface might follow the steady state curve more closely. The difference in peak nucleate fluxes may be due to the internal thermal resistance of ice which limits the flow of energy; such a resistance is much lower, and therefore the limitation is non-existent, for steady state boiling on metals.

The surface roughness of metals may be very different from that of ice which may also contribute to the above differences in the curves for steady state boiling on metals and transient boiling on water (ice).

The maximum nucleate flux for ethane boiling on water is on the order of 120 kW/m^2 (Figure 6-16). Again this flux is lower than those reported for steady state boiling on metal surfaces. An explanation similar to that given for methane applies.

The position and shape of the transition portion of the boiling curve on water is reasonable when compared to the steady state curves for boiling on metals. This could be due to the fact that ethane initially transition boils on water; thus the collapse of the vapor film need not be overcome and the temperature throughout the surface, at a given time, might be more uniform.

The boiling curve for a 90% methane, 10% ethane mixture (Figure 6-17) has a similar shape to that for methane boiling on water; the heat fluxes, however, are higher. The early localized collapse of the vapor film (due to the preferential evaporation of methane) is thought to be responsible for these higher heat fluxes.

The boiling curve, an 83% methane, 13% ethane, 4% propane mixture is given in Figure 6-18. Again, the collapse of the vapor film might

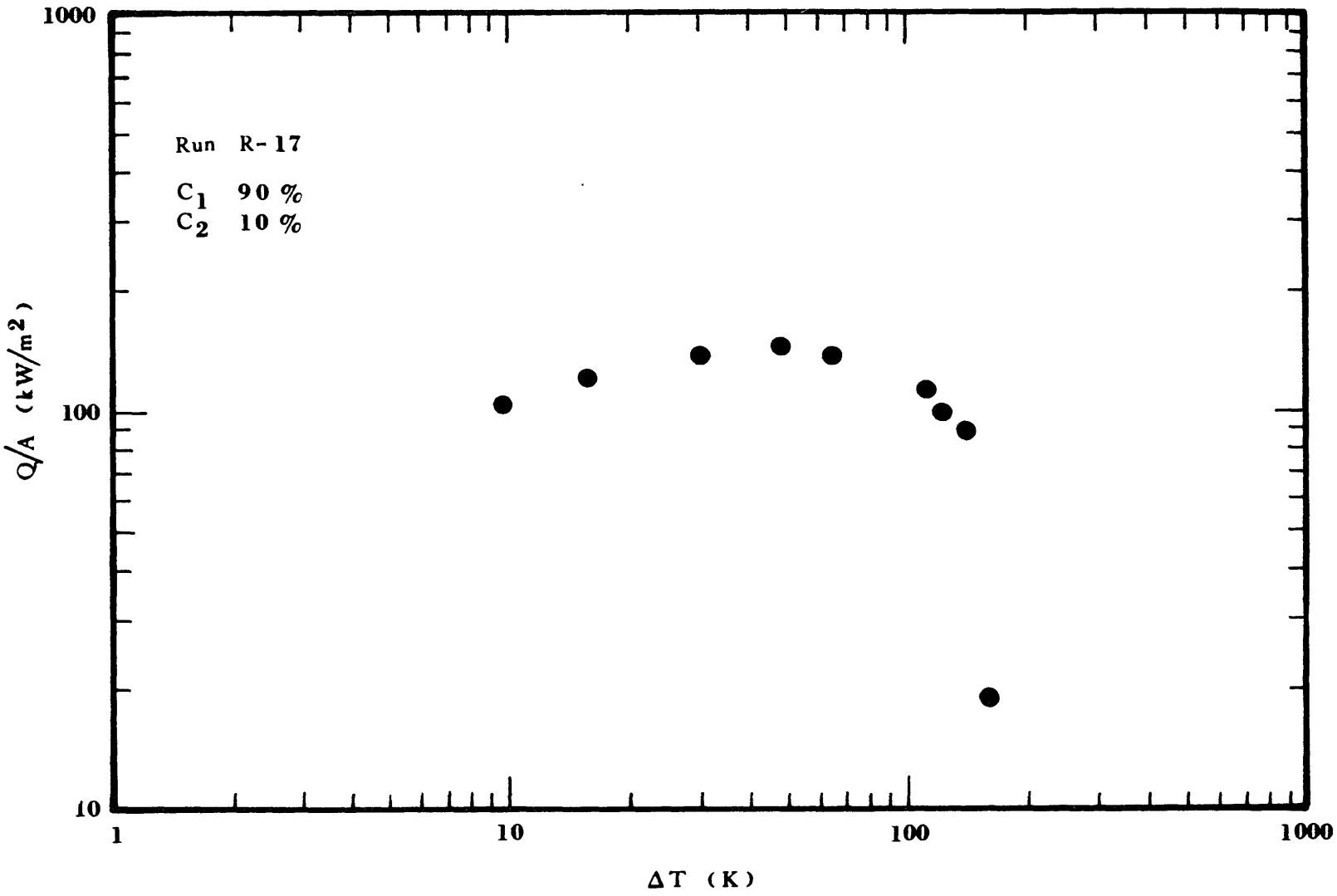

Figure 6-17 Transient Boiling of a Methane-Ethane Mixture on Water

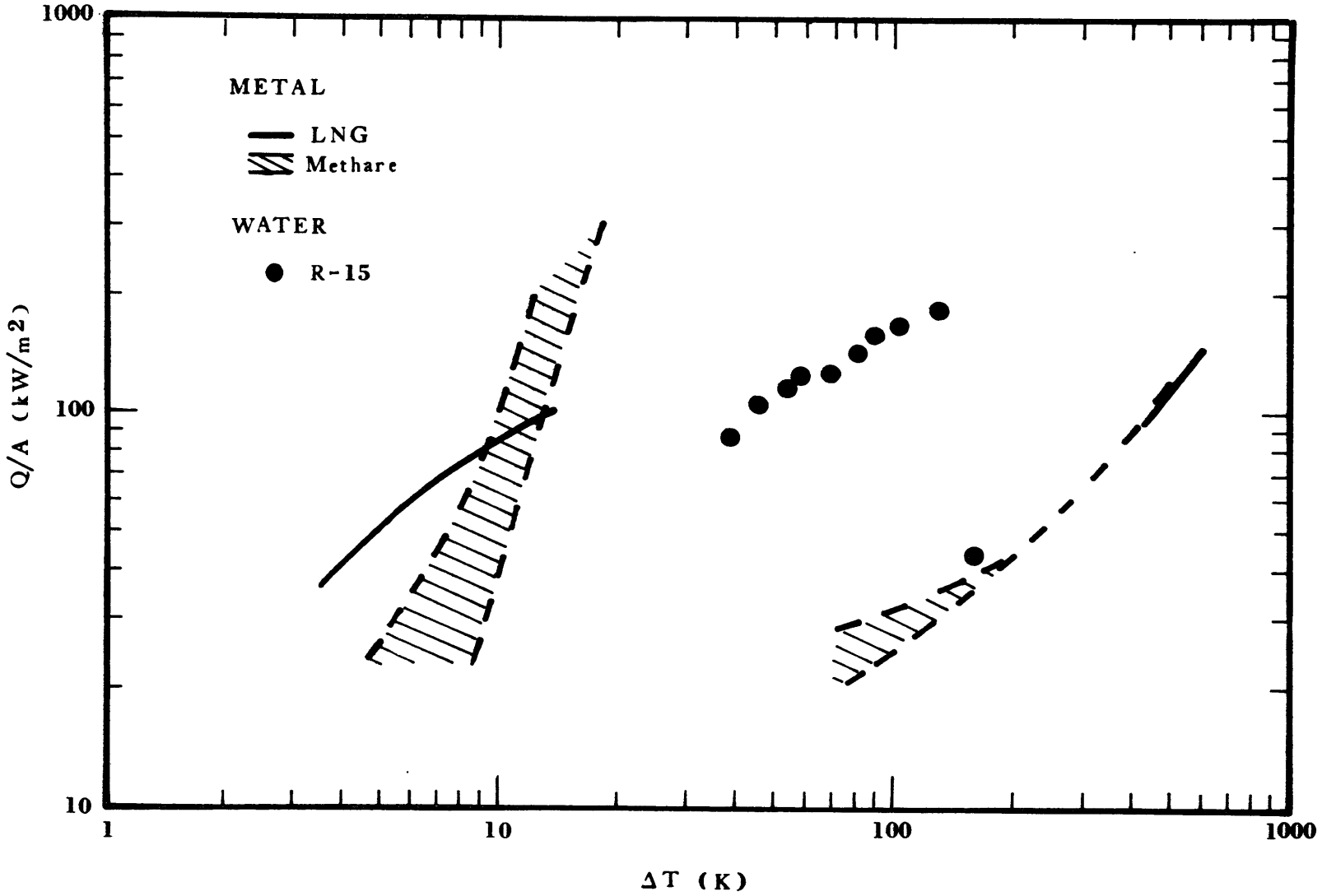

Figure 6-18 Transient Boiling of an LNG Mixture (C_1 82.5%, C_2 13.1%, C_3 4.4%) Compared to Steady State Boiling of LNG (C_1 87.5%, C_2 4.3%, C_3 1.6%, $C_4^+/N_2/CO_2$ 6.6%) on a Metal Surface

be responsible for the high heat fluxes observed for the LNG mixture boiling on water. When comparing this curve to the one reported by Brown for steady state boiling on a metal, it is interesting to note that if Brown's nucleate curve is extrapolated, it would lie reasonably close to this curve.

The lowest ΔT reported for film boiling of an LNG on a metal surface is 210 K, whereas that for methane is 70 K. Thus, it seems that even at steady state the preferential evaporation of methane causes earlier film instability by the same mechanism described in Chapter V.

Variable Grid Size Heat Transfer Model

Basically, this model replaces the differential equations for transient heat conduction with solidification (Stefan's Problem) with difference equations which are then solved numerically. The major advantages are that it allows the variation of surface temperature with time as well as the variation of thermal properties with temperature.

Consider a Taylor expansion of the temperature field

$$T_{(x+\Delta x)} = T_{(x)} + \frac{\Delta x}{1!}\frac{\partial T}{\partial x} + \frac{(\Delta x)^2}{2!}\frac{\partial^2 T}{\partial x^2} + \frac{(\Delta x)^3}{3!}\frac{\partial^3 T}{\partial x^2} + \ldots \qquad (6\text{-}71)$$

If the common approximation of neglecting second and higher order terms is made, then the first derivative can be approximated by

$$\frac{\partial T}{\partial x} \simeq \frac{T_{(x+\Delta x)} - T_{(x)}}{\Delta x} \qquad (6\text{-}72)$$

Similarly, a time deviative can be approximated by

$$\frac{\partial T}{\partial \tau} \simeq \frac{T_{(\tau+\Delta\tau)} - T_{(\tau)}}{\Delta\tau} \tag{6-73}$$

One can then use a spatial grid with increments Δx and a time grid with increments $\Delta\tau$ to approximate a solution to the heat transfer process.

Two methods can be used: the first assumes fixed increments Δx and $\Delta\tau$. The movement of the ice-water boundary must be determined at every time interval; often times this requires interpolation of temperatures since the freezing front could be located between grid points. Unless care is exercised, large errors are likely to be introduced in evaluating the spatial derivatives of the temperature field around the freezing point. This inconvenience is removed in the second method in which the ice layer is divided into $\underline{m}$ equally sized space increments; these increments increase as the ice layer grows in thickness. Similarly, the water layer is divided into $\underline{m}$ equally sized space increments as shown in Figure 6-19. Both of these methods for the solution of transient heat conduction problems involving freezing are described by Murray and Landis (1959).

For each internal point, the time derivative of the temperature is given by

$$\frac{d\theta}{d\tau} = \left(\frac{\partial\theta}{\partial x}\right)\frac{dx}{d\tau} + \frac{\partial\theta}{\partial\tau} \tag{6-74}$$

The rate of movement of each internal point is related to the movement of the freezing front,

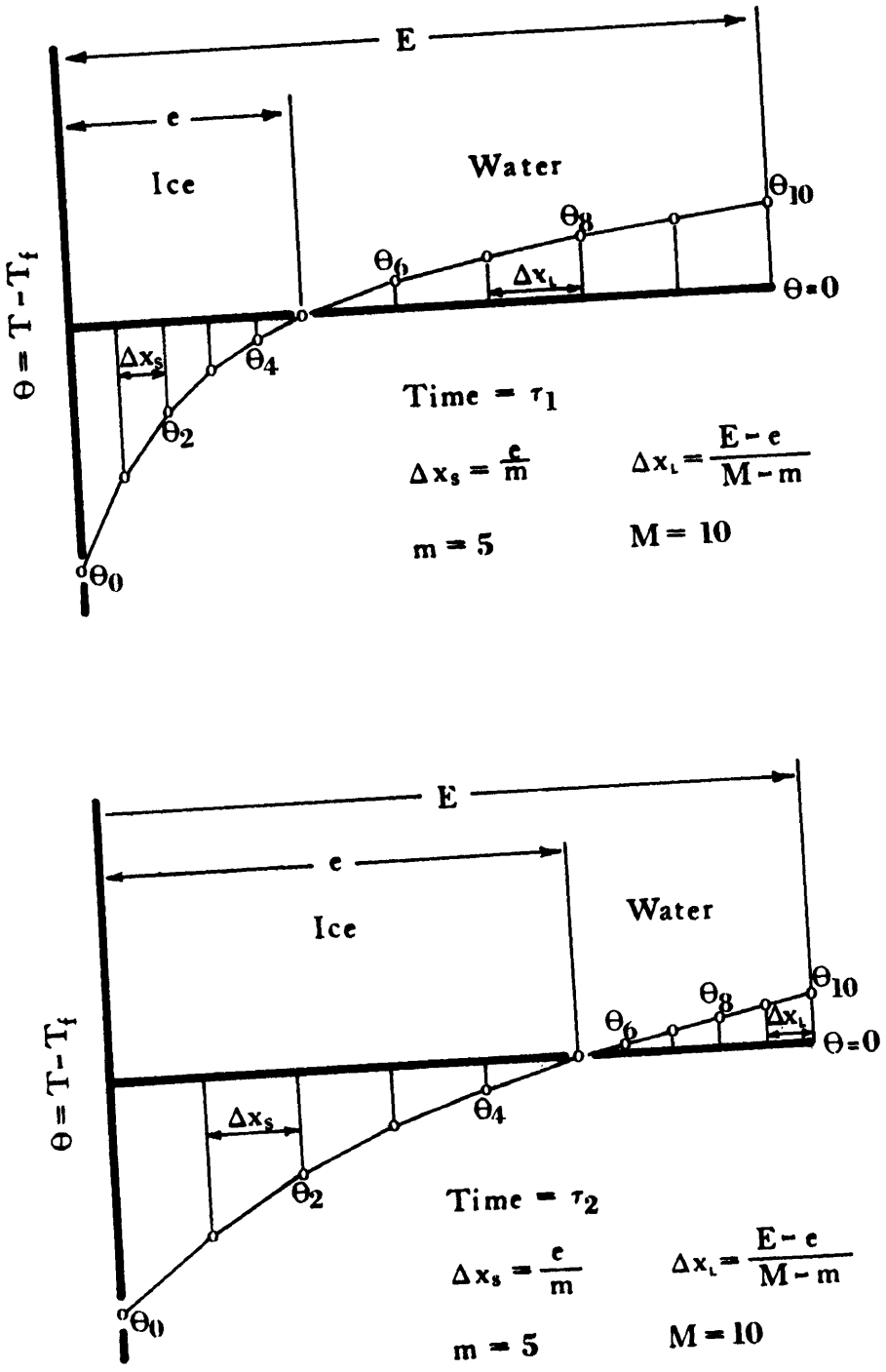

Figure 6-19 Variable Grid Size Scheme

$$\frac{1}{x}\ \frac{dx}{d\tau} = \frac{1}{e}\ \frac{de}{d\tau} \tag{6-75}$$

The transient conduction equation yields a third relationship:

$$\frac{\partial\theta}{\partial\tau} = \frac{1}{\rho C_p}\ \frac{\partial}{\partial x}\left(k\ \frac{\partial\theta}{\partial x}\right) \tag{6-76}$$

Equations (6-74), (6-75) and (6-76) can be combined to yield an expression for the time derivative of the temperature field within the ice layer:

$$\frac{d\theta_i}{d\tau} = \frac{x}{e}\ \frac{\partial\theta_i}{\partial x}\ \frac{de}{d\tau} + \frac{1}{\rho_i C_{p_i}}\ \frac{\partial}{\partial x}\left(k_i\ \frac{\partial\theta_i}{\partial x}\right) \tag{6-77}$$

For the water layer the rate of travel of the internal points is given by

$$\frac{1}{E - x}\ \frac{dx}{d\tau} = \frac{1}{E - e}\ \frac{de}{d\tau} \tag{6-78}$$

Combining Eqs. (6-74), (6-76) and (6-78) yields an expression for the time derivative of the temperature field within the water layer:

$$\frac{d\theta_w}{d\tau} = \frac{E - x}{E - e}\ \frac{\partial\theta_w}{\partial x}\ \frac{de}{d\tau} + \frac{1}{\rho_w C_{p_w}}\ \frac{\partial}{\partial x}\left(k_w\ \frac{\partial\theta_w}{\partial x}\right) \tag{6-79}$$

An expression for the rate of travel of the freezing point can be obtained by considering the fact that all the heat released during solidification must be transferred by conduction, or

$$\rho\Delta H^{fus}\ \frac{de}{d\tau} = k_i\ \frac{\partial\theta_i}{\partial x}\bigg|_{x=e} - k_w\ \frac{\partial\theta_w}{\partial x}\bigg|_{x=e} \tag{6-80}$$

Where ΔH^{fus} is the heat of fusion of ice and ρ is taken at the average of the densities of ice and water and assumed to remain constant. A value of 960 kg/m^3 is used in this study.

At this point, the differential equations can be replaced by difference equations. A three-point approximation is used for the temperature gradients in Eq. (6-80):

$$\frac{de}{d\tau} = \frac{1}{\rho_{iw}\Delta H^{fus}} \left\{ k_i \frac{\theta_{m-2} - 4\theta_{m-1} + 3\theta_m}{2(e/m)} + k_w \frac{\theta_{m+2} - 4\theta_{m+1} + 3\theta_m}{2(E-e)/(M-m)} \right\}^* \tag{6-81}$$

Similarly, Eq. (6-77), for the ice layer, can be approximated by:

$$\frac{d\theta_n}{d\tau} = \frac{n}{e}\left(\frac{\theta_{n+1} - \theta_{n-1}}{2}\right)\frac{de}{d\tau} + \frac{1}{\rho_n C_{p_n}}\left(\frac{k_{n-1/2}(\theta_{n-1} - \theta_n) - k_{n+1/2}(\theta_n - \theta_{n+1})}{(e/m)^2}\right) \tag{6-82}$$

For the water layer, Eq. (6-79) can be approximated by:

$$\frac{d\theta_n}{d\tau} = \frac{M-n}{E-e}\left(\frac{\theta_{n+1} - \theta_{n-1}}{2}\right)\frac{de}{d\tau} + \alpha_w\left(\frac{\theta_{n-1} - 2\theta_n + \theta_{n+1}}{(E-e)^2/(N-m)^2}\right) \tag{6-83}$$

Finally,

$$e_{\tau+\Delta\tau} = e_\tau + \Delta\tau \cdot \frac{de}{d\tau} \tag{6-84}$$

and

$$\theta_{n,\tau+\Delta\tau} = \theta_{n,\tau} + \Delta\tau \cdot \frac{d\theta_n}{d\tau} \tag{6-85}$$

*Note that $\theta_m = T_m - T_f = 0$ by definition of m.

As previously indicated, one of the advantages of using difference-equation approximations is the flexibility to use temperature dependent properties. In that regard, the following conventions are used in the development of this model:

k_{ice} in Eq. (6-81) is evaluated at $(\theta_{m-1} + \theta_m)/2$

ρ_n, C_{p_n} in Eq. (6-82) are evaluated at θ_n

$k_{n-1/2}$ in Eq. (6-82) is evaluated at $(\theta_{n-1} + \theta_n)/2$

$k_{n+1/2}$ in Eq. (6-82) is evaluated at $(\theta_n + \theta_{n+1})/2$

All the properties in the water layer are evaluated at the average of the freezing point and the initial temperature of the water. In this relatively small range, the properties of water do not change significantly to merit a point-by-point evaluation as in the case of ice. Physical properties for both ice and water are given in Appendix D.

Two boundary conditions are needed to solve equations (6-81) through (6-85). These conditions are

$$\left.\begin{aligned} \theta_{\tau,0} &= \frac{\tau}{\tau_{cf}} \ (T_c - T_f) && \tau \leq \tau_{cf} \\ \theta_{\tau,0} &= T_c - T_f && \tau > \tau_{cf} \end{aligned}\right\} \qquad (6\text{-}86)$$

where T_f = freezing temperature of water

T_c = cryogen's temperature

τ_{cf} = time for the total collapse of the vapor film

and

$$\theta_{\tau,N} = T_{water_0} - T_f \tag{6-87}$$

The boundary condition for the surface of the ice given by Eq. (6-86) is based on the results of the previous section in which convolution integrals were used to back calculate surface temperatures. At that time, it was shown that a reasonable approximation for the time variation of the surface temperature is a linear decrease over a time τ_{cf}, after which nucleate boiling is fully established.

Predictions made by the Variable Grid Size Heat Transfer Model (VGSHTM) for methane spilled on water are compared to experimental data in Figures 6-20 and 6-21. Ten grid points (m = 5, N = 10) and a time increment of $\Delta\tau$ = 0.005 s were used in the model for this and all other tests. The short time interval is required to maintain a stable solution to the equations. A value of 45 s was used for τ_{cf}. The agreement between the predicted mass evaporated and the experimental results is excellent up to 50 seconds. After that time the predicted values are lower than the experimental ones; at 100 seconds they are 8% lower than experimental results. The reason for these low predicted values can be seen in Figure 6-21; the predicted boiling rates are in reasonable agreement with experimental ones, except for the peak values around 40 s. The predicted values fall 10-15% short of the experimental ones. An improvement in boiling rates can be obtained by doubling the number of grid points to 20. This, however, represents a simultaneous decrease in the time interval to $\Delta\tau$ = 0.001 s to maintain a stable

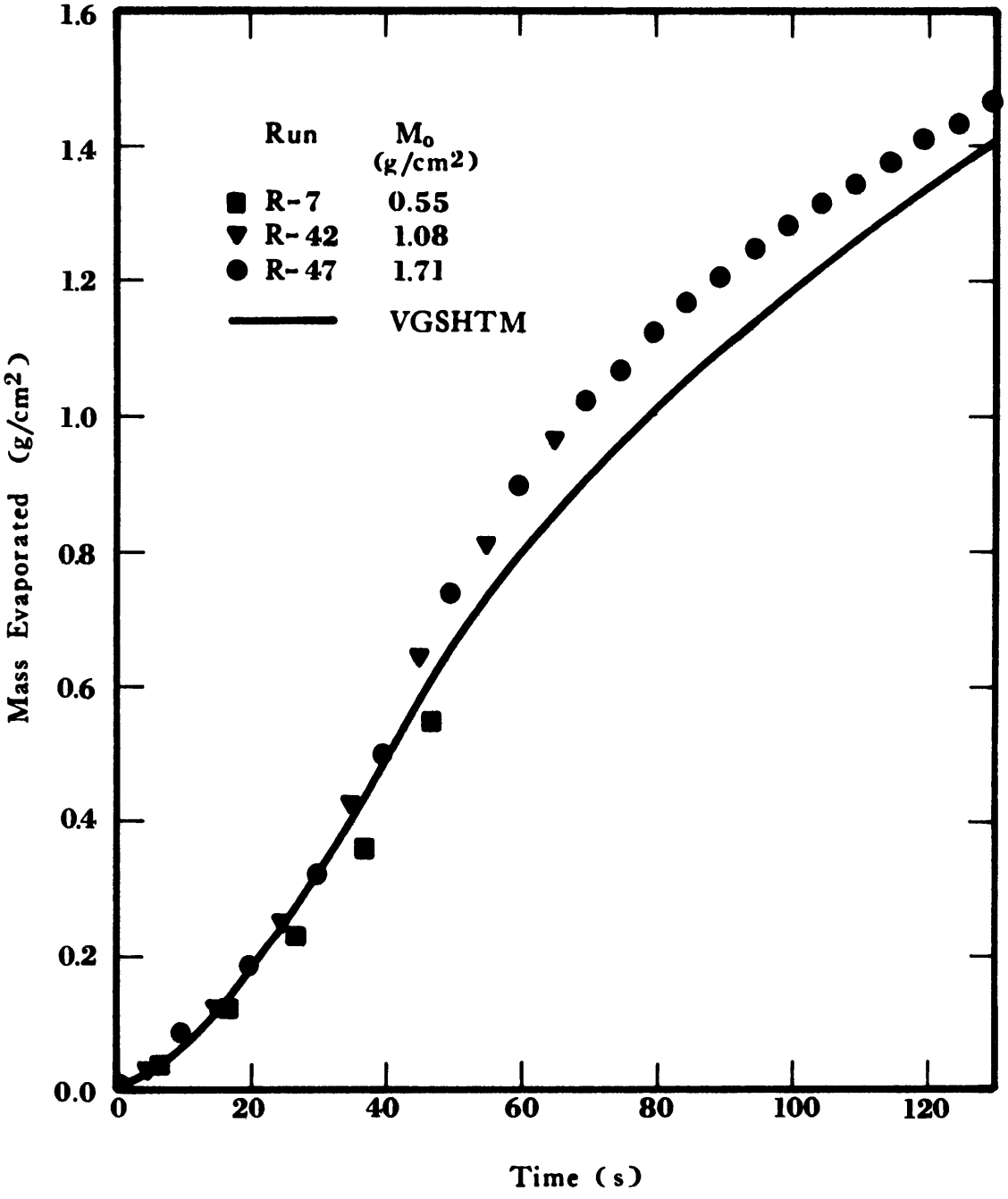

Figure 6-20 Boiling of Methane on Water. Variable Grid Size Heat Transfer Model and Experimental Data (τ_{cf} = 45 s)

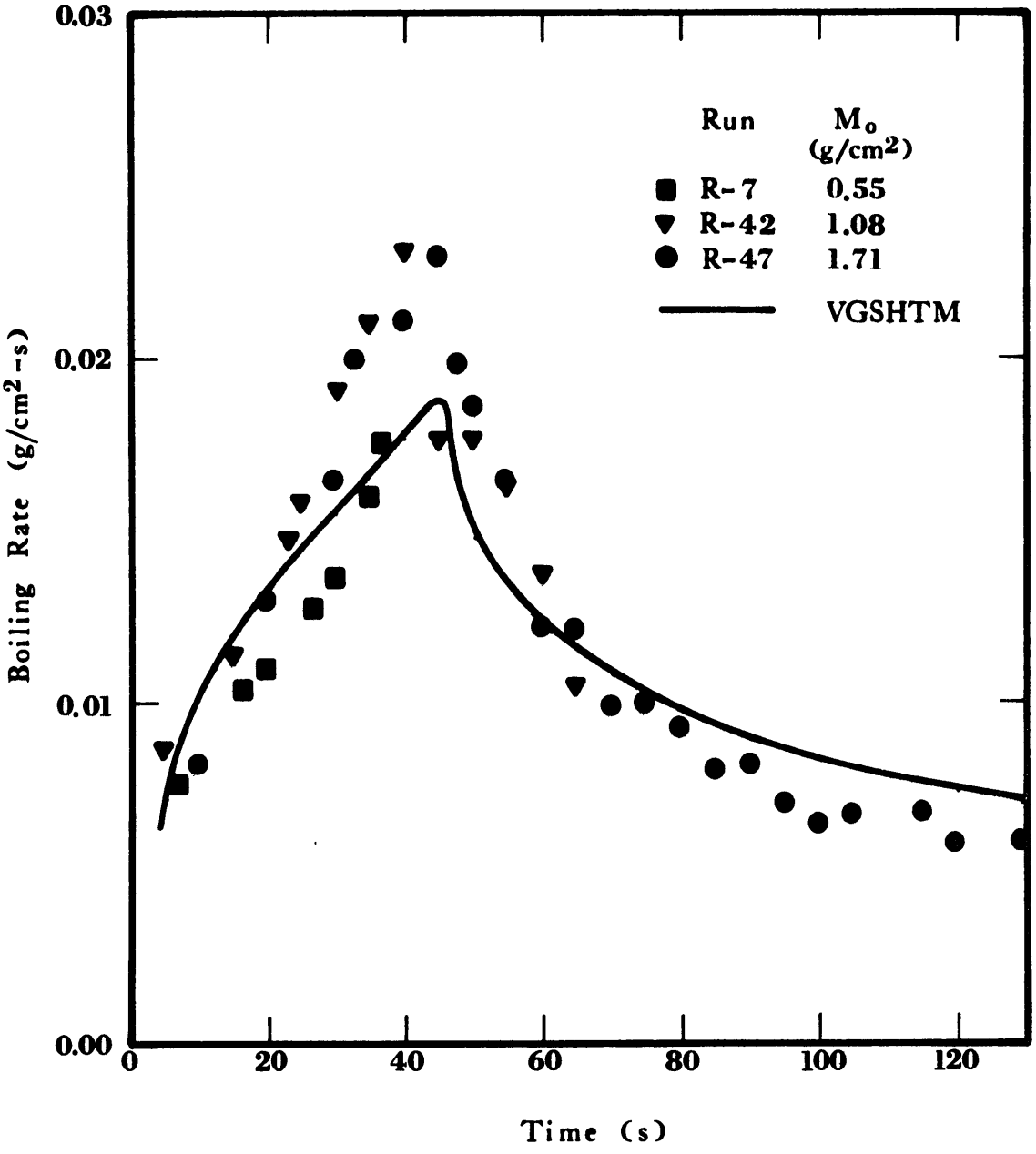

Figure 6-21 Evaporation Rates of Methane Boiling on Water. Variable Grid Size Heat Transfer Model and Experimental Data (τ_{cf} = 45 s)

solution. This is a costly improvement since the required computer time increases tenfold from 1.5 hr for N = 10 to 15 hr for N=20 (using a NOVA-840 computer).

Predictions for the evaporation of ethane on water are also compared with experimental data in Figures 6-22 and 6-23. Predictions for mass evaporated are in close agreement up to 15 seconds; thereafter the prediction underestimates the mass evaporated. At 50 s the predictions are 20% lower than experimental values and at 100 s they are 6% lower. The agreement between boiling rates predicted by the VGSHTM model and experimental ones is good, as can be seen in Figure 6-23.

Combined VGS/VLE HTM Model for LNG Mixtures

The evaporation of LNG mixtures presents a new condition as far as the heat transfer model is concerned: variation in the temperature of the cryogen due to the preferential evaporation of volatiles. One way to determine this variation in the saturation temperature of the residual LNG is to use the VLE model described in Chapter IV.

The scheme for the use of the combined Variable Grid Size/Vapor Liquid Equilibria Heat Transfer Model (VGS/VLE HTM) is shown in Figure 6-24. The VGS HTM uses the initial conditions to determine the heat flux and the consequent evaporation of cryogen. The mass evaporated is then fed into the VLE model; through a mass balance, the composition and temperature of the residual liquid are determined (see Chapter IV). If the time for the total collapse of the vapor film has been exceeded, the saturation temperature becomes the surface temperature for the heat transfer model. Otherwise, the appropriate surface temperature

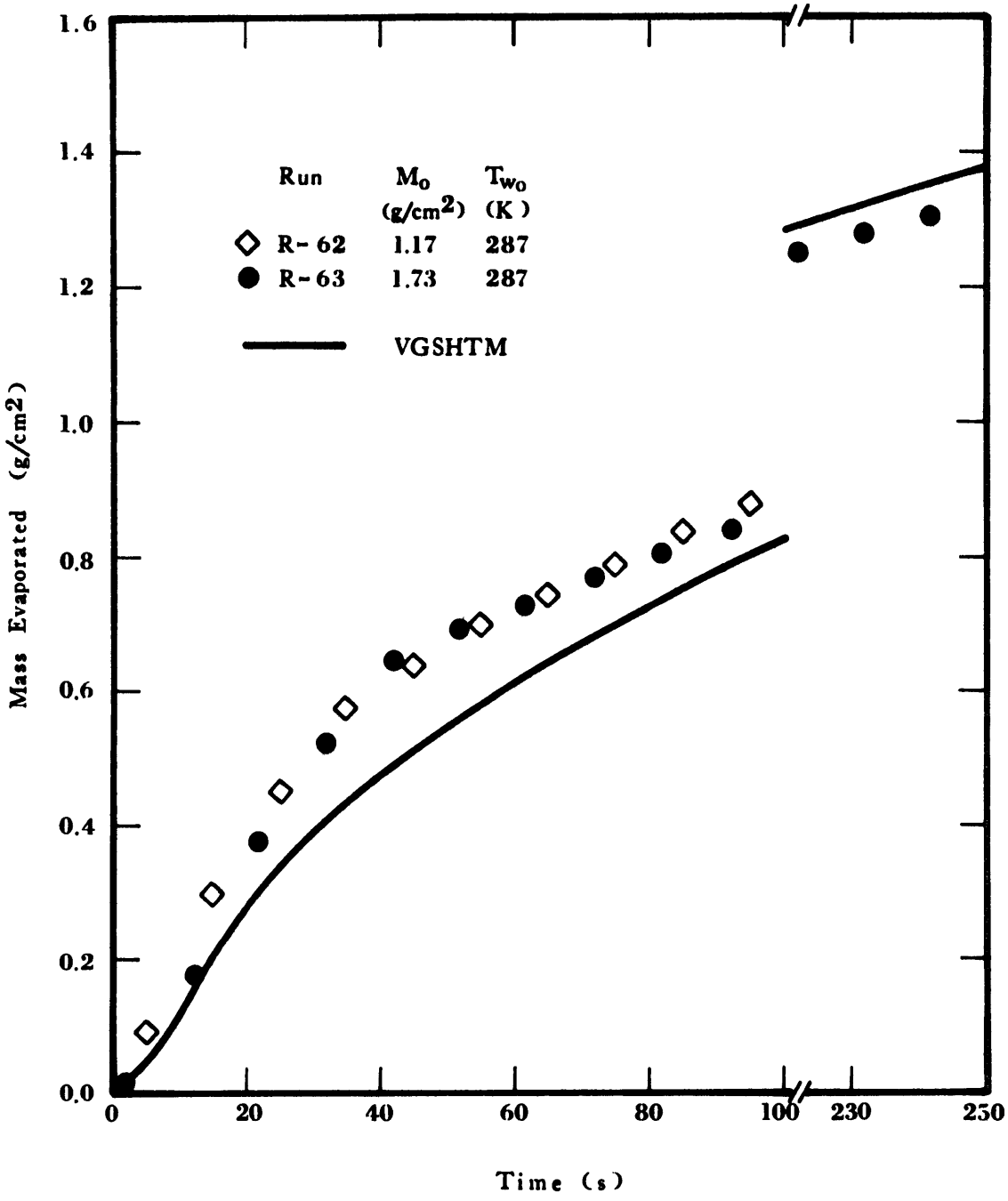

Figure 6-22 Boiling of Ethane on Water. Variable Grid Size Heat Transfer Model and Experimental Data (τ_{cf} = 13 s)

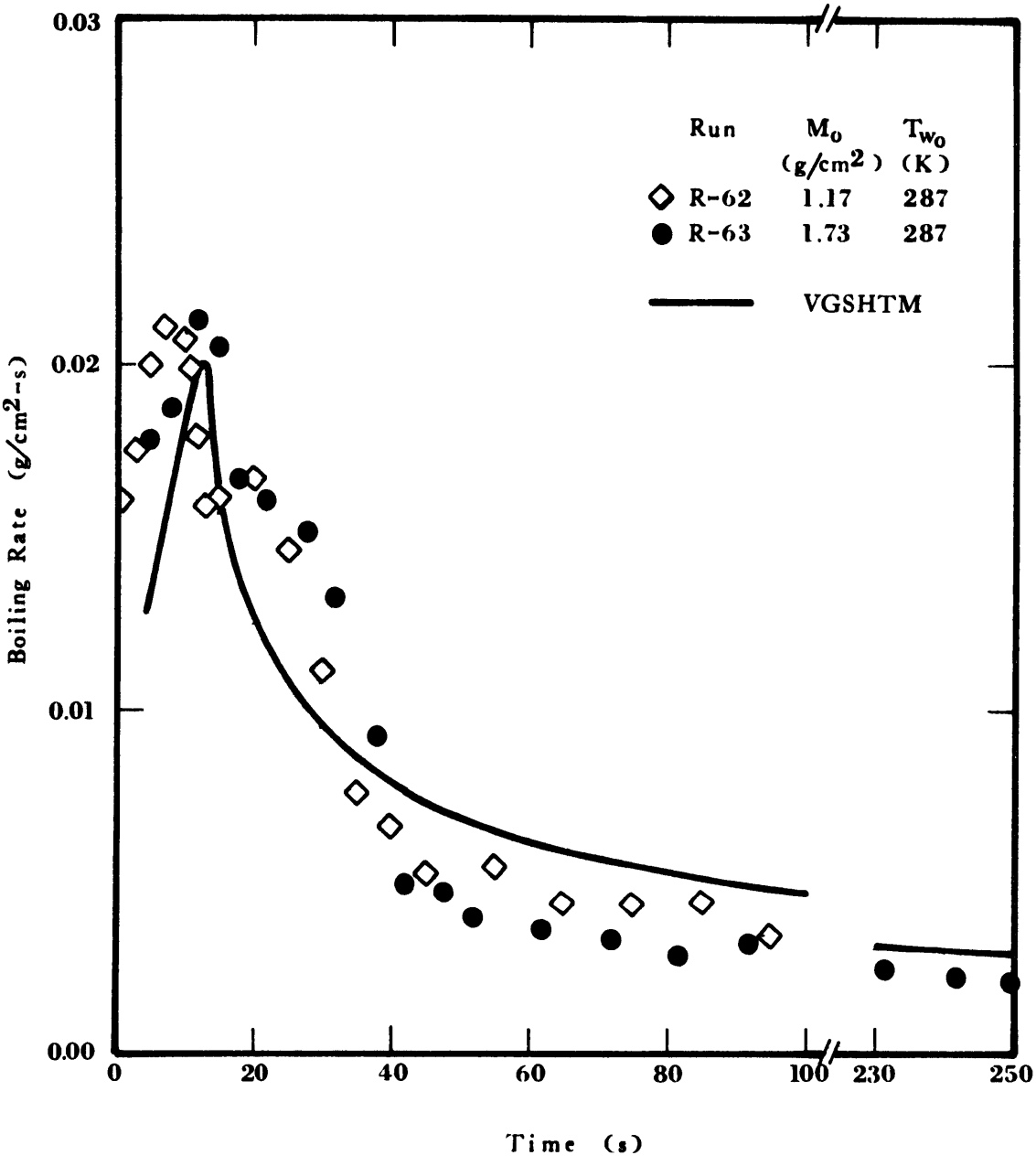

Figure 6-23 Evaporation Rates of Ethane Boiling on Water. Variable Grid Size Heat Transfer Model and Experimental Data (τ_{cf} = 13 s)

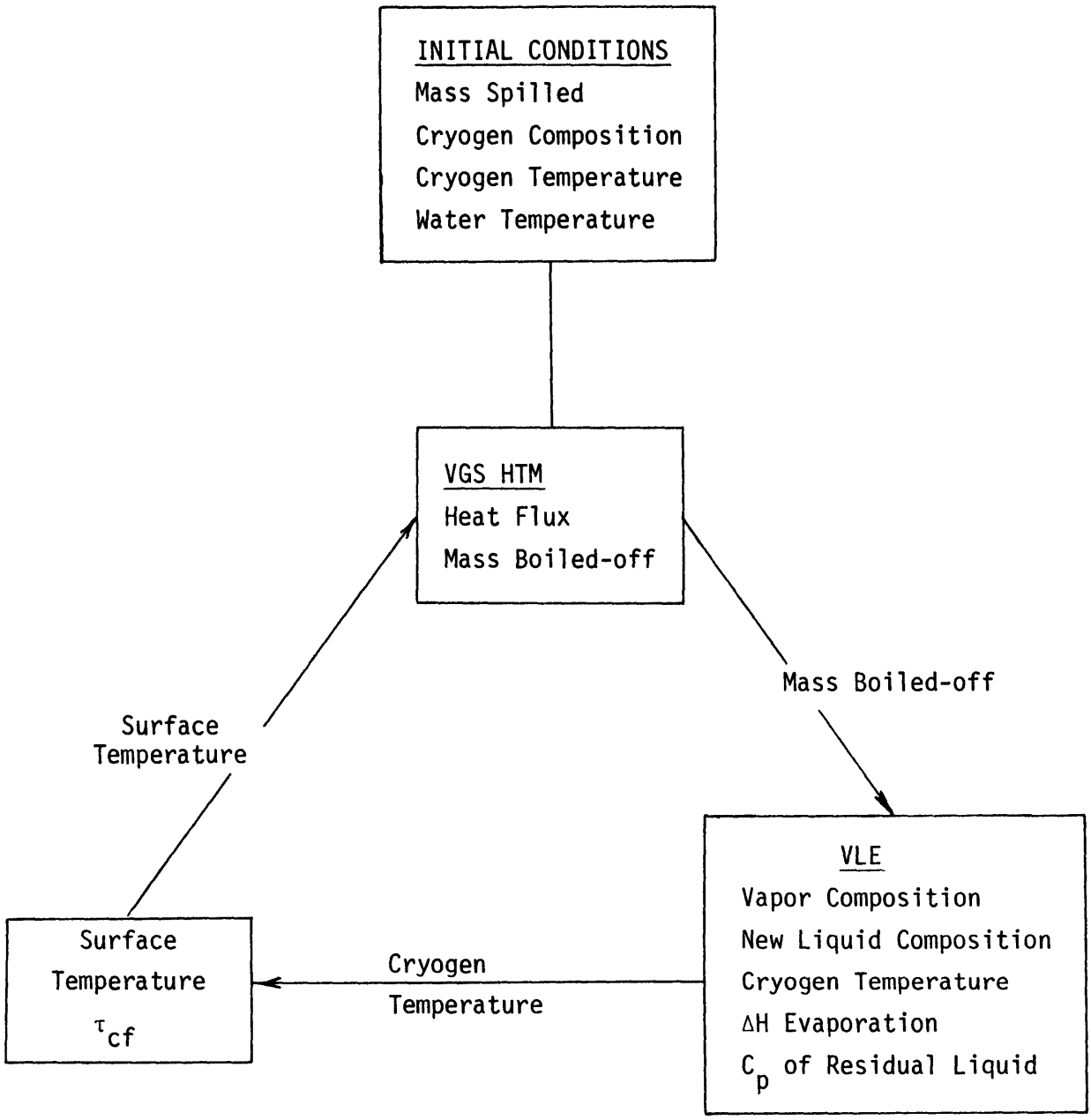

Figure 6-24 Variable Grid Size/Vapor Liquid Equilibria Heat Transfer Model (VGS/VLE HTM)

is determined by using Eq. (6-86). A very important finding made while working on the VGS/VLE HTM was that not all the heat transferred from the ice/water substrate goes toward evaporation of the cryogen. As the volatiles are exhausted, some heat is used in bringing the cryogen to the new saturation temperature. This sensible heat becomes extremely important near that time at which methane is almost completely evaporated. The saturation temperature rises rapidly and most of the heat flux goes toward warming the cryogen.

As in the case of pure components, ten grid points (N = 10) and $\Delta\tau$ = 0.005 s were used. The shift between the VGS HTM and the VLE model was made every 0.2 s. Shifting at every time increment, 0.005 s, did not change the results significantly but increased computation times prohibitively. Runs typically taking 2.5 hours with shifts every 0.2 s, took over 25 hours when shifing every 0.005 s.

The times for the collapse of the vapor film, τ_{cf}, were selected so as to best fit the experimental data. This variable is the only adjustable parameter used in the heat transfer mode. The selected values for methane-ethane mixtures are given in Figure 6-25. For ternary mixtures τ_{cf} has been correlated as follows

$$\tau_{cf} = 45\ x_{C_1} - 40\ x_{C_2}^{0.2} - 10\ x_{C_3}^{0.1}\ (s)$$

where x's are mole fractions. The following restrictions are made: $\tau_{cf} \geq 0$ and it should only be used within the LNG compositional range ($x_{C_2} \leq 0.20$, $x_{C_3} \leq 0.10$).

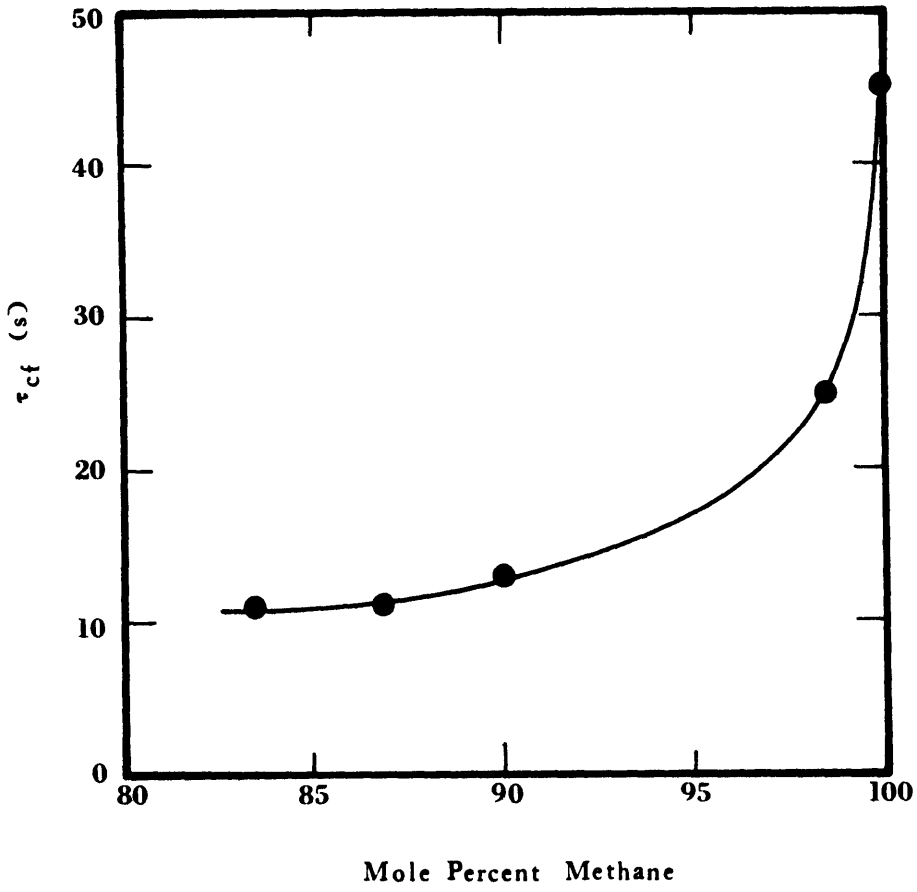

Figure 6-25 Times for Collapse of Vapor Film (τ_{cf}) for Binary Methane-Ethane Mixtures

The results predicted by the VGS/VLE HTM for binary mixtures of methane and ethane are compared to experimental data in Figures 6-26 through 6-31. The agreement for both mass evaporated and boiling rates is good.

Predictions by the VGS/VLE HTM for a binary mixture of ethane and propane are compared in Figure 6-32 and 6-33. Again, the agreement is satisfactory.

Similarly, predictions for the evaporation of ternary, methane, ethane and propane, mixtures on water are compared to experimental data in Figures 6-34 through 6-39. The agreement for both the mass evaporated and boiling rates are seen to be good.

Thus, it can be concluded that the explanations previously given for the behavior of cryogenic hydrocarbons boiling on water, i.e., initial film boiling, preferential evaporation of volatiles and vapor liquid equilibria are correct and have been proven both qualitatively and quantitatively.

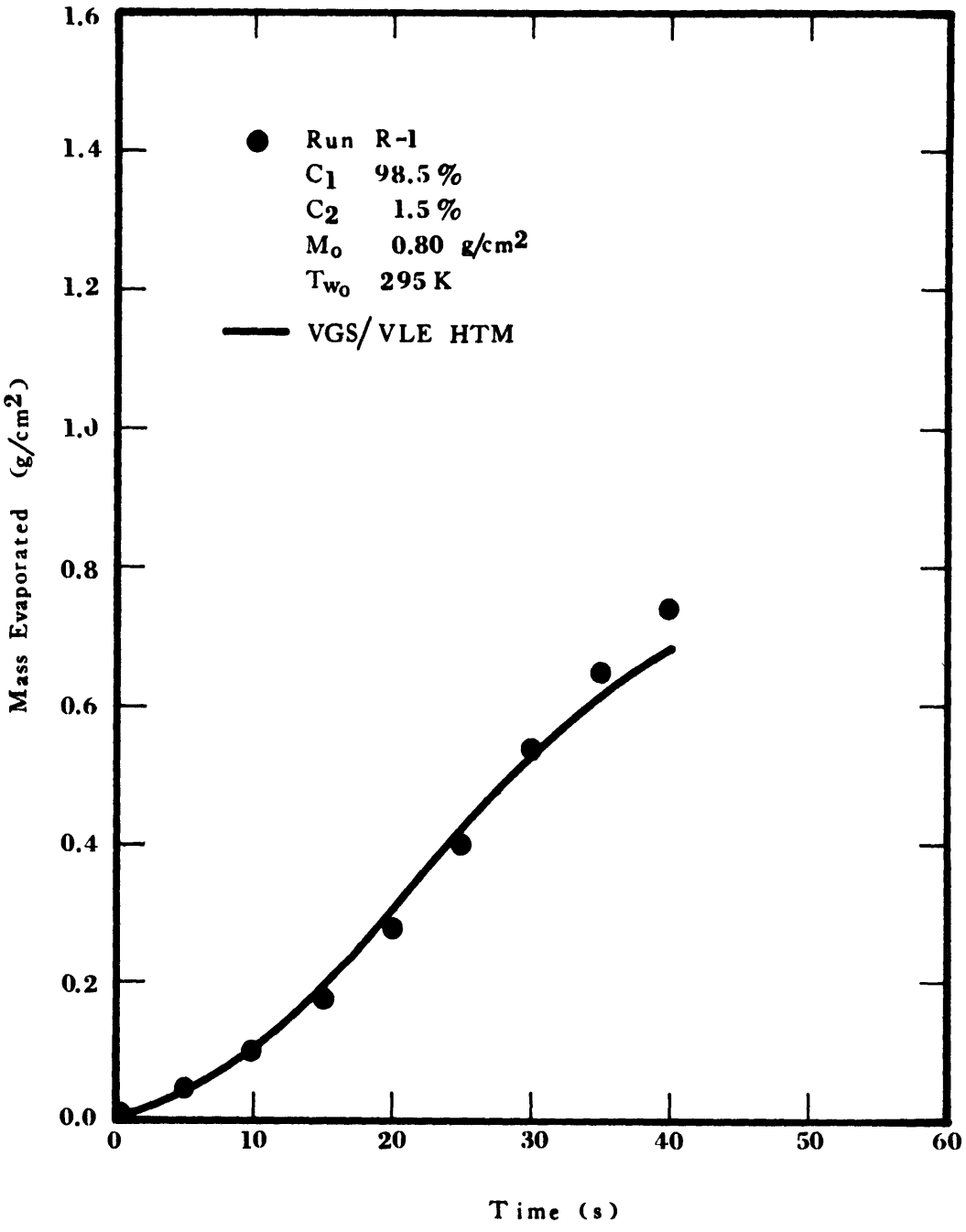

Figure 6-26 Boiling of a Methane-Ethane Mixture on Water (R-1). VGS/VLE HTM Predictions and Experimental Data (τ_{cf} = 25 s)

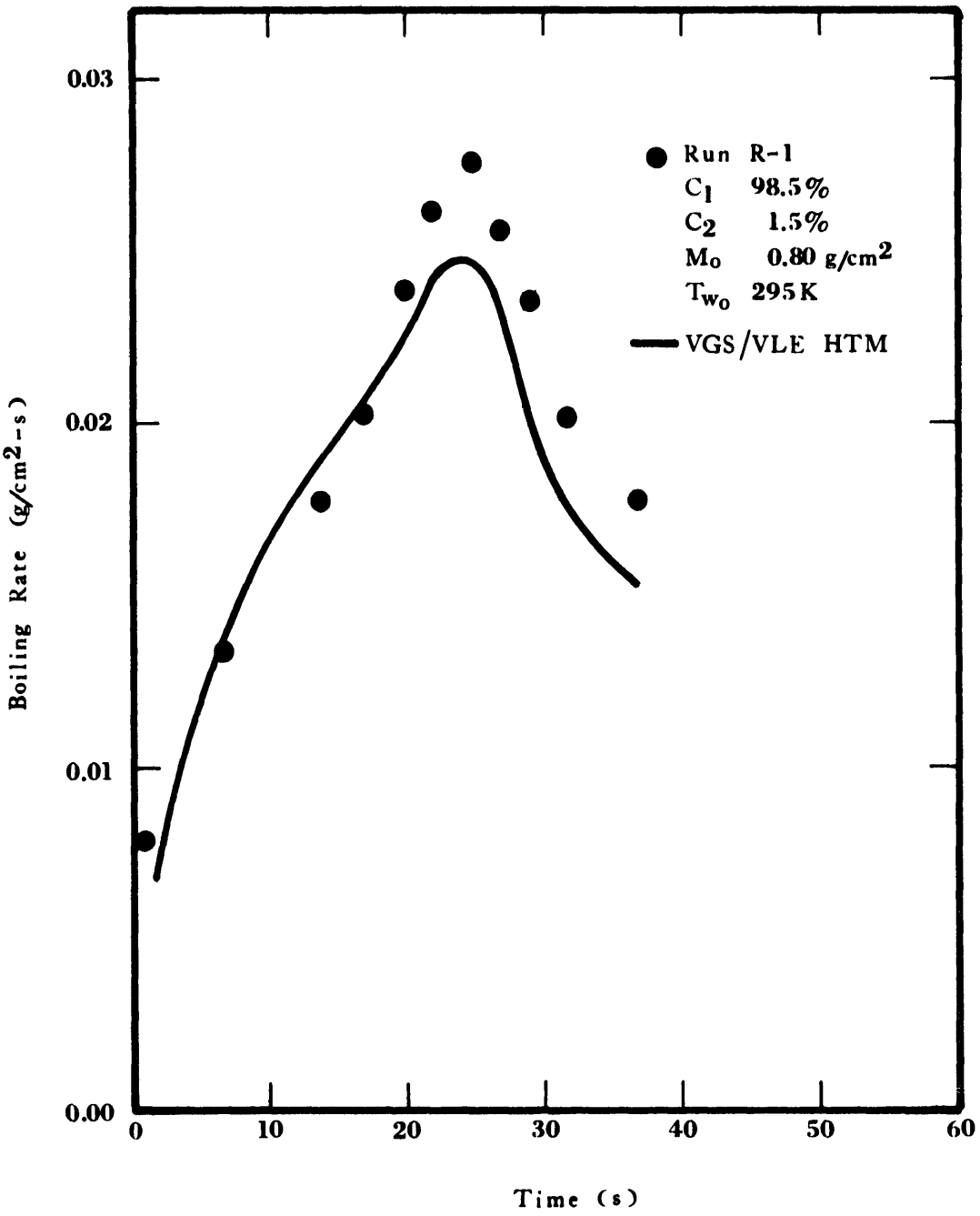

Figure 6-27 Evaporation Rates of a Methane-Ethane Mixture on Water (R-1). VGS/VLE HTM Predictions and Experimental Data (τ_{cf} = 25 s)

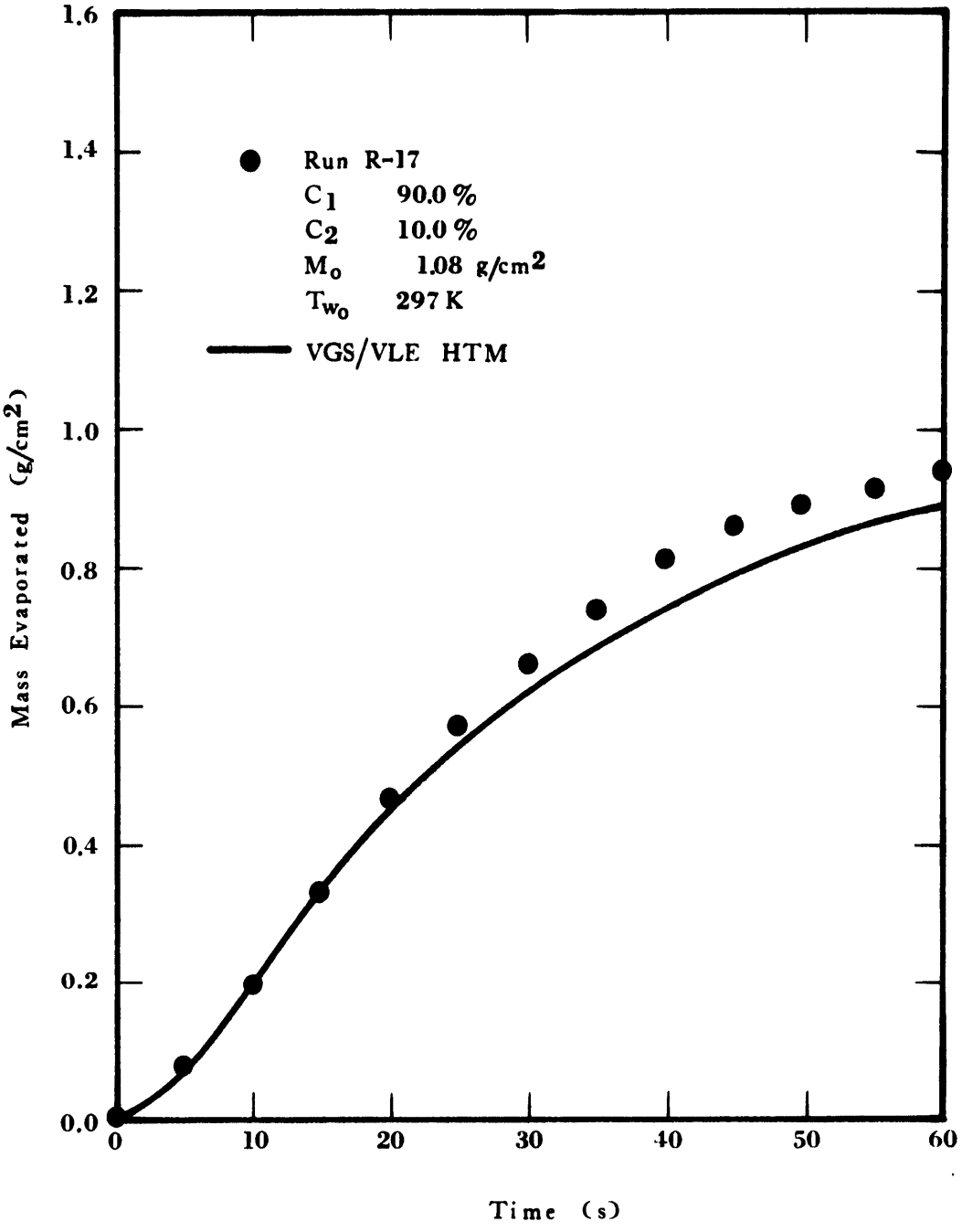

Figure 6-28 Boiling of a Methane-Ethane Mixture on Water (R-17). VGS/VLE HTM Predictions and Experimental Data (τ_{cf} = 25 s)

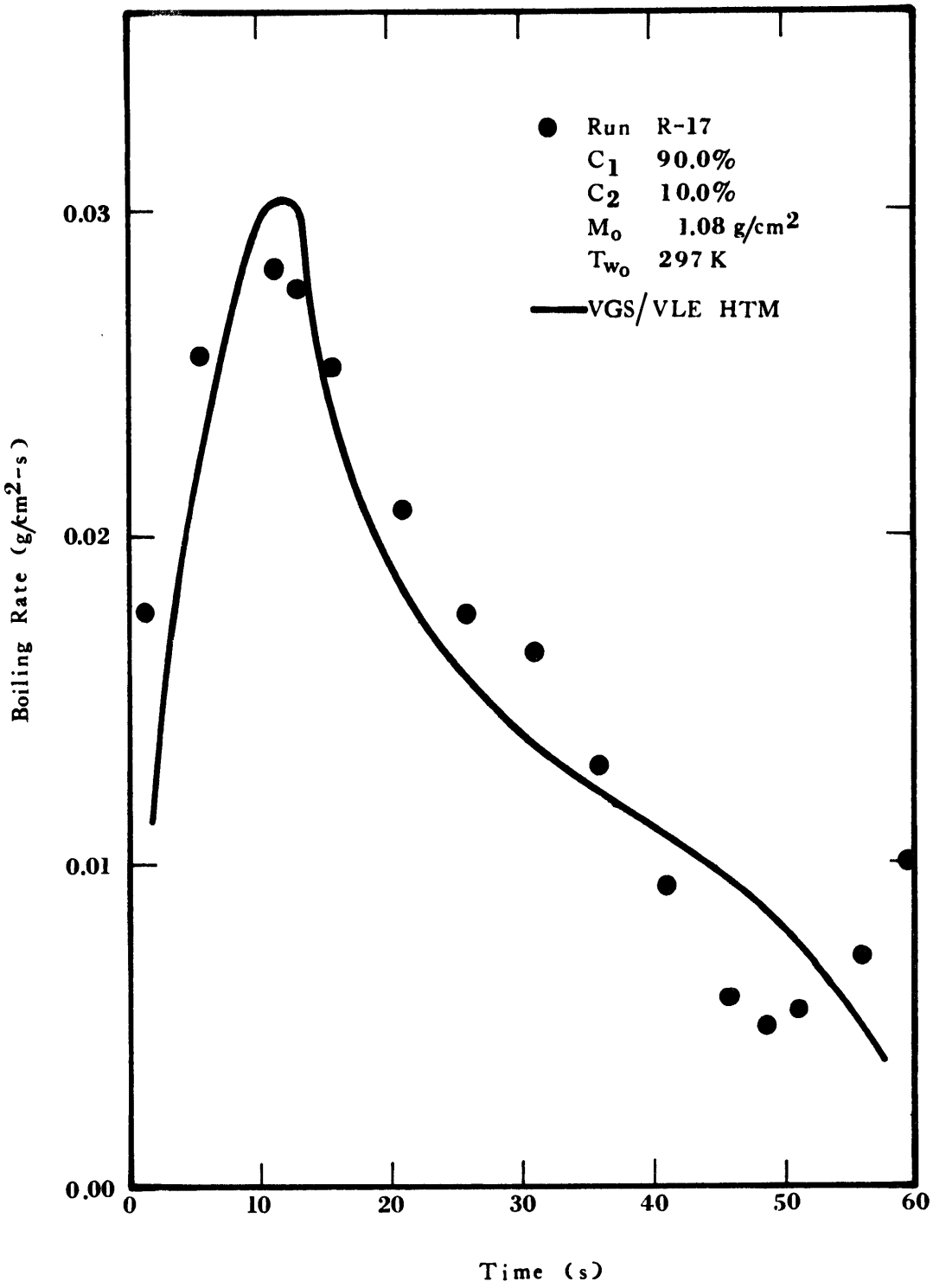

Figure 6-29 Evaporation Rates of a Methane-Ethane Mixture on Water (R-17). VGS/VLE HTM Predictions and Experimental Data (τ_{cf} = 13 s)

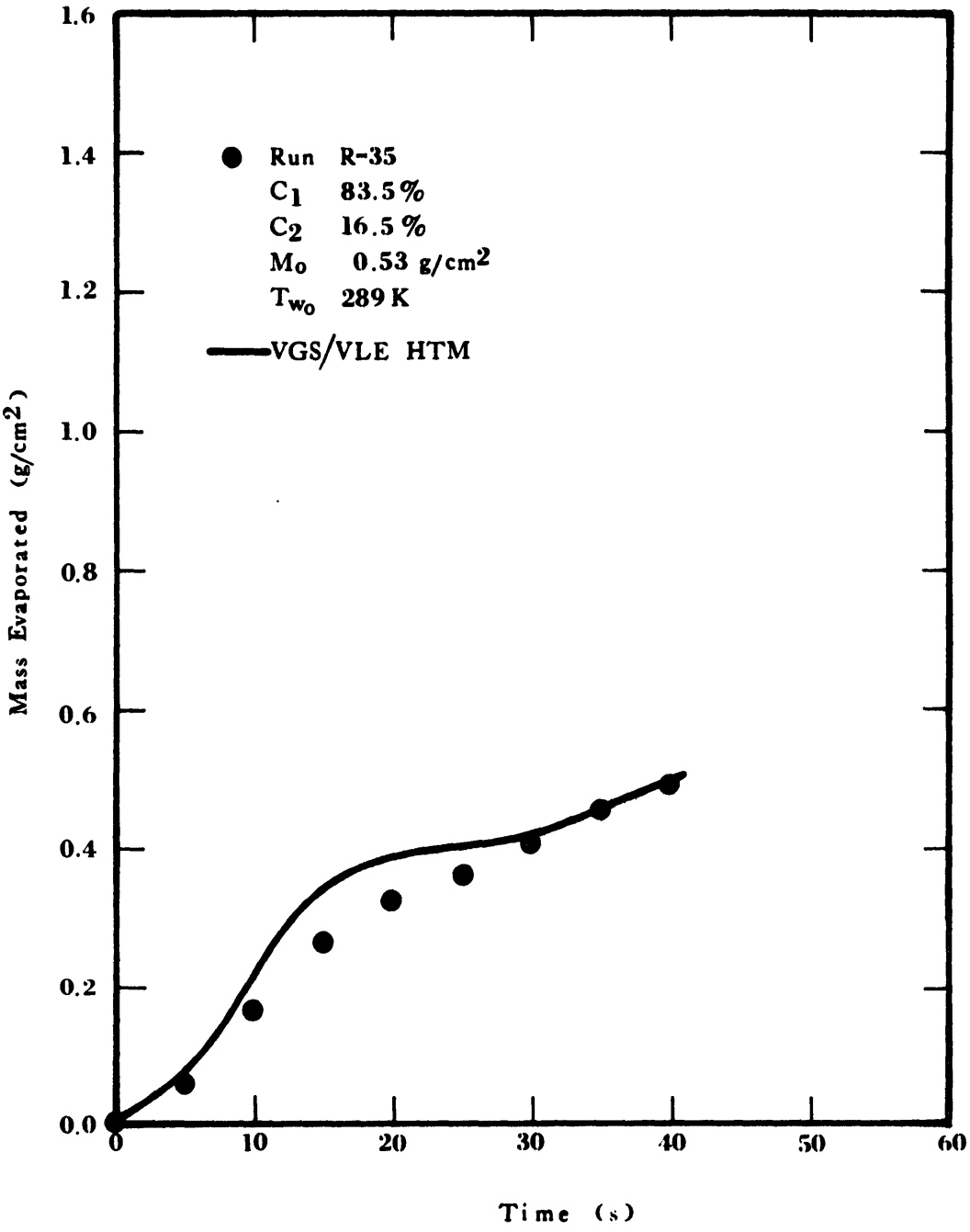

Figure 6-30 Boiling of a Methane-Ethane Mixture on Water (R-35). VGS/VLE HTM Predictions and Experimental Data (τ_{cf} = 11 s)

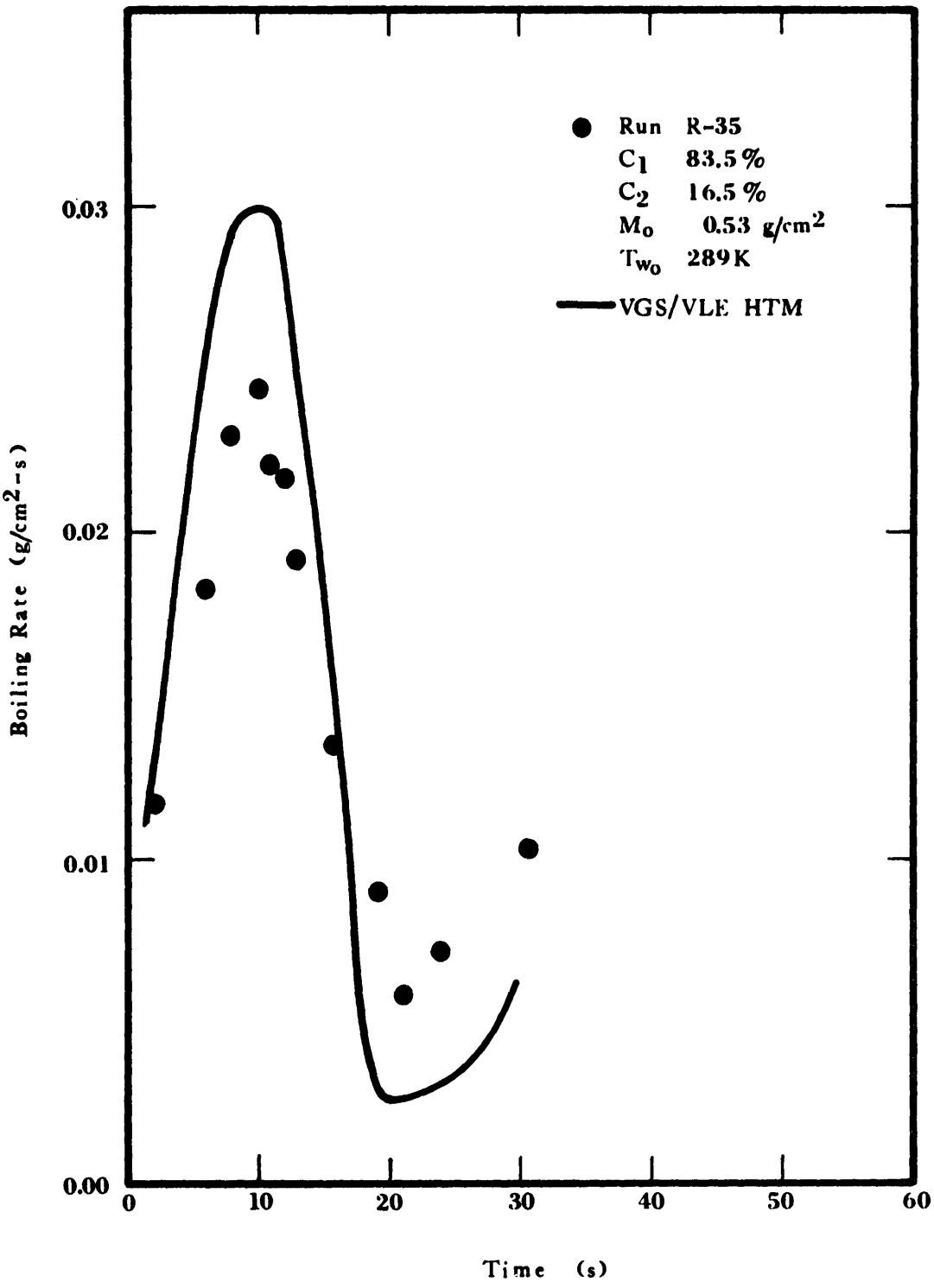

Figure 6-31 Evaporation Rates of a Methane-Ethane Mixture on Water (R-35). VGS/VLE HTM Prediction and Experimental Data (τ_{cf} = 11 s)

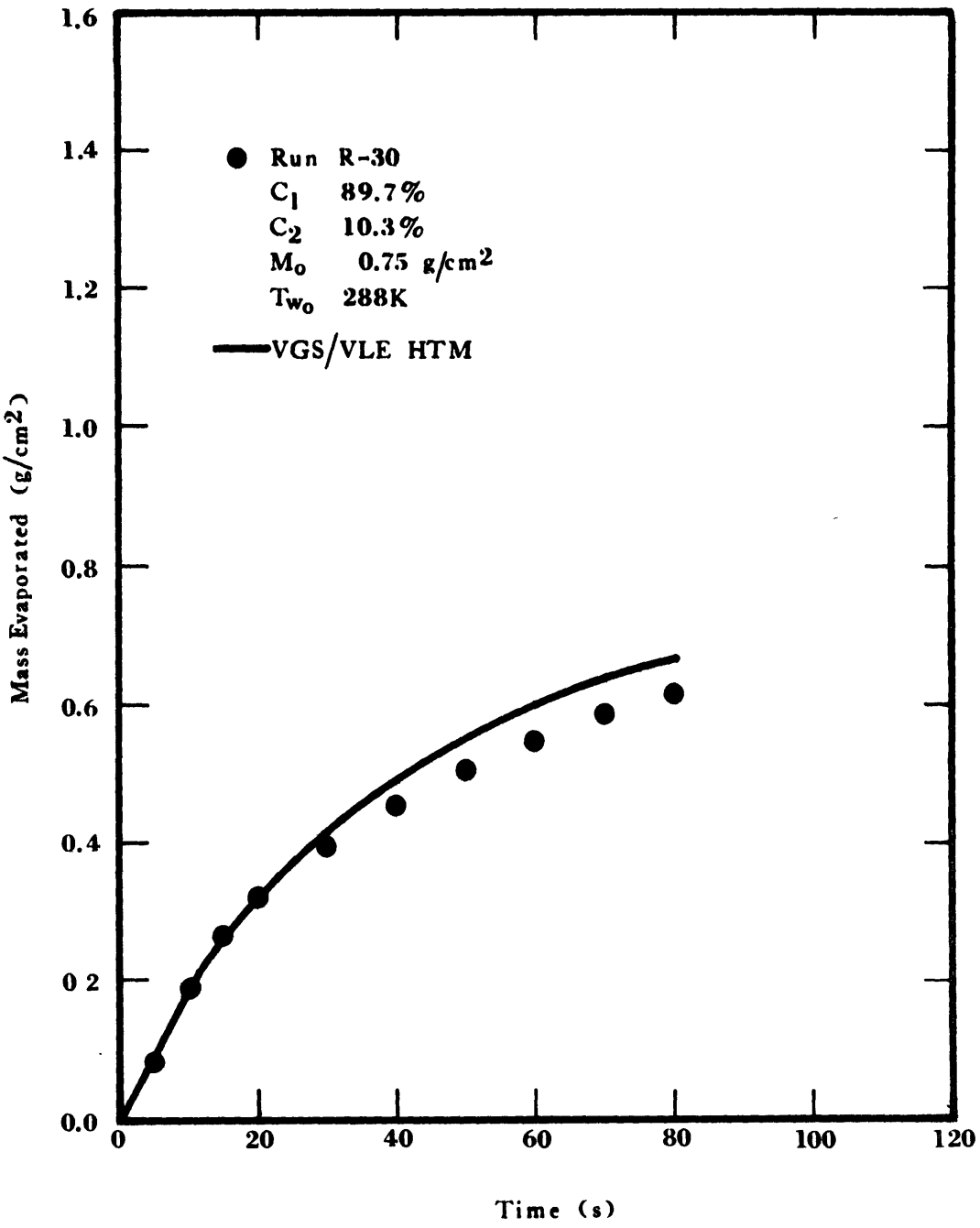

Figure 6-32 Boiling of an Ethane-Propane Mixture on Water (R-30). VGS/VLE HTM Predictions and Experimental Data (τ_{cf} = 5 s)

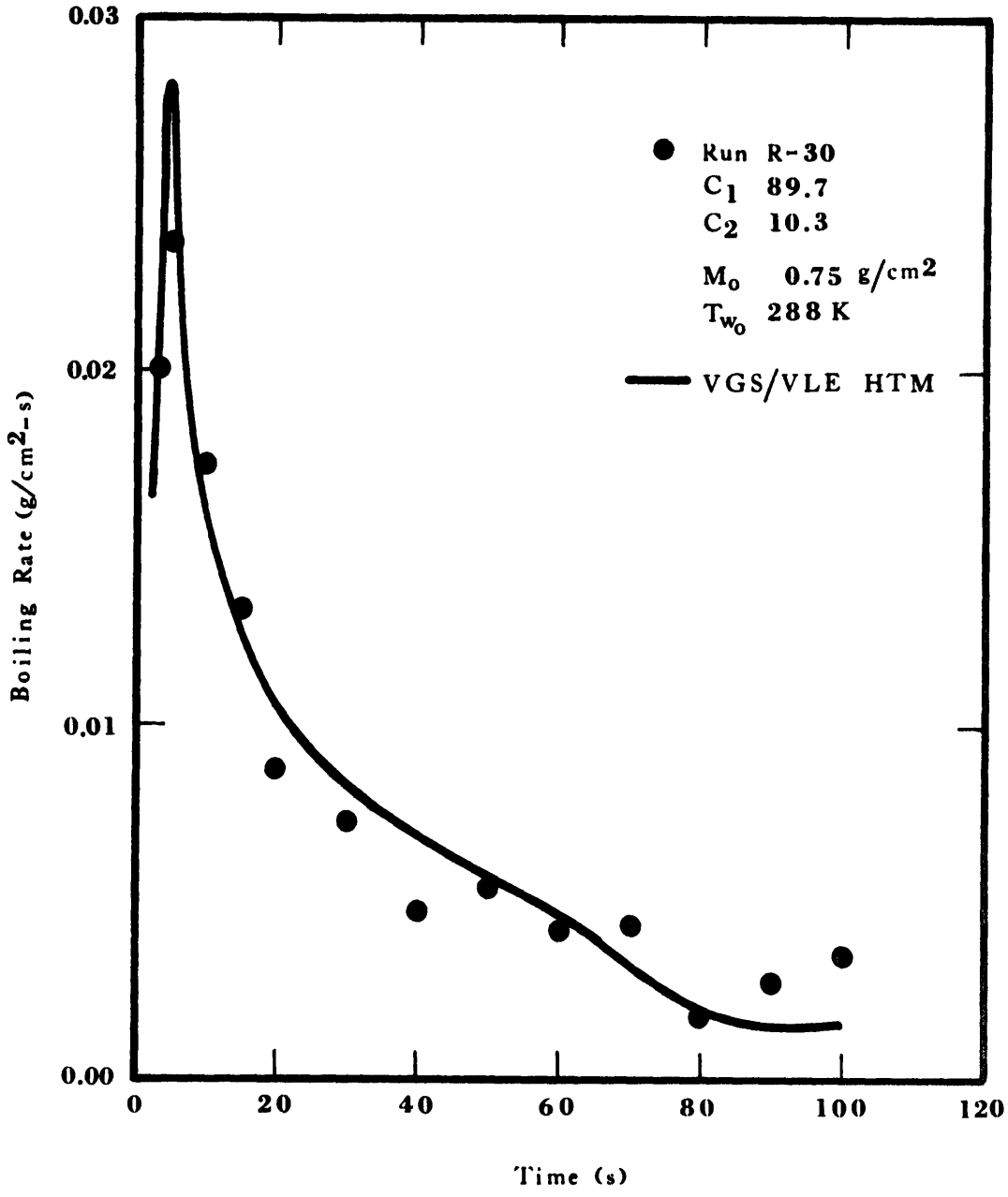

Figure 6-33 Evaporation Rates of an Ethane-Propane Mixture on Water (R-30). VGS/VLE HTM Predictions and Experimental Data (τ_{cf} = 5 s)

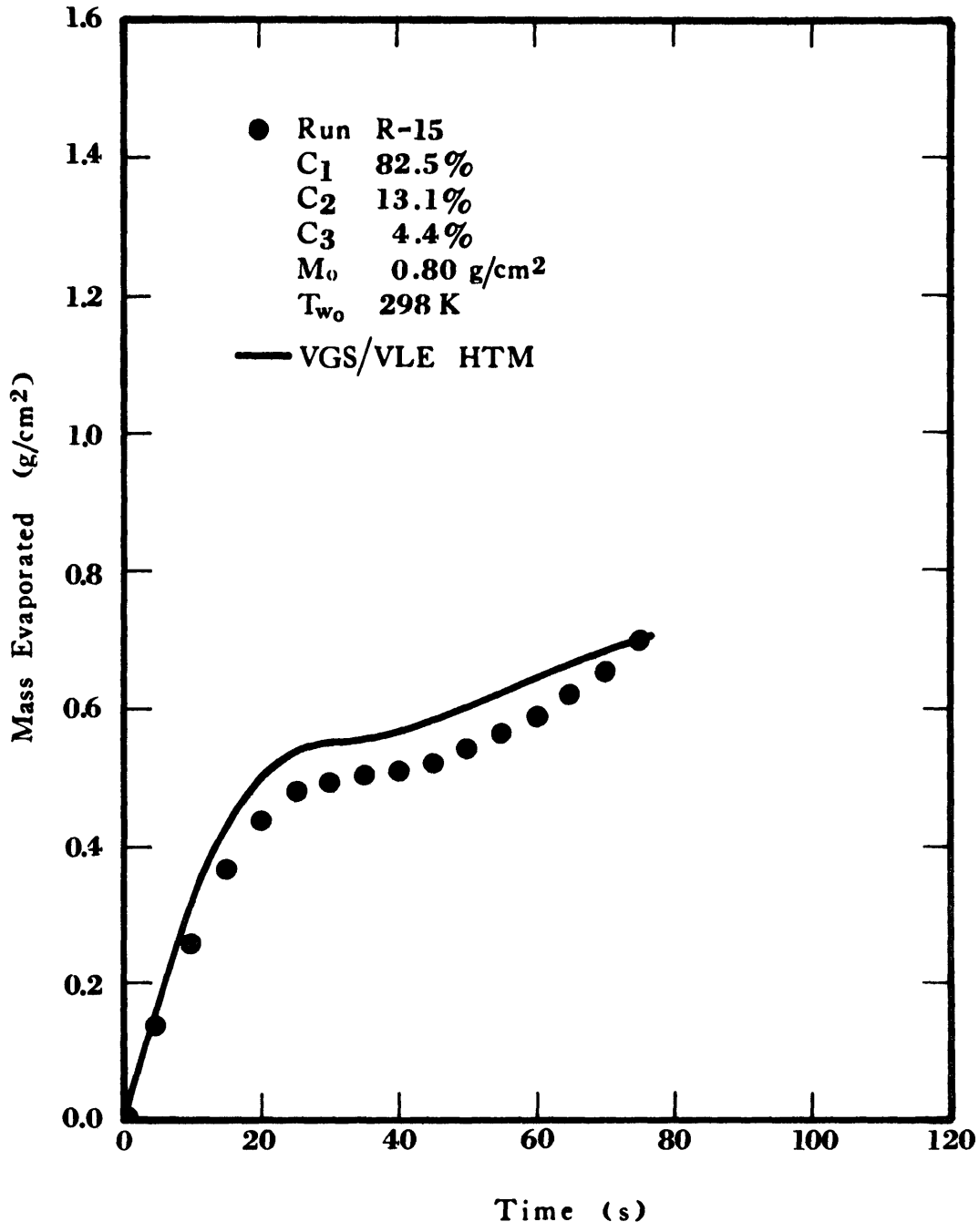

Figure 6-34 Boiling of an LNG Mixture (R-15) on Water. VGS/VLE HTM Predictions and Experimental Data (τ_{cf} = 5 s)

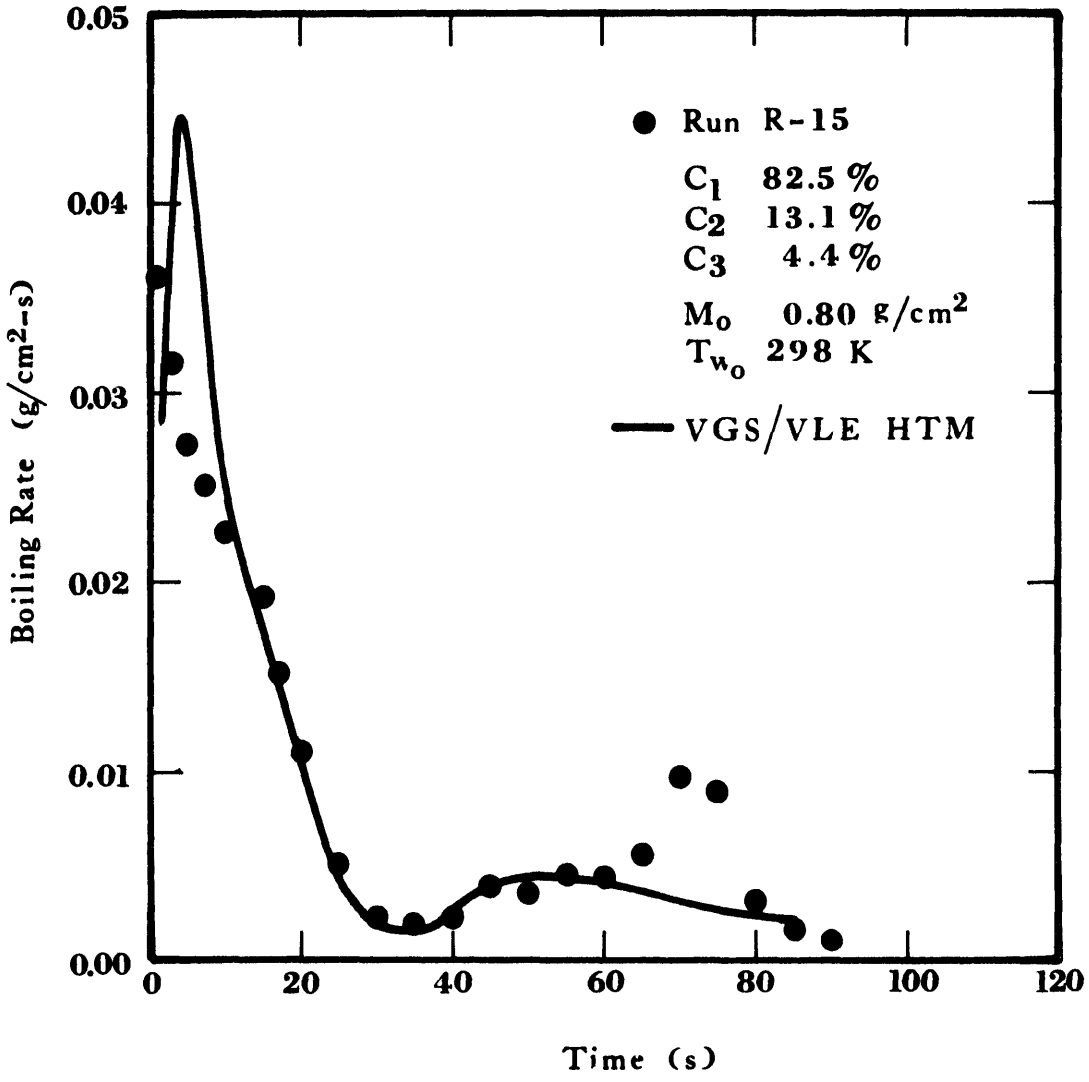

Figure 6-35 Evaporation Rates of an LNG Mixture (R-15) on Water. VGS/VLE HTM Predictions and Experimental Data (τ_{cf} = 5 s)

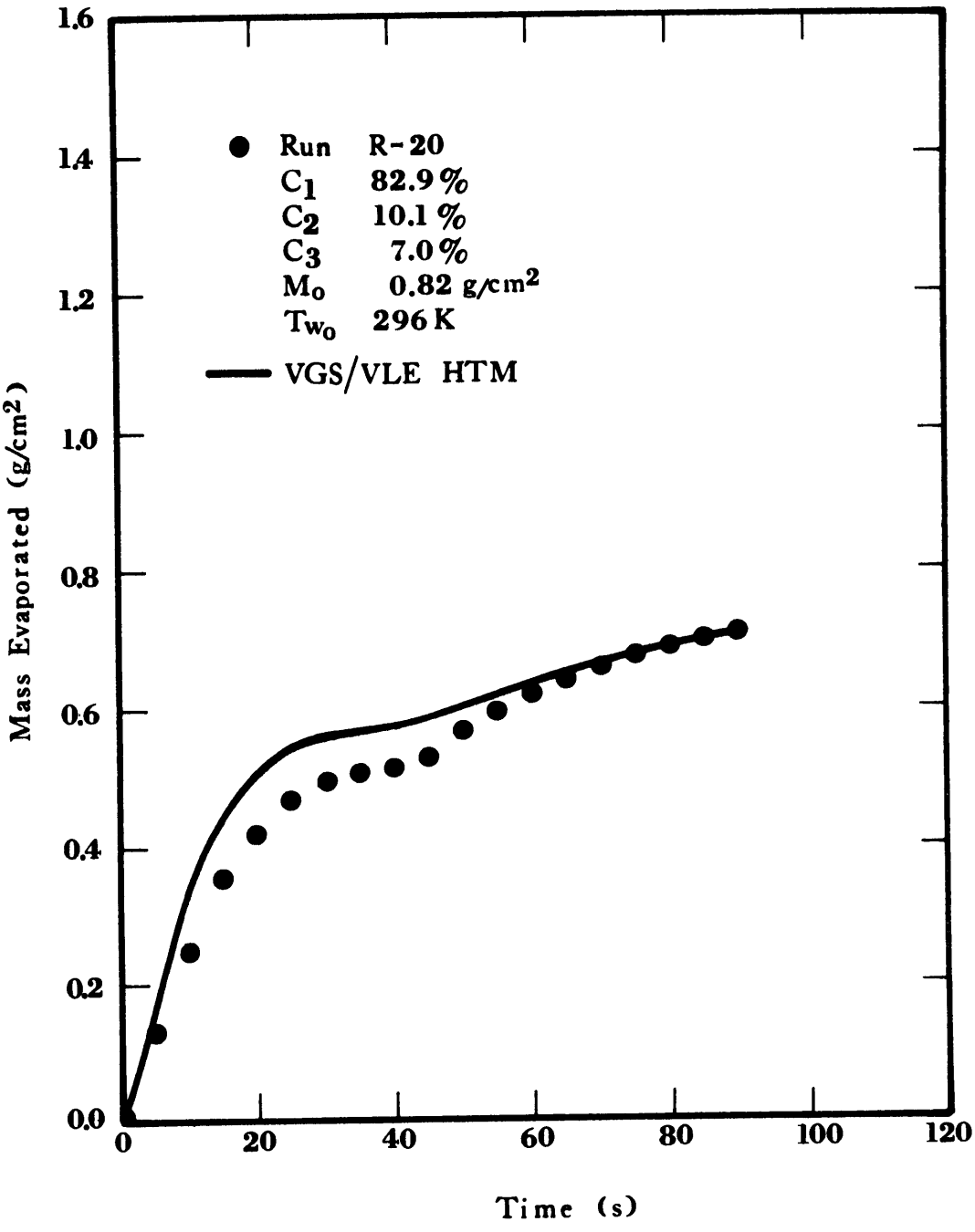

Figure 6-36 Boiling of a Methane-Ethane-Propane Mixture on Water (R-20). VGS/VLE HTM Predictions and Experimental Data (τ_{cf} = 5 s)

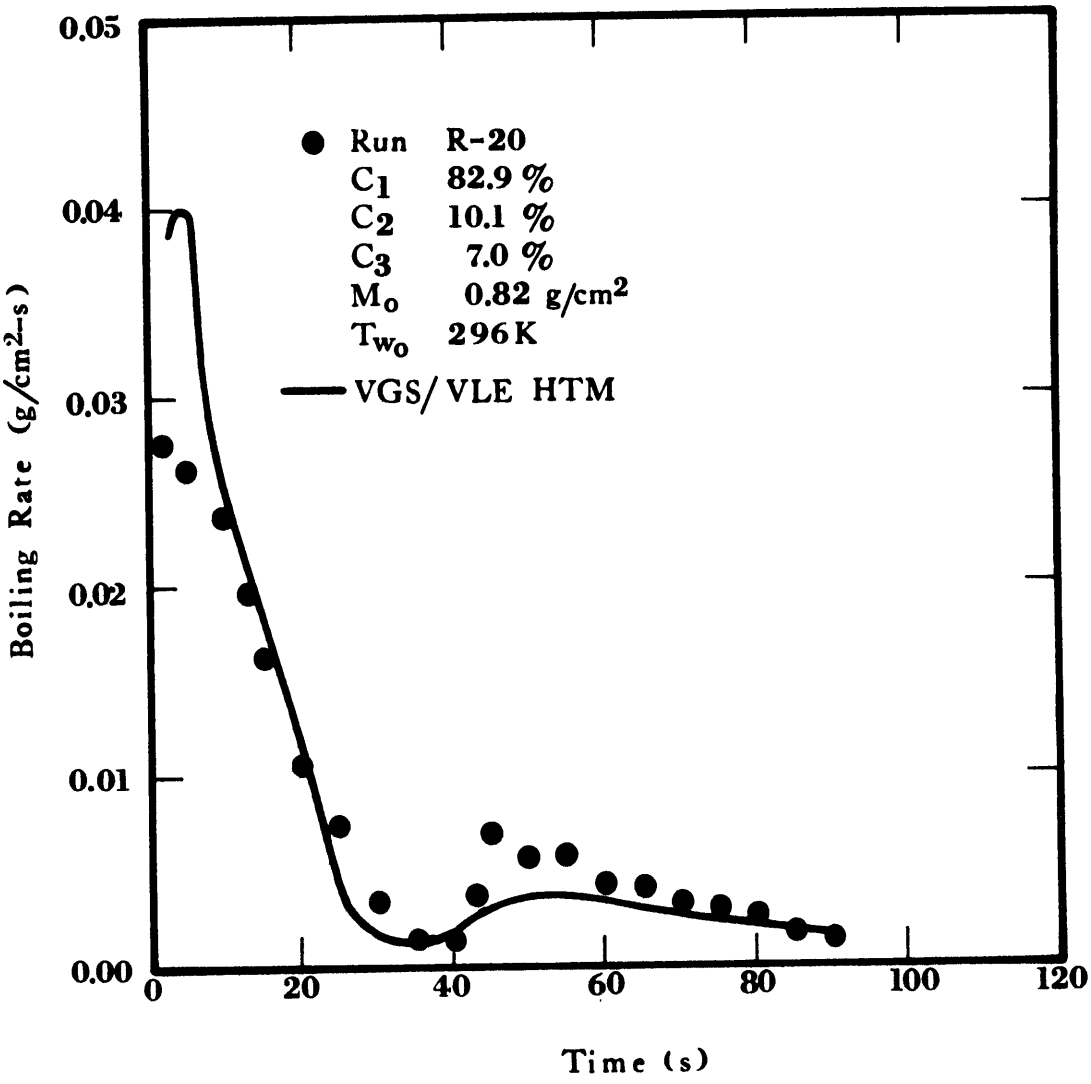

Figure 6-37 Evaporation Rates of a Methane-Ethane-Propane Mixture on Water (R-20). VGS/VLE HTM Predictions and Experimental Data (τ_{cf} = 5 s)

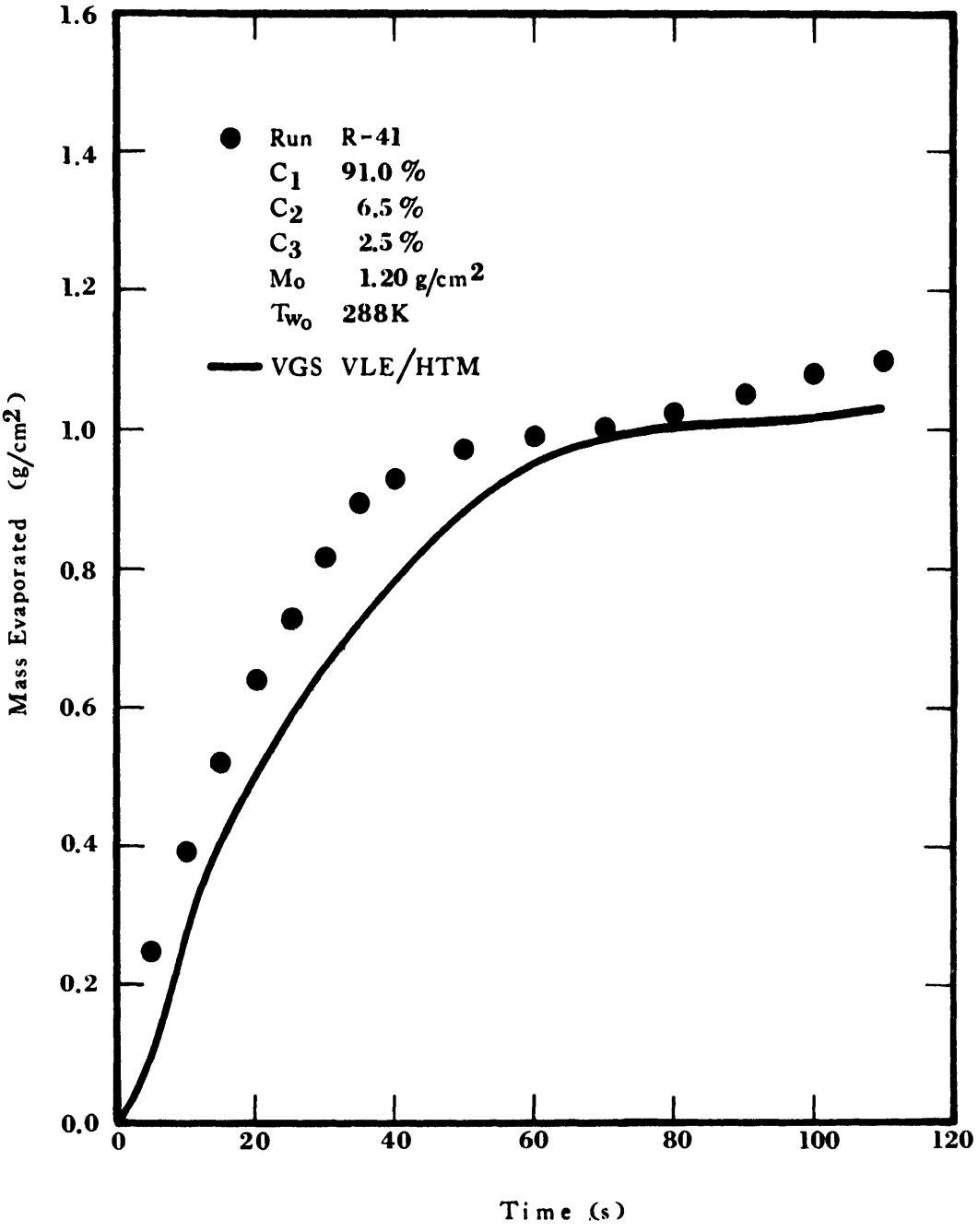

Figure 6-38 Boiling of an LNG Mixture on Water (R-41). VGS/VLE HTM Predictions and Experimental Data (τ_{cf} = 10 s)

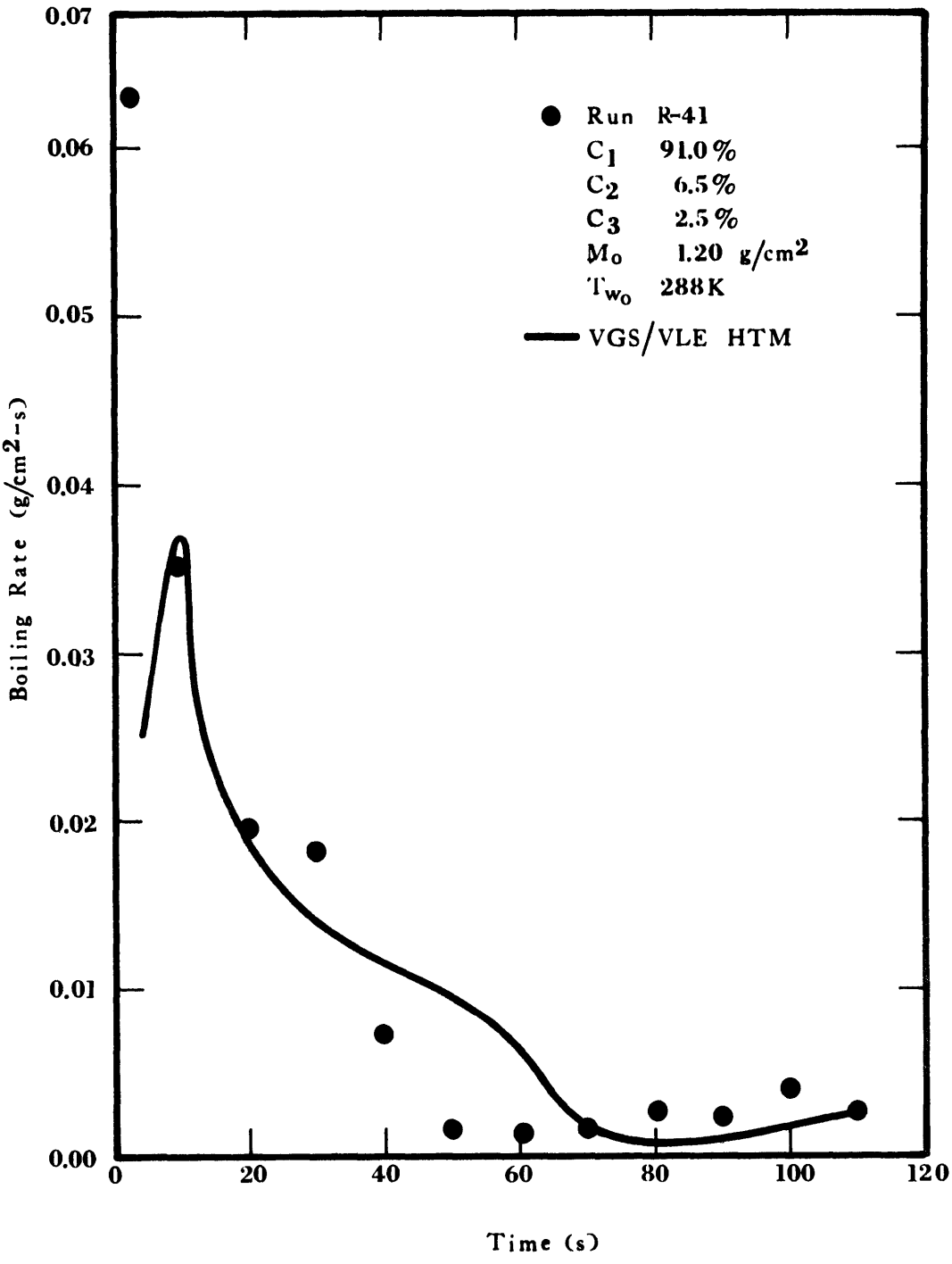

Figure 6-39 Evaporation Rates of an LNG Mixture on Water (R-41). VGS/VLE HTM Predictions and Experimental Data (τ_{cf} = 10 s)

VII. SECONDARY OBSERVATIONS REGARDING THE EVAPORATION OF LIGHT HYDROCARBONS ON WATER

Foaming

LNG mixtures have been known to foam while boiling on water (Burgess, 1970, 1972; Jeje, 1974; Vestal, 1973). In this study all methane-ethane mixtures as well as all methane-ethane-propane mixtures were found to foam. The height of the foam as well as the time it took for the foam to completely recede depended upon the composition and amount spilled.

At this point, it is worthwhile to clearly define the meaning of "foam" as it is used in this study. If the vapor bubbles formed at the substrate surface (water/ice) rise through the boiling liquid and break up upon reaching the free surface of the liquid, no foam is formed. If, however, the bubbles agglomerate and take some time before breaking up at the free surface of the boiling liquid, the liquid is said to foam.

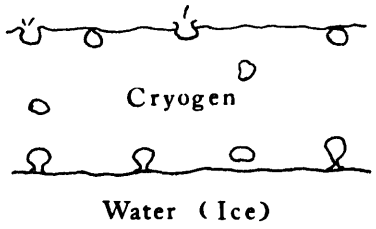

a) No Foam

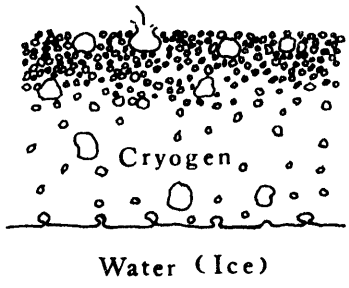

b) Foam

Ultra high purity methane (>99.97%) did not foam in any instance, whether spilled on water or ice. Similarly, research purity ethane

(>99.96%) and certified purity ethane (>99%) did not foam on either water or ice. Likewise, certified purity propane (>99%) did not foam.

Certified purity methane (∿0.1% ethane) did foam; although it was small (∿1 cm) and appeared only in the latter part of the test. These observations were made for boiling both on water and on ice.

All binary methane-ethane mixtures foamed during evaporation on water. The composition of these mixtures ranged from 80.3 to 98.5 mole percent methane and the amounts spilled ranged from 0.69 to 2.06 g/cm^2 (see Table 5-4 for more details). Typically, the height of the foam was greatest immediately after the spill, on the order of 10 cm. The amount spilled in these tests was roughly the same except for run R-38 in which twice the amount was spilled (2.06 g/cm^2). Extensive foaming took place, overflowing the boiling vessel. The height of the container was 10 cm above the water level. Since this was roughly the height of the foam in the other runs, no further analysis can be made regarding the influence of amount spilled on the height of the foam.

The time span over which a stable foam was observed exhibited a definite trend. The time at which foaming ceased was found to be slightly less than that required to boil a mass equivalent to the methane initially present in the mixture.

The foam was made up of small, stable bubbles 1-2 mm in diameter. Larger bubbles, on the order of 1-2 cm, rose quickly through the foam. The small bubbles were often seen to recirculate, agitated by the bigger and faster moving bubbles.

Binary mixtures of methane-propane (R-16 and R-25 both containing 0.2% ethane impurities, see Table 5-6) also foamed extensively. Again

a bimodal bubble distribution was observed. The bubbles, both small and large ones, were, overall, bigger than those formed by methane-ethane mixtures. The maximum foam height was about 13-15 cm, and it decreased with time.

Binary mixtures of ethane-propane did not foam. A loud crackling sound was heard while spilling the mixture from the Dewar flask. A small amount of foam (<0.5 cm) was observed in the Dewar flask while pouring the mixture.

Ternary mixtures of methane, ethane and propane foamed to a lesser or greater extent while boiling on water, depending upon their composition. Since the observations regarding foam were made while studying the boiling rates and since the foam lasted, typically, 15-25 seconds, the reported foam heights and bubble sizes are best estimates made by the observer. Due to these limitations, a definite trend (if any existed) regarding foam height could not be established for mixtures containing more than 80% methane. The maximum foam height ranged between 10 to 15 cm. For mixtures containing less than 80% methane, a definite trend could be established: if one decreased the methane content, the foam height decreased. The foam in run R-14 (C_1 75.3%, C_2 21.9%, C_3 2.8%) was only 1 cm high, and in run R-26 (C_1 78.9%, C_2 13.6%, C_3 7.5%) it reached about 3 cm in height.

The time required for the foam to recede completely was recorded more accurately. As in the case of methane-ethane mixtures, foaming stopped shortly before the mass evaporated was equivalent to the mass of methane initially present in the ternary mixture.

A satisfactory explanation for the formation of the foam is not available and only conjectures can be postulated.

During the evaporation of methane-ethane, methane-propane or methane-ethane-propane mixtures, there is a preferential evaporation of methane. At 110 K, the surface tensions of methane, ethane and propane are roughly 0.013, 0.027, 0.030 N/m, respectively (extrapolation of data by Gallant, 1968). During the formation of a bubble, methane is rapidly exhausted at the base of the bubble and the surface tension increases (enrichment in ethane and/or propane). Due to this increase in surface tension, the bubbles are pinched off at a smaller diameter than the bubbles generated with pure methane where no surface tension gradient exists. Furthermore, the collapse of the vapor film due to the lowering of the vapor pressure at the base of the bubble causes an increase in heat flux due to a direct LNG-substrate contact. The increase in energy transfer results in an increase in the frequency of bubble generation. In addition, the coalescence of these bubbles is prevented by the Marangoni effect. Due to the local exhaustion of methane in the immediate neighborhood of a bubble, the liquid film between two approaching bubbles is depleted in methane, and diffusion to the common wall is more limited than in the free walls where sufficient methane is available from the bulk. As a consequence, the interfacial tension around the common wall increases and creates a surface tension gradient. This gradient causes the flow of liquid between the approaching bubbles thereby preventing them from coalescing.

The net result is the rapid generation of a large number of very small bubbles. Furthermore, these bubbles, due to their small size,

are more difficult to rupture and rise more slowly than the larger bubbles generated with pure methane. During the initial high heat fluxes encountered in the boiling of mixtures, the rate of bubble generation is higher that the rate of bubble rupture and a "foam" is observed. Once that the heat flux begins to decrease, the foam recedes and it disappears when the heat fluxes reach very low values. The time almost coincides with the evaporation of a mass equivalent to the amount of methane initially present in the mixture. At that point, the surface of the ice layer has approached the temperature of the cryogen; when the methane in the residual liquid is almost exhausted, the temperature of the cryogen begins to increase. So the driving force for energy transfer decreases. Furthermore, most of the energy transferred at that time goes into warming up the residual cryogen and not into bubble generation (evaporation). When boiling resumes, the rate of bubble generation is low and bubbles rupture faster than they are formed. Furthermore, in the case of methane-ethane mixtures, only ethane is left and, for methane-propane mixtures, only propane remains boiling. Therefore, a surface tension gradient no longer exists. In the case of methane-ethane-propane mixtures, a residual ethane-propane mixture is left boiling, but the difference in surface tension between these components is not so severe as to cause a drastic reduction in bubble size due to early pinch-off. This also explains why ethane-propane mixtures did not foam significantly.

Solid Phase (Ice) Composition

Burgess (1972) first suggested the possibility that a hydrate might be formed after spilling LNG on water. This hypothesis was

formulated to account for the large amount of energy required to cause the vapor explosion which occurred in the previous phase of the Bureau of Mines study (Burgess, 1970). The rapid formation of hydrate which was thought to be exothermic might then have yielded that energy. The idea was abandoned after finding, experimentally, that the formation of methane-hydrate at 135 K was eight orders of magnitude slower than expected. Boyle and Kneebone (1973) also suggested the possibility of hydrate formation to account for the weight gain by the substrate after complete evaporation and subsequent weight loss after the melting of the solid phase. After evaporation stopped, the hydrates would remain with the rest of the ice. Since the hydrates contain hydrocarbons, the mass of the substrate would increase. After melting of the ice, the hydrates would decompose and the hydrocarbons would vaporize.

Direct contact between the two hydrate components (water and hydrocarbons) is required for the formation of hydrates. Consequently, the hydrates can form only during the initial hydrocarbon-water contact and during seepage of hydrocarbon through ice cracks later in the test. Since the new layers of ice form under the existing ice, the hydrates would be on the surface of the ice and in some intermediate layers if formed during cryogen seepage. Due to the non-uniformity in composition, a sophisticated chemical analysis would be required to actually identify the hydrates and their location. Nevertheless, a simple analysis of the ice layer might yield some clues.

Several experiments were carried out in which the solid phase was removed immediately upon complete evaporation of the cryogen and placed in a sealed container. After the solid melted, the vapors were

analyzed for composition. At room temperature the hydrocarbons are in the vapor phase since they are insoluble in water. The results of these tests are given in Table 7-1. The presence of hydrocarbons in the ice does not, by itself, prove that hydrates had formed after spilling a liquid hydrocarbon on water. It could also be due to a small amount of hydrocarbon trapped in the ice.

No hydrocarbons were detected in the ice formed by spilling almost pure methane (99.5%) on water. The ice formed after spilling C. P. grade ethane (IC-6) had some ethane but it amounted only to 0.1% of the volume of the container. The ice formed after spilling C. P. grade propane had some propane but, again, it only amounted to 0.7% of the container volume in run IC-3 and 0.1% in run IC-4.

Some calculations are needed to analyze these results. The volume of the sealed container where the ice was allowed to melt was 600 ml. The mass of ice placed in it was roughly 10-20 g. Thus, 0.1% of the vapor volume is 0.60 ml. At room temperature this volume represents 2.5×10^{-5} moles. For ethane, 2.5×10^{-5} moles correspond to 7.5×10^{-4} g or 1.37×10^{-3} cm^3 of liquid ethane (0.548 g/cm^3). A liquid droplet of 0.7 mm in radius has that volume and if entrapped in ice would yield the amount of ethane detected.

A similar analysis for propane will indicate that a droplet 0.8 mm in radius entrapped in ice will yield 0.1% of the container volume after evaporation (IC-4). A droplet of liquid propane 1.5 mm in radius entrapped in ice will yield 0.7% of the container volume (IC-3).

The above argument does not prove by any means that hydrate formation does not take place. It simply points out the fact that a small

TABLE 7-1

Analysis of Ice for Presence of Hydrocarbons

Run	Cryogen* Composition	Composition of* Hydrocarbons in Ice	Vapor Volume Occupied by Hydrocarbons
IC-1	67% C_1	3% C_2	9%
	19% C_2	86% C_3	
	14% C_3	3% i-C_4	
	trace C_4	9% n-C_4	
IC-2	Commercial Methane	4% C_2	12%
	93% C_1	31% C_3	
	4% C_2	31% i-C_4	
	1% C_3	34% n-C_4	
	0.5% C_4		
IC-3	C_3, C. P. Grade	100% C_3	0.7%
IC-4	C_3, C. P. Grade	100% C_3	0.1%
IC-5	99.5% C_1	0% C_1	0.0%
	0.5% C_2	0% C_2	
IC-6	C_2, C. P. Grade	100% C_2	0.1%

*Mole percent may not add up to 100 due to round off.

entrapped liquid droplet could also explain the results. In fact, a similar analysis can be made if one assumes that the hydrocarbon vapors detected are the result of hydrate decomposition. The propane hydrate has a structure of $C_3H_8 \cdot 17\ H_2O$. In run IC-3 the propane vapor volume was 0.7% of 600 ml, or 4.2 ml, which is equivalent to 1.75×10^{-4} moles. The amount of water required to form the hydrate is 17 times this value or $3. \times 10^{-3}$ moles, which is equivalent to 54 mg or 0.06 cm^3 of ice. Assuming that 10 g of 0.5 cm thick ice were sealed in the container, the cross sectional area of this ice would be 22 cm^2. Consequently, a layer 0.06/22 cm or 30 μm thick is made up of $C_3H_8 \cdot 17\ H_2O$ hydrate. The assumption of an area of 22 cm^2 gives the maximum hydrate thickness; in the experiments the boiling was extremely violent and very irregular ice was formed. The area of contact between propane and water was probably much higher than 22 cm^2.

Based on these facts, it seems that pure hydrocarbons, methane, ethane and propane, do not form hydrates when spilled on water; and if they do, the amount produced is so small that it does not have any pratical relevance.

The amounts of hydrocarbon present in the ice formed after spilling LNG mixtures are much higher than those found for pure components. The major constituents being propane and butanes. If the results for run IC-1 are analyzed in the same fashion as those for pure components, a liquid droplet 3.4 cm in radius would have to have been entrapped in ice. More likely, however, the preferential evaporation of methane and ethane would leave a film rich in propane and butane on the surface of supercooled ice with little evaporative driving force. Such a

film would only have to be 77 μm thick (ice surface area: 22 cm^2). If hydrates are assumed to have formed, the hydrate layer would be 300 μm thick. Heavier hydrocarbons form hydrates more easily and the conditions for hydrate formation are improved by decreasing the temperature; thus, one would expect the hydrates to be made up of the heavier components in the boiling mixture.

Again the above analysis does not present conclusive proof as to whether hydrates are formed or not. It does, however, point out another plausible explanation for the presence of residual hydrocarbons found after melting the ice, that of a thin liquid (subcooled heavier hydrocarbons) film remaining on the cold ice.

Regardless of whether hydrates are formed or a thin film of heavier hydrocarbons is left on the cold ice, the small amounts of hydrocarbons involved render this problem an irrelevant one for confined spills of LNG on water. In open sea spills the hydrates, if any form, will be recirculated into the water by wave motions, the hydrate will decompose and the hydrocarbon vapors mix with the evolving vapors due to boiling or condense in the residual liquid layer. Again the effect of hydrate formation would be minimal compared to the effect of the chemical composition of the cryogen on the boiling of LNG on water.

Water Pick-Up

Boyle and Kneebone (1973) placed emphasis on the so called water pick-up by boiling LNG. Should the LNG vapor cloud pick up significant amounts of water, the cloud would become more dense. This increase in density would slow the dispersion of the cloud by air.

When pure methane and nitrogen were spilled on water, a net loss in water weight was observed immediately after evaporation was completed. With LNG, however, there was a gain in weight which changed to a weight loss after the ice melted. Either some LNG was entrapped in the ice and it evaporated as the ice melted, or hydrate formation took place. Nevertheless, when LNG was spilled on ice, no weight change was observed.

Boyle and Kneebone also found the water pick-up to increase with water agitation and with decreasing amount spilled. For a spill of 0.66 g/cm^2, the water pick-up was 0.8% of the mass of LNG spilled. For a spill of 0.10 g/cm^2, it was 6.7%. In both cases the water was agitated, and in all cases the actual water loss was on the order of 1.5 g regardless of spill size. Boyle and Kneebone argue that open sea spills are more closely resembled by agitated confined spills, and then take the worst case (6.7% water pick-up) to warn that an amount of water on the order of 7-8% of the weight of LNG spilled will be picked up during evaporation. The validity of these estimates will now be reviewed in light of the results obtained in the present work.

In this study the water gained about 1 to 2 g after significant evaporation had stopped (this point is actually arbitrary since the boiling rates decrease very slowly after reaching a very low value). In almost all experiments, the melting of the ice was accelerated for expediency and during this process the weight of water was altered so in general no record of the weight of water after the ice melted could be made. In a few experiments in which the ice was left alone,

the weight gain changed into a loss ranging from 0-1 g of water. (The ice had not melted completely.) Thus, the observations made by Boyle and Kneebone regarding the loss of some water are valid.

A few experiments were made with pure methane to measure the amount of water picked up by the vapors. The amount lost was the same ($\sim$0.25 g) for spills of 0.16, 0.32, and 1.20 g/cm^2 (area = 64 cm^2). This indicates that the amount of water picked up is proportional to the contact area between the cryogen and the water and not merely a percentage of the mass of LNG spilled, as suggested by Boyle and Kneebone. Once ice forms, the water pick-up stops as was confirmed by Boyle and Kneebone. The water picked up per unit contact area, 3.9×10^{-3} g/cm^2, can be compared to the value obtained by Boyle and Kneebone of 3.8×10^{-3} g/cm^2 (1.01 g and 266 cm^2) for methane. The agreement is excellent.

Using the values for water losses given by Boyle and Kneebone, one would expect 7.5×10^{-4} g/cm^2 of water to be picked up during spills of LNG on water, in which the water is not agitated (0.2 g, 266 cm^2, 94% methane). If the water is agitated, 45×10^{-4} g/cm^2 are expected to be picked up. If the methane present is decreased to 85%, the ice will form sooner and the water pick-up will decrease to 26×10^{-4} g/cm^2 (agitated water).

Thus it would appear that the water pick-up in an open sea spill would be expected to be on the order of 25-50 $\times 10^{-4}$ g/cm^2 or 25-50 $\times 10^{-3}$ kg/m^2. To get a better feeling of what this implies in an open sea spill, the values for maximum pool radius as a function of spill size (Otterman, 1975) can be used. For a spill of 10,000 m^3

($\sim$5,000 kg) the maximum radius is 270 m or an area of 230,000 m^2 and the water pick-up would be of 5,700 kg (25×10^{-3} kg/m^2). For a spill of 100,000 m^3 ($\sim$50,000 kg), the maximum radius is 670 m or an area of 1,400,000 m^2 and the water pick-up would be 70,000 kg.

These estimates are by far greater than Boyle and Kneebone's. A scale-up of seven orders of magnitude is being made which leaves ample room for errors due to scale-up. It can be concluded, then, that some water is indeed picked up during evaporation of LNG on water. The above estimates, as well as Boyle and Kneebone's, are too rudimentary; better estimates should be obtained by actually determining the water content of the vapor cloud during unconfined spills.

VIII. CONCLUSIONS AND RECOMMENDATIONS

Conclusions

The following conclusions are made regarding the evaporation of confined spills of liquefied natural gas (LNG) and of its pure components, methane, ethane, and propane on water.

- Methane film boils on water until the ice layer formed cools sufficiently to promote nucleate boiling. The heat flux and boiling rate increase with time until nucleate boiling is fully achieved. Thereafter, the heat flux and boiling rate decrease.
- Ethane transition boils on water until the ice layer formed cools sufficiently to promote nucleate boiling. The heat fluxes increase with time until nucleate boiling is fully achieved; thereafter the heat fluxes decrease.
- Propane nucleate boils on water upon initial contact. The heat fluxes monotonically decrease with time.
- LNG mixtures undergo a preferential evaporation of the more volatile components. This preferential evaporation causes a rise in the saturation temperature of the residual liquid. The composition of the vapor and the residual liquid, as well as the saturation temperature, can be determined from vapor-liquid equilibria and mass balance considerations.
- Initially, LNG mixtures film boil on water. The preferential evaporation of methane causes a drop in the vapor pressure of the liquid in the immediate neighborhood of the base of the forming bubble. This vapor pressure drop, in turn, causes the collapse of the vapor

film; an intimate cryogen-water/ice contact is made resulting in high heat fluxes. The thin layer depleted in methane is carried by the wake of the bubble and mixes with the bulk. Fresh liquid flows to the substrate, thereby regenerating the film. The LNG/water-ice contact accelerates the formation and subsequent cooling of the ice layer, thus inhibiting the regeneration of the film. Nucleate boiling is established, thereafter the heat fluxes decrease.

- The higher the heavier hydrocarbons content in the LNG mixture, the faster the vapor film collapses and nucleate boiling is established.
- Once the methane content in the residual liquid drops to 10-20%, the saturation temperature of the liquid begins to rise rapidly. Since the temperature of the ice surface is approaching the cryogen temperature prior to the rapid change, the driving force for energy transfer decreases significantly. Furthermore, most of the energy transferred at this time is utilized in warming the residual liquid to the rising saturation temperature, thereby further reducing the evaporation rates.
- A linear decrease with time is a good approximation for the variation of substrate surface temperature with time. This finding results from the application of convolution integrals to the experimental heat fluxes.
- Based on the above considerations of film collapse, decreasing surface temperature and increasing saturation temperature, a heat transfer model, coupled with a vapor-liquid equilibria model, has been developed. This model predicts successfully and a priori the evaporation of confined spills of LNG on water.

- Pure hydrocarbons, methane, ethane and propane, do not foam while boiling on water.
- Mixtures of methane-ethane, methane-propane, methane-ethane-propane foam on water.
- Mixtures of ethane-propane do not foam on water.
- In LNG mixtures surface tension gradients at the base of forming bubbles cause an early pinch-off of the vapor bubbles at smaller diameters than in pure components. This is due to the localized exhaustion of methane which has the lowest surface tension.
- During the high initial heat fluxes, the rapid formation of a large number of these small bubbles is thought to be responsible for the formation of foam.
- The water temperature ∿1 cm below the original water surface does not change significantly. This depth is a direct function of the amount spilled.
- Methane vapors are slightly superheated (∿15 K) for spills of 0.5 g/cm^2. The superheats are negligible for spills greater than 1.5 g/cm^2.
- Ethane and propane vapors are not superheated.
- The vapors evolved during LNG spills are at the saturation temperature, determined from vapor-liquid equilibria considerations.
- Large amounts of water may be atomized and picked-up by the evolving vapors during spillage of light hydrocarbons and their mixtures on water.

Recommendations

The evaporation of confined spills of LNG on water is now sufficiently understood. Future efforts should be concentrated on the effect of the simultaneous boiling and the spreading of LNG. To this extent, the following recommendations are made.

- Determine, experimentally, the variation in composition of the residual cryogen, both with time and location, to evaluate the extent of the preferential evaporation of volatiles.
- Determine, experimentally, the characteristics and extent of ice formation, if any.
- Both of the above points will be extremely important in the development of a model to predict the evaporative behavior of LNG mixtures on an open sea.
- The best approach for determining the above characteristics is to select the composition of a mixture, the amount to be spilled, the water temperature and the degree of agitation. The spills should then be repeated, under the specified conditions, until the boiling and spreading characteristics are determined with an acceptable degree of certainty. Only at that time should variations be tried. The problem at hand is a very complex one and should be understood well for at least one case before attempting a global understanding.
- Bubbling cold nitrogen or cold methane gas through LNG might yield some clues as to the exact reason for the foam formation. This approach would prevent any preferential evaporation and the subsequent changes in surface tension.
- The water content of the vapor cloud should be measured experimentally.

APPENDIX A

EXPERIMENTAL

Electronic Balance

Real Time Computer

Computer Programs to Monitor Data Acquisition

Thermocouples

Gas Chromatograph

Electronic Balance

The load cell used in this work was a METTLER P11 with a METTLER BE13 control unit and METTLER BA26 digital readout.

This load cell system outputs an electrical signal proportional to the mass on the balance. This voltage, in turn, is fed into a NOVA 840 computer.

The measuring principle of the load cell is a force-compensating one. The block diagram for the balance is shown in Figure A-1. The beam sensor (3) determines the deflection of the balance beam which occurs during weighing. The variable-gain amplifier (4) increases the output signal of the beam sensor (3) and generates a force in the compensation system (2) by way of the range-switch (5). This force produces the counterrotational torque which returns the balance beam to the original undisturbed position. A voltage proportional to the compensating force is produced at the range selector switch (5). After being amplified (6) this signal (9) is fed into the computer. In the 1000 gram measuring range, the built-in weights used (7) are detected digitally and carried over the range selector switch (5) to the digital readout unit (8). Performance and design specifications are given in Table A-1.

It is important to realize fully the capabilities and limitations of the load cell system. The electrical output originated by the drop of a 128 g weight, from 5 cm, on the balance is shown in Figure A-2. Severe oscillations are present in the first few tenths of a second and a 100% response signal is obtained after 0.6 seconds. The output

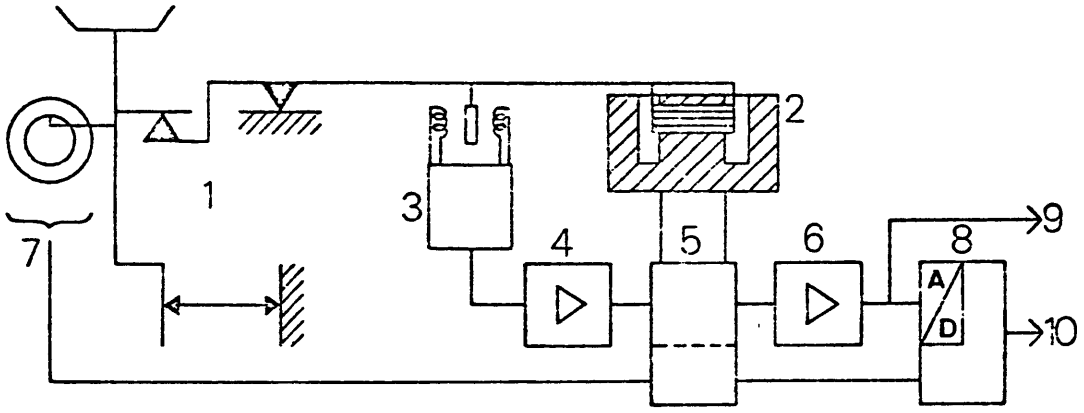

Legend

1 Mechanical top-loading balance system
2 Compensation system
3 Beam sensor
4 Variable-gain amplifier
5 Range-selector switch
6 Output amplifier
7 Digital detection of the built-in weights used including 5 kg supplementary weight
8 Digital output unit
9 Analog output signal
10 Digital output signal

Figure A-1 Block Diagram for the METTLER P11 Electronic Balance

TABLE A-1

Capacity	11000 g
Electrical range	1000 g
Weighing range	-1000/10000 g
Measured response time	
- 0 to full scale	<100 ms
- with severe oscillations (0 - 100%)	0.7 - 1.0 s
Electronical digital readout	
- 1 digital step	100 mg
- Accuracy	±100 mg
Electrical compensation range	
- Linearity	±100 mg
- Precision	±100 mg
Analog output	
- 10 V ungrounded,	-10/+10 V
internal resistance	<5 Ω
- 1 V ungrounded,	-1/+1 V
internal resistance	∿500
- 0.1 V ungrounded,	-100/+100 mV
internal resistance	∿50 Ω

originated by the drop of a 1000 g weight, from 2.5 cm, is given in Figure A-3. Again, oscillations are present at the beginning and it takes about 1 second to obtain a 100% response. A more severe case, the drop of 128 g from 18 cm is shown in Figure A-4. The oscillations are very severe but the correct 100% response signal is obtained within 1 second.

It can be concluded that data collection at time intervals of less than 0.5 second could lead to erroneous results, particularly at the time of the spill when the mass of the cryogen suddenly increases the mass of the system. An interval for data collection of one second was therefore considered accurate and convenient.

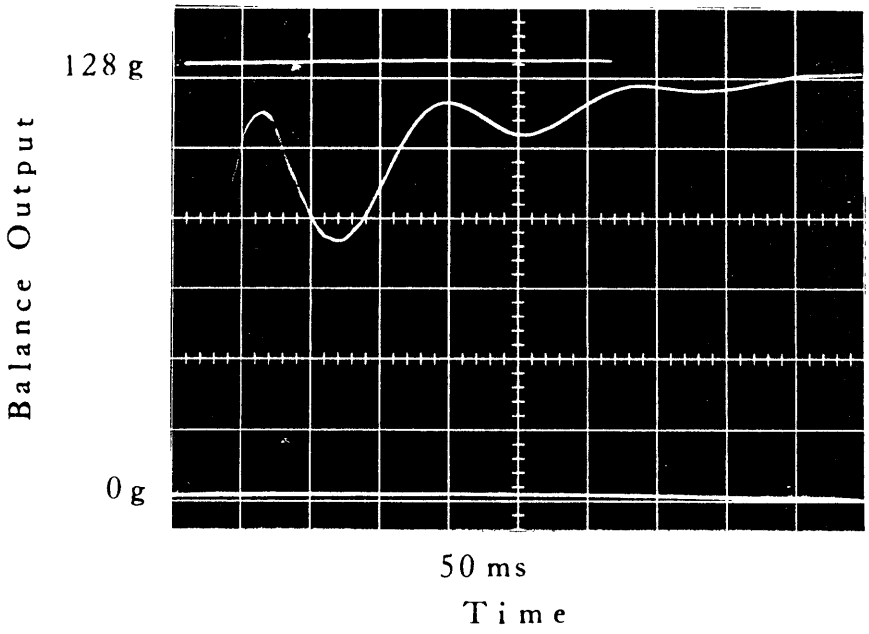

Figure A-2 Response Time of the Balance, 128 g Dropped from 5 cm

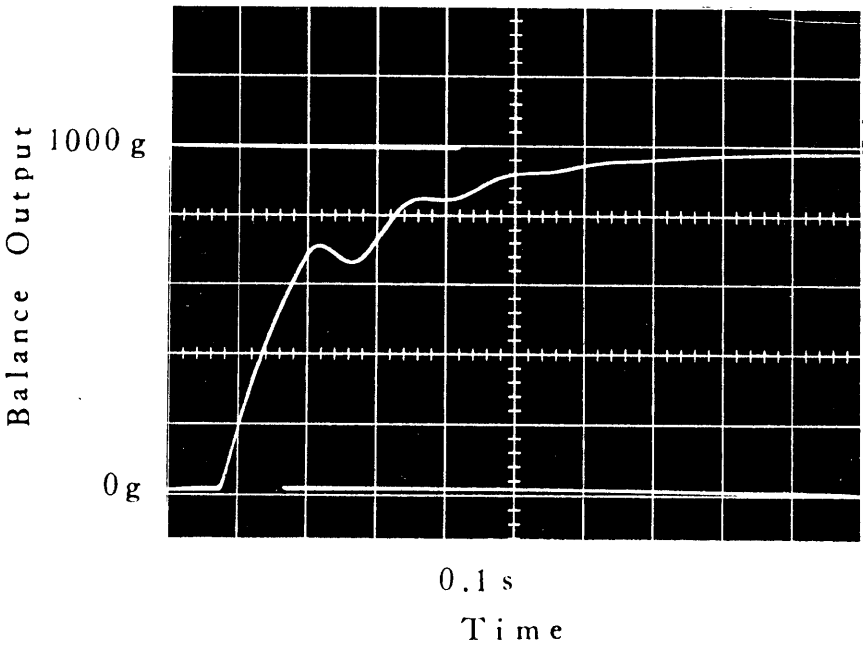

Figure A-3 Response Time of the Balance, 1000 g Dropped from 2.5 cm

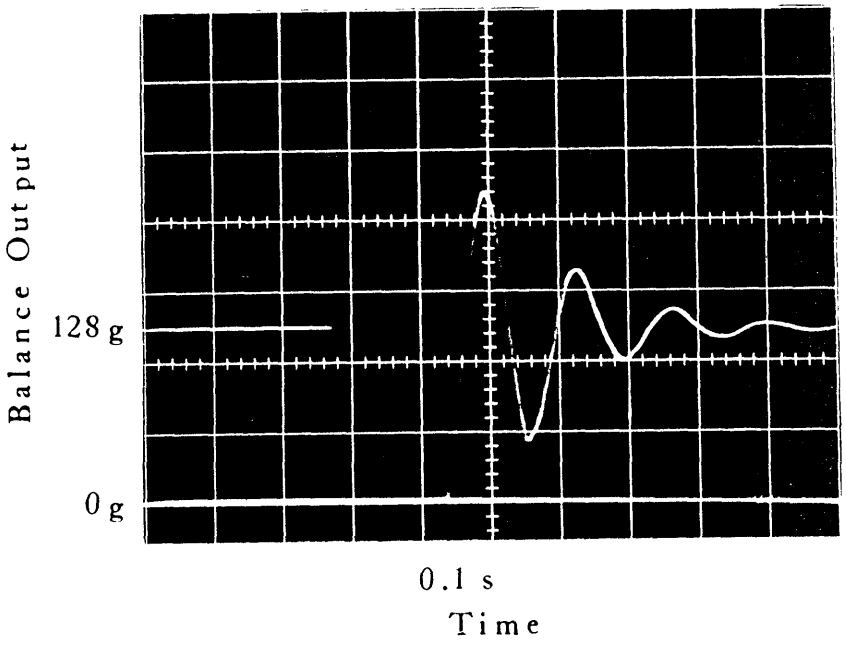

Figure A-4 Response Time of the Balance, 128 g Dropped from 18 cm

Real Time Computer

A NOVA-840, Data General Corporation, computer was used for data collection. This computer has a 24 K core memory and its central processing unit (CPU) handles 16 bit words. The memory cycle time is 800 nanoseconds; this is the rate at which instructions are executed by the CPU.

Data acquisition is controlled by a real time clock (RTC). A crystal oscillator allows the accurate generation of a sequence of pulses which are independent of the central processor timing. Available frequencies are 10, 60, 100, 1000 Hz. A frequency of 10 Hz was selected for the RTC; this allowed a maximum rate of data collection of one sample every 0.1 second. The actual sampling rate was one every second.

Two 8-channel wide range analog-input modules (Computer Products, Inc., Fort Lauderdale) were used for data input to the computer. A multi-gain analog-input routine allows the selection of the appropriate input voltage range. The input voltage is then converted to an integer number proportional to the magnitude of this input voltage. The limits of the voltage range, $+V_{max}$ and $-V_{max}$, are set to the integers +4096 and -4096, respectively. Thus if V_{max} is 10 mV and the input voltage is -5 mV, it will be converted into the integer -2048. Thirteen ranges of input voltage are available; their values are given in Table A-2. The FORTRAN variable IGAIN is used to select the appropriate value of V_{max}.

TABLE A-2

Input Ranges Available for the

Multi-Range Analog Input Modules

IGAIN	V_{max}
1	10.24 V
2	5.12 V
3	2.56 V
4	1.28 V
5	640 mV
6	320 mV
7	160 mV
8	80 mV
9	40 mV
10	20 mV
11	10 mV
12	5 mV
13	2.5 mV

The integer number is then accessible to the computer programs which control and process the data acquisition. One program reverses the input procedure; the integer generated is converted into the value of the input voltage,

$$\text{Voltage} = \frac{\text{integer}}{4096} \times V_{max}$$

This value of voltage is used in polynomials or other appropriate expressions that relate voltage to mass or temperatures. These results are then sent to a line printer and are also stored in a 1.25 megaword cartridge disk for future data retrieval and analysis.

An input voltage range of ±10.24 V was selected for the signal generated by the load cell. The balance output range was 0-10 V (0-1000 g). A simple calculation shows that after the voltage has been converted into an integer, 1 g represents 4 integer units, or alternatively one integer unit represents 0.25 g. Thus the resolution of the mass data acquisition by the computer is ±0.125 g.

Similarly for the temperature measurements a range of ±10 mV was chosen. Consequently, one integer unit represents 0.00244 mV. Assuming that the emf output of the thermocouples (Type E, Chromel-Constantan) is about 0.06 mV/K, one integer unit represents 0.04 K. The accuracy of the temperature data acquisition modules is then ±0.02 K.

Computer Programs to Monitor Data Acquisition

```
C      DATA 540 [illegible]      LOG RR [illegible]        NAME [illegible]   ALENCIA
C      THIS PROGRAM CONTROLS THE ACQUISITION OF DATA FOR THE
C           BOILING ON WATER
C      DATA FILE 2 (REFERRED AS 2 [illegible])
C      MASS ISH
C      AREA,NF,INTER,IN
C      DATA IS STORED IN INTEGER BINARY FORMAT
C      SWITCH BOARD 0 TO BEGIN RUN
C      SWITCH BOARD 0 TO DETERMINE SHIFT ZERO TIME
C      SWITCH BOARD 1 TO STOP DATA ACQUISITION
       CHANNEL 1 2 5
       EXTERNAL [illegible]
       COMMON BLK3 NC,NF,INO
       COMMON BLK4 NSTOP,LAPS,[illegible]
       COMMON BLK2 AREA,INTER
       DIMENSION NAME1(5),NAME2(5)
       NF=11
       NN=12
       TYPE "RAW DATA FILE NAME"
100    FORMAT(5A2)
       READ(NF,100)(NAME1(I),I=1,5)
       TYPE "REDUCED DATA FILE NAME"
       READ(NF,100)(NAME2(I),I=1,5)
       NF=1
       INO=2
       AREA=143
       INTER=1
       TYPE "SCAN FREQUENCY [illegible] HZ"
       TYPE "AREA [illegible] AREA"
       TYPE "TIME INTERVAL IN SEC [illegible] INTER"
```

```
      ACCEPT "TYPE 1 TO CHANGE SPECIFICATIONS  ",NCHR
      IF (NCHR.NE.1) GO TO 10
      ACCEPT "SCAN FREQUENCY     ",NF
      ACCEPT "TYPE 1 IF ARRAY LOCATION IS TO BE PRINTED    ",IDM
      ACCEPT "AREA UNIT   ",AREA
      ACCEPT "INTER SEC     ",INTER
10    CONTINUE
      NSTOP=0
      ACCEPT "TOTAL NUMBER OF CHANNELS ",NC
      CALL OPEN(1,NAME1,2,IER)
      CALL OPEN(2,NAME2,2,IER)
      WRITE(10,150)(NAME1(I),I=1,5)
150   FORMAT(1H1                 1H ,5X,"RAW DATA FILE      ",5A2)
      WRITE(10,160)(NAME2(I),I=1,5)
160   FORMAT(1H0,5X,"REDUCED DATA FILE      ",5A2)
      WRITE(12,170)AREA,NF,INTER,NC
170   FORMAT(1H0                1H0,5X,"AREA       ",F8.2,"  M2"
     11H ,5X,"NF          ",5X,I3,"  SAMPLINGS PER POINT"
     11H ,5X,"INTER       ",5X,I3,"  SEC. TIME INTERVAL"
     11H ,5X,"NC          ",5X,I3,"  CHANNELS")
      CALL [illegible]
      CALL [illegible]
      CALL [illegible]
      CALL EXIT
      END
```

```
C        NOVA 840              ING2 FR                JAIME A  VALENCIA
C     THIS TASK CONTROLS THE TIME AT WHICH THE ANALOG INPUTS
C          ARE SCANNED
      TASK TICTAC
      COMMON BLK4/ NSTOP,IAPS,IFLIF
      COMMON BLK5  IH,IM,IS
      DIMENSION IDATE(3)
      MU=12
      CALL HOLD(2,IER)
      CALL DATE(IDATE,IER)
      CALL FGTIM(IH,IM,IS)
      WRITE(MU,100) IH,IM,IS,IDATE
100   FORMAT(1H1,5X,'STARTING TIME  ',2(I2,':'),I2
     1,10X,' DATE  ',2(I2,'-'),I2)
      WRITE(MU,190)
190   FORMAT(1H0,' ',1H0,' TIME ',4X,'CRYOGEN ',7X,' T1 ',7X,' T2
     1',7X,' T3 ',7X,' T4 ',7X,' T5 ',7X,' T6 ',7X,' T7 ',7X,' T8 ',7X,' T9 ',
     I6X,' T10 ',6X,' T11 ',6X,' T12
     31H ,11X,' MASS '
     41H ,1X,'SEC',6X,' GRAMS ',12(8X,' C ')
     51H ,4('-'),4X,7('='),12(3X,6('=')))
300   CALL RELSE(2,IER)
      CALL DASW(IFLIF)
      IF(IFLIF.EQ.1) GO TO 400
      CALL FDELAY(10)
      GO TO 300
400   CALL FGTIM(IH,IM,IS)
      NSTOP=IAPS
      CALL KILL
      END
```

```
   NOVA 840                 ENG3 FR                  JAIME A  VALENCIA
C THIS TASK SCANS AND COLLECTS THE DATA FROM THE ANALOG INPUT
C      MODULES AFTER BEING ACTIVATED BY TASK TICTAC
C THE INPUT VOLTAGES ARE CONVERTED INTO INTEGERS TAKING VALUES
C BETWEEN -4096 AND +4096 DEPENDING ON THE MAGNITUD OF THE INPUT
C VOLTAGE
      TASK SCAN
      COMMON BLK1  IVOLT(16,30)
      COMMON BLK2 ITRACK(30)
      COMMON BLK3 NC,NF,INN
      COMMON BLK4 NSTOP,LAPS,IFLIP
      COMMON BLK10 IGAIN(16),ICHAN(16)
      DIMENSION INVOLT(16)
      DATA IGAIN 1 11,11,11,11,11,11,11,11,11 11 11,11,11,11,11,
      DATA ICHAN 0,1,2,3,4,5,6,7,8,9,10,11 12,13,14,15
      IARRAY=0
      LAPS=0
10    IF(NSTOP NE 0) GO TO 99
      LAPS=LAPS+1
      IARRAY=IARRAY+1
      IF(IARRAY EQ 31) IARRAY=1
      IF(INN NE 1) GO TO 15
      WRITE(MW,500) IARRAY
500   FORMAT(1H , ARRAY LOCATION  ,I4)
15    DO 25 I=1,NC
25    IVOLT(I,IARRAY)=0
      DO 50 K=1,NF
      CALL MGAIR(NC ICHAN,IGAIN,INVOLT,IER)
      DO 30 I=1,NC
30    IVOLT(I,IARRAY)=IVOLT(I,IARRAY)+INVOLT(I)
50    CONTINUE
      WRITE BINARY(1) LAPS,(IVOLT(I,IARRAY),I=1,NC)
      ITRACK(IARRAY)=LAPS
      CALL SUSP
      GO TO 10
99    CALL KILL
      END
```

```
   NUVA 840              LNG4 FR              WAINE A. VALENCIA
THIS TASK HAS THE LOWEST PRIORITY AND IS USED TO CHANGE THE
INTEGER VALUES BACK INTO THE NUMERICAL VALUE OF THE INPUT
VOLTAGE. THIS VOLTAGE IS THEN USED IN THE APPROPIATE CORRELATION
TO OBTAIN MASS OR TEMPERATURE
TASK REDUCE
REAL MASS
DIMENSION TEMP(15)
COMMON BLK1 IVOLT(16,30)
COMMON BLK2  ITRACK(30)
COMMON BLK3  NC NF INN
COMMON BLK4  NSTOP LAPS IFLIP
COMMON BLK5/IH IM IS
COMMON BLK6 AREA INTER
COMMON BLK7  MASS(500)
COMMON BLK8  IX
COMMON BLK18  ISH(500)
IFLIP=?
IDDX=1
ICHCK=0
JJ=1
NSTOP=1
WTS=0
IFLAG=0
IX=0
DO 3 IK=1,500
ISH(IK)=0
MASS(IK)=0
CONTINUE
IF(JJ EQ 31) JJ=1
ICHCK=ICHCK+1
IF(ICHCK LE LAPS) GO TO ?
CALL EDELY(5)
GO TO ?
CONTINUE
VOLT=IVOLT(1,JJ)
CORRELATION FOR MASS
WT=VOLT*1024 FLOAT(NF) 4095
DWT=WTS-WT
```

```
      DO 10 KK=2,NC
      VOLT=IVOLT(KK,JJ)
      V=VOLT*10. FLOAT(NF) 4096
      IF(V LT -5 237) GO TO 330
      IF(V GT 0 000) GO TO 340
C     CORRELATIONS FOR TEMPERATURE
      A=-0 00045358
      B1=17 046794
      B2=-0 26734292
      B3=0 016190789
      B4=-0 0006960Z
      B5=0 00013792Z5
      GO TO 350
330   A=-80 92576715
      B1=-20 576476
      B2=-4 0017909
      B3=0 87598041
      B4=0 14711677
      B5=0 0077871064
      GO TO 350
340   A=0 00137701
      B1=17 037897
      B2=-0 220683Z9
      B3=0 0055912366
      B4=-0 000337065
      B5=0 0000302242
350   TEMP(KK-1)=A+B1*V+B2*V**2+B3*V**3+B4*V**4+B5*V**5
10    CONTINUE
      IF(IX GE 500) GO TO 14
      IF(IFLIP EQ 2) GO TO 15
      IF(IFLAG EQ 1) GO TO 25
      IF(IFLAG EQ 2) GO TO 26
      IF(OUT GT -10 0) GO TO 15
      IFLAG=1
      GO TO 15
25    IF(OUT LT 0 ) GO TO 15
      IFLAG=2
      MINSS=NTS
      WRITE(12,300)
300   FORMAT(1H0, ***  TIME = 0 SEC  ***  )
```

```
 6      IX=IX+1
        ISH(IX)=(TEMP(1)+TEMP(2)+TEMP(3)) 3
        MASS(IX)=(AMASS-HT) AREA
        IDDX=1       3,27,77
        IF(IDDX NE 1) GO TO 28
        IDX=ITRACK(JJ)-IX
        IDDX=2
28      IDUMM=ITRACK(JJ)-IX
        IF(IDUMM EQ IDX) GO TO 15
        WRITE(6,351) ITRACK(JJ),IX
351     FORMAT(1H , ERROR IN INDEX  ,4X,2I6)
        GO TO 15
14      IX=IX+1
15      CONTINUE
        NCC=NC-1
        WRITE(12,200)IX,HT (TEMP(I,IK),I,IK=1,NCC)
200     FORMAT(1HO,I4,2X,13F9 2)
        HTS=HT
        IF(NSTOP NE 0) GO TO 20
        CALL PDELAY(10)
        JJ=JJ+1
        JSTOP=JSTOP+1
        GO TO 5
20      IF(JSTOP GE IAPS) GO TO 90
        JJ=JJ+1
        JSTOP=JSTOP+1
        GO TO 5
90      WRITE(12,100) IH,IM,IS
100     FORMAT(1HO, TEST ENDED AT  ,2(I2, : ),I2)
C       WRITE BINARY(2)IX,AREA,HVAP,CP,TSAT,BRMAX,HFMAX,BMMAX  3,27,77
        WRITE BINARY(2)MASS,TSH
        WRITE BINARY(2)IX,AREA,NF,INTER
        CALL CLOSE(1,IER)
        CALL CLOSE(2 IER)
        CALL EXIT
        END
```

Thermocouples

Axial heat conduction through the thermocouple wires can lead to erroneous temperature readings. In order to minimize this effect and to insure a fast response time, a minimum length of bare wire must be exposed to the fluid whose temperature is being measured.

The thermocouples are assumed to be thin rods, which are insulated at the end since, within the thermocouples, the heat flow can be assumed to be symmetrical with respect to the junction.

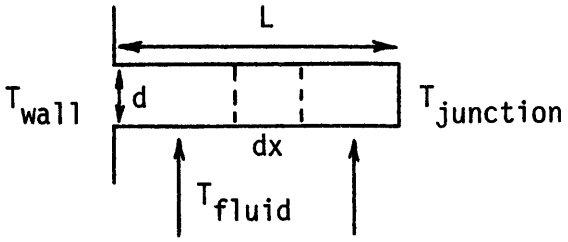

A heat balance around the element dx yields:

$$\frac{d^2\theta}{dx^2} - \frac{hC}{kA}\theta = 0$$

where:

$\theta = T_x - T_f$

$C = \pi d$

$A = \pi d^2/4$

Rewriting:

$$\frac{d^2\theta}{dx^2} - m^2\theta = 0$$

where:

$$m = \left(\frac{4h}{kd}\right)^{1/2}$$

Using the following boundary conditions:

$$\left(\frac{d\theta}{dx}\right)_{x=L} = 0$$

and

$$\theta_{x=0} = T_w - T_f$$

a solution is obtained,

$$\frac{\theta}{\theta_w} = \frac{\cosh m(L - x)}{\cosh mL}$$

At the junction (x = L),

$$\theta_j = \frac{\theta_w}{\cosh mL}$$

The following values were used for physical constants in the calculation of the bare wire length for the vapor thermocouples:

$$d = 0.0025 \text{ cm}$$

$$k_{Chromel} = 0.17 \text{ W/cm-K}$$

$$k_{Constantan} = 0.23 \text{ W/cm-K}$$

$$h = 0.002 \text{ W/cm}^2\text{-K}$$

The value of m is

$$\left(\frac{4 \times 0.002}{0.23 \times 0.0025}\right)^{1/2} = 3.75 \text{ cm}^{-1}$$

The thermal conductivity of Constantan was used since it yields the higher value for thermocouple length.

The maximum acceptable error in thermocouple reading was 0.5 K so $\theta_j = 0.5$. The maximum θ_w was 293 K - 112 K (room - cryogen) or 181 K. Therefore,

$$\cosh mL = \frac{181}{0.5} = 360$$

and $mL = 6.6$

The required length of exposed wire was 1.78 cm. The length used in the vapor thermocouples was 2 cm.

The liquid thermocouples need to be stronger than the vapor ones since the growing ice can damage them. Thermocouple wires ranging from 75 to 150 μm in diameter, or ribbon thermocouples 25 μm in thickness, were used.

Upon immersion in a liquid nitrogen bath (78 K) the ribbon thermocouples (25 μm thick ribbon, 2.3 cm long) attained a 100% response time in 220 ms (Figure A-5). Those made with 150 μm thick and 0.2 cm long leads had a response time of 400 ms (Figure A-6). For the extreme case of spilling nitrogen in a small 1.3 cm tube in which the thermocouple leads were immersed in 308 K water it took 5 seconds for a 100% response time (Figure A-7). The subsequent rise in temperature is due to the complete evaporation of nitrogen.

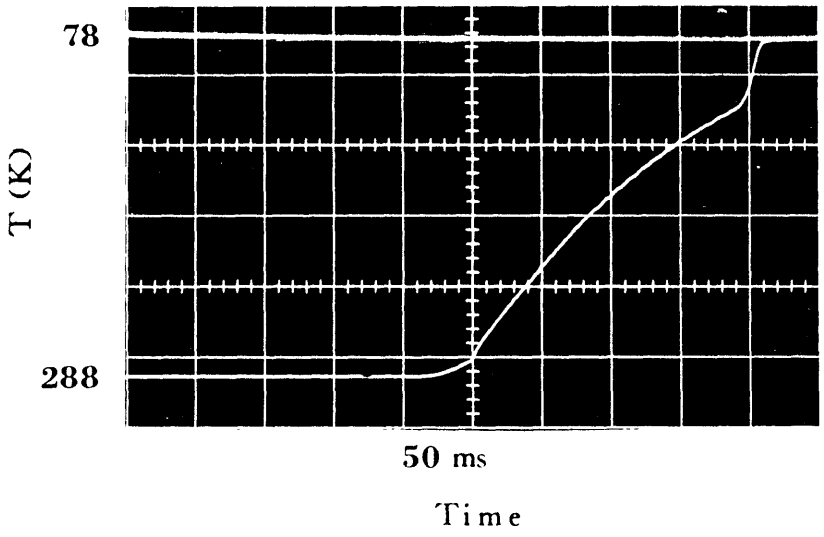

Figure A-5 Response Time for a 25 μm Thick, 2.3 cm Long Ribbon Thermocouple

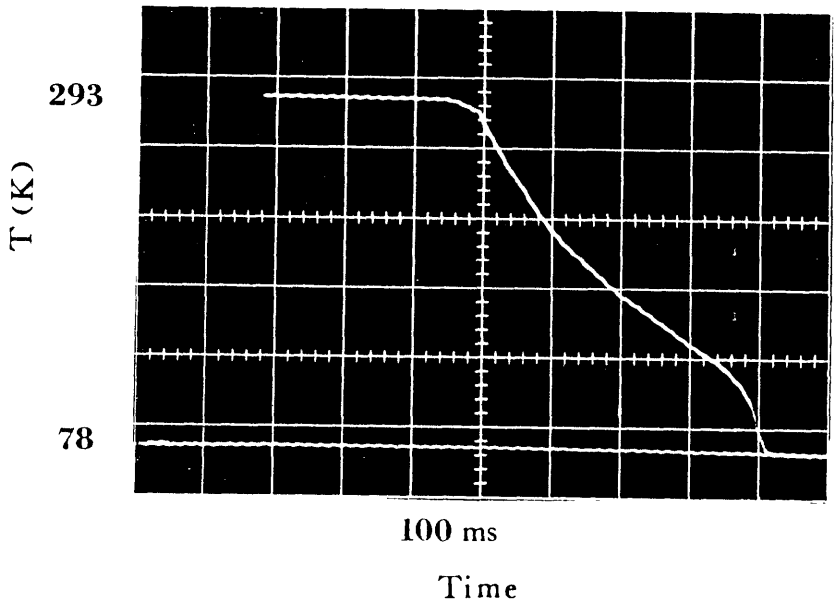

Figure A-6 Response Time for 150 μm Thick, 0.2 cm Long Lead Thermocouple

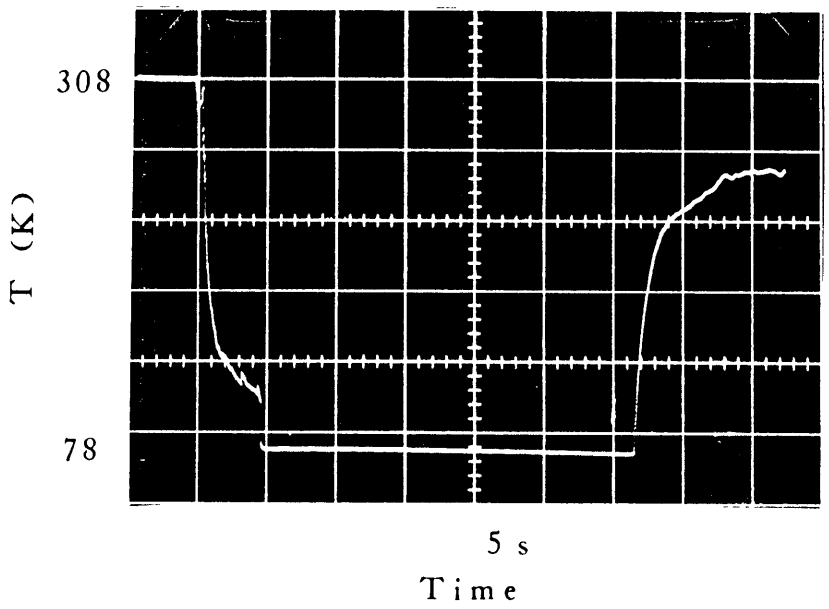

Figure A-7 Response Time of a 150 μm Thick, 0.3 cm Long Lead Thermocouple. Base of Leads in 308 K Water and Leads in Liquid Nitrogen

Gas Chromatograph

A Hewlett-Packard 700 was used to analyze the composition of LNG mixtures. The components were separated by running the mixture through a 180 cm long stainless steel column packed with Porapak-Q using helium gas as the carrier. The retention times for the various components are given in Table A-3.

After separation in the column, the gases are run through a thermal conductivity detector which outputs a voltage proportional to the amount of elute at that time. This output voltage was integrated by a Varian 477 electronic integrator or an Autolab 6300 integrator. The equipment settings are given in Table A-4.

A Microcord 44 chart recorder was used to determine the retention time of the eluting gases.

The mixture samples were removed from the sampling bulb by means of a 100 or 500 μl Precision Sampling - Pressure Lok - gas tight syringe.

TABLE A-3

Retention Times in Chromatographic Analysis

N_2	31 (s)
CH_4	38 (s)
CO_2	72 (s)
C_2H_4	120 (s)
C_2H_6	155 (s)
H_2O	280 (s)
C_3H_8	660 (s)

TABLE A-4

Settings Used in the Chromatographic Analysis

Hewlett Packard 700 Chromatograph	
Injection Point	100°C
Column	50°C
Detector	235°C
Detector Current	175 ma
Attenuation	1
Helium Flow	21 cm^3/min
Varian 477 Integrator	
Peak Width	10 (s)
Slope Sensitivity	7
Digital Baseline Corrector	5
Autolab 6300 Integrator	
Slope Sensitivity	16 (s)
Filtering	4 (s)
Noise Adjust	4
Baseline Corrector	Normal/Slow

APPENDIX B

VAPOR-LIQUID EQUILIBRIA

The Soave-Redlich-Kwong Equation

Determination of SRK Interaction Parameters, k_{ij}

Logic Diagram: Evaluation of Residual Liquid Composition

Vapor Sampling Time

Computer Programs

The Soave-Redlich-Kwong Equation

Redlich and Kwong (1949) originally proposed the following equation of state:

$$P = \frac{RT}{v - b} - \frac{a/T^{0.5}}{v(v + b)} \tag{B-1}$$

Soave (1972) modified this equation by replacing the term $a/T^{0.5}$ by a more general term a(T):

$$P = \frac{RT}{v - b} - \frac{a(T)}{v(v + b)} \tag{B-2}$$

For a pure component a and b can be found by equating the first and second derivatives of pressure with respect to temperature at the critical point:

$$a_i(T_{C_i}) = a_{C_i} = 0.42747 \frac{R^2 T_{C_i}^{\ 2}}{P_{C_i}} = \Omega_a \frac{R^2 T_{C_i}^{\ 2}}{P_{C_i}} \tag{B-3}$$

and

$$b_i = 0.08664 \frac{R\, T_{C_i}}{P_{C_i}} = \Omega_b \frac{R\, T_{C_i}}{P_{C_i}} \tag{B-4}$$

For temperatures other than the critical a_i is given by

$$a_i = \alpha_i\, a_{C_i} \tag{B-5}$$

Soave was able to correlate α_i according to the following expression,

$$\alpha_i = [1 + (0.480 + 1.574\ \omega_i - 0.176\, \omega_i^2)(1 - T_{r_i}^{\ 0.5})]^2 \tag{B-6}$$

where ω_i, the acentric factor, is defined as

$$\omega = -\log P_r^{sat} \text{ (at } T_{r=0.7}) - 1.0 \tag{B-7}$$

The fugacity coefficient of a pure component can now be calculated from the thermodynamic relationship

$$\ln \frac{f}{P} = \int_0^P \left(\frac{v}{RT} - \frac{1}{P}\right) dP \tag{B-8}$$

Since

$$P = Z \frac{RT}{v} \tag{B-9}$$

and

$$dP = \left(\frac{\partial P}{\partial v}\right)_{T,n} dv + \left(\frac{\partial P}{\partial Z}\right)_{T,n} dZ \tag{B-10}$$

Equation (B-8) can be rewritten as

$$\ln \frac{f}{P} = -\frac{1}{RT} \int_\infty^0 \left(P - \frac{RT}{v}\right) dv + \int_1^0 \left(1 - \frac{1}{Z}\right) dZ \tag{B-11}$$

Combining Eqs. (B-2) and (B-11) and integrating by parts

$$\ln \frac{f}{P} = -\frac{1}{RT} \left[RT \ln(v-b) - \frac{a}{b} \ln v + \frac{a}{b} \ln(v+b) - RT \ln v\right]_\infty^v + (Z-1) - \ln Z \tag{B-12}$$

Upon evaluation of limits, we obtain

$$\ln \frac{f}{P} = -\ln\left(\frac{v-b}{v}\right) - \frac{a}{bRT} \ln\left(\frac{v+b}{v}\right) + (Z-1) - \ln Z \tag{B-13}$$

When trying to predict thermodynamic properties of a mixture, one must use appropriate mixing rules such as:

$$a = \sum_i \sum_j x_i x_j \, (1 - k_{ij})(a_i a_j)^{1/2} \tag{B-14}$$

$$b = \sum x_i b_i \tag{B-15}$$

The interaction coefficient, k_{ij}, accounts for deviations from the simple, and commonly used, geometric mean mixing rule:

$$\theta = \sum_i \sum_j x_i x_j \, \theta_i^{1/2} \, \theta_j^{1/2} \tag{B-16}$$

Although this latter rule was found satisfactory when applied to low molecular weight hydrocarbon mixtures, it yielded less acceptable results with hydrocarbon mixtures in the presence of nitrogen.

The fugacity coefficient, ϕ_i, of component i in a mixture is given by the thermodynamic relationship (Modell and Reid, 1974)

$$\ln \phi_i = \ln \frac{f_i}{P y_i} = \int_{\infty}^{V} \left[\frac{1}{V} - \frac{1}{RT} \left(\frac{\partial P}{\partial n_i} \right)_{T,V,n_j} \right] dV - \ln Z \tag{B-17}$$

Combining Eq. (B-17) with Eq. (B-2) yields (Reid et al., 1977):

$$\ln \phi_i = \frac{b_i}{b} (Z-1) - \ln Z + \ln \frac{V}{V - b} + \frac{a}{bRT} \left\{ \frac{b_i}{b} - 2 \sum_j \frac{(1-k_{ij})(a_i a_j)^{0.5}}{a} y_i \right\} \times \ln \frac{V + b}{b} \tag{B-18}$$

where $\underline{a}$ is given by Eq. (B-14), $\underline{b}$ by Eq. (B-15), a_i by Eq. (B-5) and b_i by Eq. (B-4).

For computational purposes, the expression for the fugacity coefficient can be rewritten as

$$\ln \phi_i = \frac{b_i}{b}(Z-1) - \ln(Z-B) + \frac{A}{B}\left[\frac{b_i}{b} - 2\sum_j \frac{(1-k_{ij})(a_i a_j)^{0.5}}{} y_j\right] \ln \frac{Z+B}{Z} \quad \text{(B-19)}$$

where

$$A = \frac{aP}{R^2T^2} = \frac{P \sum\sum_{ij} x_i x_j (1 - K_{ij})(a_i a_j)^{1/2}}{R^2T^2} \quad \text{(B-20)}$$

and

$$B = \frac{bP}{RT} = \frac{P \sum_i x_i b_i}{RT} \quad \text{(B-21)}$$

The compressibility factor, Z, can be obtained by solving the cubic equation

$$Z^3 - Z^2 + Z(A - B - B^2) - AB = 0 \quad \text{(B-22)}$$

which results when A and B are combined with the SRK equation (B-2) and the thermodynamic relationship

$$Z = \frac{RT}{vP} \quad \text{(B-23)}$$

When more than one real value is obtained, the highest one is used when applying the equation to the vapor phase. The lowest value is chosen for the liquid phase.

Determination of the SRK Interaction Parameters, k_{ij}

The binary interaction parameters, k_{ij}, for the Soave-Redlich-Kwong equation were selected so as to best fit experimental data available in literature for the different binaries. The following tables compare values for pressure and vapor composition predicted with various values of k_{ij}. The effect of k_{ij} on the accuracy of SRK predictions for the methane-ethane binary is shown in Table B-1 and Figure B-1. A value of $k_{C_1-C_2} = 0.000$ was selected. The data for the methane-propane binary are given in Table B-2 and Figure B-2, for ethane-propane in Table B-3 and Figure B-3, for nitrogen-methane in Table B-4, for nitrogen-ethane in Table B-5 and for nitrogen-propane in Table B-6. The following values were selected: $k_{C_1-C_3} = 0.010$, $k_{C_2-C_3} = 0.000$, $k_{N_2-C_1} = 0.035$, $k_{N_2-C_2} = 0.035$ and $k_{N_2-C_3} = 0.120$.

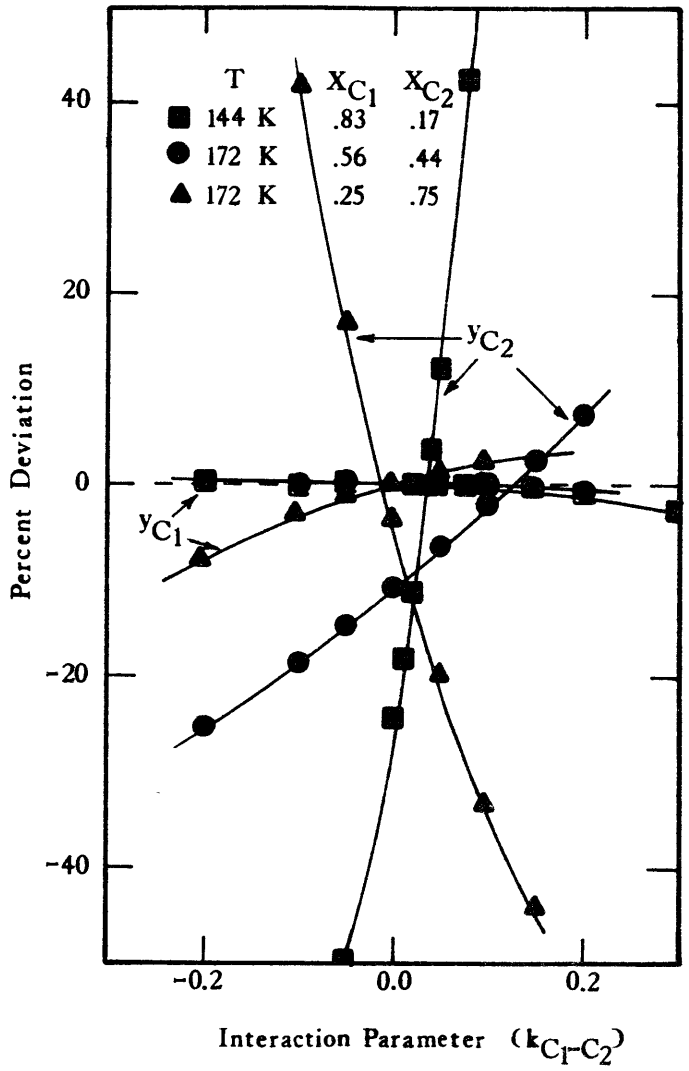

A. Effect on Vapor Composition

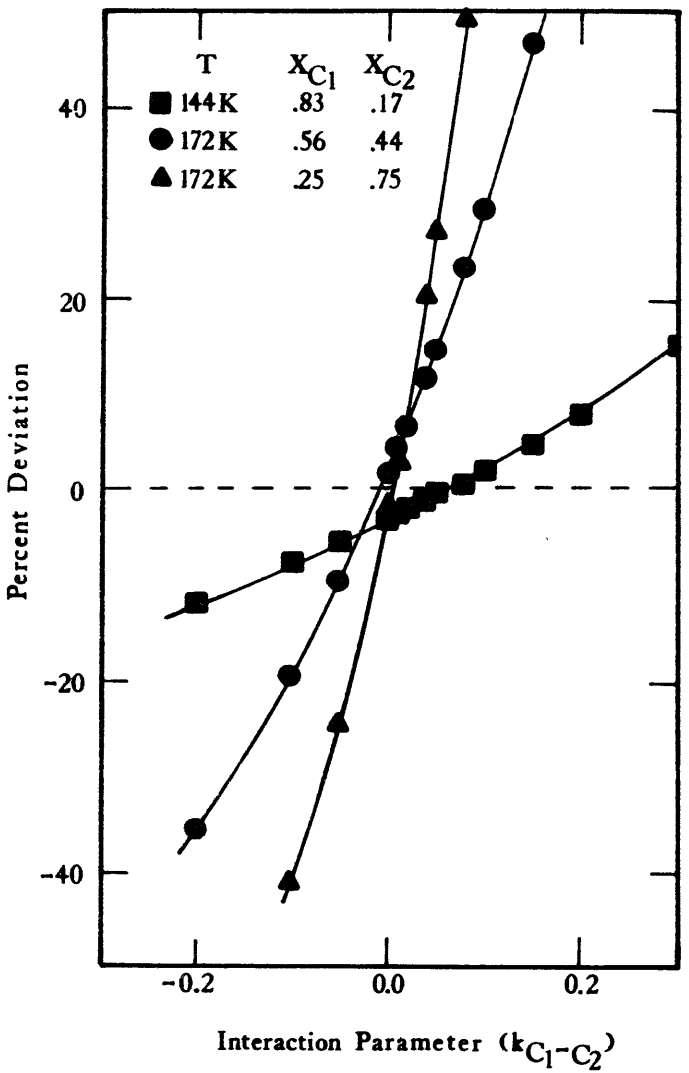

B. Effect on Pressure

Figure B-1 Effect of the Interaction Parameter on the Accuracy of VLE Predictions by the SRK Equation. Methane-Ethane System

TABLE B-1

Effect of the Interaction Parameter, k_{ij}, on the Accuracy of VLE Predictions by the SRK Equation. Methane-Ethane System*

$k_{C_1-C_2}$	T, K	Average of Absolute % Deviation P	y_{C_1}	y_{C_2}	Number of Points
0.05	283	1.8	5.6	1.8	2
	255	7.0	2.8	3.2	4
	228	9.7	6.1	6.2	5
	200	17.1	4.0	16.7	4
	172	20.8	0.8	13.4	2
	144	0.7	0.0	12.4	1
0.02	283	0.5	6.8	2.1	2
	255	3.3	2.4	3.2	4
	228	4.0	2.0	3.3	5
	200	7.7	2.6	10.9	4
	172	7.5	0.5	9.9	2
	144	2.2	0.0	11.4	1
0.01	283	1.2	7.2	2.2	2
	255	2.4	3.0	3.9	4
	228	2.3	1.6	2.4	5
	200	4.9	2.1	9.0	4
	172	3.5	0.4	8.6	2
	144	2.7	0.1	18.2	1
0.00**	283	1.9	7.5	2.3	2
	255	1.4	3.7	4.6	4
	228	1.2	1.9	1.7	5
	200	2.3	1.6	7.0	4
	172	2.0	0.3	7.2	2
	144	3.2	0.1	24.4	1
-0.05	283	5.4	9.5	2.8	2
	255	6.8	7.1	8.2	4
	228	7.3	6.8	4.3	5
	200	10.1	2.2	10.0	4
	172	16.9	0.9	15.9	2
	144	5.5	0.2	49.5	1

*Experimental data from Price and Kobayashi (1959)

**Selected value

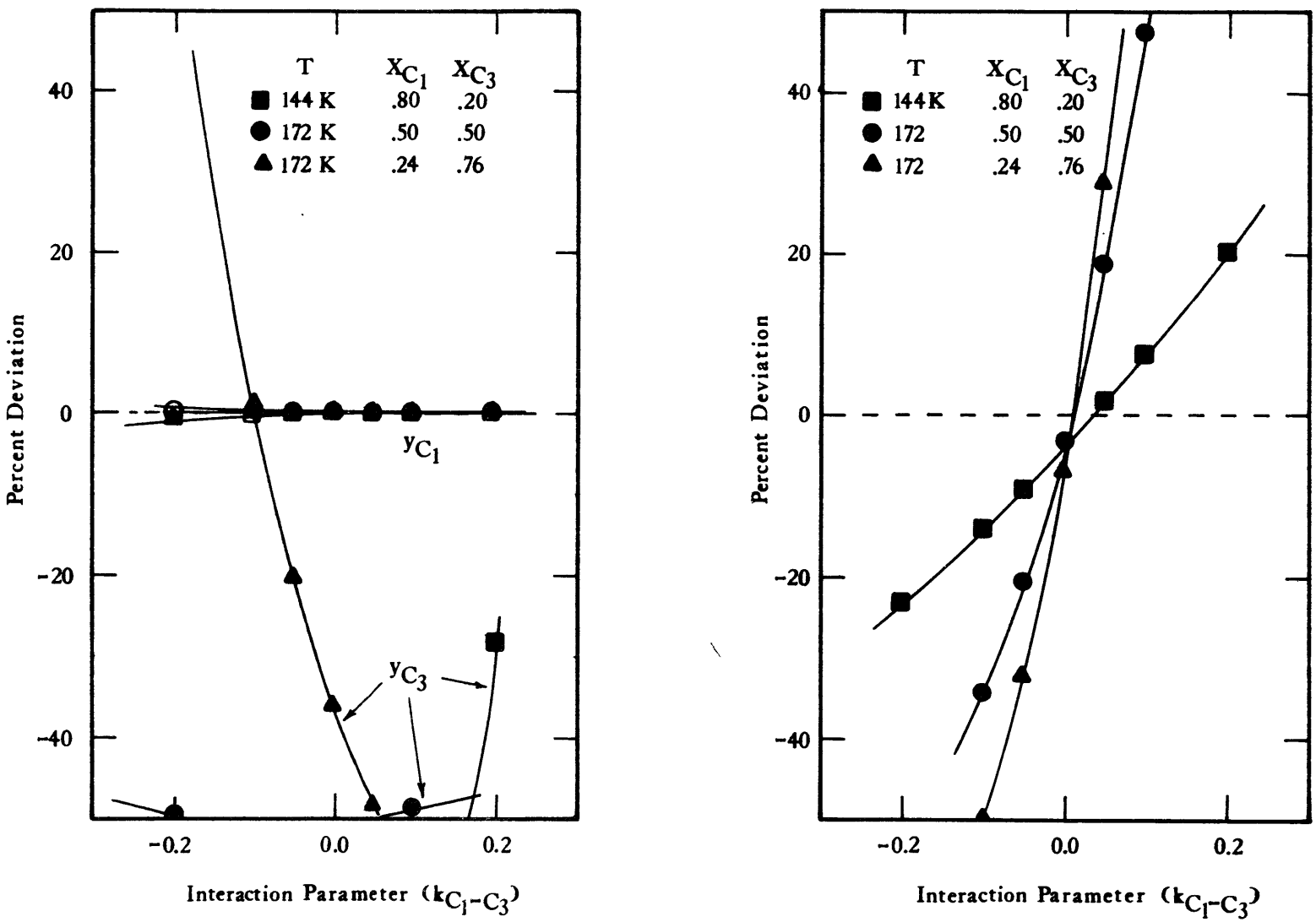

A. Effect on Vapor Composition

B. Effect on Pressure

Figure B-2 Effect of the Interaction Parameter on the Accuracy of VLE Predictions by the SRK Equation. Methane-Propane System

TABLE B-2

Effect of the Interaction Parameter, k_{ij}, on the Accuracy of VLE Predictions by the SRK Equation. Methane-Propane System*

$k_{C_1-C_3}$	T, K	Average of Absolute % Deviation P	y_{C_1}	y_{C_3}	Number of Points
0.020	200	4.9	0.6	23.3	4
	172	5.7	0.3	49.7	2
	144	1.9	0.1	84.4	1
0.015	200	4.1	0.6	23.2	4
	172	2.9	0.3	49.1	2
	144	2.4	0.1	85.0	1
0.010**	283	5.3	1.6	2.3	8
	255	1.3	1.4	6.9	9
	228	1.9	1.1	9.5	6
	200	3.5	0.6	22.9	4
	172	1.2	0.8	48.1	2
	144	3.0	0.1	85.6	1
0.005	283	6.1	1.8	2.3	8
	255	2.1	1.4	7.1	9
	228	2.4	1.0	9.5	6
	200	3.6	0.5	22.7	4
	172	2.4	0.3	47.9	2
	144	3.5	0.1	86.2	1
0.000	283	6.9	2.1	2.5	8
	255	3.4	1.4	7.5	9
	228	3.1	1.0	9.6	6
	200	4.1	0.5	22.4	4
	172	4.9	0.3	47.3	2
	144	4.0	0.1	86.8	1

*Experimental data from Price and Kobayashi (1959)

**Selected value

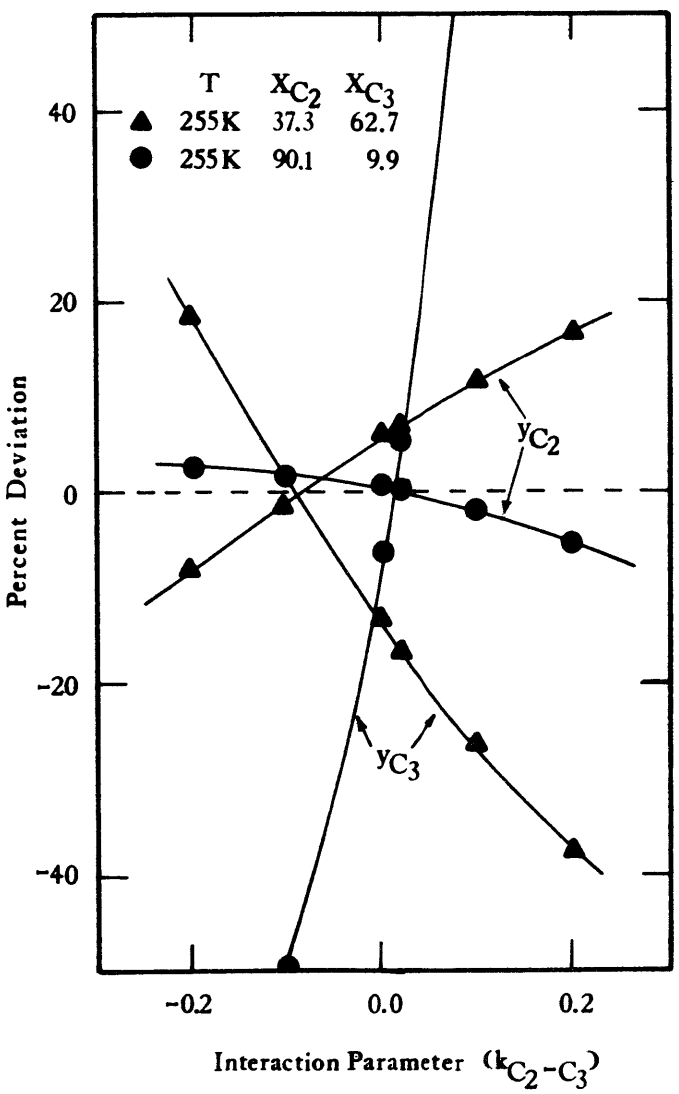

A. Effect on Vapor Composition

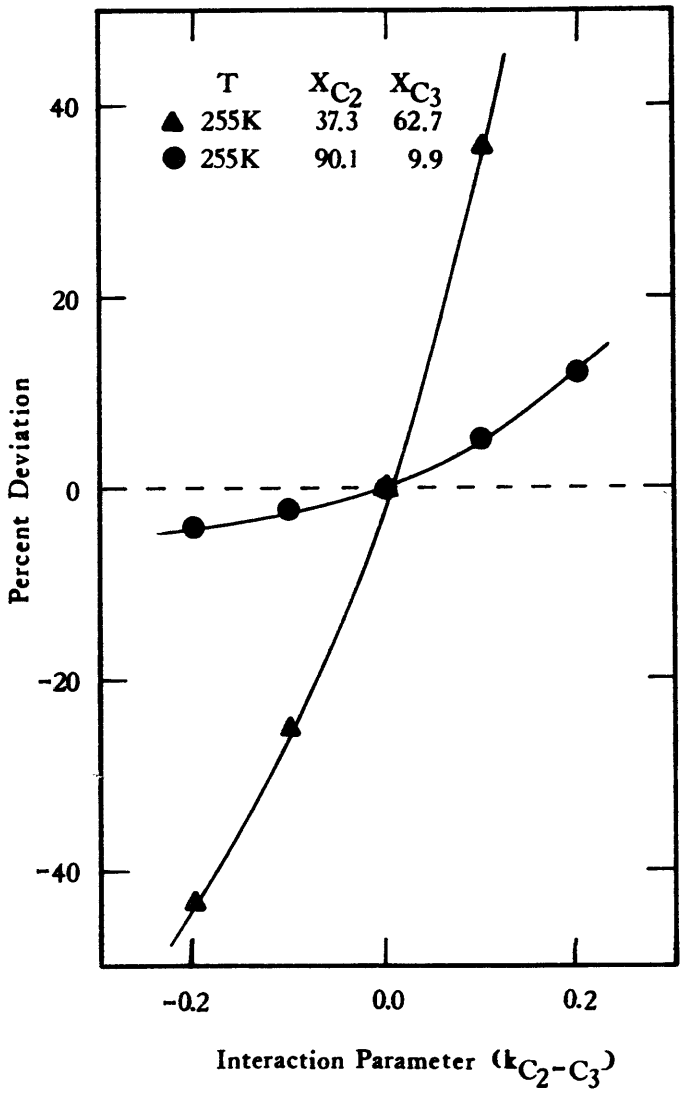

B. Effect on Pressure

Figure B-3 Effect of the Interaction Parameter on the Accuracy of SRK Predictions. Ethane-Propane System

TABLE B-3

Effect of the Interaction Parameter, k_{ij}, on the Accuracy of VLE Predictions by the SRK Equation. Ethane-Propane System*

k_{ij}	T, K	Average of Absolute % Deviation P	y_{C_2}	y_{C_3}	Number of Points
0.010	283	1.1	5.9	4.6	4
	255	1.8	3.3	7.5	2
0.005	283	0.8	5.1	4.4	4
	255	0.9	3.2	8.6	2
0.000**	283	1.0	4.3	4.2	4
	255	0.3	3.1	9.7	2
-0.005	283	1.4	3.6	4.2	4
	255	1.0	2.9	10.8	2
-0.010	283	1.7	2.9	4.9	4
	255	1.6	2.8	11.8	2

*Experimental data from Price and Kobayashi (1959)

**Selected value

TABLE B-4

Effect of the Interaction Parameter, k_{ij}, on the Accuracy of VLE Predictions by the SRK Equation. Nitrogen-Methane System*

$k_{N_2-C_1}$	T, K	Average of Absolute % Deviation P	y_{N_2}	y_{C_1}	Number of Points
0.050	114	4.3	1.6	6.1	8
	122	3.3	4.3	5.7	10
0.040	114	1.8	1.2	6.6	8
	122	1.6	3.0	5.5	10
0.035**	114	0.7	1.0	6.9	8
	122	0.8	2.4	5.6	10
0.030	114	1.1	0.8	7.3	8
	122	0.6	1.7	5.6	10
0.025	114	1.8	0.6	7.6	8
	122	1.0	1.1	5.7	10

*Experimental data from Stryjek et al. (1974a)

**Selected value

TABLE B-5

Effect of the Interaction Parameter, k_{ij}, on the Accuracy of VLE Predictions by the SRK Equation. Nitrogen-Ethane System*

$k_{N_2-C_2}$	T, K	Average of Absolute % Deviation P	y_{N_2}	y_{C_2}	Number of Points
0.060	172	19.1	1.3	16.6	10
	150	30.3	1.3	37.3	11
	139	47.8	1.7	60.6	9
0.050	172	11.3	0.9	13.0	10
	150	15.9	0.7	26.7	11
	139	25.0	1.4	53.9	9
0.040	172	6.2	1.9	14.2	10
	150	10.3	0.4	19.2	11
	139	14.8	0.9	41.7	9
0.035**	172	6.9	0.7	10.7	10
	150	9.9	0.5	20.6	11
	139	13.0	0.7	34.6	9
0.030	172	7.4	0.7	11.2	10
	150	10.2	0.7	23.0	11
	139	12.5	0.3	27.1	9
0.020	172	9.4	0.8	12.6	10
	150	14.5	0.9	26.1	11
	139	20.9	0.6	32.0	9

*Experimental data from Stryjek et al. (1974b)

**Selected value

TABLE B-6

Effect of the Interaction Parameter, k_{ij}, on the Accuracy of VLE Predictions by the SRK Equation. Nitrogen-Propane System*

$k_{N_2-C_3}$	T, K	Average of Absolute % Deviation P	y_{N_2}	y_{C_3}	Number of Points
0.150	114	396.3	1.5	596.0	6
	118	294.3	0.1	682.4	7
	122	159.8	0.1	679.7	8
0.130	114	14.1	0.0	98.4	6
	118	14.1	0.0	95.3	7
	122	11.2	0.1	219.6	8
0.120**	114	1.9	0.0	98.6	6
	118	1.1	0.0	96.4	7
	122	8.4	0.1	94.2	8
0.110	114	11.3	0.0	98.6	6
	118	12.2	0.0	96.7	7
	122	18.6	0.1	95.1	8
0.100	114	21.3	0.0	98.6	6
	118	22.1	0.0	96.8	7
	122	27.2	0.1	95.4	8

*Experimental data from Poon and Lu (1974)

**Selected value

Logic Diagram: Evaluation of Residual Liquid Composition

The substitution of a differential equation by a difference equation implies the use of small values in the difference equation so that the approximation holds.

In Chapter 4, it was found that a value of $\Delta\hat{L} \leq 0.01$ moles should be used in the evaluation of the residual liquid composition. The following diagram is a flow chart to insure that liquid compositions are evaluated using $\Delta\hat{L}$'s of less than 0.01 moles even if the mass evaporated between computer sampling intervals (1 s) is larger than 0.01 moles.

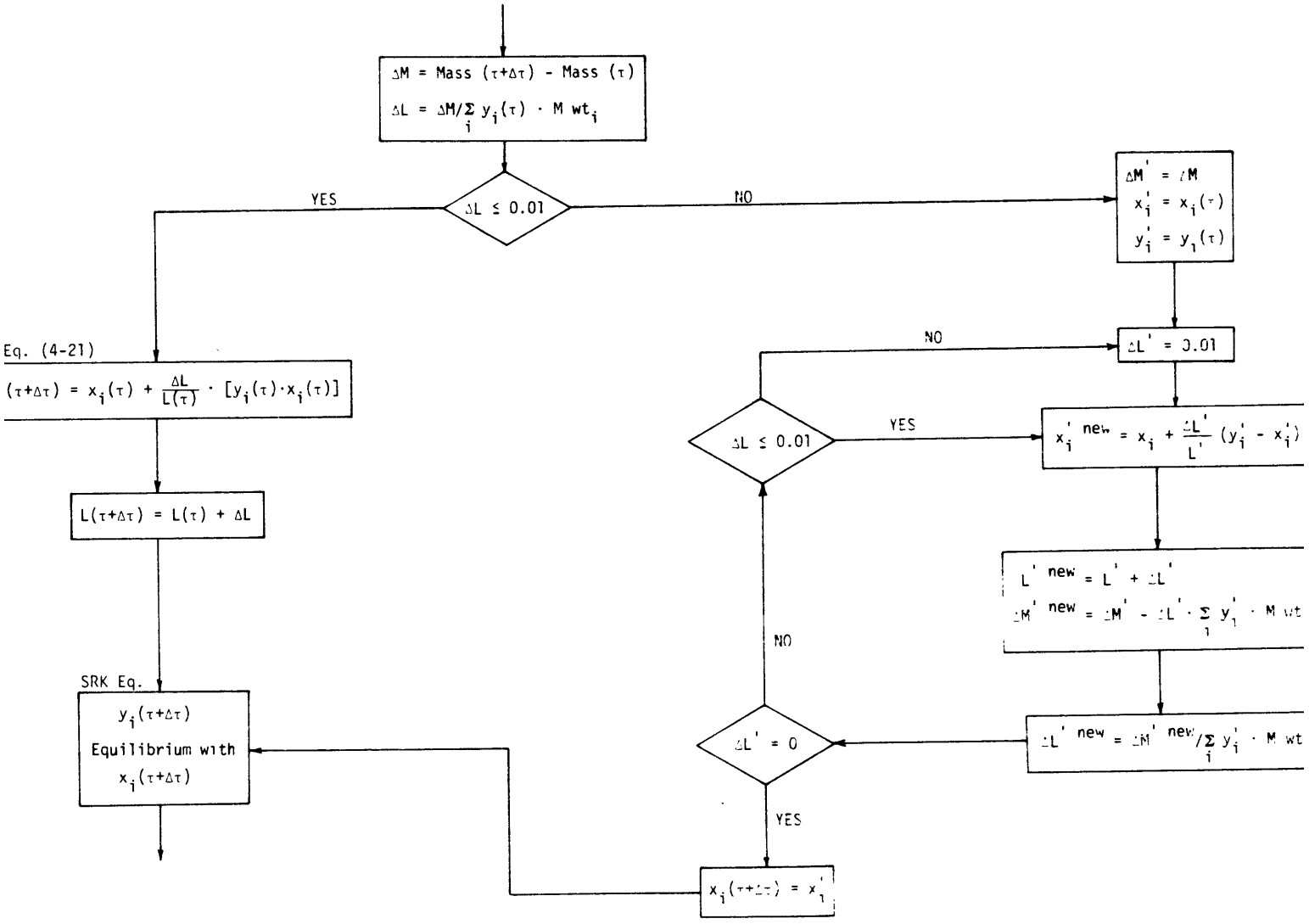

Figure B-4 Flow Chart to Insure a Value of ΔL ≤ 0.01 Moles is Used Throughout the VLE Model

Vapor Sampling Time

The following equations can be used to describe the flow rate through a tube for a given pressure drop (Bird et al., 1960).

$$f = f(Re, k/D) \tag{B-24}$$

and

$$f = \frac{(Re\ \sqrt{f})^2}{Re^2} \tag{B-25}$$

where

f = friction factor

k/D = relative roughness

Re = Reynolds number

$$Re\ \sqrt{f} = \frac{DvP}{\mu}\sqrt{\frac{(P_0 - P_L)D}{2L\rho v^2}} = \frac{D\rho}{\mu}\sqrt{\frac{(P_0 - P_L)D}{2L\rho}} \tag{B-26}$$

In the present case

$D = 0.1$ cm

$\rho = .00072$ g/cm^3

$\mu = 0.0106 \times 10^{-2}$ g/cm-s

$L = 6$ cm

$\Delta P = (760 - 1)$ mm Hg $= 1011910$ dyne/cm^2

$$Re\ \sqrt{f} = \frac{0.1 \times 0.00072}{0.0106 \times 10^{-2}}\sqrt{\frac{101 \times 10^4 \times 0.1}{2 \times 6 \times 0.00072}} = 2322$$

So if

Re = 1000	f = 5.39
10000	0.054
20000	0.0135
50000	0.0022

The friction factors for tube flow versus the Reynolds number are given in Figure 6.2-2 (Bird et al.). From this figure $Re = 3 \times 10^4$ for a smooth pipe and 2.5×10^4 for a rough one.

The volumetric flow rate is given by

$$d = \frac{\pi}{4} \, Re \, D\mu \cdot \frac{1}{\rho} \qquad \text{(B-27)}$$

and the sampling time

$$t = \frac{V}{Q} \qquad \text{(B-28)}$$

where $V = 125 \text{ cm}^3$

For a smooth pipe $Q = 347 \text{ cm}^3/\text{s}$ and $t = 0.36$ s.

For a rough pipe $Q = 289 \text{ cm}^3/\text{s}$ and $t = 0.43$ s.

Since the pressure in the sampling vessel is continuously increasing, let's assume an average ΔP of 300 mm Hg and repeat the calculations.

$$Re \sqrt{f} = 1461$$

From Figure 6.2-2 (Bird, et al.) $Re = 1.7 \times 10^4$ for smooth tubes. Q becomes $197 \text{ cm}^3/\text{s}$ and the required sampling time is 0.6 s. For a rough tube, $Re = 1.6 \times 10^4$, Q is $185 \text{ cm}^3/\text{s}$ and the sampling time is 0.7 seconds.

Computer Programs

```
C         NOVA 840        VLELNG FR                    JAIME A  VALENCIA
C         8/19/77
C         10/21/77       HVAP=SUM(X(I)*HVAP(I),  >DISK FILE
C*************************************************************************
C
C         THIS PROGRAM COMPUTES THE COMPOSITION OF THE VAPOR EVOLVED
C         WHILE BOILING LNG ON WATER
C
C         SOAVE-REDLICH-KWONG EQUATION OF STATE
C         CONSTRAINTS: P AND X
C         VARIABLES: T AND Y
C
C*************************************************************************
      REAL MWT(5),K(5),KIJ(5,5)
      REAL MASS,MOLE,MWTL
      REAL MBOFF(500)
      INTEGER CODE
      INTEGER TITLE(30),TCHK
      DIMENSION X(5),Y(5),YN(5)
      DIMENSION PC(5),TC(5),W(5)
      DIMENSION RATA(5),RATB(5),PHIL(5),PHIV(5)
      DIMENSION TB(5),DENS(5)
      DIMENSION IDATE(3),HV(5)
      DIMENSION NAME(5)
      COMMON NCOMP,PC,TC,W,TB,T,P,KIJ
      COMMON/BLKMT/MWT
      COMMON BLKMW/MW
      COMMON/BLKDM/DM,DMOLE,DENS
      MR=9
      R=8.3143
      AREA=143.
997   CONTINUE
      READ(MR,105)MW
C*************************************************************************
C
C         MR1 ALLOWS TO INPUT FROM DIFFERENT SOURCE THAN MR,EG TTY
C
C*************************************************************************
```

```
      READ(MR,105)MR1
      IF(MR1.EQ.5)CALL OPEN(5,'SCRATCH.DF',1,IER)
      CALL DATE(IDATE,IER)
      CALL FGTIM(IH,IM,IS)
      WRITE(MW,200)IH,IM,IS,IDATE
      READ(MR,110) AREA
      READ(MR,110)ERRY,ERRSY,TDEL
      READ(MR,110)DLS
      WRITE(MW,205)ERRY,ERRSY,TDEL,DLS
C*********************************************************************
C
C        ANY TITLE MAY BE PRINTED OUT IN THE OUTPUT PROVIDED THAT
C        A ' T ' IS PUNCHED IN THE FIRST COLUMN AND A BLANK CARD
C        FOLLOWS THE LAST TITLE CARD.
C
C*********************************************************************
      READ(MR,115)TCHK
401   READ(MR,115)TITLE
      IF(TITLE(1).NE.TCHK) GO TO 998
      WRITE(MW,250)(TITLE(I),I=2,30)
      GO TO 401
998   CONTINUE
      INIT=0
      CALL INPUT(MWT,DENS,MR)
C*********************************************************************
C
C        PRESSURE UNITS ARE N/M2.  USE PFAC FOR CONVERSION FACTORS.
C        TEMPERATURE IN DEGREES KELVIN.  USE TFAC1 AND TFAC2 FOR CONVERS
C          K=(X+TFAC1)/TFAC2
C        X=F        TFAC1=459.6     TFAC2=1.8
C        X=F        TFAC1=491.6     TFAC2=1.8
C        X=C        TFAC1=273.15    TFAC2=1.00
C
C*********************************************************************
      READ(MR,110)PFAC,TFAC1,TFAC2
```

```
C*************************************************************************
C
C         IFW IS USED AS A GENERAL FLAG WITH THE FOLLOWING CONVENTION:
C              6     PRINT DETAILED  CALCULATIONS OF S-R-K
C              7     PRINT INTERMEDIATE Y S AND T'S
C              8     PRINT  INTERMEDIATE X S
C              10    STORE IN DISK FILE:
C                    TIME, TEMP, X(I), Y(I)
C             ANY OTHER NUMBER WILL  NOT CAUSE ANY ACTION
C
C*************************************************************************
      READ(MR,110)(HV(J),J=1,NCOMP)
      READ(MR,105)IFW
      IF(IFW.NE.10) GO TO 330
      READ(MR,120)(NAME(I),I=1,5)
      CALL  OPEN(2,NAME,2,IER)
330   CONTINUE
      READ(MR,110)T,(Y(I),I=1,NCOMP)
      T=(T+TFAC1)/TFAC2
      READ(MR,110)P
      P=P*PFAC
      READ(MR,110)MASS
      READ(MR,110)(X(I),I=1,NCOMP)
      READ(MR,110)TMAX
      IL=TMAX+0.001
      DO 331 I=1,IL
      IF(MR1.EQ.5)READ(MR1,150)MBOFF(I)
      IF(MR1.EQ.5)GO TO 331
      READ(MR1,110) MBOFF(I)
331   CONTINUE
      IF(MR1.EQ.5)CALL CLOSE(5,IER)
      DO 332 I=1,5
      MBOFF(I)=MBOFF(5)/5.*FLOAT(I)
332   CONTINUE
```

```
      DMA=0.0
      DMASS=(MBOFF(1)-0.0)*AREA
      MWTL=0.0
      CODE=2
      TIME=0.0
      ITIM=0
      DO 333 I=1,NCOMP
      MWTL=MWTL+MWT(I)*X(I)
333   CONTINUE
      MOLE=MASS/MWTL
      WRITE(MW,300)
C*************************************************************************
C
C         IFLG  ALLOWS INITIALIZATION OF VALUES OF T FOR ITERATIONS
C         ICT   IF T DOES NOT IMPROVE BY MORE THAN 0.002 IN 15
C         CONSECUTIVE TRIALS. TERMINATE THAT ITERAION
C
C*************************************************************************
1001  CONTINUE
      IFLG=0
      ICT=0
      IYCT=0
1     CONTINUE
      CALL SETUP(AZ,BZ,X,RATA,RATB,IFW)
      CALL CUBIC(AZ,BZ,ZV,ZL,IFW)
      CALL FUGCF(X,ZL,PHIL,AZ,BZ,RATA,RATB,IFW)
2     CALL SETUP(AZ,BZ,Y,RATA,RATB,IFW)
      CALL CUBIC(AZ,BZ,ZV,ZL,IFW)
      CALL FUGCF(Y,ZV,PHIV,AZ,BZ,RATA,RATB,IFW)
      DO 5 I=1,NCOMP
      K(I)=PHIL(I)/PHIV(I)
5     CONTINUE
      CALL YNEW(X,YN,K,NCOMP,SUMY,IFW)
      DO 10 I=1,NCOMP
      IF(ABS(YN(I)-Y(I)).GT.ERRY) GO TO 20
10    CONTINUE
      GO TO 50
```

```
20      DO 25 I=1,NCOMP
        Y(I)=YN(I)
        IF(IFW.NE.7) GO TO 25
        WRITE(MW,910)I,X(I),Y(I)
25      CONTINUE
        IYCT=IYCT+1
        IF(IYCT.GT.1000)WRITE(MW,260)
        IF(IYCT.GT.1000)GO TO 54
        GO TO 2
50      CONTINUE
        EXCY=1.-SUMY
        IF(ABS(EXCY).LE.ERRSY) GO TO 54
        IYCT=IYCT+1
        IF(IYCT.GT.1000)WRITE(MW,260)
        IF(IYCT.GT.1000)GO TO 54
        IF(IFLG.NE.0) GO TO 80
        EXCY1=EXCY
        EXCY2=EXCY
        T1=T
        T2=T
        IFLG=1
80      CONTINUE
        IF(IFW.NE.7)GO TO 800
        WRITE(MW,805)EXCY,EXCY1,EXCY2,T,T1,T2
800     CONTINUE
        TEST1=EXCY*EXCY1
        IF(TEST1)81,81,85
81      CONTINUE
        T2=T
        T=(T+T1)/2
        EXCY2=EXCY
        GO TO 89
85      TEST2=EXCY*EXCY2
        IF(TEST2)86,86,88
86      CONTINUE
```

```
      T1=T
      T=(T1+T2)/2.
      EXCY1=EXCY
      GO TO 89
88    CONTINUE
      T2=T1
      T1=T
      IF(EXCY GT 0.0)T=T1+TDEL
      IF(EXCY.LT 0.0)T=T1-TDEL
      EXCY2=EXCY1
      EXCY1=EXCY
89    CONTINUE
      ICT=ICT+1
      IF(ICT LE.15)GO TO 53
      ABST1=ABS(T-T1)
      ABST2=ABS(T-T2)
      IF(ABST1 GE.0.002)GO TO 53
      IF(ABST2.GE.0.002)GO TO 53
      GO TO 54
53    CONTINUE
      IF(IFW.EQ.7)WRITE(MW,900)T
      GO TO 1
54    CONTINUE
      IF(IYCT.GT 100)IIY=IYCT/100
      IF(IYCT.GT.100)WRITE(MW,270)IIY
      IF(INIT.NE 0) GO TO 70
      H=1.0E6*(MOLE*ZL*R*T)/P/AREA
      HVAP=0
      DO 63 KK=1,NCOMP
      HVAP=HVAP+HV(KK)*X(KK)
63    CONTINUE

      DO 65 I=1,NCOMP
      XW=X(I)*100
      YW=Y(I)*100
      IF(I NE.1) GO TO 60
```

```
      WRITE(MW,420)TIME,MASS,DMA,MOLE,T,I,XW,YW,H
      IF(IFW EQ 10)WRITE(2,950)TIME,T,HVAP
      IF(IFW EQ 10)WRITE(2,951)XW,YW
      GO TO 65
60    WRITE(MW,415)I,XW,YW
      IF(IFW EQ 10)WRITE(2,951)XW,YW
65    CONTINUE
      INIT=1
70    CONTINUE
      IF(CODE EQ 0) GO TO 78
      CALL XNEW(MASS,DMASS,MOLE,X,Y,IFW,CODE,NCOMP)
      GO TO 1001
78    CONTINUE
      MASS=MASS-DMASS
      TIME=TIME+1
      ITIM=ITIM+1
      IF(TIME.GT.TMAX)GO TO 9999
      DMA=MBOFF(ITIM)
      DMASS=MBOFF(ITIM+1)-MBOFF(ITIM)
      DMASS=DMASS*AREA
      INIT=0
      IF(MASS.LE.-2.0) GO TO 9999
      IF(DMASS.LE.-2.0) GO TO 9999
      CODE=2
      GO TO 1001
9999  READ(MR,105)MORE
      IF(IFW.EQ.10)CALL CLOSE(2,IER)
      IF(MORE.EQ.0) GO TO 997
      CALL DATE(IDATE,IER)
      CALL FGTIM(IH,IM,IS)
      WRITE(MW,201)IH,IM,IS,IDATE
      TYPE *,***   RENAME SCRATCH.DF   ***
      CALL EXIT
```

```
105    FORMAT(5I3)
110    FORMAT(5F10.3)
115    FORMAT(A1,29A2)
120    FORMAT(5A2)
150    FORMAT(6X,F9.5,12F9.3)
200    FORMAT(1H1,///////
      11H ,10X,'TIME  ',2(I2,':'),I2,10X,'DATE ',2(I2,'/'),I2////)
201    FORMAT(1H0,///////
      11H ,10X,'TIME ',2(I2,':'),I2,10X,'DATE  ',2(I2,'/'),I2////)
205    FORMAT(1H0,10X,'CONSTRAINTS: P AND X'/1H ,10X,'VARIABLES: T AND Y
      1//1H0,10X,'CONVERGENCE CRITERIA'/1H ,20X,'Y (MOLE FRACTION) '
      2,E12.4/1H ,20X,'1.0 - SUMY ',7X,E12.4//1H ,10X,
      4'COARSE DELTA T   ',F10.1/1H ,10X,'MAX DELTA MOLES  ',F10.3//)
250    FORMAT(1H ,10X,29A2)
260    FORMAT(1H ,'*')
270    FORMAT(1H ,I2,'*')
300    FORMAT(1H0,1X,'TIME',7X,'RESIDUAL',7X,'BOIL-OFF ',7X,'RESIDUAL',
      24X,'TEMPERATURE',9X,'I',11X,'X(I)',11X,'Y(I) ',4X,'HYDROSTATIC'/
      31H ,2X,'SEC',11X,'MASS',11X,'MASS',10X,'MOLAR',14X,'K',51X,'HEAD'/
      41H ,19X,'G',8X,'G/CM2-S',11X,'MASS',68X,'CM'/
      51H0,5('='),4(5X,'==========='),5X,5('='),3(5X,'==========='))
415    FORMAT(1H ,70X,I5,F15.4,F15.5)
420    FORMAT(1H0,F5.0,F15.2,F15.3,2F15.2,5X,I5,F15.4,F15.5,F15.2)
805    FORMAT(1H ,'EXCY,1,2  ',3F10.5,5X,'T,1,2 ',3F10.3)
900    FORMAT(1H0,'NEW TEMPERATURE ',F10.3)
910    FORMAT(1H0,I5,'  X=   ',F10.5,5X,'Y= ',F10.5)
950    FORMAT(F10.0,F10.2,F10.2)
951    FORMAT(2F10.5)
       END
```

```
C          NOVA 840        FX2 FR        JAIME A.  VALENCIA
      SUBROUTINE INPUT(MWT,DENS,MR)
      REAL MWT(5),KIJ(5,5)
      DIMENSION PC(5),TC(5),W(5),TB(5),X(5),Y(5)
      DIMENSION  IDATE(3),NAME(5,5),DENS(5)
      COMMON NCOMP,PC,TC,W,TB,T,P,KIJ
      COMMON/BLKMW/MW
      WRITE(MW,205)
      READ(MR,100)NCOMP
      DO 10 I=1,NCOMP
      READ(MR,105)(NAME(I,J),J=1,5)
      READ(MR,110)TC(I),PC(I),W(I),TB(I),MWT(I),DENS(I)
      READ(MR,110) (KIJ(I,J),J=1,NCOMP)
      WRITE(MW,210)(NAME(I,J),J=1,5),TC(I),PC(I),W(I),TB(I),MWT(I)
     1,DENS(I)
10    CONTINUE
      WRITE(MW,220)
      DO 20 I=1,NCOMP
      DO 20 J=1,NCOMP
      WRITE(MW,225)I,J,KIJ(I,J)
20    CONTINUE
      WRITE(MW,230)
100   FORMAT(I3)
105   FORMAT(5A2)
110   FORMAT(7F10.3)
205   FORMAT(1HO//1H ,11X,'COMPONENT',7X,'CRITICAL',7X,'CRITICAL'
     1,7X,'ACENTRIC',8X,'BOILING',6X,'MOLECULAR',9X,'LIQUID'/
     21H ,24X,'TEMPERATURE',7X,'PRESSURE',9X,'FACTOR',10X,'POINT',9X,
     3'WEIGHT',8X,'DENSITY'/
     31H ,34X,'K',11X,'N/M2',29X,'K',25X,'G/CM3')
210   FORMAT(1HO,10X,5A2,5X,F10.2,5X,F10.0,5X,F10.4,5X,F10.2
     1,2(5X,F10.3))
220   FORMAT(1HO//1HO,10X,'INTERACTION PARAMETERS, K(I,J)'/)
225   FORMAT(1H ,10X,'(',I1,',',I1,') ,F8.4)
230   FORMAT(1H1,////////)
      RETURN
      END
```

```
C          NOVA 840        PX3 FR       JAIME A  VALENCIA
       SUBROUTINE SETUP(A,B,X,RATA,RATB,IFW)
       REAL M(5),KIJ(5,5)
       DIMENSION PC(5),TC(5),W(5),TB(5),X(5)
       DIMENSION RATA(5),RATB(5)
       DIMENSION TR(5),ALPHA(5)
       COMMON NCOMP,PC,TC,W,TB,T,P,KIJ
       COMMON/BLKMW/MW
C*************************************************************************
C
C      PARAMETERS IN S-R-W EQUATION
C
C*************************************************************************
       OMEGA=0.42747
       OMEGB=0.08664
       SUM1=0
       SUM2=0
       DO 20 I=1,NCOMP
       TR(I)=T/TC(I)
       M(I)=0.480+1.574*W(I)-0.176*W(I)**2
       ALPHA(I)=(1.+M(I)*(1.-TR(I)**0.5))**2
20     CONTINUE
       DO 22 I=1,NCOMP
       SUM2=SUM2+X(I)*TC(I)/PC(I)
       DO 22 J=1,NCOMP
       SUM1=SUM1+X(I)*X(J)*(1.-KIJ(I,J))*OMEGA*(TC(I)**2*ALPHA(I)/
      1PC(I)*TC(J)**2*ALPHA(J)/PC(J))**0.5
22     CONTINUE
```

```
C       PARAMETERS IN CUBIC Z EQUATION
        A=P*SUM1/T**2
        B=OMEGB*P/T*SUM2
        IF(IFW.NE.6) GO TO 25
        WRITE(MW,200)A,B
25      CONTINUE
        DO 30 I=1,NCOMP
        SUM3=0.
        DO 28 J=1,NCOMP
        SUM3=SUM3+(1.-KIJ(I,J))*X(J)*OMEGA*(TC(I)**2*ALPHA(I)/PC(I)
       1*TC(J)**2*ALPHA(J)/PC(J))**0.5
28      CONTINUE
        RATA(I)=SUM3/SUM1
        RATB(I)=TC(I)/(PC(I)*SUM2)
        IF(IFW.NE.6) GO TO 30
        WRITE(MW,210)RATA(I),RATB(I)
30      CONTINUE
200     FORMAT(1H0,' SETUP ',A,B    ,2E15.6)
210     FORMAT(1H0,'RATA,RATB ',2E15.6)
        RETURN
        END
```

```
C          NOVA 840        FX4 FR       JAIME A  VALENCIA
      SUBROUTINE CUBIC(AZ,BZ,ZV,ZL,IFW)
C     SOLUTION TO CUBIC Z EQUATION
      COMMON/BLKMW/MW
      PI=3.141596
      B=-1
      C=AZ-BZ-BZ**2
      D=-AZ*BZ
      IF(IFW NE.6) GO TO 5
      WRITE(MW,222)B,C,D
5     CONTINUE
      P=1./3.*(3.*C-B**2)
      Q=1./27.*(27.*D-9.*B*C+2.*B**3)
      R=(P/3.)**3+(Q/2.)**2
      IF(IFW NE.6) GO TO 6
      WRITE(MW,230)P,Q,R
6     CONTINUE
      IF(R)10,20,30
10    PHI=ARCOS((27.*Q**2/(-4.*P**3))**0.5)
      IF(IFW NE.6) GO TO 7
      WRITE(MW,240)PHI
7     CONTINUE
      ZZ=2.*(-P/3.)**0.5
      IF(Q.GT.0.0)ZZ=-ZZ
      Z1=ZZ*COS(PHI/3.)-B/3.
      Z2=ZZ*COS(PHI/3.+2.*PI/3.)-B/3.
      Z3=ZZ*COS(PHI/3.+4.*PI/3.)-B/3.
      ZV=Z1
      IF(Z2.GT.ZV) ZV=Z2
      IF(Z3.GT.ZV) ZV=Z3
      ZL=Z1
      IF(Z2.LT.ZL) ZL=Z2
      IF(Z3.LT.ZL) ZL=Z3
      GO TO 50
```

```
20      ZZ=2 *(-Q/2 )**3-B/3
        ZV=ZZ
        ZL=ZZ
        GO TO 50
30      CONTINUE
        IF(IFW NE 6) GO TO 35
        WRITE(MW,200)
35      CONTINUE
        AAA=-Q/2. +R**0 5
        BBB=-Q/2. -R**0 5
        IF(AAA)41,42,42
41      AA=-(-AAA)**(1. /3 )
        GO TO 45
42      AA=AAA**(1. /3. )
45      CONTINUE
        IF(BBB)46,47,47
46      BB=-(-BBB)**(1 /3. )
        GO TO 49
47      BB=BBB**(1. /3. )
49      CONTINUE
        Z1=AA+BB-B/3.
        ZV=Z1
        ZL=Z1
        IF(IFW NE 6) RETURN
        WRITE(MW,220)Z1
        RETURN
50      CONTINUE
        IF(IFW NE 6)RETURN
        WRITE(MW,220)Z1,Z2,Z3
        RETURN
200     FORMAT(1HO,' ***POSITIVE VALUE OF R *** ')
220     FORMAT(1HO,'Z1,Z2,Z3 ,3E15 5)
222     FORMAT(1HO,'CUBIC B,C,D  ,3E15 5)
230     FORMAT(1HO,'P,Q,R  ,3E15 6)
240     FORMAT(1HO,'PHI',E15 6)
        END
```

```
C          NOVA 840        PX5 FR       JAIME A. VALENCIA
      FUNCTION ARCOS(X)
      Y=SQRT(1 -X*X)/X
      ARCOS=ATAN(Y)
      RETURN
      END
```

```
C          NOVA 840        PX6 FR       JAIME A  VALENCIA
C          8/9/77
      SUBROUTINE FUGCF(X,Z,PHI,A,B,RATA,RATB,IFW)
      REAL KI,I(5,5)
      DIMENSION PC(5),TC(5),W(5),TB(5),X(5)
      DIMENSION PHI(5),RATA(5),RATB(5)
      COMMON NCOMP,PC,TC,W,TB,I,P,KI,I
      COMMON/BLKMW/MW
      DO 20 I=1 NCOMP
      PHI(I)=RATB(I)*(Z-1)-ALOG(Z-B)-(A/B)*(2 *RATA(I)-RATB(I))
     1*ALOG(1+B/Z)
      PHI(I)=EXP(PHI(I))
      IF(IFW NE 6) GO TO 20
      WRITE(MW,100)X(I),PHI(I)
20    CONTINUE
      RETURN
100   FORMAT(1HO, FUGCOF   ,2E15.6)
      END
```

```
C          NOVA 840        FX7 FR       JAIME A  VALENCIA
      SUBROUTINE YNEW(X,Y,K,NCOMP,SUMY,IFW)
      REAL K(5)
      DIMENSION X(5),Y(5)
      COMMON/BLKMW/MW
      SUMY=0
      DO 10 I=1,NCOMP
      Y(I)=K(I)*X(I)
      SUMY=SUMY+Y(I)
10    CONTINUE
      DO 15 I=1,NCOMP
      IF(IFW NE 7) GO TO 14
      WRITE(MW,200)Y(I),K(I),SUMY
14    CONTINUE
      Y(I)=Y(I)/SUMY
15    CONTINUE
200   FORMAT(1HO,' Y ',E15 6,5X, K ,E15 6, SUMY  ,E15 6)
      RETURN
      END
```

```
C          NOVA 840        FX8 FR        JAIME A  VALENCIA
C          8/19/77
C*****************************************************************
C
C          THIS SUBROUTINE COMPUTES THE NEW VALUES OF X(I)
C          SUCH THAT THE DIFFERENCE APPROXIMATION HOLDS.
C
C*****************************************************************
       SUBROUTINE XNEW(MASS,DMASS,MOLE,X,Y,IFW,CODE,NCOMP)
       INTEGER CODE
       REAL MASS,MOLE,MWT(5),MWTV
       DIMENSION X(5),Y(5)
       COMMON/BLKMT/MWT
       COMMON/BLKMW/MW
       COMMON/BLKDM/DM,DMOLE,DLS
       IF(IFW.EQ.8)WRITE(MW,210)CODE
       MWTV=0.0
       DO 10 I=1,NCOMP
       MWTV=MWTV+MWT(I)*Y(I)
10     CONTINUE
       IF(CODE.NE.1) GO TO 50
       DM=DM-DMOLE*MWTV
       IF(IFW.EQ.8)WRITE(MW,200)DM
       DMOLE=DM/MWTV
       IF(DMOLE.GT.DLS) GO TO 80
       CODE=0
       GO TO 90
50     DMOLE=DMASS/MWTV
       IF(DMOLE.GT.DLS) GO TO 60
       CODE=0
       GO TO 90
60     CODE=1
       DM=DMASS
80     DMOLE=DLS
90     CONTINUE
       CALL DELTA(X,Y,MOLE,DMOLE,IFW,NCOMP)
       MOLE=MOLE-DMOLE
       IF(IFW.EQ.8)WRITE(MW,220)CODE
       RETURN
200    FORMAT(1H0,' * XNEW *  , DM=  ',F10.5)
210    FORMAT(1H ,10X,' CODE IN ',I3)
220    FORMAT(1H ,10X,'CODE OUT ',I3)
       END
```

```
C          NOVA 840        PX9.FR          JAIME A  VALENCIA
C         8-19-77
      SUBROUTINE DELTA(X,Y,MOLE,DMOLE,IFW,NCOMP)
      REAL  MOLE
      DIMENSION X(5),Y(5)
      COMMON/BLKMW/MW
      IF(IFW EQ.8) WRITE(MW,100)MOLE,DMOLE
      DO 50  I=1,NCOMP
      X(I)=X(I)-(Y(I)-X(I))*DMOLE/MOLE
      IF(X(I) LT 1 E-10)X(I)=0.0
      IF(X(I) GT 1.0)X(I)=1.0
      IF(IFW EQ.8) WRITE(MW,110)X(I),Y(I)
50    CONTINUE
      RETURN
100   FORMAT(1H0,'* DELTA *  MOLES ',F10.3,'   DMOLE ',F10.3)
110   FORMAT(1H ,10X,' NEW X  ',F10.5,'    Y  ',F10.5)
      END
```

APPENDIX C

COMPUTATION OF BOILING RATES

Procedure

Computer Programs

Procedure

Experimental data indicated the residual liquid mass as a function of time as boiling occurred. To allow a calculation of the rate of boiling, the mass boiled was correlated with time using a simple polynomial; i.e., the correlation of the mass boiled at any time τ involved fitting a polynomial through 2n+1 points, n immediately before τ, n immediately after τ, and the mass boiled off at time τ itself. The boiling rate could then be determined by evaluating the derivative of the polynomial at time τ. For the first n points (0, 1, 2, ... n seconds), a polynomial was fitted through the first 2n+1 points; the derivatives evaluated at 0, 1, 2, ... n seconds were the respective boiling rates. Because the mass boiled off is not clearly defined in the first few seconds (it took a second or two to spill the cryogen), the error for these points is larger than the average error.

As an indication of the degree of error of the fit, both the root mean square derivation as well as the maximum absolute percent error were calculated. Furthermore, the boiling rates were integrated using one of the Newton-Cotes formulas for integration, the well known Simpson's 1/3 rule.

For each point, a selection between a polynomial of first or second order was made based on the RMS error. After the first few seconds, the maximum absolute deviation in the polynomial fits were less than 1%. Upon integration of the boiling rates, the resulting mass boiled off was typically within 1 or 2% of the experimental values.

The value of n used to determine the 2n+1 points for each polynomial was 4. However, when the boiling rates exhibited sharp peaks a value of n=2 was used.

Computer Programs

```
C          NOVA 840        BRATEN FR              JAIME A  VALENCIA
C
C       8/26/77
C       10/20/77          STORE DF       &    500 POINTS
C        FORMERLY ANALYS FR
C        RLDR BRATE SLOPE SETUP INTEG MATRIX
C        *ALLOWS FOR SEVERAL POLYNOMIAL FITS
C        ********
C
C       MAXIMUM NUMBER OF POINTS TO BE TREATED (IX-9)
C
C        ********
        REAL   MASS
        COMMON/BLK1/ MASS(500)
        COMMON/BLK2/ RATE(500)
        COMMON/BLK3/FIT(500)
        COMMON/BLK4/X(500)
        COMMON/BLK7/ SINT(500)
        DIMENSION NAME(5),IDATE(3)
        TYPE 'REDUCED DATA FILE '
        READ(11,1000)(NAME(I),I=1,5)
1000    FORMAT(5A2)
        CALL OPEN(2,NAME,1,IER)
C       SINT= DUMMY FOR ISH
        READ BINARY(2) MASS,SINT
        READ BINARY(2)IX,AREA,NF,INTER
        CALL CLOSE(2,IER)
        CALL OPEN(5, STORE DF ,2,IER)
        CALL OPEN(4, QXXX DF ',2,IER)
        TYPE 'POINTS RECORDED   ',IX
        ACCEPT 'TIME INTERVAL IN SEC   ',DELTA
        ACCEPT NUMBER OF POINTS   ',IX
        ACCEPT  MASS SPILLED  ',MSPIL
        ACCEPT  XMAX,YMAX-MASS-   ',XMX,YMX
        ACCEPT  XMAX,YMAX-RATE-   ',XMAX,YMAX
        ACCEPT  XMAX,YMAX-Q/A-   ',XMXQ,YMXQ
        ACCEPT  HVAP,IHV  - 0=CONSTANT   ',HVAP,IHV
```

```
      WRITE(12,120)(NAME(I),I=1,5)
120   FORMAT(1H1////////////
     11H ,20X, REDUCTION OF DATA FILE   ,5A2)
      CALL DATE(IDATE,IER)
      CALL FGTIM(IH,IM,IS)
      WRITE(12,130)IH,IM,IS,IDATE
130   FORMAT(1H0///1H0,20X,'TIME  ',2(I2,'   '),I2,10X,'DATE ',
     12(I2,'/'),I2)
      ACCEPT 'TYPE 1 TO CORRECT SPECIFICATIONS ',NCORR
      IF(NCORR.NE.1) GO TO 5
      TYPE 1-IX(NPOINTS) / 2-AREA / 3-HVAP / 4-CP / 5-TSAT /
      TYPE  6-BRMAX / 7-HFMAX / 8-BMMAX / 9-MASS / 10-TSH
      TYPE  TYPE 11 WHEN CORRECTIONS ARE FINISHED
700   ACCEPT 'VARIABLE NUMBER  ',NNV
      ACCEPT 'NEW VALUE ',VAL
      GO TO (701,702,703,704,705,706,707,708,709,710,720),NNV
701   IX=VAL
      GO TO 700
702   AREA=VAL
      GO TO 700
703   HVAP=VAL
      GO TO 700
704   CP=VAL
      GO TO 700
705   TSAT=VAL
      GO TO 700
706   BRMAX=VAL
      GO TO 700
707   HFMAX=VAL
      GO TO 700
708   BMMAX=VAL
      GO TO 700
709   ACCEPT 'MASS ARRAY LOCATION ',IMA
      MASS(IMA)=VAL
      GO TO 700
710   ACCEPT  TSH ARRAY LOCATION ,IMA
      TSH =VAL
      GO TO 700
720   CONTINUE
5     CONTINUE
```

```
      WRITE(12,170)AREA
170   FORMAT(1HO,,,,,,,,,,1HO,20X, AREA   ,   ,F8.2,   CM2  )
      ACCEPT  TYPE 1 TO PRINT POLYNOM  FIT AND INTG OF RATES  ,IWW
      ACCEPT  PCH 0-NOTHING 1-RATES    ,IPCH
      DO 50 I=1,500
      X(I)=FLOAT(I)*DELTA
50    CONTINUE
      IX=IX+5
      CALL  RATES(IX)
      CALL OPEN(5, STORE DF  ,2,IER)
      IF(IWW EQ 1) CALL  INTEG(IX,DELTA,MASS(1))
      WRITE(12,400)
      IX=IX-5
      XX=0
      TMB=0
      RR=MASS(1)
      WRITE(12,450)XX,TMB,TMB,RR
      DO 500 I=1,IX
      TMB=MASS(I)*AREA
      IF((MSPLL-TMB) GT. 15.0)MAX=I
      WRITE(12,450)X(I) TMB,MASS(I),RATE(I)
450   FORMAT(1H ,30X,F5.0,F15.1,2F15.5)
      IF(IPCH EQ. 1)WRITE(8,845)RR
      IF(IPCH NE 1) GO TO 890
      WRITE(8,845)RATE(I)
845   FORMAT(F12.5)
890   CONTINUE
500   CONTINUE
      CALL  RWPLT(0  ,XMX,0  ,YMX,X,MASS,1,MAX)
      CALL  RWPLT(0  ,XMAX,0  ,YMAX,X,RATE,1,MAX)
      DO 80 J=1,MAX
      IF(IHV NE 0)READ(11,200)HVAP
200   FORMAT(5F10.3)
C     FIT   DUMMY ARRAY FOR Q/A
      FIT(J)=RATE(J)*HVAP*10
      WRITE(4,799)FIT(J)
799   FORMAT(F10.2)
80    CONTINUE
```

```
      CALL CLOSE(4,IER)
      TYPE '  *** RENAME QXXX DF ***'
      CALL RWPLT(0.,XMXQ,0.,YMXQ,X,FII,1,MAX)
      IF(IWW NE 1)CALL EXIT
      WRITE(12,600)
      TMB=0
      WRITE(12,690)XX,TMB,RR
      MN=0
      DO 675 I=1,IX
      IF(I EQ 1) GO TO 655
      IF(I EQ MN) GO TO 655
      IF(MASS(I) EQ 0.0)GO TO 648
      PCTIN=(SINT(I)-MASS(I))/MASS(I)*100
      GO TO 649
648   PCTIN=0.0
649   CONTINUE
      READ BINARY(5)PCT,RMS,NORD
      WRITE(12,650)X(I),MASS(I),SINT(I),PCTIN,RATE(I),PCT,RMS
     1,NORD
650   FORMAT(1H ,5X,F5.0,2(5X,F10.3),5X,F10.2,5X,F10.5,5X,F10.2
     1,5X,F10.6,5X,I5)
      GO TO 675
655   WRITE(12,660)X(I),MASS(I),RATE(I),PCT,RMS,NORD
660   FORMAT(1H ,5X,F5.0,5X,F10.3,35X,F10.5,5X,F10.2
     1,5X,F10.6,5X,I5)
      MN=MN+2
675   CONTINUE
      CALL CLOSE(5,IER)
400   FORMAT(1H1,'',1HO,31X,' TIME ',11X,'MASS ',11X,' MASS ',8X,' BOILING '
     111H ,32X,'SEC ',5X,' BOILED-OFF',5X,' BOILED-OFF ',11X,' RATE '/
     211H ,49X,' G ',10X,' G/CM2 ',8X,' G/CM2-S'/
     331H ,30X,5(' = '),3(5X,10(' = '))/)
600   FORMAT(1H1,''/1HO,6X,'TIME ',11X,'MASS ',10X,'INTEG',8X,'% ERROR
     1,8X,' BOILING ',8X,' MAX ABS',8X,'RMS DEV ',5X,'ORDER'/
     221H ,7X,'SEC ',5X,' BOILED-OFF',8X,'OF RATE ',10X,' INTEG ',11X
     3,' RATE ',8X,' % ERROR',7X,'POLY FIT',2X,'POLY FIT'/
     441H ,20X,' G/CM2',10X,' G/CM2',23X,' G/CM2-S ',7X,'POLY FIT '/)
690   FORMAT(1H ,5X,F5.0,F15.3,30X,F15.5)
      CALL EXIT
      END
```

```
C          NOVA 840       SLOPEN FR                        JAIME A  VALENCIA
C       8/26/77
C       10/20/77            STORE DF
C       BRATE SV (FORMERLY ANAL1 SV) USES NP POINTS TO FIT A POLY OF
C          FIRST OR SECOND DEGREE,WHICHEVER FITS BEST  IT TAKES
C          THE SLOPE AT THE (NP/2+1) POINT AND THIS BECOMES THE RATE
C          OF BOILING AT THIS (NP/2+1) POINT
        SUBROUTINE RATES(IX)
        COMMON/BLK1/F(500)
        COMMON/BLK2/RATE(500)
        COMMON/BLK3/FIT(500)
        COMMON/BLK4/X(500)
        DIMENSION AA(10),BB(10)
        DIMENSION PCT(10),RAT1(10)
        DIMENSION PCT1(1),RMS1(1),NORD(1)
        ACCEPT  N POINTS PER FIT  ,NP
        DO 95 LEAD=1,IX
        LEADN=LEAD+NP-1
        N2=NP/2
        I=LEAD+2
        N=1
        CALL SETUP(N,AA,LEAD,NP,N2)
        L=0
        SMSQ=0
        DO 10 IK=LEAD,LEADN
        L=L+1
        FIT(IK)=AA(1)+AA(2)*X(IK)
        IF(F(IK).EQ.0.0)GO TO 8
        PCT(L)=(F(IK)-FIT(IK))/F(IK)*100
        GO TO 9
8       PCT(L)=0
9       CONTINUE
        PCT(L)=ABS(PCT(L))
        SMSQ=SMSQ+(F(IK)-FIT(IK))**2
        RAT1(L)=AA(2)
10      CONTINUE
        RMS1(1)=(SMSQ/(NP-1))**0.5
        PCT1(1)=AMAX1(PCT(1),PCT(2),PCT(3),PCT(4),PCT(5),PCT(6))
        NORD(1)=1
        N=2
        CALL SETUP(N,BB,LEAD,NP,N2)
        L=0
        SMSQ=0
```

```
      DO 20 IP=LEAD,LEND
      I=I+1
      FI(IP)=BB(1)+BB(2)*X(IK)+BB(3)*(X(IK))**2
      IF(F(IK).EQ.0.0)GO TO 18
      PCT(I)=(F(IP)-FI(IK))/F(IK)*100
      GO TO 19
18    PCT(I)=0.0
19    CONTINUE
      PCT(I)=ABS(PCT(I))
      SMSQ=SMSQ+(F(IK)-FI(IK))**2
20    CONTINUE
      RMS2=(SMSQ/(NP-1))**0.5
      PCT2=AMAX1(PCT(1),PCT(2),PCT(3),PCT(4),PCT(5),PCT(6))
      IF(RMS2.GT.RMS1(I)) GO TO 50
      RMS1(I)=RMS2
      PCT1(I)=PCT2
      NORD(I)=2
      I=0
      DO 25 IP=LEAD,LEND
      I=I+1
      RAT1(I)=BB(2)+2.*BB(3)*X(IK)
25    CONTINUE
50    IF(LEAD.GE.3) GO TO 70
      DO 60 KK=0,N2
      RATE(KK+1)=RAT1(KK+1)
60    CONTINUE
      GO TO 90
70    RATE(I)=RAT1(N2+I)
90    WRITE BINARY(5)PCT1(1),RMS1(1),NORD(1)
95    CONTINUE
      CALL CLOSE(5)
      RETURN
      END
```

```
C          NOVA 840          SETUPN.FR       JAIME A. VALENCIA
C          1/18/77
      SUBROUTINE SETUP(N,CC,LEAD,NP,N2)
      COMMON/BLK1/F(500)
      COMMON/BLK4/X(500)
      COMMON/BLK5/B(10,11)
      DIMENSION CC(10)
      DO 5 II=1,10
      DO 5 JJ=1,11
      B(II,JJ)=0
5     CONTINUE
      NN=N+1
      MM=N+2
      DO 15 K=1,NN
      DO 15 J=1,NN
      IF(K.EQ.1 AND J.EQ.1) GO TO 77
      SUMB=0
      LEADN=LEAD+NP-1
      DO 10 I=LEAD,LEADN
10    SUMB=SUMB+X(I)**(K-1+J-1)
      B(K,J)=SUMB
      GO TO 15
77    B(1,1)=NP
15    CONTINUE
      SUMC=0
      DO 18 I=LEAD,LEADN
18    SUMC=SUMC+F(I)
      B(1,MM)=SUMC
      DO 30 K=2,NN
      SUMC=0
      DO 20 I=LEAD,LEADN
20    SUMC=SUMC+X(I)**(K-1)*F(I)
30    B(K,MM)=SUMC
X     DO 990 IJK=1,NP-1
X     WRITE(12,980)(B(IJK,JKL),JKL=1,5)
X980  FORMAT(1H ,5E15.6)
X990  CONTINUE
      FF=F(LEAD)
      CALL PIVOT(NN,MM,CC,FF)
      RETURN
      END
```

```
C          NOV'84          INTEG FR        RAIME H  'ALENCIA
C          1.18.77
       SUBROUTINE INTEG(IX,DELTA START)
       COMMON BLK2 RATE(500)
       COMMON BLK7  SINT(500)
       FACT=DELTA/3
       DO 5 I=1 IX
       SINT(I)=0
5      CONTINUE
       SUM=RATE(1)+4 *RATE(2)+RATE(3)
       SINT(3)=SUM*FACT+START
       DO 10 I=5,IX,2
       SUM=SUM+RATE(I-2)+4 *RATE(I-1)+RATE(I)
       SINT(I)=SUM*FACT+START
10     CONTINUE
       RETURN
       END
```

```
C          NOVA 840       MATRIX FR      JAIME A  VALENCIA
C          1/18/77
      SUBROUTINE PIVOT(N,MM,X,FF)
      COMMON A(5,11)
      DIMENSION X(10)
      NITY=12
      DO 30 I=2,N
      DO 30 J=I,N
      II=I-1
      SIR=ABS(A(II,II))
      ISI=II
      DO 25 K=I,N
      IF(ABS(A(K,II)).LE.SIR) GO TO 25
      SIR=ABS(A(K,II))
      ISI=K
25    CONTINUE
      IF(SIR)440,441,440
440   DO 60 KK=II,MM
      ZZ=A(ISI,KK)
      A(ISI,KK)=A(II,KK)
60    A(II,KK)=ZZ
210   FORMAT(1H , MATRIX IS SINGULAR )
      EAC=A(I,I-1)/A(I-1,I-1)
      DO 30 J=1,MM
30    A(I,J)=A(I,J)-EAC*A(I-1,J)
      X(N)=A(N,MM)/A(N,N)
      NN=N-1
      DO 400 I=1,NN
      I=N-I
      SUM=0
      JJ=I+1
      DO 405 J=JJ,N
405   SUM=SUM+A(I,J)*X(J)
400   X(I)=(A(I,MM)-SUM)/A(I,I)
X     WRITE(NITY,220)
X220  FORMAT(1HO, SOLUTION VECTOR )
X     DO 90 I=1,N
X90   WRITE(NITY,230)I,X(I)
X230  FORMAT(1H ,I3,5X,1PE15.6)
      GO TO 99
441   WRITE(NITY,210)
      X(1)=FF
      DO 80 J=2,10
80    X(J)=0.0
99    RETURN
      END
```

APPENDIX D

HEAT TRANSFER MODELS

Properties of Ice

Properties of Water

Computer Programs

- Convolution Integral
- Variable Grid Size Heat Transfer Model
- VGS/VLE HTM

Properties of Ice

TEMPERATURE K	K KJ/S-M-K	CP KJ/KG-K	RHO KG/M3	ALPHA M2/S
273.00	0.221880E-2	0.212573E 1	0.913036E 3	0.114320E-5
270.00	0.224887E-2	0.209690E 1	0.913342E 3	0.117422E-5
260.00	0.235215E-2	0.200585E 1	0.914364E 3	0.128247E-5
250.00	0.246164E-2	0.192180E 1	0.915386E 3	0.139930E-5
240.00	0.257925E-2	0.184383E 1	0.916408E 3	0.152645E-5
230.00	0.270690E-2	0.177102E 1	0.917432E 3	0.166600E-5
220.00	0.284650E-2	0.170243E 1	0.918456E 3	0.182048E-5
210.00	0.299998E-2	0.163713E 1	0.919480E 3	0.199293E-5
200.00	0.316925E-2	0.157420E 1	0.920506E 3	0.218711E-5
190.00	0.335624E-2	0.151270E 1	0.921531E 3	0.240763E-5
180.00	0.356286E-2	0.145172E 1	0.922558E 3	0.266025E-5
170.00	0.379103E-2	0.139031E 1	0.923585E 3	0.295235E-5
160.00	0.404266E-2	0.132756E 1	0.924613E 3	0.329347E-5
150.00	0.431969E-2	0.126253E 1	0.925641E 3	0.369191E-5
140.00	0.462402E-2	0.119430E 1	0.926670E 3	0.417814E-5
130.00	0.495758E-2	0.112193E 1	0.927699E 3	0.476319E-5
120.00	0.532228E-2	0.104450E 1	0.928729E 3	0.548658E-5
110.00	0.572005E-2	0.961076E 0	0.929760E 3	0.640135E-5
100.00	0.615280E-2	0.870735E 0	0.930791E 3	0.759162E-5

Properties of Water

TEMPERATURE K	K KJ/S-M-K	CP KJ/KG-K	RHO KG/M3	ALPHA M2/S
273.50	0.553400E -3	0.421490E 1	0.999900E 3	0.131309E -6
274.50	0.556300E -3	0.421160E 1	0.999950E 3	0.132094E -6
275.50	0.558600E -3	0.420850E 1	0.999980E 3	0.132734E -6
276.50	0.560900E -3	0.420550E 1	0.999800E 3	0.133400E -6
277.50	0.563100E -3	0.420270E 1	0.999990E 3	0.133987E -6
278.50	0.565300E -3	0.420030E 1	0.999980E 3	0.134588E -6
279.50	0.567600E -3	0.419800E 1	0.999950E 3	0.135214E -6
280.50	0.569900E -3	0.419590E 1	0.999900E 3	0.135837E -6
281.50	0.572100E -3	0.419400E 1	0.999840E 3	0.136431E -6
282.50	0.574300E -3	0.419220E 1	0.999770E 3	0.137024E -6
283.50	0.576600E -3	0.419060E 1	0.999680E 3	0.137638E -6
284.50	0.578800E -3	0.418920E 1	0.999580E 3	0.138223E -6
285.50	0.581100E -3	0.418790E 1	0.999470E 3	0.138830E -6
286.50	0.583300E -3	0.418680E 1	0.999340E 3	0.139411E -6

Computer Programs

Convolution Integral

```
C         NOVA 840              CONVOL 1 FR              JAIME A  VALENCIA
C       THIS PROGRAM FINDS THE SURFACE TEMPERATURE OF A SEMI-INFINITE
C            BOD, SUBJECT TO A TIME VARYING HEAT FLUX AT THE SURFACE
C            AND UNDERGOING A PHASE TRANSFORMATION
      REAL K,K1
      DIMENSION Q(2000),NAME(5)
      COMMON/BLKQ/EXPQ(200)
      TYPE 'FILE NAME
      READ(11,100)(NAME(I),I=1,5)
      ACCEPT 'NUMBER OF POINTS ',NLIM
      ACCEPT  DELTA U ',DUS
      ACCEPT  Q/A LOST FRACTION  ,FF
      ACCEPT 'TCRYO,TF ',TC,TF
      CALL OPEN(5,NAME,2,IER)
      DO 5 I=1,NLIM
      READ(5,110)EXPQ(I)
      EXPQ(I)=EXPQ(I)*FF
5     CONTINUE
      CALL CLOSE(5,IER)
      PI=3 1415926
      ACCEPT  K1,ALPHA1,K,BETA  ,K1,ALFA1,K,BETA
      WRITE(12,300)NAME,K1,ALFA1,DUS,FF,TC,TF,K,BETA
      WRITE(12,301)
      DO 80 I=1,NLIM
      CALL DASW(IFW)
      TAU=FLOAT(I)
      DU=DUS
      UPPER=2 *SQRT(TAU)
      N=UPPER/DU+1
      NT=N-(N/2)*2
      IF(NT EQ 0)N=N+1
      DU=UPPER/(N-1)
      IF(IFW EQ 1 OR IFW EQ 9)WRITE(12,200)N,DU,TAU
```

```
      DO 20 J=1,N
      U=FLOAT(J-1)*DU
      SCRW=TAU-(U/2 )**2
      IF(IFW.EQ.1.OR.IFW.EQ.9)WRITE(12,205)U,SCRW
      CALL HEAT(F,SCRW,IFW)
      Q(J)=F
20    CONTINUE
      CALL SIMP(SMPINT,DU,N,Q,IFW)
      ZZ1=K*BETA/2 /SQRT(ALFA1)
      EPS=ERFF(ZZ1)/K1*SQRT(ALFA1/PI)
      THETA=-SMPINT*EPS
      DELT=THETA+TF-TC
      T=THETA+TF
      WRITE(12,220)TAU,THETA,EXPQ(I),DELT
80    CONTINUE
100   FORMAT(5A2)
110   FORMAT(F10.5)
200   FORMAT(1H , MAIN N,DU,TAU  ,I6,2E15.6)
205   FORMAT(1H , MAIN U,SCRW  ,2E15.6)
220    FORMAT(1H ,10X F10.1,2(10X,F10.2),10X,F10.2)
300   FORMAT(1H ////1H ,5X, FILE :    ,5A2/
     11HO,5X, K   ,E15.6,   KJ/S-M-K /
     11H ,5X, ALPHA   ,E15.6,   M2/S //
     11HO,5X, DU   ,F10.3/1H ,5X, FF   ,F10.3/
     11HO,5X, TC   ,F10.2,  K /1H ,5X, TF   ,F10.2,   K  
     11H ,5X, K  ,E15.6,10X, BETA  ,F10.5//)
301   FORMAT(1H ,16X, TIME ,15X, THETA ,17X, Q/A ,13X, DELTA T 
     11H ,19X, S ,19X, K ,15X, KW/M2 ,19X, K  )
      END
```

```
C         NOVA 840              CONVOZ FR              JAIME A  VALENCIA
C       THIS SUBROUTINE INTEGRATES THE FUNCTION F OVER
C            N POINTS
        SUBROUTINE SIMP(SMPINT,H,N,F IFW)
        DIMENSION F(2000)
        IER=N-(N 2)*2
        IF(IER EQ 0)TYPE 'SIMP IER  ,IER
        NN=N-2
        SUM=0
        DO 5 I=1,NN,2
        SUM=SUM+F(I)+4 *F(I+1)+F(I+2)
5       CONTINUE
        SMPINT=H 3. *SUM
        IF(IFW EQ 2 OR IFW EQ 9)WRITE(12,200)SMPINT,H,N
200     FORMAT(1H ,'SIMPSON : INTEG,H,N  ,2E15.6,5X,I6)
        RETURN
        END
```

```
C         NOVA 840              CONVOX FR              JAIME A  VALENCIA
C      THIS SUBROUTINE CALCULATES THE HEAT FLUXES BY INTREPOLATION
C           FOR THOSE TIMES THAT ARE NOT EXCAT MULTIPLES OF 1 SEC
       SUBROUTINE HEAT(F,SCRW,IFW)
       COMMON/BLKQ/EXPQ(200)
       I=SCRW
       IF(I EQ 0)I=I+1
       X1=I
       X2=I+1
       X3=I+2
       F1=EXPQ(I)
       F2=EXPQ(I+1)
       F3=EXPQ(I+2)
       X=SCRW
       F=(X-X2)/(X1-X2)*(X-X3)/(X1-X3)*F1
      1+(X-X1)/(X2-X1)*(X-X3)/(X2-X3)*F2
      2+(X-X1)/(X3-X1)*(X-X2)/(X3-X2)*F3
       IF(IFW EQ 3 OR IFW EQ 9)WRITE(12,200)I,F1,F2,SCRW,F
200    FORMAT(1H , HEAT ,I,F1,F2,SCRW,F   ,I5,4E15.6)
       RETURN
       END
```

```
C         NOVA 840              SULKI3 FR              JAIME A. VALENCIA
C          11/23/77
C      ERROR FUNCTION OF X
       FUNCTION ERFF(X)
       DIMENSION A(5)
       COMMON/BLLSHI/P,A
       DATA P/0 3275911/,
      1     A/0 254829592,-0 284496736,1 421413741,-1 453152027,
      2        1 061400542 9/
       IF(X)10,20,20
10     Y=-X
       GO TO 30
20     Y=X
30     T=1 0/(1 0+P*Y)
       IF(Y GT 8 3) GO TO 12
       EX=EXP(-Y*Y)
       GO TO 13
12     EX=0
13     ERFF=1 0-(T*(A(1)+T*(A(2)+T*(A(3)+T*(A(4)+T*A(5)))))*EX)
       IF(X)40,50,50
40     ERFF=-ERFF
50     CONTINUE
       IF(ABS(X) LE 1 E-10)ERFF=0 00
       RETURN
       END
```

```
C          NOVA 840                CONVOLVER               JAIME A. VALENCIA
C       THIS PROGRAM FINDS THE SURFACE TEMPERATURE OF A SEMI-INFINITE
C            BODY SUBJECT TO A TIME VARYING HEAT FLUX AT THE SURFACE
        REAL K
        DIMENSION Q(2000),NAME(5)
        COMMON/BLKQ/EXPQ(200)
        TYPE "FILE NAME"
        READ(11,100)(NAME(I),I=1,5)
        ACCEPT "NUMBER OF POINTS ",NLIM
        ACCEPT "DELTA U ",DUS
        ACCEPT "Q A LOST FRACTION ",FF
        ACCEPT "ICRYO.TICE ",IC,TICE
        CALL OPEN(5,NAME,2,IER)
        DO 5 I=1,NLIM
        READ(5,110)EXPQ(I)
        EXPQ(I)=EXPQ(I)*FF
5       CONTINUE
        CALL CLOSE(5,IER)
        PI=3.1415926
        ACCEPT "K,ALPHA ",K,ALFA
        WRITE(12,300)NAME,K,ALFA,DUS,FF,IC,TICE
        TYPE "TEMP FILE NAME"
        READ(11,100)(NAME(I),I=1,5)
        CALL OPEN(6,NAME,2,IER)
        WRITE(12,302)NAME
        WRITE(12,301)
        DO 80 I=1,NLIM
        CALL DASW(IFW)
        TAU=FLOAT(I)
        DU=DUS
        UPPER=2.*SQRT(TAU)
        N=UPPER/DU+1
        NI=N-(N/2)*2
        IF(NI.EQ.0)N=N+1
        DU=UPPER/(N-1)
        IF(IFW.EQ.1.OR.IFW.EQ.9)WRITE(12,200)N,DU,TAU
```

```
      DO 20 J=1,N
      U=FLOAT(J-1)*DU
      SCRW=TAU-(U/2 )**2
      IF(IFW EQ 1 OR IFW EQ 9)WRITE(12,205)U,SCRW
      CALL HEAT(F SCRW,IFW)
      Q(J)=F
20    CONTINUE
      CALL SIMP(SMPINT,DU,N,Q,IFW)
      THETA=-SQRT(ALFA/PI)/K*SMPINT
      DELT=THETA+TICE-TC
      T=THETA+TICE
      WRITE(6,110)T
      WRITE(12,220)TAU,THETA,EXPQ(I),DELT
80    CONTINUE
      CALL CLOSE(6,IER)
100   FORMAT(5A2)
110   FORMAT(F10 5)
200   FORMAT(1H , MAIN N,DU,TAU  ,I6,2E15 6)
205   FORMAT(1H , MAIN U,SCRW  ,2E15.6)
220    FORMAT(1H ,10X,F10 1,2(10X,F10 2),10X,F10.2)
300   FORMAT(1H /////1H ,5X,'FILE :   ',5A2//
     11H0,5X,'K    ,E15 6,'   KJ/S-M-K'/
     11H ,5X, ALPHA   ',E15 6,  M2/S'//
     11H0,5X, DU    ,F10 3/1H ,5X, FF   ,F10.3/
     11H0,5X, TC   ,F10 2,   K /1H ,5X, TICE   ,F10 2,   K'///)

301   FORMAT(1H ,16X, TIME ,15X, THETA ,17X, Q/A ,13X,'DELTA T /
     11H ,19X, S ,19X, K ,15X,'KW/M2',19X,'K'/')
302   FORMAT(1H0,5X,'TEMP FILE :  ',5A2///)
      END
```

Computer Programs

Variable Grid Size Heat Transfer Model

```
C         NOVA 840       VRBLG FR        JAIME A  VALENCIA
C       VARIABLE GRID SPACING
      REAL MBOFF
      DIMENSION TH(50), THSV(50)
      REAL K1,K2
      MR=11
      MW=12
      ACCEPT 'K1, ALFA1 ', K1, ALFA1
      ACCEPT 'K2, ALFA2 ', K2, ALFA2
      ACCEPT 'RHO, QL, HVAP ', RHO, QL, HVAP
      READ(MR,105)M,NLIM
      READ(MR,110)DTAU,EE,E
      READ(MR,110)FILMT
      READ(MR,110)TF,TCRYO,TWAT
      CALL DASW(IFW)
      THF=0.
      THC=TCRYO-TF
      THW=TWAT-TF
      NN=2*M
      R=FLOAT(M)
      P=FLOAT(NN)
      IPRT=1 /DTAU+0.1
      WRITE(MW,200)K1,ALFA1,K2,ALFA2,RHO,QL,HVAP
      WRITE(MW,201)TCRYO,TF,TWAT
      WRITE(MW,202)M,E,EE
      WRITE(MW,203)DTAU,NLIM,FILMT
      CALL TSURF(TS,TF,TCRYO,DTAU,FILMT,IFW)
      THS=TS-TF
      DO 5 I=1,M
      TH(I)=THS+(FLOAT(I)/R)*(THF-THS)
      IF(IFW.EQ.2.OR.IFW.EQ.9)WRITE(MW,210)I,TH(I)
5     CONTINUE
      DO 10 I=M,NN
      TH(I)=THF+(FLOAT(I-M)/R)*(THW-THF)
      IF(TH(I).GT.THW)TH(I)=THW
      IF(IFW.EQ.2.OR.IFW.EQ.9)WRITE(MW,210)I,TH(I)
10    CONTINUE
      MBOFF=0.
      INIT=0
      II=0
      IIT=0
15    II=II+1
      IF(II.EQ.IPRT)IIT=IIT+1
      IF(II.EQ.IPRT)II=0
      CALL DASW(IFW)
      TAU=(FLOAT(II)+FLOAT(IIT)*FLOAT(IPRT))*DTAU
      CALL TSURF(TS,TF,TCRYO,TAU,FILMT,IFW)
      THS=TS-TF
      NS=0
       IF(IFW.EQ.2.OR.IFW.EQ.9)WRITE(MW,210)NS,THS
      TPRO=(TH(M-1)+TH(M)+2.*TF)/2.
      CALL PROP(TPRO,VK1E,VCP1E,VRHO1E)
```

```
      DE=(VK1E*(TH(M-2)-4 *TH(M-1)+3 *TH(M)) (2 *E R)
     1+K2*(TH(M+2)-4 *TH(M+1)+3 *TH(M))/(2 *(EE-E) (P-R)))
     2/(RHO*CP )
      E=DE*DTAU+E
      DX1=E R
      DX2=(EE-E) (P-R)
      IF(IFN EQ 3 OR IFN EQ 9)WRITE(MW,230)E DE DX1 DX2
      MM1=M-1
      DO 30 N=1,MM1
      IF(N EQ 1)THNM1=THS
      IF(N NE 1)THNM1=TH(N-1)
      TPRO=TH(N)+TF
      CALL PROP(TPRO,VK,VCP,VRHO)
      TPRO=(THNM1+TH(N)+2 *TF) 2
      CALL PROP(TPRO,VK1,VCP1,VRHO1)
      TPRO=(TH(N)+TH(N+1)+2 *TF) 2
      CALL PROP(TPRO,VK2,VCP2,VRHO2)
      DTHDT=(VK1*(THNM1-TH(N))-VK2*(TH(N)-TH(N+1))) (VRHO*VCP*(E R)**2)
      DTH=(FLOAT(N) E)*(TH(N+1)-THNM1) 2 *DE
     1+DTHDT
      THSV(N)=DTH*DTAU+TH(N)
      IF(IFN EQ 2 OR IFN EQ 9)WRITE(MW,210)N,THSV(N)
30    CONTINUE
      THSV(M)=0
      IF(IFN EQ 2 OR IFN EQ 9)WRITE(MW,210)M,THSV(M)
      MP1=M+1
      NNM1=NN-1
      DO 50 N=MP1,NNM1
      DTH=(P-FLOAT(N)) (EE-E)*(TH(N+1)-TH(N-1)) 2 *DE
     1+ALFA2*(TH(N-1)-2 *TH(N)+TH(N+1))/((EE-E)**2 (P-R)**2)
      THSV(N)=DTH*DTAU+TH(N)
      IF(IFN EQ 2 OR IFN EQ 9)WRITE(MW,210)N,THSV(N)
50    CONTINUE
      THSV(NN)=THN
      IF(IFN EQ 2 OR IFN EQ 9)WRITE(MW,210)NN,THSV(NN)
```

```
      DTDX=(-3 *THS+4. *TH(1)-TH(2))/(2. *DX1)
      TPRO=THS+TF
      CALL PROP(TPRO,VKQA,VCPQA,VRHOQA)
      IF(IFW EQ. 5. OR. IFW. EQ. 9)WRITE(MW,220)TPRO,VKQA
      QA=VKQA*DTDX
      IF(IFW. EQ. 8. OR. IFW EQ. 9)WRITE(MW,220)TAU,QA,E
      ITEST=II-(II/IPRT)*IPRT
      IF(INIT. EQ. 0)QAS=QA
      MBOFF=MBOFF+(QAS+QA)/2. /HVAP/10. *DTAU
      IF(ITEST. EQ. 0)WRITE(MW,225)TAU,QA,TS,E,MBOFF
      QAS=QA
      INIT=1
      DO 80 IK=1,NN
      TH(IK)=THSV(IK)
80    CONTINUE
      IF(IIT. GE. NLIM)CALL EXIT
      GO TO 15
105   FORMAT(5I5)
110   FORMAT(5F10. 2)
200   FORMAT(1H ///////1H ,5X,'K1 : ',E15. 6,15X,'ALFA1 : ',
     1E15. 6/1H ,5X,'K2 : ',E15. 6,15X,'ALFA2 : ',E15. 6/
     21H ,5X,'RHO: ',E15. 6,15X,'QL : ',E15 6/
     31H ,5X,'HVAP ',E15. 6///)
201   FORMAT(1H ,5X,'TCRYO : ',F10 2/1H ,5X,'TF : ',F10. 2/
     11H ,5X,'TWAT : ',F10 2///)
202   FORMAT(1H ,5X,'M : ',I5,10X, E . ,F10 5,10X, EE : ,F10. 5///)
203   FORMAT(1H ,5X,'DTAU : ',F10. 5,10X, NLIM : ,I5///
     11H ,5X,'FILMT ',F10. 2///////)
210   FORMAT(1H ,I5,F10. 2)
220   FORMAT(1HO,5E15 6)
225   FORMAT(1H ,3(10X,F10 2),10X,F10 5,10X,F10. 5)
230   FORMAT(1H ,'E,DE,DX1,DX2 ',4E15. 6)
      END
```

```
C         NOVA 840        SUI.KI4S.FR        .JAIME A.  VALENCIA
C       SURFACE TEMPERATURE  LINEAR DROP WITH TIME
        SUBROUTINE TSURF(TS,TINIT,TCRYO,TAU,FILMT,IFW)
        IF(TAU.GT.FILMT)TS=TCRYO
        IF(TAU.GT.FILMT)GO TO 99
        TS=TINIT-(TAU/FILMT)*(TINIT-TCRYO)
99      IF(IFW.EQ.9.OR.IFW.EQ.4)WRITE(12,200)TAU,TS
200     FORMAT(1H ,'TSURF ',2F10.2)
        RETURN
        END
```

```
C         NOVA 840        SUI.KI5.FR         .JAIME A.  VALENCIA
C       PROPERTIES OF ICE
C       K IN KJ/S-M-K
C       CP IN KJ/KG-K
C       RHO IN KG/M3
        SUBROUTINE PROP(T,K,CP,RHO)
        REAL K
        A=0.128264E-1
        B=-0.915821E-4
        C=0.280440E-6
        D=-0.319791E-9
        K=A+B*T+C*T**2+D*T**3
        A=-0.617527E 0
        B=0.219018E-1
        C=-0.856677E-4
        D=0.154759E-6
        CP=A+B*T+C*T**2+D*T**3
        A=0.941138E3
        B=-0.103774E0
        C=0.306166E-5
        RHO=A+B*T+C*T**2
        RETURN
        RETURN
        END
```

Computer Programs

VGS/VLE HTM

In addition to the programs listed, the following subroutines are used:

- VLE Model (Appendix B)
  - INPUT
  - SETUP
  - CUBIC
  - ARCOS
  - FUGCF
  - YNEW
  - XNEW
  - DELTA
- Heat Transfer Models
  - TSURF
  - PROP

```
C         NOVA 840       PIPS1.FR                  JAIME A  VALENCIA
C         /77
C      10/21/77       HVAP=SUM(X(I)*HVAP(I))   >DISK FILE
C      1/14/78
C*************************************************************************
C
C         THIS PROGRAM COMPUTES THE COMPOSITION OF THE VAPOR EVOLVED
C         WHILE BOILING LNG ON WATER.
C
C         SOAVE-REDLICH-KWONG EQUATION OF STATE
C         COSTRAINTS:  P AND X
C         VARIABLES:  T AND Y
C
C*************************************************************************
       REAL MWT(5),K(5),KIJ(5,5)
       REAL MASS,MOLE,MWTL
       REAL MBOFF,MBOFFS
       INTEGER CODE
       INTEGER TITLE(30),TCHK
       DIMENSION X(5),Y(5),YN(5)
       DIMENSION PC(5),TC(5),W(5)
       DIMENSION RATA(5),RATB(5),PHIL(5),PHIV(5)
       DIMENSION TB(5),DENS(5)
       DIMENSION IDATE(3),HV(5),CP(5)
       COMMON NCOMP,PC,TC,W,TB,T,P,KIJ
       COMMON/BLKMT/MWT
       COMMON/BLKMW/MW
       COMMON/BLKDM/DM,DMOLE,DLS
       MR=9
       R=8.3143
       AREA=143.
997    CONTINUE
       READ(MR,105)MW
C*************************************************************************
C
C         MR1 ALLOWS TO INPUT FROM DIFFERENT SOURCE THAN MR,EG TTY
C
C*************************************************************************
```

```
      READ(MR,105)MR1
      CALL DATE(IDATE,IER)
      CALL FGTIM(IH,IM,IS)
      WRITE(MW,200)IH,IM,IS,IDATE
      READ(MR,110) AREA
      READ(MR,110)ERRY,ERRSY,TDEL
      READ(MR,110)DLS
      WRITE(MW,205)ERRY,ERRSY,TDEL,DLS
C*********************************************************************
C
C        ANY TITLE MAY BE PRINTED OUT IN THE OUTPUT PROVIDED THAT
C        A ' T ' IS PUNCHED IN THE FIRST COLUMN AND A BLANK CARD
C        FOLLOWS THE LAST TITLE CARD.
C
C*********************************************************************
      READ(MR,115)TCHK
401   READ(MR,115)TITLE
      IF(TITLE(1).NE.TCHK) GO TO 998
      WRITE(MW,250)(TITLE(I),I=2,30)
      GO TO 401
998   CONTINUE
      INIT=0
      CALL INPUT(MWT,DENS,MR)
C*********************************************************************
C
C        PRESSURE UNITS ARE N/M2.  USE PFAC FOR CONVERSION FACTORS.
C        TEMPERATURE IN DEGREES KELVIN  USE TFAC1 AND TFAC2 FOR CONVERS
C          K=(X+TFAC1)/TFAC2
C        X=F        TFAC1=459.6     TFAC2=1.8
C        X=F        TFAC1=491.6     TFAC2=1.8
C        X=C        TFAC1=273.15    TFAC2=1.00
C
C*********************************************************************
      READ(MR,110)PFAC,TFAC1,TFAC2
```

```
C*************************************************************************
C
C         IFW IS USED AS A GENERAL FLAG WITH THE FOLLOWING CONVENTION:
C              6    PRINT DETAILED  CALCULATIONS OF S-R-K
C              7    PRINT INTERMEDIATE Y'S AND F'S
C              8    PRINT  INTERMEDIATE X'S
C              10   STORE IN DISK FILE:
C                   TIME, TEMP, X(I), Y(I)
C             ANY OTHER NUMBER WILL NOT CAUSE ANY ACTION
C
C*************************************************************************
      READ(MR,110)(HV(J),J=1,NCOMP)
      READ(MR,110)(CP(J),J=1,NCOMP)
      READ(MR,105)IFW
      IF(IFW.NE.10) GO TO 330
330   CONTINUE
      READ(MR,110)T,(Y(I),I=1,NCOMP)
      T=(T+TFAC1)/TFAC2
      TSS=T
      READ(MR,110)P
      P=P*PFAC
      READ(MR,110)MASS
      READ(MR,110)(X(I),I=1,NCOMP)
      READ(MR,110)TMAX
      IL=TMAX+0.001
      DMA=0.0
      MBOFF=0
      MBOFF=0
      MWTL=0.0
      CODE=2
      TIME=0.0
      ITIM=0
      ITIMT=0
      DO 333 I=1,NCOMP
      MWTL=MWTL+MWT(I)*X(I)
333   CONTINUE
      MOLE=MASS/MWTL
      IW300=0
```

```
C*************************************************************************
C
C         IFLG  ALLOWS INITIALIZATION OF VALUES OF T FOR ITERATIONS
C         ICT  IF T DOES NOT IMPROVE BY MORE THAN 0 002 IN 15
C         CONSECUTIVE TRIALS, TERMINATE THAT ITERAION
C
C*************************************************************************
1001   CONTINUE
       IFLG=0
       ICT=0
       IYCT=0
1      CONTINUE
       CALL SETUP(AZ,BZ,X,RATA,RATB,IFW)
       CALL CUBIC(AZ,BZ,ZV,ZL,IFW)
       CALL FUGCF(X,ZL,PHIL,AZ,BZ,RATA,RATB,IFW)
2      CALL SETUP(AZ,BZ,Y,RATA,RATB,IFW)
       CALL CUBIC(AZ,BZ,ZV,ZL,IFW)
       CALL FUGCF(Y,ZV,PHIV,AZ,BZ,RATA,RATB,IFW)
       DO 5 I=1,NCOMP
       K(I)=PHIL(I)/PHIV(I)
5      CONTINUE
       CALL YNEW(X,YN,K,NCOMP,SUMY,IFW)
       DO 10 I=1,NCOMP
       IF(ABS(YN(I)-Y(I)).GT.ERRY) GO TO 20
10     CONTINUE
       GO TO 50
20     DO 25 I=1,NCOMP
       Y(I)=YN(I)
       IF(IFW.NE.7) GO TO 25
       WRITE(MW,910)I,X(I),Y(I)
25     CONTINUE
       IYCT=IYCT+1
       IF(IYCT.GT.1000)WRITE(MW,260)
       IF(IYCT.GT.1000)GO TO 54
       GO TO 2
50     CONTINUE
```

```
      EXCY=1. -SUMY
      IF(ABS(EXCY) LE ERRSY) GO TO 54
      IYCT=IYCT+1
            F(IYCT GT 1000)WRITE(MW,260)
      IF(IYCT GT. 1000)GO TO 54
      IF(IFLG. NE. 0) GO TO 80
      EXCY1=EXCY
      EXCY2=EXCY
      T1=T
      T2=T
      IFLG=1
80    CONTINUE
      IF(IFW. NE. 7)GO TO 800
      WRITE(MW,805)EXCY,EXCY1,EXCY2,T,T1,T2
800   CONTINUE
      TEST1=EXCY*EXCY1
      IF(TEST1)81,81,85
81    CONTINUE
      T2=T
      T=(T+T1)/2.
      EXCY2=EXCY
      GO TO 89
85    TEST2=EXCY*EXCY2
      IF(TEST2)86,86,88
86    CONTINUE
      T1=T
      T=(T1+T2)/2.
      EXCY1=EXCY
      GO TO 89
88    CONTINUE
      T2=T1
      T1=T
      IF(EXCY. GT. 0 0)T=T1+TDEL
      IF(EXCY LT. 0 0)T=T1-TDEL
      EXCY2=EXCY1
      EXCY1=EXCY
89    CONTINUE
```

```
      ICT=ICT+1
      IF(ICT .LE. 15)GO TO 53
      ABST1=ABS(T-T1)
      ABST2=ABS(T-T2)
      IF(ABST1 .GE. 0.002)GO TO 53
      IF(ABST2 .GE. 0.002)GO TO 53
      GO TO 54
53    CONTINUE
      IF(IFW .EQ. 7)WRITE(MW,900)T
      GO TO 1
54    CONTINUE
      IF(IYCT .GT. 100)IIY=IYCT/100
      IF(IYCT .GT. 100)WRITE(MW,270)IIY
      IF(INIT .NE. 0) GO TO 70
      H=1.0E6*(MOLE*ZL*R*T)/P/AREA
      HVAP=0.
      CPLIQ=0.
      DO 63 KK=1,NCOMP
      HVAP=HVAP+HV(KK)*X(KK)
      CPLIQ=CPLIQ+CP(KK)*X(KK)
63    CONTINUE
      DTCP=T-TSS
      TSS=T
      MBOFFS=MBOFF
      CALL HTM(MBOFF,T,HVAP,CPLIQ,MASS,DTCP,AREA,IPRT,DTAU)
      DMASS=(MBOFF-MBOFFS)*AREA
      IF(IW300 .EQ. 0)WRITE(MW,300)
      IW300=1
      DO 65 I=1,NCOMP
      XW=X(I)*100.
      YW=Y(I)*100.
      IF(I .NE. 1) GO TO 60
      IF(ITIM .EQ. 0)WRITE(MW,420)TIME,MASS,DMA,MOLE,T,I,XW,YW,H
      GO TO 65
60    IF(ITIM .EQ. 0)WRITE(MW,415)I,XW,YW
65    CONTINUE
      INIT=1
70    CONTINUE
```

```
      IF(CODE EQ 0) GO TO 78
      CALL XNEW(MASS,DMASS,MOLE,X,Y,IFW,CODE,NCOMP)
      GO TO 1001
78    CONTINUE
      MASS=MASS-DMASS
      ITIMT=ITIMT+1
      TIME=(FLOAT(ITIM)+FLOAT(IPRT)*FLOAT(ITIMT))*DTAU
      IF(TIME GT. TMAX)GO TO 9999
      DMA=MBOFF
      INIT=0
      IF(MASS.LE.-2.0) GO TO 9999
      CODE=2
      GO TO 1001
9999  READ(MR,105)MORE
      IF(MORE.EQ.0) GO TO 997
      CALL DATE(IDATE,IER)
      CALL FGTIM(IH,IM,IS)
      WRITE(MW,201)IH,IM,IS,IDATE
      CALL EXIT
105   FORMAT(5I3)
110   FORMAT(5F10.3)
115   FORMAT(A1,29A2)
200   FORMAT(1H1///////
     11H ,10X,'TIME ',2(I2,':'),I2,10X,'DATE ',2(I2,'/'),I2////)
201   FORMAT(1HO///////
     11H ,10X,'TIME ',2(I2,':'),I2,10X,'DATE ',2(I2,'/'),I2////)
205   FORMAT(1HO,10X,'CONSTRAINTS: P AND X'/1H ,10X,'VARIABLES: T AND Y'
     1//1HO,10X,'CONVERGENCE CRITERIA'/1H ,20X,'Y (MOLE FRACTION) '
     2,E12.4/1H ,20X,'1.0 - SUMY ',7X,E12.4//1H ,10X,
     4'COARSE DELTA T  ',F10.1/1H ,10X,'MAX DELTA MOLES ',F10.3//)
```

```
250    FORMAT(1H ,10X,29A2)
260    FORMAT(1H ,'*')
270    FORMAT(1H ,I2,  *')
300    FORMAT(1HO,1X,  TIME',7X,'RESIDUAL',7X,'BOIL-OFF',7X,  RESIDUAL',
      24X,'TEMPERATURE ,9X,'I',11X,'X(I)',11X,'Y(I) ,4X,  HYDROSTATIC'/
      31H ,2X,'SEC',11X,'MASS',11X,'MASS',10X,'MOLAR',14X,'K',51X,'HEAD'/
      41H ,19X,'G',8X,'G/CM2-S',11X,'MASS',68X,'CM'/
      51HO,5('='),4(5X,'=========='),5X,5('='),3(5X,  ========== ))
415    FORMAT(1H ,70X,I5,F15.4,F15.5)
420    FORMAT(1HO,F5.1,F15.2,F15.3,2F15.2,5X,I5,F15.4,F15.5,F15.2)
805    FORMAT(1H ,'EXCY,1,2 ',3F10.5,5X,'T,1,2  ',3F10.3)
900    FORMAT(1HO,'NEW TEMPERATURE ',F10.3)
910    FORMAT(1HO,I5,'X=  ',F10.5,5X,'Y=  ',F10.5)
       END
```

```
C         NOVA 840       PIPS2 FR         JAIME A  VALENCIA
C       VARIABLE GRID SPACING
      SUBROUTINE HTM(MBOFF,TCRYO,HVAP,CPLIQ,MASS,DTCP,AREA,IPRT,DTAU)
      REAL MBOFF,K1,K2,MASS
      COMMON/BLKHTM/TH(20),THSV(20),K1,ALFA1,K2,ALFA2,RHO,QL,M,NLIM
     1,EE,E,FILMT,TF,TWAT,THW,NN,R,P,INIT,II,IIT,QAS,IFIRST,NXCHG
      MR=11
      MW=12
      IF(IFIRST.NE.123)DTCP=0.0
      IF(IFIRST.EQ.123)GO TO 15
      ACCEPT 'K1,ALFA1  ',K1,ALFA1
      ACCEPT 'K2,ALFA2  ',K2,ALFA2
      ACCEPT 'RHO,QL  ',RHO,QL
      READ(MR,105)M,NLIM,NXCHG
      READ(MR,110)DTAU,EE,E
      READ(MR,110)FILMT
      READ(MR,110)TF,TWAT
      CALL DASW(IFW)
      THF=0
      THC=TCRYO-TF
      THW=TWAT-TF
      NN=2*M
      R=FLOAT(M)
      P=FLOAT(NN)
      IPRT=1./DTAU+0.1
      IPRT=IPRT/NXCHG
      NLIM=NLIM*NXCHG
      WRITE(MW,200)K1,ALFA1,K2,ALFA2,RHO,QL,HVAP
      WRITE(MW,201)TCRYO,TF,TWAT
      WRITE(MW,202)M,E,EE
      WRITE(MW,203)DTAU,NLIM,FILMT
      WRITE(MW,204)AREA
      CALL TSURF(TS,TF,TCRYO,DTAU,FILMT,IFW)
      THS=TS-TF
      DO 5 I=1,M
      TH(I)=THS+(FLOAT(I)/R)*(THF-THS)
      IF(IFW.EQ.2.OR.IFW.EQ.9)WRITE(MW,210)I,TH(I)
5     CONTINUE
```

```
      DO 10 I=M,NN
      TH(I)=THF+(FLOAT(I-M)/R)*(THW-THF)
      IF(TH(I) GT THW)TH(I)=THW
      IF(IFW.EQ.2.OR.IFW.EQ.9)WRITE(MW,210)I,TH(I)
10    CONTINUE
      MBOFF=0.
      INIT=0
      II=0
      IIT=0
15    II=II+1
      IF(II.EQ.IPRT)IIT=IIT+1
      IF(II.EQ.IPRT)II=0
      IF(IIT.GT.NLIM)GO TO 999
      CALL DASW(IFW)
      TAU=(FLOAT(II)+FLOAT(IIT)*FLOAT(IPRT))*DTAU
      IF(IFW.EQ.16)TYPE TAU
      CALL TSURF(TS,TF,TCRYO,TAU,FILMT,IFW)
      THS=TS-TF
      NS=0
       IF(IFW.EQ.2 OR.IFW.EQ.9)WRITE(MW,210)NS,THS
      TPRO=(TH(M-1)+TH(M)+2.*TF)/2.
      CALL PROP(TPRO,VK1E,VCP1E,VRHO1E)
      DE=(VK1E*(TH(M-2)-4.*TH(M-1)+3.*TH(M))/(2.*E/R)
     1+K2*(TH(M+2)-4.*TH(M+1)+3 *TH(M))/(2.*(EE-E)/(P-R)))
     2/(RHO*QL)
      E=DE*DTAU+E
      DX1=E/R
      DX2=(EE-E)/(P-R)
      IF(IFW.EQ.3.OR.IFW.EQ.9)WRITE(MW,230)E,DE,DX1,DX2
      MM1=M-1
      DO 30 N=1,MM1
      IF(N.EQ.1)THNM1=THS
      IF(N.NE.1)THNM1=TH(N-1)
      TPRO=TH(N)+TF
      CALL PROP(TPRO,VK,VCP,VRHO)
      TPRO=(THNM1+TH(N)+2.*TF)/2
      CALL PROP(TPRO,VK1,VCP1,VRHO1)
```

```
      TPRO=(TH(N)+TH(N+1)+2. *TF)/2
      CALL PROP(TPRO,VK2,VCP2,VRHO2)
      DTHDT=(VK1*(THNM1-TH(N))-VK2*(TH(N)-TH(N+1)))/(VRHO*VCP*(E/R)**2)
      DTH=(FLOAT(N)/E)*(TH(N+1)-THNM1)/2. *DE
     1+DTHDT
      THSV(N)=DTH*DTAU+TH(N)
      IF(IFW.EQ.2.OR.IFW.EQ.9)WRITE(MW,210)N,THSV(N)
30    CONTINUE
      THSV(M)=0.
      IF(IFW.EQ.2.OR.IFW.EQ.9)WRITE(MW,210)M,THSV(M)
      MP1=M+1
      NNM1=NN-1
      DO 50 N=MP1,NNM1
      DTH=(P-FLOAT(N))/(EE-E)*(TH(N+1)-TH(N-1))/2. *DE
     1+ALFA2*(TH(N-1)-2. *TH(N)+TH(N+1))/((EE-E)**2/(P-R)**2)
      THSV(N)=DTH*DTAU+TH(N)
      IF(IFW.EQ.2.OR.IFW.EQ.9)WRITE(MW,210)N,THSV(N)
50    CONTINUE
      THSV(NN)=THW
      IF(IFW.EQ.2.OR.IFW.EQ.9)WRITE(MW,210)NN,THSV(NN)
      DTDX=(-3 *THS+4. *TH(1)-TH(2))/(2. *DX1)
      TPRO=THS+TF
      CALL PROP(TPRO,VKQA,VCPQA,VRHOQA)
      QA=VKQA*DTDX
      IF(IFW.EQ.8.OR.IFW.EQ.9)WRITE(MW,220)TAU,QA,E
      ITEST=II-(II/IPRT)*IPRT
      IF(ITEST.NE.0)GO TO 75
      QACPL=CPLIQ*(MASS/1000)*DTCP/(AREA*1 E-4)/(DTAU*IPRT)
      IF(IFW.EQ.10.OR.IFW.EQ.9)WRITE(MW,240)TAU,QACPL,CPLIQ,MASS,DTCP
     1,AREA,DTAU
      QAT=QA
      QA=QA-QACPL
      IF(QA.LT.0.0)QA=0.0
      IF(INIT.EQ.0)QAS=QA
```

```
      MBOFF=MBOFF+(QAS+QA)/2. /HVAP/10 *(DTAU*IPRT)
      QAS=QA
      INIT=1
      IFIRST=123
      WRITE(MW,300)
      WRITE(MW,225)TAU,QACPL,QAT,TS,HVAP,E,MBOFF
      WRITE(MW,300)
      RETURN
75    CONTINUE
      DO 80 IK=1,NN
      TH(IK)=THSV(IK)
80    CONTINUE
      GO TO 15
999   CALL DATE(IDT1,IDT2,IDT3,IER)
      CALL FGTIM(IH,IM,IS)
      WRITE(MW,310)IH,IM,IS,IDT1,IDT2,IDT3
      CALL EXIT
105   FORMAT(5I5)
110   FORMAT(5F10.2)
200   FORMAT(1H /////1H ,5X,'K1 : ',E15.6,15X,' ALFA1 : ',
     1E15.6/1H ,5X,'K2 : ',E15.6,15X,'ALFA2 : ',E15.6/
     21H ,5X,'RHO: ',E15.6,15X,'QL    : ',E15.6/
     31H ,5X,'HVAP  ,E15.6///)
201   FORMAT(1H ,5X,'TCRYO : ',F10.2/1H ,5X,'TF    : ',F10.2/
     11H ,5X,'TWAT  : ',F10.2///)
202   FORMAT(1H ,5X,'M : ',I5,10X,'E : ',F10.5,10X,'EE : ',F10.5///)
203   FORMAT(1H ,5X,'DTAU : ',F10.5,10X,'NLIM :  ,I5///
     11H ,5X,'FILMT ',F10.2//)
204   FORMAT(1H ,5X,' AREA : ',F10.2/1H1)
210   FORMAT(1H ,I5,F10.2)
220   FORMAT(1H0,5E15.6)
225   FORMAT(1H ,'TAU  ',F7.2,5X,'QACPL',F7.2,5X,' QA    ',F7.2
     1,5X,'TSURF',F7.2,5X,'HVAP ',F7.2,5X,'EPS  ',F10.5,5X,'MBOFF',
     1F10.5)
230   FORMAT(1H ,'E,DE,DX1,DX2 ',4E15.6)
240   FORMAT(1H ,'TAU,QACPL,CPLIQ,MASS,DTCP,AREA,DTAU  ,7E13.5)
300   FORMAT(1H ,120('-'))
310   FORMAT(1H0////1H ,10X,'TIME ',2(I2,':'),I2,10X,'DATE  ,
     12(I2,'/'),I2//)
      END
```

BIBLIOGRAPHY

Ackermann, H., L. Bewilogua, R. Knöner, B. Kretzschmar, I. P. Usyugin, and H. Vinzelberg, "Heat Transfer in Liquid Nitrogen-Methane Mixtures Under Pressure," *Cryogenics*, 15, 657 (1975).

Ackermann, H., L. Bewilogua, A. Jahn, R. Knöner, and H. Vinzelberg, "Heat Transfer in Nitrogen-Methane Mixtures Under Pressure with Film Boiling," *Cryogenics*, 16, 497 (1976).

Berenson, P. J., "On Transition Boiling Heat Transfer from a Horizontal Surface," Ph.D. Thesis, Massachusetts Institute of Technology, Cambridge, Massachusetts (1960).

Berenson, P. J., "Experiments on Pool-Boiling Heat Transfer," *Int. J. Heat Mass Trans.*, 5, 985 (1962).

Bewilogua, L., R. Knöner, and H. Vinzelberg, "Heat Transfer in Cryogenic Liquids Under Pressure," *Cryogenics*, 15, 121 (1975).

Bird, R. B., W. E. Stewart and E. N. Lightfoot, *Transport Phenomena*, Wiley, New York (1960).

Bonilla, C. F. and A. A. Eisenberg, "Heat Transfer to Boiling Styrene and Butadiene and Their Mixtures with Water," *Ind. Eng. Chem.*, 40, 1113 (1948).

Boyle, G. I. and A. Kneebone, "Laboratory Investigations into the Characteristics of LNG Spills on Water. Evaporation, Spreading, and Vapor Dispersion," API Report 6Z32, Shell Research Ltd., Thornton Research Center, Chester, England (1973).

Brown, L. E., "Pool Boiling Heat Transfer to Liquefied Natural Gas and Liquefied Petroleum Gas," M.S. Thesis, University of Oklahoma, Norman, Oklahoma (1967).

Burgess, D. S., J. N. Murphy and M. G. Zabetakis, "Hazards Associated with the Spillage of LNG on Water," Bureau of Mines Report on Investigations RI-7448, U.S. Dept. of Interior (1970).

Burgess, D. S., J. Biordi and J. Murphy, "Hazards of Spillage of LNG into Water," MIPR No. Z-70099-9-12395, Bureau of Mines, U.S. Dept. of Interior (1972).

Carslaw, H. S. and J. C. Jaeger, *Conduction of Heat in Solids*, Oxford University at the Clarendon Press (1959).

Chang, S. D. and B. C. Y. Lu, "Vapor-Liquid Equilibria in the Nitrogen-Methane-Ethane System," *Chem. Eng. Prog. Sym. Ser.*, 63, 18 (1967).

Chueh, P. L. and J. M. Prausnitz, "Vapor-Liquid Equilibria at High Pressures. Vapor-Phase Fugacity Coefficients in Nonpolar and Quantum-Gas Mixtures," *Ind. Eng. Chem. Fundamentals*, 6, 493 (1967).

Clements, L. D., "Vapor-Liquid Change of Phase Heat Transfer Behavior of Light Hydrocarbons and Their Mixtures," Ph.D. Thesis, University of Oklahoma, Norman, Oklahoma (1973).

Dincer, A. K., "Boiling of Cryogenic Liquids on Water. The Effect of Initial Water Temperatures," M.S. Thesis, Massachusetts Institute of Technology, Cambridge, Massachusetts (1975).

Drake, E. M., A. A. Jeje and R. C. Reid, "Transient Boiling of Liquefied Cryogens on a Water Surface. I. Nitrogen, Methane, and Ethane. II. Light Hydrocarbon Mixtures," *Int. J. Heat Mass Trans.*, 18, 1361 (1975).

Erbar, J., Private communication to R. C. Reid (1973).

Erbar, J., Private communication to R. C. Reid (1977).

Fay, J. A., "Unusual Fire Hazard of LNG Tanker Spills," *Combustion Sci. and Tech.*, 7, 47 (1973).

Fortuna, G. and S. Sideman, "Direct Contact Heat Transfer Between Immiscible Liquid Layers with Simultaneous Boiling and Stirring," *Chem. Eng. Sci.*, 23, 1105 (1968).

Gallant, R. W., *Physical Properties of Hydrocarbons*, Vol. 1, Gulf Publ. Co., Houston, Texas (1968).

Hoult, D., "The Fire Hazard of LNG Spilled on Water," Proc. Conference on LNG Importation and Safety, Boston, Massachusetts, 87 (1972).

Hovestreijdt, J., "The Influence of the Surface Tension Difference on the Boiling of Mixtures," *Chem. Eng. Sci.*, 18, 631 (1963).

Jeje, A. A., "Transient Pool Boiling of Cryogenic Liquids on Water," Ph.D. Thesis, Massachusetts Institute of Technology, Cambridge, Massachusetts (1974).

Joffe, J., G. M. Schroeder and D. Zudkevitch, "Vapor-Liquid Equilibrium with the Redlich-Kwong Equation of State," *AIChE J.*, 16, 496 (1970).

Kato, M., W. K. Chung and B. C. Y. Lu, "Binary Interaction Coefficients of the Redlich-Kwong Equation of State," *Chem. Eng. Sci.*, 31, 733 (1976).

Kosky, P. G. and D. N. Lyon, "Pool Boiling Heat Transfer to Cryogenic Liquids," *AIChE J.*, 14, 372 (1968).

Kravchenko, V. A., L. F. Tolubinskaya and A. I. Pyatnichko, "Heat Transfer in Boiling of Methane at p = 1.02 bar," *Heat Transfer-Sov. Res.*, 7, 27 (1975).

Kutateladze, S. S., *Fundamentals of Heat Transfer*, Academic Press, New York (1963).

Lyon, D. N., "Pool Boiling of Cryogenic Liquids," *Chem. Eng. Prog. Sym. Ser.*, 64, 82 (1968).

Miller, S. L., "*The Clathrate Hydrates - Their Nature and Occurrence*," in *Physics and Chemistry of Ice*, edited by E. Whalley, S. J. Jones and L. W. Gold, University of Toronto Press, Canada (1973).

Modell, M. and R. C. Reid, *Thermodynamics and Its Applications*, Prentice-Hall, Inc., New Jersey (1974).

Mohammadi, S. S., "Boiling of Liquefied Petroleum Gas on Water. The Effect of Initial Mass, Spill Technique, and Composition," M.S. Thesis, Massachusetts Institute of Technology, Cambridge, Massachusetts (1977).

Murray, W. D. and F. Landis, "Numerical and Machine Solutions of Transient Heat-Conduction Problems Involving Melting or Freezing," *J. Heat Trans.*, 81, 106 (1959).

Neumann, F. (1860's) published by Riemann-Weber, *Die Partiellen Differentialgleichungen der Mathematischen Physik*, Vol. 2, p. 121 (1912).

Novakovic, M. and M. Stefanovic, "Boiling from a Mercury Surface," *Int. J. Heat Mass Trans.*, 7, 801 (1964).

Opschoor, G., "Investigations into the Spreading and Evaporation of LNG Spilled on Water," *Cryogenics*, 17, 629 (1977).

Otterman, B., "Analysis of Large LNg Spills on Water. Liquid Spread and Evaporation," *Cryogenics*, 15, 455 (1975).

Park, E. L., C. P. Colver and C. M. Sliepcevich, "Nucleate and Film Boiling Heat Transfer to Nitrogen and Methane at Elevated Pressures and Large Temperature Differences," *Advances in Cryogenic Eng., Vol. 11*, Plenum Press, New York, p. 516 (1966).

Poon, D. P. L. and B. C. Y. Lu, "Phase Equilibria for Systems Containing Nitrogen, Methane, and Propane," *Advances in Croygenic Eng., Vol. 19*, Plenum Press, New York, p. 292 (1974).

Porchey, D. V., E. L. Park and K. G. Mayhan, "A Scanning Electron Microscope Surface Study of Nucleate Pool Boiling Heat Transfer to Saturated Liquid Nitrogen," *AIChE Sym. Ser.*, 68, 162 (1972).

Porteous, W. M., "Superheating and Cryogenic Vapor Explosions," Ph.D. Thesis, Massachusetts Institute of Technology, Cambridge, Massachusetts (1975).

Prausnitz, J. M., C. A. Eckert, R. V. Orye and J. P. O'Connell, *Computer Calculations for Multicomponent Vapor-Liquid Equilibria*, Prentice-Hall, Inc., New Jersey (1967).

Price, A. R. and R. Kobayashi, "Low Temperature Vapor-Liquid Equilibrium in Light Hydrocarbon Mixtures: Methane-Ethane-Propane System," *J. Chem. Eng. Data*, 4, 40 (1959).

Redlich, O. and J. N. S. Kwong, "On the Thermodynamics of Solutions," *Chem. Rev.*, 44, 233 (1949).

Reid, R. C., J. M. Prausnitz and T. K. Sherwood, *The Properties of Gases and Liquids*, McGraw-Hill, New York (1977).

Reid, R. C. and K. A. Smith, "Boiling of Liquefied Petroleum Gas on Water," Progress Report to National Science Foundation, Grant NSF 7517445-AER, Contract EE-77-S-02-4548 (1977).

Rohsenow, W. M. and H. V. Choi, *Heat, Mass and Momentum Transfer*, Prentice-Hall, Inc., New Jersey (1961).

Sciance, C. T., C. P. Colver, and C. M. Sliepcevich, "Nucleate Pool Boiling and Burnout of Liquefied Hydrocarbon Gases," *Chem. Eng. Prog. Sym. Ser.*, 63, 109 (1967a).

Sciance, C. T., C. P. Colver, and C. M. Sliepcevich, "Film Boiling Measurements and Correlation for Liquefied Hydrocarbon Gases," *Chem. Eng. Prog. Sym. Ser.*, 63, 115 (1967b).

Sciance, C. T., C. P. Colver, and C. M. Sliepcevich, "Pool Boiling of Methane Between Atmospheric Pressure and the Critical Pressure," *Advances in Cryogenic Eng., Vol. 12*, Plenum Press, New York, p. 395 (1967c).

Sciance, C. T. and C. P. Colver, "Minimum Film-Boiling Point for Several Light Hydrocarbons," *J. Heat Trans.*, 92, 659 (1970).

Sliepcevich, C. M., H. T. Hashemi and C. P. Colver, "Heat Transfer Problems in LNG Technology," *Chem. Eng. Prog. Sym. Ser.*, 64, 120 (1968).

Soave, G., "Equilibrium Constants from a Modified Redlich-Kwong Equation of State," *Chem. Eng. Sci.*, 27, 1197 (1972).

Stefan, J., "Über die Theorie der Eisbildung, Insbesondere über die Eisbildung in Polarmaere," *Annalen der Physik und Chemie*, 42, 269 (1891).

Stryjek, R., P. S. Chappelear and R. Kobayashi, "Low Temperature Vapor-Liquid Equilibria of Nitrogen-Methane System," *J. Chem. Eng. Data*, 19, 334 (1974a).

Stryjek, R., P. S. Chappelear and R. Kobayashi, "Low Temperature Vapor-Liquid Equilibria of Nitrogen-Ethane System," *J. Chem. Eng. Data*, 19, 340 (1974b).

Tong, L. S., *Boiling Heat Transfer and Two Phase Flow*, John Wiley, New York (1965).

Van Stralen, S. J. D., "The Mechanism of Nucleate Boiling in Pure Liquids and in Binary Mixtures, Parts I, II, III, IV," *Int. J. Heat Mass Trans.*, 9, 995 (1966).

Van Stralen, S. J. D., "Bubble Growth Rates in Boiling Binary Mixtures," *British Chem. Eng.*, 12, 390 (1967).

Van Stralen, S. J. D. and W. M. Sluyter, "Local Temperature Fluctuations in Saturated Pool Boiling of Pure Liquids and Binary Mixtures," *Int. J. Heat Mass Trans.*, 12, 187 (1969).

Van Stralen, S. J. D., "The Boiling Paradox in Binary Liquid Mixtures," *Chem. Eng. Sci.*, 25, 149 (1970).

Van Stralen, S. J. D., "Nucleate Boiling in Binary System," Winter Annual Meeting ASME, New York (1970).

Van Stralen, S. J. D., C. J. J. Joosen and W. M. Sluyter, "Film Boiling of Water and an Aqueous Binary Mixture," *Int. J. Heat Mass Trans.*, 15, 2427 (1972).

Van Stralen, S. J. D., W. M. Sluyter and R. Cole, "Bubble Growth Rates in Nucleate Boiling of Aqueous Binary Systems at Subatmospheric Pressures," *Int. J. Heat Mass Trans.*, 19, 931 (1976).

Van Wijk, W. R., A. S. Vos and S. J. D. Van Stralen, "Heat Transfer to Boiling Binary Liquid Mixtures," *Chem. Eng. Sci.*, 5, 68 (1956).

Vestal, C. R., "Film Boiling Heat Transfer Between Cryogenic Liquids and Water," Ph.D. Thesis, Colorado School of Mines, Golden, Colorado (1973).

Wright, R. D. and C. P. Colver, "Saturated Pool Boiling Burnout of Ethane-Ethylene Mixtures," *Chem. Eng. Prog. Sym. Ser.*, 65, 204 (1969).

Wright, R. D., L. D. Clements and C. P. Colver, "Nucleate and Film Pool Boiling of Ethane-Ethylene Mixtures," *AIChE J.*, 17, 626 (1971).

Zudkevitch, D. and J. Joffe, "Correlation and Prediction of Vapor-Liquid Equilibria with the Redlich-Kwong Equation of State," *AIChE J.*, 16, 112 (1970).

LOCATION OF ORIGINAL DATA

The original data, computer programs and outputs are in the possession of the author. A complete copy of the above has been filed at the LNG Research Center, Department of Chemical Engineering, Massachusetts Institute of Technology.

Biographical Note

Jaime A. Valencia-Chávez was born in Arequipa, Peru in 1952. He entered the Universidad National de San Agustin in 1967. In 1970 he was awarded a scholarship to attend the University of Maryland, where he obtained a B.S. with High Honors in Chemical Engineering in December, 1973. He received the AIChE Professional Achievement Award from the AIChE National Capital Section during his senior year.

In January, 1974, he entered the Graduate Program in Chemical Engineering at the Massachusetts Institute of Technology. He fulfilled the minor requirements for the Sc.D. attending the Harvard School of Business Administration. At MIT he served as president of the Graduate Student Council of the Chemical Engineering Department.

Mr. Valencia has been associated with A. D. Little, Inc., on a part-time basis, since 1975; he will be joining A. D. Little, Inc. upon graduation from MIT.

Mr. Valencia was elected to the honorary societies of: Omicron Delta Kappa, Tau Beta Pi, Omega Chi Epsilon, Phi Kappa Phi and Sigma Xi. He is also a member of the American Institute of Chemical Engineers, American Chemical Society, and American Nuclear Society.